Spectral and Spectral Element Methods for Fractional PDEs

by

Mohsen Zayernouri

B.Sc., Mechanical Engineering, Azad University, Iran, 2004

M.Sc., Mechanical Engineering, Tehran Polytechnic, Iran, 2006

Ph.D., Mechanical Engineering, University of Utah, USA, 2010

Sc.M., Applied Mathematics, Brown University, USA, 2012

A dissertation submitted in partial fulfillment of the

requirements for the degree of Doctor of Philosophy

in The Division of Applied Mathematics at Brown University

PROVIDENCE, RHODE ISLAND

May 2015

This dissertation by Mohsen Zayernouri is accepted in its present form
by The Division of Applied Mathematics as satisfying the
dissertation requirement for the degree of Doctor of Philosophy.

Date_____ _____

George Em Karniadakis, Ph.D., Advisor

Recommended to the Graduate Council

Date_____ _____

Mark Ainsworth, Ph.D., Reader

Date_____ _____

Jan S. Hesthaven, Ph.D., Reader

Date_____ _____

Mark M. Meerschaert, Ph.D., Reader

Approved by the Graduate Council

Date_____ _____

Peter M. Weber, Dean of the Graduate School

Vitae

Mohsen Zayernouri obtained his B.Sc. in mechanical engineering from Azad University, Iran, where he was ranked first amongst the graduates in 2004. Next, he joined Tehran Polytechnic (Amirkabir University of Technology), where he acquired his M.Sc. in mechanical engineering as the top student in 2006. He received the best national M.Sc. award from Iranian Society of Mechanical Engineering (ISME), and then, he was elected into the National Foundation of Elite in Iran. Subsequently, he attended the University of Utah, USA, where he obtained his first Ph.D. in mechanical engineering in 2010. Due to his great passion and interest in mathematics and scientific computing, he joined Brown University right after defending his Ph.D. thesis at Utah to seek a second Ph.D. in applied mathematics under the advice of Prof. George Em Karniadakis. The outcome of his research at Brown on developing spectral theories and high-order methods for fractional PDEs is a series of ten journal papers, provided in the list of references.

Acknowledgements

I would like to thank my advisor, Professor George Em Karniadakis, for the great amount of trust, unique advice, and endless encouragement. I am indebted to George for many valuable opportunities he gave me during the course of this work, also for generous sharing his research experience, which provides me an important reference for my future career.

It was a privilege having such an exceptional committee of research and readers, consisting of Professor Mark Ainsworth, Professor Jan S. Hesthaven, and Professor Mark M. Meerschaert. I would like to sincerely thank them all for reading and correcting the thesis, also for their constructive feedback, which added a lot to the value of the present study.

I have learned a lot about finite-difference methods, finite element methods, spectral methods, and spectral element methods from the excellent lectures, given by Professor Ainsworth, Professor Chi-Wang Shu, and Professor Johnny Guzmann, to whom my gratitude goes. I was also fortunate to learn about the theory of probability and stochastic partial differential equations from Prof. Boris Rozovsky who will remain as a great source of inspiration in my future carrier. In addition, I would like to acknowledge Professor Anastasios Matzavinos and Professor Marco L. Bittencourt for their support and collaboration during the preparation of the last two chapters of the dissertation. Moreover, many thanks are due to our wonderful staff, especially

to Ms. Madeline Brewster, Ms. Stephanie Han, and Ms. Jean Radican for being there whenever I needed help.

I would like to express gratitude to many CRUNCHers, Mengdi Zhang, Dr. Changho Kim, Dr. Handy (Zhongqiang) Zhang, Paris Perdikaris, Minge Deng, Heyrim Cho, Dr. Minseok Choi, Dr. Xui Yang, Dr. Yue Yu, Seungjoon Lee, Yuhang, Dogkun Zhang, Ansel Blumers for all their help and many happy conservations. Moreover, I would like to thank my other friends, post-docs, senior researchers, and visitor scholars at CRUNCH group: Dr. Alireza Yazdani, Dr. Wanrong Cao, Dr. Daniele Venturi, Dr. Leopold Grinberg, Dr. Xuejin Li, Dr. Zhen Li, Dr. Fangying Song, Dr. Fanhai Zeng, Dr. Xuan Zhao, and Wei Cai for their help and interesting discussions.

I would love to especially thank my wife, Dr. Maryam Naghibolhosseini, whose love, emotional support, and encouragement made me much stronger, happier, and more faithful throughout my study at Brown and to whom this work is dedicated. At last but certainly not least, I would like to express gratitude to my precious parents, lovely brothers, and wonderful friends for their constant love, support, and friendship.

This work was supported by the Collaboratory on Mathematics for Mesoscopic Modeling of Materials (CM4) at PNNL funded by the Department of Energy, by OSD/MURI and by NSF/DMS.

To my wife

Contents

List of Tables

List of Figures

Chapter One

Introduction

Fractional partial differential equations (FPDEs) generalize the standard (integer-order) calculus and PDEs to any differential form of fractional orders. That puts existing PDEs into a subset of this larger family of mathematical models. In this context, fractional calculus is the theory, which unifies and generalizes the notions of integer-order differentiation and integration to any real- or complex-order [128, 142, 90]. Over the last decade, it has been demonstrated that many systems in science and engineering can be modelled more accurately by employing fractional-order rather than integer-order derivatives [32, 177].

Fractional PDEs open new possibilities for robust mathematical modeling of physical processes that exhibit anomalous (sub- or super-) diffusion, nonlocal interactions, self-similar structures, long memory dependence, and power-law effects. In fact, FPDEs are the right tool for exploring fractal operators and for modeling sharp interfaces in multi-phase problems, wave propagation in disordered media, and multi-scale materials. There is now an extensive amount of experimental evidence indicating that such phenomena occur in many applications in mechanics, including non-Gaussian (Levy) processes in turbulent flows, non-Newtonian fluids and rheology, non-Brownian transport phenomena in porous and disordered materials, and non-Markovian processes in multi-scale complex fluids and multi-phase applications. Moreover, there exist many other critical applications in biomechanics [115], such as anomalous thermo-fluid processes in human brain, nonlocal viscoelasticity in human red-blood-cells, and power-law stress relaxation in wall-arteries. In such applications, FPDEs naturally appear as the right governing equations leading to high-fidelity modeling and predictive simulations, which otherwise cannot be achieved using the standard PDEs.

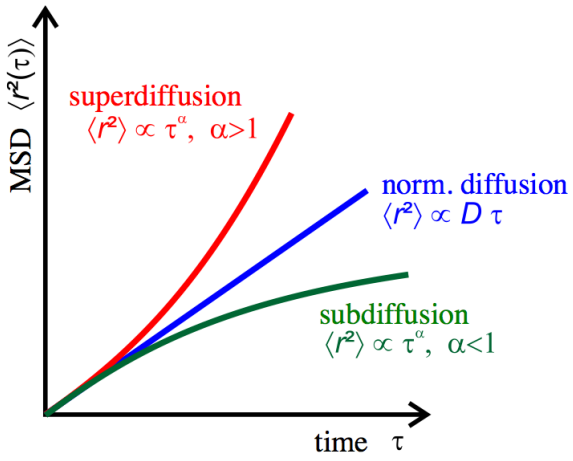

Figure 1.1: Sub-diffusion, standard diffusion, and super-diffusion.

1.0.1 Anomalous Diffusion

Anomalous diffusion is a diffusion process with a nonlinear relationship to time, in contrast to a standard diffusion process, in which the mean squared displacement (MSD), σ_r^2, of a particle is a linear function of time. Unlike the standard diffusion, anomalous diffusion is described by a power law $\sigma_r^2 \sim D\tau^\alpha$, where D is the diffusion coefficient and τ is the elapsed time. As shown in Fig. 1.1, in a typical diffusion process, $\alpha = 1$. If $\alpha > 1$, the phenomenon is called *super-diffusion*. If $\alpha < 1$, the particle undergoes sub-diffusion (see e.g., [91] and references therein).

From the particle kinetics points of view, continuum-time random walk (CTRW) is a rigorous and general mathematical model, which incorporates waiting times and/or non-Gaussian jump distributions with *divergent* second moments to account for the anomalous jumps called *Lévy flights* [126, 33, 125]. The continuous limit for such models leads to a fractional in time and/or space diffusion equation [128, 142, 90]. However in practice, many physical processes take place in bounded domains in finite times and have finite moments. Therefore, the divergent second moments may not be applicable to such processes. In order to overcome this modelling barrier,

there are different techniques such as discarding the very large jumps and employing truncated Lévy flights [120], or, adding a high-order power-law factor [161]. However, the most popular, and perhaps most rigorous approach to get finite moments, is exponentially tempering the probability of large jumps of Lévy flights, which results in tempered-stable Lévy processes with *finite* moments [33, 11, 123, 153]. The corresponding fluid (continuous) limit for such models yields the *tempered fractional* diffusion equation, which complements the previously known models in fractional calculus.

Fractional differential operators of form $\mathcal{D}_t^\nu \equiv d^\nu/dt^\nu$, where $\nu \in \mathbb{R}$, appear in many systems in science and engineering such as electrochemical processes [70], porous or fractured media [20], viscoelastic materials [117, 177], bioengineering applications [115]. For instance, it has been found that the transport dynamics in complex and/or disordered systems is governed by non-exponential relaxation patterns and *anomalous* diffusion [26, 127, 91]. For such non-Markovian processes, a time-fractional diffusion equation, in which the time-derivative emerges as $\mathcal{D}_t^\nu u(t)$, governs the evolution for the Probability Density Function (PDF). Another interesting example occurring in viscous fluid flows is the *cumulative memory* effect of the wall-friction through the boundary layer, which gives rise to fractional derivatives in equations of fluid motion [41, 84, 164].

A variety of numerical methods, originally developed for integer-order PDEs, are currently extended by several authors to FPDEs (see e.g., [64, 68, 195, 76]). Traditionally, there has been a substantial amount of work in developing finite-difference methods (FDM) for FPDEs. The notion of discretized fractional calculus was originally introduced by Lubich [113, 114] and was employed by Sanz-Serna [154] in developing a first-order FDM algorithm for partial integro-differential equations. Since then, a significant amount of work has been devoted to improving the convergence

rates of FDM schemes (see e.g., [104, 166, 111, 30]).

The main focus of this study is to construct a new mathematical platform for developing global, efficient, and highly accurate numerical algorithms for solving fractional PDEs. Although fractional partial differential equations (FPDEs) are the right mathematical models for many physical processes, the biggest challenge is their global nature and memory-dependent characteristics. That is one important reason that over the past decades these global models have not been much employed in science and engineering, and instead, simplifying Newtonian, Gaussian, and Brownian assumptions have been adopted at the cost of weakening the fidelity of resulting models. In fact, the inherent bottleneck of non-locality in fractional PDEs leads to excessive computer-memory storage requirements and insufficient computational accuracy. Utilization of local numerical methods, such as finite difference, can easily take days on a standard desktop computer, even for problems with a single dimension. Moreover, this challenge becomes even more severe when fractional PDEs are involved with multi-fractional order terms, nonlinear differential operators, or variable- and distributed-order derivatives in time and space, for which there existed no high-order numerical methods prior to our work. Given the aforementioned challenges in cases with low dimensionality, fractional PDEs in higher dimensions were computationally intractable, making real-world applications nearly impossible.

We developed a novel mathematical platform by developing a new spectral theory of fractional Sturm-Liouville eigen-problems to overcome these fundamental barriers. Our approach fractionalizes the standard family of Jacobi polynomial to a new class of fractional orthogonal functions, namely Jacobi Poly-fractonomials, which enjoy many attractive properties. We then introduced these fractional eigenfunctions as optimal basis/test functions in developing high-order Petrov-Galerkin spectral/spectral element methods for fractional ODEs/PDEs.

For fast treatment of nonlinear and multi-term fractional PDEs such as fractional Burgers equation, we have developed a new spectral method, called the fractional spectral collocation method, which introduces a new class of fractional Lagrange interpolants. For simulation of multi-scale multi-dynamics systems, we also proposed that by varying the differential order of a given governing equation as a function of space and/or time, we can capture a wide range of dynamics from diffusion to sub-diffusion or from wave dynamics transitioning back to diffusion. For such variable-order and distributed-order fractional PDEs, we have developed two fast and spectrally accurate numerical algorithms.

While almost all existing methods for fractional PDEs are applicable only in one- or at most two-dimensional problems, we developed a unified Petrov-Galerkin spectral method that solves the whole family of elliptic, hyperbolic, and parabolic fractional PDEs in high dimensions (up to ten dimensions) on just a laptop. We also aim formulated an implicit-explicit (IMEX) splitting scheme in for simulation of multi-scale and stiff problems. This algorithm provides an efficient platform in computational biology and dynamics of cell propagation. Finally, we manage to construct a novel family of fractional modal expansions for non-tensorial domains in triangle and tetrahedral elements, which can lead to formulation of FPDEs in complex geometries.

Chapter Two

Fractional Sturm-Liouville Eigen-Problems

In this chapter, we first consider a regular fractional Sturm-Liouville problem of two kinds RFSLP-I and RFSLP-II of order $\nu \in (0, 2)$. The corresponding fractional differential operators in these problems are both of Riemann-Liouville and Caputo type, of the same fractional order $\mu = \nu/2 \in (0, 1)$. We obtain the analytical eigen-solutions to RFSLP-I &-II as non-polynomial functions, which we define as Jacobi *poly-fractonomials*. These eigenfunctions are orthogonal with respect to the weight function associated with RFSLP-I &-II. Subsequently, we extend the fractional operators to a new family of singular fractional Sturm-Liouville problems of two kinds, SFSLP-I and SFSLP-II. We show that the primary regular boundary-value problems RFSLP-I&-II are indeed asymptotic cases for the singular counterparts SFSLP-I&-II. Furthermore, we prove that the eigenvalues of the singular problems are real-valued and the corresponding eigenfunctions are orthogonal. In addition, we obtain the eigen-solutions to SFSLP-I &-II analytically, also as non-polynomial functions, hence completing the whole family of the Jacobi poly-fractonomials. In the numerical examples provided in this chapter, we employ the new poly-fractonomial bases to demonstrate the exponential convergence of the approximation in agreement with the theoretical results.

2.1 Background

The Sturm-Liouville theory has been the keystone for the development of spectral methods and the theory of self-adjoint operators [3]. For many applications, the Sturm-Liouville problems (SLPs) are studied as boundary value problems [192]. However, to date mostly integer order differential operators in SLPs have been used, and such operators do not include any fractional differential operators.

In most of the Fractional Sturm-Liouville formulations presented recently, the ordinary derivatives in a traditional Sturm-Liouville problem are replaced with fractional derivatives, and the resulting problems are solved using some numerical schemes such as Adomian decomposition method [1], or fractional differential transform method, [58], or alternatively using the method of Haar wavelet operational matrix, [131]. However, in such numerical studies, round-off errors and the pseudo-spectra introduced in approximating the infinite-dimensional boundary-value problem as a finite-dimensional eigenvalue problem prohibit computing more than a handful of eigenvalues and eigenfunctions with the desired precision. Furthermore, these papers do not examine the common properties of Fractional Sturm-Liouville Problems (FSLPs) such as orthogonality of the eigenfunctions of the fractional operator in addition to the reality or complexity of the eigensolutions.

Establishing the aforementioned fundamental properties for FSLPs is very important in establishing proper numerical methods, e.g. the eiegensolutions of the RFSLP may be complex [72]. To this end, some results have been recently provided in [144, 9], where the fractional character of the problem has been considered through defining a classical Sturm-Liouville operator, extended by the term that includes a sum of the left- and right-sided fractional derivatives. More recently, a regular Fractional Sturm-Liouville problem (RFSLP) of two types has been defined in [93], where it has been shown that the the eigenvalues of the problem are real, and the eigenfunctions corresponding to distinct eigenvalues are orthogonal. However, the discreteness and simplicity of the eigenvalues have not been addressed. In addition, the spectral properties of a regular FSLP for diffusion operator have been studied in [15] demonstrating that the fractional diffusion operator is self-adjoint. The recent progress in FSLPs is promising for developing new spectral methods for fractional PDEs, however, the eigensolutions have not been obtained explicitly and

no numerical approximation results have been published so far.

The main contribution of this chapter is to develop a spectral theory for the regular and singular fractional Sturm-Liouville problems (RFSLP & SFSLP) and demonstrate its utility by constructing explicitly proper bases for numerical approximations of fractional functions. To this end, we first consider a regular problem of two kinds, i.e., RFSLP-I &-II. Then, we obtain the analytical eigensolutions to these problems explicitly for the first time. We show that the explicit eigenvalues to RFSLP-I &-II are real, discrete and simple. In addition, we demonstrate that the corresponding eigenfunctions are of non-polynomial form, called Jacobi *Poly-fractonomials*. We also show that these eigenfunctions are orthogonal and dense in $L^2_w[-1,1]$, forming a complete basis in the Hilbert space. We subsequently extend the regular problem to a singular fractional Sturm-Liouville problem again of two kinds SFSLP-I&-II, and prove that the eigenvalues of these singular problems are real and the eigenfunctions corresponding to distinct eigenvalues are orthogonal; these too are computed analytically. We show that the eigensolutions to such singular problems share many fundamental properties with their regular counterparts, with the explicit eigenfunctions of SFSLP-I&-II completing the family of the Jacobi poly-fractonomials. Finally, we complete the spectral theory for the regular and singular FSLPs by analyzing the approximation properties of the eigenfunctions of RFSLPs and SFSLPs, which are employed as basis functions in approximation theory. Our numerical tests verify the theoretical exponential convergence in approximating non-polynomial functions in $L^2_w[-1,1]$. We compare with the standard polynomial basis functions (such as Legendre polynomials) demonstrating the fast exponential convergence of the poly-fractonomial bases.

2.2 Definitions

Before defining the boundary-value problem, we start with some preliminary definitions of fractional calculus [142]. The left-sided and right-sided Riemann-Liouville integrals of order μ, when $0 < \mu < 1$, are defined, respectively, as

$$({}^{RL}_{x_L}\mathcal{I}^{\mu}_{x} f)(x) = \frac{1}{\Gamma(\mu)} \int_{x_L}^{x} \frac{f(s)ds}{(x-s)^{1-\mu}}, \quad x > x_L, \tag{2.1}$$

and

$$({}^{RL}_{x}\mathcal{I}^{\mu}_{x_R} f)(x) = \frac{1}{\Gamma(\mu)} \int_{x}^{x_R} \frac{f(s)ds}{(s-x)^{1-\mu}}, \quad x < x_R, \tag{2.2}$$

where Γ represents the Euler gamma function. The corresponding inverse operators, i.e., the left-sided and right-sided fractional derivatives of order μ, are then defined based on (2.1) and (2.2), as

$$({}^{RL}_{x_L}\mathcal{D}^{\mu}_{x} f)(x) = \frac{d}{dx}({}^{RL}_{x_L}\mathcal{I}^{1-\mu}_{x} f)(x) = \frac{1}{\Gamma(1-\mu)} \frac{d}{dx} \int_{x_L}^{x} \frac{f(s)ds}{(x-s)^{\mu}}, \quad x > x_L, \tag{2.3}$$

and

$$({}^{RL}_{x}\mathcal{D}^{\mu}_{x_R} f)(x) = \frac{-d}{dx}({}^{RL}_{x}\mathcal{I}^{1-\mu}_{x_R} f)(x) = \frac{1}{\Gamma(1-\mu)} (\frac{-d}{dx}) \int_{x}^{x_R} \frac{f(s)ds}{(s-x)^{\mu}}, \quad x < x_R. \tag{2.4}$$

Furthermore, the corresponding left- and right-sided Caputo derivatives of order $\mu \in (0, 1)$ are obtained as

$$({}^{C}_{x_L}\mathcal{D}^{\mu}_{x} f)(x) = ({}^{RL}_{x_L}\mathcal{I}^{1-\mu}_{x} \frac{df}{dx})(x) = \frac{1}{\Gamma(1-\mu)} \int_{x_L}^{x} \frac{f'(s)ds}{(x-s)^{\mu}}, \quad x > x_L, \tag{2.5}$$

and

$$({}^{C}_{x}\mathcal{D}^{\mu}_{x_R} f)(x) = ({}^{RL}_{x}\mathcal{I}^{1-\mu}_{x_R} \frac{-df}{dx})(x) = \frac{1}{\Gamma(1-\mu)} \int_{x_L}^{x} \frac{-f'(s)ds}{(x-s)^{\mu}}, \quad x < x_R. \tag{2.6}$$

The two definitions of the left- and right-sided fractional derivatives of both Riemann-Liouville and Caputo type are linked by the following relationship, which can be derived by a direct calculation

$$({}^{RL}_{x_L}\mathcal{D}^{\mu}_{x} f)(x) = \frac{f(x_L)}{\Gamma(1-\mu)(x+x_L)^{\mu}} + ({}^{C}_{x_L}\mathcal{D}^{\mu}_{x} f)(x), \tag{2.7}$$

and

$$({}^{RL}_{x}\mathcal{D}^{\mu}_{x_R} f)(x) = \frac{f(x_R)}{\Gamma(1-\mu)(x_R-x)^{\mu}} + ({}^{C}_{x}\mathcal{D}^{\mu}_{x_R} f)(x). \tag{2.8}$$

Moreover, the fractional integration-by-parts for the aforementioned fractional derivatives is obtained as

$$\int_{x_L}^{x_R} f(x)\, {}^{RL}_{x}\mathcal{D}^{\mu}_{x_R} g(x)dx = \int_{x_L}^{x_R} g(x)\, {}^{C}_{x_L}\mathcal{D}^{\mu}_{x} f(x)dx - f(x)\, {}^{RL}_{x}\mathcal{I}^{\mu}_{x_R} g(x)|^{x_R}_{x=x_L}, \tag{2.9}$$

and

$$\int_{x_L}^{x_R} f(x)\, {}^{RL}_{x_L}\mathcal{D}^{\mu}_{x} g(x)dx = \int_{x_L}^{x_R} g(x)\, {}^{C}_{x}\mathcal{D}^{\mu}_{x_R} f(x)dx + f(x)\, {}^{RL}_{x_L}\mathcal{I}^{\mu}_{x} g(x)|^{x_R}_{x=x_L}. \tag{2.10}$$

Finally, we recall a useful property of the Riemann-Liouville fractional derivatives. Assume that $0 < p < 1$ and $0 < q < 1$ and $f(x_L) = 0 \;\; x > x_L$, then

$${}^{RL}_{x_L}\mathcal{D}^{p+q}_{x} g(x) = \left({}^{RL}_{x_L}\mathcal{D}^{p}_{x}\right)\left({}^{RL}_{x_L}\mathcal{D}^{q}_{x}\right) g(x) = \left({}^{RL}_{x_L}\mathcal{D}^{q}_{x}\right)\left({}^{RL}_{x_L}\mathcal{D}^{p}_{x}\right) g(x). \tag{2.11}$$

2.3 Part I: Regular Fractional Sturm-Liouville Problems of Kind I & II

We consider a regular fractional Sturm-Liouville problem (RFSLP) of order $\nu \in (0,2)$, [93], where the differential part contains both left- and right-sided fractional derivatives, each of order $\mu = \nu/2 \in (0,1)$ as

$$ {}^{RL}\mathcal{D}^{\mu}\left[p_i(x)\,{}^{C}\mathcal{D}^{\mu}\Phi_{\lambda}^{(i)}(x)\right] + q_i(x)\Phi_{\lambda}^{(i)}(x) + \lambda w_i(x)\Phi_{\lambda}^{(i)}(x) = 0, \quad x \in [x_L, x_R], \tag{2.12} $$

where $i \in \{1,2\}$, with $i=1$ denoting the RFSLP of first kind, where ${}^{RL}\mathcal{D}^{\mu} \equiv {}^{RL}_{x}\mathcal{D}^{\mu}_{x_R}$ (i.e., right-sided Riemann-Liouville fractional derivative of order μ) and ${}^{C}\mathcal{D}^{\mu} \equiv {}^{C}_{x_L}\mathcal{D}^{\mu}_{x}$ (i.e., left-sided Caputo fractional derivative of order μ), and $i=2$ corresponding to the RFSLP of second kind in which ${}^{RL}\mathcal{D}^{\mu} \equiv {}^{RL}_{x_L}\mathcal{D}^{\mu}_{x}$ and ${}^{C}\mathcal{D}^{\mu} \equiv {}^{C}_{x}\mathcal{D}^{\mu}_{x_R}$ (i.e., respectively, left-sided Riemann-Liouville and right-sided Caputo fractional derivative of order μ). In such setting, $\mu \in (0,1)$, $p_i(x) \neq 0$, $w_i(x)$ is a non-negative weight function, and $q_i(x)$ is a potential function. Also, p_i, q_i and w_i are real-valued continuous functions in the interval $[x_L, x_R]$.

The boundary-value problem (2.12) is subject to the boundary conditions

$$ a_1\Phi_{\lambda}^{(i)}(x_L) + a_2\,{}^{RL}\mathcal{I}^{1-\mu}\left[p_i(x)\,{}^{C}\mathcal{D}^{\mu}\Phi_{\lambda}^{(i)}(x)\right]|_{x=x_L} = 0, \tag{2.13} $$

$$ b_1\Phi_{\lambda}^{(i)}(x_R) + b_2\,{}^{RL}\mathcal{I}^{1-\mu}\left[p_i(x)\,{}^{C}\mathcal{D}^{\mu}\Phi_{\lambda}^{(i)}(x)\right]|_{x=x_R} = 0, \tag{2.14} $$

where $a_1^2 + a_2^2 \neq 0$, $b_1^2 + b_2^2 \neq 0$. In this notation, ${}^{RL}\mathcal{I}^{1-\mu} \equiv {}^{RL}_{x}\mathcal{I}^{1-\mu}_{x_R}$ (i.e., right-sided Riemann-Liouville fractional integration of order $1-\mu$) when $i=1$ for RFSLP of first kind, while, ${}^{RL}\mathcal{I}^{1-\mu} \equiv {}^{RL}_{x_L}\mathcal{I}^{1-\mu}_{x}$ (i.e., left-sided Riemann-Liouville fractional integration of order $1-\mu$) when $i=2$ for RFSLP of second kind.

The problem of finding the eigenvalues λ such that the boundary-value problems (2.12)-(2.14) have non-trivial solutions yields the eigenfunction of the regular fractional Sturm-Liouville eigenvalue problem. The following theorem characterizes the eigensolutions we obtain:

Theorem 2.3.1. *[93] The eigenvalues of (2.12) are real, and the eigenfunctions, corresponding to distinct eigenvalues in each problem, are orthogonal with respect to the weight functions $w_i(x)$.*

2.3.1 Regular Boundary-Value Problem Definition

In this chapter, we shall solve two particular forms of RFSLP (2.12)-(2.14) denoted by RFSLP-I when $i = 1$ and RFSLP-II when $i = 2$ of order $\nu = 2\mu \in (0, 2)$, where the potential functions $q_i(x) = 0$, in both problems. To this end, the following non-local differential operator is defined

$$\mathcal{L}_i^{\mu} := {}^{RL}\mathcal{D}^{\mu}\left[\mathcal{K} \;\; {}^{C}\mathcal{D}^{\mu}(\cdot)\right], \tag{2.15}$$

where $\mathcal{K}$ is constant, and by the notation we introduced, $\mathcal{L}_1^{\mu} := {}^{RL}_{x}\mathcal{D}^{\mu}_{x_R}[\mathcal{K} \;\; {}^{C}_{x_L}\mathcal{D}^{\mu}_{x}(\cdot)]$ in RFSLP-I (i.e., first we take the left-sided μ-th order Caputo derivative of the function multiplied by a constant, and then we take the right-sided Riemann-Liouville derivative of order μ), and for the case of RFSLP-II we reverse the order of the right-sided and left-sided derivative for the inner and outer fractional derivatives in the operator, i.e., $\mathcal{L}_2^{\mu} := {}^{RL}_{x_L}\mathcal{D}^{\mu}_{x}[\mathcal{K} \;\; {}^{C}_{x}\mathcal{D}^{\mu}_{x_R}(\cdot)]$, where $\mu \in (0, 1)$. In fact, we have set $p_i(x) = \mathcal{K}$, a continuous non-zero constant function $\forall x \in [-1, 1]$. We referred to $\mathcal{K}$ as *stiffness* constant, which yields the regularity character to the boundary-value

problem. That being defined, we consider the RFSLP (-I & -II) as

$$\mathcal{L}_i^{\mu}\Phi_{\lambda}^{(i)}(x) + \lambda(1-x)^{-\mu}(1+x)^{-\mu}\Phi_{\lambda}^{(i)}(x) = 0, \quad i \in \{1,2\},\ x \in [-1,1]. \tag{2.16}$$

We shall solve (2.16) subject to a homogeneous Dirichlet and a homogeneous fractional *integro-differential* boundary condition to the problems RFSLP-I and RFSLP-II, respectively, as

$$\begin{aligned} \Phi_{\lambda}^{(1)}(-1) &= 0, \qquad (2.17)\\ {}^{RL}_{x}\mathcal{I}_{1}^{1-\mu}\left[\mathcal{K}\ {}^{C}_{-1}\mathcal{D}_{x}^{\mu}\Phi_{\lambda}^{(1)}(x)\right]|_{x=+1} &= 0,\\ &\textit{and,}\\ \Phi_{\lambda}^{(2)}(+1) &= 0, \qquad (2.18)\\ {}^{RL}_{-1}\mathcal{I}_{x}^{1-\mu}\left[\mathcal{K}\ {}^{C}_{x}\mathcal{D}_{1}^{\mu}\Phi_{\lambda}^{(2)}(x)\right]|_{x=-1} &= 0. \end{aligned}$$

The boundary conditions (2.17) and (2.18) are natural in non-local calculus and fractional differential equations, and they are motivated by the fractional integration-by-parts (2.9) and (2.10). In fact, the fundamental properties of eigensolutions in the theory of classical Sturm-Liouville problems are connected with the integration-by-parts formula and the choice of the boundary conditions. For instance, the continuity or discreteness of the eigen-spectrum in boundary-value problems is highly dependent on the type of boundary conditions enforced. In the setting chosen here, we shall show that the eigen-spectra of RFSLP-I and RFSLP-II are simple and fully discrete.

Remark 2.3.2. Having defined the zero-Dirichlet boundary conditions in (2.17) and (2.18), and due to the relationship between Caputo and Riemann-Liouville fractional derivatives shown in (2.7) and (2.8), above fractional differential operators $\mathcal{L}_1^{\mu}$ and $\mathcal{L}_2^{\mu}$ respectively are *identical* to $\mathcal{L}_1^{\mu} := {}^{RL}_{x}\mathcal{D}_{x_R}^{\mu}[\mathcal{K}\ {}^{RL}_{x_L}\mathcal{D}_{x}^{\mu}(\cdot)]$ and $\mathcal{L}_2^{\mu} := {}^{RL}_{x_L}\mathcal{D}_{x}^{\mu}[\mathcal{K}\ {}^{RL}_{x}\mathcal{D}_{x_R}^{\mu}(\cdot)]$

alternatively. In general, this setting and dealing only with Riemann-Liouville fractional derivatives would define the eigenvalue problem in a bigger functions space compared to the case where the middle fractional derivatives are defined of Caputo sense. However, we keep the notation as before just to make the use of the fractional integration-by-parts easier to understand in this setting.

2.3.2 Analytical Eigensolutions to RFSLP-I & -II

Here, we obtain the analytical solution $\Phi_\lambda^{(i)}(x)$ to RFSLP-I & II, (2.16), subject to the homogeneous Dirichlet and integro-differential boundary conditions (2.17) and (2.18). Before that, we recall the following lemmas for the standard Jacobi polynomials $P_n^{\alpha,\beta}$:

Lemma 2.3.3. *[5] For $\mu > 0$, $\alpha > -1$, $\beta > -1$, and $\forall x \in [-1, 1]$*

$$(1+x)^{\beta+\mu}\,\frac{P_n^{\alpha-\mu,\beta+\mu}(x)}{P_n^{\alpha-\mu,\beta+\mu}(-1)} = \frac{\Gamma(\beta+\mu+1)}{\Gamma(\beta+1)\Gamma(\mu)P_n^{\alpha,\beta}(-1)}\int_{-1}^{x}\frac{(1+s)^\beta\ P_n^{\alpha,\beta}(s)}{(x-s)^{1-\mu}}ds \quad (2.19)$$

By the left-sided Riemann-Liouville integral (2.1) and evaluating the special end-values $P_n^{\alpha-\mu,\beta+\mu}(-1)$ and $P_n^{\alpha,\beta}(-1)$, we can re-write (2.19) as

$${}^{RL}_{-1}\mathcal{I}_x^\mu\Big\{(1+x)^\beta P_n^{\alpha,\beta}(x)\Big\} = \frac{\Gamma(n+\beta+1)}{\Gamma(n+\beta+\mu+1)}(1+x)^{\beta+\mu}\,P_n^{\alpha-\mu,\beta+\mu}(x). \quad (2.20)$$

Lemma 2.3.3 can be reduced to the case when $\alpha = +\mu$ and $\beta = -\mu$ as

$${}^{RL}_{-1}\mathcal{I}_x^\mu\Big\{(1+x)^{-\mu}P_n^{\mu,-\mu}(x)\Big\} = \frac{\Gamma(n-\mu+1)}{\Gamma(n+1)}\,P_n(x), \quad (2.21)$$

where $P_n(x) = P_n^{0,0}(x)$ represents the Legendre polynomial of degree n. On the other

hand, we can set $\alpha = \beta = 0$ in (2.20) and take the fractional derivative ${}^{RL}_{-1}\mathcal{D}^{\mu}_{x}$ on both sides of (2.20) to obtain

$$ {}^{RL}_{-1}\mathcal{D}^{\mu}_{x}\Big\{(1+x)^{\mu}P_n^{-\mu,\mu}\Big\} = \frac{\Gamma(n+\mu+1)}{\Gamma(n+1)}P_n(x). \tag{2.22}$$

Lemma 2.3.4. *[5] For $\mu > 0$, $\alpha > -1$, $\beta > -1$, and $\forall x \in [-1,1]$*

$$(1-x)^{\alpha+\mu}\,\frac{P_n^{\alpha+\mu,\beta-\mu}(x)}{P_n^{\alpha+\mu,\beta-\mu}(+1)} = \frac{\Gamma(\alpha+\mu+1)}{\Gamma(\alpha+1)\Gamma(\mu)P_n^{\alpha,\beta}(+1)}\int_x^1 \frac{(1-s)^{\alpha}\;P_n^{\alpha,\beta}(s)}{(s-x)^{1-\mu}}ds \tag{2.23}$$

By the right-sided Riemann-Liouville integral (2.2) and evaluating the special end-values $P_n^{\alpha-\mu,\beta+\mu}(+1)$ and $P_n^{\alpha,\beta}(+1)$, we can re-write (2.23) as

$$ {}^{RL}_{x}\mathcal{I}^{\mu}_{1}\Big\{(1-x)^{\alpha}P_n^{\alpha,\beta}(x)\Big\} = \frac{\Gamma(n+\alpha+1)}{\Gamma(n+\alpha+\mu+1)}(1-x)^{\alpha+\mu}P_n^{\alpha+\mu,\beta-\mu}(x) \tag{2.24}$$

Similarly, Lemma 2.3.4 for the case $\alpha = -\mu$ and $\beta = +\mu$ leads to

$$ {}^{RL}_{x}\mathcal{I}^{\mu}_{1}\Big\{(1-x)^{-\mu}P_n^{-\mu,+\mu}(x)\Big\} = \frac{\Gamma(n-\mu+1)}{\Gamma(n+1)}P_n(x). \tag{2.25}$$

On the other hand, one can set $\alpha = \beta = 0$ in (2.24) and take the fractional derivative ${}^{RL}_{x}\mathcal{D}^{\mu}_{1}$ on both sides of (2.24) to obtain

$$f\,{}^{RL}_{x}\mathcal{D}^{\mu}_{1}\Big\{(1-x)^{\mu}P_n^{\mu,-\mu}\Big\} = \frac{\Gamma(n+\mu+1)}{\Gamma(n+1)}P_n(x). \tag{2.26}$$

Relations (2.21), (2.22), (2.25) and (2.26) are the key to proving the following theorem.

Theorem 2.3.5. *The exact eigenfunctions to (2.16), when $i = 1$, i.e., RFSLP-I,*

subject to (2.17) are given as

$$\Phi_n^{(1)}(x) = (1+x)^{\mu} \ P_{n-1}^{-\mu,\mu}(x), \quad \forall n \geq 1, \tag{2.27}$$

and the corresponding distinct eigenvalues are

$$\lambda_n^{(1)} = -\frac{\mathcal{K}\ \Gamma(n+\mu)}{\Gamma(n-\mu)}, \quad \forall n \geq 1. \tag{2.28}$$

Moreover, the exact eigenfunctions to (2.16), when $i = 2$, i.e., RFSLP-II subject to (2.18), are given as

$$\Phi_n^{(2)}(x) = (1-x)^{\mu} \ P_{n-1}^{\mu,-\mu}(x), \quad \forall n \geq 1 \tag{2.29}$$

where the corresponding distinct eigenvalues are given as

$$\lambda_n^{(2)} = \lambda_n^{(1)} = -\frac{\mathcal{K}\ \Gamma(n+\mu)}{\Gamma(n-\mu)}, \quad \forall n \geq 1. \tag{2.30}$$

Proof. We split the proof into three parts.

(Part a): First, we prove (2.27) and (2.28). From (2.27), it is clear that $\Phi_n^{(1)}(-1) = 0$. To check the other boundary condition, since $\Phi_n^{(1)}(-1) = 0$, by property (2.7), we could replace ${}_{-1}^{C}\mathcal{D}_x^{\mu}$ by ${}_{-1}^{RL}\mathcal{D}_x^{\mu}$, hence,

$$\begin{aligned}
\left\{ {}_{x}^{RL}\mathcal{I}_{+1}^{1-\mu} \left[\mathcal{K} \ {}_{-1}^{C}\mathcal{D}_x^{\mu} \Phi_n^{(1)}(x)\right] \right\}_{x=+1} = \\
\left\{ {}_{x}^{RL}\mathcal{I}_{+1}^{1-\mu} \left[\mathcal{K} \ {}_{-1}^{RL}\mathcal{D}_x^{\mu} \Phi_n^{(1)}(x)\right] \right\}_{x=+1} = \\
\left\{ {}_{x}^{RL}\mathcal{I}_{+1}^{1-\mu} \left[\mathcal{K} \ {}_{-1}^{RL}\mathcal{D}_x^{\mu} \left((1+x)^{\mu} \ P_{n-1}^{-\mu,\mu}(x)\right)\right] \right\}_{x=+1} =
\end{aligned}$$

(and by carrying out the fractional RL derivative in the bracket using (2.22))

$$= \left\{ {}^{RL}_{x}\mathcal{I}^{1-\mu}_{+1} \left[\mathcal{K} \, \frac{\Gamma(n+\mu)}{\Gamma(n)} P_{n-1}(x) \right] \right\}_{x=+1} =$$
$$\mathcal{K} \, \frac{\Gamma(n+\mu)}{\Gamma(n)} \left\{ {}^{RL}_{x}\mathcal{I}^{1-\mu}_{+1} \left[P f_{n-1}(x) \right] \right\}_{x=+1}.$$

By working out the fractional integration using (2.24) (when $\alpha = \beta = 0$), we obtain

$$\mathcal{K} \Big\{ (1-x)^{\mu} P^{\mu,-\mu}_{n-1} \Big\}_{x=+1} = 0.$$

Now, we need to show that (2.27) indeed satisfies (2.16), when $i = 1$, with the eigenvalues (2.28). First, we take the fractional integration of order μ on both sides of (2.16) taking $i = 1$,

$$\mathcal{K} \; {}^{C}_{-1}\mathcal{D}^{\mu}_{x} \Phi^{(1)}_{n}(x) = -\lambda \, {}^{RL}_{x}\mathcal{I}^{\mu}_{+1} \Big\{ (1-x)^{-\mu} (1+x)^{-\mu} \Phi^{(1)}_{n}(x) \Big\}.$$

Substituting (2.27) and replacing the Caputo derivative by the Riemann-Liouville one, thanks to (2.7), we obtain

$$\mathcal{K} \; {}^{RL}_{-1}\mathcal{D}^{\mu}_{x} \left[(1+x)^{\mu} \;\; P^{-\mu,\mu}_{n-1}(x) \right] = -\lambda \, {}^{RL}_{x}\mathcal{I}^{\mu}_{+1} \Big\{ (1-x)^{-\mu} \;\; P^{-\mu,\mu}_{n-1}(x) \Big\}.$$

Finally, the fractional derivative on the left-hand side and the fractional integration on the right-hand side are worked out using (2.22) and (2.25), respectively, as

$$\mathcal{K} \, \frac{\Gamma(n+\mu)}{\Gamma(n)} \; P_{n-1}(x) = -\lambda \frac{\Gamma(n-\mu)}{\Gamma(n)} \;\; P_{n-1}(x).$$

Since, $P_{n-1}^{\alpha+1,-\beta-1}(x)$ is non-zero almost everywhere in $[-1,1]$, we can cancel this term out from both sides and get

$$\lambda \equiv \lambda_n^{(1)} = -\frac{\mathcal{K}\ \Gamma(n+\mu)}{\Gamma(n-\mu)},\ \ \forall n \geq 1,$$

which shows that the eigenvalues of RFSLP-I are real-valued and discrete. In fact, this result agrees with Theorems 3.1. Moreover, the orthogonality of the eigenfunctions (2.27) with respect to $w_1(x) = (1-x)^{-\mu}(1+x)^{-\mu}$ is shown as

$$\int_{-1}^{1} w_1(x)\Phi_k^{(1)}(x)\Phi_j^{(1)}(x)dx = \int_{-1}^{1} w_1(x)\left[(1+x)^{\mu}\right]^2\ \ P_{k-1}^{-\mu,\mu}(x)\ \ P_{j-1}^{-\mu,\mu}(x)dx =$$
$$\int_{-1}^{1}(1-x)^{-\mu}(1+x)^{\mu}\ \ P_{k-1}^{-\mu,\mu}(x)\ \ P_{j-1}^{-\mu,\mu}(x)dx$$
$$= C_k^{-\mu,\mu}\delta_{kj}$$

where, $C_k^{-\mu,\mu}$ denotes the orthogonality constant of the family of Jacobi polynomials with parameters $^{-\mu,\mu}$.

(Part b): The proof of the eigen-solution to RFSLP-II, (2.29) and (2.30), follows the same steps as in Part a. It is clear that $\Phi_n^{(2)}(1) = 0$. To check the other boundary condition in (2.18), since $\Phi_n^{(2)}(1) = 0$, by (2.8), we can replace ${}_x^C\mathcal{D}_1^{\mu}$ by ${}_x^{RL}\mathcal{D}_1^{\mu}$; hence, by substituting in (2.29), and working out the middle fractional derivative using (2.26),

$$\left\{ {}_x^{RL}\mathcal{I}_{+1}^{1-\mu}\left[\mathcal{K}\ {}_x^C\mathcal{D}_1^{\mu}\Phi_n^{(1)}(x)\right]\right\}_{x=-1} =$$
$$\mathcal{K}\ \frac{\Gamma(n)}{\Gamma(n+\mu)}\left\{ {}_{-1}^{RL}\mathcal{I}_x^{1-\mu}\left[P_{n-1}(x)\right]\right\}_{x=-1} =$$

and by working out the fractional integration using (2.24) (when $\alpha = \beta = 0$), we

obtain

$$\mathcal{K}\Big\{(1+x)^{\mu}P_{n-1}^{-\mu,+\mu}\Big\}_{x=-1}=0.$$

To check if (2.29) satisfies (2.16), when $i=2$, we can substitute (2.29) into (2.16) and carry out the fractional integration of order μ on both sides using (2.20). Then, by working out the fractional derivative on the left-hand side using (2.25) we verify that (2.29) satisfies the boundary-value problem, provided that (2.30) are the real-values distinct eigenvalues of RFSLP-II.

Finally, the orthogonality of the eigenfunctions (2.29) with respect to $w_2(x)=(1-x)^{-\mu}(1+x)^{-\mu}$ is shown as

$$\int_{-1}^{1} w_2(x)\Phi_k^{(2)}(x)\Phi_j^{(2)}(x)dx=\int_{-1}^{1}(1-x)^{\mu}(1+x)^{-\mu}\ P_{k-1}^{\mu,-\mu}(x)\ P_{j-1}^{\mu,-\mu}(x)dx$$
$$=C_k^{\mu,-\mu}\delta_{kj}$$

where, $C_k^{\mu,-\mu}$ represents the orthogonality constant of the family of Jacobi polynomials with parameters $^{\mu,-\mu}$.

(Part c): It is left to prove that the set $\{\Phi_n^{(i)}(x) : n=1,2,\cdots\}$ forms a basis for the infinite-dimensional Hilbert space $L_w^2[-1,1]$, and $\lambda_n^{(i)}$, the corresponding eigenvalue for each n, is simple. Let $f(x)\in L_w^2[-1,1]$ and then clearly $g(x)=$

$(1 \pm x)^{\mu} f(x) \in L^2_w[-1,1]$, as well when $\mu \in (0,1)$. Hence

$$\begin{aligned}
\|\sum_{n=1}^{N} a_n \Phi_n^{(i)}(x) - f(x)\|_{L^2_w[-1,1]} &= \\
\|\sum_{n=1}^{N} a_n (1 \pm x)^{\mu} P_{n-1}^{\mp\mu,\pm\mu}(x) - f(x)\|_{L^2_w[-1,1]} &= \\
\|(1 \pm x)^{\mu} \left(\sum_{n=1}^{N} a_n P_{n-1}^{\mp\mu,\pm\mu}(x) - (1 \pm x)^{-\mu} f(x) \right) \|_{L^2_w[-1,1]} &= \\
\|(1 \pm x)^{\mu} \left(\sum_{n=1}^{N} a_n P_{n-1}^{\mp\mu,\pm\mu}(x) - g(x) \right) \|_{L^2_w[-1,1]} &\leq \quad \text{(by Cauchy-Schwartz)} \\
\|(1 \pm x)^{\mu}\|_{L^2_w[-1,1]} \| \sum_{n=1}^{N} a_n P_{n-1}^{\mp\mu,\pm\mu}(x) - g(x)\|_{L^2_w[-1,1]} &\leq \\
c\| \sum_{n=1}^{N} a_n P_{n-1}^{\mp\mu,\pm\mu}(x) - g(x)\|_{L^2_w[-1,1]}, &
\end{aligned}$$

where the upper signs are corresponding to RFSLP-I, $i = 1$, and the lower signs are corresponding to the case $i = 2$, i.e., RFSLP-II. Hence,

$$\lim_{N\to\infty} \| \sum_{n=1}^{N} a_n \Phi_n^{(i)}(x) - f(x)\|_{L^2_w[-1,1]} \leq \lim_{N\to\infty} c\| \sum_{n=1}^{N} a_n P_{n-1}^{\mp\mu,\pm\mu}(x) - g(x)\|_{L^2_w[-1,1]} = 0, \tag{2.31}$$

by Weierstrass theorem. Therefore, $\sum_{n=1}^{N} a_n \Phi_n^{(i)}(x) \xrightarrow{L^2_w} f(x)$, implying that $\{\Phi_n^{(i)}(x) : n = 1, 2, \cdots\}$ is dense in the Hilbert space and it forms a basis for $L^2_w[-1,1]$.

To show the simplicity of the eigenvalues, assume that corresponding to the eigenvalue $\lambda_j^{(i)}$, there exits another eigenfunction $\Phi_j^{(i)*}(x) \in L^2_w[-1,1]$ in addition to $\Phi_j^{(i)}(x)$, which is by Theorem 2.3.1 orthogonal to the rest of the eigenfunctions $\Phi_n^{(i)}(x),\ n \neq j$. By the density of the eigenfunctions set, i.e., (2.31), we can represent

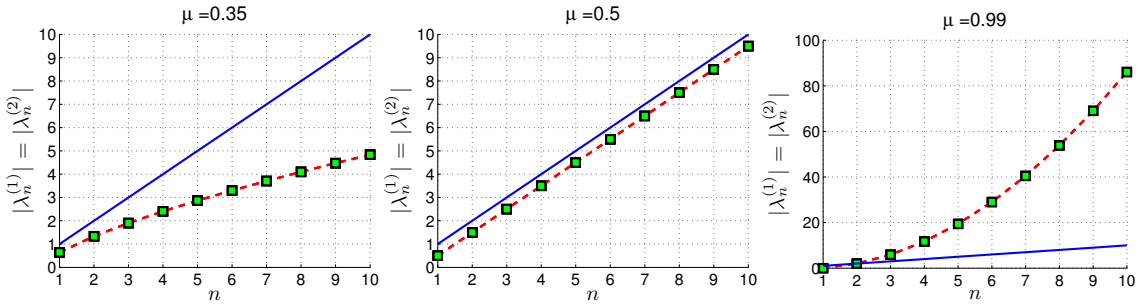

Figure 2.1: Magnitude of the eigenvalues of RFSLP-I and RFSLP-II, $|\lambda_n^{(1)}| = |\lambda_n^{(2)}|$, versus n, corresponding to $\mu = 0.35$, left: sublinear growth, $\mu = 0.5$, middle: linear growth, and $\mu = 0.99$, right: superlinear-subquadratic growth. The blue line denotes the linear growth.

$\Phi_j^{(i)*}(x)$ as

$$\Phi_j^{(i)*}(x) = \sum_{n=1}^{\infty} a_n \Phi_n^{(i)}(x). \tag{2.32}$$

Now, by multiplying both sides by $\Phi_k^{(i)}(x)$, $k = 1, 2, \cdots$ and $k \neq j$, and integrating with respect to the weight function $w(x)$ we obtain

$$\begin{aligned} \int_{-1}^{1} w(x)\Phi_j^{(i)*}(x)\Phi_k^{(i)}(x)dx &= \sum_{n=1}^{\infty} a_n \int_{-1}^{1} w(x)\Phi_n^{(i)}(x)\Phi_k^{(i)}(x)dx \\ &= a_k C_k \neq 0, \end{aligned} \tag{2.33}$$

which contradicts to Theorem 2.3.1. Therefore, the eigenvalues $\lambda_n^{(i)}$ are simple, and this completes the proof. □

The growth of the magnitude of the eigenvalues of RFSLP-I &-II, $|\lambda_n^i|$, $i \in \{1, 2\}$, is plotted in Fig. 2.1, corresponding to three values of $\mu = 0.35$, $\mu = 0.5$, and $\mu = 0.99$. We observe that there are two growth modes, depending on either $\mu \in (0, 1/2)$, where a sublinear growth in $|\lambda_n^1| = |\lambda_n^2|$ is observed, or, $\mu \in (1/2, 1)$, where a superlinear-subquadratic growth mode is noticed. The case $\mu = 1/2$ leads to an exactly linear growth mode.

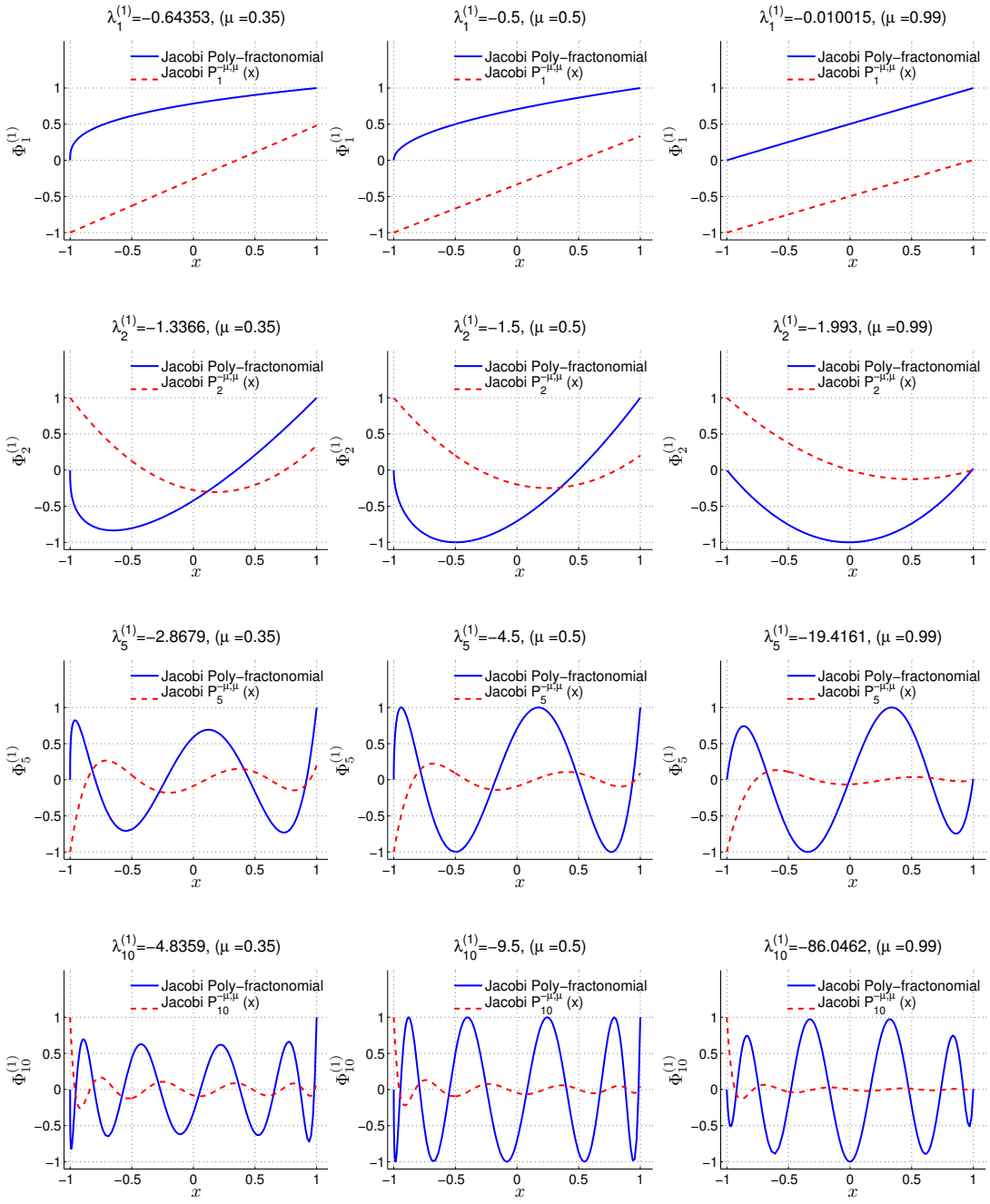

Figure 2.2: Eigenfunctions of RFSLP-I, $\Phi_n^{(1)}$, versus x, for $n = 1$ (first row), $n = 2$ (second row), $n = 5$ (third row), and $n = 10$ (last row), corresponding to the fractional order $\mu = \nu/2 = 0.35$ (left column), $\mu = \nu/2 = 0.5$ (middle column), and $\mu = \nu/2 = 0.99$ (right column).

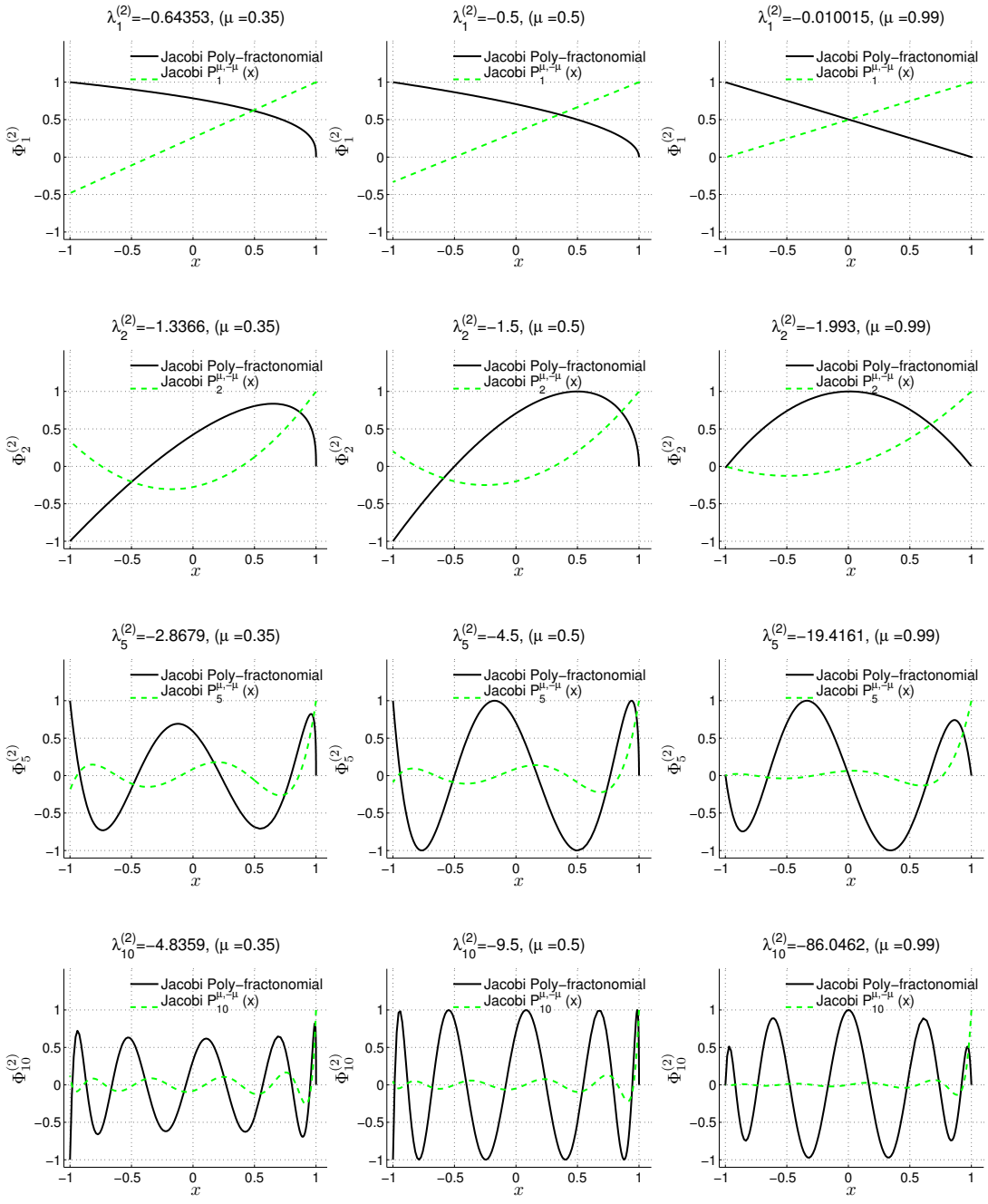

Figure 2.3: Eigenfunctions of RFSLP-II, $\Phi_n^{(2)}$, versus x, for $n = 1$ (first row), $n = 2$ (second row), $n = 5$ (third row), and $n = 10$ (last row), corresponding to the fractional order $\mu = \nu/2 = 0.35$ (left column), $\mu = \nu/2 = 0.5$ (middle column), and $\mu = \nu/2 = 0.99$ (right column).

In order to visually get more sense of how the eigensolutions look like, in Fig. 2.2 we plot the eigenfunctions of RFSLP-I, $\Phi_n^{(1)}(x)$ of different orders and corresponding to different values of μ used in Fig. 2.1. In each plot we compare the eigensolutions with the corresponding standard Jacobi polynomials $P_n^{-\mu,\mu}(x)$. In a similar fashion, we plot the eigenfunctions of RFSLP-II, $\Phi_n^{(2)}(x)$, of different orders compared to $P_n^{+\mu,-\mu}(x)$ in Fig. 2.3.

So far, the eigenfunctions have been defined in the interval $[-1,1]$. The following lemma provides a useful shifted definition of the $\Phi_n^{(i)}$, which is not only more convenient to work with but also helps exploit some interesting properties.

Lemma 2.3.6. *The shifted eigensolutions to RFSLP-I&-II, denoted by* $\widetilde{\Phi}_n^{(i)}(t)$, $i \in \{1,2\}$, *are given by*

$$\widetilde{\Phi}_n^{(i)}(t) = 2^{\mu} \sum_{j=0}^{n-1} (-1)^{n+j-1} \binom{n-1+j}{j} \binom{n-1+(-1)^{i+1}\mu}{n-1-j} t^{j+\mu}, \tag{2.34}$$

where $t \in [0,1]$ *in the mapped domain, in case of RFSLP-I, and* $t \in [-1,0]$ *in RFSLP-II.*

Proof. We first obtain the shifted RFSLP-I by performing an affine mapping from interval $[-1,1]$ to $[0,1]$. To do so, we recall the power expansion of the Jacobi polynomial $P_n^{\alpha,\beta}(x)$ as

$$P_n^{\alpha,\beta}(x) = \sum_{j=0}^{n} \binom{n+\alpha+\beta+j}{j} \binom{n+\alpha}{n-j} \left(\frac{x-1}{2}\right)^j, \quad x \in [-1,1] \tag{2.35}$$

and from the properties of the Jacobi polynomials we have

$$P_n^{\alpha,\beta}(-x) = (-1)^n P_n^{\beta,\alpha}(x). \tag{2.36}$$

We obtain the shifted eigensolution $\widetilde{\Phi}_n^{(1)}(t)$ utilizing (2.35) and (2.36) in (2.27) and performing the change of variable $x = 2t - 1$ as

$$\widetilde{\Phi}_n^{(1)}(t) = 2^{\mu} \sum_{j=0}^{n-1} (-1)^{n+j-1} \binom{n-1+j}{j} \binom{n-1+\mu}{n-1-j} t^{j+\mu}. \tag{2.37}$$

In order to obtain the shifted $\widetilde{\Phi}_n^{(2)}(t)$, we follow the same steps, except that this time we do the change of variable $x = -2t + 1$, which maps $[-1, 1]$ to $[-1, 0]$. □

Definition 2.3.7. A *fractonomial* is defined as a function $f : \mathbb{C} \to \mathbb{C}$ of non-integer power, denoted as $t^{k+\mu}$, where $k \in \mathbb{Z}^+$ and $\mu \in (0, 1)$, in which the power can be represented as a sum of an integer and non-integer number. Moreover, denoted by $\mathcal{F}_e^{n+\mu}$ is the *fractal expansion set*, which is defined as the set of all fractonomials of order less than or equal $n + \mu$ as

$$\mathcal{F}_e^{n+\mu} = span\{t^{k+\mu} : \ \mu \in (0, 1) \ and \ k = 0, 1, \cdots, n\}. \tag{2.38}$$

Remark 2.3.8. All fractonomials are zero-valued at $t = 0$. Moreover, asymptotically, when $\mu \to 0$, a fractonomial of order $n + \mu$ approaches the monomial t^n.

Definition 2.3.9. A *Poly-fractonomial* of order $n + \mu < \infty$, $n \in \{0, 1, 2, \cdots, N < \infty\}$, and $\mu \in (0, 1)$, is defined as a linear combination of the elements in the fractal expansion set $\mathcal{F}_e^{n+\mu}$, as

$$F_{n+\mu}(t) = a_0\, t^{\mu} + a_1\, t^{1+\mu} + \cdots + a_n\, t^{n+\mu}$$

where $a_j \in \mathbb{C}$, $j \in \{0, 1, \cdots, n\}$ are constants. Moreover, denoted by $\mathbb{F}^{n+\mu}$ is the space of all poly-fractonomials up to order $n + \mu$. By Remark 2.3.8, all elements in $\mathbb{F}^{n+\mu}$ asymptotically approach the corresponding standard polynomial of order n with coefficients a_j.

Remark 2.3.10. It is observed that $\mathbb{F}^{n+\mu} \subset L^2_w$ since $\mu \in (0,1)$, and hence, all poly-fractonomials in $\mathbb{F}^{n+\mu}$ can be represented as an infinite sum in terms of the shifted eigenfunctions of RFSLP-I&-II. It is true by the density of the eigenfunction in L^2_w, shown in (Part c) of the proof in Theorem 2.3.5.

Lemma 2.3.11. *Any fractional Caputo derivative of order $\mu \in (0,1)$ of all polynomials up to degree N lies in the space of Poly-fractonomials $\mathbb{F}^{n+\widetilde{\mu}}$, where $n = N-1$, and $\widetilde{\mu} = 1-\mu \in (0,1)$.*

Proof. Let $f(t) = \sum_{j=0}^{N} a_j t^j$ be an arbitrary polynomial of order N, i.e., $a_N \neq 0$. From [142] and for $\mu \in (0,1)$, we have

$$ {}^{C}_{0}\mathcal{D}^{\mu}_{t} t^k = \begin{cases} 0, & k < \mu, \\ \frac{\Gamma(k+1)}{\Gamma(k+1-\mu)} t^{k-\mu}, & 0 < \mu \leq k. \end{cases} \tag{2.39} $$

Hence, by (2.39),

$$ {}^{C}_{0}\mathcal{D}^{\mu}_{t} f(t) = \sum_{j=0}^{N} a_j \, {}^{C}_{0}\mathcal{D}^{\mu}_{t} t^j = \sum_{j=1}^{N} a_j \frac{\Gamma(j+1)}{\Gamma(j+1-\mu)} t^{j-\mu} = \sum_{j=1}^{N} b_j t^{j-\mu}, \tag{2.40} $$

where $b_j = \frac{\Gamma(j+1)}{\Gamma(j+1-\mu)} a_j$. Taking $n = N-1$ and $\widetilde{\mu} = 1-\mu \in (0,1)$, and the fact that $b_N = \frac{\Gamma(j+1)}{\Gamma(j+1-\mu)} a_N \neq 0$ completes the proof. □

Theorem 2.3.12. *The shifted eigensolutions to (2.16), $\widetilde{\Phi}^{(i)}_n(t)$, $n \in \mathbb{N}$ and $n < \infty$, form a complete hierarchical basis for the finite-dimensional space of poly-fractonomials $\mathbb{F}_{n-1+\mu}$, where $\mu \in (0,1)$.*

Proof. From (2.34), it is clear that

$$ dim\, \mathbb{F}_{n-1+\mu} = dim\{\widetilde{\Phi}^{(i)}_k, k \in \{1, 2, \cdots, n\}\}. \tag{2.41} $$

Moreover, we can re-write (2.34) as

$$\mathbb{T}\ \vec{t} = \vec{\Phi}^{(i)}, \tag{2.42}$$

where,

$$\vec{t} = \begin{pmatrix} t^{\mu} \\ t^{1+\mu} \\ \vdots \\ t^{n-1+\mu} \end{pmatrix}, \quad \text{and} \quad \vec{\Phi}^{(1)} = \begin{pmatrix} \Phi_1^{(i)}(t) \\ \Phi_2^{(i)}(t) \\ \vdots \\ \Phi_n^{(i)}(t) \end{pmatrix},$$

and finally, $\mathbb{T} = \{T_{jk}\}_{j,k=1}^{n}$ is an $n \times n$ matrix obtained as

$$\mathbb{T} = \{T_{jk}\}_{j,k=1}^{n} = (-1)^{k+j-1} \begin{pmatrix} k-1+j \\ j \end{pmatrix} \begin{pmatrix} k-1+(-1)^{i+1}\mu \\ k-1-j \end{pmatrix},$$

which is a *lower-triangular* matrix. Thanks to the orthogonality of the $\Phi_n^{(i)}$, the eigenfunctions are linearly independent, therefore, the matrix $\mathbb{T}$ is invertible. Let $\mathcal{T} = \mathbb{T}^{-1}$, which is also lower-triangular. Hence,

$$\vec{t} = \mathcal{T}\ \vec{\Phi}^{(i)}. \tag{2.43}$$

In other words, each element in the poly-fractonomial space $\mathbb{F}_{n-1+\mu}$, say $t^{m+\mu}$, $0 \leq m \leq n-1$, can be uniquely represented through the following expansion

$$t^{m+\mu} = \sum_{j=1}^{n} c_j\ \Phi_j^{(i)}(t) = \sum_{j=1}^{n} \{\mathcal{T}_{mj}\}\ \Phi_j^{(i)}(t) = \sum_{j=1}^{m} \{\mathcal{T}_{mj}\}\ \Phi_j^{(i)}(t), \tag{2.44}$$

where the last equality holds since $\mathcal{T}$ is a lower-triangular matrix. As seen in (2.38), the fractal expansion set $\mathcal{F}_e^{n+\mu} \subset \mathcal{F}_e^{n+1+\mu}$, which indicates that the shifted eigen-solutions $\widetilde{\Phi}_n^{(i)}$ form a *hierarchical* expansion basis set. $\square$

2.3.3 Properties of the Eigensolution to RFSLP-I & -II

Next, we list a number of properties of the solutions to RFSLP-I & II (2.16):

- **Non-polynomial nature**:

  From $\Phi_n^{(i)}(x)$ shown in (2.27) when $i = 1$, and in (2.29) corresponding to $i = 2$, it is understood that the eigenfunctions exhibit a non-polynomial behaviour, thanks to the multiplier $(1 \pm x)^{\mu}$ of fractional power. Hence, to distinguish them from the standard Jacobi polynomials, we refer to $\Phi_n^{(i)}(x)$ as *Jacobi Poly-fractonomial* of order $n + \mu$.

- **Asymptotic eigenvalues** $\lambda_n^{(i)}$:

  The growth in the magnitude of eigenvalues in RFSLP with n is dependent on the fractional derivative order μ, as shown in (2.30). Since $\mu \in (0, 1)$, there are two modes of growth in the magnitude of $\lambda_n^{(i)}$, the *sublinear* mode corresponding to $0 < \mu < 1/2$, and *superlinear-subquadratic* mode which corresponds to $1/2 < \mu < 1$. Particularly, when $\mu = 1/2$, the eigenvalues grow linearly with n. Hence, the asymptotic values are summarized as

$$|\lambda_n^{(i)}| = \begin{cases} \mathcal{K}n^2, & \mu \to 1, \\ \mathcal{K}n & \mu \to 1/2, \\ \mathcal{K} & \mu \to 0. \end{cases} \tag{2.45}$$

- **Recurrence relations**:

Thanks to the hierarchical property of the eigenfunctions $\Phi_n^{(i)}$, we obtain the following recurrence relations:

$$\begin{aligned}
\Phi_1^{(i)}(x) &= (1 \pm x)^{\mu}, \\
\Phi_2^{(i)}(x) &= (1 \pm x)^{\mu}(x \mp \mu), \\
&\vdots \\
a_n \Phi_{n+1}^{(i)}(x) &= b_n x \Phi_n^{(i)}(x) - c_n \Phi_{n-1}^{(i)}(x) \\
a_n &= 4n^2(n-1) \\
b_n &= 2n(2n-1)(2n-2) \\
c_n &= 4n(n-1 \mp \mu)(n-1 \pm \mu),
\end{aligned} \tag{2.46}$$

where the upper signs correspond to $i = 1$, solution to RFSLP-I, and the lower signs correspond to RFSLP-II when $i = 2$.

- **Orthogonality**:

$$\begin{aligned}
&\int_{-1}^{1} (1-x)^{-\mu}(1+x)^{-\mu}\Phi_k^{(i)}(x)\Phi_m^{(i)}(x)dx = \\
&\int_{-1}^{1} (1-x)^{\alpha_i}(1+x)^{\beta_i} P_{k-1}^{\alpha_i,\beta_i}(x) P_{m-1}^{\alpha_i,\beta_i}(x)dx = \mathcal{J}_k^{\alpha_i,\beta_i}\delta_{kj}
\end{aligned} \tag{2.47}$$

$$\mathcal{J}_k^{\alpha_i,\beta_i} = \frac{2}{2k-1}\frac{\Gamma(k+\alpha_i)\Gamma(k+\beta_i)}{(k-1)!\,\Gamma(k)}, \tag{2.48}$$

where $(\alpha_1, \beta_1) = (-\mu, \mu)$ and $(\alpha_2, \beta_2) = (\mu, -\mu)$.

- **Fractional derivatives**:

$$\begin{aligned} {}^{RL}_{-1}\mathcal{D}^{\mu}_{x}\Phi^{(1)}_{n} = {}^{C}_{-1}\mathcal{D}^{\mu}_{x}\Phi^{(1)}_{n} &= \\ {}^{RL}_{x}\mathcal{D}^{\mu}_{1}\Phi^{(2)}_{n} = {}^{C}_{x}\mathcal{D}^{\mu}_{1}\Phi^{(2)}_{n} &= \frac{\Gamma(n+\mu)}{\Gamma(n)}P_{n-1}(x), \end{aligned} \tag{2.49}$$

where $P_{n-1}(x)$ denotes that standard Legendre polynomial of order $n-1$.

- **Orthogonality of the fractional derivatives**:

$$\int_{-1}^{1} \mathcal{D}^{\mu}\Phi^{(i)}_{k}\, \mathcal{D}^{\mu}\Phi^{(i)}_{j} dx = \left(\frac{\Gamma(k+\mu)}{\Gamma(k)}\right)^{2} \frac{2}{2k-1}\delta_{kj}, \tag{2.50}$$

where $\mathcal{D}^{\mu}$ can be either ${}^{RL}_{-1}\mathcal{D}^{\mu}_{x}$ or ${}^{C}_{-1}\mathcal{D}^{\mu}_{x}$, when $i=1$, and can be either ${}^{RL}_{x}\mathcal{D}^{\mu}_{1}$ or ${}^{C}_{x}\mathcal{D}^{\mu}_{1}$ when $i=2$.

- **First derivatives**:

$$\frac{d\Phi^{(1)}_{n}(x)}{dx} = \mu(1+x)^{\mu-1}P^{-\mu,\mu}_{n-1}(x) + \frac{n}{2}(1+x)^{\mu}P^{1-\mu,1+\mu}_{n-2}(x), \tag{2.51}$$

$$\frac{d\Phi^{(2)}_{n}(x)}{dx} = -\mu(1-x)^{\mu-1}P^{\mu,-\mu}_{n-1}(x) + \frac{n}{2}(1-x)^{\mu}P^{1+\mu,1-\mu}_{n-2}(x). \tag{2.52}$$

- **Special values**:

$$\Phi^{(1)}_{n}(-1) = 0, \tag{2.53}$$

$$\Phi^{(1)}_{n}(+1) = 2^{\mu}\begin{pmatrix} n-1-\mu \\ n-1 \end{pmatrix} \tag{2.54}$$

$$\Phi_n^{(2)}(+1) = 0, \tag{2.55}$$

$$\Phi_n^{(2)}(-1) = (-1)^{n-1}\Phi_n^{(1)}(+1). \tag{2.56}$$

2.4 Part II: Singular Fractional Sturm-Liouville Problems of Kind I & II

In the second part of this chapter, we begin with our definition of the singular fractional Sturm-Liouville of first kind I (SFSLP-I) and second kind II (SFSLP-II) of order $\nu = 2\mu \in (0, 2)$, with parameters $-1 < \alpha < 2 - \mu$, and $-1 < \beta < \mu - 1$ in SFSLP-I ($i = 1$), and $-1 < \alpha < \mu - 1$, and $-1 < \beta < 2 - \mu$ in SFSLP-II ($i = 2$), for $x \in [-1, 1]$ as

$$\begin{aligned} {}^{RL}\mathcal{D}^{\mu}\Big\{(1-x)^{\alpha+1}(1+x)^{\beta+1}\ {}^{C}\mathcal{D}^{\mu}\mathcal{P}^{(i)}(x)\Big\} + \Lambda^{(i)}(1-x)^{\alpha+1-\mu}(1+x)^{\beta+1-\mu}\ \mathcal{P}^{(i)}(x) \\ = 0. \end{aligned} \tag{2.57}$$

where the fractional order $\mu \in (0, 1)$ and $i \in \{1, 2\}$, where $i = 1$ denotes the SFSLP-I in which ${}^{RL}\mathcal{D}^{\mu} \equiv {}^{RL}_{x}\mathcal{D}^{\mu}_{+1}$ and ${}^{C}\mathcal{D}^{\mu} \equiv {}^{C}_{-1}\mathcal{D}^{\mu}_{x}$; also $i = 2$ corresponds to the RFSLP-II where ${}^{RL}\mathcal{D}^{\mu} \equiv {}^{RL}_{-1}\mathcal{D}^{\mu}_{x}$ and ${}^{C}\mathcal{D}^{\mu} \equiv {}^{C}_{x}\mathcal{D}^{\mu}_{+1}$. The singular boundary-value problem is subject to the following boundary conditions

$$\mathcal{P}^{(i)}(\ (-1)^i\ ) = 0, \tag{2.58}$$

$$\Big\{\ {}^{RL}\mathcal{I}^{1-\mu}\left[p(x)\,{}^{C}\mathcal{D}^{\mu}\mathcal{P}^{(i)}(x)\right]\Big\}_{x=(-1)^{i+1}} = 0, \tag{2.59}$$

where ${}^{RL}\mathcal{I}^{1-\mu} \equiv {}^{RL}_{x}\mathcal{I}^{1-\mu}_{+1}$ when $i = 1$ in SFSLP-I, and ${}^{RL}\mathcal{I}^{1-\mu} \equiv {}^{RL}_{-1}\mathcal{I}^{1-\mu}_{x}$ in case of $i = 2$ in SFSLP-II; $p(x) = (1-x)^{\alpha+1}(1+x)^{\beta+1}$, used in the fractional differential operator in (2.57), vanishes at the boundary ends $x = \pm 1$. We also note that the weight function $w(x) = (1-x)^{\alpha+1-\mu}(1+x)^{\beta+1-\mu}$ in (2.57) is a non-negative function.

Theorem 2.4.1. *The eigenvalues of SFSLP-I &-II (2.57)-(2.59) are real-valued, moreover, the eigenfunctions corresponding to distinct eigenvalues of SFSLP-I &-II (2.57)-(2.59) are orthogonal with respect to the weight function*

$$w(x) = (1-x)^{\alpha+1-\mu}(1+x)^{\beta+1-\mu}$$

Proof. (*Part a*): Let $\mathcal{L}_i^{\alpha,\beta;\mu}$ be the fractional differential operator of order 2μ as

$$\mathcal{L}_i^{\alpha,\beta;\mu} := {}^{RL}\mathcal{D}^{\mu}\Big\{(1-x)^{\alpha+1}(1+x)^{\beta+1}\ {}^{C}\mathcal{D}^{\mu}(\cdot)\Big\}, \tag{2.60}$$

and assume that $\Lambda^{(i)}$ is the eigenvalue of (2.57)-(2.59) corresponding the the eigenfunction $\eta^{(i)}(x)$, where $i \in \{1, 2\}$. Then the following set of equations are valid for $\eta^{(i)}(x)$

$$\mathcal{L}_i^{\alpha,\beta;\mu}\eta^{(i)}(x) + \Lambda^{(i)}w(x)\eta^{(i)}(x) = 0. \tag{2.61}$$

subject to the boundary conditions

$$\eta^{(i)}(\ (-1)^i\ ) = 0,$$
$$\Big\{\ {}^{RL}\mathcal{I}^{1-\mu}\left[p(x)\,{}^{C}\mathcal{D}^{\mu}\eta^{(i)}(x)\right]\Big\}_{x=(-1)^{(i+1)}} = 0,$$

and its complex conjugate $\bar{\eta}^{(i)}(x)$

$$\mathcal{L}_I^{\alpha,\beta;\mu}\bar{\eta}^{(i)}(x) + \bar{\Lambda}^{(i)}w(x)\bar{\eta}^{(i)}(x) = 0, \tag{2.62}$$

corresponding to the following boundary conditions

$$\begin{aligned} \bar{\eta}^{(i)}(\ (-1)^i\ ) &= 0, \\ \left\{ {}^{RL}\mathcal{I}^{1-\mu}\left[p(x)\,{}^{C}\mathcal{D}^{\mu}\bar{\eta}^{(i)}(x)\right]\right\}_{x=(-1)^{i+1}} &= 0, \end{aligned}$$

Now, we multiply (2.61) by $\bar{\eta}^{(i)}(x)$, and (2.62) by $\eta^{(i)}(x)$ and subtract them as

$$(\Lambda^{(i)} - \bar{\Lambda}^{(i)})w(x)\eta^{(i)}(x)\bar{\eta}^{(i)}(x) = \eta^{(i)}(x)\mathcal{L}_i^{\alpha,\beta;\mu}\bar{\eta}^{(i)}(x) - \bar{\eta}^{(i)}(x)\mathcal{L}_i^{\alpha,\beta;\mu}\eta^{(i)}(x). \tag{2.63}$$

Integrating over the interval $[-1, 1]$ and utilizing the fractional integration-by-parts (2.9) and (2.10), we obtain

$$\begin{aligned} (\Lambda^{(i)} - \bar{\Lambda}^{(i)})\int_{-1}^{+1} w(x)|\eta^{(i)}(x)|^2dx \ &= \\ -\eta(\ (-1)^{i+1}\ )\left\{ {}^{RL}\mathcal{I}^{1-\mu}\left[p(x)\,{}^{C}\mathcal{D}^{\mu}\eta^{(i)}(x)\right]\right\}_{x=(-1)^{i+1}} & \\ +\bar{\eta}^{(i)}(\ (-1)^{i+1}\ )\left\{ {}^{RL}\mathcal{I}^{1-\mu}\left[p(x)\,{}^{C}\mathcal{D}^{\mu}\bar{\eta}^{(i)}(x)\right]\right\}_{x=(-1)^{i+1}} & \\ +\eta(\ (-1)^i\ ) - \bar{\eta}(\ (-1)^i\ ), & \end{aligned} \tag{2.64}$$

where we re-iterate that ${}^{RL}\mathcal{I}^{1-\mu} \equiv {}^{RL}_{x}\mathcal{I}^{1-\mu}_{+1}$ and ${}^{C}\mathcal{D}^{\mu} \equiv {}^{C}_{-1}\mathcal{D}^{\mu}_{x}$ when $i = 1$ in SFSLP-I, also ${}^{RL}\mathcal{I}^{1-\mu} \equiv {}^{RL}_{-1}\mathcal{I}^{1-\mu}_{x}$ and ${}^{C}\mathcal{D}^{\mu} \equiv {}^{C}_{x}\mathcal{D}^{\mu}_{+1}$in case of $i = 2$, i.e., SFSLP-II. Now, by

applying the boundary conditions for $\eta^{(i)}(x)$ and $\bar{\eta}^{(i)}(x)$ we obtain

$$(\Lambda^{(i)} - \bar{\Lambda}^{(i)}) \int_{-1}^{+1} w(x)|\eta^{(i)}(x)|^2 dx = 0 \tag{2.65}$$

Therefore, $\Lambda^{(i)} = \bar{\Lambda}^{(i)}$ because $\eta^{(i)}(x)$ is a non-trivial solution of the problem, and $w(x)$ is non-negative in interval $[-1, 1]$.

(*Part b*): Now, we prove the second statement on the orthogonality of the eigenfunctions with respect to the weight function $w(x)$. Assume that $\eta_1^{(i)}(x)$ and $\eta_2^{(i)}(x)$ are two eigenfunctions corresponding to two distinct eigenvalues $\Lambda_1^{(i)}$ and $\Lambda_2^{(i)}$, respectively. Then they both satisfy (2.57)-(2.59) as

$$\mathcal{L}_i^{\alpha,\beta;\mu} \eta_1^{(i)}(x) + \Lambda_1^{(i)} w(x) \eta_1^{(i)}(x) = 0. \tag{2.66}$$

subject to

$$\eta_1^{(i)}(\ (-1)^i\ ) = 0,$$
$$\left\{ {}^{RL}\mathcal{I}^{1-\mu} \left[p(x)\, {}^{C}\mathcal{D}^{\mu} \eta_1^{(i)}(x) \right] \right\}_{x=(-1)^{i+1}} = 0,$$

and

$$\mathcal{L}_i^{\alpha,\beta;\mu} \eta_2^{(i)}(x) + \Lambda_2^{(i)} w(x) \eta_2^{(i)}(x) = 0, \tag{2.67}$$

corresponding to the following boundary conditions

$$\eta_2(\ (-1)^i\ ) = 0,$$
$$\left\{ {}^{RL}\mathcal{I}^{1-\mu}\left[p(x)\,{}^{C}\mathcal{D}^{\mu}\eta_2^{(i)}(x)\right]\right\}_{x=(-1)^{(i+1)}} = 0.$$

It can be shown that

$$(\Lambda_1^{(i)} - \Lambda_2^{(i)})w(x)\eta_1^{(i)}(x)\eta_2^{(i)}(x) = \eta_1^{(i)}(x)\mathcal{L}_i^{\alpha,\beta;\mu}\eta_2^{(i)}(x) - \eta_2^{(i)}(x)\mathcal{L}_i^{\alpha,\beta;\mu}\eta_1^{(i)}(x). \quad (2.68)$$

Integrating over the interval $[-1,1]$ yields

$$\begin{aligned}(\Lambda_1^{(i)} - \Lambda_2^{(i)})\int_{-1}^{+1} w(x)\eta^{(i)}(x)\eta_2^{(i)}(x)dx \;\; &= \\ -\eta_1(+1)\left\{ {}^{RL}\mathcal{I}^{1-\mu}\left[p(x)\,{}^{C}\mathcal{D}^{\mu}\eta_1^{(i)}(x)\right]\right\}_{x=+1} &\\ +\eta_2^{(i)}(+1)\left\{ {}^{RL}\mathcal{I}^{1-\mu}\left[p(x)\,{}^{C}\mathcal{D}^{\mu}\eta_2^{(i)}(x)\right]\right\}_{x=+1} &\\ +\eta_1^{(i)}(-1) - \eta_2^{(i)}(-1), &\end{aligned} \quad (2.69)$$

and using fractional integration-by-parts (2.9) and (2.10), also since $\Lambda_1^{(i)} - \Lambda_2^{(i)} \neq 0$, we obtain

$$\int_{-1}^{+1} w(x)\eta_1^{(i)}(x)\eta_2^{(i)}(x)dx = 0, \quad (2.70)$$

which completes the proof. □

Theorem 2.4.2. *The exact eigenfunctions of SFSLP-I (2.57)-(2.59), when $i = 1$, are given as*

$$\mathcal{P}_n^{(1)}(x) = {}^{(1)}\mathcal{P}_n^{\alpha,\beta,\mu}(x) = (1+x)^{-\beta+\mu-1}\ \ P_{n-1}^{\alpha-\mu+1,-\beta+\mu-1}(x), \quad (2.71)$$

and the corresponding distinct eigenvalues are

$$\Lambda_n^{(1)} = {}^{(1)}\Lambda_n{}^{\alpha,\beta,\mu} = -\frac{\Gamma(n-\beta+\mu-1)\Gamma(n+\alpha+1)}{\Gamma(n-\beta-1)\Gamma(n+\alpha-\mu+1)}, \tag{2.72}$$

and furthermore, the exact eigenfunctions to SFSLP-II (2.57)-(2.59), in case of $i = 2$*, are given as*

$$\mathcal{P}_n^{(2)}(x) = {}^{(2)}\mathcal{P}_n^{\alpha,\beta,\mu}(x) = (1-x)^{-\alpha+\mu-1}\ \ P_{n-1}^{-\alpha+\mu-1,\beta-\mu+1}(x), \tag{2.73}$$

and the corresponding distinct eigenvalues are

$$\Lambda_n^{(2)} = {}^{(2)}\Lambda_n^{\alpha,\beta,\mu} = -\frac{\Gamma(n-\alpha+2\mu-1)\Gamma(n+\beta+1)}{\Gamma(n-\alpha+\mu-1)\Gamma(n+\beta-\mu+1)}. \tag{2.74}$$

Proof. The proof follows similar steps as shown in Theorem 2.3.5. Hence, we only prove (2.71) and (2.72) in detail.

From (2.71), it is clear that ${}^{(1)}\mathcal{P}_n^{\alpha,\beta,\mu}(-1) = 0$. So, we need to make sure that the other boundary condition is satisfied. Since ${}^{(1)}\mathcal{P}_n^{\alpha,\beta,\mu}(-1) = 0$, the property (2.7) helps in replacing ${}_{-1}^{C}\mathcal{D}_x^{\mu}$ by ${}_{-1}^{RL}\mathcal{D}_x^{\mu}$. Consequently,

$$\begin{aligned}
\left\{ {}_{x}^{RL}\mathcal{I}_{+1}^{1-\mu}\left[p(x)\,{}_{-1}^{C}\mathcal{D}_x^{\mu}\ \ {}^{(1)}\mathcal{P}_{n-1}^{\alpha,\beta,\mu}(x)\right]\right\}_{x=+1} &= \\
\left\{ {}_{x}^{RL}\mathcal{I}_{+1}^{1-\mu}\left[p(x)\,{}_{-1}^{RL}\mathcal{D}_x^{\mu}\ \ {}^{(1)}\mathcal{P}_{n-1}^{\alpha,\beta,\mu}(x)\right]\right\}_{x=+1} &= \\
\left\{ {}_{x}^{RL}\mathcal{I}_{+1}^{1-\mu}\left[p(x)\,{}_{-1}^{RL}\mathcal{D}_x^{\mu}\left((1+x)^{-\beta+\mu-1}\ \ P_{n-1}^{\alpha-\mu+1,\,-\beta+\mu-1}(x)\right)\right]\right\}_{x=+1} &=
\end{aligned}$$

and by carrying out the fractional RL derivative using Lemma 2.3.3

$$= \left\{ {}^{RL}_{x}\mathcal{I}^{1-\mu}_{+1} \left[p(x) \frac{\Gamma(n-1-\beta+\mu)}{\Gamma(n-1-\beta)} (1+x)^{-1-\beta} P^{1+\alpha,-1-\beta}_{n-1} \right] \right\}_{x=+1} =$$
$$\frac{\Gamma(n-1-\beta+\mu)}{\Gamma(n-1-\beta)} \left\{ {}^{RL}_{x}\mathcal{I}^{1-\mu}_{+1} \left[(1-x)^{1+\alpha} P^{1+\alpha,-1-\beta}_{n-1} \right] \right\}_{x=+1}$$

and by working out the fractional integration using Lemma 2.3.4 we obtain

$$\frac{\Gamma(n-1-\beta+\mu)}{\Gamma(n-1-\beta)} \frac{\Gamma(n+\alpha+1)}{\Gamma(n+\alpha-\mu+1)} \left\{ (1-x)^{2+\alpha-\mu} P^{1+\alpha,-1-\beta}_{n-1} \right\}_{x=+1} = 0.$$

The next step is to show that (2.71) satisfies (2.57) with eigenvalues (2.72). First, we take a fractional integration of order μ on both sides of (2.57) and substitute (2.71). Then, again by replacing the Caputo derivative by the Riemann-Liouville one, thanks to (2.7), we obtain

$$(1-x)^{\alpha+1}(1+x)^{\beta+1} \, {}^{RL}_{-1}\mathcal{D}^{\mu}_{x} \left[(1+x)^{-\beta+\mu-1} \; P^{\alpha-\mu+1,\,-\beta+\mu-1}_{n-1}(x) \right] =$$
$$-\Lambda^{(1)} \, {}^{RL}_{x}\mathcal{I}^{\mu}_{+1} \left\{ (1-x)^{\alpha+1-\mu} \; P^{\alpha-\mu+1,\,-\beta+\mu-1}_{n-1}(x) \right\}.$$

Finally, the fractional derivative on the left-hand side and the fractional integration on the right-hand side is worked out using (2.22) and (2.24) as

$$\frac{\Gamma(n-1-\beta+\mu)}{\Gamma(n-1-\beta)} (1-x)^{\alpha+1} \; P^{\alpha+1,-\beta-1}_{n-1}(x) =$$
$$-\Lambda^{(1)} \frac{\Gamma(n+\alpha+\mu+1)}{\Gamma(n+\alpha+1)} (1-x)^{\alpha+1} \; P^{\alpha+1,-\beta-1}_{n-1}(x).$$

By a similar argument on the $(1-x)^{\alpha+1} \; P^{\alpha+1,-\beta-1}_{n-1}(x)$ being non-zero almost every-

where, we can cancel this term out on both sides and obtain

$$\Lambda^{(1)} \equiv {}^{(1)}\Lambda_n^{\alpha,\beta,\mu} = -\frac{\Gamma(n-\beta+\mu-1)\Gamma(n+\alpha+1)}{\Gamma(n-\beta-1)\Gamma(n+\alpha-\mu+1)}.$$

Now, we need to check Theorem 2.4.1, to see if (2.72) verifies that the eigenvalues are indeed real-valued and distinct, and the orthogonality of the eigenfunctions with respect to $w(x) = (1-x)^{1+\alpha-\mu}(1+x)^{1+\beta-\mu}$ is valid:

$$\int_{-1}^{1} w(x)\, {}^{(1)}\mathcal{P}_k^{\alpha,\beta,\mu}(x)\, {}^{(1)}\mathcal{P}_j^{\alpha,\beta,\mu}(x)dx =$$
$$\int_{-1}^{1} w(x)\left[(1+x)^{-\beta+\mu-1}\right]^2 \;\; P_{k-1}^{\alpha-\mu+1,\,-\beta+\mu-1}(x) \;\; P_{j-1}^{\alpha-\mu+1,\,-\beta+\mu-1}(x)dx =$$
$$\int_{-1}^{1} (1-x)^{1+\alpha-\mu}(1+x)^{-\beta+\mu-1} \;\; P_{k-1}^{\alpha-\mu+1,-\beta+\mu-1}(x) \;\; P_{j-1}^{\alpha-\mu+1,-\beta+\mu-1}(x)dx$$
$$= \int_{-1}^{1} (1-x)^{\alpha^*}(1+x)^{\beta^*} \;\; P_{k-1}^{\alpha^*,\beta^*}(x) \;\; P_{j-1}^{\alpha^*,\beta^*}(x)dx = C^{\alpha^*,\beta^*}(k-1)\delta_{kj},$$

where $\alpha^* = \alpha-\mu+1$, $\beta^* = -\beta+\mu-1$, and denoted by $C^{\alpha^*,\beta^*}(k)$ is the orthogonality constant of the family of Jacobi polynomials.

The simplicity of the eigenvalues can be also shown in a similar fashion as Part c in the proof of Theorem 2.3.5, and this completes the proof. □

Lemma 2.4.3. *The shifted eigenfunctions to SFSLP-I&-II, denoted by* ${}^{(i)}\widetilde{\mathcal{P}}_n^{\alpha,\beta,\mu}(t)$, *are given as*

$${}^{(i)}\widetilde{\mathcal{P}}_n^{\alpha,\beta,\mu}(t) = 2^{\widetilde{\mu}^{(i)}} \sum_{j=0}^{n-1} (-1)^{n+j-1} \binom{n-1+j}{j} \binom{n+(-1)^{i+1}\widetilde{\mu}^{(1)}-1}{n-1-j} t^{j+\widetilde{\mu}^{(i)}}, \tag{2.75}$$

where in case of the SFLSP-I (i=1), $t \in [0,1]$, $\widetilde{\mu}^{(1)} = -\beta+\mu-1$ *and* $0 < \widetilde{\mu}^{(1)} < \mu$, *and for SFSLP-II (i = 2),* $t \in [-1,0]$, $\widetilde{\mu}^{(2)} = -\alpha+\mu-1$ *also* $0 < \widetilde{\mu}^{(2)} < \mu$.

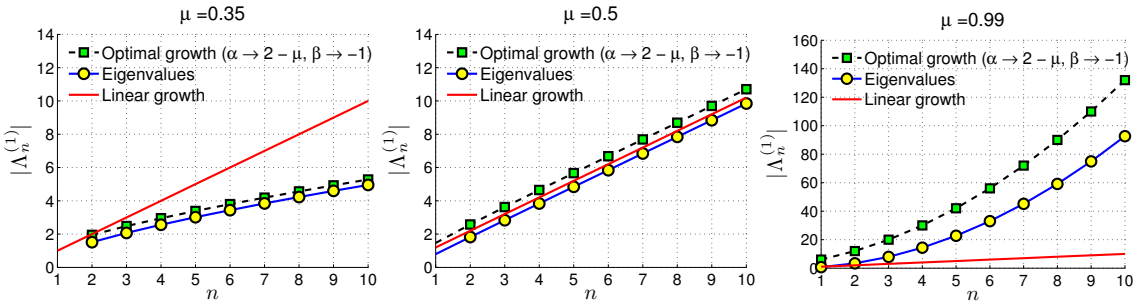

Figure 2.4: Magnitude of the eigenvalues of SFSLP-I, $|\Lambda_n^{(1)}|$, versus n, corresponding to $\alpha = 0$ and $\beta = -0.7$, corresponding to different fractional order $\mu = 0.35$, left: sublinear growth, $\mu = 0.5$, middle: linear growth, and $\mu = 0.99$, right: superlinear-subquadratic growth. Here we compare the growth of the eigenvalues to the optimal case when $\alpha \to 2 - \mu$ and $\beta \to -1$.

Proof. The proof follows the one in Lemma 2.3.6. □

Theorem 2.4.4. *The shifted eigensolutions to (2.57),* ${}^{(i)}\widetilde{\mathcal{P}}_n^{\alpha,\beta,\mu}(t)$*, form a complete hierarchical basis for the finite-dimensional space of poly-fractonomials* $\mathbb{F}_{n-1+\widetilde{\mu}^{(i)}}$*, where* $\widetilde{\mu}^{(1)} = -\beta+\mu-1$ *and* $\widetilde{\mu}^{(2)} = -\alpha+\mu-1$*, where* $0 < \widetilde{\mu}^{(1)} < \mu$*, also* $0 < \widetilde{\mu}^{(2)} < \mu$*.*

Proof. The proof follows the one in Theorem 2.3.12. □

The growth of the magnitude in the eigenvalues of SFSLP-I, $|\Lambda_n^{(1)}|$, exhibits a similar behaviour as one observed in RFSLP-I-&-II. However, there are another two degrees of freedom in the choice of parameters α and β, which affect the magnitude of the eigenvalues. It turns out that in case of SFSLP-I ($i = 1$), the optimal highest magnitude is achieved when $\alpha \to 2 - \mu$ and $\beta \to -1$, $\forall \mu \in (0, 1)$. The growth of the $|\Lambda_n^{(1)}|$ corresponding to three values of $\mu = 0.35$, $\mu = 0.5$, and $\mu = 0.99$ is shown in Fig. 2.4. Again, we observe about the two growth modes of $|\Lambda_n^{(1)}|$, depending on either $\mu \in (0, 1/2)$, where a sublinear growth in $|\Lambda_n^1|$ is observed, or, $\mu \in (1/2, 1)$, where a superlinear-subquadratic growth mode is valid; the case $\mu = 1/2$ leads to an exactly linear growth mode. Corresponding to the aforementioned fractional orders μ, in Fig. 2.5, we plot the eigenfunctions of SFSLP-I, $\mathcal{P}_n^{(1)}(x)$, of different orders and corresponding to different values of μ used in Fig. 2.4. In a similar fashion,

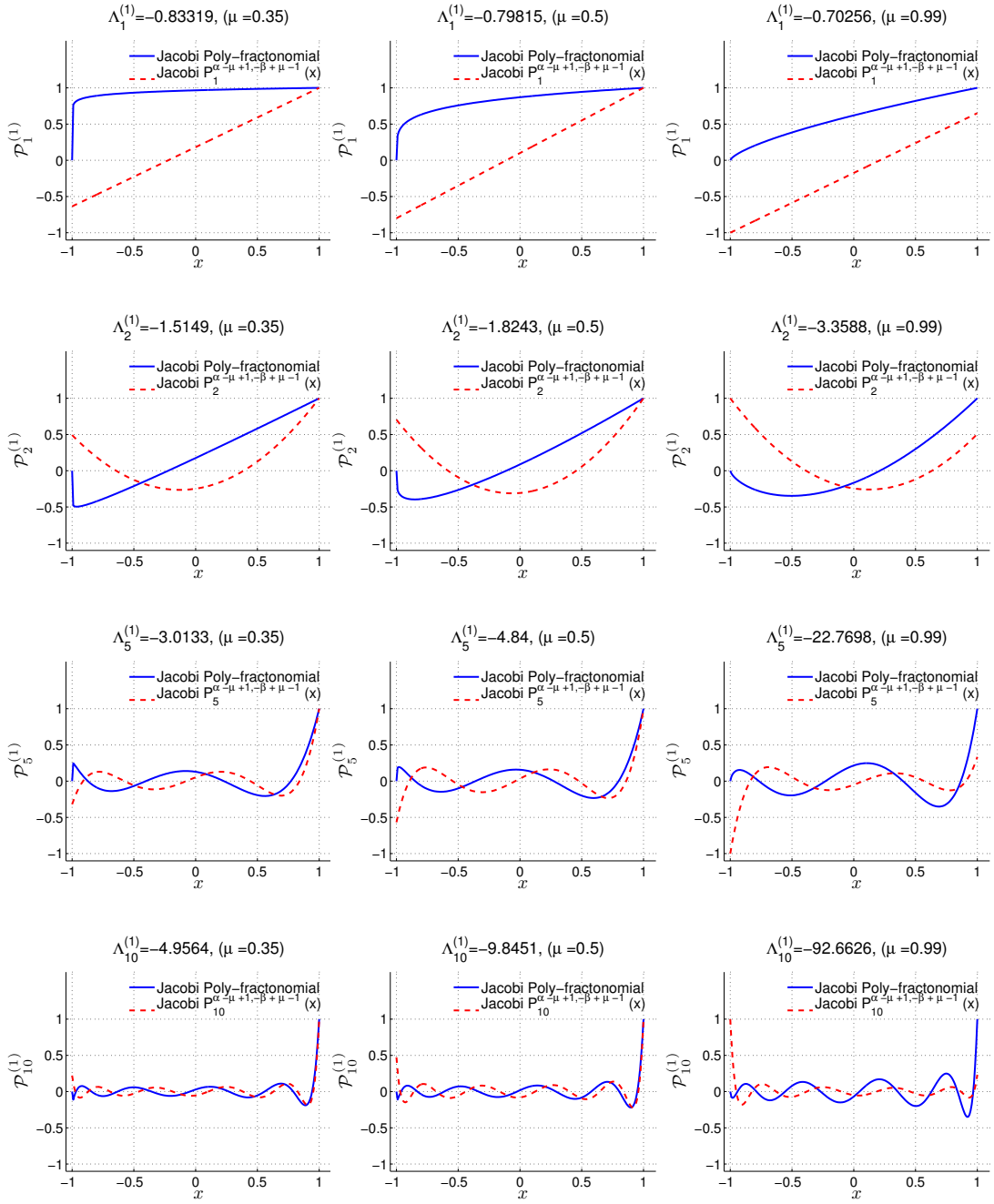

Figure 2.5: Eigenfunctions of SFSLP-I, $\mathcal{P}_n^{(1)}$, versus x, for $n = 1$ (first row), $n = 2$ (second row), $n = 5$ (third row), and $n = 10$ (last row), corresponding to the fractional order $\mu = \nu/2 = 0.35$ (left column), $\mu = \nu/2 = 0.5$ (middle column), and $\mu = \nu/2 = 0.99$ (right column). Here, we take the same values $\alpha = 0$ and $\beta = -0.7$, as shown in Fig. 2.4

.

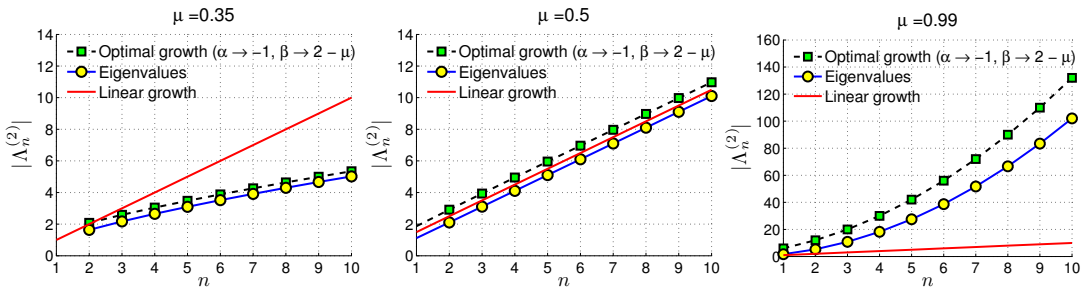

Figure 2.6: Magnitude of the eigenvalues of SFSLP-II, $|\Lambda_n^{(2)}|$, versus n, corresponding to $\alpha = -0.7$ and $\beta = 0$, corresponding to different fractional order $\mu = 0.35$, left: sublinear growth, $\mu = 0.5$, middle: linear growth, and $\mu = 0.99$, right: superlinear-subquadratic growth. Here we compare the growth of the eigenvalues to the optimal case when $\alpha \to -1$ and $\beta \to 2 - \mu$.

we compare the eigensolutions with the corresponding standard Jacobi polynomials $P_n^{\alpha-\mu+1,-\beta+\mu-1}(x)$ in each plot.

In Fig. 2.6, the growth of the magnitude in $\Lambda_n^{(2)}$, corresponding to three values of $\mu = 0.35$, $\mu = 0.5$, and $\mu = 0.99$ is plotted. In SFSLP-II ($i = 2$), the optimal highest magnitude in the eigenvalues is achieved when $\alpha \to -1$ and $\beta \to 2-\mu$. Moreover, in Fig. 2.7, we plot the eigenfunctions of SFSLP-II, $\mathcal{P}_n^{(2)}(x)$, of different fractional orders and corresponding to different μ used in Fig. 2.6. This time, we compare the eigensolutions with the corresponding standard Jacobi polynomials $P_n^{-\alpha+\mu-1,\beta-\mu+1}(x)$ in each plot.

2.4.1 Properties of the Eigen-solutions to SFSLP-I&-II

We list a number of properties of the eigensolutions to SFSLP-I &-II as follows.

- **Non-polynomial nature**:

  From (2.71) and (2.73), the eigenfunctions exhibit a non-polynomial (fractal) behaviour, thanks to the fractonomial multipliers $(1 + x)^{-\beta+\mu-1}$ in SFSLP-

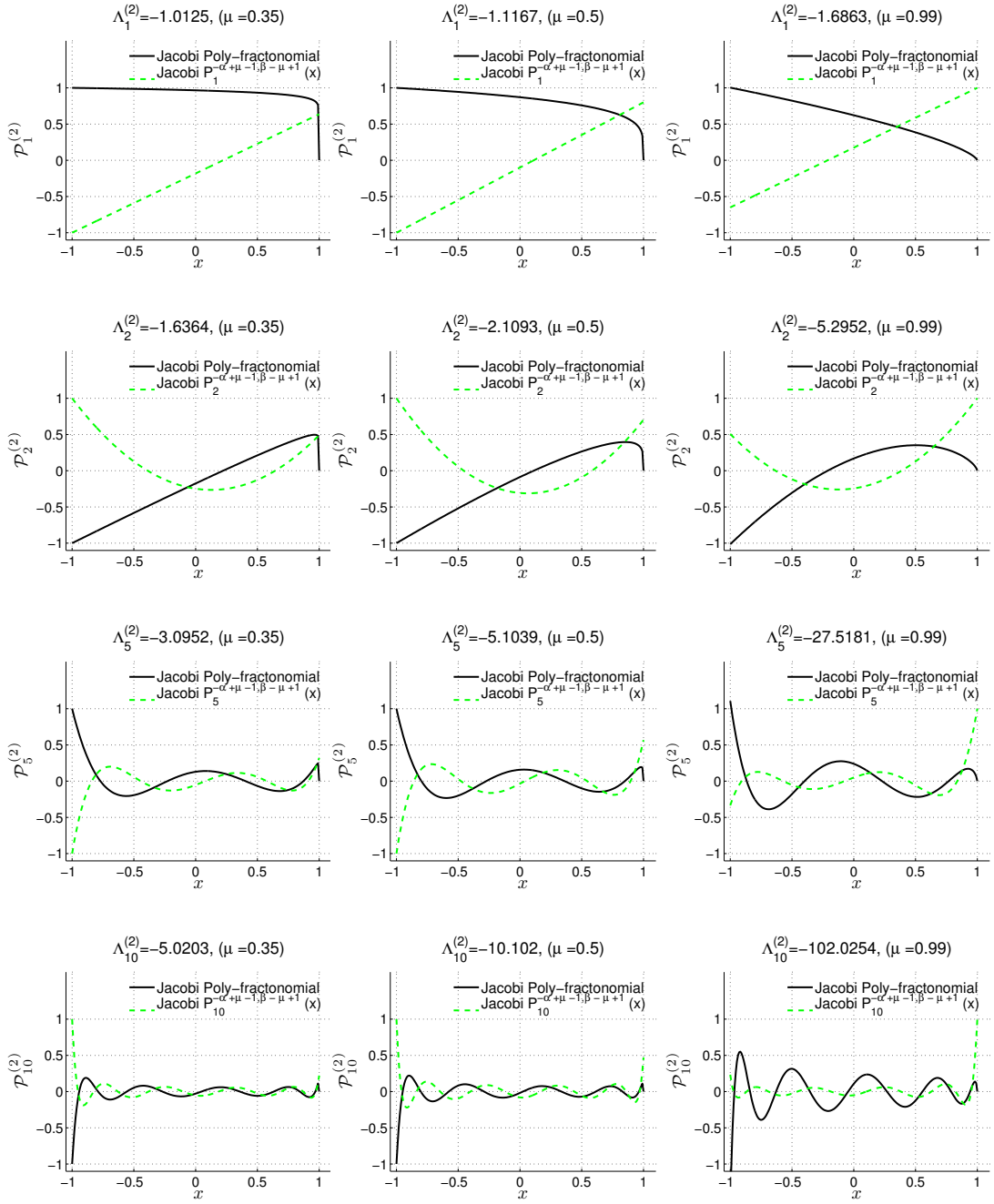

Figure 2.7: Eigenfunctions of SFSLP-II, $\mathcal{P}_n^{(2)}$, versus x, for $n = 1$ (first row), $n = 2$ (second row), $n = 5$ (third row), and $n = 10$ (last row), corresponding to the fractional order $\mu = \nu/2 = 0.35$ (left column), $\mu = \nu/2 = 0.5$ (middle column), and $\mu = \nu/2 = 0.99$ (right column). Here, we take the same values $\alpha = -0.7$ and $\beta = 0$, as shown in Fig. 2.6

.

I and $(1-x)^{-\alpha+\mu-1}$ in SFSLP-II. Indeed, these poly-fractonomials are the generalization of those introduced in RFSLP (2.27) and (2.29). We realize that when $\alpha \to -1$ and $\beta \to -1$ simultaneously, the eigen-solutions to the singular problems SFSLP-I&-II, only *asymptotically*, approach to that of the regular counterparts. However, special attention should be taken due to the fact that when $\alpha \to -1$ and $\beta \to -1$, the governing equations (2.57) then become *non-singular* and equivalent to the regular problems RFSLP-I&-II (2.16) at the first place.

Here, we refer to ${}^{(i)}\mathcal{P}_n^{\alpha,\beta,\mu}(x)$ as the *generalization of the whole family of the Jacobi Poly-Fractonomial* corresponding to the triple ${}^{\alpha,\beta,\mu}$, where $-1 < \alpha < 2-\mu$, and $-1 < \beta < \mu - 1$ in SFSLP-I ($i = 1$), and $-1 < \alpha < \mu - 1$, and $-1 < \beta < 2 - \mu$ in SFSLP-II ($i = 2$).

- **Asymptotic eigenvalues** $\Lambda_n^{(i)}$:

The growth in the magnitude of eigenvalues in SFSLP with n is dependent on three parameters: the fractional derivative order μ, α and β. From (2.72) and (2.74), it is easy to show that α and β only affect the magnitude and not the behaviour (i.e., order) of the growth. As shown in (2.30), since $\mu \in (0, 1)$, there are two modes of growth in the magnitude of $\Lambda_n^{(i)}$ referred to as *sublinear* mode corresponding to $0 < \mu < 1/2$, and *superlinear-subquadratic* mode which corresponds to $1/2 < \mu < 1$. Particularly, when $\mu = 1/2$, the eigenvalues grow linearly with n. The optimal highest magnitude of $\Lambda_n^{(1)}$ achieved when $\alpha \to 2-\mu$ and $\beta \to -1$ in SFSLP-I, and in case of the SFSLP-II when $\alpha \to -1$ and $\beta \to 2-\mu$ the optimal eigenvalues are obtained. The asymptotic cases are

summarized as

$$|\Lambda_n^{(i)}| = \begin{cases} n^2, & \mu \to 1, \\ n & \mu \to 1/2, \\ 1 & \mu \to 0. \end{cases} \tag{2.76}$$

- **Recurrence relations**:

  A recurrence relations is obtained for the Jacobi poly-fractonomials ${}^{(i)}\mathcal{P}_n^{\alpha,\beta,\mu}(x)$ as

$$\begin{aligned} {}^{(1)}\mathcal{P}_1^{\alpha,\beta,\mu}(x) &= (1+x)^{-\beta+\mu-1}, \\ {}^{(1)}\mathcal{P}_2^{\alpha,\beta,\mu}(x) &= \frac{1}{2}(1+x)^{-\beta+\mu-1}\left[\alpha+\beta-2\mu+2+(\alpha-\beta+2)x\right], \\ &\vdots \\ a_n\,{}^{(1)}\mathcal{P}_{n+1}^{\alpha,\beta,\mu}(x) &= (b_n+c_n x)\,{}^{(1)}\mathcal{P}_n^{\alpha,\beta,\mu}(x) - d_n\,{}^{(1)}\mathcal{P}_{n-1}^{\alpha,\beta,\mu}(x) \\ a_n &= 2n(n+\alpha-\beta)(2n+\alpha-\beta-2) \\ b_n &= (2n-\alpha+\beta-1)(\alpha-\beta)(\alpha+\beta-2\mu+2) \\ c_n &= (2n-\alpha+\beta)(2n-\alpha+\beta-1)(2n-\alpha+\beta-2) \\ d_n &= 2(n-\alpha+\mu-2)(n+\beta-\mu)(2n-\alpha+\beta) \end{aligned} \tag{2.77}$$

and

$$\begin{aligned}
{}^{(2)}\mathcal{P}_1^{\alpha,\beta,\mu}(x) &= (1-x)^{-\alpha+\mu-1}, \\
{}^{(2)}\mathcal{P}_2^{\alpha,\beta,\mu}(x) &= \frac{1}{2}(1-x)^{-\alpha+\mu-1}\left[-\alpha-\beta+2\mu-2+(-\alpha+\beta+2)x\right], \\
&\vdots \\
a_n^{*\,(2)}\mathcal{P}_{n+1}^{\alpha,\beta,\mu}(x) &= (b_n^*+c_n^*x)\,{}^{(2)}\mathcal{P}_n^{\alpha,\beta,\mu}(x) - d_n^{*\,(2)}\mathcal{P}_{n-1}^{\alpha,\beta,\mu}(x) \\
a_n^* &= 2n(n-\alpha+\beta)(2n-\alpha+\beta-2) \\
b_n^* &= (2n-\alpha+\beta-1)(\alpha-\beta)(\alpha+\beta-2\mu+2) \\
c_n^* &= (2n+\alpha+\beta)(2n+\alpha+\beta-1)(2n+\alpha+\beta-2) \\
d_n^* &= 2(n+\alpha-\mu)(n-\beta+\mu-2)(2n+\alpha-\beta)
\end{aligned} \tag{2.78}$$

- **Orthogonality**:

$$\int_{-1}^{1}(1-x)^{\alpha+1-\mu}(1+x)^{\beta+1-\mu}\;{}^{(i)}\mathcal{P}_k^{\alpha,\beta,\mu}(x)\;{}^{(i)}\mathcal{P}_j^{\alpha,\beta,\mu}(x)dx = {}^{(i)}\mathcal{C}_k^{\alpha,\beta}\delta_{kj}, \tag{2.79}$$

where,

$${}^{(1)}\mathcal{C}_k^{\alpha,\beta} = \frac{2^{\alpha-\beta+1}}{2k+\alpha-\beta-1}\frac{\Gamma(k+\alpha-\mu+1)\Gamma(k-\beta+\mu-1)}{(k-1)!\;\Gamma(k+\alpha-\beta)}$$

and

$${}^{(2)}\mathcal{C}_k^{\alpha,\beta} = \frac{2^{-\alpha+\beta+1}}{2k-\alpha+\beta-1}\frac{\Gamma(k-\alpha+\mu-1)\Gamma(k+\beta-\mu+1)}{(k-1)!\;\Gamma(k-\alpha+\beta)}$$

- **Fractional derivatives**:

$$ {}^{RL}_{-1}\mathcal{D}_x^{-\beta+\mu+1}\left({}^{(1)}\mathcal{P}_n^{\alpha,\beta,\mu}\right) = {}^{C}_{-1}\mathcal{D}_x^{-\beta+\mu+1}\left({}^{(1)}\mathcal{P}_n^{\alpha,\beta,\mu}\right) = \frac{\Gamma(n+\mu)}{\Gamma(n)} P_{n-1}^{\alpha-\beta,0}(x) \tag{2.80} $$

and

$$ {}^{RL}_{x}\mathcal{D}_1^{-\alpha+\mu-1}\left({}^{(2)}\mathcal{P}_n^{\alpha,\beta,\mu}\right) = {}^{C}_{x}\mathcal{D}_1^{-\alpha+\mu-1}\left({}^{(2)}\mathcal{P}_n^{\alpha,\beta,\mu}\right) = \frac{\Gamma(n+\mu)}{\Gamma(n)} P_{n-1}^{0,\beta-\alpha}(x) \tag{2.81} $$

where $P_{n-1}^{\alpha-\beta,0}(x)$ and $P_{n-1}^{0,\beta-\alpha}(x)$ denote the standard Jacobi polynomials.

- **First derivatives**:

$$ \begin{aligned} \frac{d}{dx}\left({}^{(1)}\mathcal{P}_n^{\alpha,\beta,\mu}(x)\right) = {} & (-\beta+\mu-1)(1+x)^{-\beta+\mu-2} P_{n-1}^{\alpha-\mu+1,-\beta+\mu-1}(x) + \\ & \frac{1}{2}(n+\alpha-\beta)(1+x)^{-\beta+\mu-1} P_{n-2}^{\alpha-\mu+2,-\beta+\mu}(x) \end{aligned} $$

and

$$ \begin{aligned} \frac{d}{dx}\left({}^{(2)}\mathcal{P}_n^{\alpha,\beta,\mu}(x)\right) = {} & (+\alpha-\mu+1)(1-x)^{-\alpha+\mu-2} P_{n-1}^{-\alpha+\mu-1,\beta-\mu+1}(x) + \\ & \frac{1}{2}(n-\alpha+\beta)(1-x)^{-\alpha+\mu-1} P_{n-2}^{-\alpha+\mu,\beta-\mu+2}(x) \end{aligned} $$

- **Special values**:

$$ \begin{aligned} {}^{(1)}\mathcal{P}_n^{\alpha,\beta,\mu}(-1) &= 0, \\ {}^{(1)}\mathcal{P}_n^{\alpha,\beta,\mu}(+1) &= 2^{-\beta+\mu-1}\binom{n+\alpha-\mu}{n-1} \end{aligned} \tag{2.82} $$

and

$$
\begin{aligned}
{}^{(2)}\mathcal{P}_n^{\alpha,\beta,\mu}(+1) &= 0, \\
{}^{(2)}\mathcal{P}_n^{\alpha,\beta,\mu}(-1) &= 2^{-\alpha+\mu-1}\begin{pmatrix} n+\beta-\mu \\ n-1 \end{pmatrix}
\end{aligned} \tag{2.83}
$$

2.5 Numerical Approximation

As discussed in Sec. 2.4.1, taking $\alpha = \beta = -1$ in SFLP-I&-II essentially eliminates the singularity in the definition of SFSLP-I&-II (2.57). Accordingly, we are not allowed to take such values for α and β, unless asymptotically, in the SFSLP-I&-II. However, the Jacobi poly-fractonomials ${}^{(i)}\mathcal{P}_n^{\alpha,\beta,\mu}(x)$, $i \in \{1,2\}$, regardless of where they are coming from, are the generalization of the poly-fractonomials $\Phi_n^{(i)}(x)$ which are known as the eigenfunctions of FSLP-I&-II. Therefore, we can represent the whole family of the Jacobi poly-fractonomials ${}^{(i)}\mathcal{P}_n^{\alpha,\beta,\mu}(x)$ as

$$
{}^{(i)}\mathcal{P}_n^{\alpha,\beta,\mu}(x) = \begin{cases} \text{Eigenfunctions of RFSLPs in (2.16)}, & \alpha = \beta = -1, \\ \text{Eigenfunctions of SFSLPs in (2.57)}, & \textit{Otherwise}, \end{cases} \tag{2.84}
$$

where $i \in \{1,2\}$.

By Theorems 2.3.12 and 2.4.4, we can employ such basis functions for numerical approximation. In such setting, we can study the approximation properties of the family of Jacobi poly-fractonomials ${}^{(i)}\mathcal{P}_n^{\alpha,\beta,\mu}(x)$ in a unified fashion. To this end, we

represent a function $f(x) \in L^2_w[-1,1]$ as

$$f(x) \approx f_N(x) = \sum_{n=1}^{N} \hat{f}_n \ \ {}^{(i)}\mathcal{P}_n^{\alpha,\beta,\mu}(x), \ \ x \in [-1,1] \tag{2.85}$$

where $f(x)$ satisfied the same boundary conditions as ${}^{(i)}\mathcal{P}_n^{\alpha,\beta,\mu}(x)$ in (2.85). Now, the main question is how fast the expansion coefficients $\hat{f}_n$ decay. By multiplying (2.85) by $\mathcal{L}_i^{\alpha,\beta;\mu}({}^{(i)}\mathcal{P}_k^{\alpha,\beta,\mu}(x))$, $k = 1, 2, \cdots, N$, and integrating in the interval $[-1,1]$, we obtain

$$\int_{-1}^{1} f(x)\mathcal{L}_i^{\alpha,\beta;\mu}\left({}^{(i)}\mathcal{P}_k^{\alpha,\beta,\mu}(x)\right) \ dx = \int_{-1}^{1}\left(\sum_{n=1}^{N} \hat{f}_n \ \ {}^{(i)}\mathcal{P}_n^{\alpha,\beta,\mu}(x)\right)\mathcal{L}_i^{\alpha,\beta;\mu}\left({}^{(i)}\mathcal{P}_k^{\alpha,\beta,\mu}(x)\right) dx,$$

where, $\mathcal{L}_i^{\alpha,\beta;\mu}({}^{(i)}\mathcal{P}_k^{\alpha,\beta,\mu}(x))$ on the right-hand side can be substituted by the right-hand side of (2.57), i.e., $-\Lambda_n^{(i)} w(x)\, {}^{(i)}\mathcal{P}_k^{\alpha,\beta,\mu}(x)$ as

$$\int_{-1}^{1} f(x)\mathcal{L}_i^{\alpha,\beta;\mu}\left({}^{(i)}\mathcal{P}_n^{\alpha,\beta,\mu}(x)\right) \ dx = \sum_{n=1}^{N} -\hat{f}_n\, \Lambda_n^{(i)} \int_{-1}^{1} (1-x)^{\alpha+1-\mu}(1+x)^{\beta+1-\mu} \ \ {}^{(i)}\mathcal{P}_n^{\alpha,\beta,\mu}(x)\, {}^{(i)}\mathcal{P}_k^{\alpha,\beta,\mu}(x),$$

and thanks to the orthogonality property (2.79) we get

$$\hat{f}_k = \frac{-1}{{}^{(i)}\mathcal{C}_k^{\alpha,\beta}\ \Lambda_k^{(i)}} \int_{-1}^{1} f(x)\mathcal{L}_i^{\alpha,\beta;\mu}\left({}^{(i)}\mathcal{P}_k^{\alpha,\beta,\mu}(x)\right) \ dx,$$

or equivalently by (2.60),

$$\hat{f}_k = \frac{-1}{{}_{(i)}\mathcal{C}_k^{\alpha,\beta}\ \Lambda_k^{(i)}} \int_{-1}^{1} f(x)\, {}^{RL}\mathcal{D}^{\mu}\Big\{(1-x)^{\alpha+1}(1+x)^{\beta+1}\ {}^{C}\mathcal{D}^{\mu}\ \Big({}^{(i)}\mathcal{P}_k^{\alpha,\beta,\mu}(x)\Big)\Big\}\, dx. \tag{2.86}$$

We recall that $i = 1$ corresponds to ${}^{RL}\mathcal{D}^{\mu} \equiv {}_{x}^{RL}\mathcal{D}_{+1}^{\mu}$ and ${}^{C}\mathcal{D}^{\mu} \equiv {}_{-1}^{C}\mathcal{D}_{x}^{\mu}$, also when $i = 2$ we have ${}^{RL}\mathcal{D}^{\mu} \equiv {}_{-1}^{RL}\mathcal{D}_{x}^{\mu}$ and ${}^{C}\mathcal{D}^{\mu} \equiv {}_{x}^{C}\mathcal{D}_{+1}^{\mu}$. Now, by carrying out the fractional integration-by-parts (2.9) and (2.10), we get

$$\hat{f}_k = \frac{-1}{{}_{(i)}\mathcal{C}_k^{\alpha,\beta}\ \Lambda_k^{(i)}} \int_{-1}^{1} (1-x)^{\alpha+1}(1+x)^{\beta+1} \left({}^{C}\mathcal{D}^{\mu}\, f(x)\right) \left({}^{C}\mathcal{D}^{\mu}\ {}^{(i)}\mathcal{P}_k^{\alpha,\beta,\mu}(x)\right)\, dx, \tag{2.87}$$

which is equivalent to

$$\begin{aligned}\hat{f}_k = \frac{-1}{{}_{(i)}\mathcal{C}_k^{\alpha,\beta}\ \Lambda_k^{(i)}} \int_{-1}^{1} (1-x)^{\alpha+1}(1+x)^{\beta+1} \left({}^{C}\mathcal{D}^{\mu}\ {}^{(i)}\mathcal{P}_k^{\alpha,\beta,\mu}(x)\right)\ \left({}^{C}\mathcal{D}^{\mu}\, f(x)\right) dx \\ - {}^{(i)}\mathcal{P}_k^{\alpha,\beta,\mu}(x)\, {}_{x}^{RL}\mathcal{I}_{x_R}^{\mu} f(x)|_{x=-1}^{+1}.\end{aligned} \tag{2.88}$$

We realize that the last term in (2.88) is identically zero. Again, by the fractional integration-by-parts (2.9) and (2.10), we obtain

$$\hat{f}_k = \frac{-1}{{}_{(i)}\mathcal{C}_k^{\alpha,\beta}\ \Lambda_k^{(i)}} \int_{-1}^{1} {}^{(i)}\mathcal{P}_k^{\alpha,\beta,\mu}(x)\, {}^{RL}\mathcal{D}^{\mu}\Big\{(1-x)^{\alpha+1}(1+x)^{\beta+1}\ {}^{C}\mathcal{D}^{\mu}\, f(x)\Big\}\, dx.$$

or equivalently

$$\hat{f}_k = \frac{-1}{{}_{(i)}\mathcal{C}_k^{\alpha,\beta}\ \Lambda_k^{(i)}} \int_{-1}^{1} {}^{(i)}\mathcal{P}_k^{\alpha,\beta,\mu}(x) \mathcal{L}_i^{\alpha,\beta;\mu}\left[\, f(x)\right] dx,$$

if denoted by $f_{(1)}(x) \equiv \mathcal{L}_i^{\alpha,\beta;\mu}\left[\, f(x)\right] \in L_w^2[-1,1]$. By carrying out the fractional integration-by-parts another $(m-1)$ times, and setting $f_{(m)}(x) \equiv \mathcal{L}_i^{\alpha,\beta;\mu}\left[\, f_{(m-1)}(x)\right] \in$

$L^2_w[-1,1]$, we obtain

$$|\hat{f}_k| \approx \frac{C}{|\Lambda_k^{(i)}|^m}\|f_{(m)}(x)\|_{L^2_w}, \quad k = 1, 2, \cdots, N. \tag{2.89}$$

Consequently, if the function $f(x) \in C^\infty[-1,1]$, we recover the spectral decay of the expansion coefficients $\hat{f}_k$ since m can be chosen arbitrarily large.

Remark 2.5.1. Although when $0 < \mu < 1/2$ the magnitude of the eigenvalues grows sublinearly, such decay behavior does not affect fundamentally the exponential character of the decay in the coefficients coefficients if $f(x)$ possesses the required regularity.

2.5.1 Numerical Tests

In the following examples, we test the convergence rate in approximating some poly-fractonomials in addition to some other type of functions involving fractional character. By Theorems 2.3.12 and 2.4.4, we can exactly represent any poly-fractonomial $F_{N+\mu}$ of order $N+\mu$ in terms of the first N regular Jacobi fractal basis functions (2.16), or alternatively, using the first N singular Jacobi fractal basis functions (2.75). However, this is not the case when other types of basis functions, such as the standard (shifted) Legendre polynomials $\widetilde{P}_n(x)$, are employed.

We first approximate the simplest fractal function $f(t) = \sqrt{t}$ using our regular and singular Jacobi poly-fractonomials, where we see that only *one* term is needed to exactly represent the fractonomial, i.e., $f(t) = f_1(t)$. To make a comparison, we also plot the the L^2-norm error in terms of N, the number of expansion terms in (2.85) in Fig. 2.8 (left), when the standard Legendre polynomials are employed as the basis functions. Moreover, we represent the poly-fractonomial $f(t) = t^{1/3} + t^{4+1/3} + t^{7+1/3}$

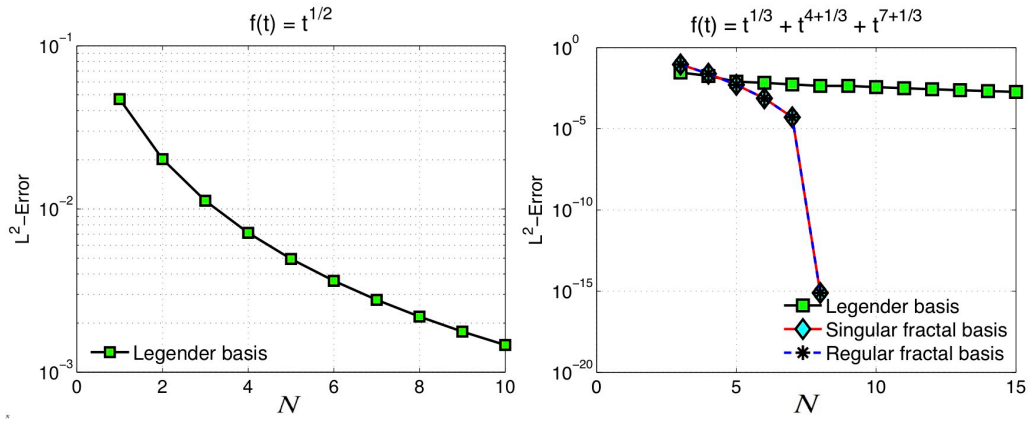

Figure 2.8: L^2-norm error $\|f(t) - f_N(t)\|_{L^2}$ versus n, the number of expansion terms in (2.85) when Legendre polynomials are used as the basis functions. Here, $f(t)$ is a poly-fractonomial; left: $f(t) = \sqrt{t}$, where only one term, i.e., ${}^{(i)}\mathcal{P}^{\alpha,\beta,\mu}{}_1$ is needed to exactly capture $\sqrt{t}$, and right: $f(t) = t^{1/3} + t^{4+1/3} + t^{7+1/3}$; here $\alpha = \beta = 0$.

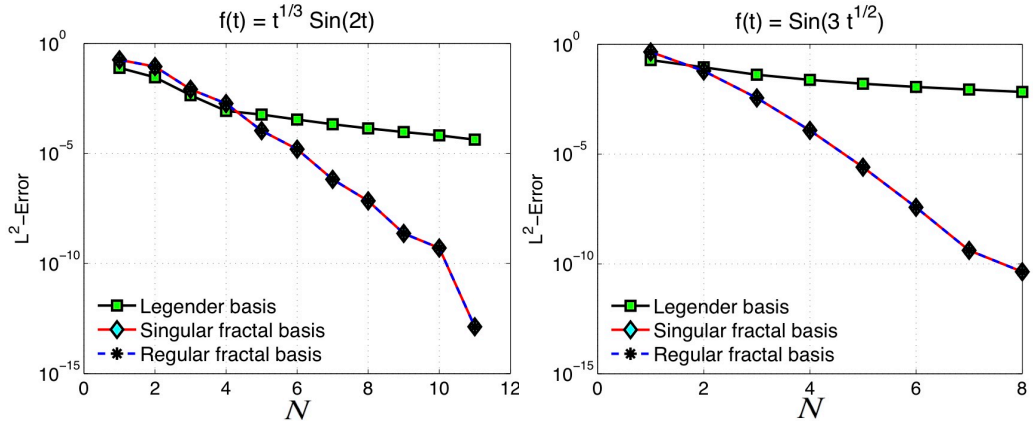

Figure 2.9: L^2-norm error $\|f(t) - f_N(t)\|_{L^2}$ versus N, the number of expansion terms in (2.85), where $f(t)$ is not a poly-fractonomial; left: $f(t) = t^{1/3}\sin(2t)$, and right: $f(t) = \sin(3\sqrt{t})$; here $\alpha = \beta = 0$.

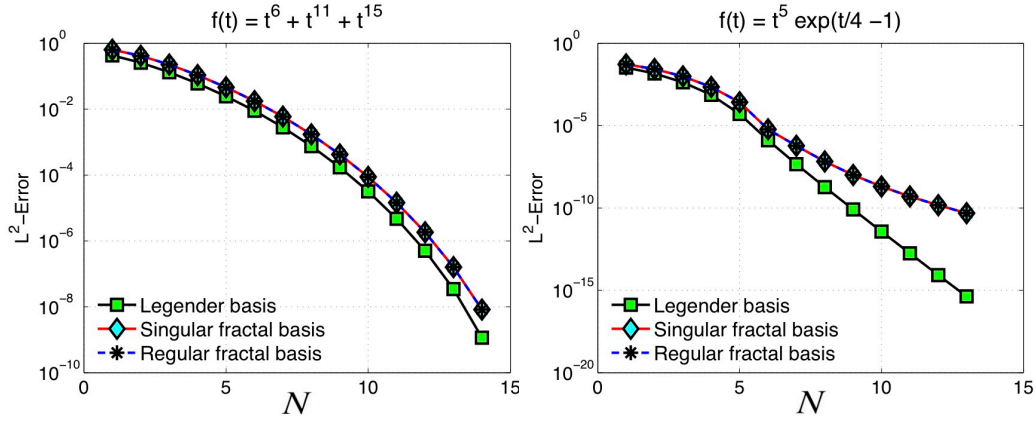

Figure 2.10: L^2-norm error $\|f(t) - f_N(t)\|_{L^2}$ versus N, the number of expansion terms in (2.85), where $f(t)$ is a polynomial; left: $f(t) = t^6 + t^{11} + t^{15}$, and right: $f(t) = t^5 \exp t/4 - 1$; here $\alpha = \beta = 0$.

by our regular and singular Jacobi poly-fractonomials to compare the efficiency of such expansion functions to other standard polynomial bases. The fast (super) spectral convergence of the our fractal basis functions shown in Fig. 2.8 (right), compared to that of the Legendre expansion, highlights the efficiency of Jacobi poly-fractonomial basis functions in approximating non-polynomial functions. Next, we approximate another two functions which are not poly-fractonomials. In Fig. 2.9, we show the L^2-norm error in (2.85), where the convergence to $f(t) = t^{1/3}\sin(2t)$ is shown on the left and the error in the approximation of $f(t) = \sin(3\sqrt{t})$ is plotted on the right. Once again, we observe spectral (exponential) convergence of (2.85) when the regular and the singular eigenfunctions are employed as the basis functions, compared to the case when the standard Legendre polynomials are employed. Finally, we also test how well smooth functions are approximated using a non-polynomial basis in Fig. 2.10. As expected, we see that the Legendre polynomial basis is outperforming the poly-fractonomial basis but only slightly and we still observe expoential convergence of the latter. Here we employed $\mu = 1/2$ for the both RFSLP and SFSLP bases but other choices are also possible to optimize the convergence rate.

Chapter Three

Tempered Fractional Sturm-Liouville Eigen-Problems

Continuum-time random walk is a general model for particle kinetics, which allows for incorporating waiting times and/or non-Gaussian jump distributions with divergent second moments to account for Lévy flights. Exponentially tempering the probability distribution of the waiting times and the anomalously large displacements results in tempered-stable Lévy processes with *finite* moments, where the fluid (continuous) limit leads to the tempered fractional diffusion equation. The development of fast and accurate numerical schemes for such non-local problems requires a new spectral theory and suitable choice of basis functions. In this chapter, we introduce two classes of regular and singular tempered fractional Sturm-Liouville problems of two kinds (TFSLP-I and TFSLP-II) of order $\nu \in (0, 2)$. In the regular case, the corresponding tempered differential operators are associated with tempering functions $p_I(x) = \exp(2\tau)$ and $p_{II}(x) = \exp(-2\tau)$, $\tau \geq 0$, respectively in the regular TFSLP-I and TFSLP-II, which do not vanish in $[-1, 1]$. In contrast, the corresponding differential operators in the singular setting are associated with different forms of $p_I(x) = \exp(2\tau)(1-x)^{1+\alpha}(1+x)^{1+\beta}$ and $p_{II}(x) = \exp(-2\tau)(1-x)^{1+\alpha}(1+x)^{1+\beta}$, vanishing at $x = \pm 1$ in the singular TFSLP-I and TFSLP-II, respectively. The aforementioned tempered fractional differential operators are both of tempered Riemann-Liouville and tempered Caputo type of fractional order $\mu = \nu/2 \in (0, 1)$. We prove the well-posedness of the boundary-value problems and that the eigenvalues of the regular tempered problems are real-valued and the corresponding eigenfunctions are orthogonal. Next, we obtain the explicit eigensolutions to the TFSLP-I & -II as non-polynomial functions, which we define as *tempered Jacobi poly-fractonomials*. These eigenfunctions are orthogonal with respect to the weight function associated with the TFSLP-I & -II. Finally, we introduce these eigenfunctions as new basis (and test) functions for spectrally-accurate approximation of functions and tempered-fractional differential operators. To this end, we further develop a Petrov-Galerkin spectral method for solving tempered fractional ODEs (TFODEs), followed by the corre-

sponding stability and convergence analysis, which validates the achieved spectral convergence in our simulations.

3.1 Background

In order to develop efficient numerical schemes for tempered non-local operators, it is important to first formulate a proper spectral theory for tempered fractional eigenproblems. In the standard calculus, the Sturm-Liouville problem (SLP) has been a fruitful resource for the development of spectral methods, spectral/hp element methods, and the theory of self-adjoint operators [3, 192]. However, mostly integer order differential operators in SLPs have been used, and such operators do not include any fractional differential operators. Over the last decade, it has been demonstrated that many systems in science and engineering can be modelled more accurately by employing fractional-order rather than integer-order derivatives [32, 177, 47, 115]. In most Fractional Sturm-Liouville formulations, the ordinary derivatives in a traditional Sturm-Liouville problem are replaced with fractional derivatives, and the resulting problems are approximated using a variety of numerical schemes [1, 58, 131]. However, approximating such an infinite-dimensional non-local operators in a finite-dimensional space can be challenging. It turns out that the linear systems resulting from these numerical methods quickly become ill-conditioned, which may suffer from round-off errors and the pseudo-spectra. That would prohibit computing the eigenvalues and eigenfunctions with the desired precision.

Establishing the basic properties of Fractional Sturm-Liouville Problems (FSLPs) such as orthogonality of the eigenfunctions, the nature of eigenvalues, etc, is the first step. Qi and Chen in [144], also Atanackovic and Stankovic in [9], considered a

classical Sturm-Liouville operator including a sum of the left- and right-sided fractional derivatives. Bas and Metin [15], Klimek and Agrawal [93], Zayernouri and Karniadakis [187], also Rivero et.al. [149], defined different classes of fractional SturmLiouville operators and investigated the properties of the corresponding eigenfunctions and the eigenvalues. In addition, in [92], the exact eigen-solutions are obtained in terms of the standard Legendre polynomials. Recently, Zayernouri and Karniadakis in [187] have formulated regular and singular FSLPs of kind-I and -II, and obtained explicit eigensolutions, in the form of *Jacobi poly-fractonomials* given by

$$ {}^{(1)}\mathcal{P}_n^{\alpha,\beta,\mu}(x) = (1+x)^{-\beta+\mu-1} P_{n-1}^{\alpha-\mu+1,-\beta+\mu-1}(x), \quad x \in [-1,1], \tag{3.1} $$

with $\mu \in (0,1)$, $-1 \leq \alpha < 2-\mu$, and $-1 \leq \beta < \mu - 1$, which represent the eigenfunctions of the singular problem of first kind, and

$$ {}^{(2)}\mathcal{P}_n^{\alpha,\beta,\mu}(x) = (1-x)^{-\alpha+\mu-1} P_{n-1}^{-\alpha+\mu-1\,,\,\beta-\mu+1}(x), \quad x \in [-1,1], \tag{3.2} $$

where $-1 < \alpha < \mu - 1$ and $-1 < \beta < 2-\mu$, and $\mu \in (0,1)$, are eigenfunctions of the singular problem of second kind. In addition, they showed that these eigenfunctions have similar properties to those with non-fractional setting such as orthogonality, recurrence relations, fractional derivatives and integration formula, etc. Jacobi poly-fractonomials have been successfully employed as basis and test functions in developing spectrally-accurate Petrov-Galerkin spectral and discontinuous spectral element methods in [189, 188] and fractional spectral collocation methods in [190] for a variety of FODEs and FPDEs including multi-term FPDEs and the non-linear space-fractional Burgers' equation.

In this chapter, we consider FSLPs corresponding to *tempered fractional* boundary-value problems and formulate both regular and singular Tempered Fractional Sturm-

Liouville Problems (TFSLPs) of two kinds. We prove the well-posedness of the boundary-value problems, that the eigenvalues of the tempered problems are real-valued, the corresponding eigenfunctions are orthogonal, and obtain the corresponding explicit eigenfunctions as *tempered Jacobi poly-fractonomials*. We employ these eigenfunctions as basis (and test) functions in a Petrov-Galerkin spectral method for approximating tempered fractional ODEs (TFODEs).

3.2 Definitions

We start with some preliminary definitions of fractional and tempered fractional calculus following [142, 33, 123]. The left-sided and the right-sided *tempered* Riemann-Liouville fractional integrals of order $\mu \in (0,1)$ are defined as

$$({}^{RL}_{x_L}\mathbb{I}^{\mu,\tau}_{x})f(x) = \Big(e^{-\tau x}\ {}^{RL}_{x_L}\mathcal{I}^{\mu}_{x}\ e^{\tau x}\Big)f(x) = \frac{1}{\Gamma(\mu)}\int_{x_L}^{x}\frac{e^{-\tau(x-s)}f(s)ds}{(x-s)^{1-\mu}}, \quad x > x_L, \quad (3.3)$$

and

$$({}^{RL}_{x}\mathbb{I}^{\mu,\tau}_{x_R})f(x) = \Big(e^{\tau x}\ {}^{RL}_{x}\mathcal{I}^{\mu}_{x_R}\ e^{-\tau x}\Big)f(x) = \frac{1}{\Gamma(\mu)}\int_{x}^{x_R}\frac{e^{-\tau(s-x)}f(s)ds}{(s-x)^{1-\mu}}, \quad x < x_R, \quad (3.4)$$

respectively, where Γ represents the Euler gamma function. When $\tau = 0$, the tempered fractional integrations (3.3) and (3.4) reduce to the standard Riemann-Liouville fractional integrations $({}^{RL}_{x_L}\mathcal{I}^{\mu}_{x})f(x)$ and $({}^{RL}_{x}\mathcal{I}^{\mu}_{x_R})f(x)$, respectively.

The corresponding *tempered* Riemann-Liouville fractional derivative of order μ

with tempering parameter $\tau \geq 0$ are given by

$$({}^{RL}_{x_L}\mathbb{D}^{\mu,\tau}_{x})f(x) = \left(e^{-\tau x}\ {}^{RL}_{x_L}\mathcal{D}^{\mu}_{x}\ e^{\tau x}\right)f(x) = \frac{e^{-\tau x}}{\Gamma(1-\mu)}\frac{d}{dx}\int_{x_L}^{x}\frac{e^{\tau s}\,f(s)ds}{(x-s)^{\mu}}, \quad x > x_L, \tag{3.5}$$

and

$$({}^{RL}_{x}\mathbb{D}^{\mu,\tau}_{x_R})f(x) = \left(e^{\tau x}\ {}^{RL}_{x}\mathcal{D}^{\mu}_{x_R}\ e^{-\tau x}\right)f(x) = \frac{e^{\tau x}}{\Gamma(1-\mu)}\frac{d}{dx}\int_{x}^{x_R}\frac{e^{-\tau s}\,f(s)ds}{(s-x)^{\mu}}, \quad x < x_R. \tag{3.6}$$

An alternative approach in defining the tempered fractional derivatives is based on the left- and right-sided *tempered* Caputo derivatives of order $\mu \in (0,1)$, defined respectively, as

$$({}^{C}_{x_L}\mathbb{D}^{\mu,\tau}_{x})f(x) = \left(e^{-\tau x}\ {}^{C}_{x_L}\mathcal{D}^{\mu}_{x}\ e^{\tau x}\right)f(x) = \frac{e^{-\tau x}}{\Gamma(1-\mu)}\int_{x_L}^{x}\frac{[e^{\tau s}\,f(s)]'ds}{(x-s)^{\mu}}, \quad x > x_L, \tag{3.7}$$

and

$$({}^{C}_{x}\mathbb{D}^{\mu,\tau}_{x_R})f(x) = \left(e^{\tau x}\ {}^{C}_{x}\mathcal{D}^{\mu}_{x_R}\ e^{-\tau x}\right)f(x) = \frac{e^{\tau x}}{\Gamma(1-\mu)}\int_{x}^{x_R}\frac{[e^{-\tau s}\,f(s)]'ds}{(s-x)^{\mu}}, \quad x < x_R. \tag{3.8}$$

Similarly, if $\tau = 0$, the tempered fractional derivatives (3.5) and (3.6) reduce to the standard Riemann-Liouville fractional integrations $({}^{RL}_{x_L}\mathcal{D}^{\mu}_{x})f(x)$ and $({}^{RL}_{x}\mathcal{D}^{\mu}_{x_R})f(x)$, in addition, (3.7) and (3.8) reduce to the Caputo fractional integrations $({}^{C}_{x_L}\mathcal{D}^{\mu}_{x})f(x)$ and $({}^{C}_{x}\mathcal{D}^{\mu}_{x_R})f(x)$, respectively. The corresponding relationships between the tempered Riemann-Liouville and tempered Caputo fractional derivatives when $\mu \in (0,1)$ are given by

$$({}^{TRL}_{x_L}\mathbb{D}^{\mu,\tau}_{x})f(x) = \frac{f(x_L)}{\Gamma(1-\mu)(x-x_L)^{\mu}} + ({}^{TC}_{x_L}\mathbb{D}^{\mu,\tau}_{x})f(x), \tag{3.9}$$

and

$$({}^{TRL}_{x}\mathbb{D}^{\mu}_{x_R})f(x) = \frac{f(x_R)}{\Gamma(1-\mu)(x_R-x)^{\mu}} + ({}^{TC}_{x}\mathbb{D}^{\mu,\tau}_{x_R})f(x). \tag{3.10}$$

These definitions coincide with each other when boundary-values vanish. Moreover, let $\Omega = [x_L, x_R]$, the corresponding fractional integrations by parts for the aforementioned fractional derivatives are obtained as

$$\Big(f(x), {}^{RL}_{x}\mathcal{D}^{\mu}_{x_R} g(x)\Big)_{\Omega} = \Big(g(x), {}^{C}_{x_L}\mathcal{D}^{\mu}_{x} f(x)\Big)_{\Omega} - f(x)\, {}^{RL}_{x}\mathcal{I}^{\mu}_{x_R} g(x)|^{x_R}_{x=x_L}, \tag{3.11}$$

and

$$\Big(f(x), {}^{RL}_{x_L}\mathcal{D}^{\mu}_{x} g(x)\Big)_{\Omega} = \Big(g(x), {}^{C}_{x}\mathcal{D}^{\mu}_{x_R} f(x)\Big)_{\Omega} + f(x)\, {}^{RL}_{x_L}\mathcal{I}^{\mu}_{x} g(x)|^{x_R}_{x=x_L}, \tag{3.12}$$

where $(\cdot,\cdot)_{\Omega}$ represents the standard L^2 inner product. We note that (3.11) and (3.12) are also valid when the fractional derivatives and integrals are replaced with their tempered counterparts.

By $H^s(\mathbb{R})$, $s \geq 0$, we denote the Fractional Sobolev space on $\mathbb{R}$, defined as

$$H^s(\mathbb{R}) = \{v \in L^2(\mathbb{R}) |\ (1 + |\omega|^2)^{\frac{s}{2}} \mathcal{F}(v)(\omega) \in L^2(\mathbb{R})\}, \tag{3.13}$$

which is endowed with the norm

$$\|\cdot\|_{s,\mathbb{R}} = \|(1 + |\omega|^2)^{\frac{s}{2}} \mathcal{F}(\cdot)(\omega)\|_{L^2(\mathbb{R})}, \tag{3.14}$$

where $\mathcal{F}(v)$ represents the Fourier transform of v. Subsequently, we denote by $H^s([-1,1])$, $s \geq 0$ the Fractional Sobolev space on the finite closed interval $[-1,1]$, defined as

$$H^s([-1,1]) = \{v \in L^2(\mathbb{R}) |\ \exists \tilde{v} \in H^s(\mathbb{R})\ \ s.t.\ \ \tilde{v}|_{[-1,1]} = v\}, \tag{3.15}$$

with the norm

$$\|\cdot\|_{s,[-1,1]} = \inf_{\tilde{v}\in H^s(\mathbb{R}),\tilde{v}|_{[-1,1]}=v} \|\cdot\|_{s,\mathbb{R}}. \tag{3.16}$$

We note that the definition of $H^s([-1,1])$ and the corresponding norm relies on the Fourier transformation of the function. Other useful norms associated with $H^s([-1,1])$ have been also introduced in [108],

$$\|\cdot\|_{l,s,[-1,1]} = \left(\|\cdot\|^2_{L^2([-1,1])} + \|\, {}^{RL}_{x_L}\mathcal{D}^{\mu}_{x}(\cdot)\|^2_{L^2([-1,1])}\right)^{\frac{1}{2}}, \tag{3.17}$$

and

$$\|\cdot\|_{r,s,[-1,1]} = \left(\|\cdot\|^2_{L^2([-1,1])} + \|\, {}^{RL}_{x}\mathcal{D}^{\mu}_{x_R}(\cdot)\|^2_{L^2([-1,1])}\right)^{\frac{1}{2}}, \tag{3.18}$$

such that $\|\cdot\|_{l,s,[-1,1]}$, $\|\cdot\|_{r,s,[-1,1]}$, and $\|\cdot\|_{s,[-1,1]}$ are shown to be equivalent. The following lemmas provide alternative ways of carrying out fractional integration-by-parts, equivalent to (3.12) and (3.12) in the following.

Lemma 3.2.1. *[108]: For all $0 < \xi \leq 1$, if $u \in H^1([a,b])$ such that $u(a) = 0$, and $w \in H^{\xi/2}([a,b])$, then*

$$({}_a\mathcal{D}_s^{\xi}u, w)_{\Omega} = ({}_a\mathcal{D}_s^{\xi/2}u\,,\, {}_s\mathcal{D}_b^{\xi/2}w\,)_{\Omega}, \tag{3.19}$$

where $(\cdot,\cdot)_{\Omega}$ represents the standard inner product in $\Omega = [a,b]$.

Lemma 3.2.2. *[108]: For all $0 < \xi \leq 1$, if $u \in H^1([a,b])$ such that $u(b) = 0$ and $w \in H^{\xi/2}([a,b])$, then*

$$({}_s\mathcal{D}_b^{\xi}u, w)_{\Omega} = ({}_s\mathcal{D}_b^{\xi/2}u\,,\, {}_a\mathcal{D}_s^{\xi/2}w\,)_{\Omega}. \tag{3.20}$$

Remark 3.2.3. It is easy to check that Lemma 3.2.1 and 3.2.2 also hold when the standard Riemann-Liouville fractional derivatives are replaced with their corresponding tempered derivatives.

3.3 Well-posedness

Let $\Omega = [-1, 1]$, $\mu \in (0, 1)$, and

$$\mathcal{L}_I(\cdot) := {}^{RL}_{x}\mathcal{D}^{\mu}_{1}\Big[\, p_I(x)\ {}^{C}_{-1}\mathcal{D}^{\mu}_{x}\,(\cdot)\,\Big], \tag{3.21}$$

in which $p_I(x)$ is non-vanishing and continuous in Ω. We define the following bilinear form

$$a_I(u, v) = (\mathcal{L}_I u, v)_{\Omega}. \tag{3.22}$$

for some $v(x)$. Assuming $u(-1) = 0$, we have $\mathcal{L}_I = {}^{RL}_{x}\mathcal{D}^{\mu}_{1}[\, p_I(x)\ {}^{RL}_{-1}\mathcal{D}^{\mu}_{x}\,(\cdot)\,]$ by virtue of the property (3.9). By plugging it into (3.22) and carrying out the fractional integration by parts (3.11), we obtain

$$\begin{aligned} a_I(u, v) &= (\mathcal{L}_I u, v)_{\Omega} \qquad (3.23)\\ &= \Big({}^{RL}_{x}\mathcal{D}^{\mu}_{1}[\, p_I(x)\ {}^{RL}_{-1}\mathcal{D}^{\mu}_{x}\, u(x)\,]\,,\, v\Big)_{\Omega}\\ &= \Big(p_I(x)\ {}^{RL}_{-1}\mathcal{D}^{\mu}_{x}\, u\,,\ {}^{RL}_{-1}\mathcal{D}^{\mu}_{x}\, v\Big)_{\Omega} - v(x)\ {}^{RL}_{x}\mathcal{I}^{\mu}_{1}({}^{RL}_{-1}\mathcal{D}^{\mu}_{x}u)|^{1}_{x=-1}\\ &= \Big(p_I(x)\ {}^{RL}_{-1}\mathcal{D}^{\mu}_{x}\, u\,,\ {}^{RL}_{-1}\mathcal{D}^{\mu}_{x}\, v\Big)_{\Omega}, \end{aligned}$$

if we further assume that $v(-1) = {}^{RL}_{x}\mathcal{I}^{\mu}_{1}({}^{RL}_{-1}\mathcal{D}^{\mu}_{x}u)|_{x=1} = 0$. Now, let

$$U_I = \{u \in C(\Omega)\ \Big|\ \| {}^{RL}_{-1}\mathcal{D}^{\mu}_{x}\, u\|_{L^2(\Omega), p_I(x)} < \infty,\ and\ u(-1) = {}^{RL}_{x}\mathcal{I}^{\mu}_{1}({}^{RL}_{-1}\mathcal{D}^{\mu}_{x}u)|_{x=1} = 0\}, \tag{3.24}$$

and

$$V_I = \{v \in C(\Omega)\ \Big|\ \| {}^{RL}_{-1}\mathcal{D}^{\mu}_{x}\, v\|_{L^2(\Omega), p_I(x)} < \infty,\ and\ v(-1) = 0\}. \tag{3.25}$$

We observe that $V_I \supset U_I$. Therefore, for convenience and in order to adopt a Galerkin (rather than Petrov-Galerkin) method, we choose $U_I = U_I \cap V_I$ to be the space of

trial and test functions u and v, respectively. Hence, taking $\mathcal{L}_I u = \lambda w_I(x) u$ with respect to the positive weight function $w_I(x)$, the regular eigenvalue problem of first kind reads as: find $u \in U_I$ such that

$$a_I(u,v) := (\mathcal{L}_I u, v)_\Omega = (\lambda u, v)_{\Omega, w_I(x)}, \quad \forall v \in U_I, \tag{3.26}$$

or equivalently,

$$\Big({}^{RL}_{-1}\mathcal{D}^{\mu}_{x}\, u\,,\, {}^{RL}_{-1}\mathcal{D}^{\mu}_{x}\, v \Big)_{\Omega, p_I(x)} - \lambda (u,v)_{\Omega, w_I(x)} = 0, \quad \forall v \in U_I. \tag{3.27}$$

Following similar steps, we define the following fractional differential operator

$$\mathcal{L}_{II}(\cdot) := {}^{RL}_{-1}\mathcal{D}^{\mu}_{x}\Big[\, p_{II}(x)\ {}^{C}_{x}\mathcal{D}^{\mu}_{1}\,(\cdot)\,\Big], \tag{3.28}$$

in which the non-vanishing $p_{II}(x)$ is continuous in Ω. The corresponding bilinear form $a_{II}(u,v)$ is then defined as

$$a_{II}(u,v) = (\mathcal{L}_{II} u, v)_\Omega. \tag{3.29}$$

Now, assuming $u(1) = 0$, it is easy to verify that $\mathcal{L}_{II} = {}^{RL}_{-1}\mathcal{D}^{\mu}_{x}[\, p_{II}(x)\ {}^{RL}_{x}\mathcal{D}^{\mu}_{1}\,(\cdot)\,]$ by virtue of the property (3.10). By plugging it into (3.29) and carrying out the fractional integration-by-parts (3.12), we obtain

$$\begin{aligned} a_{II}(u,v) &= \Big(p_{II}(x)\ {}^{RL}_{x}\mathcal{D}^{\mu}_{1}\, u\,,\, {}^{RL}_{x}\mathcal{D}^{\mu}_{1}\, v \Big)_\Omega - v(x)\, {}^{RL}_{-1}\mathcal{I}^{\mu}_{x}({}^{RL}_{x}\mathcal{D}^{\mu}_{1} u)|^{1}_{x=-1} \\ &= \Big(p_{II}(x)\ {}^{RL}_{x}\mathcal{D}^{\mu}_{1}\, u\,,\, {}^{RL}_{x}\mathcal{D}^{\mu}_{1}\, v \Big)_\Omega, \end{aligned} \tag{3.30}$$

when $v(1) = {}^{RL}_{-1}\mathcal{I}^{\mu}_{x}({}^{RL}_{x}\mathcal{D}^{\mu}_{1}u)|_{x=-1} = 0$. Now, let

$$U_{II} = \{u \in C(\Omega) \,\Big|\, \| {}^{RL}_{x}\mathcal{D}^{\mu}_{1}\, u\|_{L^2(\Omega),p_{II}(x)} < \infty, \textit{ and } u(1) = {}^{RL}_{-1}\mathcal{I}^{\mu}_{x}({}^{RL}_{x}\mathcal{D}^{\mu}_{1}u)|_{x=-1} = 0\}, \tag{3.31}$$

and

$$V_{II} = \{v \in C(\Omega) \,\Big|\, \| {}^{RL}_{x}\mathcal{D}^{\mu}_{1}\, v\|_{L^2(\Omega),p_{II}(x)} < \infty, \textit{ and } v(1) = 0\}. \tag{3.32}$$

Here, we also observe that $V_{II} \supset U_{II}$. Therefore, we choose $U_{II} = U_{II} \cap V_{II}$ to be the trial and test function spaces. Subsequently, by $\mathcal{L}_{II}u = \lambda w_{II}(x)u$ with respect to the positive weight function $w_{II}(x)$, the second regular fractional eigenvalue problem reads as: find $u \in U_{II}$ such that

$$\Big({}^{RL}_{x}\mathcal{D}^{\mu}_{1}\, u\,,\, {}^{RL}_{x}\mathcal{D}^{\mu}_{1}\, v\Big)_{\Omega,p(x)} - \lambda(u,v)_{\Omega,w_{II}(x)} = 0, \quad \forall v \in U_{II}. \tag{3.33}$$

Remark 3.3.1. The construction of the aforementioned eigenvalue problems of first and second kind can be similarly done by replacing all left- and right-righted fractional derivatives/integrals to their corresponding tempered counterparts.

Theorem 3.3.2. *Let $p_I(x) = p_{II}(x) = 1$. Then, the regular eigenvalue problem of first kind, $\mathcal{L}_I u(x) = \lambda w_I(x)u(x)$, subject to the boundary conditions $u(-1) = {}^{RL}_{x}\mathcal{I}^{\mu}_{1}({}^{RL}_{-1}\mathcal{D}^{\mu}_{x}u)|_{x=1} = 0$ and the second regular eigenvalue problem, $\mathcal{L}_{II}u(x) = \lambda w_{II}(x)u(x)$, subject to $u(1) = {}^{RL}_{-1}\mathcal{I}^{\mu}_{x}({}^{RL}_{x}\mathcal{D}^{\mu}_{1}u)|_{x=-1} = 0$ are well-posed.*

Proof. We first observe that U_I is a Hilbert space, moreover, $a_I(u,v)$ and $a_{II}(u,v)$ are linear and continuous. To this end, we need the following conclusion by Lemma 2.4 in [108], which states that there are positive constants C_1 and C_2 such that for

any $w \in H^{\mu}([a,b])$,

$$C_1 \int_a^b {}^{RL}_{a}\mathcal{D}^{\mu}_{x} w(x)\, {}^{RL}_{x}\mathcal{D}^{\mu}_{b} w(x) dx \leq \| {}^{RL}\mathcal{D}^{\mu} w(x)\|^2 \leq C_2 \int_a^b {}^{RL}_{a}\mathcal{D}^{\mu}_{x} w(x)\, {}^{RL}_{x}\mathcal{D}^{\mu}_{b} w(x) dx. \tag{3.34}$$

in which ${}^{RL}\mathcal{D}^{\mu}$ can is either ${}^{RL}_{a}\mathcal{D}^{\mu}_{x}$ or ${}^{RL}_{x}\mathcal{D}^{\mu}_{b}$. Hence, $a_I(u,v) \geq C_I \|u\|_{U_I}$ and $a_{II}(u,v) \geq C_{II}\|u\|_{U_{II}}$, so the bilinear forms are coercive and by Lax-Milgram lemma these problems are wellposed. □

3.4 Regular TFSLPs of Kind I & II

After this preparation and setting the underlying spaces, we now introduce the following regular TFSLP of order $\nu = 2\mu \in (0,2)$,

$${}^{TRL}\mathbb{D}^{\mu,\tau}\Big[\, p_i(x)\, {}^{TC}\mathbb{D}^{\mu,\tau}\, F^{(i)}_{\lambda}(x)\,\Big] + \lambda\, w_i(x)\, F^{(i)}_{\lambda}(x) = 0, \quad x \in [x_L, x_R], \tag{3.35}$$

where $i = 1,2$, with $i = 1$ denoting the regular TFSLP of first kind, in which ${}^{TRL}\mathbb{D}^{\mu,\tau} \equiv {}^{TRL}_{x}\mathbb{D}^{\mu,\tau}_{x_R}$ and ${}^{TC}\mathbb{D}^{\mu,\tau} \equiv {}^{TC}_{x_L}\mathbb{D}^{\mu,\tau}_{x}$. Moreover, $i = 2$ corresponds to the regular TFSLP of second kind where ${}^{TRL}\mathbb{D}^{\mu,\tau} \equiv {}^{TRL}_{x_L}\mathbb{D}^{\mu,\tau}_{x}$ and ${}^{TC}\mathbb{D}^{\mu,\tau} \equiv {}^{TC}_{x}\mathbb{D}^{\mu,\tau}_{x_R}$. In such setting, $\mu \in (0,1)$, $\tau \geq 0$, $p_i(x) \neq 0$, and $w_i(x)$ is a non-negative weight function. In addition, we assume that p_i and w_i are real-valued continuous functions in the interval $[x_L, x_R]$. The tempered fractional boundary-value problem (3.35) is subject to the following boundary conditions

$$a_1 F^{(i)}_{\lambda}(x_L) + a_2\, {}^{TRL}\mathbb{I}^{1-\mu,\,\tau}\Big[\, p_i(x)\, {}^{TC}\mathbb{D}^{\mu,\tau} F^{(i)}_{\lambda}(x)\,\Big]\,|_{x=x_L} = 0, \tag{3.36}$$

$$b_1 F^{(i)}_{\lambda}(x_R) + b_2\, {}^{TRL}\mathbb{I}^{1-\mu,\,\tau}\Big[\, p_i(x)\, {}^{TC}\mathbb{D}^{\mu,\tau} F^{(i)}_{\lambda}(x)\Big]\,|_{x=x_R} = 0, \tag{3.37}$$

where $a_1^2 + a_2^2 \neq 0$, $b_1^2 + b_2^2 \neq 0$. Here, ${}^{TRL}\mathbb{I}^{1-\mu,\,\tau} \equiv {}^{TRL}_{x}\mathbb{I}^{1-\mu,\,\tau}_{x_R}$ when $i = 1$ for the regular TFSLP of first kind, while, ${}^{TRL}\mathbb{I}^{1-\mu,\,\tau} \equiv {}^{TRL}_{x_L}\mathbb{I}^{1-\mu,\,\tau}_{x}$ when $i = 2$ for the regular TFSLP of second kind.

Theorem 3.4.1. *The eigenvalues of the regular TFSLP of kind-I and -II (3.35) subject to the non-local boundary conditions* (3.36) *and* (3.37) *are real, and the eigenfunctions corresponding to distinct eigenvalues are orthogonal with respect to the weight functions $w_i(x)$.*

Proof. We first consider the first regular problem when $i = 1$:

$$ {}^{TRL}_{x}\mathbb{D}^{\mu,\tau}_{x_R}\Big[\; p_1(x)\; {}^{TC}_{x_L}\mathbb{D}^{\mu,\tau}_{x}\; F^{(1)}_{\lambda}(x)\;\Big] \;+\; \lambda\, w_1(x)\, F^{(1)}_{\lambda}(x) = 0. $$

Now, by the definition of the tempered derivatives ${}^{TRL}_{x}\mathbb{D}^{\mu,\tau}_{x_R}$ and ${}^{TC}_{x_L}\mathbb{D}^{\mu,\tau}_{x}$, we can re-write the first problem as

$$ e^{\tau x}\, {}^{RL}_{x}\mathcal{D}^{\mu}_{x_R} e^{-\tau x}\Big[\; p_i(x)\, e^{-\tau x}\, {}^{C}_{x_L}\mathcal{D}^{\mu}_{x} e^{\tau x}\; F^{(1)}_{\lambda}(x)\;\Big] \;+\; \lambda\, w_1(x)\, F^{(1)}_{\lambda}(x) = 0, $$

where we multiply both sided by $e^{-\tau x}$ to obtain

$$ {}^{RL}_{x}\mathcal{D}^{\mu}_{x_R}\Big[\; e^{-2\tau x} p_1(x)\; {}^{C}_{x_L}\mathcal{D}^{\mu}_{x}\Big(e^{\tau x}\; F^{(1)}_{\lambda}(x)\Big)\;\Big] \;+\; \lambda\, e^{-2\tau x} w_1(x)\Big(\, e^{\tau x} F^{(1)}_{\lambda}(x)\Big) = 0. $$

By taking $P_1(x) \equiv e^{-2\tau x} p_1(x)$ and $W_1(x) \equiv e^{-2\tau x} w_1(x)$, and $\Phi^{(1)}_{\lambda}(x) \equiv e^{\tau x}\; F^{(1)}_{\lambda}(x)$, we transform the tempered boundary-value problem of first kind to

$$ {}^{RL}_{x}\mathcal{D}^{\mu}_{x_R}\Big[\; P_1(x)\; {}^{C}_{x_L}\mathcal{D}^{\mu}_{x}\Phi^{(1)}_{\lambda}(x)\;\Big] \;+\; \lambda\, W_1(x)\Phi^{(1)}_{\lambda}(x) = 0. \tag{3.38} $$

Clearly, $P_1(x) \neq 0$ and $W_1(x)$ are continuous functions in $[x_L, x_R]$. Moreover, we obtain the boundary conditions corresponding to this change of variables (functions)

from (3.36) and (3.37) by employing the definitions of the tempered fractional integration as

$$a_1\Phi_\lambda^{(1)}(x_L) + a_2\, {}^{RL}_{x}\mathcal{I}^{1-\mu}_{x_R}\Big[\, P_1(x)\, {}^{C}_{x_L}\mathcal{D}^{\mu}_{x}\Phi_\lambda^{(1)}(x)\,\Big]\,|_{x=x_L} = 0, \tag{3.39}$$

$$b_1\Phi_\lambda^{(1)}(x) + b_2\, {}^{RL}_{x}\mathcal{I}^{1-\mu}_{x_R}\Big[\, P_1(x)\, {}^{C}_{x_L}\mathcal{D}^{\mu}_{x}\Phi_\lambda^{(1)}(x)\Big]\,|_{x=x_R} = 0. \tag{3.40}$$

Following [93], the transformed eigen-problem has real-valued eigenvalues eigenfunctions. Moreover, the corresponding eigenfunctions to distinct eigenvalues are orthogonal with respect to $W_1(x)$. Clearly, the transformed problem (3.38) subject to (3.39) and (3.40) shares the same eigenvalues with the original problem (3.35) subject to (3.36) and (3.37), when $i = 1$. Therefore, the eigenvalues of the regular TFSLP of first kind are real-valued. Moreover, let $\xi_1^{(1)}$ and $\xi_2^{(1)}$ be eigenfunctions corresponding to two distinct eigenvalues λ_1 and λ_2. Then, by the orthogonality of the transformed problem, we have

$$\int_{x_L}^{x_R} \xi_1^{(1)}(x)\, \xi_2^{(1)}(x)\, W_1(x)dx = 0,$$

that can be re-written by the inverse transformation of the eigenfunctions as

$$\int_{x_L}^{x_R} \Big(e^{\tau x}\Xi_1^{(1)}(x)\Big)\, \Big(e^{\tau x}\Xi_2^{(1)}(x)\Big)\, e^{-2\tau x} w_1(x)dx = 0,$$

or

$$\int_{x_L}^{x_R} \Xi_1^{(1)}(x)\; \Xi_2^{(1)}(x)\; w_1(x)dx = 0,$$

where $\Xi_1^{(1)}(x)$ and $\Xi_2^{(1)}(x)$ are the corresponding real-valued eigenfunctions associated with the distinct eigenvalues λ_1 and λ_2.

When $i = 2$, we follow similar steps by taking $P_2(x) \equiv e^{2\tau x}p_2(x)$ and $W_2(x) \equiv e^{2\tau x}w_2(x)$, and $\Phi_\lambda^{(2)}(x) \equiv e^{-\tau x}\; F_\lambda^{(2)}(x)$ and through the transformation of the tempered boundary-value problem of second kind, we complete the proof.

□

3.4.1 Regular Tempered Eigen-Problems

We specifically solve two regular TFSLPs, denoted by regular TFSLP-I and -II of order $\nu = 2\mu \in (0, 2)$, by choosing particular forms $p_i(x)$ and $w_i(x)$. To this end, the following tempered non-local differential operator is defined

$$\mathcal{L}_i^{\mu,\tau} := {}^{RL}\mathbb{D}^{\mu,\tau}\left[e^{(-1)^{i+1}2\tau}\ {}^{C}\mathbb{D}^{\mu,\tau}(\cdot)\right], \quad i = 1, 2, \tag{3.41}$$

where $\mathcal{L}_1^{\mu} := {}^{RL}_{x}\mathbb{D}^{\mu,\tau}_{x_R}[e^{2\tau}\ {}^{C}_{x_L}\mathbb{D}^{\mu,\tau}_{x}(\cdot)]$ in the regular TFSLP-I, and for the case of the regular TFSLP-II, we reverse the order of the right-sided and left-sided tempered derivative for the inner and outer fractional derivatives in the operator, i.e., $\mathcal{L}_2^{\mu} := {}^{RL}_{x_L}\mathbb{D}^{\mu,\tau}_{x}[e^{-2\tau}\ {}^{C}_{x}\mathbb{D}^{\mu,\tau}_{x_R}(\cdot)]$, where $\mu \in (0, 1)$. We note that the term $e^{(-1)^{i+1}2\tau} \neq 0$, $\forall x \in [x_L, x_R]$, yields the regularity character to the tempered boundary-value problem. That being defined, we consider the regular TFSLP (-I & -II) as

$$\mathcal{L}_i^{\mu,\tau} F_\lambda^{(i)}(x) + \lambda\, e^{(-1)^{i+1}2\tau}\ (1-x)^{-\mu}(1+x)^{-\mu}\ F_\lambda^{(i)}(x) = 0, \quad i = 1, 2,\ x \in [-1, 1]. \tag{3.42}$$

We shall solve (3.42) subject to a homogeneous Dirichlet and a homogeneous fractional *integro-differential* boundary condition

$$\begin{aligned} F_\lambda^{(1)}(-1) &= 0, \\ {}^{TRL}_{x}\mathbb{I}_1^{1-\mu,\tau}\left[e^{2\tau}\ {}^{TC}_{-1}\mathbb{D}^{\mu,\tau}_{x} F_\lambda^{(1)}(x)\right]|_{x=+1} &= 0, \end{aligned} \tag{3.43}$$

and

$$\begin{aligned} F_{\lambda}^{(2)}(+1) &= 0, \\ {}^{TRL}_{-1}\mathbb{I}_{x}^{1-\mu,\tau}\left[e^{-2\tau}\ {}^{TC}_{x}\mathbb{D}_{1}^{\mu,\tau}F_{\lambda}^{(2)}(x)\right]|_{x=-1} &= 0, \end{aligned} \tag{3.44}$$

which are enforced on the regular TFSLP-I and TFSLP-II, respectively.

3.4.2 Explicit Eigensolutions to the regular TFSLP-I & -II

Next, we obtain the analytical solution $F_{\lambda}^{(i)}(x)$ to the regular TFSLP-I & II, (3.42), subject to the homogeneous Dirichlet and integro-differential boundary conditions (3.43) and (3.44).

Theorem 3.4.2. *The exact eigenfunctions to (3.42), when $i = 1$, i.e., the regular TFSLP-I, subject to (3.43) are given by*

$$F_{n}^{(1)}(x) = e^{-\tau x}(1+x)^{\mu}\ P_{n-1}^{-\mu,\mu}(x), \quad \forall n \geq 1, \tag{3.45}$$

and the corresponding distinct eigenvalues are

$$\lambda_{n}^{(1)} = -\frac{\Gamma(n+\mu)}{\Gamma(n-\mu)}, \quad \forall n \geq 1. \tag{3.46}$$

Moreover, the exact eigenfunctions to (3.42), when $i = 2$, i.e., the regular TFSLP-II subject to (3.44), are given as

$$F_{n}^{(2)}(x) = e^{\tau x}(1-x)^{\mu}\ P_{n-1}^{\mu,-\mu}(x), \quad \forall n \geq 1 \tag{3.47}$$

with the corresponding distinct eigenvalues, given by

$$\lambda_n^{(2)} = \lambda_n^{(1)} = -\frac{\Gamma(n+\mu)}{\Gamma(n-\mu)}, \quad \forall n \geq 1. \tag{3.48}$$

Proof. First, we prove (3.45) and (3.46). Clearly, $F_n^{(1)}(-1) = 0$. Therefore, by (3.9), we substitute ${}^{TC}_{-1}\mathbb{D}^{\mu,\tau}_x$ by ${}^{TRL}_{-1}\mathcal{D}^{\mu,\tau}_x$, hence,

$$\begin{aligned}
\left\{ {}^{TRL}_{x}\mathbb{I}^{1-\mu,\,\tau}_{+1} \left[e^{2\tau x} \;\; {}^{TC}_{-1}\mathbb{D}^{\mu,\tau}_x F_n^{(1)}(x) \right] \right\}_{x=+1} = \\
\left\{ {}^{TRL}_{x}\mathbb{I}^{1-\mu,\,\tau}_{+1} \left[e^{2\tau x} \;\; {}^{TRL}_{-1}\mathbb{D}^{\mu,\tau}_x F_n^{(1)}(x) \right] \right\}_{x=+1} = \\
\left\{ {}^{TRL}_{x}\mathbb{I}^{1-\mu,\,\tau}_{+1} \left[e^{2\tau x} \;\; {}^{TRL}_{-1}\mathbb{D}^{\mu,\tau}_x \left(e^{-\tau x} (1+x)^{\mu} \;\; P_{n-1}^{-\mu,\mu}(x) \right) \right] \right\}_{x=+1} = \\
\left\{ e^{\tau x} \, {}^{RL}_{x}\mathcal{I}^{1-\mu}_{+1} \; e^{-\tau x} \left[e^{2\tau x} e^{-\tau x} \;\; {}^{RL}_{-1}\mathcal{D}^{\mu}_x e^{\tau x} \left(e^{-\tau x} (1+x)^{\mu} \;\; P_{n-1}^{-\mu,\mu}(x) \right) \right] \right\}_{x=+1} = \\
\left\{ e^{\tau x} \, {}^{RL}_{x}\mathcal{I}^{1-\mu}_{+1} \left[\; {}^{RL}_{-1}\mathcal{D}^{\mu}_x \left((1+x)^{\mu} \;\; P_{n-1}^{-\mu,\mu}(x) \right) \right] \right\}_{x=+1}
\end{aligned} \tag{3.49}$$

Following [5, 187] and for $\mu > 0$, $\alpha > -1$, $\beta > -1$, $\forall x \in [-1, 1]$ we have:

$${}^{RL}_{-1}\mathcal{I}^{\mu}_x \Big\{ (1+x)^{\beta} P_n^{\alpha,\beta}(x) \Big\} = \frac{\Gamma(n+\beta+1)}{\Gamma(n+\beta+\mu+1)} (1+x)^{\beta+\mu} \, P_n^{\alpha-\mu,\beta+\mu}(x), \tag{3.50}$$

and

$${}^{RL}_{x}\mathcal{I}^{\mu}_1 \Big\{ (1-x)^{\alpha} P_n^{\alpha,\beta}(x) \Big\} = \frac{\Gamma(n+\alpha+1)}{\Gamma(n+\alpha+\mu+1)} (1-x)^{\alpha+\mu} P_n^{\alpha+\mu,\beta-\mu}(x). \tag{3.51}$$

The relation (3.50) can be reduced to the case when $\alpha = +\mu$ and $\beta = -\mu$ as

$${}^{RL}_{-1}\mathcal{I}^{\mu}_x \Big\{ (1+x)^{-\mu} P_n^{\mu,-\mu}(x) \Big\} = \frac{\Gamma(n-\mu+1)}{\Gamma(n+1)} \, P_n(x), \tag{3.52}$$

where $P_n(x) = P_n^{0,0}(x)$ represents the Legendre polynomial of degree n. On the other hand, we can set $\alpha = \beta = 0$ in (3.50) and take the fractional derivative ${}^{RL}_{-1}\mathcal{D}^{\mu}_x$ on

both sides of (3.50) to obtain

$$ {}^{RL}_{-1}\mathcal{D}^{\mu}_{x}\Big\{(1+x)^{\mu}P_n^{-\mu,\mu}\Big\} = \frac{\Gamma(n+\mu+1)}{\Gamma(n+1)}P_n(x). \tag{3.53} $$

Now, by carrying out the fractional Riemann-Liouville derivative in the bracket of (3.49) using (3.53), we obtain

$$ \Big\{e^{\tau x}\,{}^{RL}_{x}\mathcal{I}^{1-\mu}_{+1}\left[\frac{\Gamma(n+\mu)}{\Gamma(n)}P_{n-1}(x)\right]\Big\}_{x=+1} = e^{\tau x}\,\frac{\Gamma(n+\mu)}{\Gamma(n)}\Big\{\,{}^{RL}_{x}\mathcal{I}^{1-\mu}_{+1}\left[P_{n-1}(x)\right]\Big\}_{x=+1}. $$

By working out the fractional integration using (3.51) (when $\alpha=\beta=0$), we obtain

$$ \Big\{e^{\tau x}(1-x)^{\mu}P^{\mu,-\mu}_{n-1}(x)\Big\}_{x=+1} = 0, \tag{3.54} $$

hence, $F_n^{(1)}(x)$ satisfies the boundary conditions.

Next, we show that (3.45) indeed satisfies (3.42), when $i=1$, with the eigenvalues (3.46). First, we multiply both sides of (3.42) by $e^{-\tau x}$ and then take the fractional integration of order μ on both sides when $i=1$ to obtain

$$ e^{-\tau x}\,e^{2\tau x}\;\,{}^{TC}_{-1}\mathbb{D}^{\mu,\tau}_{x}F_n^{(1)}(x) = -\lambda\,{}^{RL}_{x}\mathcal{I}^{\mu}_{+1}\Big\{e^{-\tau x}\,e^{2\tau x}(1-x)^{-\mu}(1+x)^{-\mu}F_n^{(1)}(x)\Big\}. $$

Substituting (3.45) and replacing the Caputo derivative by the Riemann-Liouville

one, we obtain

$$ {}^{RL}_{-1}\mathcal{D}^{\mu}_{x}\left[(1+x)^{\mu}\ P^{-\mu,\mu}_{n-1}(x)\right] = -\lambda\, {}^{RL}_{x}\mathcal{I}^{\mu}_{+1}\Big\{(1-x)^{-\mu}\ P^{-\mu,\mu}_{n-1}(x)\Big\}. $$

Finally, the fractional derivative on the left-hand side and the fractional integration on the right-hand side are worked out using (3.52) and (3.53), respectively, as

$$ \frac{\Gamma(n+\mu)}{\Gamma(n)}\ P_{n-1}(x) = -\lambda\frac{\Gamma(n-\mu)}{\Gamma(n)}\ P_{n-1}(x), $$

and therefore

$$ \lambda \equiv \lambda^{(1)}_{n} = -\frac{\Gamma(n+\mu)}{\Gamma(n-\mu)},\ \ \forall n \geq 1. $$

The orthogonality of the eigenfunctions (3.45) with respect to $w_1(x) = e^{2\tau x}\ (1-x)^{-\mu}(1+x)^{-\mu}$ is checked as

$$ \begin{aligned} \int_{-1}^{1} w_1(x)F^{(1)}_{k}(x)F^{(1)}_{j}(x)dx &= \int_{-1}^{1} w_1(x)e^{-2\tau x}\ \left[(1+x)^{\mu}\right]^2\ P^{-\mu,\mu}_{k-1}(x)\ P^{-\mu,\mu}_{j-1}(x)dx \\ &= \int_{-1}^{1}(1-x)^{-\mu}(1+x)^{\mu}\ P^{-\mu,\mu}_{k-1}(x)\ P^{-\mu,\mu}_{j-1}(x)dx \\ &= C^{-\mu,\mu}_{k}\delta_{kj}, \end{aligned} $$

where $C^{-\mu,\mu}_{k}$ denotes the orthogonality constant corresponding to Jacobi polynomials with parameters $^{-\mu,\mu}$. Similar steps can be taken for the second tempered eigenproblem when $i = 2$.

□

The eigenfunctions of the regular TFSLP-I & -II are *non-polynomial* functions

due to their particular structure i.e., the multiplier $e^{\mp\tau x}\,(1 \pm x)^{\mu}$. These eigenfunctions in fact generalize the existing *Jacobi poly-fractonomial* functions $(1 \pm x)^{\mu} P_{n-1}^{\mp\mu,\pm\mu}(x)$, introduced in [187] as the exact eigenfunctions of the regular fractional (non-tempered) Sturm-Liouville problems (RFSLP-I & -II). We note that when the tempering parameter $\tau = 0$, they reduce to the Jacobi poly-fractonomials. Here, to distinguish the tempered eigenfunctions from them, we refer to $F_n^{(i)}(x)$ as *Tempered Jacobi poly-fractonomial*. Clearly, when $\tau = 0$ and $\mu \to 1$ or 0, the tempered Jacobi poly-fractonomials (3.45) and (3.47) coincide with the well-known Jacobi polynomials, which are the eigenfunctions of the standard (integer-order) Sturm-Liouville problem.

Remark 3.4.3. The regular TFSLP-I & -II share the same eigenvalues with RFSLP-I & -II in [187]. We note that the growth in the magnitude of eigenvalues with respect to n is dependent on the fractional derivative order μ. The asymptotic values are obtained as

$$|\lambda_n^{(i)}| = \begin{cases} n^2, & \mu \to 1, \\ n, & \mu \to 1/2, \\ 1, & \mu \to 0. \end{cases} \tag{3.55}$$

Hence, there are two modes of growth in the magnitude of $\lambda_n^{(i)}$, the *sublinear* mode corresponding to $0 < \mu < 1/2$, and *superlinear subquadratic* mode corresponding to $1/2 < \mu < 1$. In particular, when $\mu = 1/2$, the eigenvalues grow linearly with n.

3.4.3 Properties of the Eigenfunctions of the regular TFSLP-I & -II

Next, we list a number of important properties of the solutions to the regular TFSLP-I & II, in (3.42):

- **Recurrence relations**:

$$\begin{aligned} F_1^{(i)}(x) &= e^{\mp\tau x}(1 \pm x)^{\mu}, \\ F_2^{(i)}(x) &= e^{\mp\tau x}(1 \pm x)^{\mu}(x \mp \mu), \\ &\vdots \\ a_n F_{n+1}^{(i)}(x) &= b_n x F_n^{(i)}(x) - c_n F_{n-1}^{(i)}(x) \\ a_n &= 4n^2(n-1) \\ b_n &= 2n(2n-1)(2n-2) \\ c_n &= 4n(n-1\mp\mu)(n-1\pm\mu), \end{aligned} \tag{3.56}$$

  where the upper signs correspond to $i = 1$, solution to the regular TFSLP-I, and the lower signs correspond to the regular TFSLP-II when $i = 2$.

- **Orthogonality**:

$$\int_{-1}^{1} e^{\pm 2\tau x}(1-x)^{-\mu}(1+x)^{-\mu}\ F_k^{(i)}(x) F_m^{(i)}(x) dx = \mathcal{J}_k^{\alpha_i,\beta_i}\delta_{kj},$$

$$\mathcal{J}_k^{\alpha_i,\beta_i} = \frac{2}{2k-1}\frac{\Gamma(k+\alpha_i)\Gamma(k+\beta_i)}{(k-1)!\ \Gamma(k)}, \tag{3.57}$$

  where $(\alpha_1, \beta_1) = (-\mu, \mu)$ and $(\alpha_2, \beta_2) = (\mu, -\mu)$.

- **Fractional derivatives**:

$$ {}^{TRL}_{-1}\mathbb{D}^{\mu,\tau}_{x} F^{(1)}_n(x) = {}^{TC}_{-1}\mathbb{D}^{\mu,\tau}_{x} F^{(1)}_n(x) = e^{-\tau x}\frac{\Gamma(n+\mu)}{\Gamma(n)} P_{n-1}(x), \quad (3.58) $$

$$ {}^{TRL}_{x}\mathbb{D}^{\mu,\tau}_{1} F^{(2)}_n(x) = {}^{TC}_{x}\mathbb{D}^{\mu,\tau}_{1} F^{(2)}_n(x) = e^{\tau x}\frac{\Gamma(n+\mu)}{\Gamma(n)} P_{n-1}(x), \quad (3.59) $$

  where $P_{n-1}(x)$ denotes the standard Legendre polynomial of order $n-1$.

- **Special values**:

$$ F^{(1)}_n(-1) = 0, \quad F^{(1)}_n(+1) = e^{-\tau}\, 2^{\mu} \begin{pmatrix} n-1-\mu \\ n-1 \end{pmatrix} \quad (3.60) $$

$$ F^{(2)}_n(+1) = 0, \quad F^{(2)}_n(-1) = e^{\tau}(-1)^{n-1} F^{(1)}_n(+1). \quad (3.61) $$

3.5 Singular Tempered Fractional Problems

In the regular setting $p_i(x)$ did not vanish in $[-1,1]$, and here, we aim to generalize it to singular eigen-problems, in which $p_i(x) = e^{(-1)^{i+1}2\tau}\ (1-x)^{\alpha+1}(1+x)^{\beta+1}$ that vanishes at the boundary points. We present the definition of the singular TFSLPs-I and singular TFSLPs-II of order $\nu = 2\mu \in (0,2)$, associated this time with the additional parameters $-1 < \alpha < 2-\mu$, and $-1 < \beta < \mu - 1$ in the singular TFSLP-I ($i=1$), and $-1 < \alpha < \mu - 1$, and $-1 < \beta < 2-\mu$ in the singular TFSLP-II ($i=2$),

for $x \in [-1,1]$ as

$$
\begin{aligned}
{}^{RL}\mathbb{D}^{\mu,\,\tau}\Big\{e^{(-1)^{i+1}2\tau}\ (1-x)^{\alpha+1}(1+x)^{\beta+1}\ {}^{C}\mathbb{D}^{\mu,\,\tau}\ \mathbb{P}^{(i)}(x)\Big\} \\
+\Lambda^{(i)}e^{(-1)^{i+1}2\tau}\ (1-x)^{\alpha+1-\mu}(1+x)^{\beta+1-\mu}\ \mathbb{P}^{(i)}(x)=0.
\end{aligned}
\tag{3.62}
$$

where $\tau \geq 0$, $\mu \in (0,1)$ and $i = 1, 2$. Similar to the regular setting, $i = 1$ denotes the singular TFSLP-I in which ${}^{RL}\mathbb{D}^{\mu,\,\tau} \equiv {}^{TRL}_{x}\mathbb{D}^{\mu,\,\tau}_{+1}$ and ${}^{TC}\mathbb{D}^{\mu,\,\tau} \equiv {}^{TC}_{-1}\mathbb{D}^{\mu\ \tau}_{x}$, also, $i = 2$ corresponds to the singular TFSLP-II where ${}^{TRL}\mathbb{D}^{\mu,\,\tau} \equiv {}^{TRL}_{-1}\mathbb{D}^{\mu,\,\tau}_{x}$ and ${}^{TC}\mathbb{D}^{\mu,\,\tau} \equiv {}^{TC}_{x}\mathbb{D}^{\mu,\,\tau}_{+1}$. The singular problem (3.62) is subject to

$$
\mathbb{P}^{(i)}(\ (-1)^{i}\ ) = 0, \tag{3.63}
$$

$$
\Big\{\,{}^{TRL}\mathbb{I}^{1-\mu,\,\tau}\left[p_i(x)\,{}^{TC}\mathbb{D}^{\mu,\tau}\mathbb{P}^{(i)}(x)\right]\Big\}_{x=(-1)^{i+1}} = 0, \tag{3.64}
$$

in which we follow the same definitions as in the regular problems i.e., ${}^{TRL}\mathbb{I}^{1-\mu,\,\tau} \equiv {}^{TRL}_{x}\mathbb{I}^{1-\mu,\,\tau}_{+1}$ when $i = 1$ in the singular TFSLP-I, and ${}^{TRL}\mathbb{I}^{1-\mu,\,\tau} \equiv {}^{TRL}_{-1}\mathbb{I}^{1-\mu,\,\tau}_{x}$ in case of $i = 2$ in the singular TFSLP-II; $p_i(x) = e^{(-1)^{i+1}2\tau}\ (1-x)^{\alpha+1}(1+x)^{\beta+1}$ and $w_i(x) = e^{(-1)^{i+1}2\tau}\ (1-x)^{\alpha+1-\mu}(1+x)^{\beta+1-\mu}$ in (3.62), which is a non-negative function.

Theorem 3.5.1. *The eigenvalues of the singular TFSLP-I & -II (3.62)-(3.64) are real-valued, and the eigenfunctions corresponding to distinct eigenvalues of (3.62)-(3.64) are orthogonal with respect to the weight function*

$$
w_i(x) = e^{(-1)^{i+1}2\tau}\ (1-x)^{\alpha+1-\mu}(1+x)^{\beta+1-\mu}.
$$

Moreover, the exact eigenfunctions of the singular TFSLP-I (3.62)-(3.64), when $i = 1$*, are given as*

$$
\mathbb{P}^{(1)}_{n}(x) = {}^{(1)}\mathbb{P}^{\alpha,\beta,\mu}_{n}(x) = e^{-\tau x}(1+x)^{-\beta+\mu-1}\ P^{\alpha-\mu+1,-\beta+\mu-1}_{n-1}(x), \tag{3.65}
$$

and the corresponding distinct eigenvalues are

$$\Lambda_n^{(1)} = {}^{(1)}\Lambda_n{}^{\alpha,\beta,\mu} = -\frac{\Gamma(n-\beta+\mu-1)\Gamma(n+\alpha+1)}{\Gamma(n-\beta-1)\Gamma(n+\alpha-\mu+1)}. \tag{3.66}$$

In addition, the exact eigenfunctions to the singular TFSLP-II (3.62)-(3.64), in case of $i = 2$, are given as

$$\mathbb{P}_n^{(2)}(x) = {}^{(2)}\mathbb{P}_n^{\alpha,\beta,\mu}(x) = e^{\tau x}(1-x)^{-\alpha+\mu-1}\ \ P_{n-1}^{-\alpha+\mu-1,\beta-\mu+1}(x), \tag{3.67}$$

and the corresponding distinct eigenvalues are

$$\Lambda_n^{(2)} = {}^{(2)}\Lambda_n^{\alpha,\beta,\mu} = -\frac{\Gamma(n-\alpha+2\mu-1)\Gamma(n+\beta+1)}{\Gamma(n-\alpha+\mu-1)\Gamma(n+\beta-\mu+1)}. \tag{3.68}$$

Proof. By the definition of the tempered fractional derivatives and integrations, it is easy to check that (3.62) can be transformed into the singular fractional Sturm-Liouville in [187] through $W_i^{(2)} = e^{(-1)^i 2\tau x} w_i(x)$, $P_i^{(2)} = e^{(-1)^i 2\tau x} p_i(x)$, and $\mathcal{P}^{(i)}(x) = e^{(-1)^{i+1} 2\tau x}\mathbb{P}^{(i)}(x)$. Then, readily, the proof is complete following Theorem 4.1 and Theorem 4.2 in [187]. □

Remark 3.5.2. In the earlier work [187], the standard singular Sturm-Liouville problem was generalized to the fractional (non-tempered) Sturm-Liouville problems (SFSLP-I & -II) and the singular Jacobi poly-fractonomials of first and second kind given in (3.1) and (3.2), which were explicitly obtained as the eigenfunctions. Here, the tempered Jacobi poly-fractonomials involves another parameter i.e., $\tau \geq 0$, which further generalizes the existing singular fractional eigenfunctions, and they in fact complete the whole family of tempered Jacobi poly-fractonomials. Moreover, we note that the singular TFSLP-I & -II also share the same eigenvalues, hence the same asymptotic values, with SFSLP-I & -II as in [187].

3.5.1 Properties of the Eigen-solutions to the singular TFSLP-I&-II

We list a number of properties of the eigensolutions to the singular TFSLP-I &-II as follows.

- **Recurrence relations**:

  A recurrence relations is obtained for the tempered Jacobi poly-fractonomials ${}^{(i)}\mathbb{P}_n^{\alpha,\beta,\mu}(x)$ of first kind, when $i = 1$:

$$
\begin{aligned}
{}^{(1)}\mathbb{P}_1^{\alpha,\beta,\mu}(x) &= e^{-\tau x}(1+x)^{-\beta+\mu-1}, \\
{}^{(1)}\mathbb{P}_2^{\alpha,\beta,\mu}(x) &= \frac{1}{2}e^{-\tau x}(1+x)^{-\beta+\mu-1}\left[\alpha+\beta-2\mu+2+(\alpha-\beta+2)x\right], \\
&\vdots \\
a_n\,{}^{(1)}\mathbb{P}_{n+1}^{\alpha,\beta,\mu}(x) &= (b_n+c_n x)\,{}^{(1)}\mathbb{P}_n^{\alpha,\beta,\mu}(x) - d_n\,{}^{(1)}\mathbb{P}_{n-1}^{\alpha,\beta,\mu}(x) \\
a_n &= 2n(n+\alpha-\beta)(2n+\alpha-\beta-2) \\
b_n &= (2n-\alpha+\beta-1)(\alpha-\beta)(\alpha+\beta-2\mu+2) \\
c_n &= (2n-\alpha+\beta)(2n-\alpha+\beta-1)(2n-\alpha+\beta-2) \\
d_n &= 2(n-\alpha+\mu-2)(n+\beta-\mu)(2n-\alpha+\beta)
\end{aligned}
$$

and second kind when $i = 2$:

$$\begin{aligned}
{}^{(2)}\mathbb{P}_1^{\alpha,\beta,\mu}(x) &= e^{\tau x}(1-x)^{-\alpha+\mu-1}, \\
{}^{(2)}\mathbb{P}_2^{\alpha,\beta,\mu}(x) &= \frac{1}{2}e^{\tau x}(1-x)^{-\alpha+\mu-1}\left[-\alpha-\beta+2\mu-2+(-\alpha+\beta+2)x\right], \\
&\vdots \\
a_n^{*\,(2)}\mathbb{P}_{n+1}^{\alpha,\beta,\mu}(x) &= (b_n^* + c_n^* x)\,{}^{(2)}\mathbb{P}_n^{\alpha,\beta,\mu}(x) - d_n^{*\,(2)}\mathbb{P}_{n-1}^{\alpha,\beta,\mu}(x) \\
a_n^* &= 2n(n-\alpha+\beta)(2n-\alpha+\beta-2) \\
b_n^* &= (2n-\alpha+\beta-1)(\alpha-\beta)(\alpha+\beta-2\mu+2) \\
c_n^* &= (2n+\alpha+\beta)(2n+\alpha+\beta-1)(2n+\alpha+\beta-2) \\
d_n^* &= 2(n+\alpha-\mu)(n-\beta+\mu-2)(2n+\alpha-\beta)
\end{aligned}$$

- **Orthogonality**:

$$\int_{-1}^{1} e^{\pm 2\tau x}(1-x)^{\alpha+1-\mu}(1+x)^{\beta+1-\mu}\ {}^{(i)}\mathbb{P}_k^{\alpha,\beta,\mu}(x)\ {}^{(i)}\mathbb{P}_j^{\alpha,\beta,\mu}(x)dx = {}^{(i)}\mathcal{C}_k^{\alpha,\beta}\delta_{kj}, \tag{3.69}$$

$$\begin{aligned}
{}^{(1)}\mathcal{C}_k^{\alpha,\beta} &= \frac{2^{\alpha-\beta+1}}{2k+\alpha-\beta-1}\frac{\Gamma(k+\alpha-\mu+1)\Gamma(k-\beta+\mu-1)}{(k-1)!\,\Gamma(k+\alpha-\beta)} \\
{}^{(2)}\mathcal{C}_k^{\alpha,\beta} &= \frac{2^{-\alpha+\beta+1}}{2k-\alpha+\beta-1}\frac{\Gamma(k-\alpha+\mu-1)\Gamma(k+\beta-\mu+1)}{(k-1)!\,\Gamma(k-\alpha+\beta)}
\end{aligned}$$

- **Fractional derivatives**:

$$\begin{aligned}
{}^{RL}_{-1}\mathbb{D}_x^{-\beta+\mu+1,\tau}\left({}^{(1)}\mathbb{P}_n^{\alpha,\beta,\mu}\right) &= {}^{C}_{-1}\mathbb{D}_x^{-\beta+\mu+1,\tau}\left({}^{(1)}\mathbb{P}_n^{\alpha,\beta,\mu}\right) = e^{\tau x}\frac{\Gamma(n+\mu)}{\Gamma(n)}P_{n-1}^{\alpha-\beta,0}(x) \\
{}^{RL}_{x}\mathcal{D}_1^{-\alpha+\mu-1,\tau}\left({}^{(2)}\mathbb{P}_n^{\alpha,\beta,\mu}\right) &= {}^{C}_{x}\mathcal{D}_1^{-\alpha+\mu-1,\tau}\left({}^{(2)}\mathbb{P}_n^{\alpha,\beta,\mu}\right) = e^{-\tau x}\frac{\Gamma(n+\mu)}{\Gamma(n)}P_{n-1}^{0,\beta-\alpha}(x)
\end{aligned}$$

where $P_{n-1}^{\alpha-\beta,0}(x)$ and $P_{n-1}^{0,\beta-\alpha}(x)$ denote the standard Jacobi polynomials.

- **Special values**:

$$
\begin{aligned}
{}^{(1)}\mathbb{P}_n^{\alpha,\beta,\mu}(-1) &= 0, \quad {}^{(1)}\mathbb{P}_n^{\alpha,\beta,\mu}(+1) = 2^{-\beta+\mu-1}\binom{n+\alpha-\mu}{n-1}e^{-\tau} \\
{}^{(2)}\mathbb{P}_n^{\alpha,\beta,\mu}(+1) &= 0, \quad {}^{(2)}\mathbb{P}_n^{\alpha,\beta,\mu}(-1) = 2^{-\alpha+\mu-1}\binom{n+\beta-\mu}{n-1}e^{-\tau}
\end{aligned}
$$

3.6 Approximability of the Tempered Eigenfunctions

We introduce the tempered eigenfunctions (regular and singular) as new basis functions in $L^2_{w_i}[-1,1]$. Then, we discuss how fast the expansion coefficients of the approximation would decay with N.

Theorem 3.6.1. *The set of regular eigenfunctions* $\{F_n^{(i)}(x) : n = 1, 2, \cdots\}$ *and the singular eigenfunctions* $\{{}^{(i)}\mathbb{P}_n^{\alpha,\beta,\mu}(x) : n = 1, 2, \cdots\}$ *each forms a basis for the infinite-dimensional Hilbert space* $L^2_{w_i}[-1,1]$*, and the corresponding eigenvalues* $\lambda_n^{(i)}$ *and* $\Lambda_n^{(i)}$ *are simple.*

Proof. It suffices to prove the regular part with the singular part following similar steps. Let $f(x) \in L^2_{w_i}[-1,1]$ and then clearly $g(x) = e^{\pm\tau x}(1 \pm x)^{-\mu} f(x) \in L^2_{w_i}[-1,1]$ as well when $\mu \in (0,1)$. Considering the upper signs to correspond to the regular TFSLP-I, $i = 1$, and the lower signs to correspond to the case $i = 2$, i.e., the regular

TFSLP-II, we have

$$\begin{aligned}
\|\sum_{n=1}^{N} a_n F_n^{(i)}(x) - f(x)\|_{L^2_{w_i}[-1,1]} &= \\
\|e^{\mp\tau x}(1\pm x)^{\mu}\left(\sum_{n=1}^{N} a_n P_{n-1}^{\mp\mu,\pm\mu}(x) - e^{\pm\tau x}(1\pm x)^{-\mu} f(x)\right)\|_{L^2_{w_i}[-1,1]} &= \\
\|e^{\mp\tau x}(1\pm x)^{\mu}\|_{L^2_{w_i}[-1,1]}\|\sum_{n=1}^{N} a_n P_{n-1}^{\mp\mu,\pm\mu}(x) - g(x)\|_{L^2_{w_i}[-1,1]} &\leq \\
c\|\sum_{n=1}^{N} a_n P_{n-1}^{\mp\mu,\pm\mu}(x) - g(x)\|_{L^2_{w_i}[-1,1]}.&
\end{aligned}$$

Therefore by Weierstrass theorem, the set of tempered eigenfunctions $\{F_n^{(i)}(x) : n = 1, 2, \cdots\}$ is dense in the Hilbert space and it forms a basis for $L^2_{w_i}[-1, 1]$.

To show the simplicity of the eigenvalues, assume that corresponding to the eigenvalue $\lambda_j^{(i)}$, there exits another eigenfunction $F_j^{(i)*}(x) \in L^2_{w_i}[-1, 1]$ in addition to $F_j^{(i)}(x)$, which is by Theorem 3.4.1 is orthogonal to the rest of the eigenfunctions $F_n^{(i)}(x),\ n \neq j$. By the density of the eigenfunctions set, i.e., (3.70), we can represent $F_j^{(i)*}(x)$ as

$$F_j^{(i)*}(x) = \sum_{n=1}^{\infty} a_n F_n^{(i)}(x). \tag{3.70}$$

Now, by multiplying both sides by $F_k^{(i)}(x)$, $k = 1, 2, \cdots$ and $k \neq j$, and integrating with respect to the weight function $w_i(x)$ we obtain

$$\int_{-1}^{1} w_i(x) F_j^{(i)*}(x) F_k^{(i)}(x) dx = \sum_{n=1}^{\infty} a_n \int_{-1}^{1} w_i(x) F_n^{(i)}(x) F_k^{(i)}(x) dx = a_k C_k \neq 0, \tag{3.71}$$

which contradicts Theorem 3.4.1, and this completes the proof. □

3.6.1 Spectral Approximation using Singular Tempered Basis ${}^{(i)}\mathbb{P}_n^{\alpha,\beta,\mu}(x)$, $\mu \in (0,1)$

Next, we study the approximation properties of the family of Jacobi poly-fractonomials ${}^{(i)}\mathbb{P}_n^{\alpha,\beta,\mu}(x)$ by representing $f(x) \in L_w^2[-1,1]$ as

$$f(x) \approx \sum_{n=1}^{N} \hat{f}_n \ {}^{(i)}\mathbb{P}_n^{\alpha,\beta,\mu}(x), \ \ x \in [-1,1]. \tag{3.72}$$

Here, we need to understand how fast the expansion coefficients $\hat{f}_n$ decay by N. To this end, we multiply (3.72) by $\mathcal{L}_i^{\alpha,\beta;\mu}({}^{(i)}\mathbb{P}_k^{\alpha,\beta,\mu}(x))$, $k = 1, 2, \cdots, N$, and carry out the integration over $[-1,1]$ to obtain:

$$\int_{-1}^{1} f(x)\mathcal{L}_i^{\alpha,\beta;\mu}\left({}^{(i)}\mathbb{P}_k^{\alpha,\beta,\mu}(x)\right) \ dx = \int_{-1}^{1}\left(\sum_{n=1}^{N} \hat{f}_n \ {}^{(i)}\mathbb{P}_n^{\alpha,\beta,\mu}(x)\right)\mathcal{L}_i^{\alpha,\beta;\mu}\left({}^{(i)}\mathbb{P}_k^{\alpha,\beta,\mu}(x)\right)dx,$$

where $\mathcal{L}_i^{\alpha,\beta;\mu}({}^{(i)}\mathbb{P}_k^{\alpha,\beta,\mu}(x))$ on the right-hand side can be substituted by the right-hand side of (3.62), i.e., $-\Lambda_n^{(i)} w(x)\, {}^{(i)}\mathbb{P}_k^{\alpha,\beta,\mu}(x)$ as

$$\int_{-1}^{1} f(x)\mathcal{L}_i^{\alpha,\beta;\mu}\left({}^{(i)}\mathbb{P}_n^{\alpha,\beta,\mu}(x)\right) \ dx = \sum_{n=1}^{N} -\hat{f}_n \, \Lambda_n^{(i)} \int_{-1}^{1} (1-x)^{\alpha+1-\mu}(1+x)^{\beta+1-\mu} \ {}^{(i)}\mathbb{P}_n^{\alpha,\beta,\mu}(x)\, {}^{(i)}\mathbb{P}_k^{\alpha,\beta,\mu}(x),$$

and by the orthogonality property (3.69) we get

$$\hat{f}_k = \frac{-1}{{}^{(i)}\mathcal{C}_k^{\alpha,\beta} \ \Lambda_k^{(i)}} \int_{-1}^{1} f(x)\, {}^{RL}\mathbb{D}^{\mu}\Big\{(1-x)^{\alpha+1}(1+x)^{\beta+1} \ {}^{C}\mathbb{D}^{\mu} \ \left({}^{(i)}\mathbb{P}_k^{\alpha,\beta,\mu}(x)\right)\Big\} \ dx. \tag{3.73}$$

Now, by carrying out the fractional integration-by-parts using Lemmas 3.2.1 and 3.2.2, we obtain

$$\hat{f}_k = \frac{-1}{{}^{(i)}\mathcal{C}_k^{\alpha,\beta}\ \Lambda_k^{(i)}} \int_{-1}^{1} (1-x)^{\alpha+1}(1+x)^{\beta+1} \left({}^{C}\mathbb{D}^{\mu}\ {}^{(i)}\mathbb{P}_k^{\alpha,\beta,\mu}(x) \right)\ \left({}^{C}\mathbb{D}^{\mu}\, f(x) \right) dx. \tag{3.74}$$

Again, by Lemmas 3.2.1 and 3.2.1, we obtain

$$\hat{f}_k = \frac{-1}{{}^{(i)}\mathcal{C}_k^{\alpha,\beta}\ \Lambda_k^{(i)}} \int_{-1}^{1} {}^{(i)}\mathbb{P}_k^{\alpha,\beta,\mu}(x)\, {}^{RL}\mathbb{D}^{\mu} \Big\{ (1-x)^{\alpha+1}(1+x)^{\beta+1}\ {}^{C}\mathbb{D}^{\mu}\, f(x) \Big\}\, dx.$$

or equivalently

$$\hat{f}_k = \frac{-1}{{}^{(i)}\mathcal{C}_k^{\alpha,\beta}\ \Lambda_k^{(i)}} \int_{-1}^{1} {}^{(i)}\mathbb{P}_k^{\alpha,\beta,\mu}(x) \mathcal{L}_i^{\alpha,\beta;\mu} \left[f(x) \right] dx,$$

if denoted by $f_{(1)}(x) \equiv \mathcal{L}_i^{\alpha,\beta;\mu} \left[f(x) \right] \in L_w^2[-1,1]$. By carrying out the fractional integration-by-parts another $(m-1)$ times, and setting $f_{(m)}(x) \equiv \mathcal{L}_i^{\alpha,\beta;\mu} \left[f_{(m-1)}(x) \right] \in L_w^2[-1,1]$, we obtain

$$|\hat{f}_k| \approx \frac{C_{sing.}}{|\Lambda_k^{(i)}|^m} \|f_{(m)}(x)\|_{L_w^2}, \quad k = 1, 2, \cdots, N. \tag{3.75}$$

Consequently, when $m \to \infty$ and $f_{(m)}(x) \in L_w^2[-1,1]$, we recover the spectral decay of the expansion coefficients $\hat{f}_k$.

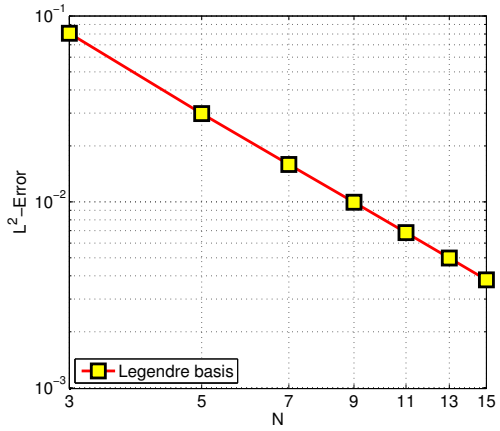

Figure 3.1: L^2- error, $\|f - f_N\|_{L^2}$ in approximating $f(x) = e^{-x}(1+x)^{1/2}$ versus N, the number of terms in the expansion (3.76) when, instead, the Legendre polynomials are used as the basis functions.

3.6.2 Numerical Approximation

Here, we test the performance of the tempered Jacobi poly-fractonomials as basis functions in approximating some tempered functions, involved with some fractional character, also in developing a Petrov-Galerkin method for tempered fractional ODEs (TFODEs), followed with the wellposedness and convergence analyses.

Function Approximation

Following Theorem 3.6.1, we employ tempered eigenfunctions as a complete basis, next we examine their efficiency in approximating $f(x) \in L^2_{w_1}[-1,1]$. We note that both regular and singular tempered bases share the same structure. Hence, taking $\alpha, \beta \to -1$, we represent $f(x)$ in $x \in [-1,1]$ as

$$f(x) \approx \sum_{n=1}^{N} \hat{f}_n \, {}^{(i)}\mathbb{P}_n^{-1,-1,\mu}(x) = \sum_{n=1}^{N} \hat{f}_n e^{-\tau x}(1+x)^{\mu} P_{n-1}^{-\mu,\mu}(x), \qquad (3.76)$$

In order to obtain the unknown coefficients $\hat{f}_n$, we multiply both sides of (3.76) by $w_1(x)F_m^{(1)}(x)$ and integrate over $[-1,1]$, where by the orthogonality property of the eigenfunctions (see Theorem 3.4.1), we obtain

$$\hat{f}_m = \frac{1}{\mathcal{J}_m}\Big(f(x), F_m^{(1)}(x)\Big)_{L^2_{w_1}([-1,1])} \tag{3.77}$$

where $\mathcal{J}_m$ is given by (3.57).

In Fig. 3.1, we plot the log-log L^2- error of approximating $f(x) = e^{-x}(1+x)^{1/2}$, the simplest tempered fractonomial, versus N, the number of terms in the expansion (3.76) when, instead, the Legendre polynomials are used as the basis functions. While only one term is needed to accurately capture $f(x)$ employing the tempered poly-fractonomials, this plot exhibits the deficiency of using standard polynomials to approximate functions whose (higher) derivatives happen to be singular on the boundaries. Moreover, in Fig. 3.2, we compare the performance of tempered and Legendre bases in approximating $f(x) = \sin\Big(\pi e^{-x}(1+x)^{1/2}\Big)$ (left), and $f(x) = (1+x)^{2/3}\exp(-x)\sin(\pi x)$ (right), where the tempered poly-fractonomials outperform the Legendre polynomials by orders of magnitude.

Petrov-Galerkin Method For Tempered Fractional Differential Equations

We now test the efficiency of the tempered poly-fractonomials in solving some tempered fractional differential equations (FDEs). To this end, we develop a Petrov-Galerkin spectral method for the following problem:

$$\begin{aligned} {}^{TRL}_{-1}\mathbb{D}_x^{2\mu,\tau}u(x) &= f(x), \quad x \in (-1,1], \\ u(-1) &= 0, \end{aligned} \tag{3.78}$$

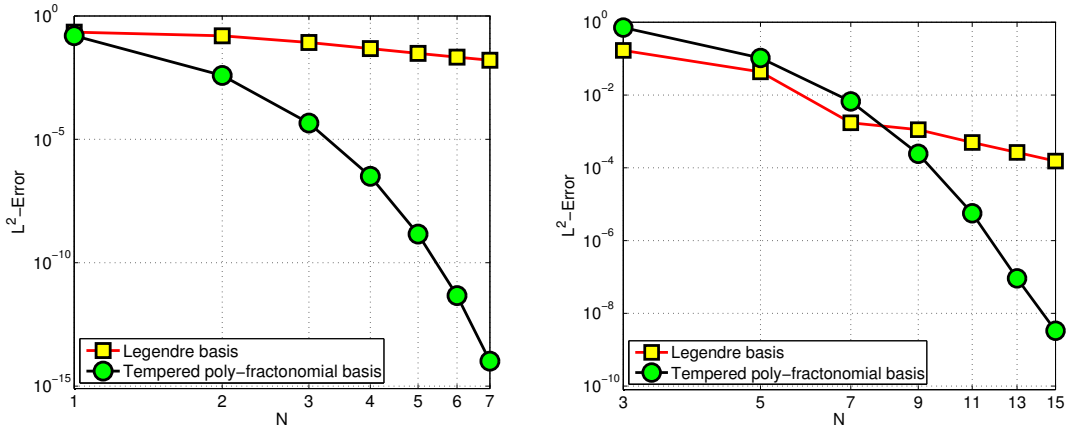

Figure 3.2: L^2- error, $\|f - f_N\|_{L^2}$ in approximating $f(x) = \sin\left(\pi e^{-x}(1+x)^{1/2}\right)$ (left), and $f(x) = (1+x)^{2/3}\exp(-x)\sin(\pi x)$ (right) versus N, the number of terms in the expansion (3.76) when both the tempered poly-fractonomial bases and Legendre bases are utilized.

where $\tau \geq$ and $2\mu \in (0,1)$. We choose $U_N \subset U_I$ to be the space of basis (trial) functions, defined in terms of the following eigenfunction of first kind as

$$U_N = \{F_n^{(1)}(x), \quad \forall n \geq 1\}, \tag{3.79}$$

whose elements i.e., any linear combinations of $F_n^{(1)}(x) = e^{-\tau x}(1+x)^{\mu}\ P_{n-1}^{-\mu,\mu}(x)$, satisfy the left-boundary condition. Here, we note that when $\alpha, \beta \to -1$, the singular bases approach the regular ones. For simplicity and to avoid dealing with extra parameters α and β, we set them to -1. Moreover, we consider $V_N \subset U_{II}$ as the space of test functions to be constructed as

$$V_N = \{F_n^{(2)}(x), \quad \forall n \geq 1\}, \tag{3.80}$$

where we recall $F_n^{(2)}(x) = e^{\tau x}(1+x)^{\mu}\ P_{n-1}^{\mu,-\mu}(x)$. Noting Remark 3.2.3, it is straightforward to check that $\forall u \in U_N$ and $w \in V_N$, we have the following bilinear form

$$a(u,w) = \left({}^{TRL}_{-1}\mathbb{D}^{2\mu}_{x,\tau}u, w\right)_{\Omega} = \left({}^{TRL}_{-1}\mathbb{D}^{\mu,\tau}_{x}u\,,\ {}^{TRL}_{x}\mathbb{D}^{\mu,\tau}_{1}w\right)_{\Omega}. \tag{3.81}$$

Hence, we consider the corresponding weak form of (3.78), which reads as: find $u_N \in U_N$ such that

$$a(u_N, w) := \Big({}^{TRL}_{-1}\mathbb{D}_x^{\mu,\tau} u_N \, , \, {}^{TRL}_{x}\mathbb{D}_1^{\mu,\tau} w \Big)_\Omega = \Big(f, w \Big)_\Omega, \quad \forall w \in V_N, \tag{3.82}$$

which becomes equivalent to the strong form (3.78) when $u_N \approx u$ possesses sufficient smoothness. Next, we seek the approximate solution u_N of the form

$$u_N(x) = \sum_{n=1}^{N} b_n F_n^{(1)}(x), \tag{3.83}$$

where b_n are the unknown expansion coefficients. By plugging (3.83) into ((3.82)), which enforces the residual $R_N(x) = {}^{TRL}_{-1}\mathbb{D}_x^{2\mu} u_N(x) - f(t)$ to be L^2-orthogonal to all elements in V_N, we obtain

$$\sum_{n=1}^{N} b_n \Big({}^{TRL}_{-1}\mathbb{D}_x^{\mu} F_n^{(1)}(x) \, , \, {}^{TRL}_{x}\mathbb{D}_1^{\mu} F_k^{(2)}(x) \Big)_\Omega = \Big(f(x) \, , \, F_k^{(2)}(x) \, , \Big)_\Omega, \quad k = 1, 2, \cdots, N,$$

which yields a *diagonal* stiffness matrix on the left-hand side, due to (3.58) and (3.59), whose diagonal entries are given by $\gamma_k = \Big(\Gamma(\frac{k+\mu}{\Gamma(k)} \Big)^2 \frac{2}{2k-1}$. Consequently, we obtain the expansion coefficients as

$$b_k = \frac{1}{\gamma_k} \Big(f \, , \; F_k^{(2)}(x) \Big)_\Omega. \tag{3.84}$$

In Fig. 3.3, we study the convergence of the proposed Petrov-Galerkin scheme. We plot the log-log L^2-error versus N, the number of expansion terms in (3.83), corresponding to the limit fractional orders $2\mu = 1/10$ and $2\mu = 9/10$, considering two different exact solutions: (i) $u(x) = e^{-x}(1+x)^5$ (left), and (ii) $u(x) = e^{1+x+x^2}(1+$

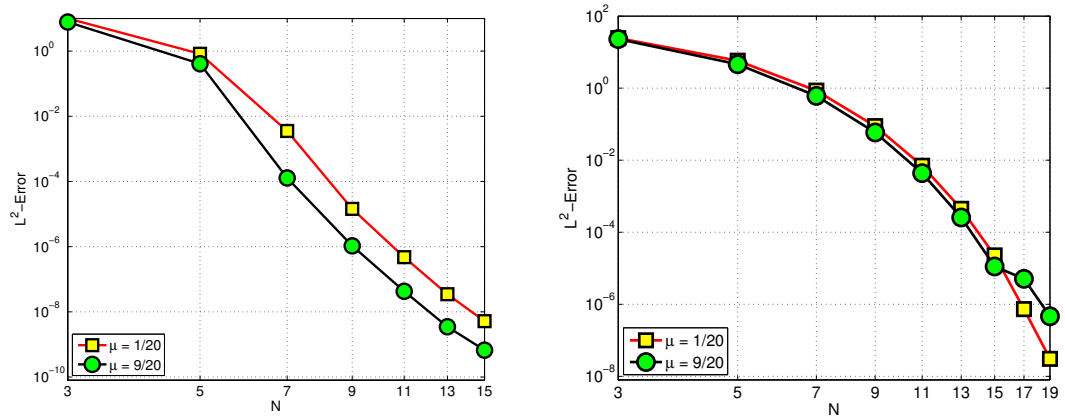

Figure 3.3: Petrov-Galerkin scheme for TFODE (3.78): L^2-error versus N, the number of expansion terms in (3.83), corresponding to the limit fractional orders $2\mu = 1/10$ and $2\mu = 9/10$. Here, the exact solutions are $u(x) = e^{-x}(1+x)^5$ (left) and $u(x) = e^{1+x+x^2}(1+x)^2$ (right).

$x)^2$ (right). These plots show the spectral mode of convergence in the Petrov-Galerkin spectral method. In what follows, we further provide the stability and convergence analysis of the method.

3.6.3 Stability and Convergence Analysis

We carry out the discrete stability analysis given the pair of $U_N \subset U_I$ and $V_N \subset V_I$.

Case I) $0 < \mu < 1/2$**:** we represent u_N as

$$u_N(x) = \sum_{n=1}^{N} \hat{u}_n F_n^{(1)}(x), \tag{3.85}$$

and choose v_N to be the following linear combination of elements in V_N as

$$v_N(x) = \sum_{k=1}^{N} \hat{u}_n F_n^{(2)}(x). \tag{3.86}$$

Hence, we obtain

$$\begin{aligned} a(u_N, v_N) &= \Big({}_{-1}\mathbb{D}_x^{\mu,\tau} u_N \, , {}_x\mathbb{D}_1^{\mu,\tau} v_N \Big)_\Omega \\ &= \sum_{n=1}^{N} \hat{u}_n \sum_{k=1}^{N} \hat{u}_k \int_{-1} {}_{-1}\mathbb{D}_x^{\mu,\tau} F_n^{(1)}(x) \, {}_x\mathbb{D}_1^{\mu} F_n^{(2)}(x) \, dx \\ &= \sum_{n=1}^{N} \hat{u}_n \frac{\Gamma(n+\mu)}{\Gamma(n)} \sum_{k=1}^{N} \hat{u}_k \frac{\Gamma(k+\mu)}{\Gamma(k)} \int_{-1}^{1} P_{n-1}(x) P_{k-1}(x) \, dx \\ &= \sum_{n=1}^{N} \hat{u}_n^2 \Big(\frac{\Gamma(n+\mu)}{\Gamma(n)} \Big)^2 \, \frac{2}{2n-1}. \end{aligned} \tag{3.87}$$

Moreover, we have

$$\begin{aligned} \|v_N\|_V^2 &= \| \, {}_x\mathbb{D}_1^{\mu,\tau} v_N \|_{L^2([-1,1])}^2 = \int_{-1}^{1} \Big(\sum_{k=1}^{N} \hat{u}_k \, {}_x\mathbb{D}_1^{\mu,\tau} F_k^{(2)}(x) \Big)^2 dx \\ &= \int_{-1}^{1} \Big(\sum_{k=1}^{N} \hat{u}_k e^{\tau x} \frac{\Gamma(k+\mu)}{\Gamma(k)} P_{n-1}(x) \Big)^2 dx, \end{aligned} \tag{3.88}$$

by which we observe that

$$\begin{aligned} \|v_N\|_V^2 &\geq C_1^2 \int_{-1}^{1} \Big(\sum_{k=1}^{N} \hat{u}_k \frac{\Gamma(k+\mu)}{\Gamma(k)} P_{n-1}(x) \Big)^2 dx = C_1^2 a(u_N, v_N) \\ \|v_N\|_V^2 &\leq C_2^2 \int_{-1}^{1} \Big(\sum_{k=1}^{N} \hat{u}_k \frac{\Gamma(k+\mu)}{\Gamma(k)} P_{n-1}(x) \Big)^2 dx = C_2^2 a(u_N, v_N) \end{aligned} \tag{3.89}$$

where $C_1 = \min_{-1\leq x\leq 1}(|e^{\tau x}|)$ and $C_2 = \max_{-1\leq x\leq 1}(|e^{\tau x}|)$. We can obtain similar results for $\|u_N\|_U^2$ as

$$c_1^2 a(u_N, v_N) \leq \|u_N\|_U^2 \leq c_2^2 a(u_N, v_N), \tag{3.90}$$

where $c_1 = \min_{-1\leq x\leq 1}(|e^{-\tau x}|)$ and $c_2 = \max_{-1\leq x\leq 1}(|e^{-\tau x}|)$. Hence, there exists a positive constant C such that $\|v_N\|_V \leq \mathcal{C}\|u_N\|_U$, by which and using the right

inequality of (3.90) we obtain

$$\sup_{v_N \in V_N} \frac{a(u_N, v_N)}{\|v_N\|_V} \geq \frac{\frac{1}{c_2^2}\|u_N\|_U^2}{\mathcal{C}\|u_N\|_U} = \frac{1}{\mathcal{C}\, c_2^2}\|u_N\|_U, \quad \forall u_N \in U_N, \tag{3.91}$$

that is stability is guaranteed for $\beta = \frac{1}{\mathcal{C}\, c_2^2}$. Therefore, Céa's lemma holds:

$$\|u - u_N\|_U \leq (1 + \frac{M}{\beta})\|u - \widetilde{u}_N\|_U, \quad \forall \widetilde{u}_N \in U_N, \tag{3.92}$$

in which the continuity constant $M = 1$. Next, in order to obtain the corresponding (projection) error estimates, we expand the exact solution u, when $2\mu \in (0, 1)$, in terms of the following infinite series of tempered Jacobi polyfractonomials

$$u(x) = \sum_{n=1}^{\infty} \hat{u}_n e^{-\tau x}(1 + x)^{\mu} P_{n-1}^{-\mu,\mu}(x). \tag{3.93}$$

Here, we would like to bound $\|u - u_N\|_U$ in terms of higher-order derivatives. We first note that

$$\begin{aligned} {}_{-1}\mathbb{D}_x^{r+\mu,\tau} u(x) &= e^{-\tau x}[{}_{-1}\mathcal{D}_x^{r+\mu}\, e^{-\tau x} u(x)] = e^{-\tau x}[\frac{d^r}{dx^r}\, {}_{-1}\mathcal{D}_x^{\mu}\, e^{-\tau x} u(x)] \\ &= \sum_{n=1}^{\infty} \hat{u}_n \frac{\Gamma(n+\mu)}{\Gamma(n)} e^{-\tau x} \frac{d^r}{dx^r}[P_{n-1}(x)], \end{aligned}$$

where

$$\frac{d^r}{dx^r}[P_{n-1}(x)] = \begin{cases} \frac{(n-1+r)!}{2r(n-1)!} P_{n-1-r}^{r,r}(x), & r \leq n, \\ 0, & r > n. \end{cases}$$

Therefore,

$${}_{-1}\mathcal{D}_x^{r+\mu} u(x) = \sum_{n=r}^{\infty} \hat{u}_n \frac{\Gamma(n+\mu)}{\Gamma(n)} \frac{(n-1+r)!}{2r(n-1)!} e^{-\tau x} P_{n-1-r}^{r,r}(x).$$

Hence,

$$\|(1-x)^{r/2}(1+x)^{r/2}\,{}_{-1}\mathbb{D}_x^{r+\mu}u(x)\| =$$
$$\int_{-1}^{1}(1-x)^r(1+x)^r\Big(\sum_{n=r}^{\infty}\hat{u}_n\frac{\Gamma(n+\mu)}{\Gamma(n)}\frac{(n-1+r)!}{2r(n-1)!}e^{-\tau x}P_{n-1-r}^{r,r}(x)\Big)^2 =$$
$$\sum_{n=r}^{\infty}\Big(\hat{u}_n\frac{\Gamma(n+\mu)}{\Gamma(n)}\frac{(n-1+r)!}{2r(n-1)!}\Big)^2\int_{-1}^{1}e^{-2\tau x}(1-x)^r(1+x)^r(P_{n-1-r}^{r,r}(x))^2dx \geq$$
$$C\sum_{n=r}^{\infty}\Big(\hat{u}_n\frac{\Gamma(n+\mu)}{\Gamma(n)}\frac{(n-1+r)!}{2r(n-1)!}\Big)^2\int_{-1}^{1}(1-x)^r(1+x)^r(P_{n-1-r}^{r,r}(x))^2dx$$
$$C\sum_{n=r}^{\infty}\Big[\hat{u}_n\frac{\Gamma(n+\mu)}{\Gamma(n)}\Big]^2\frac{2}{2n+1}\frac{(n-1+r)!}{(n-1-r)!}.$$

where C could be any positive constant greater that the minimum of $e^{-\tau x}$ in $[-1,1]$. Noting that $\frac{(n-1+r)!}{(n-1-r)!}$ is minimized when $n=N+1$, we have

$$\begin{aligned}
\|u-u_N\|_U^2 &\leq \sum_{n=N+1}^{\infty}\Big[\hat{u}_n\frac{\Gamma(n+\mu)}{\Gamma(n)}\Big]^2 \\
&\leq \sum_{n=N+1}^{\infty}\Big[\hat{u}_n\frac{\Gamma(n+\mu)}{\Gamma(n)}\Big]^2\frac{(n-1+r)!}{(n-1-r)!}\frac{(N-r)!}{(N+r)!} \\
&\leq \frac{1}{C}\frac{(N-r)!}{(N+r)!}\|\,{}_{-1}\mathbb{D}_x^{r+\mu}u(x)\|_{L^2([-1,1])}^2 \\
&\leq cN^{-2r}\|\,{}_{-1}\mathbb{D}_x^{r+\mu}u(x)\|_{L^2([-1,1])}^2 \qquad (3.94)
\end{aligned}$$

where $r\geq 1$ and $2\mu\in(0,1)$.

Chapter Four

Petrov-Galerkin Spectral Method and Discontinuous Galerkin Method for Fractional ODEs

Current discretizations of fractional differential equations lead to numerical solutions of low order of accuracy. Here in this chapter, we present different methods for fractional ODEs that lead to exponentially fast decay of the error. First, we develop a Petrov-Galerkin (PG) spectral method for Fractional Initial Value Problems (FIVPs) of the form ${}_0\mathcal{D}_t^\nu u(t) = f(t)$ and Fractional Final Value Problems (FFVPs) ${}_t\mathcal{D}_T^\nu u(t) = g(t)$, where $\nu \in (0, 1)$, subject to Dirichlet initial/final conditions. These schemes are developed based on a new spectral theory for fractional Sturm-Liouville problems (FSLPs), which has been recently developed in [187]. Specifically, we obtain solutions to FIVPs and FFVPs in terms of the new fractional (non-polynomial) basis functions, called *Jacobi polyfractonomials*, which are the eigenfunctions of the FSLP of *first* kind (FSLP-I). Correspondingly, we employ another space of test functions as the span of polyfractonomial eigenfunctions of the FSLP of *second* kind (FSLP-II). Subsequently, we develop a Discontinuous Spectral Method (DSM) of Petrov-Galerkin type for the aforementioned FIVPs and FFVPs, where the basis functions do not satisfy the initial/final conditions. Finally, we extend the DSM scheme to a discontinuous spectral element method (DSEM) for efficient longer time-integration and adaptive refinement. In these discontinuous schemes, we employ the *asymptotic* eigensolutions to FSLP-I&-II, which are of Jacobi polynomial forms, as basis and test functions. Our numerical tests confirm the exponential/algebraic convergence, respectively, in p- and h-refinements, for various test-cases with integer and fractional-order solutions.

4.1 Background

Over the last two decades, the notion of fractional derivative has been extended to many ordinary fractional differential equations (FODEs) such as fractional Cauchy

equation, fractional Gauss equations [51, 90] and fractional Sturm-Liouville equation [93], in addition to a variety of fractional partial differential equations (FPDEs) such as fractional Fokker-Planck equation [14], fractional Burgers' equation [163], and fractional advection-diffusion equation [67]. In these problems, the corresponding differential operators can be defined based on different but closely related ways. The extension of existing numerical methods for integer-order differential equations ([64, 106, 68, 195, 77] and references therein) to their corresponding fractional differential equations (FDEs) is not trivial. While the approximation of these models is computationally demanding due to their long-range *history*-dependence, the development of numerical schemes in this area does not have a long history, and has undergone a fast evolution. Depending on how (temporal $\mathcal{D}_t^\nu$ or spatial $\mathcal{D}_x^\nu$) fractional derivatives are discretized and according to their order of accuracy, different classes of numerical methods have been developed in the literature.

4.1.1 Finite Difference Methods (FDM)

To our knowledge, Lubich [113, 114] is the pioneer of the idea of *discretized fractional calculus* within the spirit of finite difference method (FDM). Later, Sanz-Serna [154] adopted the idea of Lubich and presented a temporal semi-discrete algorithm for partial integro-differential equations, which was first order accurate. Sugimoto [163] also employed a FDM for approximating the fractional derivative emerging in Burgers' equation. Later on, the paper of Metzler et. al. [127] opened a new horizon toward FPDEs by introducing a fractional dynamics approach to time-fractional diffusion. Subsequently, Gorenflo et. al. [63] adopted a finite-difference scheme by which they could generate discrete models of random walk in such anomalous diffusion. Diethelm et al. proposed a predictor-corrector scheme in addition to a

fractional Adams method [51, 53]. After that, Langlands and Henry [104] considered the fractional diffusion equation, and analyzed the L^1 scheme for the time-fractional derivative. Sun and Wu [166] also constructed a difference scheme with L^∞ approximation of time-fractional derivative. In order to develop and analyze higher order FDM schemes Lin and Xu [111] analyzed a FDM for the discretization of the time-fractional diffusion equation with order $(2-\alpha)$. Kumar and Agrawal [99] proposed a block-by-block method for a class of fractional initial value problems which later Huang et al. [69] proved that it enjoys a rate of convergence of at least 3. Recently, Cao and Xu [30] rigorously developed the scheme to $(3+\alpha)$-th order, $\alpha \in (0,1)$. To the best of knowledge, this is the highest-order and the most recent FDM scheme for discretization of fractional derivatives.

Although implementation of such FDM approaches is relatively easy, their biggest issue is that the accuracy is limited. Moreover, these approaches suffer from heavy cost of computing the long-ranged memory in discretization of the fractional derivatives at each point. In fact, FDM is inherently a *local* approach whereas fractional derivatives are essentially *global* (nonlocal) differential operators. This property would suggest that global schemes such as *Spectral Methods* (SMs) are more appropriate tools for discretizing fractional differential equations.

4.1.2 Spectral Methods (SMs)

Unlike the attention put on developing FDM schemes, very little effort has been put on developing rigorous high-order spectral methods. A Fourier SM was utilized by Sugimoto [163] in a fractional Burgers' equation, linearized by Taylor expansion, and a spline-based collocation method was employed by Blank [25] for numerical treatment of a class of FODEs. This approach was later employed by Rawashdeh [147] for

solving fractional integro-differential equations. In these works, the expected high convergence rate was not observed and no error/stability analysis was carried out. Lin and Xu [111] developed a hybrid scheme for time-fractional diffusion problem, treating the time-fractional derivative using FDM and discretizing the *integer-order* spatial derivative by a Legendre SM. In such mixed approaches, the error associated with the low-order temporal accuracy can easily dominate the global error, for instance when the time-dependent portion of the exact solution is discontinuous, or if is a monomial of form t^n, where n is sufficiently large, or is a smooth function e.g., $\sin(n\pi t)$. The idea of collocation was later adopted by Khader [86], where he proposed a Chebyshev collocation method for the discretization of the space-fractional diffusion equation. More recently, Khader and Hendy [87] developed a Legendre pseudospectral method for fractional-order delay differential equations.

The collocation and pseudospectral schemes for fractional equations are relatively easy to implement but their performance has not been tested thoroughly. For instance, when the exact solution is of polynomial form it is claimed that a fast convergence is observed. However, for other test-cases no such exponential-like convergence is achieved. The first fundamental work on spectral methods for FPDEs was done by Li and Xu [108, 109] who developed a time-space SM for time-fractional diffusion equation. To the best of our knowledge, they were the first who achieved *exponential* convergence in their numerical tests in agreement with their error analysis. However, in this scheme, the corresponding stiffness and mass matrices are dense and gradually become ill-conditioned when the fractional order α tends to small values. Moreover, this approach is not effective e.g., when the forcing term exhibits discontinuity in the time-domain. This, in turn, motivates the use of domain decomposition and *Finite Element Methods* (FEM) and *Spectral Element Methods* (SEM) in the context of fractional calculus.

4.1.3 Spectral/hp Element Methods

A theoretical framework for the least-square finite-element approximation of a fractional order differential equation was developed by Fix [60], where optimal error estimates are proven for piecewise linear trial elements. The main hurdle to overcome in FEM is the non-local nature of the fractional operator which leads to large dense matrices; even construction of such matrices presents difficulties [151]. There are, however, a number of recent works already employed in this area using FEM to obtain more efficient schemes. McLean and Mustapha [122] developed a piecewise-constant discontinuous Galerkin method for the time discretization of a sub-diffusion equation. Hanert [66] also considered the use of a Chebyshev spectral element method for the numerical solution of the fractional-order transport. Recently, the idea of the least-square FEM [60] was extended to the spectral element method by Carella [31]. Despite the spectral expansion, these schemes are not properly formulated and fail to achieve exponential convergence.

In this chapter, we develop exponentially accurate numerical schemes of Petrov-Galerkin type for the FODEs of form ${}_0\mathcal{D}_t^\nu u(t) = f(t)$ and ${}_t\mathcal{D}_T^\nu u(t) = f(t)$, introduced, respectively, as Fractional Initial Value Problem (FIVP) and Fractional Final Value Problem (FFVP) subject to Dirichlet initial conditions. To this end, we first develop a Petrov-Galerkin (PG) spectral method whose corresponding stiffness matrix is *diagonal*. Subsequently, we develop a Discontinuous Spectral Method (DSM) of Petrov-Galerkin type with *exact* quadrature rules for the aforementioned FIVPs and FFVPs. This scheme is also extended to a discontinuous spectral element method (DSEM) for efficient longer time-integrations and adaptive refinement. These schemes are developed based on a new spectral theory for fractional Sturm-Liouville problems (FSLPs), which has been recently developed in [187]. In order to test the perfor-

mance of our schemes, p-refinement and h-refinement tests are performed for a range of test cases, where the exact solution is a monomial t^n, $n \in \mathbb{N}$, fractonomial $t^{n+\mu}$, $\mu \in (0,1)$, (see [187]), smooth functions of form $t^p \sin(n\pi t)$, $p \in \mathbb{N}$, fractional functions $t^{n_1+\mu_1} \sin(n\pi t^{n_2+\mu_2})$, $n_1, n_2 \in \mathbb{N}$ and $\mu_1, \mu_2 \in (0,1)$, or any combinations of these functions. We also include a case with strong discontinuity in the forcing term $f(t)$, demonstrating that the use of DSEM yields exponential convergence in that case too.

4.2 Notation and Definitions

We first introduce the simplest fractional ordinary differential equation (FODE), which forms a building block for the construction of other fractional differential operators. Here, we define the Fractional Initial Value Problem (FIVP) of order $\nu \in (0,1)$ as

$$\begin{aligned} {}_0\mathcal{D}_t^{\nu} u(t) &= f(t), \quad t \in (0,T], \\ u(0) &= u_0, \end{aligned} \tag{4.1}$$

where ${}_0\mathcal{D}_t^{\nu}$ denotes the left-sided Reimann-Liouville fractional derivative of order $\nu \in (0,1)$ following [142], defined as

$${}_0\mathcal{D}_t^{\nu} u(t) = \frac{1}{\Gamma(1-\nu)} \frac{d}{dt} \int_0^t \frac{u(s)ds}{(t-s)^{\nu}}, \quad t > 0, \tag{4.2}$$

where Γ represents the Euler gamma function.

Next, we define the corresponding Fractional Final Value Problem (FFVP) of

order $\nu \in (0,1)$, for which the final value of the unknown solution is given as

$$\begin{aligned} {}_t\mathcal{D}_T^{\nu} u(t) &= g(t), \quad t \in [0,T), \\ u(T) &= u_T, \end{aligned} \tag{4.3}$$

where ${}_t\mathcal{D}_T^{\nu}$ represents the right-sided Reimann-Liouville fractional derivative of order $\nu \in (0,1)$, defined as

$${}_t\mathcal{D}_T^{\nu} u(t) = \frac{1}{\Gamma(1-\nu)} \Big(\frac{-d}{dt}\Big) \int_t^T \frac{u(s)ds}{(s-t)^{\nu}}, \quad t < T. \tag{4.4}$$

We also define the fractional differential operators in (4.1) and (4.3) to be the Caputo fractional derivatives ${}_0^C\mathcal{D}_t^{\nu}$ and ${}_t^C\mathcal{D}_T^{\nu}$, respectively. In fact, these fractional operators can be defined by (11.2) and (4.4), in which the order of the integration and first derivative is reversed. However, the two definitions are linked by the following relationships

$${}_0\mathcal{D}_t^{\nu} u(t) = \frac{u(0)}{\Gamma(1-\nu)t^{\nu}} + {}_0^C\mathcal{D}_t^{\nu} u(t), \tag{4.5}$$

and

$${}_t\mathcal{D}_T^{\nu} u(t) = \frac{u(t_T)}{\Gamma(1-\nu)(T-t)^{\nu}} + {}_t^C\mathcal{D}_T^{\nu} u(t). \tag{4.6}$$

Hence, when $u_0 = 0$ and $u_T = 0$ in (4.1) and (4.3), these problems become identical to the corresponding problems with the Caputo derivatives by virtue of (4.5) and (4.6).

4.3 Petrov-Galerkin (PG) Spectral Method

First, we develop a spectral method for the FIVP (4.1), subject to homogeneous Dirichlet initial conditions. Then, we generalize the scheme for non-zero Dirichlet

initial conditions.

4.3.1 Basis Functions

Our spectral scheme is based upon a new spectral theory for fractional Sturm-Liouville eigen-problems (FSLP), developed in [187]. Accordingly, we seek the solution to the FIVPs in terms of the new fractional (non-polynomial) basis functions, called *Jacobi polyfractonomials*, which are the eigenfunctions of the FSLP of first kind, explicitly obtained as

$$ {}^{(1)}\mathcal{P}_n^{\alpha,\beta,\mu}(x) = (1+x)^{-\beta+\mu-1} P_{n-1}^{\alpha-\mu+1,-\beta+\mu-1}(x), \quad x \in [-1,1], \tag{4.7} $$

where $P_{n-1}^{\alpha-\mu+1,-\beta+\mu-1}(x)$ are the standard Jacobi polynomials in which $\mu \in (0,1)$, $-1 \leq \alpha < 2-\mu$, and $-1 \leq \beta < \mu - 1$. Particularly, ${}^{(1)}\mathcal{P}_n^{\alpha,\beta,\mu}(x)$ represent the eigenfunctions of the *singular* FSLP of first kind (SFSLP-I) when $\alpha \neq -1$ and $\beta \neq -1$; otherwise ${}^{(1)}\mathcal{P}_n{}^{\mu}(x) \equiv {}^{(1)}\mathcal{P}_n^{-1,-1,\mu}(x)$ denote the eigenfunctions of the *regular* FSLP of first kind (RFSLP-I). Moreover, it has been shown in [187] that both sets of regular $\{{}^{(1)}\mathcal{P}_n{}^{\mu}(x)\}_{n=1}^{N}$ and singular bases $\{{}^{(1)}\mathcal{P}_n^{\alpha,\beta,\mu}(x)\}_{n=1}^{N}$ (for some $N \in \mathbb{N}$) have identical approximating properties when $\alpha = \beta$. Hence, in this work and for simplicity, we employ the fractional eigenfunctions for $\alpha = \beta = -1$:

$$ {}^{(1)}\mathcal{P}_n{}^{\mu}(x) = (1+x)^{\mu} P_{n-1}^{-\mu,\mu}(x), \quad x \in [-1,1], \tag{4.8} $$

as our basis functions. Now, let $u_0 = 0$ and $t \in [0,T]$. Then,

$$ {}^{(1)}\widetilde{\mathcal{P}}_n{}^{\mu}(t) = \Big(\frac{2}{T}\Big)^{\mu} t^{\mu} P_{n-1}^{-\mu,\mu}(\, x(t)\,) \tag{4.9} $$

represent the shifted basis functions of fractional order $(n-1+\mu)$ that is obtained through the affine mapping $x = 2t/T - 1$, transforming the standard interval $[-1, 1]$ to $[0, T]$. From the properties of the eigensolutions in [187], the left-sided Riemann-Liouville fractional derivative of (6.10) is given as

$$\begin{aligned} {}_0\mathcal{D}_t^{\mu}\left({}^{(1)}\widetilde{\mathcal{P}}_n^{\mu}(\,x(t)\,)\right) &= \left(\frac{2}{T}\right)^{\mu} {}_{-1}\mathcal{D}_x^{\mu}\left({}^{(1)}\mathcal{P}_n^{\mu}(x)\right) \\ &= \left(\frac{2}{T}\right)^{\mu} \frac{\Gamma(n+\mu)}{\Gamma(n)} P_{n-1}(\,x(t)\,), \end{aligned} \tag{4.10}$$

stating that the μ^{th} order fractional derivative of such fractional (non-polynomial) basis functions of order $(n-1+\mu)$ is a standard Legendre polynomials of integer order $(n-1)$. Moreover, since $u(0) = u_0 = 0$, the aforementioned Riemann-Liouville fractional derivative is identical to the one of Caputo type by virtue of (4.5).

4.3.2 Test Functions

In order to obtain the variational form in the Petrov-Galerkin spectral method, we test (4.1) against a different set of test functions, which are in fact the eigenfunctions of the FSLP of second kind, explicitly obtained in [187] as

$${}^{(2)}\mathcal{P}_k^{\alpha,\beta,\mu}(x) = (1-x)^{-\alpha+\mu-1} P_{k-1}^{-\alpha+\mu-1,\beta-\mu+1}(x), \quad x \in [-1, 1], \tag{4.11}$$

which belong to another family of the Jacobi polyfractonomials, where this time $-1 \leq \alpha < 1-\mu$, and $-1 \leq \beta < 2\mu - 1$. By the same argument made in Sec. 4.3.1, we employ the following fractional test functions

$${}^{(2)}\mathcal{P}_k^{\mu}(x) = (1-x)^{\mu} P_{k-1}^{\mu,-\mu}(x), \quad x \in [-1, 1], \tag{4.12}$$

in our weak formulation. By carrying out the same affine mapping $x = 2t/T - 1$, we can obtain the shifted test functions

$$ {}^{(2)}\widetilde{\mathcal{P}}_k^{\mu}(\,x(t)\,) = (\frac{2}{T})^{\mu}\,(T-t)^{\mu} P_{k-1}^{\mu,-\mu}(\,x(t)\,), \tag{4.13} $$

corresponding to the interval $[0, T]$. Now, following [187], the right-sided Riemann-Liouville fractional derivative of (6.18) is obtained as

$$ \begin{aligned} {}_t\mathcal{D}_T^{\mu}\left({}^{(2)}\widetilde{\mathcal{P}}_k^{\mu}(t)\right) &= \left(\frac{2}{T}\right)^{\mu} {}_x\mathcal{D}_{+1}^{\mu}\left({}^{(2)}\mathcal{P}_k^{\mu}(x)\right) \\ &= \left(\frac{2}{T}\right)^{\mu} \frac{\Gamma(k+\mu)}{\Gamma(k)} P_{k-1}(\,x(t)\,) \\ &= {}_0\mathcal{D}_t^{\mu}\left({}^{(1)}\widetilde{\mathcal{P}}_k^{\mu}(t)\right), \end{aligned} \tag{4.14} $$

where the last equality holds by (C.37). The relations in (C.38) also hold for the Caputo fractional derivatives thanks to (4.6).

Having defined the basis and test functions, next we will present the Petrov-Galerkin spectral method by recalling the following lemma.

Lemma 4.3.1. *[108]: For all $0 < \xi < 1$, if $u \in H^1([0,T])$ and $w \in H^{\xi/2}([0,T])$, then*

$$ ({}_0\mathcal{D}_t^{\xi} u, w)_{[0,T]} = (\,{}_0\mathcal{D}_t^{\xi/2} u\,,\, {}_t\mathcal{D}_T^{\xi/2} w\,)_{[0,T]}, \tag{4.15} $$

where $(\cdot,\cdot)_{[0,T]}$ denotes the standard inner product in the interval $[0,T]$.

4.3.3 PG Spectral Method for the FIVP

In FIVP (4.1), we seek an approximate solution of the form

$$u(t) \approx u_N(t) = \sum_{n=1}^{N} a_n \, {}^{(1)}\widetilde{\mathcal{P}}_n^{\mu}(t), \tag{4.16}$$

where a_n are the unknown expansion coefficients to be determined. By plugging (7.59) into (4.1), we obtain the residual $R_N(t)$ as

$$R_N(t) = {}_0\mathcal{D}_t^{\nu} u_N(t) - f(t)$$

to be L^2-orthogonal to all elements in the set of test functions $\{ {}^{(2)}\widetilde{\mathcal{P}}_k^{\mu}(\, x(t)\,) : \; k = 1, 2, \cdots, N\}$ as

$$\sum_{n=1}^{N} a_n \int_0^T {}_0\mathcal{D}_t^{\nu} \, {}^{(1)}\widetilde{\mathcal{P}}_n^{\mu}(t) \;\; {}^{(2)}\widetilde{\mathcal{P}}_k^{\mu}(\, x(t)\,)\, dt = \int_0^T f(t) \;\; {}^{(2)}\widetilde{\mathcal{P}}_k^{\mu}(\, x(t)\,)\, dt.$$

Now, we choose $\mu = \nu/2$, and by Lemma 6.3.4, we obtain

$$\sum_{n=1}^{N} a_n \int_0^T {}_0\mathcal{D}_t^{\mu} \, {}^{(1)}\widetilde{\mathcal{P}}_n^{\mu}(t) \;\; {}_t\mathcal{D}_T^{\mu} \, {}^{(2)}\widetilde{\mathcal{P}}_k^{\mu}(\, x(t)\,)\, dt = \int_0^T f(t) \;\; {}^{(2)}\widetilde{\mathcal{P}}_k^{\mu}(\, x(t)\,)\, dt,$$

where by (C.37) and (C.38) we obtain

$$\sum_{n=1}^{N} a_n \Big(\frac{2}{T}\Big)^{2\mu} \left(\frac{n+\mu}{n}\right) \left(\frac{k+\mu}{k}\right) \int_0^T P_{n-1}(\, x(t)\,) P_{k-1}(\, x(t)\,)\, dt =$$

$$\sum_{n=1}^{N} a_n \Big(\frac{2}{T}\Big)^{2\mu-1} \left(\frac{n+\mu}{n}\right)^2 \frac{2}{2n-1} \delta_{nk} =$$

$$\int_0^T f(t) \;\; {}^{(2)}\widetilde{\mathcal{P}}_k^{\mu}(\, x(t)\,)\, dt,$$

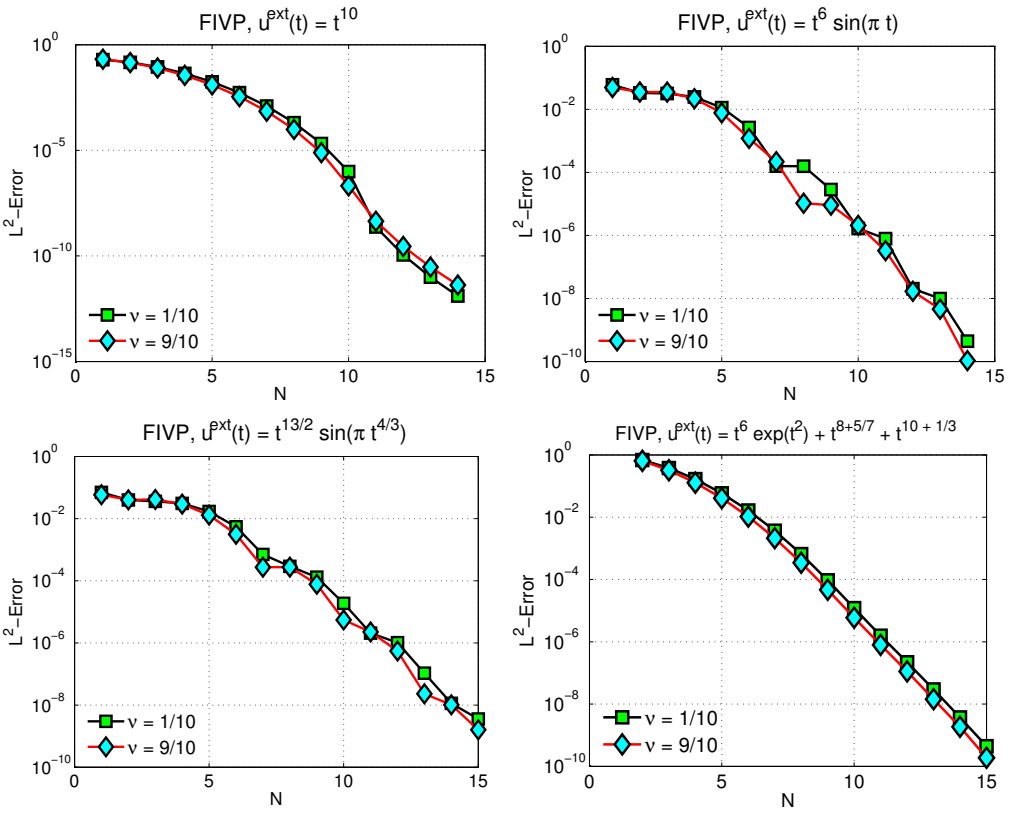

Figure 4.1: PG spectral method for FIVP: log-linear L^2-error of the numerical solution to ${}_0\mathcal{D}_t^{\nu} u(t) = f(t)$, $t \in [0,1]$, versus N, the order-index in (7.59), corresponding to $\nu = 1/10$ and $9/10$: (top-left) the exact solution $u^{ext}(t) = t^{10}$, (top-right) $u^{ext}(t) = t^6 \sin(\pi t)$, (bottom-left) $u^{ext}(t) = t^{13/2} \sin(\pi t^{4/3})$, and (bottom-right) $u^{ext}(t) = t^6 \exp(t^2) + t^{8+5/7} + t^{10+1/3}$.

which yields a *diagonal* stiffness matrix on the left-hand side, whose diagonal entries are given by $\gamma_k = (\frac{2}{T})^{2\mu-1} \left(\frac{k+\mu}{k}\right)^2 \frac{2}{2k-1}$. Consequently, we obtain the expansion coefficients as

$$a_k = \frac{1}{\gamma_k} \int_0^T f(t) \ {}^{(2)}\widetilde{\mathcal{P}}_k^{\mu}(\, x(t)\,)\, dt. \tag{4.17}$$

For the case of non-homogeneous initial conditions when $u(0) = u_0 \neq 0$, we employ the method of *lifting a known solution*, where we decompose the solution $u(t)$ into two parts as

$$u(t) = u_{\mathcal{H}}(t) + u_{\mathcal{D}}, \tag{4.18}$$

in which $u_{\mathcal{H}}(t)$ corresponds to the homogeneous solution and $u_{\mathcal{D}} \equiv u_0$ is the non-zero initial condition, given in (4.1). We substitute (5.50) into (4.1) and take the fractional derivative on the known $u_{\mathcal{D}}$ to the right hand-side to obtain

$$\begin{aligned} {}_0\mathcal{D}_t^{\nu} u_{\mathcal{H}}(t) &= h(t), \quad t \in (0, T], \\ u_{\mathcal{H}}(0) &= 0, \end{aligned} \tag{4.19}$$

where $h(t) = f(t) - \frac{u_{\mathcal{D}}}{\Gamma(1-\nu)\, t^{\nu}}$. We note that if we replace the fractional derivative in (4.19) by a Caputo one, the same scheme can be used, where this time $h(t) \equiv f(t)$, since the Caputo fractional derivative of the constant initial value $u_0 (= u_{\mathcal{D}})$ is identically zero.

In Fig.4.1, we present numerical results obtained using the PG spectral method to solve the fractional initial-value problem ${}_0\mathcal{D}_t^{\nu} u(t) = f(t),\ t \in [0, 1]$, corresponding to $\nu = 1/10$ and $9/10$. Here we consider four different exact solutions (i) monomial $u^{ext}(t) = t^{10}$, (ii) smooth function $u^{ext}(t) = t^6 \sin(\pi t)$, (iii) fractional function $u^{ext}(t) = t^{13/2} \sin(\pi t^{4/3})$, and finally (iv) combination of fractonomials (see [187]) and a smooth function $u^{ext}(t) = t^6 \exp(t^2) + t^{8+5/7} + t^{10+1/3}$. In all aforementioned cases exponential convergence is observed.

4.3.4 PG Spectral Method for the FFVP

The numerical scheme for the FFVP (4.3) is similar to the one we developed in Sec. 4.3.3, except that we interchange the space of basis and test functions in the new scheme. In fact, we choose $\{{}^{(2)}\widetilde{\mathcal{P}}_j^{\mu}(t) : j = 1, 2, \cdots, N\}$ to be set of basis functions, and we consider $\{{}^{(1)}\widetilde{\mathcal{P}}_k^{\mu}(t) : k = 1, 2, \cdots, N\}$ as the set of test functions in deriving

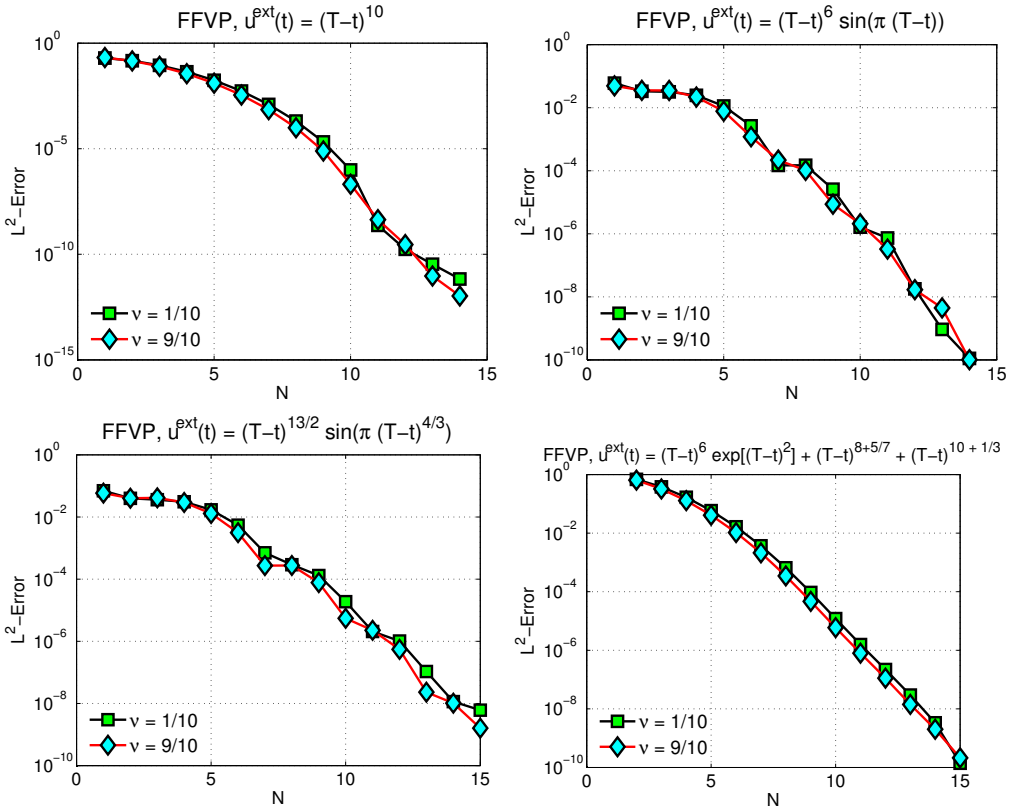

Figure 4.2: PG spectral method for FFVP: log-linear L^2-error of the approximate solution to ${}_t\mathcal{D}_T^{\nu} u(t) = f(t)$, $t \in [0,1]$, versus N, the order-index in (4.20), corresponding to $\nu = 1/10$ and $9/10$: (top-left) the exact solution $u^{ext}(t) = (T-t)^{10}$, (top-right) the exact solution $u^{ext}(t) = (T-t)^6 \sin(\pi(T-t))$, (bottom-left) the exact solution $u^{ext}(t) = (T-t)^{13/2} \sin(\pi(T-t)^{4/3})$, and (bottom-right) the exact solution $u^{ext}(t) = (T-t)^6 \exp[(T-t)^2] + (T-t)^{8+5/7} + (T-t)^{10+1/3}$.

the variational form. Here, we seek the approximate solution to (4.3) of form

$$u(t) \approx u_N(t) = \sum_{j=1}^{N} b_j \, {}^{(2)}\widetilde{\mathcal{P}}_j^{\mu}(t), \tag{4.20}$$

where b_j are the unknown expansion coefficients. By plugging (4.20) into (4.3) and requiring the corresponding residual function $R_N(t)$ to be L^2-orthogonal to each element in the set of the test functions, we obtain the unknown coefficients as

$$b_k = \frac{1}{\gamma_k} \int_0^T f(t) \; {}^{(1)}\widetilde{\mathcal{P}}_k^{\mu}(\, x(t)\,)\, dt. \tag{4.21}$$

When $u(T) = u_T \neq 0$, we employ again the method of lifting a known solution. We then decompose $u(t)$ as shown in (5.50) and substitute it into (4.3) to obtain the following equivalent finite-value problem

$$\begin{aligned} {}_t\mathcal{D}_T^{\nu} u_{\mathcal{H}}(t) &= w(t), \qquad t \in [0, T), \\ u_{\mathcal{H}}(T) &= 0, \end{aligned} \tag{4.22}$$

where $w(t) = f(t) - \frac{u_T}{\Gamma(1-\nu)\,(T-t)^{\nu}}$. In Fig. 4.2, we present numerical results obtained by the PG spectral method to solve the fractional final-value problem ${}_t\mathcal{D}_T^{\nu} u(t) = f(t)$, $t \in [0, 1]$, corresponding to $\nu = 1/10$ and $9/10$. We consider four different exact solutions (i) monomial $u^{ext}(t) = (T-t)^{10}$, (ii) smooth function $u^{ext}(t) = (T-t)^6 \sin(\pi(T-t))$, (iii) fractional function $u^{ext}(t) = (T-t)^{13/2} \sin(\pi(T-t)^{4/3})$, and finally (iv) combination of fractonomials and a smooth function $u^{ext}(t) = (T-t)^6 \exp((T-t)^2) + (T-t)^{8+5/7} + (T-t)^{10+1/3}$. In all of these test cases again we obtain exponential convergence.

4.4 Discontinuous Methods

In spectral methods developed for FIVP (4.1) and FFVP (4.3), the basis functions naturally satisfy the homogeneous initial conditions; however for the case of non-homogeneous initial conditions, we needed to decompose the solution and slightly modify the problem. Next, we present a new *discontinuous spectral element* method to be efficiently employed in *long-time* integration and possible adaptive refinement. To this end, the following lemmas are useful:

Lemma 4.4.1. *[5] For* $\mu > 0$, $\alpha > -1$, $\beta > -1$, *and* $\forall x \in [-1, 1]$

$$(1+x)^{\beta+\mu}\,\frac{P_n^{\alpha-\mu,\beta+\mu}(x)}{P_n^{\alpha-\mu,\beta+\mu}(-1)} = \frac{\Gamma(\beta+\mu+1)}{\Gamma(\beta+1)\Gamma(\mu)P_n^{\alpha,\beta}(-1)}\int_{-1}^{x}\frac{(1+s)^{\beta}\;P_n^{\alpha,\beta}(s)}{(x-s)^{1-\mu}}ds. \quad (4.23)$$

By the definition of the left-sided Riemann-Liouville integral and evaluating the special end-values $P_n^{\alpha-\mu,\beta+\mu}(-1)$ and $P_n^{\alpha,\beta}(-1)$, we can re-write (10.16) as

$${}^{RL}_{-1}\mathcal{I}_x^{\mu}\Big\{(1+x)^{\beta}P_n^{\alpha,\beta}(x)\Big\} = \frac{\Gamma(n+\beta+1)}{\Gamma(n+\beta+\mu+1)}(1+x)^{\beta+\mu}\,P_n^{\alpha-\mu,\beta+\mu}(x). \quad (4.24)$$

Now, by taking the fractional derivative ${}^{RL}_{-1}\mathcal{D}_x^{\mu}$ on both sides of (5.15) when $\beta = -\mu$ we obtain

$${}^{RL}_{-1}\mathcal{D}_x^{\mu}\Big\{P_n^{\alpha-\mu,0}(x)\Big\} = \frac{\Gamma(n+1)}{\Gamma(n-\mu+1)}(1+x)^{-\mu}P_n^{\alpha,\,-\mu}(x). \quad (4.25)$$

Lemma 4.4.2. *[5] For* $\mu > 0$, $\alpha > -1$, $\beta > -1$, *and* $\forall x \in [-1, 1]$

$$(1-x)^{\alpha+\mu}\,\frac{P_n^{\alpha+\mu,\beta-\mu}(x)}{P_n^{\alpha+\mu,\beta-\mu}(+1)} = \frac{\Gamma(\alpha+\mu+1)}{\Gamma(\alpha+1)\Gamma(\mu)P_n^{\alpha,\beta}(+1)}\int_{x}^{1}\frac{(1-s)^{\alpha}\;P_n^{\alpha,\beta}(s)}{(s-x)^{1-\mu}}ds. \quad (4.26)$$

By the definition of the right-sided Riemann-Liouville integral and evaluating the

special end-values $P_n^{\alpha-\mu,\beta+\mu}(+1)$ and $P_n^{\alpha,\beta}(+1)$, we can re-write (10.17) as

$$ {}^{RL}_{x}\mathcal{I}_1^{\mu}\Big\{(1-x)^{\alpha}P_n^{\alpha,\beta}(x)\Big\} = \frac{\Gamma(n+\alpha+1)}{\Gamma(n+\alpha+\mu+1)}(1-x)^{\alpha+\mu}P_n^{\alpha+\mu,\beta-\mu}(x). \tag{4.27} $$

In a similar fashion, by taking the fractional derivative ${}^{RL}_{x}\mathcal{D}_{-1}^{\mu}$ on both sides of (6.21) when $\alpha = -\mu$ we obtain

$$ {}^{RL}_{x}\mathcal{D}_1^{\mu}\Big\{P_n^{0,\beta-\mu}(x)\Big\} = \frac{\Gamma(n+1)}{\Gamma(n-\mu+1)}(1-x)^{-\mu}P_n^{-\mu,\beta}(x). \tag{4.28} $$

The relations (10.18) and (10.20) are useful in computing the corresponding stiffness matrix in the discontinuous scheme presented in the following section.

In the following, we first develop a discontinuous spectral (single-element) scheme for FIVPs (4.1) and FFVPs (4.3) and subsequently we extend it to a discontinuous spectral element method in which we partition the computational domain into non-overlapping elements.

4.4.1 Discontinuous Spectral Method (DSM; Single-Element)

We first introduce the spaces of basis and test functions to be employed in the discontinuous scheme for the FIVPs (4.1). Let $(-\beta+\mu-1) \to 0$ in (8.2), then ${}^{(1)}\mathcal{P}_n^{\alpha,\beta,\mu}(x) \to P_{n-1}^{\alpha-\mu+1,0}(x)$, where $\alpha-\mu+1 = \eta \in (0,1)$, since $-1 \le \alpha < 2-\mu$ and $-1 \le \beta < \mu-1$, recalling from [187]. Hence, in the mapped interval $[0,T]$, we define the space of basis functions as

$$ V_N = span\{\widetilde{P}_j^{\,\eta,0}(\,x(t)\,) : \eta \in (0,1), \text{and } j = 0,1,\cdots,N\}. \tag{4.29} $$

In a similar fashion, if we let $(-\alpha+\mu-1)\to 0$, then ${}^{(2)}\mathcal{P}_n^{\alpha,\beta,\mu}(x)\to P_{n-1}^{0,\beta-\mu+1}(x)$, where $\beta-\mu+1=\chi\in(0,1)$. In fact in this case $-1\le\beta<2-\mu$ and $-1\le\alpha<\mu-1$. Hence, we define the space of test functions as

$$\mathcal{V}_N=span\{\widetilde{P}_k^{\,0,\chi}(\,x(t)\,):\chi\in(0,1),\text{and }k=0,1,\cdots,N\}. \tag{4.30}$$

We call $\widetilde{P}_j^{\,\eta,0}(\,x(t)\,)$ and $\widetilde{P}_k^{\,0,\chi}(\,x(t)\,)$ *asymptotic eigenfunctions* of FSLP-I & -II, which are *polynomials*.

Remark 4.4.3. We shall show how this choice of basis and test polynomial functions leads to efficient and exact calculation of the stiffness matrices arising in the corresponding variational forms using standard Gauss-Legendre quadrature rules.

FIVP (Single-Element)

We follow a discontinuous spectral method (DSM) of Petrov-Galerkin kind and seek an approximate solution to (4.1), where $u(0)=u_D\neq 0$ generally, in the form

$$u_N(t)=\sum_{n=0}^{N}c_n\,\widetilde{P}_j^{\,\eta,0}(\,x(t)\,), \tag{4.31}$$

which $\forall\vartheta(t)\in\mathcal{V}_N$ satisfies the following variational form obtained from (4.1) in the time-interval $I=[0,T]$

$$\Big(\,{}_{0^+}\mathcal{D}_t^{\nu/2}u_N(t)\;,\;{}_t\mathcal{D}_T^{\nu/2}\vartheta(t)\,\Big)_I\;-\frac{\vartheta(T)T^{1-\nu}}{(1-\nu)\Gamma(1-\nu)}[\![u_N(0)]\!]=\Big(\,f(t),\vartheta(t)\Big)_I, \tag{4.32}$$

where $(\cdot,\cdot)_I$ denotes the standard inner-product in the interval I, and $[\![u_N(0)]\!]=u_N(0^+)-u_N(0^-)=u_N(0^+)-u_D$ represents the jump discontinuity of the solution

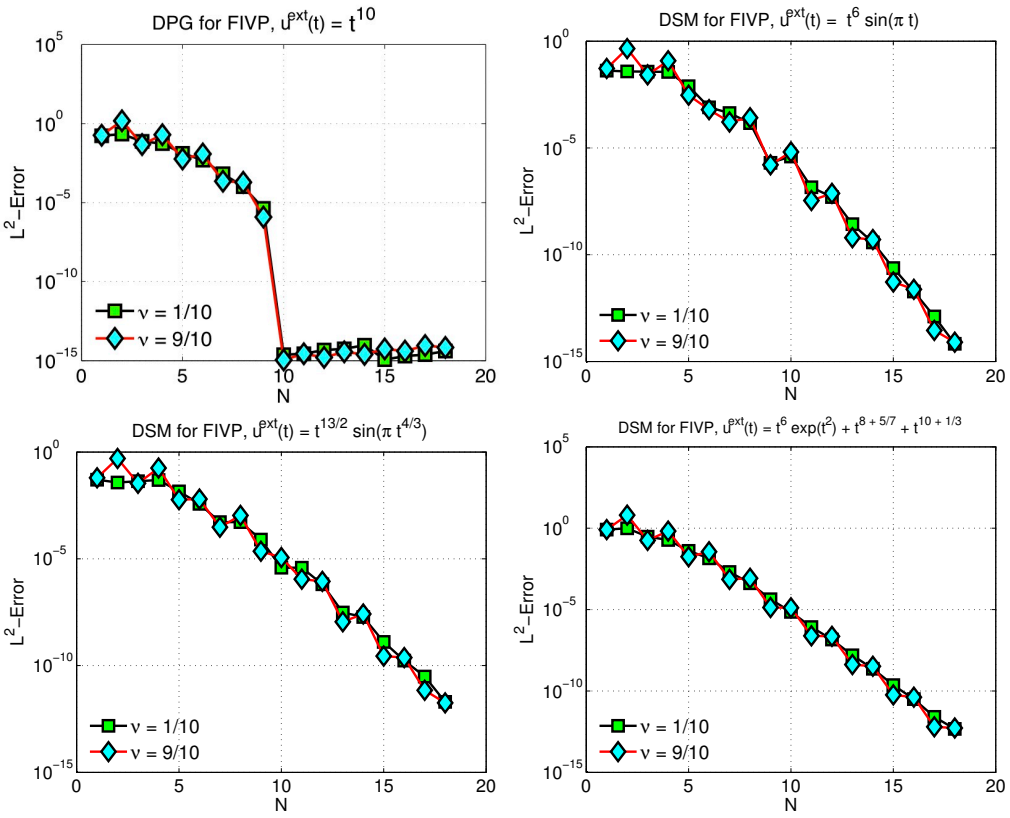

Figure 4.3: Discontinuous spectral method for FIVP: log-linear L^2-error of the approximate solution to ${}_0\mathcal{D}_t^{\nu} u(t) = f(t)$, $t \in [0,1]$, versus N, the polynomial order in (5.62), corresponding to $\nu = 1/10$ and $9/10$: (top-left) the exact solution $u^{ext}(t) = t^{10}$, (top-right) the exact solution $u^{ext}(t) = t^6 \sin(\pi t)$, (bottom-left) the exact solution $u^{ext}(t) = t^{13/2} \sin(\pi t^{4/3})$, and (bottom-right) the exact solution $u^{ext}(t) = t^6 \exp(t^2) + t^{8+5/7} + t^{10+1/3}$.

at the initial condition, and $\vartheta(T)$ is the test-function evaluated at the end of the time-interval. In A.1, we provide the derivation of the scheme (5.63).

We then choose $\eta = \chi = \nu/2$, and by substituting (5.62) into the scheme (5.63),

and taking $\vartheta(t) = \widetilde{P}_k^{\,0,\chi}(\,x(t)\,)$ for $k = 0, 1, \cdots, N$, we obtain

$$\sum_{n=0}^{N} c_n \tag{4.33}$$
$$\Big\{ \int_0^T {}_{0^+}\mathcal{D}_t^{\nu/2} \widetilde{P}_n^{\,\nu/2,\,0}(\,x(t)\,)\ {}_t\mathcal{D}_{T^-}^{\eta} \widetilde{P}_k^{\,0,\nu/2}(\,x(t)\,)\,dt - \frac{\widetilde{P}_k^{\,0,\,\nu/2}(T) T^{1-\nu}}{(1-\nu)\Gamma(1-\nu)} \widetilde{P}_n^{\,\nu/2,\,0}(0^+) \Big\}$$
$$= \int_0^T f(t)\, \widetilde{P}_k^{\,0,\nu/2}(\,x(t)\,)\,dt - \frac{\widetilde{P}_k^{\,0,\,\nu/2}(T) T^{1-\nu}}{(1-\nu)\Gamma(1-\nu)} u_D,$$

where by virtue of (10.18) and (10.20) and explicitly evaluating the end points $\widetilde{P}_k^{\,\nu/2,\,0}(T^-) \equiv 1$ and $\widetilde{P}_n^{\,\nu/2,\,0}(0^+) \equiv (-1)^n$, (5.64) yields the following linear system

$$\mathcal{S}\ \vec{\mathbf{c}} = \vec{\mathbf{F}} \tag{4.34}$$

where $\mathcal{S}$ denotes the corresponding $N \times N$ stiffness matrix whose entries are obtained as

$$\mathcal{S}[k,n] = \Lambda_{kn} \int_0^T t^{-\nu/2}\ (T-t)^{-\nu/2}\, \widetilde{P}_n^{\,\nu,\,-\nu/2}(\,x(t)\,) \widetilde{P}_k^{\,-\nu/2,\nu}(\,x(t)\,)\ dt + \frac{(-1)^{n+1}\, T^{1-\nu}}{(1-\nu)\Gamma(1-\nu)}, \tag{4.35}$$

where Λ_{kn} is computed explicitly as

$$\Lambda_{kn} \;=\; \frac{\Gamma(k+1)}{\Gamma(k-\nu/2+1)} \frac{\Gamma(n+1)}{\Gamma(n-\nu/2+1)}. \tag{4.36}$$

In (5.65), we also compute the load-vector $\vec{\mathbf{F}}$ of size N as

$$\mathbf{F}[k] = \int_0^T f(t)\, \widetilde{P}_k^{\,0,\nu/2}(\,x(t)\,)\,dt - \frac{T^{1-\nu}}{(1-\nu)\Gamma(1-\nu)}\ u_D \tag{4.37}$$

Remark 4.4.4. The stiffness matrix $\mathcal{S}$ is a full matrix whose entries satisfy $\mathcal{S}[k,n] = (-1)^{k+n}\mathcal{S}[n,k]$. Hence, we need to compute only half of the entries. Moreover, such entries can be computed *exactly* using the following Gauss quadrature rule thanks to the weight function $t^{-\nu/2}\,(T-t)^{-\nu/2}$ arising from the choice of the basis and test functions

$$\int_0^T t^{-\nu/2}\,(T-t)^{-\nu/2}\,\widetilde{P}_n^{\,\nu,\,-\nu/2}(\,x(t)\,)\widetilde{P}_k^{\,-\nu/2,\nu}(\,x(t)\,)\,dt \approx \sum_{j=1}^{N+1} \widetilde{P}_n^{\,\nu,\,-\nu/2}(\,t_j\,)\widetilde{P}_k^{\,-\nu/2,\nu}(\,t_j\,)\omega_j. \tag{4.38}$$

This is true since $\widetilde{P}_n^{\,\nu,\,-\nu/2}\widetilde{P}_k^{\,-\nu/2,\nu} \in P_{2N}$ for all $n,k = 1,2,\cdots,N$. Here, t_k's are the Gauss-Lobatto-Jacobi (GLJ) quadrature points in the interval $[0,T]$ given by

$$t_j = \frac{T}{2}\Big(\xi_j^{-\nu/2,-\nu/2} + 1\Big),\ j = 1,2,\cdots,N+1, \tag{4.39}$$

where $\xi_j^{-\nu/2,-\nu/2}$ are the standard quadrature GLJ points in $[-1,1]$, and the corresponding weights are obtained as

$$\omega_j = (\frac{T}{2})^{1-\nu}\rho_j^{-\nu/2,-\nu/2},\ j = 1,2,\cdots,N+1, \tag{4.40}$$

in which $\rho_j^{-\nu/2,-\nu/2}$ represents the standard GLJ quadrature weights associated with the Jacobi parameters $^{-\nu/2,-\nu/2}$.

FFVPs (Single-Element)

We now modify the DSM scheme (5.63) for solving the FFVPs (4.3), simply by switching the space of the basis and test functions employed in (5.63), where this

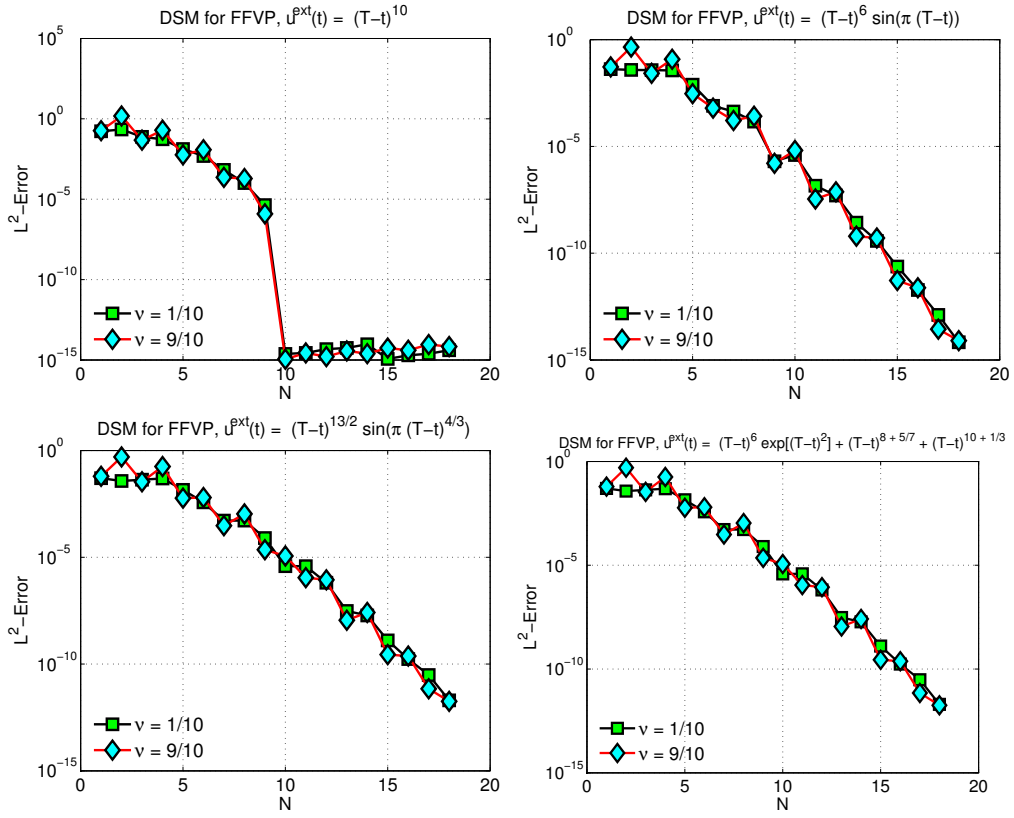

Figure 4.4: Discontinuous spectral method for FFVP: log-linear L^2-error of the approximate solution to ${}_t\mathcal{D}_T^{\nu}u(t) = f(t),\ t \in [0,1]$, versus N, the polynomial order in (4.41), corresponding to $\nu = 1/10$ and $9/10$: (top-left) the exact solution $u^{ext}(t) = (T-t)^{10}$, (top-right) the exact solution $u^{ext}(t) = (T-t)^6 \sin(\pi(T-t))$, (bottom-left) the exact solution $u^{ext}(t) = (T-t)^{13/2} \sin(\pi(T-t)^{4/3})$, and (bottom-right) the exact solution $u^{ext}(t) = (T-t)^6 \exp[(T-t)^2] + (T-t)^{8+5/7} + (T-t)^{10+1/3}$.

time we employ (5.61) as our basis space and instead we use (5.60) as the set of test functions. Then, we seek the approximate solution to (5.63) where we choose $u(T) = u_D \neq 0$, in the form

$$u_N(t) = \sum_{n=0}^{N} \hat{c}_n \, \widetilde{P}_j^{\,0,\chi}(\, x(t)\,), \tag{4.41}$$

which $\forall \vartheta(t) \in V_N$ (set of test functions) satisfies the following variational form

$$\Big(\, {}_t\mathcal{D}_{T^-}^{\nu/2} u_N(t) \;,\; {}_{0^+}\mathcal{D}_t^{\nu/2} \vartheta(t) \Big)_I \; + \frac{\vartheta(0^+) T^{1-\nu}}{(1-\nu)\Gamma(1-\nu)} [\![u_N(T)]\!] = \Big(f(t), \vartheta(t) \Big)_I, \tag{4.42}$$

where $[\![u_N(T)]\!] = u_N(T^+) - u_N(T^-) = u_D - u_N(T^-)$ represents the jump discontinuity of the solution at the initial condition, and finally $\vartheta(0^+)$ is the test-function evaluated at the beginning of the time-interval. In A.1, we provide the derivation of the scheme (4.42).

In Figs. 4.3 and 4.4, we present numerical results obtained by the DSM scheme to solve the fractional initial-value problem ${}_0\mathcal{D}_t^{\nu} u(t) = f(t),\ t \in [0,1]$, and finite-value problem ${}_t\mathcal{D}_T^{\nu} u(t) = f(t),\ t \in [0,1]$, corresponding to $\nu = 1/10$ and $9/10$. For the sake of comparison, we consider the same test cases utilized in Fig. 4.1 and 4.2. Exponential convergence of both schemes in Figs. 4.3 and 4.4 is demonstrated.

4.4.2 Discontinuous Spectral Element Method (DSEM; Multi-Element)

Now, we partition the time-interval $[0,T]$ into N_{el} non-overlapping time-elements, $I_e = [t_{e-\frac{1}{2}}, t_{e+\frac{1}{2}}]$ such that $\cup_{e=1}^{N_{el}} I_e = [0,T]$. Next, we expand the solution in each

element I_e in terms of some basis functions, which are discontinuous at the interfaces of elements and test the problem against another set of test functions psace. Here, we construct our basis and test functions based upon (5.60) and (5.61), employed in the development of the DPG scheme, as

$$V_h^N = \{v : v\Big|_{I_e} \in V_N(I_e), e = 1, 2, \cdots, N_{el}\}, \tag{4.43}$$

and

$$\mathcal{V}_h^N = \{v : v\Big|_{I_e} \in \mathcal{V}_N(I_e), e = 1, 2, \cdots, N_{el}\}, \tag{4.44}$$

In our discontinuous spectral element method, we seek an approximate solution to (4.1) on e^{th} time-element in the form

$$u_N^e(t) = \sum_{n=1}^{N} \mathcal{C}_n \, \widetilde{P}_j^{\,\eta,0}(\, x^e(t)\,), \tag{4.45}$$

which $\forall \vartheta^e(t) \in \mathcal{V}_h^N$ satisfies the following bilinear form originated from projecting (4.1) onto $\vartheta^e(t)$ in the time-interval $I_e = [t_{e-\frac{1}{2}}, t_{e+\frac{1}{2}}]$ as

$$\Big(\, {}_{t^+_{e-1/2}}\mathcal{D}_t^{\nu/2} u_N^e(t)\ ,\ {}_t\mathcal{D}^{\nu/2}_{t^-_{e+1/2}} \vartheta^e(t)\,\Big)_{I_e} - \frac{\vartheta^e(t^-_{e+1/2})(\Delta t)_e^{1-\nu}}{(1-\nu)\Gamma(1-\nu)} [\![u_N^e(t_{e-1/2})]\!] = \Big(\, f(t), \vartheta(t)\Big)_{I_e} - \mathcal{H}_e, \tag{4.46}$$

beginning form the first element, i.e., $e = 1$, and marching element-by-element along the time-axis to the $e = N_{el}$. Here, $(\Delta t)_e$ emerges the time-length of the element I_e. We note that the only difference between the scheme (5.79) and the discontinuous spectral (single-element) method in (5.63) is the *history-term* $\mathcal{H}_e$ appearing on the right-hand side of (5.79). We shall explain how this term represents an extra

history-load included in (5.79). We first write $\mathcal{H}_e$ in the following convenient and computationally efficient form as

$$\mathcal{H}_e \;=\; \vartheta^e(t)F_e(t)\Big|_{t=t^+_{e-1/2}}^{t=t^-_{e+1/2}} - \Big(\, F_e(t)\,,\, \frac{d}{dt}\vartheta^e(t)\Big)_{I_e}, \tag{4.47}$$

where $F_e(t)$ is the *history function* associated with element I_e

$$F_e(t) = \sum_{\epsilon=1}^{e-1}\sum_{\delta=0}^{N} \tau_\delta (t-s)^{\delta+1-\nu} u_N^{(\delta)\epsilon}(s)\Big|_{s=t^+_{\epsilon-1/2}}^{s=t^-_{\epsilon+1/2}} \tag{4.48}$$

in which $\tau_\delta = -1/[\Gamma(1-\nu)\prod_{m=0}^{\delta}(m+1-\nu)]$ is decaying with rate $(\delta-\nu)!$, $\delta = 0, 1, \cdots, N$, and $u_N^{(\delta)\epsilon}$ represents the δ-th derivative of the solution in I_ϵ to be only evaluated at the boundaries of I_ϵ. We recall that the approximate solution in each element is obtained in terms of the basis functions which are Jacobi-polynomials in (5.60) whose derivatives can be obtained recursively thanks to their hierarchical structure. Hence, $F_e(t)$ is a *poly-fractonomial* of degree $N+\mu$, where $\mu = 1-\nu \in (0,1)$, defined in [187]. Furthermore, we note that when we take $N_{el} = 1$ in the DSEM scheme, the history-load term $\mathcal{H}_e = 0$, then the scheme becomes identical to the DSM scheme (5.63). In A.2, we provide the complete derivation of the scheme (5.79).

Remark 4.4.5. In order to shed light on the interpretation of such history term in (5.81) we obtain an alternative representation for the history term (see A.2) as

$$\mathcal{H}_e = -\sum_{\epsilon=1}^{e-1} \Big\{ \Big(\; {}_{s_\epsilon^0}\mathcal{D}_t^\nu u_N^{\epsilon *}(t)\,,\, \vartheta^e(t)\,\Big)_{I_e}\Big|_{s_\epsilon^0=t^+_{\epsilon-1/2}}^{s_\epsilon^0=t^-_{\epsilon+1/2}}, \tag{4.49}$$

where we have continuously extended the solution u_N^ϵ from the corresponding element I_ϵ to the present element I_e, denoted by $u_N^{\epsilon *}$, such that $u_N^{\epsilon *}\Big|_{I_\epsilon} = u_N^\epsilon$. Such a representation implies that the history of the present element I_e respects the structure of the

fractional ODE (4.1) on the left-hand side. Therefore, assuming any time-continuous extension of the past solution in I_ϵ to I_e, an *extra load* term emerges as a history contribution to the present element.

In order to obtain the corresponding linear system, we choose $\eta = \chi = \nu/2$, and by substituting (5.78) into the scheme (5.79), and taking $\vartheta^e(t) = \widetilde{P}_k^{\,0,\chi}(\,x^e(t)\,)$ for $k = 0, 1, \cdots, N$ and $e = 1, 2, \cdots, N_{el}$, we obtain

$$\sum_{n=0}^{N} \mathcal{C}_{\,n}^{\,e} \Big\{ \int_{I_e} {}_{t_{e-1/2}^{+}}\mathcal{D}_t^{\nu/2} \widetilde{P}_n^{\,\nu/2,\,0}(\,x^e(t)\,)\ {}_{t}\mathcal{D}_{t_{e+1/2}^{-}}^{\nu/2} \widetilde{P}_k^{\,0,\nu/2}(\,x^e(t)\,)\,dt + (-1)^{n+1}(\Delta t)_e^{1-\nu}\kappa_v \Big\}$$
$$= \int_{I_e} f(t)\,\widetilde{P}_k^{\,0,\nu/2}(\,x^e(t)\,)\,dt \;-\; \kappa_v\,(\Delta t)_e^{1-\nu}(u_N^{e-1})^R \;-\; \mathcal{H}_{e,k},$$

in which $\kappa_v = 1/[(1-\nu)\Gamma(1-\nu)]$, and hence by Lemma 6.3.4, we obtain

$$\sum_{n=0}^{N} \mathcal{C}_{\,n}^{\,e} \Big\{ \Lambda_{kn} \int_{I_e} w^e(t) \widetilde{P}_n^{\,\nu,\,-\nu/2}(\,x^e(t)\,)\ \widetilde{P}_k^{\,-\nu/2,\nu}(\,x^e(t)\,)\,dt \;\;+\;\; (-1)^{n+1}(\Delta t)_e^{1-\nu}\kappa_v \Big\}$$
$$= \int_{I_e} f(t)\,\widetilde{P}_k^{\,0,\nu/2}(\,x^e(t)\,)\,dt \;-\; \kappa_v\,(\Delta t)_e^{1-\nu}(u_N^{e-1})^R \;-\; \mathcal{H}_{e,k},$$

where $w^e(t) = (t - t_{e-1/2})^{-\nu/2}(t_{e+1/2} - t)^{-\nu/2}$ and the term $(u_N^{e-1})^R$ represents the solution we have already obtained for in element I_{e-1}, which is evaluated at the right boundary. We note that for $e = 1$, $(u_N^0)^R$ is equal to the initial condition $u(0) = u_D$. The corresponding linear system in element I_e is then obtained as

$$\mathcal{S}_e \vec{\mathbf{c}}_e = \vec{\mathbf{F}}_e \tag{4.50}$$

where $\mathcal{S}_e$ denotes the corresponding $N \times N$ *local* stiffness matrix in I_e whose entries

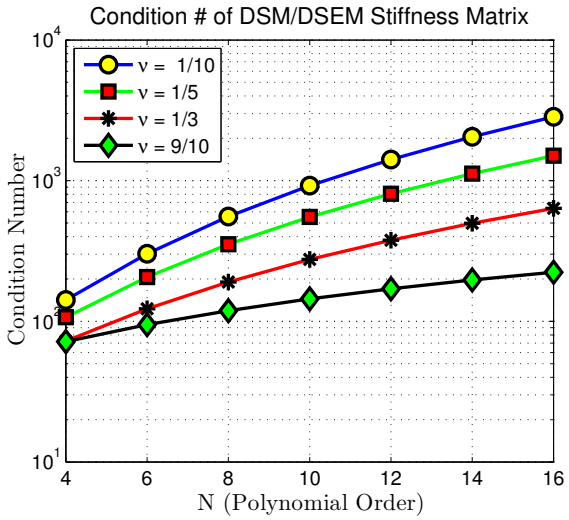

Figure 4.5: Condition number of the stiffness matrix obtained in DSM/DSEM in terms of the polynomial order N and corresponding to different values of the fractional order ν. We observe that the condition number grows roughly as $N^{3-\nu}$.

are obtained as

$$\mathcal{S}_e[k,n] = \Lambda_{kn} \int_{I_e} w^e(t) \widetilde{P}_n^{\nu,-\nu/2}(\, x^e(t)\,)\ \widetilde{P}_k^{-\nu/2,\nu}(\, x^e(t)\,)\, dt \ \ + \ \ (-1)^{n+1} (\Delta t)_e^{1-\nu} \kappa_v \tag{4.51}$$

in which Λ_{kn} is explicitly given in (5.72). In (4.50), we also compute the local load-vector $\vec{\mathbf{F}}_e$ of size N as

$$\mathbf{F}_e[k] = \int_{I_e} f(t)\, \widetilde{P}_k^{\,0,\nu/2}(\, x^e(t)\,)\, dt \ - \ \kappa_v\, (\Delta t)_e^{1-\nu} (u_N^{e-1})^R \ - \ \mathcal{H}_{e,k}, \tag{4.52}$$

in which $\mathcal{H}_{e,k}$ is given by

$$\mathcal{H}_{e,k} = F_e(t^-_{e+1/2}) + (-1)^{k+1} F_e(t^+_{e-1/2}) - \Big(F_e(t)\,,\ \frac{d}{dt}\, \widetilde{P}_k^{\,0,\nu/2}(\, x^e(t)\,)\Big)_{I_e} \tag{4.53}$$

Remark 4.4.6. Similarly to DSM, the stiffness matrix $\mathcal{S}_e$ in DSEM scheme is also a full matrix, whose entries similarly follow the property $\mathcal{S}_e[k,n] = (-1)^{k+n} \mathcal{S}_e[n,k]$.

By the same argument, due to the weight function $w_e(t)$ appearing as a result of the choice of the basis and test functions the entries of $\mathcal{S}_e$ can be computed *exactly* using a standard quadrature rule. By performing local element operations and considering an affine mapping from of the physical element to the standard one, we can efficiently compute the entries of $\mathcal{S}_e$ as

$$\begin{aligned} \mathcal{S}_e[k,n] = \Lambda_{kn} \int_{I_e} w_e(t)\, \widetilde{P}_n^{\nu,-\nu/2}(\, x^e(t)\,) \widetilde{P}_k^{-\nu/2,\nu}(\, x^e(t)\,)\; dt \;\; &= \qquad (4.54) \\ J \cdot \Lambda_{kn} \int_{-1}^{+1} (1-x)^{-\nu/2}(1+x)^{-\nu/2}\, P_n^{\nu,-\nu/2}(\, x\,) P_k^{-\nu/2,\nu}(\, x\,)\; dx \;\; &= \\ J \cdot \mathcal{S}_e^{st}[k,n], & \end{aligned}$$

where $J = [(\Delta t)_e/2]^{1-\nu}$ represents the Jacobian of the transformation and $\mathcal{S}^{st}$ denotes the stiffness matrix on the *standard* element in the interval $[-1,1]$, obtained as

$$\mathcal{S}^{st}[k,n] = \Lambda_{kn} \sum_{j=1}^{N+1} P_n^{\nu,-\nu/2}(\, x_j\,) P_k^{-\nu/2,\nu}(\, x_j\,) \rho_j^{-\nu/2,-\nu/2}, \qquad (4.55)$$

in which x_j's are the standard Gauss-Lobatto-Jacobi (GLJ) quadrature points in the interval $[-1,1]$ and ρ_j represent the corresponding weights. The relation (4.55) shows that in order to compute $\mathcal{S}_e$ in each element, we only need to obtain $\mathcal{S}_e^{st}$ once and multiply it to the corresponding Jacobian in each element. Clearly, on a uniform mesh where $(\Delta t)_1 = (\Delta t)_2 = \cdots = (\Delta t)_{N_{el}} = T/N_{el}$, the stiffness matrix is invariant in each element and we compute it only *once* for the entire of the simulation.

In addition, we study the condition number of the stiffness matrix in the DSEM and DSM schemes versus the fractional order ν and polynomial order N in Fig. 4.5. This plot shows that as ν decreases the condition number of the stiffness matrix increases. It can be attributed to the fact that the singularity in the definition of the fractional derivative in (4.1), also the ones appearing in the weight functions

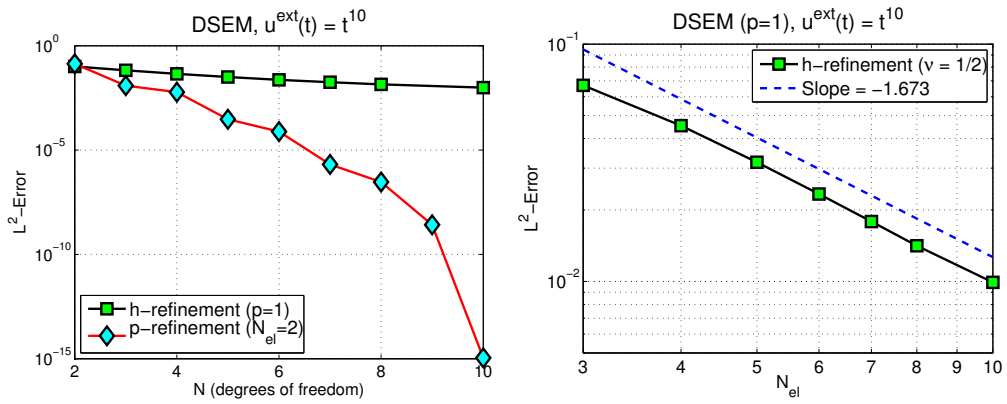

Figure 4.6: DSEM for FIVP: L^2-error of the approximate solution to FIVP ${}_0\mathcal{D}_t^\nu u(t) = f(t),\ t \in [0,1]$,, corresponding to $\nu = 1/2$; (left): log-linear plot of p-refinement compared to the h-refinement versus the degrees of freedom N; and (right): log-log plot of the error versus the number of elements N_{el}. Here, the exact solution is $u^{ext}(t) = t^{10}$.

$w(t)$ (DSM) and $w^e(t)$ (DSEM) become stronger as the fractional order ν possesses smaller values. It would suggest that the *global* character of the fractional differential operator in our problem becomes more significant as ν, leading to higher stiffness condition numbers. However, we notice in Fig. 4.5 that as $\nu \to 1$, we recover the standard condition number of the stiffness matrix corresponding to the integer-order (non-fractional) problem.

4.4.3 Numerical Tests for DSEM

The L^2-error of the approximate solution to FIVP ${}_0\mathcal{D}_t^\nu u(t) = f(t),\ t \in [0,1]$, using discontinuous spectral element method (DSEM), corresponding to $\nu = 1/2$ is shown in Fig. 4.6, where the exact solution is $u^{ext}(t) = t^{10}$. We compare the log-linear plot of p-refinement on the left to the h-refinement, where we observe the exponential convergence in the p-refinement and the algebraic convergence in the h-refinement. We show the algebraic convergence rate to be -1.673 in the log-log L^2-error plot on the right for $p = 1$ (linear element).

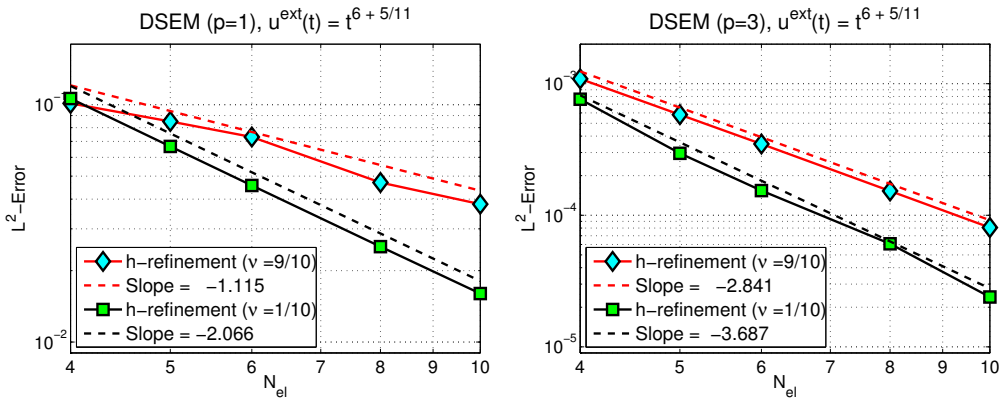

Figure 4.7: DSEM for FIVP: log-log L^2-error plot of the approximate solution to FIVP ${}_0\mathcal{D}_t^{\nu}u(t) = f(t),\ t \in [0,1]$, corresponding to $\nu = 1/10$ and $9/10$ versus the number of elements N_{el}. Here, the exact solution is $u^{ext}(t) = t^{6+5/11}$.

Next, we are going to examine the effect of the fractional order $\nu \in (0,1)$ on the order of algebraic convergence, where we require the exact solution to possess enough smoothness. To this end, we present the log-log L^2-error plot of the approximate solution to FIVP ${}_0\mathcal{D}_t^{\nu}u(t) = f(t),\ t \in [0,1]$, obtained using DSEM and corresponding to $\nu = 1/10$ and $9/10$ in Fig. 4.7. The exact solution in this numerical test is $u^{ext}(t) = t^{2+1/10}$, and the algebraic order of convergence obtained is -1.115 and -2.066 corresponding to $\nu = 1/10$ and $9/10$ respectively, when piecewise linear basis functions are employed. In the other test (Fig. 4.7; right), we employ piecewise cubic basis functions and we observe the convergence order to be -3.687 and -2.841 corresponding to $\nu = 9/10$ and $1/10$ respectively.

In the next test case, we address the issue of the long-time integration. Moreover, we observe that in some cases when the exact solution does not possess enough smoothness p-refinement may not be the best choice of improving the finite element space V_N. Accordingly, we take the FIVP ${}_0\mathcal{D}_t^{\nu}u(t) = f(t),\ t \in [0,10]$, where $\nu = 1/2$, for *long-time* integration in which the exact solution is $u^{ext}(t) = t^{1+1/10}$. The L^2-error of the approximate solution to the aforementioned problem using DSEM is shown in Fig. 4.8. The h-refinement top plot exhibits algebraic convergence with rates -1.890

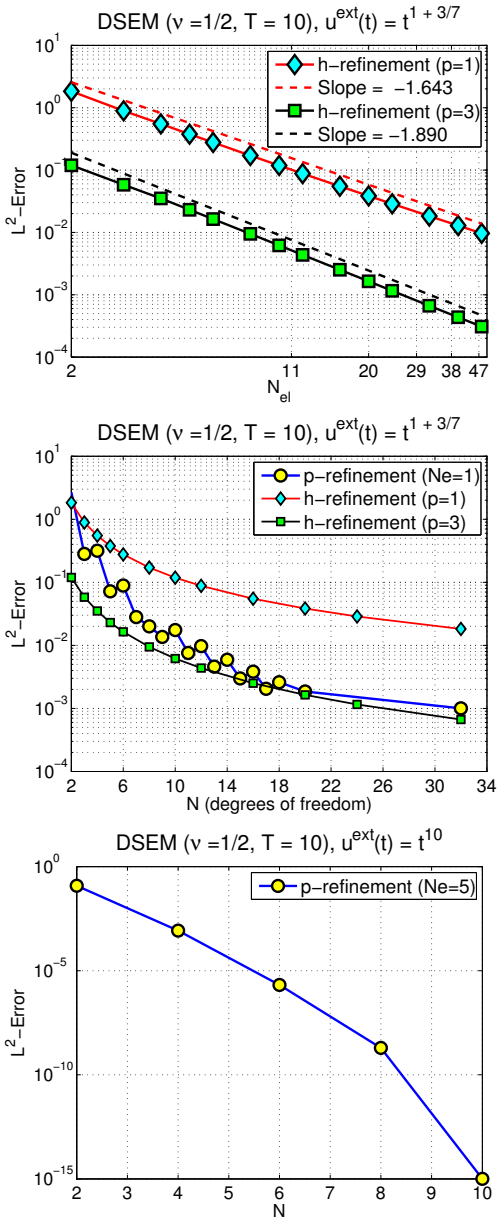

Figure 4.8: Long time integration: L^2-error of the approximate solution to FIVP ${}_0\mathcal{D}_t^{\nu} u(t) = f(t),\ t \in [0, 10]$, corresponding to $\nu = 1/2$ obtained using the discontinuous spectral element method (DSEM); (top): log-log plot of the h-refinement versus the number of elements N_{el}; (middle): log-linear plot of the error versus the number of degrees of freedom N, compared to the p-refinement; and (bottom) log-linear plot of the error versus the polynomial order in each element in the p-refinement. Here, the exact solution for the top and the middle plots is $u^{ext}(t) = t^{1+3/7}$, and we add to the regularity of the exact solution in the bottom plot where $u^{ext}(t) = t^{10}$.

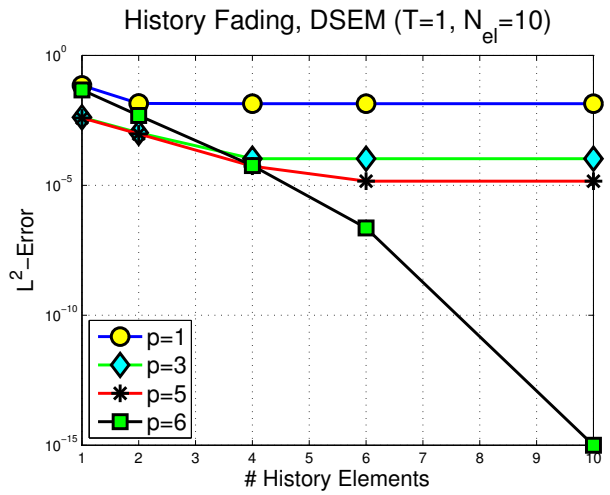

Figure 4.9: History fading in DSEM: the L^2-error of the numerical solution to FIVP ${}_0\mathcal{D}_t^\nu u(t) = f(t),\ t \in [0,1]$, corresponding to $\nu = 1/10$ and different polynomial order p, versus the number of the past elements considered in computation of history function (5.81). Here, the exact solution is $u^{ext}(t) = t^6$.

and -1.643 corresponding to $\nu = 1/10$ and $9/10$ respectively. In the middle plot, the log-linear plot of the error versus the number of degrees of freedom N, compared to the p-refinements is shown. We observe that the aforementioned h-refinements are shown to be lower and upper bounds for the decay of the error in the p-refinements. If we now increase the smoothness in the exact solution as presented in the lower plot, we recover the exponential convergence using p-refinement where we partition the domain into $N_{el} = 5$ elements.

Finally, we examine the idea of *memory fading/truncation* in the calculation of the history term (5.80). In this technique we do not take all the past elements into account at the expense of losing accuracy, and instead, an *effective history length* is chosen to calculate (5.80). Such an effective length is well-known to be dependent mainly on the fractional order ν. In fact, the greater ν in ${}_0\mathcal{D}_t^\nu u(t)$ the less history-length is needed since as $\nu \to 1$, we approach ${}_0\mathcal{D}_t^\nu \to d/dt$, which is completely a *local* operator for which no history is required. To this end, we solve ${}_0\mathcal{D}_t^\nu u(t) = f(t),\ t \in [0,1]$, partitioning the domain into $N_{el} = 10$ non-overlapping

uniform elements when the fractional order is $\nu = 1/10$. As shown in Fig. 4.9, in order to get the convergence down to machine precision, higher modes demand longer history lengths; therefore we need to include the whole history to achieve such an accuracy. We emphasize that such a phenomenon is independent of the discretization method and is solely due to the global nature of the fractional differential operators.

4.5 Discussion

We conclude this chapter by comparing the performance of the developed schemes with the finite difference method (FDM) developed in [111], where the fractional derivative ${}_0\mathcal{D}_t^\nu u(t)$ is represented as

$$ {}_0\mathcal{D}_t^\nu u(t) = \frac{1}{\Gamma(2-\nu)} \sum_{j=0}^{k} b_j \frac{u(t_{k+1-j}) - u(t_{k-j})}{(\Delta t)^\nu} + r_{\Delta t}^{k+1}, \tag{4.56} $$

where $r_{\Delta t}^{k+1} \leq C_u(\Delta t)^{2-\nu}$ and $b_j := (j+1)^{1-\nu} - j^{1-\nu}, j = 0, 1, \cdots, k$; a central difference method has been employed to approximate the kernel in the fractional derivative.

In Fig. 4.10, we have solved (4.1) using DSEM for having the $T = 10$; we plot the normalized L^2-error versus the number of the elements ($= T/\Delta t$) corresponding to the fractional order $\nu = 1/10$ and $\nu = 9/10$. In DSEM, we utilized both piecewise linear ($p = 1$) and piecewise cubic ($p = 3$) basis functions. First, we observe that when $\nu = 1/10$, DSEM ($p = 1$) performs slightly better than FDM in terms of the rate of the convergence in the range of h-refinement examined (see Fig. 4.10; Left). By increasing the fractional order to $\nu = 9/10$, we obtain a good agreement between the rate of convergence in FDM and DSEM ($p = 1$). However,

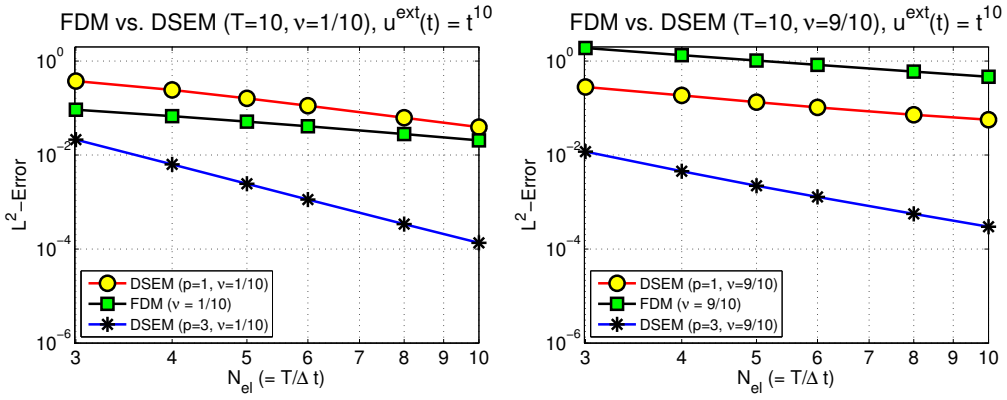

Figure 4.10: Finite difference method versus discontinuous spectral element method (DSEM); L^2-norm error (normalized by the L^2-norm of the exact solution) of the approximate solution to ${}_0\mathcal{D}_t^{\nu} u(t) = f(t)$, $T = 10$, corresponding to (Left): $\nu = 1/10$ and (Right): $\nu = 9/10$.

increasing the polynomial order p (from 1 to 3), DSEM leads to a noticeable faster convergence rate.

In addition to the fast convergence of the high-order methods developed in this work, we show that the computational cost (number of operations) in PG, DSM and DSEM asymptotically increases as $\mathcal{O}(N)$, $\mathcal{O}(N^3)$, $\mathcal{O}(N_{el}^2\ N^3)$, respectively, where N represents the polynomial order employed, and N_{el} denotes the number of elements. In contrast, the computational cost of FDM grows as N_g^2, where N_g stands for the number of the grid-points in the computational domain. Moreover, we compute the CPU time (in seconds) required for solving (4.1) corresponding to $\nu = 1/10$, $1/2$, and $9/10$ in Table 4.1, where the exact solution is $u^{ext}(t) = t^6$ and the integration time $T = 1$. We developed all codes in Wolfram *Mathematica* 8.0.4.0.

Although the implementation of FDM is simpler than the schemes developed in this study, it turns out that FDM becomes computationally prohibited, especially when we ask for slightly higher accurate results and ν is not necessarily close to zero. For instance, in order to reach the L^2-error of order 10^{-6} using FDM, we needed to include $N_g = 7500$ grid-points when $\nu = 1/2$. By increasing the fractional-order to $\nu = 9/10$, *Mathematica* ran out of memory and the error level 10^{-6} was not

achieved. In fact, it highlights the strong sensitivity of the CPU time in FDM on the fractional-order ν, in addition to the accuracy dependency of FDM on ν as shown in (4.56). In contrast, the corresponding memory allocation and CPU time in our schemes were considerably less than what needed in FDM. As shown in Table 4.1, while we *exactly* capture the solution by just setting the polynomial order to $N = 6$ in DSM and DSEM in all cases, the CPU time taken in FDM to reach the error level 10^{-6} (when $\nu = 1/2$) was almost 6500 times larger than that in PG spectral method, 1500 times larger than CPU time in DSM, and 850 times larger than that in DSEM. We also performed the CPU time comparison shown in Table 4.1 for the four test-cases shown in Fig. 4.1, and we obtained similar results.

Table 4.1: CPU time (seconds) on a Intel (Xeon X5550) 2.67GHz processor, corresponding to PG spectral method, DSM, DSEM, and FDM for solving ${}_0\mathcal{D}_t^{\nu} u(t) = f(t)$, $u(0) = 0$, and the exact solution is $u^{ext}(t) = t^6$. Here, N denotes the expansion order in PG spectral method, DSM, and DSEM with $N_{el} = 2$ (in each element), also N_g represents the number of grid points in FDM, and the simulation time is set to $T = 1$.

($\nu = 1/10$)

L^2-norm Error	PG Spectral Method	DSM	DSEM ($N_{el} = 2$)	FDM
$\mathcal{O}(10^{-4})$	($N = 6$) 0.0749885	($N = 5$) 0.251108	×	($N_g = 48$) 0.048815
$\mathcal{O}(10^{-5})$	×	×	($N = 5$) 0.390158	($N_g = 180$) 0.24374
$\mathcal{O}(10^{-6})$	($N = 7$) 0.0969855	($N = 6$) 0.344162 (exact)	($N = 6$) 0.652402 (exact)	($N_g = 640$) 3.74287

($\nu = 1/2$)

L^2-norm Error	PG Spectral Method	DSM	DSEM ($N_{el} = 2$)	FDM
$\mathcal{O}(10^{-4})$	($N = 6$) 0.0584915	($N = 5$) 0.235509	($N = 4$) 0.256461	($N_g = 340$) 0.966354
$\mathcal{O}(10^{-5})$	×	×	($N = 5$) 0.374215	($N_g = 1600$) 23.0223
$\mathcal{O}(10^{-6})$	($N = 7$) 0.073489	($N = 6$) 0.336951 (exact)	($N = 6$) 0.565914 (exact)	($N_g = 7500$) 480.12

($\nu = 9/10$)

L^2-norm Error	PG Spectral Method	DSM	DSEM ($N_{el} = 2$)	FDM
$\mathcal{O}(10^{-4})$	($N = 6$) 0.076988	($N = 5$) 0.244935	×	($N_g = 3000$) 74.5901
$\mathcal{O}(10^{-5})$	×	×	($N = 5$) 0.389906	($N_g = 23000$) 3348.96
$\mathcal{O}(10^{-6})$	($N = 7$) 0.097985	($N = 6$) 0.343947 (exact)	($N = 6$) 0.645917 (exact)	Running Out of Memory

Chapter Five

Fractional Delay Differential Equations

In this chapter, we aim to develop a spectrally accurate Petrov-Galerkin (PG) spectral method for fractional delay differential equations (FDDEs). This scheme is developed based on a new spectral theory for fractional Sturm-Liouville problems (FSLPs), which has been recently presented in [187]. Specifically, we obtain solutions to FDDEs in terms of new non-polynomial basis functions, called *Jacobi polyfractonomials*, which are the eigenfunctions of the FSLP of *first* kind (FSLP-I). Correspondingly, we employ another space of test functions as the span of polyfractonomial eigenfunctions of the FSLP of *second* kind (FSLP-II). We prove the wellposedness of the problem and carry out the corresponding stability and error analysis of the PG spectral method. In contrast to standard (non-delay) fractional differential equations (FDEs), the delay character of FDDEs might induce solutions, which are either non-smooth or piecewise smooth. In order to effectively treat such cases, we first develop a discontinuous spectral method (DSM) of Petrov-Galerkin type for FDDEs, where the basis functions do not satisfy the initial conditions. Consequently, we extend the DSM scheme to a discontinuous spectral element method (DSEM) for possible adaptive refinement and long time-integration. In DSM and DSEM schemes, we employ the *asymptotic* eigensolutions to FSLP-I&-II, which are of Jacobi polynomial form, both as basis and test functions. Our numerical tests demonstrate spectral convergence for a wide range of FDDE model problems with different benchmark solutions.

5.1 Background

Time-fractional differential equations (FDEs) appear in science and engineering applications as mathematical models representing sub-diffusive transport with long history effects. Examples are chemical and contaminant transport in heterogeneous

aquifers [10], transport of passive tracers carried by fluid flow in a porous medium in groundwater hydrology [156], propagation of mechanical diffusive waves in viscoelastic media [116], long-time memory in financial time series [139], etc. More applications of FDEs in the fields of physics, biology, chemistry and finance can be found in [4, 89, 155].

In some of these systems with sub-diffusive processes, the future state is to some extent determined by their history. For such problems, delay terms cannot be omitted in spite of the whole history being considered by the FDEs. For example, many automatic control systems with feedback contain time delay [105, 160]; time delay may also exist in random walk [133]. In modeling HIV infection of $CD4^+T$-cells, time delay describes the time between infection of $CD4^+T$-cells and the emission of viral particles on a cellular level [44, 181].

Mathematical Model: The scalar time-fractional differential equation with constant time delay (FDDEs) has the general form:

$$\begin{aligned} {}_0\mathcal{D}_t^{\nu} u(t) &= f\Big(t, u(t), u(\,t-\tau\,)\Big), \quad t \in [0,T], \\ u(t) &= \xi(t), t \in [-\tau, 0], \end{aligned} \tag{5.1}$$

where τ is a positive fixed delay, $0 < \nu \leq 1$, the function $f : [0,T] \times \mathbb{R} \times \mathbb{R} \to \mathbb{R}$, and $\xi(t)$ is the given solution at the initial time-segment. Here, the fractional differential operator ${}_0\mathcal{D}_t^{\nu}$ can be defined in many closely connected ways as the generalization of the *integer-order* time-derivative to a *fractional-order* one. In the limit-case as $\nu \to 1$, equation (5.1) becomes $u'(t) = f(t, u(t), u(t-\tau))$, which is the classical delay differential equation (DDE). For properties of analytical solutions and numerical

methods for DDEs, we refer to [16, 65]. If the delay term $u(\,t-\tau\,)$ is not present, it reduces to a time-fractional differential equation ${}_0\mathcal{D}_t^{\nu}u(t) = f(t, u(t))$. For existence, uniqueness and stability of analytical solutions of FDEs, see [50, 142].

There are also other types of time delay in modeling of industrial and engineering problems. For instance, wave motion in the overhead supply line to an electrified railway system is modeled by $y'(x) = f(y(x), y(qx))$ with initial condition $y(0)$, where $0 \leq x < \infty$, $0 < q < 1$ and qx is called pantograph delay; for more details see [79, 62, 2].

Literature Review: Recently, many authors have studied the properties of FDDEs theoretically. Deng et al. [48] used Laplace transform and the characteristic equation to study the stability of n-dimensional linear FDDEs. Lakshmikantham [102] developed the basic theory for the initial value problems for fractional functional differential equations (substitute $u(t-\tau)$ with $u_t(s) = u(t+s)$, $-\tau \leq s \leq 0$ in (5.1)), and he discussed both local and global existence of solutions. Moreover, the existence and stability of solutions of linear fractional system with input and state delays are discussed in [105, 160]. In addition, Morgado, Ford and Lima [129] discussed existence, uniqueness and stability of analytical solution for the one-dimensional linear version of equation (5.1); for more results see [19, 78, 97, 175]. Moreover, existence and uniqueness of impulsive differential equations of fractional order with infinite delay has been studied in [18, 17].

The time delay in (5.1) causes the solution at current time to rely on the solution information at certain past time. Furthermore, due to the definition of the fractional order derivative, it is a nonlocal operator, which means that the fractional order derivative requires a longer history of the solution at previous time-steps than what the delay term provides. In fact, in the former case, the solution at a time t_n

only depends on the solution at t_{n-1} and a certain previous time-step $t_n - \tau$, while in the latter, it depends on the whole history $t < t_n$. When the time delay τ is comparatively large, computations may run into storage problems when high accuracy is demanded and a small time-step size is taken. The globality of the non-integer order derivative makes the design of accurate and fast methods more difficult. In view of finite-difference approaches and multi-step/multi-stage time-integration methods, it is a big challenge when all the past history of the solution has to be saved in order to compute the solution at the current time. This would prohibit large-scale simulation of systems characterized by FDDEs especially where highly accurate simulations are needed. Hence, due to the global nature of such problems, developing high-order global numerical methods for FDDEs is an effective approach to overcome this barrier.

Spectral methods and discontinuous Galerkin (DG) methods for time and/or space discretization of FDEs have been employed before. Li and Xu [110] proposed a spectral method for temporal discretization of the time-fractional diffusion equation and provided *a priori* error estimates. In [130], Mustapha and Mclean applied a piecewise-linear DG method for time discretization and proved its super-convergence at the nodes. Khader et al. [85] developed a spectral collocation method based on the generalized Laguerre polynomials for solving multi-term fractional orders initial value problems. For finite-difference methods and other numerical methods for FDEs, see [61, 107, 132, 141].

With respect to FDDEs, a number of works have appeared in the literature. Khader and Hendy [87] proposed a Legendre pseudo-spectral method. Bhalekar [21] transformed the FDDE to the Volterra integral equation for which they provided an algorithm based upon a composite trapezoidal quadrature formula and a predictor-corrector method. Wang [176] provided an iterative algorithm and proved that it

is convergent to Grünwald-Letnibov derivative under Lipschitz conditions. In [167], Sweilam et al. studied the Chebyshev spectral method for the fractional order logistic differential equation with two delays. They also considered the fractional complex transform and variational iteration method to solve the equation.

Motivation: The objective of our paper is to develop generalized and spectrally accurate spectral and spectral element methods for deterministic FDDEs ${}_0\mathcal{D}_t^{\nu}u(t) = h(t) - A(t)u(t) - B(t)u(g_\tau(t))$ subject to homogeneous Dirichlet initial condition. To this end, we first develop a Petrov-Galerkin (PG) spectral method whose corresponding stiffness matrix is *diagonal* and the corresponding *mass* and *delay mass* matrices are obtained exactly. Moreover, we study the wellposedness of the problem and then carry out the corresponding stability and convergence analysis of our scheme. Subsequently, we develop a discontinuous spectral method (DSM) of Petrov-Galerkin type with *exact* quadrature rules for the aforementioned FDDEs. This scheme is also extended to a discontinuous spectral element method (DSEM) for efficient longer time-integrations and adaptive refinement. These schemes are developed based on a new spectral theory for fractional Sturm-Liouville problems (FSLPs) in [187] and in continuation to the recent work on high-order methods for (non-delay) fractional ODEs [189]. In addition, these eigenfunctions have been recently employed as *space-time* bases for solving fractional advection equation in [188], and, their corresponding *nodal* representations were used to develop fractional spectral collocation methods for non-delay fractional ODEs/PDEs [190].

We examine a wide range of exact solutions with constant and time-dependent coefficients $A(t)$ and $B(t)$. We consider the delay term $u(g_\tau(t))$ to be of $u(t-\tau)$, pantograph type $u(qt)$ and harmonic delay form $u(q\sin(\pi t))$. Consistently, in all the aforementioned test cases and schemes, spectral convergence of the L^2-norm error is

achieved. We furthermore examine delay problems whose exact solutions are discontinuous and by employing the DSEM scheme we recover the spectral convergence.

5.2 Notation and Problem Definition

For simplicity, we rewrite the FDDE of order $\nu \in (0, 1]$ as

$$\begin{aligned} {}_0\mathcal{D}_t^\nu u(t) &= h(t) - A(t)u(t) - B(t)u(g_\tau(t)), t \in [0, T], \\ u(0) &= u_0(t), \quad t \in [g_\tau(0), 0], \end{aligned} \tag{5.2}$$

where $u(g_\tau(t))$ is the term with time delay (we call it delay term in the following) and $g_\tau(t)$ could be $t - \tau$, qt or another function of t with $g_\tau(0) \leq 0$ and $g_\tau(t) \leq t$ for $t > 0$. Here, $u_0(t)$ is the initial function when $g_\tau(0) < 0$ and the initial value when $g_\tau(0) = 0$. We choose $u_0(t) \equiv u_0$ in all cases in this paper. ${}_0\mathcal{D}_t^\nu$ denotes the left-sided Reimann-Liouville fractional derivative of order $\nu \in (0, 1]$ following [142], defined as

$${}_0\mathcal{D}_t^\nu u(t) = \frac{1}{\Gamma(1-\nu)} \frac{d}{dt} \int_0^t \frac{u(s)ds}{(t-s)^\nu}, \quad t > 0, \tag{5.3}$$

where Γ represents the Euler gamma function. We could also define the fractional differential operators in (5.2) to be the Caputo fractional derivatives ${}_0^C\mathcal{D}_t^\nu$. In fact, this fractional operator can be defined by (5.3), where the order of the integration and differentiation is reversed. However, the two definitions are closely linked by the following relationship

$${}_0\mathcal{D}_t^\nu u(t) = \frac{u(0)}{\Gamma(1-\nu)\ t^\nu} + {}_0^C\mathcal{D}_t^\nu u(t). \tag{5.4}$$

Hence, when $u_0 = 0$ in (5.2), these problems become identical to the corresponding problems with the Caputo derivatives by virtue of (5.4).

5.3 Petrov-Galerkin Spectral Method: Continuous & Single-Domain

As the first step, we develop a Petrov-Galerkin (PG) spectral method for the FDDE (5.2), subject to homogeneous Dirichlet initial conditions. To this end, we introduce the proper spaces of *basis* and *test* functions, where the basis functions satisfy the homogeneous initial-condition exactly. Later, we shall show how this scheme can be generalized for any non-zero Dirichlet initial conditions. Hence, we denote the following spaces

$$\begin{aligned} U_N &= span\{t^{\mu} P_n^{-\mu,\mu}(\frac{2}{T}t - 1),\ n = 0, 1, \cdots, N-1\}, \\ W_N &= span\{(T-t)^{\mu} P_n^{\mu,-\mu}(\frac{2}{T}t - 1),\ n = 0, 1, \cdots, N-1\}. \end{aligned}$$

Then, the numerical scheme is to find $u_N \in U_N$ such that

$$({}_0\mathcal{D}_t^{\mu} u_N, {}_t\mathcal{D}_T^{\mu} w) = (h - Au_N - Bu_{N,g_\tau}, w), \quad w \in W_N. \tag{5.5}$$

In what follows, we further elaborate on the choice of basis and test functions and their key properties.

5.3.1 Space of Basis Functions

Here, we employ

$$ {}^{(1)}\mathcal{P}_n^{\,\mu}(x) = (1+x)^{\mu} P_{n-1}^{-\mu,\mu}(x), \quad x \in [-1,1], \tag{5.6} $$

as our basis functions, which are the explicit fractional eigenfunctions of fractional Sturm-Liouville problem in [187]. Now, let $u_0 = 0$ and $t \in [0,T]$. Then,

$$ {}^{(1)}\widetilde{\mathcal{P}}_n^{\,\mu}(t) = \left(\frac{2}{T}\right)^{\mu} t^{\mu} P_{n-1}^{-\mu,\mu}(\,x(t)\,) \tag{5.7} $$

represent the shifted basis functions of fractional order $(n-1+\mu)$ that is obtained through the affine mapping $x = 2t/T - 1$, transforming the standard interval $[-1,1]$ to $[0,T]$. From the properties of the eigensolutions in [187], the left-sided Riemann-Liouville fractional derivative of (5.7) is given as

$$ {}_0\mathcal{D}_t^{\,\mu}\left({}^{(1)}\widetilde{\mathcal{P}}_n^{\,\mu}(\,t\,)\right) = \left(\frac{2}{T}\right)^{\mu} {}_{-1}\mathcal{D}_x^{\,\mu}\left({}^{(1)}\mathcal{P}_n^{\,\mu}(x)\right) = \left(\frac{2}{T}\right)^{\mu} \frac{\Gamma(n+\mu)}{\Gamma(n)} P_{n-1}(\,x(t)\,), \tag{5.8} $$

stating that the μ^{th} order fractional derivative of such fractional (non-polynomial) basis functions of order $(n-1+\mu)$ is a standard Legendre polynomials of integer order $(n-1)$. Moreover, since $u(0) = u_0 = 0$, the aforementioned Riemann-Liouville fractional derivative is identical to the one of Caputo type by virtue of (5.4).

5.3.2 Space of Test Functions

We test (5.2) against a different set of test functions, which are eigenfunctions of the FSLP of second kind, explicitly obtained in [187] as

$$ {}^{(2)}\mathcal{P}_k^{\mu}(x) = (1-x)^{\mu} P_{k-1}^{\mu,-\mu}(x), \quad x \in [-1,1], \tag{5.9} $$

in our weak formulation. By carrying out the same affine mapping $x = 2t/T - 1$, we can obtain the shifted test functions

$$ {}^{(2)}\widetilde{\mathcal{P}}_k^{\mu}(\,t\,) = (\frac{2}{T})^{\mu}\,(T-t)^{\mu} P_{k-1}^{\mu,-\mu}(\,x(t)\,), \tag{5.10} $$

corresponding to the interval $[0,T]$. Now, following [187], the right-sided Riemann-Liouville fractional derivative of (5.10) is obtained as

$$ {}_t\mathcal{D}_T^{\mu}\left({}^{(2)}\widetilde{\mathcal{P}}_k^{\mu}(t)\right) = \left(\frac{2}{T}\right)^{\mu} {}_x\mathcal{D}_{+1}^{\mu}\left({}^{(2)}\mathcal{P}_k^{\mu}(x)\right) = \left(\frac{2}{T}\right)^{\mu} \frac{\Gamma(k+\mu)}{\Gamma(k)} P_{k-1}(\,x(t)\,). \tag{5.11} $$

Having defined the basis and test functions, next we recall the following lemma in order to obtain the variational form in the Petrov-Galerkin spectral method.

Lemma 5.3.1. *[108]: For all $0 < \xi < 1$, if $u \in H^1([0,T])$ such that $u(0) = 0$ and $w \in H^{\xi/2}([0,T])$, then*

$$ ({}_0\mathcal{D}_t^{\xi} u, w)_{[0,T]} = (\,{}_0\mathcal{D}_t^{\xi/2} u\,,\, {}_t\mathcal{D}_T^{\xi/2} w\,)_{[0,T]}, \tag{5.12} $$

where $(\cdot,\cdot)_{[0,T]}$ denotes the standard inner product in the interval $[0,T]$.

The following lemmas are also useful in our analysis throughout the paper.

Lemma 5.3.2. *[5] For $\mu > 0$, $\alpha > -1$, $\beta > -1$, and $\forall x \in [-1, 1]$*

$$(1+x)^{\beta+\mu} \frac{P_n^{\alpha-\mu,\beta+\mu}(x)}{P_n^{\alpha-\mu,\beta+\mu}(-1)} = \frac{\Gamma(\beta+\mu+1)}{\Gamma(\beta+1)\Gamma(\mu)P_n^{\alpha,\beta}(-1)} \int_{-1}^{x} \frac{(1+s)^{\beta}\ P_n^{\alpha,\beta}(s)}{(x-s)^{1-\mu}} ds, \quad (5.13)$$

and

$$(1-x)^{\alpha+\mu} \frac{P_n^{\alpha+\mu,\beta-\mu}(x)}{P_n^{\alpha+\mu,\beta-\mu}(+1)} = \frac{\Gamma(\alpha+\mu+1)}{\Gamma(\alpha+1)\Gamma(\mu)P_n^{\alpha,\beta}(+1)} \int_{x}^{1} \frac{(1-s)^{\alpha}\ P_n^{\alpha,\beta}(s)}{(s-x)^{1-\mu}} ds. \quad (5.14)$$

By the definition of the left-sided Riemann-Liouville integral ${}^{RL}_{-1}\mathcal{I}^{\mu}_{x}$ and evaluating the special end-values $P_n^{\alpha-\mu,\beta+\mu}(-1)$ and $P_n^{\alpha,\beta}(-1)$, we can re-write (10.16) as

$${}^{RL}_{-1}\mathcal{I}^{\mu}_{x}\Big\{(1+x)^{\beta}P_n^{\alpha,\beta}(x)\Big\} = \frac{\Gamma(n+\beta+1)}{\Gamma(n+\beta+\mu+1)}(1+x)^{\beta+\mu}\ P_n^{\alpha-\mu,\beta+\mu}(x). \quad (5.15)$$

Now, by taking the fractional derivative ${}^{RL}_{-1}\mathcal{D}^{\mu}_{x}$ on both sides of (5.15) when $\beta = -\mu$ we obtain

$${}^{RL}_{-1}\mathcal{D}^{\mu}_{x}\Big\{P_n^{\alpha-\mu,0}(x)\Big\} = \frac{\Gamma(n+1)}{\Gamma(n-\mu+1)}(1+x)^{-\mu}P_n^{\alpha,\,-\mu}(x). \quad (5.16)$$

By the definition of the right-sided Riemann-Liouville integral ${}^{RL}_{x}\mathcal{I}^{\mu}_{1}$ and evaluating the special end-values $P_n^{\alpha-\mu,\beta+\mu}(+1)$ and $P_n^{\alpha,\beta}(+1)$, we can re-write (10.17) as

$${}^{RL}_{x}\mathcal{I}^{\mu}_{1}\Big\{(1-x)^{\alpha}P_n^{\alpha,\beta}(x)\Big\} = \frac{\Gamma(n+\alpha+1)}{\Gamma(n+\alpha+\mu+1)}(1-x)^{\alpha+\mu}P_n^{\alpha+\mu,\beta-\mu}(x). \quad (5.17)$$

In a similar fashion, by taking the fractional derivative ${}^{RL}_{x}\mathcal{D}^{\mu}_{-1}$ on both sides of (6.21) when $\alpha = -\mu$ we obtain

$${}^{RL}_{x}\mathcal{D}^{\mu}_{1}\Big\{P_n^{0,\beta-\mu}(x)\Big\} = \frac{\Gamma(n+1)}{\Gamma(n-\mu+1)}(1-x)^{-\mu}P_n^{-\mu,\beta}(x). \quad (5.18)$$

5.3.3 Stability and Error Analysis

We consider (5.2) under the following assumption:

Assumption 5.3.3. A and B are constants and $u(g_\tau(t)) = u(t-\tau)$.

Let h be a continuous function on $[0,T]$ also the initial condition $\phi(t)$ be continuous on $[-\tau,0]$. We denote by $\|v\|$ the L^2-norm of v over the domain $[0,T]$. Define the norm $\|v\|_\mu = (\|v\|^2 + \|{}_0\mathcal{D}_t^\mu v\|^2)^{1/2}$ and its associated Sobolev space

$$H^\mu([0,T]) = \left\{v | v, {}_0\mathcal{D}_t^\mu v \in L^2([0,T])\right\}. \tag{5.19}$$

The space $H^{-\mu}([0,T])$ is the dual of $H^\mu([0,T])$ with respect to the L^2-inner product. We denote the norm in $H^{-\mu}([0,T])$ by $\|\cdot\|_{-\mu}$. The space $C([0,T])$ is the space of continuous functions over $[0,T]$ with maximum norm.

Wellposedness of Problem (5.2)

Theorem 5.3.4. *Assume that the function h is continuous on $[0,T]$, $\phi(t) = 0$ and $\varepsilon := A - |B| + C_p^{-1} > 0$, where the constant C_p is from the following Poincare inequality*

$$\|v\|^2 \le C_p \int_0^T {}_0\mathcal{D}_t^\mu v(t)\, {}_t\mathcal{D}_T^\mu v(t) dt, \quad \forall v \in H^\mu([0,T]) \cap \{v | v \in C[0,T],\, v(0) = 0\}. \tag{5.20}$$

Then for any $0 < \nu < 1$, there exists a constant $C > 0$ such that the solution of the problem (5.2) *sunder the assumption* (5.3.3)*, u, satisfies*

$$\|{}_0\mathcal{D}_t^\mu u\| + \|u\| \le C \|h\|_{-\mu}, \tag{5.21}$$

where C depends on A, B, C_p, μ and T.

Proof. We recall that there exists a unique continuous solution to (5.2) sunder the assumption (5.3.3), see [129]. Define the following bilinear form: for $u \in H^\mu([0,T])$ and $v \in H^\mu([0,T])$

$$a(u,v) := \int_0^T {}_0\mathcal{D}_t^\mu u(t)\, {}_t\mathcal{D}_T^\mu v(t)dt + A\int_0^T u(t)v(t)dt + B\int_0^T u_\tau(t)v(t)\,dt. \quad (5.22)$$

and the linear functional $\mathcal{F}(v) = \int_0^T h(t)v(t)dt$. We first prove the coercivity. We need the following conclusion, see e.g. [110, Lemma 2.4]: there are positive constants C_1 and C_2, such that for any $v \in H^\mu([0,T])$

$$C_1\int_0^T {}_0\mathcal{D}_t^\mu v(t)\, {}_t\mathcal{D}_T^\mu v(t)dt \le \|{}_0\mathcal{D}_t^\mu v\|^2 \le C_2\int_0^T {}_0\mathcal{D}_t^\mu v(t)\, {}_t\mathcal{D}_T^\mu v(t)dt. \quad (5.23)$$

By Cauchy inequality, (5.20) and (5.23), we have

$$\begin{aligned} a(u,u) &= \int_0^T {}_0\mathcal{D}_t^\mu u(t)\, {}_t\mathcal{D}_T^\mu u(t)\,dt + A\|u\|^2 + B\int_0^T u_\tau(t)u(t)\,dt \\ &\ge \int_0^T {}_0\mathcal{D}_t^\mu u(t)\, {}_t\mathcal{D}_T^\mu u(t)\,dt + (A-|B|)\|u\|^2 \\ &= \int_0^T {}_0\mathcal{D}_t^\mu u(t)\, {}_t\mathcal{D}_T^\mu u(t)\,dt + (\varepsilon - C_p^{-1})\|u\|^2 \\ &\ge \min(1,\varepsilon C_p)\int_0^T {}_0\mathcal{D}_t^\mu u(t)\, {}_t\mathcal{D}_T^\mu u(t)\,dt \ge C_2^{-1}\min(1,\varepsilon C_p)\,\|{}_0\mathcal{D}_t^\mu u\|^2. \end{aligned}$$

Then we conclude from here and (5.23) that there exists a constant $C > 0$ such that

$$a(u,u) \ge C\|u\|_\mu^2. \quad (5.24)$$

It can be readily checked that by the Cauchy inequality, (5.23) and the fact that

$\| {}_t\mathcal{D}_T^\mu v\|_{L^2([0,T])}$ is equivalent to $\| {}_0\mathcal{D}_t^\mu v\|_{L^2([0,T])}$ (see e.g. [59]), we have

$$a(u,v) \le (C_2 + |A| + |B|) \|u\|_\mu \|v\|_\mu . \tag{5.25}$$

The linear functional $\mathcal{F}(v)$ is bounded by $|\mathcal{F}(v)| \le \|v\|_\mu \|h\|_{-\mu}$. Then by (5.24), (5.25) and Lax-Millgram therorem, we have the well-posedness of the following problem: given any $h \in H^{-\mu}([0,T])$, find $u \in H^\mu([0,T])$, such that

$$a(u,v) = F(v), \quad v \in H^\mu([0,T]),$$

and thus (5.21) holds. □

Stability and Error Estimates of the Numerical Solution

We note that (5.2) sunder the assumption (5.3.3) can be written in an equivalent form

$$\begin{aligned} u(t) &= {}_0\mathcal{I}_t^\mu {}_0\mathcal{I}_t^\mu [h - Au - Bu_\tau],\ t \in [0,T], \\ u(t) &= 0,\ t \in [-\tau, 0]. \end{aligned} \tag{5.26}$$

Defining $v = {}_t\mathcal{D}_T^\mu w$, where $w \in W_N$. By the property of the fractional integral (6.21) and derivative (5.11), we have $w = {}_t\mathcal{I}_T^\mu v$ and $v \in V_N$, where

$$V_N = span\{P_n(\frac{2}{T}t - 1),\ n = 0, 1, \cdots, N-1\}.$$

Then the numerical scheme (5.5) can be written in an equivalent form:

$$({}_0\mathcal{D}_t^{\mu} u_N, v) = ({}_0\mathcal{I}_t^{\mu}[h - Au_N - Bu_{N,\tau}], v), \quad \forall v \in V_N. \tag{5.27}$$

where we have used the argument of integration by parts (5.3.1) and the projection P_N from $L^2([0,T])$ to V_N is defined by

$$(z - P_N z, v) = 0, \quad \forall v \in V_N.$$

When $z \in H^r([0,T])$ and $r \geq 0$, we then have, see [29, Chapter 5]

$$\|P_N z - z\| \leq CN^{-r} \left\|\partial_x^r z\right\|. \tag{5.28}$$

Then we can represent (5.27) by

$$P_{N0}\mathcal{D}_t^{\mu} u_N = P_{N0}\mathcal{I}_t^{\mu}[h - Au_N - Bu_{N,\tau}], \tag{5.29}$$

or simply, by ${}_0\mathcal{D}_t^{\mu} u_N \in V_N$,

$${}_0\mathcal{D}_t^{\mu} u_N = P_{N0}\mathcal{I}_t^{\mu}[h - Au_N - Bu_{N,\tau}]. \tag{5.30}$$

Noticing that ${}_0\mathcal{D}_t^{\mu} u_N \in V_N$ and take ${}_0\mathcal{I}_t^{\mu}$ over both side of (5.29), we have

$$P_N^{\mu} u_N = P_{N0}^{\mu}\mathcal{I}_t^{\mu} P_{N0}\mathcal{I}_t^{\mu}[h - Au_N - Bu_{N,\tau}], \tag{5.31}$$

where $P_N^{\mu} u_N = t^{\mu} P_N(t^{-\mu} u_N)$ or we can simply write

$$u_N = {}_0\mathcal{I}_t^{\mu} P_{N0}\mathcal{I}_t^{\mu}[h - Au_N - Bu_{N,\tau}], \tag{5.32}$$

because ${}_0\mathcal{I}_t^\mu V_N = U_N$ which can be readily checked by the the property of the fractional integral (5.15).

The numerical solution (5.32) can be rewritten as

$$\begin{aligned} u_N + A\,{}_0\mathcal{I}_t^\nu u_N + B\,{}_0\mathcal{I}_t^\nu u_{N,\tau} &= {}_0\mathcal{I}_t^\mu P_{N0}\mathcal{I}_t^\mu[-Au_N - Bu_{N,\tau}] - {}_0\mathcal{I}_t^\nu[-Au_N - Bu_{N,\tau}] \\ &\quad + {}_0\mathcal{I}_t^\mu P_{N0}\mathcal{I}_t^\mu h. \end{aligned}$$

By Theorem 5.3.4, we have

$$\|{}_0\mathcal{D}_t^\mu u_N\| + \|u_N\| \le C(\|P_{N0}\mathcal{I}_t^\mu[-Au_N - Bu_{N,\tau}] - {}_0\mathcal{I}_t^\mu[-Au_N - Bu_{N,\tau}]\| + \|P_{N0}\mathcal{I}_t^\mu h\|). \tag{5.33}$$

It requires to estimate $\|P_{N0}\mathcal{I}_t^\mu[-Au_N - Bu_{N,\tau}] - {}_0\mathcal{I}_t^\mu[-Au_N - Bu_{N,\tau}]\|$. We have

$$\begin{aligned} &\|P_{N0}\mathcal{I}_t^\mu[-Au_N - Bu_{N,\tau}] - {}_0\mathcal{I}_t^\mu[-Au_N - Bu_{N,\tau}]\| \\ \le\ & CN^{-\mu}\,\|-Au_N - Bu_{N,\tau}\| \le CN^{-\mu}\,\|u_N\|\,. \end{aligned} \tag{5.34}$$

where we have used (5.28) and the fact that

$$\|{}_0\mathcal{I}_t^\mu v\|_{H^\mu} \le C\,\|v\|\,.$$

Then by (5.33), we have

$$\|{}_0\mathcal{D}_t^\mu u_N\| + \|u_N\| \le CN^{-\mu}\,\|u_N\| + \|{}_0\mathcal{I}_t^\mu h\|\,. \tag{5.35}$$

When $h = 0$, we take N to $+\infty$, we have $\|u_N\| = 0$ and thus $u_N = 0$. This proves

the stability of the numerical scheme (5.5) .

Theorem 5.3.5 (Convergence rate)**.** *In addition to the assumptions in Theorem 5.3.4, assume also that the solution to* (5.2) *under the assumption* (5.3.3) $u \in H^m([0,T])$ *and* $t^{-\mu}u \in H^k([0,T])$ *and* $h \in H^r([0,T])$*. Let* u_N *be the solution to* (5.2) *under the assumption* (5.3.3)*. Then there exists a positive constant* C *independent of* N *such that*

$$\|u - u_N\| \leq C(N^{-\mu-r}\|\partial_t^r h\| + N^{-m+\mu}\|\partial_t^m u\| + N^{-\mu-k}\left\|\partial_t^k(t^{-\mu}u)\right\|). \tag{5.36}$$

Moreover, we have

$$\|u - u_N\| \leq C(N^{-\mu-r}\|\partial_t^r h\|_{\omega^{r,r}} + N^{-m+\mu}\|\partial_t^m u\|_{\omega^{m,m}} + N^{-\mu-k}\left\|\partial_t^k(t^{-\mu}u)\right\|_{\omega^{k,k}}), \tag{5.37}$$

when all the weighted norms are bounded. Here $\|v\|_{\omega^{r,r}} = (\int_0^T v^2 t^r (T-t)^r\, dt)^{1/2}$.

Proof. Let $e_N = u_N - P_N^\mu u$ and $\eta = P_N^\mu u - u$. By (5.26) and (5.31), we have the following error equation,

$$\begin{aligned} e_N + A\,{}_0\mathcal{I}_t^\nu e_N + B\,{}_0\mathcal{I}_t^\nu e_{N,\tau} &= {}_0\mathcal{I}_t^\mu P_{N0}\mathcal{I}_t^\mu[-Ae_N - Be_{N,\tau}] - {}_0\mathcal{I}_t^\nu[-Ae_N - Be_{N,\tau}] \\ &\quad + {}_0\mathcal{I}_t^\mu P_{N0}\mathcal{I}_t^\mu[-A\eta - B\eta_\tau] + [{}_0\mathcal{I}_t^\mu P_{N0}\mathcal{I}_t^\mu h - {}_0\mathcal{I}_t^\nu h] \\ &\quad + [{}_0\mathcal{I}_t^\mu P_{N0}\mathcal{I}_t^\mu\,{}_0\mathcal{D}_t^\nu u - {}_0\mathcal{I}_t^\nu\,{}_0\mathcal{D}_t^\nu u], \end{aligned}$$

where we also used the fact that ${}_0\mathcal{D}_t^\mu u = {}_0\mathcal{I}_t^\mu[h - Au(t) - Bu_\tau]$.

Similar to the proof of (5.33) and (5.35), we have

$$\begin{aligned}\|{}_0\mathcal{D}_t^\mu e_N\| + \|e_N\| &\leq C\left\|P_{N0}\mathcal{I}_t^\mu[-Ae_N - Be_{N,\tau}] - {}_0\mathcal{I}_t^\mu[-Ae_N - Be_{N,\tau}]\right\| \\ &\quad + \|P_{N0}\mathcal{I}_t^\mu[-A\eta - B\eta_\tau]\| + \left\|{}_0\mathcal{I}_t^\mu P_{N0}\mathcal{I}_t^\mu h - {}_0\mathcal{I}_t^\mu h\right\| \\ &\quad + \left\|P_{N0}\mathcal{I}_t^\mu {}_0\mathcal{D}_t^\nu u - {}_0\mathcal{I}_t^\mu {}_0\mathcal{D}_t^\nu u\right\|. \end{aligned} \tag{5.38}$$

Similar to the proof of (5.34), we have

$$\begin{aligned}\left\|P_{N0}\mathcal{I}_t^\mu[-Ae_N - Be_{N,\tau}] - {}_0\mathcal{I}_t^\mu[-Ae_N - Be_{N,\tau}]\right\| &\leq CN^{-\mu}\|e_N\|, \\ \left\|P_{N0}\mathcal{I}_t^\mu h - {}_0\mathcal{I}_t^\mu h\right\| &\leq CN^{-\mu-r}\left\|\partial_t^r h\right\|, \\ \left\|P_{N0}\mathcal{I}_t^\mu {}_0\mathcal{D}_t^\nu u - {}_0\mathcal{I}_t^\mu {}_0\mathcal{D}_t^\nu u\right\| &\leq CN^{-m+\mu}\left\|\partial_t^m u\right\|. \end{aligned} \tag{5.39}$$

Recall that $\eta = P_N^\mu u - u$ and $P_N^\mu u = t^\mu P_N(t^{-\mu}u)$. Then by (5.28), we have

$$\|P_{N0}\mathcal{I}_t^\mu[-A\eta - B\eta_\tau]\| \leq CN^{-\mu}\|A\eta + B\eta_\tau\| \leq CN^{-\mu}\|\eta\| \leq CN^{-\mu-k}\left\|\partial_t^k(t^{-\mu}u)\right\|. \tag{5.40}$$

Then by (5.38), (5.39) and (5.40), we obtain (5.36) via the triangle inequality. The estimate (5.37) can be obtained similarly if we use the following estimate (see e.g. [40])

$$\|P_N z - z\| \leq CN^{-r}\left\|\partial_x^r z\right\|_{\omega^{r,r}}.$$

instead of the estimate (5.28). □

Remark 5.3.6. It is possible to obtain a sharper estimate for the convergence rate when the solutions and h belongs to some subspace of the employed Sobolev spaces. For example, when the solution belongs to some weighted Sobolev spaces, such as in [40], we can have better smoothness indices and may obtain better convergence rate. In other words, the present error estimate is general and thus it may be conservative for many situations.

5.3.4 Implementation of the PG Spectral Method

In FDDE (5.2), we seek an approximate solution of the form

$$u(t) \approx u_N(t) = \sum_{n=1}^{N} a_n \, {}^{(1)}\widetilde{\mathcal{P}}_n^{\mu}(t), \tag{5.41}$$

where a_n are the unknown expansion coefficients to be determined. By plugging (5.41) into (5.2), we obtain the residual $R_N(t)$ as

$$R_N(t) = {}_0\mathcal{D}_t^{\nu} u_N(t) + A(t)u_N(t) + B(t)u_N(\, g_\tau(t)\,) - h(t)$$

to be L^2-orthogonal to all elements in the set of test functions $\{{}^{(2)}\widetilde{\mathcal{P}}_k^{\mu}(\,t\,) : \; k = 1, 2, \cdots, N\}$. Next, we choose $\mu = \nu/2$, and by Lemma 5.3.1, we obtain

$$\begin{aligned}
\sum_{n=1}^{N} a_n \int_0^T {}_0\mathcal{D}_t^{\mu} \, {}^{(1)}\widetilde{\mathcal{P}}_n^{\mu}(t) \;\, {}_t\mathcal{D}_T^{\mu} \, {}^{(2)}\widetilde{\mathcal{P}}_k^{\mu}(\,t\,)\, dt \;\; &+ \\
\sum_{n=1}^{N} a_n \Big[\int_0^T A(t) \, {}^{(1)}\widetilde{\mathcal{P}}_n^{\mu}(t) \;\, {}^{(2)}\widetilde{\mathcal{P}}_k^{\mu}(\,t\,)\, dt \Big] \;\; &+ \\
\sum_{n=1}^{N} a_n \Big[\int_0^T B(t) \, {}^{(1)}\widetilde{\mathcal{P}}_n^{\mu}(\, g_\tau(t)\,) \;\, {}^{(2)}\widetilde{\mathcal{P}}_k^{\mu}(\,t\,)\, dt \Big] \;\; &= \\
\int_0^T h(t) \;\, {}^{(2)}\widetilde{\mathcal{P}}_k^{\mu}(\,t\,)\, dt, &
\end{aligned} \tag{5.42}$$

where by (5.8) and (5.11) we obtain the stiffness term, i.e., the first term of (5.42), as

$$\begin{aligned}
&\sum_{n=1}^{N} a_n \int_0^T {}_0\mathcal{D}_t^{\mu} \, {}^{(1)}\widetilde{\mathcal{P}}_n^{\mu}(t) \;\, {}_t\mathcal{D}_T^{\mu} \, {}^{(2)}\widetilde{\mathcal{P}}_k^{\mu}(\,t\,)\, dt \;\; = \\
&\sum_{n=1}^{N} a_n \Big(\frac{2}{T}\Big)^{2\mu-1} \, \left(\frac{\Gamma(n+\mu)}{\Gamma(n)}\right)^2 \frac{2}{2n-1}\delta_{nk},
\end{aligned} \tag{5.43}$$

in which δ_{nk} denotes the Kronecker delta and it highlights that this scheme yields a *diagonal* stiffness matrix on the left-hand side. By substituting (5.43) back into (5.42) we obtain the following linear system

$$\mathcal{S}_{tot}\ \vec{\mathbf{a}} = \vec{\mathbf{F}} \tag{5.44}$$

in which $\vec{\mathbf{a}}$ denotes the vector of unknown coefficients, $\vec{\mathbf{F}}$ represents the load-vector whose components are obtained as

$$\begin{aligned} \vec{\mathbf{F}}_k = \int_0^T h(t)\ {}^{(2)}\widetilde{\mathcal{P}}_k^{\mu}(\,t\,)\,dt &= (\frac{2}{T})^{\mu}\int_0^T (T-t)^{\mu}h(t)\,P_{k-1}^{\mu,-\mu}(x(t))\,dt \\ &\approx (\frac{2}{T})^{\mu}\sum_{q=0}^{Q} w_q h(t_q) P_{k-1}^{\mu,-\mu}(x(t_q)), \end{aligned} \tag{5.45}$$

where in this context, $\{w_q\}_{q=1}^{Q}$ and $\{t_q\}_{q=1}^{Q}$ are the Gauss-Lobatto-Jacobi quadrature weights and points corresponding to the Jacobi weight function $(T-t)^{\mu}t^0$. Finally $\mathcal{S}_{tot}$ is the corresponding $N \times N$ matrix obtained as

$$\mathcal{S}_{tot} = \mathbf{S} + \mathbf{M} + \mathbf{M}^{delay}, \tag{5.46}$$

where $\mathbf{S}$ is the diagonal $N \times N$ stiffness matrix, whose diagonal entries are given as

$$\mathbf{S}_{kk} = (\frac{2}{T})^{2\mu-1}\ \left(\frac{\Gamma(k+\mu)}{\Gamma(k)}\right)^2 \frac{2}{2k-1}, \tag{5.47}$$

$\mathbf{M}$ denotes the $A(t)$-weighted $N \times N$ mass matrix whose entries are given as

$$\begin{aligned} \mathbf{M}_{kn} &= \int_0^T A(t)\ {}^{(2)}\widetilde{\mathcal{P}}_k^{\mu}(\,t\,)\ {}^{(1)}\widetilde{\mathcal{P}}_n^{\mu}(t)\,dt, \\ &\approx (\frac{2}{T})^{2\mu}\sum_{q=1}^{Q_M} w_q A(t_q) P_{k-1}^{\mu,-\mu}(x(t_q)) P_{n-1}^{-\mu,\mu}(x(t_q)), \end{aligned} \tag{5.48}$$

in which w_q and t_q denote the Gauss-Lobatto-Jacobi weights and quadrature points associated with the weight function $(T-t)^{\mu}\, t^{\mu}$. Moreover, $\mathbf{M}^{delay}$ represents the corresponding $N \times N$ delay mass matrix associated with the weight function $B(t)$, given as

$$\mathbf{M}_{kn}^{delay} = \int_0^T B(t)\, {}^{(2)}\widetilde{\mathcal{P}}_k^{\mu}(\, t\,)\ {}^{(1)}\widetilde{\mathcal{P}}_n^{\mu}(g_\tau(t))\, dt. \tag{5.49}$$

Based on the choice of the delay function $g_\tau(t)$, we can obtain proper quadrature rules. For instance, if $g_\tau(t) = t - \tau$ then

$$\begin{aligned} \mathbf{M}_{kn}^{delay} &= (\frac{2}{T})^{2\mu} \int_\tau^T (T-t)^{\mu}\, (t-\tau)^{\mu}\, B(t) P_{k-1}^{\mu,-\mu}(x(t))\ P_{n-1}^{-\mu,\mu}(x(t-\tau))\, dt \\ &\approx (\frac{2}{T})^{2\mu} \sum_{q=1}^{Q_{M_d}} w_q B(t_q) P_{k-1}^{\mu,-\mu}(x(t_q)) P_{n-1}^{-\mu,\mu}(x(t_q-\tau)), \end{aligned}$$

where w_q and t_q represent the Gauss-Lobatto-Jacobi weights and quadrature points associated with the weight function $(T-t)^{\mu}\,(t-\tau)^{\mu}$. Alternatively, when we employ a pantograph delay function of form $g_\tau(t) = ct$, we obtain the entries of the delay mass matrix via

$$\mathbf{M}_{kn}^{delay} \approx c^{\mu} (\frac{2}{T})^{2\mu} \sum_{q=1}^{Q_{M_d}} w_q B(t_q) P_{k-1}^{\mu,-\mu}(x(t_q)) P_{n-1}^{-\mu,\mu}(x(ct_q)),$$

where, this time, w_q and t_q are the weights and quadrature points corresponding to $(T-t)^{\mu}\, t^{\mu}$.

Remark 5.3.7. In the aforementioned quadrature rules, $\approx$ can be replaced by $=$ if $f(t)$, $A(t)$ and $B(t)$ are nice functions by choosing Q, Q_M, and Q_{M_d} sufficiently large in the numerical simulations.

For the case of non-homogeneous initial conditions when $u(0) = u_0 \neq 0$, we

employ the method of *lifting a known solution*, where we decompose the solution $u(t)$ into two parts as

$$u(t) = u_{\mathcal{H}}(t) + u_{\mathcal{D}}, \tag{5.50}$$

in which $u_{\mathcal{H}}(t)$ corresponds to the homogeneous solution and $u_{\mathcal{D}} \equiv u_0$ is the non-zero initial condition, given in (5.2). We substitute (5.50) into (5.2) and take the fractional derivative of the known $u_{\mathcal{D}}$ to the right hand-side to obtain

$$\begin{aligned} {}_0\mathcal{D}_t^{\nu} u_{\mathcal{H}}(t) &= L(t) - A(t)u(t) - B(t)u(\, g_\tau(t)\,), \quad t \in (0, T], \\ u_{\mathcal{H}}(0) &= 0, \end{aligned} \tag{5.51}$$

where $L(t) = h(t) - \frac{u_{\mathcal{D}}}{\Gamma(1-\nu)\, t^{\nu}}$. Then, Theorem 5.3.4 holds since $L(t) \in H^{-\mu}([0, T])$. Moreover, we note that if we replace the fractional derivative in (5.51) by a Caputo one, the same scheme can be used, where this time $h(t) \equiv L(t)$, since the Caputo fractional derivative of the constant initial value $u_0 (= u_{\mathcal{D}})$ is identically zero.

5.3.5 Numerical Examples for PG Spectral Method

We shall examine our PG spectral method for solving FDDE (5.2) for different cases. We consider the following model problems in which: (i) A and B are constant and the delay term is represented as $u(t - \tau)$, (ii) $A(t)$ and $B(t)$ are time-dependent yet the delay term is introduced as $u(t-\tau)$, and (iii) A and B are constant but the delay term is represented as $u(qt)$, known as *pantograph* delay, furthermore as $u(q \sin(\pi t))$, introduced as *harmonic* delay for some real-valued q. In each model problem, we

shall consider the following two exact solutions, one as a *monomial*

$$u^{ext}(t) \;=\; \begin{cases} u_0 = 0, & t \in [-\tau, 0], \\ t^{10}, & t \in (0, T], \end{cases} \tag{5.52}$$

and the other one as a *fractional* function given as

$$u^{ext}(t) \;=\; \begin{cases} u_0 = 0, & t \in [-\tau, 0], \\ t^{13/2}\sin(\pi t^{4/3}), & t \in (0, T]. \end{cases} \tag{5.53}$$

However, the corresponding forcing term $h(t)$ is specifically obtained in each model problem separately. In all test-cases, we set the simulation time $T = 1$, and we examine two extreme values of fractional orders $\nu = 1/0$ and $9/10$. For each model problem, we present the corresponding log-linear L^2-error of the numerical solution versus N, the order-index in (5.41) to assess the convergence rate.

Model Problem 3.4.1: *Constant $A = B = 1$, and delay term $u(t-\tau)$.*

As the first example, we consider the following FDDE:

$$\begin{aligned} {}_0\mathcal{D}_t^{\nu} u(t) &= h(t) - u(t) - u(\,t - \tau\,), \quad t \in (0, 1], \\ u(t) &= 0, \quad t \in [-\tau, 0], \end{aligned} \tag{5.54}$$

where τ is taken as a fraction of the whole simulation time T. We obtain the corresponding linear system from (5.44), where the stiffness matrix and the mass matrix are obtained by (5.47), and (5.48), respectively, in which $A = B = 1$. Given

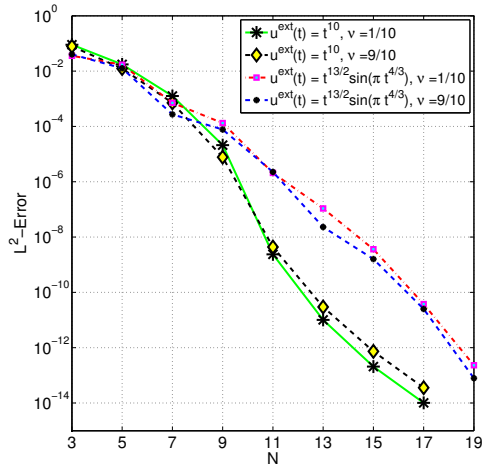

$(u^{ext} = t^{10})$		
N	$\nu = 1/10$	$\nu = 9/10$
5	11.4377	12.5547
9	39.5841	33.9166
13	25.7409	25.0707
$(u^{ext}(t) = t^{\frac{13}{2}} \sin(\pi t^{\frac{4}{3}}))$		
4	6.72783	6.6938
8	20.3891	20.8804
16	23.7527	23.3847

Figure 5.1: Model problem 3.4.1 with $A = B = 1$ and delay term of form $u(t-\tau)$; (Left): log-linear L^2-error of the numerical solution to (5.54), versus N, the order-index in (5.41), corresponding to $u^{ext}(t) = t^{10}$ and $u^{ext}(t) = t^{13/2}\sin(\pi t^{4/3})$, also associated with $\nu = 1/10$ and $\nu = 9/10$ in each case. Here, the simulation time $T = 1$. (Right): the rate of convergence $|\log(\frac{\|\epsilon_2\|_2}{\|\epsilon_1\|_2})/\log(\frac{N_2}{N_1})|$.

the analytical solutions, the corresponding forcing term $h(t)$, associated with the monomial solution (5.52), is obtained as

$$h(t) = \begin{cases} \frac{\Gamma(11)}{\Gamma(11-\nu)} t^{10-\nu} + t^{10}, & t \in [0, \tau], \\ \frac{\Gamma(11)}{\Gamma(11-\nu)} t^{10-\nu} + t^{10} + (t-\tau)^{10}, & t \in (\tau, T]. \end{cases} \tag{5.55}$$

Hence, $h(t)$ corresponds to the following fractional analytical solution (5.53):

$$h(t) = \begin{cases} \sum_{j=0}^{\infty} \frac{(-1)^j}{(2j+1)!} \pi^{2j+1} \frac{\Gamma(\frac{53+16j}{6})}{\Gamma(\frac{53+16j}{6} - \nu)} \; t^{\frac{47+16j}{6} - \nu} + t^{13/2} \sin(\pi t^{4/3}), & t \in [0, \tau], \\ \sum_{j=0}^{\infty} \frac{(-1)^j}{(2j+1)!} \pi^{2j+1} \frac{\Gamma(\frac{53+16j}{6})}{\Gamma(\frac{53+16j}{6} - \nu)} \; t^{\frac{47+16j}{6} - \nu} + t^{13/2} \sin(\pi t^{4/3}) + \\ (t-\tau)^{13/2} \sin\Big(\pi (t-\tau)^{4/3}\Big), & t \in (\tau, T]. \end{cases}$$

correspondingly, the load-vector $\vec{\mathbf{F}}_k$ is obtained by plugging $h(t)$ in (5.45).

In Fig. 5.1 (left), we present the log-linear L^2-error plot corresponding to fractional order $\nu = 1/10$ and $9/10$, where we have examined both the exact solutions,

given in (5.52) and (5.53). The first observation we make is that the results are *independent* of the time-delay τ, where error plots corresponding to $\tau = T/8$, $T/4$ and $T/2$ coincide for each ν. Moreover, we observe that the rate of convergence for the case of $u^{ext}(t) = t^{10}$ is higher than what is achieved when $u^{ext}(t) = t^{13/2}\sin(\pi t^{4/3})$. We explain this by the fact that $u^{ext}(t) = t^{10}$ is infinitely-many differentiable in contract to the fractional function $u^{ext}(t) = t^{13/2}\sin(\pi t^{4/3})$, which is not as smooth as the monomial case.

In addition, we obtain the rate of convergence in the Model Problem 3.4.1. in Fig. 5.1 (right). While the theory conservatively estimates the rate of convergence in the case of $u^{ext} = t^{10}$ (using the weighted norm) as $21 - \nu$, also, in the case of $u^{ext} = t^{13/2}\sin(\pi t^{4/3})$ the rate is estimated as $16.6 - \nu$, the table of convergence represents faster rates.

Model Problem 3.4.2: *Time-Dependent $A(t)$ and $B(t)$ with delay term $u(t-\tau)$.*

As the second example, we consider

$$\begin{aligned} {}_0\mathcal{D}_t^{\nu} u(t) &= h(t) - A(t)u(t) - B(t)u(\,t-\tau\,), \quad t \in (0,1], \\ u(t) &= 0, \quad t \in [-\tau, 0], \end{aligned} \tag{5.56}$$

where τ is taken as a constant, and similar to the previous test-problem, to be a fraction of the whole simulation time T. We consider two choices for $A(t)$ and $B(t)$: (i) a cubic function $A(t) = B(t) = t^2 - t^3$ and (ii) harmonic function $A(t) = B(t) = \sin(\pi t)$. For each choice of $A(t)$ and $B(t)$, we separately consider the exact solutions shown in (5.52) and (5.53).

In a similar fashion, in Fig. 5.2-left and corresponding to $A(t) = B(t) = t^2 - t^3$,

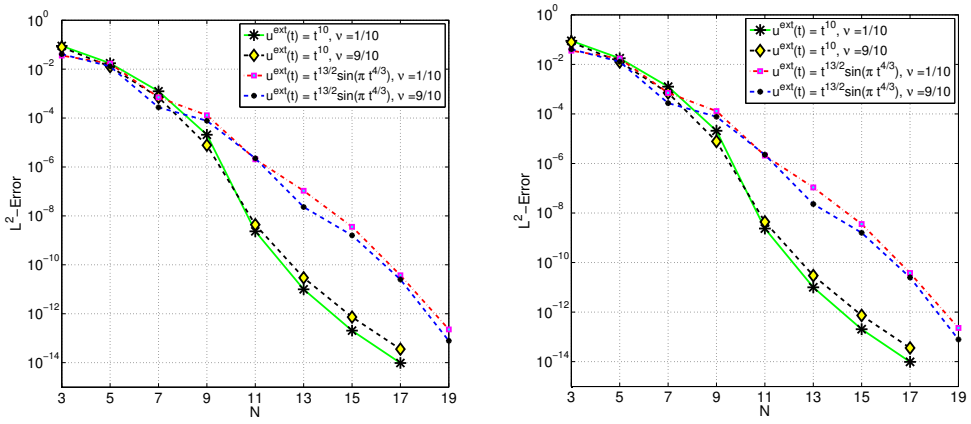

Figure 5.2: Model problem 5.4.2 with time-dependent $A(t) = B(t)$ and delay term of form $u(t-\tau)$: log-linear L^2-error of the numerical solution to (5.56), versus N, the order-index in (5.41), corresponding to $A(t) = B(t) = t^2 - t^3$ (left) and $A(t) = B(t) = \sin(\pi t)$ (right). Here, $\nu = 1/10$ and $\nu = 9/10$, also exact solutions $u^{ext}(t) = t^{10}$ and $u^{ext}(t) = t^{13/2}\sin(\pi t^{4/3})$ in each case, where the simulation time $T = 1$.

we present the log-linear L^2-error plot corresponding to fractional order $\nu = 1/10$ and $9/10$, where we make similar observations. Again, we demonstrate the spectral convergence, independent of the value of the time-delay τ for each ν, where we have examined $\tau = T/8$, $T/4$, and $T/2$. This model problem demonstrates that our PG spectral method can be effectively employed for time-dependent coefficient FDDEs with the same ease. In Fig. 5.2-right, we plot the log-linear L^2-error plot corresponding to fractional order $\nu = 1/10$ and $9/10$ for the case of $A(t) = B(t) = \sin(\pi t)$, where we make similar observations.

Model Problem 3.4.3: *Constant A and B, with delay term $u(qt)$ & $u(q\sin(\pi t))$.*

As the third model problem, we consider the following FDDE

$$\begin{aligned} {}_0\mathcal{D}_t^{\nu} u(t) &= h(t) - u(t) - u(\, g_\tau(t)\,), \qquad t \in (0,1], \\ u(t) &= 0, \qquad t \in [-\tau, 0], \end{aligned} \tag{5.57}$$

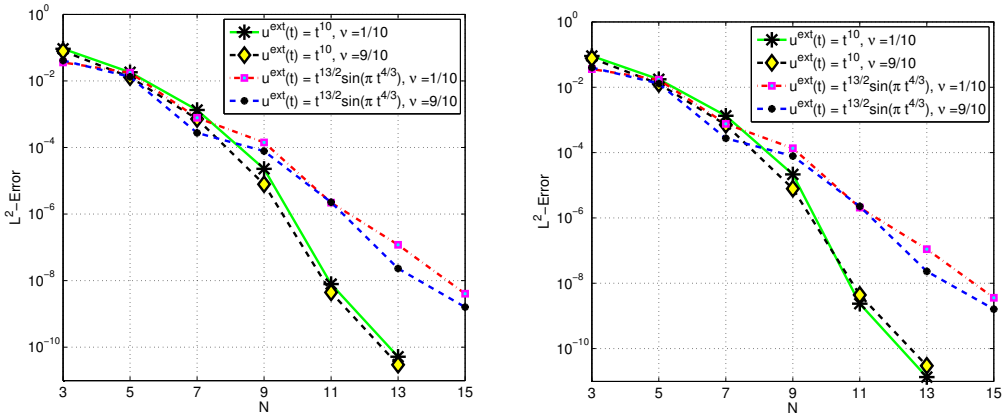

Figure 5.3: Pantograph & harmonic FDDEs: log-linear L^2-error of the numerical solution to (5.57), versus N, the order-index in (5.41), corresponding to pantograph delay term $u(\,g_\tau(t)\,) = u(\,qt\,)$ (left) and harmonic delay term $u(\,g_\tau(t)\,) = u(\,q\sin(\pi t)\,)$ (right); here $\nu = 1/10$ and $\nu = 9/10$, $u^{ext}(t) = t^{10}$ and $u^{ext}(t) = t^{13/2}\sin(\pi t^{4/3})$ in each case, where the simulation time $T = 1$.

where we have set $A = B = 1$ and have modified the time delay term as $u(\,g_\tau(t)\,)$. Here, we consider two forms of $g_\tau(t)$; in the first test-case, we consider the pantograph delay $g_\tau(t) = qt$. Subsequently, we set $g_\tau(t) = q\sin(\pi t)$, as a harmonic delay time term. We note that having such type of the delay term does not require the definition of the solution in $[-\tau, 0]$. Now, for each delay term we provide the forcing term $h(t)$ as

$$h(t) = \frac{\Gamma(11)}{\Gamma(11-\nu)} t^{10-\nu} + t^{10} + (t-\tau)^{10}, \quad t \in [0,T], \tag{5.58}$$

corresponding to the exact solution $u^{ext}(t) = t^{10}$, also

$$\begin{aligned} h(t) &= \sum_{j=0}^{\infty} \frac{(-1)^j}{(2j+1)!}\pi^{2j+1} \frac{\Gamma(\frac{53+16j}{6})}{\Gamma(\frac{53+16j}{6}-\nu)}\, t^{\frac{47+16j}{6}-\nu} + t^{13/2}\sin(\pi t^{4/3}) \\ &+ (t-\tau)^{13/2}\sin(\pi(t-\tau)^{4/3}), \quad t \in [0,T], \end{aligned} \tag{5.59}$$

associated with the exact solution $u^{ext}(t) = t^{13/2}\sin(\pi t^{4/3})$. In Fig. 5.3-left corresponding to $u(\,g_\tau(t)\,) = u(qt)$, and in Fig. 5.3-right corresponding to $u(\,g_\tau(t)\,) = u(qt)$, $q \leq \frac{1}{\pi}$, we present the log-linear L^2-error of the numerical solution to (5.57),

versus N, the order-index in (5.41). For both pantograph and harmonic delay problems and independent of the modulation coefficient q, we obtain the spectral convergence.

5.4 Discontinuous Galerkin (DG) Schemes

The most obvious difference between FDEs and FDDEs is the initial data. For FDDEs we usually provide not just the value of the solution at the initial point, but also the history with the certain length related to τ, that is, the solution at times prior to the initial point. The fact that FDDEs have an initial history may lead to a discontinuity of the exact solution or some higher derivatives of the exact solution [57]. The property is important when solving FDDEs numerically, because general high-order numerical methods are intended for problems with solutions belonging to higher Sobolev spaces. Interestingly in such cases, the points on which the exact solution become non-smooth are always related to the time delay. For problems with constant time delays, such points are residing at $t = \tau, 2\tau, \cdots$. This property and the useful information of the behaviour of the exact solution could be exploited to develop high-order numerical methods in a multi-element and discontinuous fashion.

Next, we present a new *Discontinuous Spectral Method* (DSM) to be later extended to a *Discontinuous Spectral Element Method* (DSEM) for efficient adaptive refinement.

The relations (10.18) and (10.20) are useful in computing the corresponding stiffness matrix in the discontinuous scheme presented in the following section.

Next, we first develop a discontinuous spectral (single-element) scheme for FDDE

(5.2) and subsequently we extend it to a discontinuous spectral element method in which we partition the computational domain into non-overlapping elements, which allows us to develop a spectrally accurate scheme for the FDDEs where the exact solution is only piecewise continuous.

5.4.1 Discontinuous Spectral Method (DSM; Single-Domain)

In the mapped interval $[0, T]$, we define the space of basis functions as

$$\mathbb{V}_N = span\{\widetilde{P}_j^{\,\eta,0}(\,x(t)\,) : \eta \in (0,1), \text{and } j = 0, 1, \cdots, N\}. \tag{5.60}$$

We also define the space of test functions as

$$\mathcal{V}_N = span\{\widetilde{P}_k^{\,0,\chi}(\,x(t)\,) : \chi \in (0,1), \text{and } k = 0, 1, \cdots, N\}. \tag{5.61}$$

We note that $\mathcal{V}_N \equiv \mathbb{V}_N$, however, we adopt this representation for efficient implementation of the scheme. We call $\widetilde{P}_j^{\,\eta,0}(\,x(t)\,)$ and $\widetilde{P}_k^{\,0,\chi}(\,x(t)\,)$ *asymptotic eigenfunctions* of FSLP-I & -II, which are *polynomials*. We shall show how this choice of basis and test polynomial functions leads to efficient and exact calculation of the stiffness matrices arising in the corresponding variational forms using standard Gauss-Legendre quadrature rules.

We follow a discontinuous Galerkin spectral method and seek an approximate solution to (5.2), where $u(0) = u_D \neq 0$ generally, in the form

$$u_N(t) = \sum_{n=0}^{N} c_n\, \widetilde{P}_n^{\,\eta,0}(\,x(t)\,), \tag{5.62}$$

which $\forall \vartheta(t) \in \mathcal{V}_N$ satisfies the following variational form obtained from (5.2) in

$I = (0, T]$ (see [189], also Lemma 3.5 in [188])

$$\Big({}_{0^+}\mathcal{D}_t^{\nu/2} u_N(t) \ , \ {}_t\mathcal{D}_T^{\nu/2} \vartheta(t) \Big)_I + \Big(A(t) u_N(t) \ , \vartheta(t) \Big)_I + \Big(B(t) u_N(g_\tau(t)) \ , \vartheta(t) \Big)_I - \frac{\vartheta(T^-) T^{1-\nu}}{(1-\nu)\Gamma(1-\nu)} [\![u_N(0)]\!] = \Big(h(t), \vartheta(t) \Big)_I, \tag{5.63}$$

where $(\cdot, \cdot)_I$ denotes the standard inner-product in the interval I, $[\![u_N(0)]\!] = u_N(0^+) - u_N(0^-) = u_N(0^+) - u_D$ represents the jump discontinuity of the solution at the initial condition, and $\vartheta(T)$ is the test-function evaluated at the end of the time-interval.

We then choose $\eta = \chi = \nu/2$, and by substituting (5.62) into the scheme (5.63), and taking $\vartheta(t) = \widetilde{P}_k^{\,0,\chi}(\, x(t)\,)$ for $k = 0, 1, \cdots, N$, we obtain

$$\begin{aligned} \sum_{n=0}^{N} c_n \Big\{ \int_0^T {}_t\mathcal{D}_{T^-}^{\eta} \widetilde{P}_k^{\,0,\nu/2}(\, x(t)\,) \ {}_{0^+}\mathcal{D}_t^{\nu/2} \widetilde{P}_n^{\,\nu/2,\,0}(\, x(t)\,) \ dt \Big\} \\ + \sum_{n=0}^{N} c_n \Big\{ \int_0^T A(t) \widetilde{P}_k^{\,0,\nu/2}(\, x(t)\,) \widetilde{P}_n^{\,\nu/2,\,0}(\, x(t)\,) \ dt \Big\} \\ + \sum_{n=0}^{N} c_n \Big\{ \int_0^T B(t) \widetilde{P}_k^{\,0,\nu/2}(\, x(t)\,) \, \widetilde{P}_n^{\,\nu/2,\,0}(\, x(\, g_\tau(t)\,)\,) \ dt \Big\} \\ - \sum_{n=0}^{N} c_n \Big\{ \frac{\widetilde{P}_k^{\,0,\nu/2}(T) T^{1-\nu}}{(1-\nu)\Gamma(1-\nu)} \widetilde{P}_n^{\,\nu/2,\,0}(0^+) \Big\} \\ = \int_0^T h(t) \, \widetilde{P}_k^{\,0,\nu/2}(\, x(t)\,) \, dt - \frac{\widetilde{P}_k^{\,0,\nu/2}(T^-) T^{1-\nu}}{(1-\nu)\Gamma(1-\nu)} u_D, \end{aligned} \tag{5.64}$$

where by virtue of (10.18) and (10.20) and explicitly evaluating the end-points $\widetilde{P}_k^{\,\nu/2,\,0}(T^-) \equiv 1$ and $\widetilde{P}_n^{\,\nu/2,\,0}(0^+) \equiv (-1)^n$, (5.64) yields the following linear system

$$\mathbb{S}_{tot} \ \vec{\mathbf{c}} = \vec{\mathbb{F}} \tag{5.65}$$

in which $\vec{\mathbf{c}}$ denotes the vector of unknown coefficients, $\vec{\mathbb{F}}$ represents the load-vector whose components are obtained as

$$\vec{\mathbb{F}}_k = \int_0^T h(t)\, \widetilde{P}_k^{\,0,\nu/2}(\, x(t)\,)\, dt - \frac{\widetilde{P}_k^{\,0,\nu/2}(T^-)T^{1-\nu}}{(1-\nu)\Gamma(1-\nu)} u_D, \tag{5.66}$$

and $\mathbb{S}_{tot}$ is the corresponding $(N+1)\times(N+1)$ matrix obtained as

$$\mathbb{S}_{tot} = \mathbf{S}^{dis} + \mathbf{M}^{dis} + \mathbf{M}^{dis,delay} + \mathbf{J}^{jump}, \tag{5.67}$$

where $\mathbf{J}_{jump}$ denotes a $(N+1)\times(N+1)$ jump matrix whose entries are obtained as

$$\mathbf{J}_{kn}^{jump} = \frac{(-1)^{n+1}\, T^{1-\nu}}{(1-\nu)\Gamma(1-\nu)}, \tag{5.68}$$

and $\mathbf{M}^{dis,delay}$ represents the corresponding $(N+1)\times(N+1)$ delay mass matrix associated with the weight function $B(t)$, given as

$$\mathbf{M}_{kn}^{dis,delay} = \int_0^T B(t)\widetilde{P}_k^{\,0,\nu/2}(\, x(t)\,)\, \widetilde{P}_n^{\,\nu/2,\,0}(\, x(\, g_\tau(t)\,)\,)\ dt. \tag{5.69}$$

Moreover, $\mathbf{M}^{dis}$ is the $A(t)$-weighted $(N+1)\times(N+1)$ mass matrix whose entries are given as

$$\mathbf{M}_{kn}^{dis} = \int_0^T A(t)\widetilde{P}_k^{\,0,\nu/2}(\, x(t)\,)\ \widetilde{P}_n^{\,\nu/2,\,0}(\, x(t)\,)\ dt, \tag{5.70}$$

and finally $\mathbf{S}^{dis}$ denotes the corresponding $(N+1)\times(N+1)$ stiffness matrix whose entries are obtained by Lemma 5.3.2 as

$$\mathbf{S}_{kn}^{dis} = \Lambda_{kn} \int_0^T t^{-\nu/2}\ (T-t)^{-\nu/2}\, \widetilde{P}_n^{\,\nu,\,-\nu/2}(\, x(t)\,)\widetilde{P}_k^{\,-\nu/2,\nu}(\, x(t)\,)\ dt \tag{5.71}$$

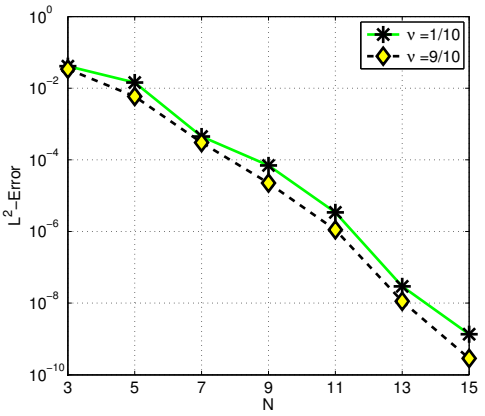

Figure 5.4: Discontinuous spectral method (DSM): log-linear L^2-error of the numerical solution to (5.2), where $A(t) = B(t) = 1$ and the exact solution is given as $u^{ext}(t) = t^{13/2}\sin(\pi t^{4/3})$, versus N, the order-index in (5.62). Here, the simulation time $T = 1$.

where Λ_{kn} is computed explicitly as

$$\Lambda_{kn} \quad = \quad \frac{\Gamma(k+1)}{\Gamma(k-\nu/2+1)}\frac{\Gamma(n+1)}{\Gamma(n-\nu/2+1)}. \tag{5.72}$$

Remark 5.4.1. The stiffness matrix $\mathbf{S}^{dis}$ is a full matrix whose entries satisfy $\mathbf{S}^{dis}_{kn} = (-1)^{k+n}\mathbf{S}^{dis}_{kn}$. Hence, we need to compute only half of the entries. Moreover, such entries can be computed *exactly* using the following Gauss quadrature rule thanks to the weight function $t^{-\nu/2}\,(T-t)^{-\nu/2}$ arising from the choice of the basis and test functions

$$\int_0^T t^{-\nu/2}\,(T-t)^{-\nu/2}\,\widetilde{P}_n^{\,\nu,\,-\nu/2}(\,x(t)\,)\widetilde{P}_k^{\,-\nu/2,\nu}(\,x(t)\,)\,dt \approx \sum_{j=1}^{N+1}\widetilde{P}_n^{\,\nu,\,-\nu/2}(\,t_j\,)\widetilde{P}_k^{\,-\nu/2,\nu}(\,t_j\,)\omega_j. \tag{5.73}$$

This is true since $\widetilde{P}_n^{\,\nu,\,-\nu/2}\widetilde{P}_k^{\,-\nu/2,\nu} \in P_{2N}$ for all $n, k = 1, 2, \cdots, N$. Here, t_k's are the Gauss-Lobatto-Jacobi (GLJ) quadrature points in the interval $(0, T]$ given by

$$t_j = \frac{T}{2}\Big(\xi_j^{-\nu/2,-\nu/2} + 1\Big),\ j = 1, 2, \cdots, N+1, \tag{5.74}$$

following [189] and Lemma 3.5 in [188], where $\xi_j^{-\nu/2,-\nu/2}$ are the standard quadrature GLJ points in $[-1,1]$, and the corresponding weights are obtained as

$$\omega_j = (\frac{T}{2})^{1-\nu}\rho_j^{-\nu/2,-\nu/2},\ j = 1, 2, \cdots, N+1, \tag{5.75}$$

in which $\rho_j^{-\nu/2,-\nu/2}$ represents the standard GLJ quadrature weights associated with the Jacobi parameters $^{-\nu/2,-\nu/2}$.

Numerical Example for DSM Scheme

In order to demonstrate the performance of the DSM scheme (5.63), we solve for ${}_0\mathcal{D}_t^{\mu}u(t) = -u(t) - u(t-\tau) + h(t),\ t \in [0,1]$ subject to a homogeneous Dirichlet initial condition. We plot the corresponding log-linear L^2-error of the numerical solution versus N, the order-index in (5.62) in Fig. 5.4, corresponding to $\nu = 1/10$ and $\nu = 9/10$. The time delay is taken as $\tau = T/8$, $T/4$, and $T/2$, where the convergence results again appear to be independent of τ. Here the exact solution is chosen as $u^{ext}(t) = t^{13/2}\sin(\pi t^{4/3})$. We show that our DSM scheme yields spectral convergence with respect to N, similar to the PG method.

In addition to this test-case, we have examined our DSM scheme for other examples shown in Sec. 5.3.5, recovering the expected rate of convergence successfully. Moreover, we recall that DSM is still a single-domain spectral method, in which the basis functions employed in the expansion (5.41) do not satisfy the initial condition this time. In what follows, we extend this scheme to a *multi-element* method for efficient discontinuity capturing and possible long time-integration.

5.4.2 Discontinuous Spectral Element Method (DSEM; Multi-Element)

Now, we partition the time-interval $[0, T]$ into N_{el} non-overlapping time-elements, $I_e = [t_{e-\frac{1}{2}}, t_{e+\frac{1}{2}}]$ such that $\cup_{e=1}^{N_{el}} I_e = [0, T]$. Next, we expand the solution in each element I_e in terms of some basis functions, which are discontinuous at the interfaces of elements and test the problem against another set of test functions space. Here, we construct our basis and test functions based upon (5.60) and (5.61), employed in the development of the DSM scheme, as

$$V_h^N = \{v : v\Big|_{I_e} \in V_N(I_e), e = 1, 2, \cdots, N_{el}\}, \tag{5.76}$$

and

$$\mathcal{V}_h^N = \{v : v\Big|_{I_e} \in \mathcal{V}_N(I_e), e = 1, 2, \cdots, N_{el}\}, \tag{5.77}$$

In our discontinuous spectral element method, we seek an approximate solution to (5.2) on e^{th} time-element in the form

$$u_N^e(t) = \sum_{n=1}^{N} \mathcal{C}_n \, \widetilde{P}_j^{\,\eta,0}(\, x^e(t)\,), \tag{5.78}$$

which $\forall \vartheta^e(t) \in \mathcal{V}_h^N$ satisfies the following bilinear form originated from projecting (5.2) onto $\vartheta^e(t)$ in the time-interval $I_e = (t_{e-\frac{1}{2}}, t_{e+\frac{1}{2}}]$ as

$$\begin{aligned} \Big({}_{t^+_{e-1/2}}\mathcal{D}_t^{\nu/2} u_N^e(t) \, , \, {}_t\mathcal{D}^{\nu/2}_{t^-_{e+1/2}} \vartheta^e(t) \Big)_{I_e} + \Big(A(t)\, u_N^e(t) \, , \, \vartheta^e(t) \Big)_{I_e} + \\ \Big(B(t)\, u_N^e(\, g_\tau(t)\,) \, , \, \vartheta^e(t) \Big)_{I_e} - \frac{\vartheta^e(t^-_{e+1/2})(\Delta t)_e^{1-\nu}}{(1-\nu)\Gamma(1-\nu)} [\![u_N^e(t_{e-1/2})]\!] = \\ \Big(h(t), \vartheta(t) \Big)_{I_e} - \mathcal{H}_e, \end{aligned} \tag{5.79}$$

beginning form the first element, i.e., $e = 1$, and marching element-by-element along the time-axis to the $e = N_{el}$. Here, $(\Delta t)_e$ denotes the time-length of the element I_e. We note that the only difference between the scheme (5.79) and the discontinuous spectral (single-element) method in (5.63) is the *history-term* $\mathcal{H}_e$ appearing on the right-hand side of (5.79). We shall explain how this term represents an extra *history-load* included in (5.79). We first write $\mathcal{H}_e$ in the following convenient and computationally efficient form as

$$\mathcal{H}_e \;=\; \vartheta^e(t) F_e(t) \Big|_{t=t^+_{e-1/2}}^{t=t^-_{e+1/2}} - \Big(F_e(t) \, , \, \frac{d}{dt} \vartheta^e(t) \Big)_{I_e}, \tag{5.80}$$

where $F_e(t)$ is the *history function* associated with element I_e

$$F_e(t) = \sum_{\epsilon=1}^{e-1} \sum_{\delta=0}^{N} \tau_\delta (t-s)^{\delta+1-\nu} u_N^{(\delta)\epsilon}(s) \Big|_{s=t^+_{\epsilon-1/2}}^{s=t^-_{\epsilon+1/2}} \tag{5.81}$$

in which $\tau_\delta = -1/[\Gamma(1-\nu) \prod_{m=0}^{\delta}(m+1-\nu)]$ is decaying with rate $(\delta-\nu)!$, $\delta = 0, 1, \cdots, N$, and $u_N^{(\delta)\epsilon}$ represents the δ-th derivative of the solution in I_ϵ to be only evaluated at the boundaries of I_ϵ. We recall that the approximate solution in each element is obtained in terms of the basis functions which are Jacobi-polynomials

in (5.60) whose derivatives can be obtained recursively thanks to their hierarchical structure. Hence, $F_e(t)$ is a *polyfractonomial* of degree $N+\mu$, where $\mu = 1-\nu \in (0,1)$, defined in [187]. Furthermore, we note that when we take $N_{el} = 1$ in the DSEM scheme, the history-load term $\mathcal{H}_e = 0$, then the scheme becomes identical to the DSM scheme (5.63).

In order to obtain the corresponding linear system, we choose $\eta = \chi = \nu/2$. Then, by substituting (5.78) into the scheme (5.79), taking $\vartheta^e(t) = \widetilde{P}_k^{\,0,\chi}(\,x^e(t)\,)$ for $k = 0, 1, \cdots, N$ and $e = 1, 2, \cdots, N_{el}$, and by Lemma 5.3.1 we obtain

$$
\begin{aligned}
\sum_{n=0}^{N} \mathcal{C}_{\,n}^{\,e} \quad & \Big\{ \quad \Lambda_{kn} \int_{I_e} w^e(t) \widetilde{P}_n^{\,\nu,\,-\nu/2}(\,x^e(t)\,)\ \widetilde{P}_k^{\,-\nu/2,\nu}(\,x^e(t)\,)\,dt \Big\} \\
& + \quad \sum_{n=0}^{N} \mathcal{C}_{\,n}^{\,e} \Big\{ \int_{I_e} A(t) \widetilde{P}_k^{\,0,\nu/2}(\,x^e(t)\,)\ \widetilde{P}_n^{\,\nu/2,\,0}(\,x^e(t)\,)\,dt \Big\} \\
& + \quad \sum_{n=0}^{N} \mathcal{C}_{\,n}^{\,e} \Big\{ \int_{I_e} B(t) \widetilde{P}_k^{\,0,\nu/2}(\,x^e(\,g_\tau(t)\,)\,)\ \widetilde{P}_n^{\,\nu/2,\,0}(\,x^e(t)\,)\,dt \Big\} \\
& + \quad \sum_{n=0}^{N} \mathcal{C}_{\,n}^{\,e} \Big\{ (-1)^{n+1} (\Delta t)_e^{1-\nu} \kappa_v \Big\} \\
& = \quad \int_{I_e} h(t)\, \widetilde{P}_k^{\,0,\nu/2}(\,x^e(t)\,)\,dt \;-\; \kappa_v\,(\Delta t)_e^{1-\nu} (u_N^{e-1})^R \;-\; \mathcal{H}_{e,k},
\end{aligned}
$$

in which $\kappa_v = 1/[(1-\nu)\Gamma(1-\nu)]$, $w^e(t) = (t - t_{e-1/2})^{-\nu/2}(t_{e+1/2} - t)^{-\nu/2}$ and the term $(u_N^{e-1})^R$ represents the solution we have already obtained in element I_{e-1}, which is evaluated at the right boundary. We note that for $e = 1$, $(u_N^0)^R$ is equal to the initial condition $u(0) = u_D$. The corresponding linear system in element I_e is then obtained as

$$
\mathbb{S}_{tot}^{e}\ \vec{\mathbf{c}^e} = \vec{\mathbb{F}^e} \tag{5.82}
$$

in which $\vec{\mathbf{c}^e}$ denotes the vector of unknown coefficients and $\mathbb{S}^e_{tot}$ is the corresponding $(N+1)\times(N+1)$ matrix obtained as

$$\mathbb{S}^e_{tot} = \mathbf{S}^e + \mathbf{M}^e + \mathbf{M}^{e,delay} + \mathbf{J}^e, \tag{5.83}$$

where $\mathbf{J}_e$ denotes a $(N+1)\times(N+1)$ jump matrix whose entries are obtained as

$$\mathbf{J}^e_{kn} = \frac{(-1)^{n+1}\,(\Delta t)_e^{1-\nu}}{(1-\nu)\Gamma(1-\nu)}, \tag{5.84}$$

and $\mathbf{M}^{e,delay}$ represents the corresponding $(N+1)\times(N+1)$ delay mass matrix for element "e", associated with the weight function $B(t)$, given as

$$\mathbf{M}^{e,delay}_{kn} = \int_{I_e} B(t)\widetilde{P}_k^{\,0,\nu/2}(\,x^e(\,g_\tau(t)\,)\,)\;\widetilde{P}_n^{\,\nu/2,\,0}(\,x^e(t)\,)\,dt. \tag{5.85}$$

Moreover, $\mathbf{M}^e$ is the $A(t)$-weighted $(N+1)\times(N+1)$ mass matrix whose entries are given as

$$\mathbf{M}^e_{kn} = \int_{I_e} A(t)\widetilde{P}_k^{\,0,\nu/2}(\,x^e(t)\,)\;\widetilde{P}_n^{\,\nu/2,\,0}(\,x^e(t)\,)\,dt \tag{5.86}$$

and $\mathbf{S}^e$ denotes the corresponding $(N+1)\times(N+1)$ stiffness matrix whose entries are obtained as

$$\mathbf{S}^e_{kn} = \Lambda_{kn}\int_{I_e} w^e(t)\widetilde{P}_n^{\,\nu,\,-\nu/2}(\,x^e(t)\,)\;\widetilde{P}_k^{\,-\nu/2,\nu}(\,x^e(t)\,)\,dt \tag{5.87}$$

in which Λ_{kn} is explicitly given in (5.72). In (5.82), $\vec{\mathbb{F}^e}$ represents the load-vector, associated with local element I_e, whose components are obtained as

$$\vec{\mathbb{F}}_{ek} = \int_{I_e} h(t)\,\widetilde{P}_k^{\,0,\nu/2}(\,x^e(t)\,)\,dt \;-\; \kappa_v\,(\Delta t)_e^{1-\nu}(u_N^{e-1})^R \;-\; \mathcal{H}_{e,k}, \tag{5.88}$$

in which $\mathcal{H}_{e,k}$ is given by

$$\mathcal{H}_{e,k} = F_e(t^-_{e+1/2}) + (-1)^{k+1} F_e(t^+_{e-1/2}) - \Big(F_e(t)\,,\, \frac{d}{dt}\, \widetilde{P}_k^{\,0,\nu/2}(\, x^e(t)\,) \Big)_{I_e}. \tag{5.89}$$

Remark 5.4.2. Similarly to DSM, the stiffness matrix $\mathbf{S}^e$ in DSEM scheme is also a full matrix, whose entries follow the property $\mathbf{S}^e_{kn} = (-1)^{k+n}\mathbf{S}^e_{nk}$. By the same argument, due to the weight function $w_e(t)$ appearing as a result of the choice of the basis and test functions the entries of $\mathbf{S}^e$ can be computed *exactly* using a standard quadrature rule. By performing local element operations and considering an affine mapping from of the physical element to the standard one, we can efficiently compute the entries of $\mathbf{S}^e$ as

$$\begin{aligned} \mathbf{S}^e_{kn} = \Lambda_{kn} \int_{I_e} w_e(t)\, \widetilde{P}_n^{\,\nu,\,-\nu/2}(\, x^e(t)\,) \widetilde{P}_k^{\,-\nu/2,\nu}(\, x^e(t)\,)\, dt \;\; &= \\ J \cdot \Lambda_{kn} \int_{-1}^{+1} (1-x)^{-\nu/2}(1+x)^{-\nu/2}\, P_n^{\,\nu,\,-\nu/2}(\, x\,) P_k^{\,-\nu/2,\nu}(\, x\,)\, dx \;\; &= \\ J \cdot \mathbf{S}^{e,st}_{kn}, & \end{aligned} \tag{5.90}$$

where $J = [(\Delta t)_e/2]^{1-\nu}$ represents the Jacobian of the transformation and $\mathcal{S}^{e,st}$ denotes the stiffness matrix on the *standard* element in the interval $[-1,1]$, obtained as

$$\mathbf{S}^{e,st}_{kn} = \Lambda_{kn} \sum_{j=1}^{N+1} P_n^{\,\nu,\,-\nu/2}(\, x_j\,) P_k^{\,-\nu/2,\nu}(\, x_j\,) \rho_j^{-\nu/2,-\nu/2}, \tag{5.91}$$

in which x_j's are the standard Gauss-Lobatto-Jacobi (GLJ) quadrature points in the interval $[-1,1]$ and ρ_j represent the corresponding weights. The relation (5.91) shows that in order to compute $\mathbf{S}^e$ in each element, we only need to obtain $\mathbf{S}^{e,st}$ once and multiply it to the corresponding Jacobian in each element. Clearly, on a uniform mesh where $(\Delta t)_1 = (\Delta t)_2 = \cdots = (\Delta t)_{N_{el}} = T/N_{el}$, the stiffness matrix is invariant

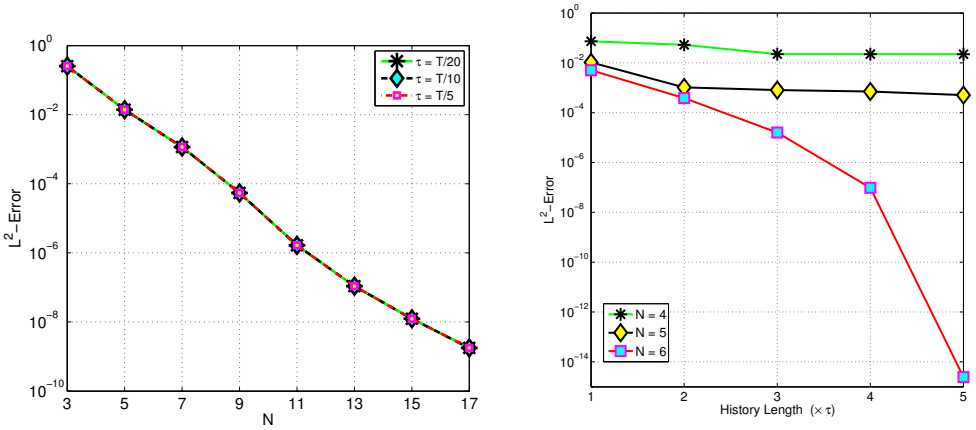

Figure 5.5: (Left): long time-integration using DSEM: log-linear L^2-error of the numerical solution to ${}_0\mathcal{D}_t^{1/2}u(t) = -u(t) - u(t-\tau) + h(t),\ t \in [0, 10]$, where the exact solution is given as $u^{ext}(t) = \sin(4\pi t/T)$ and $N_{el} = 4$, versus N, the order-index in (5.78). Here, the simulation time is set to $T = 10$. (Right): memory fading effect: log-linear L^2-error of the numerical solution to ${}_0\mathcal{D}_t^{1/10}u(t) = -u(t) - u(t-\tau) + h(t),\ t \in [0, 2]$, where the exact solution is given as $u^{ext}(t) = t^6$ and $N_{el} = 2$, versus history length (to be multiplied by τ). Here, N denotes the maximum polynomial order utilized in the expansion (5.78). Here, the simulation time is set to $T = 2$.

in each element and we compute it only *once* for the entire course of the simulation.

5.4.3 Numerical Examples for DSEM scheme

One can check that the DSEM scheme can be successfully employed in all model problems, introduced in Sec. 5.3.5, with the expected exponential convergence. Here, we demonstrate the performance of DSEM in the particular case of long time-integration of FDDEs with constant coefficients and constant time delay. Moreover, since there is an extra *history* term arising in DSEM scheme, we shall study the effect of *memory fading*, in which only a portion of the history information is taken into account.

Model Problem 4.3.2: Long Time-Integration

To examine the effectiveness of DSEM in carrying out long-time integration of FDDEs, we consider a case where the the exact solution is given as

$$u^{ext}(t) \;=\; \begin{cases} u_0 = 0, & t \in [-\tau, 0], \\ \sin(4\pi t/T), & t \in (0, T], \end{cases} \tag{5.92}$$

where $T = 10$. By setting $N_{el} = 4$ and performing p-refinement, we plot the log-linear L^2-error of the numerical solution to ${}_0\mathcal{D}_t^{1/2} u(t) = -u(t) - u(t-\tau) + h(t),\ t \in [0, T]$, versus N, the order-index in (5.78) in Fig. 5.5 (left). We take three values of time delay $\tau = 0.5$, (T/20), $\tau = 1$, (T/10), and $\tau = 2$, (T/5). The exponential convergence of error is shown to be independent of τ in long time-integrations as well.

Model Problem 4.3.3: Memory Fading

We now examine the idea of *memory fading/truncation* in the calculation of the history term (5.80). In this technique we do not take all the past elements into account at the expense of losing accuracy, and instead, an *effective history length* is chosen to calculate (5.80). Such an effective length is well-known to be dependent mainly on the fractional order ν. In fact, the greater ν in ${}_0\mathcal{D}_t^{\nu} u(t)$ the less history-length is needed since as $\nu \to 1$, we approach ${}_0\mathcal{D}_t^{\nu} \to d/dt$, which is a *local* operator for which no history is required. To this end, we solve ${}_0\mathcal{D}_t^{1/10} u(t) = -u(t) - u(t-\tau) + h(t),\ t \in [0, 1]$, partitioning the domain into $N_{el} = 2$ uniform elements when the fractional order is $\nu = 1/10$ and $\tau = T/10$. As shown in Fig. 5.5 (right), in order to get the convergence down to machine precision, higher modes demand longer history lengths; therefore we need to include the whole history to achieve such an accuracy.

We emphasize that such a phenomenon is independent of the discretization method and is solely due to the global nature of the fractional differential operators.

5.5 Discussion

We compare the computation performance of the developed schemes with the finite difference method (FDM) developed in [111], where the fractional derivative ${}_0\mathcal{D}_t^\nu u(t)$ is represented as

$$ {}_0\mathcal{D}_t^\nu u(t) = \frac{1}{\Gamma(2-\nu)} \sum_{j=0}^{k} b_j \frac{u(t_{k+1-j}) - u(t_{k-j})}{(\Delta t)^\nu} + r_{\Delta t}^{k+1}, \tag{5.93} $$

where $r_{\Delta t}^{k+1} \leq C_u (\Delta t)^{2-\nu}$ and $b_j := (j+1)^{1-\nu} - j^{1-\nu}, j = 0, 1, \cdots, k$. We solve (5.2), where $A = B = 1$, and τ is taken as constant. We compare the computational cost of solving such FDDE using FDM and the three high-order methods developed here. We note that the number of operations in PG, DSM and DSEM schemes asymptotically increases as $\mathcal{O}(N)$, $\mathcal{O}(N^3)$, $\mathcal{O}(N_{el}^2\ N^3)$, respectively, where N represents the polynomial order employed, and N_{el} denotes the number of elements. Moreover, the computational cost of FDM grows as N_g^2, where N_g stands for the number of the grid-points in the computational domain.

We also compute the CPU time (in seconds) required for solving (5.2) corresponding to $\nu = 1/10$, $\nu = 1/2$, and $9/10$ in Table 5.1, where the exact solution is $u^{ext}(t) = t^6$ and the integration time $T = 1$. We furthermore present the CPU time (in seconds) taken by the aforementioned schemes when the exact solution is $u^{ext}(t) = t^{13/2} \sin(\pi\, t^{4/3})$ in Table 5.2, corresponding to $\nu = 1/10$, $\nu = 1/2$, and $9/10$. We developed the codes in *Mathematica 8*. Clearly, the implementation of FDM

is simpler than our schemes. Moreover, FDM appears to be comparable with our high-order schemes in terms of CPU time when $\nu \in (0, 1/2)$ for the given range of accuracy (i.e., L^2- error $\geq 10^{-6}$). However, it turns out that FDM becomes computationally prohibited, especially when we ask for slightly higher accurate results, also when the fractional order $\nu \in [1/2, 1)$. For instance, Table 5.2 clearly shows that reaching the L^2-error of order 10^{-6} in FDM leads to running out of memory and this accuracy is not achieved when $\nu = 9/10$.

In the other example shown in Table 5.2, FDM for the case $\nu = 1/2$ appears to be almost 50 times more CPU time-consuming than DSEM, 75 times more costly than DSM, and 150 times slower than PG spectral method when $u^{ext}(t) = t^{13/2} \sin(\pi\, t^{4/3})$. We also repeated this test for the case where the exact solution $u^{ext}(t) = t^{10}$. In this case, while we *exactly* captured the solution by just setting the polynomial order to $N = 6$ in all cases, the CPU time taken in FDM when $\nu = 1/2$ was almost 200 times larger than that in DSEM and DSM, and is roughly 100 times bigger than the CPU time demanded by PG spectral method. Similar to the previous case, reaching the L^2-error of order 10^{-6} in FDM leaded to running out of memory and this accuracy was not achieved when $\nu = 9/10$.

Table 5.1: CPU time (seconds) on a Intel (Xeon X5550) 2.67GHz processor, corresponding to PG spectral method, DSM, DSEM, and FDM for solving ${}_0\mathcal{D}_t^{\nu}u(t)+u(t)+u(t-\tau)=f(t)$, $u(0)=0$, and the exact solution is $u^{ext}(t)=t^6$. Here, N denotes the expansion order in PG spectral method, DSM, and DSEM with $N_{el}=2$ (in each element), also N_g represents the number of grid points in FDM, and the simulation time is set to $T=1$.

($\nu=1/10$)

L^2-norm Error	PG Spectral Method	DSM	DSEM ($N_{el}=2$)	FDM
$\mathcal{O}(10^{-4})$	($N=8$) 2.84157	($N=5$) 1.3393	($N=5$) 2.02553	($N_g=48$) 0.048993
$\mathcal{O}(10^{-5})$	($N=9$) 3.86191	$\times$	$\times$	($N_g=180$) 0.25846
$\mathcal{O}(10^{-6})$	($N=10$) 5.10322	($N=6$) 2.14667 (exact)	($N=6$) 2.54888 (exact)	($N_g=640$) 3.75593

($\nu=1/2$)

L^2-norm Error	PG Spectral Method	DSM	DSEM ($N_{el}=2$)	FDM
$\mathcal{O}(10^{-4})$	($N=8$) 2.73908	($N=5$) 1.3258	($N=5$) 2.05569	($N_g=340$) 0.966354
$\mathcal{O}(10^{-5})$	($N=9$) 3.73393	$\times$	$\times$	($N_g=1600$) 23.4289
$\mathcal{O}(10^{-6})$	($N=10$) 4.92675	($N=6$) 2.11268 (exact)	($N=6$) 2.52712 (exact)	($N_g=7500$) 482.26

($\nu=9/10$)

L^2-norm Error	PG Spectral Method	DSM	DSEM ($N_{el}=2$)	FDM
$\mathcal{O}(10^{-4})$	($N=8$) 2.84057	($N=5$) 1.3428	($N=5$) 2.16667	($N_g=3000$) 75.2966
$\mathcal{O}(10^{-5})$	($N=9$) 3.80792	$\times$	$\times$	($N_g=23000$) 3352.53
$\mathcal{O}(10^{-6})$	($N=10$) 5.05573	($N=6$) 2.14167 (exact)	($N=6$) 2.56261 (exact)	Running Out of Memory

Table 5.2: CPU time (seconds) on a Intel (Xeon X5550) 2.67GHz processor, corresponding to PG spectral method, DSM, DSEM, and FDM for solving ${}_0\mathcal{D}_t^{\nu} u(t) + u(t) + u(t-\tau) = f(t)$, $u(0) = 0$, and the exact solution is $u^{ext}(t) = t^{13/2}\sin(\pi\, t^{4/3})$. Here, N denotes the expansion order in PG spectral method, DSM, and DSEM with $N_{el} = 2$ (in each element), also N_g represents the number of grid points in FDM, and the simulation time is set to $T = 1$.

$(\nu = 1/10)$

L^2-norm Error	PG Spectral Method	DSM	DSEM ($N_{el} = 2$)	FDM
$\mathcal{O}(10^{-4})$	$(N = 7)$ 2.90106	$(N = 9)$ 6.43152	$(N = 9)$ 8.99263	$(N_g = 48)$ 0.393939
$\mathcal{O}(10^{-5})$	$(N = 9)$ 5.04973	$(N = 11)$ 11.5942	$(N = 11)$ 17.5835	$(N_g = 200)$ 1.12583
$\mathcal{O}(10^{-6})$	$(N = 11)$ 8.14076	$(N = 2)$ 15.3367	$(N = 12)$ 23.5779	$(N_g = 760)$ 6.85696

$(\nu = 1/2)$

L^2-norm Error	PG Spectral Method	DSM	DSEM ($N_{el} = 2$)	FDM
$\mathcal{O}(10^{-4})$	$(N = 7)$ 2.87756	$(N = 9)$ 6.51001	$(N = 9)$ 9.1976	$(N_g = 340)$ 2.17417
$\mathcal{O}(10^{-5})$	$(N = 9)$ 4.99024	$(N = 11)$ 11.5367	$(N = 11)$ 16.9739	$(N_g = 1600)$ 28.8981
$\mathcal{O}(10^{-6})$	$(N = 11)$ 7.99078	$(N = 2)$ 15.0037	$(N = 12)$ 22.7535	$(N_g = 7500)$ 1137.6

$(\nu = 9/10)$

L^2-norm Error	PG Spectral Method	DSM	DSEM ($N_{el} = 2$)	FDM
$\mathcal{O}(10^{-4})$	$(N = 7)$ 2.85357	$(N = 9)$ 6.38253	$(N = 9)$ 9.04712	$(N_g = 2000)$ 62.9404
$\mathcal{O}(10^{-5})$	$(N = 9)$ 4.96675	$(N = 11)$ 11.3878	$(N = 11)$ 16.9654	$(N_g = 16000)$ 1968
$\mathcal{O}(10^{-6})$	$(N = 11)$ 8.05677	$(N = 12)$ 14.1633	$(N = 12)$ 22.4631	Running Out of Memory

Chapter Six

Spectral Element Methods for Fractional Advection Equation

We develop spectral element methods for time- and space- Fractional Advection Equation (TSFAE) of the form ${}_0\mathcal{D}_t^{\tau}u(x,t)+\theta\ {}_0\mathcal{D}_x^{\nu}u(x,t) = f(x,t)$, of order $\tau \in (0,1]$, $\nu \in (0,1)$, subject to Dirichlet initial/boundary conditions. We present two exponentially accurate and efficient methods for *global* discretization of both the temporal and spatial terms, instead of employing traditional low-order time-integration methods. To this end, we first develop a Petrov-Galerkin in time and discontinuous Galerkin in space (PG-DG) method, where we carry out the time-integration using a single time-domain spectral method (SM), and we perform the spatial discretization using the discontinuous spectral/*hp* element method (DSEM). This scheme also leads to a more efficient time-integration when the time-derivative is integer-order i.e., $\tau = 1$. We develop the *SM-DSEM* scheme based on a new spectral theory for fractional Sturm-Liouville problems (FSLPs), recently presented in [187]. We choose the corresponding space-time bases from the span of tensor product of the introduced eigenfunctions. Specifically, we employ the eigenfunctions of the FSLP of *first* kind (FSLP-I), called *Jacobi polyfractonomial*s, as temporal bases. We also employ the corresponding *asymptotic* eigensolutions to FSLP-I, which are Jacobi polynomials, as spatial basis. Next, we construct a different test function space, defined as the span of tensor product of polyfractonomial eigenfunctions of the FSLP of *second* kind (FSLP-II), as the temporal test functions, and the corresponding *asymptotic* eigensolutions to FSLP-II, as the spatial ones. Subsequently, we extend the PG-DG to a *DG-DG* scheme employing DG method in both time and space. In this scheme, both time-integration and spatial discretization are performed in an DSEM fashion (DSEM-DSEM). Our numerical tests confirm the expected exponential-like/algebraic convergence, respectively, in corresponding *p*- and *h*-refinements in various test-cases, and show a four-order of magnitude speed-up compared to finite-difference discretizations.

6.1 Background

The notion of fractional differential operators has been rapidly extended to many fractional partial differential equations (FPDEs) such as fractional Burgers' equation [163], fractional Fokker-Planck equation [14], and fractional advection-diffusion equation [67]. However, the extension of existing numerical methods, developed for integer-order PDEs (see e.g., [64, 106, 68, 195, 77] and references therein) to their corresponding FPDEs is not a straightforward task. It is mainly because of the *non-local* nature and long-range *history*-dependence of fractional differential operators. However, the development of numerical schemes in this area has received enormous attention and has undergone a fast evolution in recent years. Most of numerical methods developed for integer-order PDEs have been applied to FPDEs; methods such as Finite Difference Methods (FDM), Spectral Methods (SM), and Finite/Spectral Element Methods (FEM/SEM).

As indicated in previuous chapters, the implementation of FDM approaches (see e.g., [51, 104, 166, 30]) is relatively easy, however, the challenging issue in FDM is that the convergence is *algebraic* and the accuracy is limited. Moreover, FDM suffers from the heavy cost of computing the long-range memory since FDM is inherently a *local* approach whereas fractional derivatives are essentially *global* (nonlocal). This fact would suggest global schemes such as spectral methods may be more appropriate tools for discretizing FPDEs.

The early works in SM were developed in [163, 25, 147] employing collocation approaches. The idea of collocation was later adopted by Khader [86], who proposed a Chebyshev collocation method for the discretization of the space-fractional diffusion equation. More recently, Khader and Hendy [87] developed a Legendre pseudospec-

tral method for fractional-order delay differential equations. The aforementioned schemes are relatively easy to implement however their performance has not been tested rigorously or systematically and only limited cases have been examined. The first fundamental work on spectral methods for FPDEs was done by Li and Xu [108, 109], which was based on the early work of Fix and Roop [60]. They developed a time-space SM for time-fractional diffusion equation, where the spatial term is integer-order, with exponential convergence. In this scheme, the corresponding stiffness and mass matrices however are dense and gradually become ill-conditioned when the fractional order tends to small values. Hence, due to the nature of single-domain spectral methods, carrying out long-time and/or adaptive integration using such a SM becomes prohibited. Moreover, we note that the expected fast convergence in SMs is achieved only when the solution belongs to higher Sobolev spaces and possesses high regularity. This motivates employing domain decomposition and developing proper finite element methods in addition to spectral element methods in an efficient form.

Unlike the great effort put on developing FDM and the considerable work done on SM schemes, very little attention has been put on developing rigorous high-order FEM and SEM methods. Fix and Roop [60] developed the first theoretical framework for the least-square FEM approximation of a fractional order differential equation, where optimal error estimates are proven for piecewise linear elements. However, Roop [151] later showed that the main hurdle to overcome in FEM is the non-local nature of the fractional operator, which leads to large dense matrices; he showed that even the construction of such matrices presents difficulties. Among other rigoours works, McLean and Mustapha [122] developed a piecewise-constant Discontinuous Galerkin (DG) method for the time-discretization of a sub-diffusion equation. A Chebyshev-SEM for fractional-order transport was adopted by Hanert

[66], and later on, the idea of the least-square FEM was extended to SEM by Carella [31]. Recently, Deng and Hesthevan [49], also Xu and Hesthaven [179] developed Local Discontinuous Galerkin (LDG) methods for solving space-fractional diffusion and advection-diffusion problems with optimal accuracy.

In our earlier study in [189], we developed efficient and highly accurate Petrov-Galerkin (PG) spectral and discontinuous Galerkin (DG) spectral element methods for FODEs of the form ${}_0\mathcal{D}_t^\tau u(t) = f(t)$ and ${}_t\mathcal{D}_T^\tau u(t) = f(t)$, $\tau \in (0,1)$, subject to Dirichlet initial conditions. The goal of the present study is to generalize the aforementioned schemes to linear hyperbolic FPDEs, where the corresponding temporal and spatial stiffness/mass matrices co-exist. The main contribution of this paper is the development of highly accurate and efficient methods for time- and space- Fractional Advection Equation (TSFAE) of the form ${}_0\mathcal{D}_t^\tau u(x,t) + \theta\ {}_0\mathcal{D}_x^\nu u(x,t) = f(x,t)$, of order $\tau \in (0,1]$, $\nu \in (0,1)$. We accomplish this following the spectral theory on the fractional Sturm-Liouville eigen-problem, recently developed in [187], where the corresponding eigenfunctions, called *Jacobi polyfractonomial*s, are employed as basis and test functions.

The TSFAE problem is of physical and mathematical importance. From the view point of transport kinetics, this equation governs the PDF of the continuous-time random walk (CTRW) limit processes, known as $\tau\&\nu$-stable Lévy processes with strictly positive jumps and waiting times when the spatial order $\nu \in (0,1)$ [124]. In fluid mechanics, the aforementioned equation when $\tau = 1/2$ and $\nu \to 1$ has been shown to be equivalent to the governing equations in Stokes first and second problems after performing a proper change of variable through Laplace transform [98]. From the mathematical development point of view, our approach is analogous to the first DG method, developed in 1973 [148] for time-independent linear advection equations that paved the way for further development of DG schemes for other

PDEs. The present study provides a suitable platform for further development of PG-DG methods for higher-order FPDEs such as fractional wave or advection-diffusion equation. Here in this study, the major feature of our schemes is the *global* and multi-element discretization of the temporal term, in addition to the spatial term, rather than utilizing traditional low-order time-integration methods, particularly when $\tau = 1$.

We first develop a Petrov-Galerkin in time and discontinuous Galerkin in space (PG-DG) method, where we carry out the time-integration using a SM-type discretization, and we perform the spatial discretization using the discontinuous spectral/hp element method (DSEM). This scheme is in contrast to the traditional approaches (e.g., see [111]) which treat the temporal term using FDM and discretize the spatial term by SM. In fact, in such mixed FDM-SM schemes, the high-order spatial descretization can be easily polluted by the low accuracy of the time-integration. Here, we develop the *SM-DSEM* scheme based on a new spectral theory for fractional Sturm-Liouville problems (FSLPs), introduced in [187], which provides proper spaces of basis and test functions. Subsequently, we extend the PG-DG to a DG-DG scheme, in which both time-integration and spatial discretization are performed in an hp-element fashion (*DSEM-DSEM*). In contrast to common FEM/SEM methods, in which the construction of the corresponding mass and stiffness matrices is challenging (see e.g., [151]), all the aforementioned matrices in our methods are constructed *exactly* and *efficiently*.

6.2 Problem Definition

We consider the following linear time- and space-Fractional Advection Equation (TSFAE)

$$\begin{aligned} {}_0\mathcal{D}_t^\tau u(x,t) + \theta\ {}_0\mathcal{D}_x^\nu u(x,t) &= f(x,t), \quad (x,t) \in [0,L] \times [0,T], \\ u(x,0) &= g(x), \\ u(0,t) &= h(t), \end{aligned} \tag{6.1}$$

where $\theta > 0$, $g \in C[0,L]$ and $h \in C[0,T]$, such that $g(0) = h(0) = 0$. Moreover, denoted by ${}_0\mathcal{D}_t^\tau u(x,t)$ is the left-sided Reimann-Liouville time-fractional derivative of order $\tau \in (0,1]$ following [142], defined as

$${}_0\mathcal{D}_t^\tau u(x,t) = \frac{1}{\Gamma(1-\tau)} \frac{\partial}{\partial t} \int_0^t \frac{u(x,s)}{(t-s)^\tau}\, ds, \quad t > 0, \quad x \in [0,L], \tag{6.2}$$

in which Γ represents the Euler gamma function. In (6.2), as $\nu \to 1$, the *global* (non-local) operator ${}_0\mathcal{D}_t^\tau u(x,t) \to \partial u(x,t)/\partial t$, recovering the *local* first-order partial derivative with respect to t. Also, ${}_0\mathcal{D}_x^\nu u(x,t)$ denotes the left-sided Reimann-Liouville space-fractional derivative of order $\nu \in (0,1)$, defined as

$${}_0\mathcal{D}_x^\nu u(x,t) = \frac{1}{\Gamma(1-\nu)} \frac{\partial}{\partial x} \int_0^x \frac{u(z,t)}{(x-z)^\nu}\, dz, \quad x > 0, \quad t \in [0,T]. \tag{6.3}$$

We could also define the fractional derivatives in (6.1) to be of Caputo fractional derivative sense i.e, ${}_0^C\mathcal{D}_t^\tau$ and ${}_0^C\mathcal{D}_x^\nu$, respectively, defined as

$${}_0^C\mathcal{D}_t^\tau u(x,t) = \frac{1}{\Gamma(1-\tau)} \int_0^t \frac{\partial u(x,s)/\partial s}{(t-s)^\tau}\, ds, \quad t > 0, \quad x \in [0,L], \tag{6.4}$$

and

$$ {}_0^C\mathcal{D}_x^\nu u(x,t) = \frac{1}{\Gamma(1-\nu)} \int_0^x \frac{\partial u(z,t)/\partial z}{(x-z)^\nu}\, dz, \quad x > 0, \quad t \in [0,T]. \tag{6.5} $$

These fractional operators are defined in fact by interchanging the order of the integration and differentiation in (6.2) and (6.3). However, the two definitions are closely linked by the following relationships

$$ {}_0\mathcal{D}_t^\tau u(x,t) = \frac{g(x)}{\Gamma(1-\tau)\ t^\tau} + {}_0^C\mathcal{D}_t^\tau u(x,t), \tag{6.6} $$

and

$$ {}_0\mathcal{D}_x^\nu u(x,t) = \frac{h(t)}{\Gamma(1-\nu)\ x^\nu} + {}_0^C\mathcal{D}_x^\nu u(x,t), \tag{6.7} $$

By virtue of (6.6) and (6.7), the TSFAE (6.1) becomes identical to the corresponding problem with the Caputo fractional derivatives when $g(x) = h(t) = 0$. Without loss of generality, we consider (6.1) subject to homogeneous Dirichlet initial and boundary conditions in this study. Moreover, we note that when the aforementioned fractional derivatives apply to a *univariate* function, the corresponding partial derivative is replaced by an *ordinary* derivative one.

6.3 PG-DG Method: SM-in-Time & DSEM-in-Space

We develop a PG-DG method for (6.1), where the time-fractional order $\tau \in (0,1]$ and space-fractional order $\nu \in (0,1)$, subject to homogeneous Dirichlet initial/boundary conditions. Here, we aim rather than utilizing traditional low-order time-integrators such as FDM when $\tau \in (0,1)$, or Adams families when $\tau = 1$, to treat the temporal term $\forall \tau \in (0,1]$ globally by employing a spectral method (SM) in the single

time-domain $[0, T]$. Moreover, we perform the spatial discretization by a Discontinuous Spectral Element Method (DSEM). In the SM-DSEM scheme, we partition the computational domain into N_{el} non-overlapping *space-time* elements, $\Omega_e = [x_{e-1/2}, x_{e+1/2}] \times [0, T]$, such that $\cup_{e=1}^{N_{el}} \Omega_e = [0, L] \times [0, T]$. In SM-DSEM, the new eigensolutions, introduced in [187], yield new sets of *basis* and *test* functions, properly suited for our Petrov-Galerkin framework.

6.3.1 Basis Functions

In SM-DSEM, we represent the solution in each space-time element Ω_e in terms of special basis functions, constructed as the tensor product of the the eigenfunctions in the following manner. We first recall the following *Jacobi polyfractonomials*, obtained as the eigenfunctions of the FSLP of first kind explicitly in [187] as

$$ {}^{(1)}\mathcal{P}_n^{\alpha,\beta,\mu}(x) = (1+x)^{-\beta+\mu-1} P_{n-1}^{\alpha-\mu+1,-\beta+\mu-1}(x), \quad x \in [-1, 1], \tag{6.8} $$

where $P_{n-1}^{\alpha-\mu+1,-\beta+\mu-1}(x)$ are the standard Jacobi polynomials in which $\mu \in (0, 1)$, $-1 \leq \alpha < 2 - \mu$, and $-1 \leq \beta < \mu - 1$. Particularly, ${}^{(1)}\mathcal{P}_n^{\alpha,\beta,\mu}(x)$ represent the eigenfunctions of the *singular* FSLP of first kind (SFSLP-I) when $\alpha \neq -1$ and $\beta \neq -1$; otherwise ${}^{(1)}\mathcal{P}_n^{\mu}(x) \equiv {}^{(1)}\mathcal{P}_n^{-1,-1,\mu}(x)$ denote the eigenfunctions of the *regular* FSLP of first kind (RFSLP-I). The eigenfunctions (6.8) are the baseline of our space-time basis construction.

To define the *spatial* basis in the interval $[x_{e-1/2}, x_{e+1/2}]$, let the fractional power of the multiplier term in (6.8) $(-\beta + \mu - 1) \to 0$, then ${}^{(1)}\mathcal{P}_n^{\alpha,\beta,\mu}(x) \to P_{n-1}^{\alpha-\mu+1,0}(x)$, where $\alpha - \mu + 1 = \eta \in (0, 1)$, since $-1 \leq \alpha < 2 - \mu$ and $-1 \leq \beta < \mu - 1$, recalling from [187]. Hence, through an affine mapping from $[-1, 1]$ to $[x_{e-1/2}, x_{e+1/2}]$, we

define the spatial basis as

$$\widetilde{P}_m^{\,\eta,0}(\,x^e\,),\ m=0,1,2,\cdots,\quad x^e\in[x_{e-1/2},x_{e+1/2}], \tag{6.9}$$

which are Jacobi polynomials associated with the parameters η and 0.

In order to define the *temporal* basis in the interval $[0,T]$, we recall that the regular $\{^{(1)}\mathcal{P}_n^{\,\mu}(x)\}_{n=1}^N$ and singular $\{^{(1)}\mathcal{P}_n^{\alpha,\beta,\mu}(x)\}_{n=1}^N$ sets (for some $N\in\mathbb{N}$) have identical approximating properties when $\alpha=\beta$. Hence, by choosing $\alpha=\beta=-1$ and through the affine mapping $x(t)=2t/T-1$, from the standard interval $[-1,1]$ to $[0,T]$ we define our temporal basis as

$$^{(1)}\widetilde{\mathcal{P}}_n^{\,\mu}(t)=\Big(\frac{2}{T}\Big)^{\mu}t^{\mu}P_{n-1}^{-\mu,\mu}(\,x(t)\,),\ n=1,2,\cdots,\quad t\in[0,T], \tag{6.10}$$

known as *shifted* Jacobi polyfractonomial of fractional order $(n-1+\mu)$. Now, having defined the spatial and temporal functions in (6.9) and (6.10), we construct the space-time trial (basis) space V^e as

$$V^e\equiv span\{\widetilde{P}_m^{\,\eta,0}(\,x^e\,)\ ^{(1)}\widetilde{\mathcal{P}}_n^{\,\mu}(t):m=0,1,\ldots,M,n=1,2,\ldots,N\}, \tag{6.11}$$

where we shall approximate the solution to (6.1) in terms of a linear combination of elements in V^e. The corresponding space-time basis functions are then *discontinuous* in space at the interfaces of elements Ω_e, $e=1,2,\cdots,N_{el}$, while they satisfy the homogeneous initial condition in the single time-domain. We note that the corresponding *nodal* representation of (6.10) has been recently employed in developing fractional spectral collocation methods for fractional ODEs/PDEs [190].

Fractional Derivatives of the Bases

The following lemma is useful to obtain the space-fractional derivative of the spatial basis $\widetilde{P}_m^{\,\eta,0}(\,x^e\,)$.

Lemma 6.3.1. *[5] For* $\mu > 0$, $\alpha > -1$, $\beta > -1$, *and* $\forall x \in [-1, 1]$

$$(1+x)^{\beta+\mu}\,\frac{P_m^{\alpha-\mu,\beta+\mu}(x)}{P_m^{\alpha-\mu,\beta+\mu}(-1)} = \frac{\Gamma(\beta+\mu+1)}{\Gamma(\beta+1)\Gamma(\mu)P_m^{\alpha,\beta}(-1)}\int_{-1}^{x}\frac{(1+s)^{\beta}\;P_m^{\alpha,\beta}(s)}{(x-s)^{1-\mu}}ds. \quad (6.12)$$

By the definition of the left-sided Riemann-Liouville integral ${}_{-1}\mathcal{I}_x^{\mu}$ (see e.g. [142]) and evaluating the special end-values $P_m^{\alpha-\mu,\beta+\mu}(-1)$ and $P_m^{\alpha,\beta}(-1)$, we can re-write (6.12) as

$${}_{-1}\mathcal{I}_x^{\mu}\Big\{(1+x)^{\beta}P_m^{\alpha,\beta}(x)\Big\} = \frac{\Gamma(m+\beta+1)}{\Gamma(m+\beta+\mu+1)}(1+x)^{\beta+\mu}\,P_m^{\alpha-\mu,\beta+\mu}(x). \quad (6.13)$$

Now, by taking the fractional derivative ${}_{-1}\mathcal{D}_x^{\mu}$ on both sides of (6.13) when $\beta = -\mu$ we obtain

$${}_{-1}\mathcal{D}_x^{\mu}\Big\{P_m^{\alpha-\mu,0}(x)\Big\} = \frac{\Gamma(m+1)}{\Gamma(m-\mu+1)}(1+x)^{-\mu}P_m^{\alpha,\,-\mu}(x). \quad (6.14)$$

Moreover, from the properties of the eigensolutions in [187], the left-sided Riemann-Liouville fractional derivative of (6.10) is given as

$${}_0\mathcal{D}_t^{\,\mu}\Big({}^{(1)}\widetilde{\mathcal{P}}_n^{\,\mu}(t)\Big) = \Big(\frac{2}{T}\Big)^{\mu}\,\frac{\Gamma(n+\mu)}{\Gamma(n)}P_{n-1}(\,x(t)\,), \quad (6.15)$$

stating that the μ^{th} order fractional derivative of such fractal (non-polynomial) basis functions of order $(n-1+\mu)$ is a standard Legendre polynomial of integer order $(n-1)$.

6.3.2 Test Functions

In order to construct the space of test functions, we recall the following Jacobi polyfractonomials, introduced as the eigensolutions of the FSLP of *second* kind, obtained explicitly as

$$ {}^{(2)}\mathcal{P}_n^{\alpha,\beta,\mu}(x) = (1-x)^{-\alpha+\mu-1} P_{n-1}^{-\alpha+\mu-1\,,\,\beta-\mu+1}(x), \quad x \in [-1,1], \tag{6.16} $$

in [187], where $-1 < \alpha < \mu - 1$ and $-1 < \beta < 2 - \mu$, and $\mu \in (0,1)$. Particularly ${}^{(2)}\mathcal{P}_n^{\alpha,\beta,\mu}(x)$ denote the eigenfunctions of the *singular* FSLP of second kind (SFSLP-II) when $\alpha \neq -1$ and $\beta \neq -1$, also ${}^{(2)}\mathcal{P}_n{}^{\mu}(x) \equiv {}^{(2)}\mathcal{P}_n^{-1,-1,\mu}(x)$ denote the eigenfunctions of the *regular* FSLP of first kind (RFSLP-II). In a similar fashion, we employ the eigenfunctions (6.16) as the baseline of construction for our space-time test functions.

To define the *spatial* test functions in the interval $[x_{e-1/2}, x_{e+1/2}]$, we set the power of the fractional multiplier in (6.16) $(-\alpha + \mu - 1) \to 0$, then ${}^{(2)}\mathcal{P}_n^{\alpha,\beta,\mu}(x) \to P_{n-1}^{0,\beta-\mu+1}(x)$, where $\beta - \mu + 1 = \chi \in (0,1)$. Hence, we define the spatial basis as

$$ \widetilde{P}_i{}^{0,\chi}(\,x^e\,), \;\; i = 0,1,2,\cdots, \quad x^e \in [x_{e-1/2}, x_{e+1/2}], \tag{6.17} $$

which are Jacobi polynomials associated with the parameters 0 and χ. We also define the *temporal* basis in the interval $[0,T]$ by choosing $\alpha = \beta = -1$ in (6.16) and mapping from the standard interval $[-1,1]$ to $[0,T]$ as

$$ {}^{(2)}\widetilde{\mathcal{P}}_j{}^{\mu}(\,t\,) = (\frac{2}{T})^{\mu}\,(T-t)^{\mu} P_{j-1}^{\mu,-\mu}(\,x(t)\,), \;\; j = 1,2,\cdots, \quad t \in [0,T]. \tag{6.18} $$

Now, having defined the spatial and temporal functions in (6.17) and (6.18), we

construct the space-time test space $\mathcal{V}^e$ as

$$\mathcal{V}^e \equiv span\{\widetilde{P}_i^{\,0,\chi}(\,x^e\,)\;{}^{(2)}\widetilde{\mathcal{P}}_j^{\,\mu}(\,t\,) : i = 0, 1, \ldots, M, j = 1, 2, \ldots, N\}, \tag{6.19}$$

where we test the problem (6.1) against the elements in $\mathcal{V}^e$.

Fractional Derivatives of the Test Functions

We use the following lemma to calculate the space-fractional derivative of the spatial test functions $\widetilde{P}_i^{\,0,\chi}(\,x^e\,)$.

Lemma 6.3.2. *[5] For $\mu > 0$, $\alpha > -1$, $\beta > -1$, and $\forall x \in [-1, 1]$*

$$(1-x)^{\alpha+\mu}\,\frac{P_i^{\alpha+\mu,\beta-\mu}(x)}{P_i^{\alpha+\mu,\beta-\mu}(+1)} = \frac{\Gamma(\alpha+\mu+1)}{\Gamma(\alpha+1)\Gamma(\mu)P_i^{\alpha,\beta}(+1)}\int_x^1 \frac{(1-s)^\alpha\; P_i^{\alpha,\beta}(s)}{(s-x)^{1-\mu}}ds. \tag{6.20}$$

Once again by the definition of the right-sided Riemann-Liouville integral ${}_x\mathcal{I}_1^\mu$ (see e.g. [142]) and evaluating the special end-values $P_i^{\alpha-\mu,\beta+\mu}(+1)$ and $P_i^{\alpha,\beta}(+1)$, we can re-cast (10.17) as

$${}_x\mathcal{I}_1^\mu\Big\{(1-x)^\alpha P_i^{\alpha,\beta}(x)\Big\} = \frac{\Gamma(i+\alpha+1)}{\Gamma(i+\alpha+\mu+1)}(1-x)^{\alpha+\mu}P_i^{\alpha+\mu,\beta-\mu}(x). \tag{6.21}$$

In a similar fashion, by taking the fractional derivative ${}_x\mathcal{D}_{-1}^\mu$ on both sides of (6.21) when $\alpha = -\mu$ we obtain

$${}_x\mathcal{D}_1^\mu\Big\{P_i^{0,\beta-\mu}(x)\Big\} = \frac{\Gamma(i+1)}{\Gamma(i-\mu+1)}(1-x)^{-\mu}P_i^{-\mu,\beta}(x). \tag{6.22}$$

The relations (6.14) and (10.20) are useful in computing the corresponding spatial *stiffness* matrix in the discontinuous SM-DSEM.

Next, following [187], the right-sided Riemann-Liouville fractional derivative of (6.18) is obtained as

$$ {}_t\mathcal{D}_T^{\mu}\left({}^{(2)}\widetilde{\mathcal{P}}_j^{\mu}(t)\right) \;=\; \left(\frac{2}{T}\right)^{\mu}\frac{\Gamma(j+\mu)}{\Gamma(j)}P_{j-1}(\,x(t)\,). \tag{6.23} $$

The relations (C.37) and (C.38) will be employed in computing the corresponding temporal *stiffness* matrix in the SM-DSEM scheme.

Remark 6.3.3. The Jacobi polynomials $P_i^{0,\chi}(x)$ in (6.19) and $P_m^{\eta,0}(x)$ in (6.9) have been previously utilized by Li and Xu [108], where they formulated exact quadrature rules for the corresponding temporal matrices arising in their Galerkin method. Here, we obtain and interpret the aforementioned polynomials as the asymptotic forms of the polyfractonomial eigen-functions of FSLPs, and employ them in a discontinuous Petrov-Galerkin framework.

The following lemma is useful in carrying out the temporal fractional integration-by-parts in the development of the SM-DSEM scheme.

Lemma 6.3.4. *[108]: For all* $0 < \xi < 1$*, if* $u \in H^1([a,b])$*, such that* $u(a) = 0$*, and* $w \in H^{\xi/2}([a,b])$*, then*

$$ ({}_a\mathcal{D}_s^{\xi}u, w)_{\Omega} = (\,{}_a\mathcal{D}_s^{\xi/2}u\,,\,{}_s\mathcal{D}_b^{\xi/2}w\,)_{\Omega}, \tag{6.24} $$

where $(\cdot,\cdot)_{\Omega}$ *represents the standard inner product in* $\Omega = [a,b]$*.*

Next, we prove the following lemma that is useful in deriving the weak form in the DSEM-DSEM scheme and discretizing the spatial advection term using the discontinuous spectral element method.

Lemma 6.3.5. *For all* $0 < \xi < 1$*, if* $u \in H^1([a,b])$ *and* $w \in H^{\xi/2}([a,b])$*, then*

$$(\ {}_{a^+}\mathcal{D}_s^{\xi} u, w \ )_\Omega = (\ {}_{a^+}\mathcal{D}_s^{\xi/2} u \ , \ {}_s\mathcal{D}_b^{\xi/2} w \ )_\Omega. \tag{6.25}$$

Proof. Let $u(a) = u_D \neq 0$ (constant). Then,

$$\begin{aligned}
(\ {}_{a^+}\mathcal{D}_s^{\xi} u, w \ )_\Omega &= (\ {}_{a^+}\mathcal{D}_s^{\xi}(u - u_D) \ , \ w \ )_\Omega + (\ {}_{a^+}\mathcal{D}_s^{\xi} u_D \ , \ w \ )_\Omega, \\
&= (\ {}_{a^+}\mathcal{D}_s^{\xi/2}(u - u_D) \ , \ {}_x\mathcal{D}_s^{\xi/2} w \ )_\Omega + (\ {}_{a^+}\mathcal{D}_s^{\xi} u_D \ , \ w \ )_\Omega, \ \textit{by Lemma 6.3.4} \\
&= ({}_{a^+}\mathcal{D}_s^{\xi/2} u, {}_x\mathcal{D}_s^{\xi/2} w \ )_\Omega - ({}_{a^+}\mathcal{D}_s^{\xi/2} u_D, {}_x\mathcal{D}_s^{\xi/2} w \ )_\Omega + ({}_{a^+}\mathcal{D}_s^{\xi} u_D, w \ )_\Omega.
\end{aligned}$$

Now, it remains to show that $({}_{a^+}\mathcal{D}_s^{\xi} u_D, w \ )_\Omega = ({}_{a^+}\mathcal{D}_s^{\xi/2} u_D, {}_x\mathcal{D}_s^{\xi/2} w \ )_\Omega$. We note that the lower-terminal of the fractional derivative now is a^+ and not a. Therefore, it does not contradict the previous lemma. Moreover, we can always represent u_D in terms of $Q_n(s) \in C_0^\infty([a,b])$ such that $\forall s \in (a,b), \lim_{N\to\infty} \sum_{n=1}^{N} c_n Q_n(s)$ converges to u_D in a point-wise fashion. Hence,

$$\begin{aligned}
({}_{a^+}\mathcal{D}_s^{\xi} u_D \quad , \quad w \ )_\Omega &= ({}_{a^+}\mathcal{D}_s^{\xi} \lim_{N\to\infty} \sum_{n=1}^{N} c_n Q_n(s), w \ )_\Omega \\
&= (\lim_{N\to\infty} \sum_{n=1}^{N} c_n [{}_{a^+}\mathcal{D}_s^{\xi/2} Q_n(s)], {}_s\mathcal{D}_b^{\xi/2} w \ )_\Omega, \ \textit{by Lemma 6.3.4 since } Q_n(s) \in C_0^\infty([a,b]) \\
&= ({}_{a^+}\mathcal{D}_s^{\xi/2} u_D, {}_s\mathcal{D}_b^{\xi/2} w \ )_\Omega.
\end{aligned}$$

□

6.3.3 Implementation of SM-DSEM Scheme

Now, we implement the SM-DSEM scheme to solve TSFAE (6.1), where we seek the solution in $\Omega_e = [x_{e-1/2}, x_{e+1/2}] \times [0, T]$ in terms of the linear combination of elements in the basis function space V^e of the form

$$u^e_{MN}(x,t) = \sum_{m=0}^{M} \sum_{n=1}^{N} \hat{u}^e_{MN} \tilde{P}^{\eta,0}_m(x^e)\ {}^{(1)}\tilde{\mathcal{P}}^{\mu}_n(t). \tag{6.26}$$

The ultimate step of the SM-DSEM scheme is to obtain a linear system corresponding to (6.1) of the form

$$\mathsf{A}\ \hat{\mathbf{U}}^e \mathsf{B}\ +\ \mathsf{C}\, \hat{\mathbf{U}}^e \mathsf{D} = \mathsf{E}, \tag{6.27}$$

for some matrices A, B, C, D, and E, where $\hat{\mathbf{U}}^e$ is the matrix of unknown coefficient in Ω_e and $(\hat{\mathbf{U}}^e)_{mn} = \hat{u}^e_{mn}$. The linear system (6.27) is called *Lyapunov* matrix equation for which there are several numerical approaches introduced (see e.g., [71, 137, 152, 174] and references therein). To this end, we require the solution (6.26) to satisfy the following variational (weak) form as

$$\begin{aligned} \Big({}_0\mathcal{D}^{\tau/2}_t u^e_{MN}(x,t)\ ,\ {}_t\mathcal{D}^{\tau/2}_T v^e(x,t)\Big)_{\Omega_e} \ &+\ \theta \left({}_{x^+_{e-1/2}}\mathcal{D}^{\nu/2}_x u^e_{MN}(x,t)\ ,\ {}_x\mathcal{D}^{\nu/2}_{x^-_{e+1/2}} v^e(x,t)\right)_{\Omega_e} \\ &+\ \gamma_e \Big(\llbracket u^e_{MN}(x_{e-1/2},t)\rrbracket\, ,\, v^e(x^-_{e+1/2},t)\Big)_{[0,T]} \\ &=\ \Big(f(x,t), v^e(x,t)\Big)_{\Omega_e} - \theta \cdot \mathcal{H}^x_e, \end{aligned} \tag{6.28}$$

$\forall v^e(x,t) \in \mathcal{V}^e$, beginning from the first space-time element, i.e., $e = 1$, and marching element-by-element along the x-axis to $e = N_{el}$. In (6.28), $\gamma_e = -\frac{\theta(\Delta x)^{1-\nu}_e}{(1-\nu)\Gamma(1-\nu)}$, $\llbracket u^e_{MN}(x_{e-1/2},t)\rrbracket$ represents the jump discontinuity of the solution at $x = x_{e-1/2}$ as

Construct S_t and M_t ;
for $e = 1$*;* $e = N_{el}$ **do**
  Construct M_x^e, S_x^e, and η^e ;
  if $e = 1$ **then**
    $\mathcal{H}_e^x = 0$;
  else
    Compute $\mathcal{H}_e^x$ then construct $\mathcal{F}^e$;
  end
  Solve $M_x^e \hat{\mathbf{U}}^e S_t^T + (\theta S_x^e + \gamma_e\ \eta^e)\, \hat{\mathbf{U}}^e M_t^T = \mathcal{F}^e$;
end

Algorithm 1: First PG-DG Method: a pseudocode for the SM-DSEM scheme, employed in a non-uniformly partitioned domain.

a function of time $t \in [0, T]$, $(\Delta x)_e = x_{e+1/2} - x_{e-1/2}$ is the (spatial) length of the e-th sub-domain; also $(\cdot,\cdot)_{\Omega_e}$ and $(\cdot,\cdot)_{[0,T]}$ represent, respectively, the standard inner product in the space-time element Ω_e, i.e.,

$$\Big(f(x,t), g(x,t)\Big)_{\Omega_e} = \int_0^T \int_{x^+_{e-1/2}}^{x^-_{e+1/2}} f(x,t) g(x,t)\ dx\ dt,$$

and the standard inner product in the time interval $[0, T]$ is defined as

$$\Big(p(t), q(t)\Big)_{[0,T]} = \int_0^T p(t)\, q(t)\ dt.$$

Finally, $\mathcal{H}_e^x$ is the *history-load* term, which we shall obtain in a convenient and computationally efficient form shortly.

We obtain the corresponding linear system by plugging the expansion (6.26) into the weak form (6.28), taking $v^e(x,t) = \widetilde{P}_i^{\,0,\chi}(\,x^e\,)\ {}^{(2)}\widetilde{\mathcal{P}}_j^{\,\mu}(\,t\,)$, and choosing $\eta = \chi = \nu/2$ and $\mu = \tau/2$ as the following Lyapunov matrix equation

$$M_x^e \hat{\mathbf{U}}^e S_t^T \ + \ (\theta S_x^e + \gamma_e \eta^e)\, \hat{\mathbf{U}}^e M_t^T = \mathcal{F}^e, \tag{6.29}$$

where η^e is a constant matrix associated with e-th element and $\hat{\mathbf{U}}^e$ is the unknown $(M+1)\times N$ matirx of coefficients. Moreover, the matrices S_t and M_t represent the corresponding temporal stiffness and mass matrices, also S_x^e and M_x^e denote the spatial stiffness and mass matrices, associated with element Ω_e, respectively. Finally, in (6.29), $\mathcal{F}^e$ is the total load matrix and the superscript ^{T} is the transpose operation.

In Algorithm 1, we present the necessary steps in the SM-DSEM scheme, where the computational domain is assumed to be non-uniformly partitioned. However, dealing with uniform elements, the matrices S_t, M_t, M_x^e, and S_x^e are constructed *once* at a preprocessing step. In the following, we obtain the aforementioned matrices *efficiently* and *exactly*.

Temporal Stiffness Matrix: S_t is an $N\times N$ *diagonal* matrix whose entries are obtained using (C.37) and (C.38) as

$$\begin{aligned}(S_t)_{jn} &= \int_0^T {}_tD_T^{\tau/2}\ {}^{(2)}\tilde{\mathcal{P}}_j^{\tau/2}(t)\,{}_0D_t^{\tau/2}\ {}^{(1)}\tilde{\mathcal{P}}_n^{\tau/2}(t)dt \\ &= \delta_{jn}\left(\frac{2}{T}\right)^{\tau-1}\left(\frac{\Gamma(n+\tau/2)}{\Gamma(n)}\right)^2\frac{2}{2n-1},\end{aligned} \tag{6.30}$$

in which δ_{jn} is the Kronecker delta.

Temporal Mass Matrix: M_t is also an $N\times N$ matrix whose entries are obtained as

$$(M_t)_{jn} = \int_0^T {}^{(2)}\tilde{\mathcal{P}}_j^{\tau/2}(t)\,{}^{(1)}\tilde{\mathcal{P}}_n^{\tau/2}(t)\ dt, \tag{6.31}$$

which can be computed exactly by mapping $[0,T]$ to the reference element $[-1,1]$ and employing the Gauss-Lobatto-Jacobi (GLJ) quadrature rule as follows:

$$
\begin{aligned}
(M_t)_{jn} &= J_t \cdot \int_{-1}^{1} {}^{(2)}\tilde{\mathcal{P}}_j^{\tau/2}(t(s))\,{}^{(1)}\tilde{\mathcal{P}}_n^{\tau/2}(t(s))\; ds \qquad (6.32)\\
&= J_t \cdot \int_{-1}^{1} (1-s)^{\tau/2}\,(1+s)^{\tau/2}\; P_{j-1}^{\tau/2,-\tau/2}(s) P_{n-1}^{-\tau/2,\tau/2}(s) ds\\
&= J_t \cdot \sum_{k=0}^{Q-1} w_k^{\tau/2,\tau/2}\; P_{k-1}^{\tau/2,-\tau/2}(s_k)\, P_{n-1}^{-\tau/2,\tau/2}(s_k),
\end{aligned}
$$

when $2Q-3 = 2(N-1)$. In (6.32), $J_t = (T/2)$ represents the Jacobian of the transformation, also $\{s_k\}_{k=0}^{Q-1}$ and $\{w_k^{\tau/2,\tau/2}\}_{k=0}^{Q-1}$ are the corresponding quadrature points and weights, associated with GLJ rule.

Spatial Stiffness Matrix: S_x^e is an $(M+1)\times(M+1)$ matrix whose entries are obtained as

$$
(S_x^e)_{im} = \int_{x_{e-1/2}}^{x_{e+1/2}} {}_{x_{e-1/2}}\mathcal{D}_x^{\nu/2}\tilde{P}_i^{\nu/2,0}(x)\,{}_x\mathcal{D}_{x_{e+1/2}}^{\nu/2}\tilde{P}_m^{0,\nu/2}(x)dx, \qquad (6.33)
$$

which can be computed exactly by mapping $[x_{e-1/2}, x_{e+1/2}]$ to the reference element $[-1,1]$ and employing another Gauss-Lobatto-Jacobi (GLJ) rule corresponding to a different weight function as follows:

$$
\begin{aligned}
(S_x^e)_{im} &= C_x^e \cdot \int_{-1}^{1} {}_{-1}\mathcal{D}_z^{\nu/2}\tilde{P}_i^{\nu/2,0}(x(z))\,{}_z\mathcal{D}_1^{\nu/2}\tilde{P}_m^{0,\nu/2}(x(z))dz \qquad (6.34)\\
&= C_x^e \cdot \Lambda_{im} \int_{-1}^{1} (1-z)^{-\nu/2}\,(1+z)^{-\nu/2}\; P_i^{\nu,-\nu/2}(z)\, P_m^{-\nu/2,\nu}(z)\\
&= C_x^e \cdot \Lambda_{im} \sum_{k=0}^{M} P_i^{\nu,-\nu/2}(z_k) P_m^{-\nu/2,\nu}(z_k)\rho_k^{-\nu/2,-\nu/2},
\end{aligned}
$$

where $C_x^e = (2/\Delta x_e)^{\nu-1}$, also

$$\Lambda_{im} = \frac{\Gamma(i+1)}{\Gamma(i-\nu/2+1)} \frac{\Gamma(m+1)}{\Gamma(m-\nu/2+1)}.$$

Moreover, $\{z_k\}_{k=0}^M$ and $\{\rho_k\}_{k=0}^M$ are the corresponding Gauss-Lobato-Jacobi (GLJ) quadrature points and weights in the interval $[-1,1]$, associated with the weight function $(1-z)^{-\nu/2}(1+z)^{-\nu/2}$. Here, we have used the relations (6.14) and (10.20) to obtain

$$\begin{aligned} {}_{-1}\mathcal{D}_z^{\nu/2} P_m^{\nu/2,0}(z) &= \frac{\Gamma(m+1)}{\Gamma(m-\tau/2+1)}(1+z)^{-\nu/2} P_m^{\nu,-\nu/2}(z), \\ {}_{z}\mathcal{D}_1^{\nu/2} P_i^{0,\nu/2}(z) &= \frac{\Gamma(i+1)}{\Gamma(i-\tau/2+1)}(1-z)^{-\nu/2} P_i^{-\nu/2,\nu}(z), \end{aligned}$$

in the reference element, employed in (6.34).

Spatial Mass Matrix: M_x^e is also an $(M+1)\times(M+1)$ matrix whose entries are defined as

$$(M_x^e)_{im} = \int_{x_{e-1/2}}^{x_{e+1/2}} \tilde{P}_i^{0,\nu/2}(x_e)\tilde{P}_m^{\nu/2,0}(x_e)dx, \tag{6.35}$$

where, we compute the mass matrix exactly as well using the standard Gauss-Lobato-Legendre (GLL) rule by choosing Q so that $2Q-3=2M$

$$\begin{aligned} (M_x^e)_{im} &= J_x^e \int_{-1}^{1} P_i^{0,\nu/2}(x(\xi))P_m^{\nu/2,0}(x(\xi))d\xi \\ &= J_x^e \sum_{k=0}^{Q} w_k P_i^{0,\nu/2}(\xi_k)P_m^{\nu/2,0}(\xi_k), \end{aligned} \tag{6.36}$$

where $J_x^e = (\Delta x_e)/2 = 1/2(x_{e+1/2} - x_{e-1/2})$ is the Jacobian of the transformation.

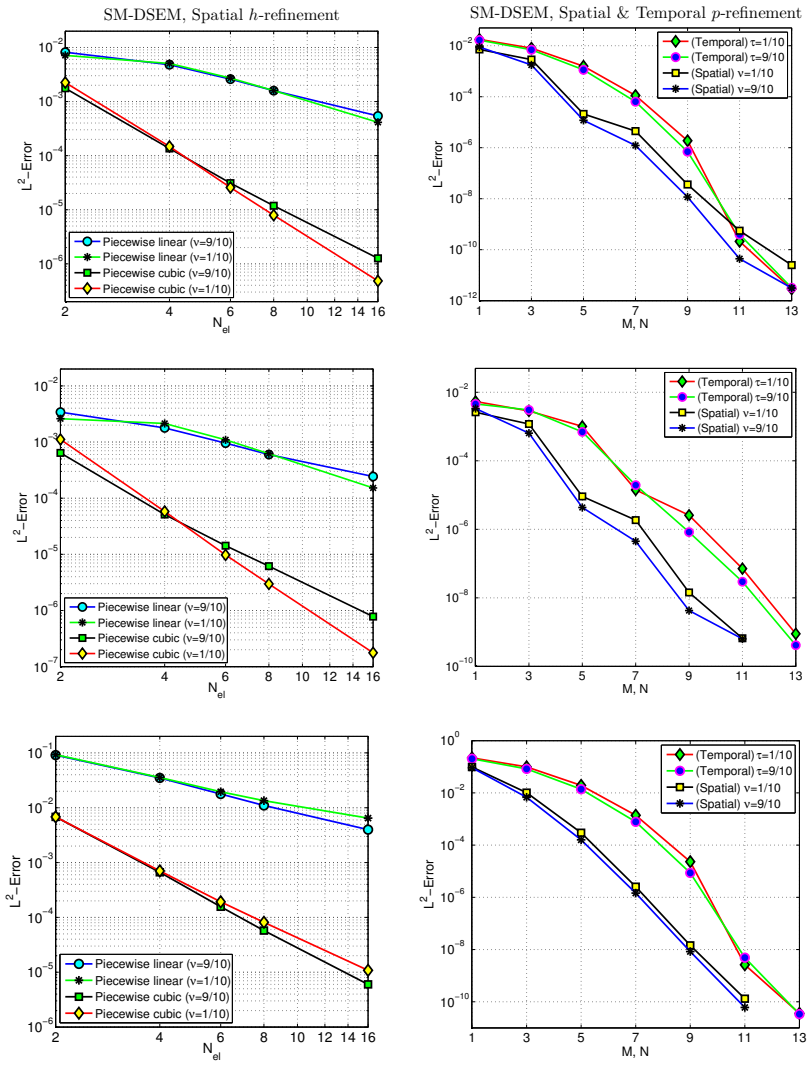

Figure 6.1: SM-DSEM; (Left) *h-refinement*: log-log L^2-error versus number of elements N_{el}, corresponding to piecewise linear/cubic spatial bases and $\nu = 1/10{,}9/10$ while $\tau = 1/2$; (Right) *p-refinement*: log-linear L^2-error versus M/N the spatial/temporal order-indices in (6.26). In the spatial p-refinement, the spatial orders are $\nu = 1/10$ and $9/10$ while $\tau = 1/2$, also in the temporal p-refinement $\tau = 1/10$ and $9/10$ while $\nu = 1/2$. The first row corresponds to $u^{ext}(x,t) = t^{10}\, x^{13/2} \sin(\pi x^{4/3})$, the second row to $u^{ext}(x,t) = t^6 \sin(\pi t)\, [x^{13/2} \sin(\pi x^{4/3})]$, and the third row to $u(x,t) = t^{10}[x^6 \exp(x^2) + x^{8+5/7} + x^{10+1/3}]$.

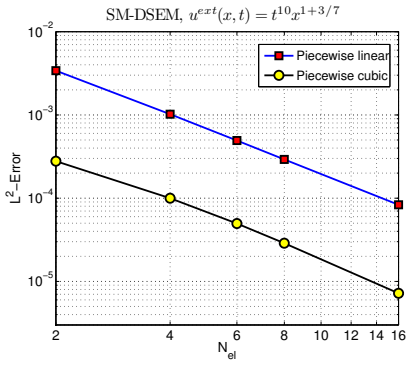

Figure 6.2: SM-DSEM: *h-refinement*: log-log L^2-error versus number of elements N_{el}, corresponding to piecewise linear/cubic spatial bases, temporal order $N = 13$ fixed, $\tau = \nu = 1/2$, and the exact solution $u^{ext}(x,t) = t^{10}\, x^{1+3/7}$.

Constant Matrix: η^e is also an $(M+1)\times(M+1)$ matrix whose entries are defined as

$$\begin{aligned} (\,\eta^e\,)_{im} &= P_i^{0,\nu/2}(+1)\, P_m^{\nu/2,0}(-1) \\ &= P_m^{\nu/2,0}(-1) \\ &= (-1)^m, \end{aligned} \tag{6.37}$$

for $m = 0, 1, 2, \cdots, M$.

Total Load Matrix $\mathcal{F}^e$ is an $(M+1)\times(N)$ matrix defined in terms of the aforementioned stiffness and mass matrices

$$\mathcal{F}^e = F^e - \gamma_e \eta^e \hat{\mathbf{U}}^{e-1} M_t^T - \theta\, \mathcal{H}_e^x \tag{6.38}$$

in which $F^e = (f(x,t), v^e(x,t))_{\Omega_e}$, $\hat{\mathbf{U}}^{e-1}$ denotes the coefficient matrix, known in the previously resolved element I_{e-1}, and we obtain the history-load term $\mathcal{H}_e^x$ in a

computationally efficient form as

$$(\mathcal{H}_e^x)_{ij} = F_e(x)P_i^{0,\nu/2}(x)\Big|_{x=x_{e-1/2}^+}^{x=x_{e+1/2}^-} - \int_{x_{e-1/2}}^{x_{e+1/2}} F_e(x)\frac{d}{dx}P_i^{0,\nu/2}(x)\,dx, \tag{6.39}$$

in which $F_e(x)$ represents the history function associated with the current element Ω_e

$$F_e(x) = \sum_{\varepsilon=1}^{e-1} F_e^{\varepsilon}(x), \tag{6.40}$$

consisting of all the past element contributions as

$$F_e^{\varepsilon}(x) = \sum_{m,n} \hat{u}_{mn}^{\varepsilon}\,(M_t)_{jn} \sum_{\delta=0}^{M} \Big(C_\delta \cdot (x-s)^{\delta+1-\nu}\Big)\tilde{P}_m^{\nu/2,0(\delta)}(s)\Big|_{s=s_{\varepsilon-1/2}^+}^{s=s_{\varepsilon+1/2}^-}, \tag{6.41}$$

where $\tilde{P}_m^{\nu/2,0(\delta)}(s)$ represents the δ-th derivative of $\tilde{P}_m^{\nu/2,0}(s)$. The coefficient $C_\delta = -1/\{\Gamma(1-\nu)\prod_{k=0}^{\delta}(k+1-\nu)\}$ decays in a factorial fashion with respect to δ. We note that when $e=1$, there is no history introduced into the problem, hence $(\mathcal{H}_1^x)_{ij} \equiv 0$.

In Fig. 6.1, we present the h-refinement (left panel), and p-refinement (right panel) tests for SM-DSEM. For the case of h-refinement, we present the log-log L^2-error versus the number of elements N_{el}, corresponding to piecewise linear/cubic spatial bases and $\nu = 1/10,\ 9/10$ while $\tau = 1/2$. Associated with the p-refinement, we plot the log-linear L^2-error versus M or N the spatial/temporal order-indices in (6.26). In the spatial p-refinement, the spatial orders $\nu = 1/10$ and $9/10$ while $\tau = 1/2$, also in the temporal p-refinement $\tau = 1/10$ and $9/10$ while $\nu = 1/2$. The first row corresponds to $u^{ext}(x,t) = t^{10}\,x^{13/2}\sin(\pi x^{4/3})$, the second row to $u^{ext}(x,t) = t^6\sin(\pi t)\,[x^{13/2}\sin(\pi x^{4/3})]$, and the third row to $u(x,t) = t^{10}[x^6\exp(x^2) + x^{8+5/7} + x^{10+1/3}]$. We observe an exponential-like convergence in p-refinement and

the algebraic convergence in h-refinement.

In all above cases, the exact solutions are relatively smooth. We examine a case where the exact solution does not belong to higher Sobolev spaces. For this case, we confirm the success of h-refinement in Fig. 6.2. In this plot, we present the log-log L^2-error versus number of elements N_{el}, corresponding to piecewise linear/cubic spatial bases, temporal order $N = 13$ fixed, $\tau = \nu = 1/2$, and the exact solution $u^{ext}(x,t) = t^{10}\, x^{1+3/7}$, which is not smooth with respect to x.

6.4 Time-integration using SM-DSEM when $\tau = 1$

We recall that SM-DSEM works equally well when the temporal time-derivative order τ tends to 1. In general, a PDE/FPDE, which is first-order in time, reads as

$$\frac{\partial u}{\partial t} = F(u; x, t), \tag{6.42}$$

where particularly in view of (6.1), the operator $F(u; x, t)$ is given as

$$F(u; x, t) = f(x, t) - \theta\ {}_0\mathcal{D}_x^{\nu} u(x, t),$$

Here, we regard the PG-DG method as an alternative scheme for *exponentially* accurate time-integration for a general $F(u; x, t)$, rather than utilizing existing *algebraically* accurate methods, including *multi-step* methods such as the Adams family and stiffly-stable schemes, also *multi-stage* approaches such as the Runge-Kutta method.

The idea of employing SM-DSEM when $\tau = 1$ is simply based on the useful

Table 6.1: CPU time (seconds) on a dual-core 2.9 GHz Intel processor, corresponding to the third-order in time SSS-DSEM, AB-DSEM, AM-DSEM, and our high-order SM-DSEM scheme all with two elements in space and polynomial order $M = 3$. The spatial fractional order is $\nu = 1/2$ and the temporal time-order is $\tau = 1$. Here, the simulation time $T = 1$.

L^2-Error	SSS-DSEM	AB-DSEM	AM-DSEM	SM-DSEM
$\mathcal{O}(10^{-4})$	8.5830	15.9770	9.2260	$(N = 7)$ 11.2020
$\mathcal{O}(10^{-8})$	117.423	328.655	136.976	$(N = 13)$ 28.634
$\mathcal{O}(10^{-9})$	233.153	652.611	272.125	$(N = 15)$ 37.619
$\mathcal{O}(10^{-10})$	463.874	1302.793	685.618	$(N = 17)$ 48.919

property by which a full first-order derivative d/dt can be decomposed into a product of the sequential $(\frac{1}{2})$-th order derivatives ${}_0\mathcal{D}_t^{1/2}\,{}_0\mathcal{D}_t^{1/2}$, a result that is not valid in the standard (integer-order) calculus. Hence, by virtue of the *fractional* integration-by-parts (see Lemma 6.3.4), such a decomposition artificially induces *non-locality* to the temporal term in the corresponding weak form. Therefore, it provides an appropriate framework for *global* (spectral) treatment of the temporal term using SM-DSEM.

To demonstrate the efficiency of SM-DSEM when ${}_0\mathcal{D}_t^{\tau} \to d/dt$, we compare the computational cost of SM-DSEM with that of the multi-step methods such as Stiffly-Stable Scheme (SSS), Adams-Bashforth (AB), and Adams-Moulton (AM). To this end, we recall these schemes to integrate (9.81) in time, where we employ DSEM to discretize the spatial domain as before. However, we note that our approach is independent of the type of the spatial discretization.

In Table 6.1, we present the CPU time (seconds) corresponding to the backward and forward multi-step time-integration schemes introduced along with that of our SM-DSEM. We particularly compare the CPU time in the third-order SSS-DSEM , AB-DSEM , AM-DSEM and our SM-DSEM developed in Sec. 6.3.3. We choose the exact solution to be $u^{ext}(x,t) = x^3 t^{13/2} \sin(\pi t^{4/3})$, where we consider two elements in space and setting the polynomial order $M = 3$ to accurately resolve the spatial

solution. Moreover, we set the spatial fractional order to $\nu = 1/2$ and set the temporal time-order to the integer value $\tau = 1$. Among the multi-step methods, we observe SSS-DSEM to be more efficient than AB-DSEM and AM-DSEM specially at smaller error-levels. Moreover, Table 6.1 shows that all the aforementioned schemes are comparable in terms of the CPU time at the relatively large L^2-error $\mathcal{O}(10^{-4})$. However, SM-DSEM outperforms all the multi-step methods by about one order of magnitude speed-up at smaller error-levels.

6.5 DG-DG Method: DSEM-in-Time & DSEM-in-Space

We extend our SM-DSEM scheme to another method, which is more appropriate for adaptive and/or long time-integration of (6.1). The idea is to discretize both the space- and time-domain employing DSEM in an *hp*-element fashion. We set $\tau \in (0,1)$ and $\nu \in (0,1)$ in (6.1), subject to homogeneous Dirichlet initial/boundary conditions. In DSEM-DSEM, we first decompose the space-domain $[0, L]$ into N_{el}^x non-overlapping sub-intervals $I_{\widetilde{e}}^x = [x_{\widetilde{e}-1/2}\,,\, x_{\widetilde{e}+1/2}]$ and the time-domain $[0, T]$ into N_{el}^t sub-intervals $I_{\widehat{e}}^t = [t_{\widehat{e}-1/2}\,,\, t_{\widehat{e}+1/2}]$. Next, we partition the whole computational domain $\Omega = [0, L] \times [0, T]$ into $\mathcal{N}^{el} = N_{el}^x \cdot N_{el}^t$ *structured* space-time elements $\Omega_e \equiv I_{\widetilde{e}}^x \times I_{\widehat{e}}^t$ such that $\cup_{e=1}^{\mathcal{N}^{el}} \Omega_e = \Omega$. In this setting, the element number "e" corresponds to a particular pair of the spatial sub-interval number "$\widetilde{e}$" and the temporal one "$\widehat{e}$", respectively.

6.5.1 Basis and Test Function Spaces in DSEM-DSEM Scheme

We construct the basis function space $\mathbf{V}^e$ as the tensor product of the asymptotic (temporal and spatial) eigenfunctions, presented in Sec. 6.3.3, as

$$\mathbf{V}^e \equiv span\{\widetilde{P}_m^{\eta^x,0}(\, x_{\widetilde{e}}\,)\, \widetilde{P}_n^{\eta^t,0}(\, t_{\widehat{e}}\,) : m = 0, 1, \ldots, M, n = 0, 1, \ldots, N\}, \tag{6.43}$$

where η^x, $\eta^t \in (0, 1)$ and the temporal bases $\widetilde{P}_n^{\eta^t,0}(\, t_{\widehat{e}}\,)$ are Jacobi polynomials, defined in the time-interval $I_{\widehat{e}}^t = [t_{\widehat{e}-1/2}\,,\, t_{\widehat{e}+1/2}]$ as the asymptotic eigenfunction $P_n^{\eta^t,0}(\,\xi\,)$ through an affine mapping from the standard domain $[-1, 1]$ to the physical time-subdomain $I_{\widehat{e}}^t$. We approximate the solution to (6.1) in Ω_e in terms of linear combination of elements in $\mathbf{V}^e$. In our Petrov-Galerkin DSEM-DSEM scheme, we construct the space of test functions $\mathbb{V}^e$, constructed as

$$\mathbb{V}^e \equiv span\{\widetilde{P}_i^{\,0,\chi^x}(\, x_{\widetilde{e}}\,)\, \widetilde{P}_j^{\,0,\chi^t}(\, t_{\widehat{e}}\,) : i = 0, 1, \ldots, M, j = 0, 1, \ldots, N\}, \tag{6.44}$$

where we test problem (6.1) against elements in $\mathbb{V}^e$.

6.5.2 Implementation of DSEM-DSEM Scheme

The space-time basis functions in our DSEM-DSME are *discontinuous* in both space and time at the interfaces of the two-dimensional (time-space) element Ω_e. Here, we seek the approximation solution to (6.1), restricted in element Ω_e, of the form

$$u(x,t)\Big|_{\Omega_e} \approx u_{MN}^e(x,t) = \sum_{m=0}^{M}\sum_{n=0}^{N} \overline{u}_{mn}^{\,e} \widetilde{P}_m^{\eta^x,0}(\, x_{\widetilde{e}}\,)\,, \widetilde{P}_n^{\eta^t,0}(\, t_{\widehat{e}}\,). \tag{6.45}$$

Once again the ultimate step in our DSEM-DSEM scheme is to construct a linear system corresponding to (6.2) of Lyapunov form (6.27). To this end, we require the solution (6.45) to satisfy the following weak form is

$$
\begin{aligned}
\left({}_{t^{+}_{\widehat{e}-1/2}}\mathcal{D}^{\tau/2}_{t} u^{e}_{MN}(x,t)\,,\, {}_{t}\mathcal{D}^{\tau/2}_{t^{-}_{\widehat{e}+1/2}} v^{e}(x,t) \right)_{\Omega_e} &+ \theta \left({}_{x^{+}_{\widetilde{e}-1/2}}\mathcal{D}^{\nu/2}_{x} u^{e}_{MN}(x,t)\,,\, {}_{x}\mathcal{D}^{\nu/2}_{x^{-}_{\widetilde{e}+1/2}} v^{e}(x,t) \right)_{\Omega_e} \\
&+ \gamma^{x}_{\widetilde{e}} \left([\![u^{e}_{MN}(x_{\widetilde{e}-1/2}\,,\, t)]\!]\,,\; v^{e}(x^{-}_{\widetilde{e}+1/2}\,,\, t) \right)_{I^{t}_{\widehat{e}}} \\
&+ \gamma^{t}_{\widehat{e}} \left([\![u^{e}_{MN}(x\,,\, t_{\widehat{e}-1/2})]\!]\,,\; v^{e}(x\,,\, t^{-}_{\widehat{e}+1/2}) \right)_{I^{x}_{\widetilde{e}}} \\
&= \Big(f(x,t), v^{e}(x,t) \Big)_{\Omega_e} - \theta \cdot \mathcal{H}^{x}_{\widetilde{e}} - \mathcal{H}^{t}_{\widehat{e}}
\end{aligned}
\tag{6.46}
$$

$\forall v^{e}(x,t) \in \mathbb{V}^{e}$. In (6.46),

$$
\gamma^{x}_{\widetilde{e}} = -\frac{\theta (\Delta x)^{1-\nu}_{\widetilde{e}}}{(1-\nu)\Gamma(1-\nu)}, \tag{6.47}
$$

also

$$
\gamma^{t}_{\widehat{e}} = -\frac{(\Delta t)^{1-\tau}_{\widehat{e}}}{(1-\tau)\Gamma(1-\tau)}, \tag{6.48}
$$

where $(\Delta x)_{\widetilde{e}} = x_{\widetilde{e}+1/2} - x_{\widetilde{e}-1/2}$ and $(\Delta t)_{\widehat{e}} = t_{\widehat{e}+1/2} - t_{\widehat{e}-1/2}$. Moreover, $[\![u^{e}_{MN}(x_{\widetilde{e}-1/2}\,,\, t)]\!]$ denotes the (spatial) jump discontinuity of the solution at $x = x_{\widetilde{e}-1/2}$ as a function of time $t \in I^{t}_{\widehat{e}}$ and $[\![u^{e}_{MN}(x\,,\, t_{\widehat{e}-1/2})]\!]$ is the (temporal) jump discontinuity of the solution at $t = t_{\widehat{e}-1/2}$ as a function of space $x \in I^{x}_{\widetilde{e}}$. Similarly, $(\cdot,\cdot)_{\Omega_e}$, $(\cdot,\cdot)_{I^{t}_{\widehat{e}}}$, and $(\cdot,\cdot)_{I^{x}_{\widetilde{e}}}$ are, respectively, the standard inner product in the local space-time element Ω_e

$$
\Big(f(x,t), g(x,t) \Big)_{\Omega_e} = \int_{I^{t}_{\widehat{e}}} \int_{I^{x}_{\widetilde{e}}} f(x,t) g(x,t)\; dx\; dt,
$$

the inner product in $I_{\widehat{e}}^t$, defined as

$$\Big(p(t), q(t)\Big)_{I_{\widehat{e}}^t} = \int_{t_{\widehat{e}-1/2}^+}^{t_{\widehat{e}+1/2}^-} p(t)\, q(t)\; dt,$$

and the inner product in $I_{\widetilde{e}}^x$

$$\Big(Y(x), W(x)\Big)_{I_{\widetilde{e}}^x} = \int_{x_{\widetilde{e}-1/2}^+}^{x_{\widetilde{e}+1/2}^-} Y(x)\, W(x)\; dx,$$

Finally, in (6.46), $\mathcal{H}_{\widetilde{e}}^x$ and $\mathcal{H}_{\widehat{e}}^t$ represent the corresponding *spatial history-load* and *temporal history-load* term, which we compute in an efficient fashion similarly as presented in Sec. 6.3.3.

Next, we obtain the corresponding linear system resulting from our DSEM-DSEM scheme by substituting the solution (6.45) into the weak form (6.46), taking $v^e(x,t) = \widetilde{P}_i^{\,0,\chi^x}(\,x_{\widetilde{e}}\,)\,\widetilde{P}_j^{\,0,\chi^t}(\,t_{\widehat{e}}\,)$, and choosing $\eta^x = \chi^x = \nu/2$ and $\mu = \tau/2$ as another *Lyapunov* equation

$$M_x^{\widetilde{e}}\;\overline{\mathbf{U}}^{\,e}\;\left(S_t^{\widehat{e}\;T} + \gamma_{\widehat{e}}^{\,t}\eta^{\widehat{e}}\right)\;+\;\left(\theta S_x^{\widetilde{e}} + \gamma_{\widetilde{e}}^{\,x}\eta^{\widetilde{e}}\right)\;\overline{\mathbf{U}}^{\,e}\;M_t^{\widehat{e}\;T} = \mathbb{F}^e, \tag{6.49}$$

where we recall that the element number "e" is associated with the pair of "$\widetilde{e}$" and "$\widehat{e}$", the spatial and temporal sub-intervals $I_{\widetilde{e}}^x$ and $I_{\widehat{e}}^t$. In the Lyapunov system (6.49), $\overline{\mathbf{U}}^{\,e}$ is the $(M+1)\times(N+1)$ matrix of unknown coefficient associated with Ω_e whose entries are $\overline{\mathbf{U}}_{mn}^{\,e} = \overline{u}_{mn}^{\,e}$. In addition, the spatial matrices $S_x^{\widetilde{e}}$, $M_x^{\widetilde{e}}$, and $\eta^{\widetilde{e}}$ represent the corresponding $(M+1)\times(M+1)$ spatial stiffness, mass, and the constant matrices, respectively, which are identical to those obtained in (6.34), (6.36) and (6.37), by setting "e" to "$\widetilde{e}$". Moreover, $S_t^{\widehat{e}}$, $M_t^{\widehat{e}}$, and $\eta^{\widehat{e}}$ are, respectively, the temporal stiffness, mass, and constant matrices.

In Algorithm 2, we present the corresponding pseudocode for our DSEM-DSEM

for $e = 1$; $e = N_{el}$ **do**
  Construct $M_x^{\widetilde{e}}$, $S_x^{\widetilde{e}}$, $\eta^{\widetilde{e}}$, also $M_t^{\widehat{e}}$, $S_t^{\widehat{e}}$, and $\eta^{\widehat{e}}$;
  if $e = 1$ **then**
    $\mathcal{H}_{\widetilde{e}}^{x} = 0$ and $\mathcal{H}_{\widehat{e}}^{t} = 0$;
  else
    Compute $\mathcal{H}_{\widetilde{e}}^{x}$ and $\mathcal{H}_{\widehat{e}}^{t}$ then construct $\mathbb{F}^e$;
  end
  Solve $M_x^{\widetilde{e}}\ \overline{\mathbf{U}}^{\,e}\ (S_t^{\widehat{e}\,T} + \gamma_{\widehat{e}}{}^{t}\eta^{\widehat{e}})\ +\ (\theta S_x^{\widetilde{e}} + \gamma_{\widetilde{e}}{}^{x}\eta^{\widetilde{e}})\ \overline{\mathbf{U}}^{\,e}\ M_t^{\widehat{e}\,T} = \mathbb{F}^e$;
end

Algorithm 2: Pseudocode of DSEM-DSEM scheme, employed in a non-uniform structured partitioned domain.

scheme, where the computational space- and time-domain are assumed to be non-uniformly partitioned. As before, if the elements are uniform, we construct the matrices $M_x^{\widetilde{e}}$, $S_x^{\widetilde{e}}$, $\eta^{\widetilde{e}}$, also $M_t^{\widehat{e}}$, $S_t^{\widehat{e}}$, and $\eta^{\widehat{e}}$ only *once* at a preprocessing step. In the following, we present the construction of the corresponding temporal matrices.

Temporal Stiffness Matrix: $S_t^{\widehat{e}}$ is an $(N+1)\times(N+1)$ matrix whose entries are obtained as

$$
\begin{aligned}
(\,S_t^{\widehat{e}}\,)_{jn} &= \int_{t_{\widehat{e}-1/2}}^{t_{\widehat{e}+1/2}} {}_{t_{\widehat{e}-1/2}}\mathcal{D}_t^{\tau/2}\tilde{P}_j^{\tau/2,0}(t_{\widehat{e}})\ {}_{t}\mathcal{D}_{t_{\widehat{e}+1/2}}^{\tau/2}\tilde{P}_n^{0,\tau/2}(t_{\widehat{e}})dt \qquad (6.50)\\
&= C_t^{\widehat{e}}\cdot\Lambda_{im}^{t}\ \sum_{k=0}^{N} P_j^{\tau,-\tau/2}(z_k)P_n^{-\tau/2,\tau}(z_k)\rho_k^{-\tau/2,-\tau/2}
\end{aligned}
$$

which we compute *exactly* by mapping $[t_{\widehat{e}-1/2}, t_{\widehat{e}+1/2}]$ to the reference element $[-1,1]$ and performing a GLJ rule similar to (6.34). Here, $C_t^{\widehat{e}} = \{2/(\Delta t)_{\widehat{e}}\}^{\tau-1}$, also

$$
\Lambda_{jn}^{t} = \frac{\Gamma(j+1)}{\Gamma(j-\tau/2+1)}\frac{\Gamma(n+1)}{\Gamma(n-\tau/2+1)}.
$$

Moreover, $\{z_k\}_{k=0}^{N}$ and $\{\rho_k\}_{k=0}^{N}$ are the corresponding Gauss-Lobato-Jacobi (GLJ) quadrature points and weights in the interval $[-1,1]$, associated with the weight function $(1-z)^{-\tau/2}\,(1+z)^{-\tau/2}$.

Temporal Mass Matrix: ${M_t}^{\widehat{e}}$ is also an $(N+1)\times(N+1)$ matrix whose entries are obtained as

$$\begin{aligned}(\,{M_t}^{\widehat{e}}\,)_{jn} &= = \int_{t_{\widehat{e}-1/2}}^{t_{\widehat{e}+1/2}} \tilde{P}_j^{0,\tau/2}(t_{\widehat{e}})\tilde{P}_n^{\tau/2,0}(t_{\widehat{e}})dx \\ &= J_t^{\widehat{e}}\sum_{k=0}^{Q} w_k P_j^{0,\tau/2}(\xi_k)P_m^{\tau/2,0}(\xi_k),\end{aligned} \tag{6.51}$$

in which $J_t^{\widehat{e}} = (\Delta x)_{\widehat{e}}/2$ is the Jacobian of the transformation from the time sub-interval to the standard element. Here, we compute the mass matrix *exactly* based on the standard Gauss-Lobato-Legendre (GLL) rule and choosing$Q$ so that $2Q-3=2N$ similar to (6.32).

Constant Matrix: $\eta^{\widehat{e}}$ is also an $(M+1)\times(M+1)$ matrix whose entries are defined as

$$\begin{aligned}(\,\eta^{e}\,)_{jn} &= P_j^{0,\tau/2}(+1)\,P_n^{\tau/2,0}(-1) \\ &= (-1)^n,\end{aligned} \tag{6.52}$$

for $j,\, n = 0,1,2,\cdots,N$.

Total Load Matrix: $\mathbb{F}^e$ is an $(M+1)\times(N+1)$ matrix defined as

$$\mathbb{F}^e = \mathbf{F}^e - \gamma_{\widetilde{e}}^{\,x}\,\left(\eta^{\widetilde{e}}\;\hat{\mathbf{U}}^{e-1}{M_t^{\widehat{e}}}^{\,T}\right) - \gamma_{\widehat{e}}^{\,t}\,\left({M_x^{\widetilde{e}}}^{\,T}\;\hat{\mathbf{U}}^{e-1}\;\eta^{\widehat{e}}\right) - \theta\,\mathcal{H}_{\widetilde{e}}^{x} - \mathcal{H}_{\widehat{e}}^{t} \tag{6.53}$$

in which $\mathbf{F}^e = (f(x,t), v^e(x,t))_{\Omega_e}$, $\hat{\mathbf{U}}^{e-1}$ denotes the coefficient matrix, known in the previously resolved element Ω_{e-1}, and we obtain the spatial and temporal history-load terms $\mathcal{H}^x_{\widetilde{e}}$ and $\mathcal{H}^t_{\widehat{e}}$ in a similar computationally efficient form as

$$(\mathcal{H}^x_{\widetilde{e}})_{ij} = \left. F_e(x) P_i^{0,\nu/2}(x) \right|_{x=x^+_{\widetilde{e}-1/2}}^{x=x^-_{\widetilde{e}+1/2}} - \int_{x_{\widetilde{e}-1/2}}^{x_{\widetilde{e}+1/2}} F_e(x) \frac{d}{dx} P_i^{0,\nu/2}(x)\, dx, \tag{6.54}$$

and

$$(\mathcal{H}^t_{\widehat{e}})_{ij} = \left. G_e(t) P_j^{0,\tau/2}(t) \right|_{t=t^+_{\widehat{e}-1/2}}^{t=t^-_{\widehat{e}+1/2}} - \int_{t_{\widehat{e}-1/2}}^{t_{\widehat{e}+1/2}} G_e(t) \frac{d}{dt} P_j^{0,\tau/2}(t)\, dt, \tag{6.55}$$

respectively. We then obtain the corresponding spatial history functions $F_e(x)$ in (6.40), setting "e" to "$\widetilde{e}$". Similarly, we obtain the temporal history function $G_e(x)$ associated with the current element Ω_e as

$$G_e(t) = \sum_{\varepsilon=1}^{\widehat{e}-1} G^{\varepsilon}_{\widehat{e}}(t), \tag{6.56}$$

in which

$$G^{\varepsilon}_{\widehat{e}}(t) = \sum_{m,n} \hat{u}^{\varepsilon}_{mn} \, (M^{\widetilde{e}}_x)_{im} \sum_{\delta=0}^{N} \Big(C^t_\delta \cdot (t-s)^{\delta+1-\tau} \Big) \tilde{P}_n^{\tau/2,0(\delta)}(s) \Big|_{s=s^+_{\varepsilon-1/2}}^{s=s^-_{\varepsilon+1/2}}, \tag{6.57}$$

where the coefficient $C^t_\delta = -1/\{\Gamma(1-\tau)\prod_{k=0}^{\delta}(k+1-\tau)\}$.

We have examined the DSEM-DSEM for all the test-cases presented previously successfully. Here, we examine DSEM-DSEM for log-time integration. In Fig. 6.3, and corresponding to the simulation time $T = 10$ and $\tau = \nu = 1/2$, we plot the log-linear L^2-error versus the temporal order-index N in (6.45). We partition the

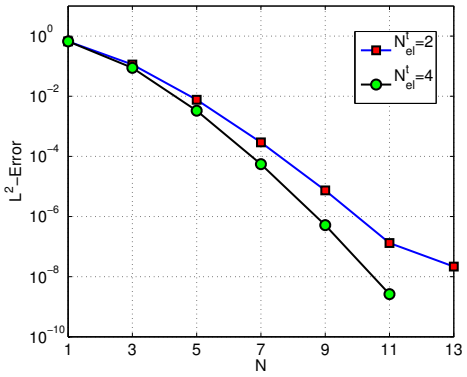

Figure 6.3: DSEM-DSEM; Long-time integration: log-linear L^2-error versus the temporal order-index N in (6.45), corresponding to $N^t_{el} = 2$ and 4 temporal sub-intervals, also $N^x_{el} = 2$ spatial sub-intervals kept fixed, i.e., total $N_{el} = N^x_{el}.N^t_{el} = 4$ and 8 space-time elements. Here, the simulation time $T = 10$ and $\tau = \nu = 1/2$.

whole computational domain into 4 and 8 element by choosing $N^t_{el} = 2$ and 4, also $N^x_{el} = 2$ fixed. While we have increased the simulation time from $T = 1$ to $T = 10$, we recover the exponential convergence in DSEM-DSEM.

6.6 Discussion

Although we have formulated the aforementioned methods when (6.1) is subject to *homogeneous* Dirichlet boundary and initial conditions, i.e., $h(t) = g(x) = 0$, these schemes are equally valid when *inhomogeneous* conditions are enforced. In such cases, we first homogenize the problem by the method of *lifting a known solution*. Using this trick, we first set the solution $u(x,t) = u^H(x,t) + g(x) + h(t)$, and then substitute in (6.1). Hence, we obtain a modified/homogenized TSFAE of the form

$$\begin{aligned} {}_0\mathcal{D}^{\tau}_t u^H(x,t) + \theta\ {}_0\mathcal{D}^{\nu}_x u^H(x,t) &= \widetilde{f}(x,t), \quad (x,t) \in [0,L] \times [0,T], \qquad (6.58) \\ u^H(x,0) &= 0, \\ u^H(0,t) &= 0, \end{aligned}$$

Table 6.2: Inhomogeneous boundary conditions: $p-$refinement in the spatial dimension for Case-I: $u^{ext}(x,t) = t^{3+1/2}\cos(\pi x)$, and the for Case-II: $u^{ext}(x,t) = t^{10}[exp(x^2) + 10\pi]$. Here, we set $T = L = 1$, $\tau = \nu = 1/2$ and $N = 15$.

M	L^2-Error, Case-I	L^2-Error, Case-II
1	0.0384286	0.334819
3	0.0007635	0.001144
5	4.98×10^{-6}	1.71×10^{-5}
7	6.18×10^{-8}	1.54×10^{-7}

where $\widetilde{f} = f - ({}_0\mathcal{D}_t^{\tau} + \theta\ {}_0\mathcal{D}_x^{\nu})\{h(t) + g(x)\}$, and we recall that $h(0) = g(0)$. For demonstration of the generality of the schemes presented, we solve (6.1) subject to inhomogeneous boundary conditions e.g., using SM-DSEM. We consider the following two test-cases: (i) the exact solution $u^{ext}(x,t) = t^{3+1/2}\cos(\pi x)$, corresponding to the time-variable inhomogeneous boundary condition $u(0,t) = h(t) = t^{3+1/2}$, and (ii) the exact solution $u^{ext}(x,t) = t^{10}[exp(x^2) + 10\pi]$, in which the boundary condition is given by $u(0,t) = h(t) = 10\pi t^{10}$. We solve the problem by taking $T = L = 1$, setting $\tau = \nu = 1/2$, and keeping $N = 15$ in all simulations. In Table 6.2, we show the corresponding $p-$refinements for the aforementioned problems, where we achieve an exponential-like convergence in both cases.

We finally conclude the work by comparing the performance of the developed methods with the finite difference method (FDM) developed in [111], where the fractional derivative ${}_0\mathcal{D}_t^{\nu}u(t)$ is represented as

$$ {}_0\mathcal{D}_t^{\tau}u(x,t) = \frac{1}{\Gamma(2-\tau)}\sum_{j=0}^{k} a_j \frac{u(x,t_{k+1-j}) - u(x,t_{k-j})}{(\Delta t)^{\tau}} + r_{\Delta t}^{k+1}, \tag{6.59} $$

where $r_{\Delta t}^{k+1} \leq C_u(\Delta t)^{2-\tau}$ and $a_j := (j+1)^{1-\tau} - j^{1-\tau}, j = 0, 1, \cdots, k$; where a similar

Table 6.3: CPU time (seconds) on a dual-core 2.9 GHz Intel processor, corresponding to PG-SM, PG-DSEM and FDM with $\nu = 1/2$ (kept constant), when the exact solution is $u(x,t) = t^3x^3$. In all cases, we set spatial polynomials order $M = 3$, and we set $\Omega = [0,1] \times [0,1]$.

$\tau = 1/10$

Error	SM-DSEM	DSEM-DSEM($N_{el}^x = N_{el}^t = 2$)	FDM($N_g^t = 200$)
$\mathcal{O}(10^{-4})$	3.69	–	($N_g^x = 10$) 15.705
$\mathcal{O}(10^{-5})$	4.69	(exact) 4.09	($N_g^x = 40$) 173.385

$\tau = 1/2$

Error	SM-DSEM	DSEM-DSEM($N_{el}^x = N_{el}^t = 2$)	FDM($N_g^t = 200$)
$\mathcal{O}(10^{-4})$	3.64	–	($N_g^x = 50$) 253.771
$\mathcal{O}(10^{-5})$	4.58	(exact) 4.01	($N_g^x = 300$) 12128.341

$\tau = 9/10$

Error	SM-DSEM	DSEM-DSEM($N_{el}^x = N_{el}^t = 2$)	FDM($N_g^t = 200$)
$\mathcal{O}(10^{-4})$	3.60	–	($N_g^x = 500$) $5.89 \cdot 10^4$
$\mathcal{O}(10^{-5})$	4.55	(exact) 4.13	($N_g^x = 2000$) Out of Memory

formulation can be obtained for the spatial fractional derivative as

$$ {}_0\mathcal{D}_x^{\nu} u(x,t) = \frac{1}{\Gamma(2-\nu)} \sum_{j=0}^{k} b_j \frac{u(x, t_{k+1-j}) - u(x, t_{k-j})}{(\Delta x)^{\nu}} + r_{\Delta x}^{k+1}. \tag{6.60} $$

where $b_j := (j+1)^{1-\nu} - j^{1-\nu}, j = 0, 1, \cdots, k$.

In Table 6.3, we compute the CPU time (in seconds), required for solving (6.1), corresponding to three temporal fractional orders $\tau = 1/10$, $1/2$, and $9/10$, where we keep the spatial fractional order $\nu = 1/10$ fixed. Here, the exact solution is $u(x,t) = t^3x^3$ and the integration time $T = 1$ and the spatial domain size $L = 1$. We compare SM-DSEM with ($N_{el} = 1$) and ($N_{el} = 2$) elements with FDM.

We first observe that our schemes are not sensitive to the fractional order τ, however, the CPU time in FDM is shown to be strongly dependent on τ. It is actually consistent with the fact that the order of accuracy of FDM is $\mathcal{O}((\Delta t)^{2-\tau} + (\Delta x)^{2-\nu})$. Here, we set the relatively big error-levels $\mathcal{O}(10^{-4})$ and $\mathcal{O}(10^{-5})$ for comparison, also the spatial fractional order $\nu = 1/2$ was kept constant. We observe that when τ is very small, FDM and our methods become comparable in terms of computational cost. However, increasing τ to $1/2$ and $9/10$, the cost of FDM becomes *two to four orders of magnitude* greater than that in our methods, depending on the error level and τ. Moreover, we observe that when τ is close to one, FDM becomes almost first-order accurate in time, which leads to a significant amount of memory storage that might not be available on a PC. Clearly, for higher values of ν, even larger memory allocation is required; moreover, the CPU time will significantly be increased in FDM. Regarding DSEM-DSEM and for all the aforementioned cases, we obtain the *exact* solution by setting $N = M = 3$.

Chapter Seven

Fractional Spectral Collocation Method

In this chapter, we develop a spectrally accurate Fractional Spectral Collocation Method (FSCM) for solving steady-state and time-dependent Fractional PDEs (FPDEs). We first introduce a new family of interpolants, called *fractional Lagrange interpolants*, which satisfy the Kronecker delta property at collocation points. We perform such a construction following a spectral theory recently developed in [187] for fractional Sturm-Liouville eigenproblems. Subsequently, we obtain the corresponding fractional differentiation matrices, and we solve a number of linear FODEs in addition to linear and nonlinear FPDEs to investigate the numerical performance of the fractional collocation method. We first examine space-fractional advection-diffusion problem and generalized space-fractional multi-term FODEs. Next, we solve FPDEs including time- and space-fractional advection-diffusion equation, time- and space-fractional multi-term FPDEs, and finally the space-fractional Burgers' equation. Our numerical results confirm the exponential convergence of the fractional collocation method.

7.1 Background

Galerkin/Petrov-Galerkin (PG) projection type schemes have in general difficulties in the treatment of nonlinear FPDEs and multi-term FPDEs, since no straightforward variational form can be efficiently obtained for such problems. The *collocation* schemes for fractional equations are relatively easy to implement and they can overcome the aforementioned challenges. The idea of collocation was proposed by Khader in [86], who presented a Chebyshev collocation method for the discretization of the space-fractional diffusion equation. More recently, Khader and Hendy [87] developed a Legendre pseudospectral method for fractional-order delay differential equations. However, in these works only linear problems have been considered and

the performance of such methods has not been fully investigated.

The aim of this study is to develop an exponentially accurate fractional spectral collocation method (FSCM) for solving steady-state and time-dependent Fractional PDEs (FPDEs). In this chapter, we introduce *fractional Lagrange interpolants*, which satisfy the Kronecker delta property at collocation points. Moreover, we obtain the corresponding fractional differentiation matrices. Next, we solve a number of linear and nonlinear FPDEs to investigate the numerical performance of the fractional collocation method. In this section, we examine steady-state problems such as space-fractional advection-diffusion problem and generalized space-fractional multi-term problems, in addition to time-dependent FPDEs such as time- and space-fractional advection-diffusion equation, time- and space- fractional multi-term FPDEs, and finally the space-fractional Burgers' equation. We demonstrate the exponential convergence of FSCM.

7.2 Notation and Definitions

Before presenting our fractional spectral collocation method, we start with some preliminary definitions of fractional calculus [142]. The left-sided and right-sided Riemann-Liouville fractional derivatives of order μ, when $0 < \mu < 1$, are defined as

$$({}^{RL}_{-1}\mathcal{D}^{\mu}_{x} f)(x) = \frac{1}{\Gamma(1-\mu)} \frac{d}{dx} \int_{-1}^{x} \frac{f(s)ds}{(x-s)^{\mu}}, \quad x > -1, \tag{7.1}$$

and

$$({}^{RL}_{x}\mathcal{D}^{\mu}_{1} f)(x) = \frac{1}{\Gamma(1-\mu)} (\frac{-d}{dx}) \int_{x}^{1} \frac{f(s)ds}{(s-x)^{\mu}}, \quad x < 1. \tag{7.2}$$

Furthermore, the corresponding left- and right-sided Caputo derivatives of order $\mu \in (0,1)$ are obtained as

$$({}_{-1}^{C}\mathcal{D}_{x}^{\mu} f)(x) = \frac{1}{\Gamma(1-\mu)} \int_{-1}^{x} \frac{f'(s)ds}{(x-s)^{\mu}}, \quad x > -1, \tag{7.3}$$

and

$$({}_{x}^{C}\mathcal{D}_{1}^{\mu} f)(x) = \frac{1}{\Gamma(1-\mu)} \int_{-1}^{x} \frac{-f'(s)ds}{(x-s)^{\mu}}, \quad x < 1. \tag{7.4}$$

The two definitions of fractional derivatives of Riemann-Liouville and Caputo type are closely linked by the following relationship

$$({}_{-1}^{RL}\mathcal{D}_{x}^{\mu} f)(x) = \frac{f(-1)}{\Gamma(1-\mu)(x+1)^{\mu}} + ({}_{-1}^{C}\mathcal{D}_{x}^{\mu} f)(x), \tag{7.5}$$

and

$$({}_{x}^{RL}\mathcal{D}_{1}^{\mu} f)(x) = \frac{f(1)}{\Gamma(1-\mu)(1-x)^{\mu}} + ({}_{x}^{C}\mathcal{D}_{1}^{\mu} f)(x). \tag{7.6}$$

We also recall a useful property of the Riemann-Liouville fractional derivatives. Assume that $0 < p \leq 1$ and $0 < q \leq 1$ and $f(-1) = 0 \;\; x > -1$, then

$${}_{-1}^{RL}\mathcal{D}_{x}^{p+q} f(x) = \left({}_{-1}^{RL}\mathcal{D}_{x}^{p}\right)\left({}_{-1}^{RL}\mathcal{D}_{x}^{q}\right) f(x) = \left({}_{-1}^{RL}\mathcal{D}_{x}^{q}\right)\left({}_{-1}^{RL}\mathcal{D}_{x}^{p}\right) f(x). \tag{7.7}$$

Finally, from [142] and for $\mu \in (0,1)$, we have

$${}_{0}^{C}\mathcal{D}_{x}^{\mu} x^{k} = \begin{cases} 0, & k < \mu, \\ \frac{\Gamma(k+1)}{\Gamma(k+1-\mu)} x^{k-\mu}, & 0 < \mu \leq k. \end{cases} \tag{7.8}$$

In this paper, we deal with fractional problems with *homogeneous* boundary/initial conditions. Hence, from now on, we drop the type of the fractional derivative and represent them by $\mathcal{D}^{\mu}$. Clearly, any problem with non-homogeneous boundary/initial conditions can be converted to a corresponding homogeneous one through (7.5) and

(7.6).

7.3 Fractional Lagrange interpolants

In standard collocation methods, interpolation operators are the key to circumvent the need for evaluating the inner products in Galerkin and Petrov-Galerkin type spectral methods. To this end, we define a set of *interpolation points* $\{x_i\}_{i=1}^N$ on which the corresponding Lagrange interpolants are obtained. Moreover, to form a collocation method, we require the residual to vanish on the same set of grid points called *collocation points* $\{y_i\}_{i=1}^N$. In general, these residual-vanishing points do not need to be same as the interpolation points. Our fractional collocation scheme is inspired by a new spectral theory developed for fractional Sturm-Liouville eigenproblems (FSLP) in [187], by which we solve

$$\begin{aligned} {}_0\mathcal{D}_t^{\tau} u(x,t) &= \mathcal{L}^{\nu} u(x,t), \quad x \in [-1,1],\ t \in [0,T], \\ u(x,0) &= g(x), \\ u(-1,t) &= 0, \quad \nu \in (0,1), \\ u(-1,t) = u(1,t) &= 0, \quad \nu \in (1,2), \end{aligned} \tag{7.9}$$

in which $\tau \in (0,1)$ and $\mathcal{L}^{\nu}$ denotes a fractional differential operator, where ν denotes the highest fractional order. We represent the solution to (7.9) in terms of new fractal (non-polynomial) basis functions, called *Jacobi polyfractonomials*, which are the eigenfunctions of the FSLP of first kind, explicitly obtained as

$${}^{(1)}\mathcal{P}_n^{\alpha,\beta,\mu}(x) = (1+x)^{-\beta+\mu-1} P_{n-1}^{\alpha-\mu+1,-\beta+\mu-1}(x), \quad x \in [-1,1], \tag{7.10}$$

where $P_{n-1}^{\alpha-\mu+1,-\beta+\mu-1}(x)$ are the standard Jacobi polynomials in which $\mu \in (0,1)$, $-1 \leq \alpha < 2-\mu$, and $-1 \leq \beta < \mu - 1$. It has been shown that eigenfunctions with $\alpha = \beta$ exhibit identical approximating properties when they are utilized as basis functions. Hence, we consider the polyfractonomial eigenfunctions corresponding to $\alpha = \beta = -1$ as

$$ {}^{(1)}\mathcal{P}_n^{\mu}(x) = (1+x)^{\mu} P_{n-1}^{-\mu,\mu}(x), \quad x \in [-1,1]. \tag{7.11} $$

From the properties of the eigensolutions in [187], the left-sided fractional derivative of (7.11), of both Riemann-Liouville and Caputo sense, is given as

$$ {}_{-1}\mathcal{D}_x^{\mu}\left({}^{(1)}\mathcal{P}_n^{\mu}(\,x\,)\right) \;=\; \frac{\Gamma(n+\mu)}{\Gamma(n)} P_{n-1}(\,x\,), \tag{7.12} $$

where $P_{n-1}(\,x\,)$ denotes a Legendre polynomial of order $(n-1)$. In our fractional collocation method, we seek solutions

$$ u_N \in V_N^{\mu} = span\{{}^{(1)}\mathcal{P}_n^{\mu}(x), 1 \leq n \leq N\}, \tag{7.13} $$

$\mu \in (0,1), x \in [-1,1]$, of the form

$$ u_N(x) = \sum_{j=1}^{N} \hat{u}_j \; {}^{(1)}\mathcal{P}_j^{\mu}(x). \tag{7.14} $$

This polyfractonomial *modal* expansion can also be alternatively expressed as a *nodal* expansion as

$$ u_N(x) = \sum_{j=1}^{N} u_N(x_j)\, h_j^{\mu}(x), \tag{7.15} $$

where $h_j^{\mu}(x)$ represent *fractional Lagrange interpolants* and are defined using the aforementioned interpolations points $-1 = x_1 < x_2 < \cdots < x_N = 1$. The inter-

polants $h_j^{\mu}(x)$ are all of fractional order $(N+\mu-1)$ and defined as

$$h_j^{\mu}(x) = \Big(\frac{x-x_1}{x_j-x_1}\Big)^{\mu} \prod_{\substack{k=1 \\ k\neq j}}^{N} \Big(\frac{x-x_k}{x_j-x_k}\Big), \;\; 2 \leq j \leq N. \tag{7.16}$$

Here, we call the superscript μ *interpolation parameter* to be set prior to solving (7.9). We note that a general FPDE however can be associated with multiple fractional differentiation orders ν_k, $k = 1, 2, \cdots, K$, for some positive integer K. We shall show how to set μ just from the fractional orders ν_k, given in the problem.

Remark 7.3.1. Because of the homogeneous Dirichlet boundary condition(s) in (7.9), we only construct $h_j^{\mu}(x)$ for $j = 2, 3, \cdots, N$ when maximum fractional order $\nu \in (0, 1)$, for which we set $u_N(-1) = 0$. Moreover, when $\nu \in (1, 2)$, there are only $(N-2)$ fractional Lagrange interpolants $h_j^{\mu}(x)$, $j = 2, 3, \cdots, N-1$, to construct since we impose $u_N(\pm 1) = 0$.

The fractional interpolants, shown in (11.19), satisfy the Kronecker delta property, i.e., $h_j^{\mu}(x_k) = \delta_{jk}$, at interpolation points, however they vary as a polyfractonomial between x_k's. We employ these interpolants as fractional *nodal* basis functions in (7.15), where they mimic the key structure of the eigenfunctions (7.11), utilized as fractional *modal* bases in the expansion (7.14).

7.3.1 Fractional differentiation matrix $\mathbf{D}^\sigma$, $0 < \sigma < 1$

Next, we obtain the differentiation matrix $\mathbf{D}^\sigma$ of a general fractional order $\sigma \in (0, 1)$. We substitute (11.19) in (7.15) and take the σ-th order fractional derivative as

$$\begin{aligned}
{}_{-1}\mathcal{D}_x^{\,\sigma} u_N(\,x\,) &= {}_{-1}\mathcal{D}_x^{\,\sigma}\Big[\sum_{j=2}^{N} u_N(x_j)\, h_j^{\mu}(x)\Big] \\
&= \sum_{j=2}^{N} u_N(x_j)\ {}_{-1}\mathcal{D}_x^{\,\sigma}\Big[h_j^{\mu}(x)\Big] \\
&= \sum_{j=2}^{N} u_N(x_j)\ {}_{-1}\mathcal{D}_x^{\,\sigma}\Big[\Big(\frac{x-x_1}{x_j-x_1}\Big)^{\mu}\prod_{\substack{k=1\\k\neq j}}^{N}\Big(\frac{x-x_k}{x_j-x_k}\Big)\Big] \\
&= \sum_{j=2}^{N} u_N(x_j)\ {}_{-1}\mathcal{D}_x^{\,\sigma}\Big[(1+x)^{\mu}\mathsf{P}_j(x)\Big]\, a_j \qquad (7.17)
\end{aligned}$$

where $a_j = \frac{1}{(x_j-x_1)^{\mu}}$, and $\mathsf{P}_j(x) = \prod_{\substack{k=1\\k\neq j}}^{N}\Big(\frac{x-x_k}{x_j-x_k}\Big)$, $j = 2, 3, \cdots, N$, are all polynomials of order $(N-1)$, which can be represented exactly in terms of Jacobi polynomials $P_{n-1}^{-\mu,\mu}(x)$ as

$$\mathsf{P}_j(x) = \sum_{n=1}^{N} \beta_n^j P_{n-1}^{-\mu,\mu}(x). \qquad (7.18)$$

We note that the unknown coefficients β_n^j can be obtained analytically. Plugging (C.1) into (7.17), we obtain

$$\begin{aligned}
{}_{-1}\mathcal{D}_x^{\,\mu} u_N(\,x\,) &= \sum_{j=2}^{N} u_N(x_j)\ {}_{-1}\mathcal{D}_x^{\,\sigma}\Big[(1+x)^{\mu}\sum_{n=1}^{N}\beta_n^j P_{n-1}^{-\mu,\mu}(x)\Big]\, a_j \\
&= \sum_{j=2}^{N} u_N(x_j) a_j \sum_{n=1}^{N}\beta_n^j\ {}_{-1}\mathcal{D}_x^{\,\sigma}\Big[(1+x)^{\mu}P_{n-1}^{-\mu,\mu}(x)\Big],\ \text{by (7.11)}, \\
&= \sum_{j=2}^{N} u_N(x_j) a_j \sum_{n=1}^{N}\beta_n^j\ {}_{-1}\mathcal{D}_x^{\,\sigma}\Big[{}^{(1)}\mathcal{P}_n^{\,\mu}(x)\Big],\ \text{by (7.12)}. \qquad (7.19)
\end{aligned}$$

I) The Particular Case $\sigma = \mu \in (0, 1)$

In this case, we use the property (7.12) and obtain

$$ {}_{-1}\mathcal{D}_x^{\sigma} u_N(\,x\,) \;=\; \sum_{j=2}^{N} u_N(x_j) a_j \sum_{n=1}^{N} \beta_n^j \Big[\frac{\Gamma(n+\mu)}{\Gamma(n)} P_{n-1}(\,x\,) \Big]. \tag{7.20} $$

Consequently, we take the interpolation and collocation points to be identical, also recalling Remark 7.3.1 and by evaluating ${}_{-1}\mathcal{D}_x^{\mu} u_N(\,x\,)$ at the collocation points $\{x_i\}_{i=2}^{N}$ we obtain

$$ \begin{aligned} {}_{-1}\mathcal{D}_x^{\mu} u_N(\,x\,)\Big|_{x_i} \;&=\; \sum_{j=2}^{N} u_N(x_j) a_j \sum_{n=1}^{N} \beta_n^j \Big[\frac{\Gamma(n+\mu)}{\Gamma(n)} P_{n-1}(\,x_i\,) \Big], \\ &=\; \sum_{j=2}^{N} \mathbf{D}_{ij}^{\mu}\; u_N(x_j), \end{aligned} \tag{7.21} $$

where $\mathbf{D}_{ij}^{\mu}$ are the entries of the $(N-1) \times (N-1)$ *fractional differentiation matrix* $\mathbf{D}^{\mu}$, obtained as

$$ \mathbf{D}_{ij}^{\mu} = \frac{1}{(x_j+1)^{\mu}} \sum_{n=1}^{N} \frac{\Gamma(n+\mu)}{\Gamma(n)}\, \beta_n^j\, P_{n-1}(\,x_i\,). \tag{7.22} $$

II) The General Case $\sigma \in (0, 1)$

This case is important when the fractional differential operator is associated with multiple fractional derivatives of different order. To obtain the fractional differentiation matrix in this case, we perform an affine mapping from $x \in [-1, 1]$ to $s \in [0, 1]$

through $s = (x+1)/2$, and re-write (C.2) as

$$\begin{aligned} {}_{-1}\mathcal{D}_x^{\sigma} u_N(x) &= \sum_{j=2}^{N} u_N(x_j) a_j \sum_{n=1}^{N} \beta_n^j \; {}_{-1}\mathcal{D}_{x(s)}^{\sigma} \Big[{}^{(1)}\mathcal{P}_n^{\mu}(x(s)) \Big], \\ &= \sum_{j=2}^{N} u_N(x_j) a_j \sum_{n=1}^{N} \beta_n^j \, (\frac{1}{2})^{\sigma} \; {}_0\mathcal{D}_s^{\sigma} \Big[{}^{(1)}\mathcal{P}_n^{\mu}(x(s)) \Big], \end{aligned} \tag{7.23}$$

where ${}^{(1)}\mathcal{P}_n^{\mu}(x(s))$ denotes the *shifted basis* that can be represented as

$${}^{(1)}\mathcal{P}_n^{\mu}(x(s)) = 2^{\mu} \sum_{q=0}^{n-1} (-1)^{n+q-1} \binom{n-1+q}{q} \binom{n-1+\mu}{n-1-q} s^{q+\mu}. \tag{7.24}$$

Substituting (7.24) into (7.23) we have

$$\begin{aligned} &{}_{-1}\mathcal{D}_x^{\sigma} u_N(x) = \\ &2^{\mu-\sigma} \sum_{j=2}^{N} u_N(x_j) a_j \sum_{n=1}^{N} \beta_n^j \sum_{q=0}^{n-1} (-1)^{n+q-1} \binom{n-1+q}{q} \binom{n-1+\mu}{n-1-q} \, {}_0\mathcal{D}_s^{\sigma} \Big[s^{q+\mu} \Big], \end{aligned}$$

in which ${}_0\mathcal{D}_s^{\sigma} \Big[s^{q+\mu} \Big]$, can be evaluated exactly by (7.8), and finally by an inverse transformation we obtain the σ-fractional derivative of the approximate solution as

$${}_{-1}\mathcal{D}_x^{\sigma} u_N(x) = \sum_{j=2}^{N} u_N(x_j) \Big[a_j \sum_{n=1}^{N} \beta_n^j \sum_{q=\lceil \sigma-\mu \rceil}^{n-1} b_{nq} \, (x+1)^{q+\mu-\sigma} \Big], \tag{7.25}$$

in which $\lceil \sigma - \mu \rceil$ denotes the ceiling of $\sigma - \mu$ and

$$b_{nq} = (-1)^{n+q-1} (\frac{1}{2})^q \binom{n-1+q}{q} \binom{n-1+\mu}{n-1-q} \frac{\Gamma(q+\mu+1)}{\Gamma(q+\mu-\sigma+1)}. \tag{7.26}$$

Now, similarly by evaluating ${}_{-1}\mathcal{D}_x^{\mu} u_N(\,x\,)$ at the collocation points $\{x_i\}_{i=2}^{N}$,

$$\begin{aligned} {}_{-1}\mathcal{D}_x^{\sigma} u_N(\,x\,)\Big|_{x_i} &= \sum_{j=2}^{N} u_N(x_j)\Big[a_j \sum_{n=1}^{N} \beta_n^j \sum_{q=\lceil \sigma-\mu \rceil}^{n-1} b_{nq}\,(x_i+1)^{q+\mu-\sigma}\Big], \\ &= \sum_{j=2}^{N} \mathbf{D}_{ij}^{\sigma}\; u_N(x_j), \end{aligned} \tag{7.27}$$

where $\mathbf{D}_{ij}^{\sigma}$ are the entries of the $(N-1)\times(N-1)$ fractional differentiation matrix $\mathbf{D}^{\sigma}$, computed as

$$\mathbf{D}_{ij}^{\sigma} = \frac{1}{(x_j+1)^{\mu}} \sum_{n=1}^{N} \beta_n^j \sum_{q=\lceil \sigma-\mu \rceil}^{n-1} b_{nq}\,(x_i+1)^{q+\mu-\sigma}. \tag{7.28}$$

7.3.2 Fractional differentiation matrix $\mathbf{D}^{1+\sigma}$, $0<\sigma<1$

As before, we split the derivation into two parts.

I) The Particular Case $\sigma = \mu$

The fractional derivative matrix $\mathbf{D}^{1+\sigma}$ when $\sigma=\mu$ can be directly obtained following (7.7) and by taking the first derivative of (C.3) as

$$\begin{aligned} {}_{-1}\mathcal{D}_x^{1+\mu} u_N(\,x\,) &= \frac{d}{dx}\Big[\,{}_{-1}\mathcal{D}_x^{\mu} u_N(\,x\,)\Big] \\ &= \frac{d}{dx}\sum_{j=2}^{N} u_N(x_j) a_j \sum_{n=1}^{N} \beta_n^j \Big[\frac{\Gamma(n+\mu)}{\Gamma(n)} P_{n-1}(\,x\,)\Big] \\ &= \sum_{j=2}^{N} u_N(x_j) a_j \sum_{n=1}^{N} \beta_n^j \Big[\frac{\Gamma(n+\mu)}{\Gamma(n)} \frac{dP_{n-1}(\,x\,)}{dx}\Big] \\ &= \sum_{j=1}^{N} u_N(x_j) a_j \sum_{n=2}^{N} \beta_n^j \Big[\frac{\Gamma(n+\mu)}{\Gamma(n)} \frac{n}{2} P_{n-2}^{1,1}(\,x\,)\Big]. \end{aligned}$$

Similarly, we can evaluate ${}_{-1}\mathcal{D}_x^{1+\mu} u_N(\,x\,)$ at the collocation points $\{x_i\}_{i=1}^N$ to obtain

$$\begin{aligned} {}_{-1}\mathcal{D}_x^{1+\mu} u_N(\,x\,)\Big|_{x_i} &= \sum_{j=1}^{N} u_N(x_j) a_j \sum_{n=2}^{N} \beta_n^j \Big[\frac{\Gamma(n+\mu)}{\Gamma(n)} \frac{n}{2} P_{n-2}^{1,1}(\,x_i\,)\Big] \\ &= \sum_{j=1}^{N} \mathbf{D}_{ij}^{1+\mu}\; u_N(x_j), \end{aligned} \tag{7.29}$$

where $\mathbf{D}_{ij}^{1+\mu}$ are the entries of the fractional differentiation matrix $\mathbf{D}^{1+\mu}$, provided as

$$\mathbf{D}_{ij}^{1+\mu} = \frac{1}{(x_j+1)^{\mu}} \sum_{n=2}^{N} \beta_n^j \Big[\frac{\Gamma(n+\mu)}{\Gamma(n)} \frac{n}{2} P_{n-2}^{1,1}(\,x_i\,)\Big]. \tag{7.30}$$

II) Case $\sigma \neq \mu$

For the case $\sigma \neq \mu$, it suffices to take the first derivative of (7.25) in terms of x as

$$\begin{aligned} \frac{d}{dx}\Big[\,{}_{-1}\mathcal{D}_x^{\sigma} u_N(\,x\,)\Big] &= \sum_{j=2}^{N} u_N(x_j) a_j \sum_{n=1}^{N} \beta_n^j \sum_{q=\lceil \sigma-\mu \rceil}^{n-1} b_{nq} \frac{d}{dx}\Big[(x+1)^{q+\mu-\sigma}\Big], \\ &= \sum_{j=2}^{N} u_N(x_j)\Big[a_j \sum_{n=1}^{N} \beta_n^j \sum_{q=\lceil \sigma-\mu \rceil}^{n-1} b_{nq}^{*}\,(x+1)^{q+\mu-\sigma-1}\Big], \end{aligned}$$

where by evaluating the above expression at the collocation points, we obtain:

$$\begin{aligned} {}_{-1}\mathcal{D}_x^{1+\sigma} u_N(\,x\,)\Big|_{x=x_i} &= \sum_{j=2}^{N} u_N(x_j)\Big[a_j \sum_{n=1}^{N} \beta_n^j \sum_{q=\lceil \sigma-\mu \rceil}^{n-1} b_{nq}^{*}\,(x_i+1)^{q+\mu-\sigma-1}\Big], \\ &= \sum_{j=2}^{N} \mathbf{D}_{ij}^{1+\sigma} u_N(x_j), \end{aligned} \tag{7.31}$$

in which $\mathbf{D}_{ij}^{1+\sigma}$ are the entries of $\mathbf{D}^{1+\sigma}$, computed as

$$\mathbf{D}_{ij}^{1+\sigma} = \frac{1}{(x_j+1)^{\mu}}\Big[\sum_{n=1}^{N} \beta_n^j \sum_{q=\lceil \sigma-\mu \rceil}^{n-1} b_{nq}^{*}\,(x_i+1)^{q+\mu-\sigma-1}\Big], \tag{7.32}$$

where $b^*_{nq} = (q + \mu - \sigma)b_{nq}$, see (11.22).

Remark 7.3.2. We note that the coefficients β^j_n, shown in (C.1), are obtained only *once* and are utilized as many as times needed to calculate $\mathbf{D}^\sigma$ or $\mathbf{D}^{1+\sigma}$ of any order $\sigma \in (0, 1)$.

7.3.3 Collocation/interpolation points

In principle, the collocation and interpolation points can be chosen arbitrarily. However, the right choice of the collocation/interpolation points is the key to obtaining efficient schemes resulting in well-conditioned linear systems. Here, we examine five methods which yield different sets of collocation/interpolation points for the construction of the differentiation matrix $\mathbf{D}^{\sigma_1}$, and $\mathbf{D}^{1+\sigma_2}$, $\sigma_1, \sigma_2 \in (0, 1)$. For a general FODEs/FPDEs where both $\mathbf{D}^{\sigma_1}$ and $\mathbf{D}^{1+\sigma_2}$ may appear, we consider N collocation points of *Gauss-Lobatto* type in order to include both boundary points. We refer to the aforementioned points as:

(i) *Equidistant points*: this choice is inspired by the well-known *Fourier* collocation points, and we obtain the N points as $x_i = -1 + \frac{2(i-1)}{N-1}$, $i = 1, 2, \cdots, N$.

(ii) *Roots of* ${}^{(1)}\widetilde{\mathcal{P}}^{\mu}_{M}(\,x\,) = (1+x)^{\mu} P^{-\mu,\mu}_{M-1}(x)$: the M zeros of such Jacobi polyfractonomial are essentially *Gauss-Radau* points, obtained through finding the $(M-1)$ roots of the Jacobi polynomial $P^{-\mu,\mu}_{M-1}(x)$ in addition to the left-boundary point $x = -1$ due to the fractional multiplier term. Setting $M = N - 1$ and including the right boundary-point $x = 1$ provides the N collocation/interpolation points needed.

(iii) *Roots of* ${}_{-1}\mathcal{D}^{\mu}_{x}[\ {}^{(1)}\mathcal{P}^{\mu}_{M}(\,x\,)\ ]$: the corresponding $M - 1$ roots are *Gauss* points, which lie in the interior domain in this case. Here, we can think of these colloca-

tion/interpolation points as the (fractional) *extrema* of the Jacobi polyfractonomial ${}^{(1)}\mathcal{P}_M^{\mu}(\,x\,)$ because we compute the roots of the (fractional) derivative of the eigenfunction. We perform such root finding easily using the property (7.12) and equivalently obtaining the $M-1$ roots of *Legendre* polynomial $P_{M-1}(x)$. Finally, we set $M = N-2$ and add both the left- and right-boundary points $x = -1$ and $x = 1$ to provide the N points needed.

(iv) *Chebyshev roots,* $-\cos(\frac{(2j+1)}{M}\,\frac{\pi}{2})$, $j = 0, 1, \cdots, M-1$: the M roots of Chebyshev polynomial $T_M(x)$ are also *Gauss* points. Hence, we set $M = N-2$ and similarly add both the left- and right-boundary points $x = -1$ and $x = 1$.

(v) *Roots of* $dT_{N+1}(x)/dx$, *i.e.,* $-\cos(\frac{j\pi}{N-1})$, $j = 0, 1, \cdots, N-1$: this choice provides the N collocation/interpolation points which are the *extrema* points of the Chebyshev polynomial $T_{N+1}(x)$ roots. These N points are essentially of *Gauss-Lobatto* type and the boundary-points $x = \pm 1$ are included automatically.

In order to examine the efficiency of each choice of collocation/interpolation points, we consider two canonical steady-state problems, namely one-dimensional (1-D) steady-state space-fractional advection equation and 1-D steady-state space-fractional diffusion problem. In these test-cases, we compare the obtained accuracy in addition to the condition number of the corresponding linear system for the five aforementioned choices of the collocation/interpolation points.

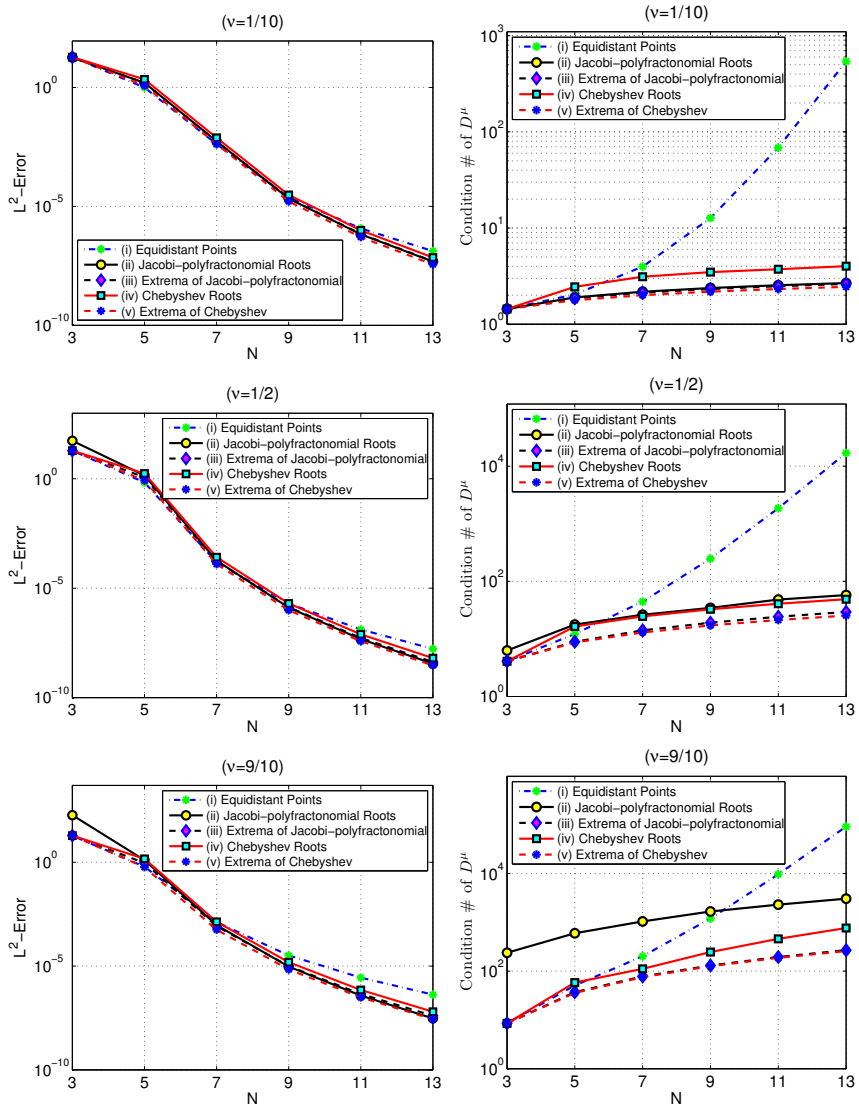

Figure 7.1: Steady-state fractional advection problem: log-linear L^2-norm error of the numerical solution to ${}_{-1}\mathcal{D}_x^{\nu} u(x) = f(x)$, $x \in [-1, 1]$, versus N, employing different collocation/interpolation points (left column), and the corresponding condition number of the linear system resulting from each choice of collocation/interpolation points (right column). The first row is associated with the fractional order $\nu = \mu = 1/10$, the middle row is corresponding to $\nu = \mu = 1/2$, and the bottom row corresponds to the fractional order $\nu = \mu = 9/10$.

Steady-state fractional advection equation

First, we consider the simplest FODE that is the following space-fractional advection equation of order $\nu \in (0,1)$:

$$\begin{aligned} {}_{-1}\mathcal{D}_x^{\nu} u(\,x\,) &= f(x), \quad x \in [-1,1], \\ u(-1) &= 0. \end{aligned} \tag{7.33}$$

We seek the solution to (7.33) in the form $u_N(x) = \sum_{j=2}^{N} u_N(x_j)\, h_j^{\mu}(x)$ (note that $u_N(x_1) = u_N(-1) = 0$). Then, by adopting one the collocation/interpolation points presented in Sec. 7.3.3, and requiring the residual

$$R_N^{adv}(x) = {}_{-1}\mathcal{D}_x^{\nu} u(\,x\,) - f(x) \tag{7.34}$$

to vanish on the collocation points, and finally setting $\nu = \mu$, we obtain

$$\sum_{j=2}^{N} \mathbf{D}_{ij}^{\mu}\; u_N(x_j) - f(x_i) = 0, \tag{7.35}$$

for $i = 2, 3, \cdots, N$. Hence, the collocation scheme leads to the following linear system:

$$\mathbf{D}^{\mu} \vec{\mathbf{u}_N} = \vec{\mathbf{f}}, \tag{7.36}$$

in which $\mathbf{D}^{\mu}$ is the corresponding $(N-1)\times(N-1)$ fractional differentiation matrix given in (C.4).

Corresponding to the force-term $f(x) = \frac{\Gamma(7+9/17)}{\Gamma(7+9/17-\nu)}\ (1+x)^{6+9/17-\nu}$, the analytical solution to (7.33) is obtained as $u^{ext}(x) = (1+x)^{6+9/17}$, which is a fractional-order

function. Having such an exact solution, we show the log-linear L^2-norm error of the numerical solution to (7.33), versus N, in Fig. 7.1. On the left panel, we employ different collocation/interpolation points, and we present the corresponding condition number of the linear system resulting from each choice of collocation/interpolation points on the right panel. We examine also three fractional order, where the first row is associated with the fractional order $\nu = \mu = 1/10$, the middle row corresponds to $\nu = \mu = 1/2$, and the bottom row corresponds to $\nu = \mu = 9/10$. We first observe that our fractional collocation method yields exponential convergence (decay of the L^2-error with N) in each case. We also observe that the roots of ${}_{-1}\mathcal{D}_x^{\nu}[\ {}^{(1)}\mathcal{P}_M^{\nu}(\,x\,)\ ]$, denoted as (fractional) extrema of the Jacobi polyfractonomials, are the best points among all cases. It is shown that not only this choice leads to the best accuracy (lowest error level), but also it results in the lowest condition number with the slowest growth with respect to N.

Steady-state fractional diffusion problem

Next, we examine a higher-order FODE that is a space-fractional diffusion equation of order $1+\nu$, $\nu \in (0,1)$:

$$\begin{aligned} {}_{-1}\mathcal{D}_x^{1+\nu} u(\,x\,) &= f(x), \quad x \in [-1,1], \\ u(\pm 1) &= 0, \end{aligned} \tag{7.37}$$

to analyze the performance of the higher differentiation matrices. We seek solutions to (7.37) in the form $u_N(x) = \sum_{j=2}^{N-1} u_N(x_j)\, h_j^{\mu}(x)$, where $u_N(x_1) = u_N(-1) = u_N(x_N) = u_N(+1) = 0$. Similarly, by requiring the residual to vanish on any choice

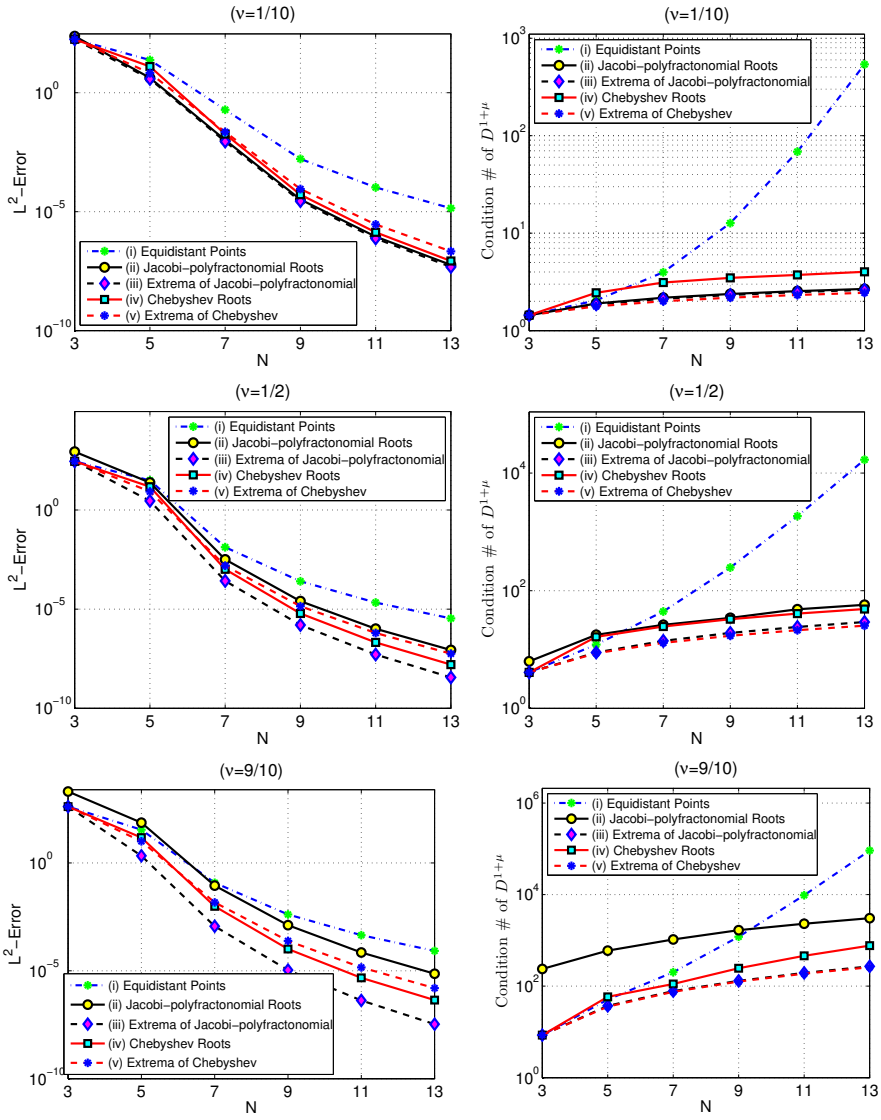

Figure 7.2: Steady-state fractional diffusion problem: log-linear L^2-norm error of the numerical solution to ${}_{-1}\mathcal{D}_x^{1+\nu} u(x) = f(x)$, $x \in [-1, 1]$, versus N, employing different collocation/interpolation points (left column), and the corresponding condition number of the linear system resulting from each choice of collocation/interpolation points (right column). The first row is associated with the fractional order $\nu = \mu = 1/10$ (of total order 1.1), the middle row is corresponding to $\nu = \mu = 1/2$ (of total order 1.5), and the bottom row corresponds to the fractional order $\nu = \mu = 9/10$ (of total order 1.9).

of the collocation points given in Sec. 7.3.3 and setting $\mu = \nu$, we obtain

$$\sum_{j=2}^{N} \mathbf{D}_{ij}^{1+\mu} \; u_N(x_j) - f(x_i) = 0, \tag{7.38}$$

for $i = 2, 3, \cdots, N-1$, which leads to the following linear system:

$$\mathbf{D}^{1+\mu} \vec{\mathbf{u}_N} = \vec{\mathbf{f}}, \tag{7.39}$$

in which $\mathbf{D}^{1+\mu}$ is the corresponding $(N-2)\times(N-2)$ fractional differentiation matrix given in (11.26). Having the same analytical solution taken in previous case and in a similar fashion, we present log-linear L^2-norm error of the numerical solution to ${}_{-1}\mathcal{D}_x^{1+\nu} u(\,x\,) = f(x)$, versus N, in Fig. 7.2 on the left panel, where different collocation/interpolation points are utilized. We also show the corresponding condition number of the linear system resulting from each choice on the right panel. This numerical experiment is also in agreement with our previous observation which again highlights that the roots of ${}_{-1}\mathcal{D}_x^{\nu}[\;{}^{(1)}\mathcal{P}_M^{\nu}(\,x\,)\;]$, denoted as (fractional) extrema of the Jacobi polyfractonomials, are the best points.

7.4 Numerical Tests

Having established the best choice of the collocation points in the previous section, we now present further numerical test-cases. In fact, many applications might involve fractional differential operators consisting of multiple fractional derivative terms possibly with different fractional order. In this section, we solve a number of linear and nonlinear FPDEs to investigate the performance of our fractional collocation method.

7.4.1 Steady-state Problems

We first examine two linear steady-state problems: (i) space-fractional advection-diffusion equation, and (ii) space-fractional multi-term FODEs. Here, we take a step-by-step approach to show how the fractional spectral collocation method can be employed to solve different problems with almost the same ease.

Steady-state fractional advection-diffusion

Here, we consider a two-term equation that describes the dynamics of steady-state fractional advection-diffusion problem. Particularly, we are interested in the following case

$$\begin{aligned} c\ {}_{-1}\mathcal{D}_x^{\nu_1} u(x) - K\ {}_{-1}\mathcal{D}_x^{1+\nu_2} u(x) &= f(x), \quad x \in [-1,1], \\ u(\pm 1) &= 0, \end{aligned} \tag{7.40}$$

where ν_1 and $\nu_2 \in (0,1)$.

Remark 7.4.1. Problem (7.33) was associated only with a single fractional order ν, for which we could perform the interpolation (7.15). However, in (7.40), the fractional differential operator generally is associated with two fractional orders. Hence, we need to specify a *representative fractional order*, ν_{rep}, to do interpolation operation at the collocation points. Such ν_{rep} can be simply set as the average of the fractional orders in (7.40), or as the $\max/\min\{\nu_1, \nu_2\}$.

This time, we seek the solution to (7.40) as $u_N(x) = \sum_{j=2}^{N-1} u_N(x_j)\, h_j^{\mu}(x)$ considering $\mu = \nu_{rep}$, where due to the homogeneous boundary conditions, $u_N(x_1) = u_N(-1) = 0 = u_N(1) = u_N(x_N)$ we construct $h_j^{\mu}(x)$ only for $j = 2, 3, \cdots, N-1$.

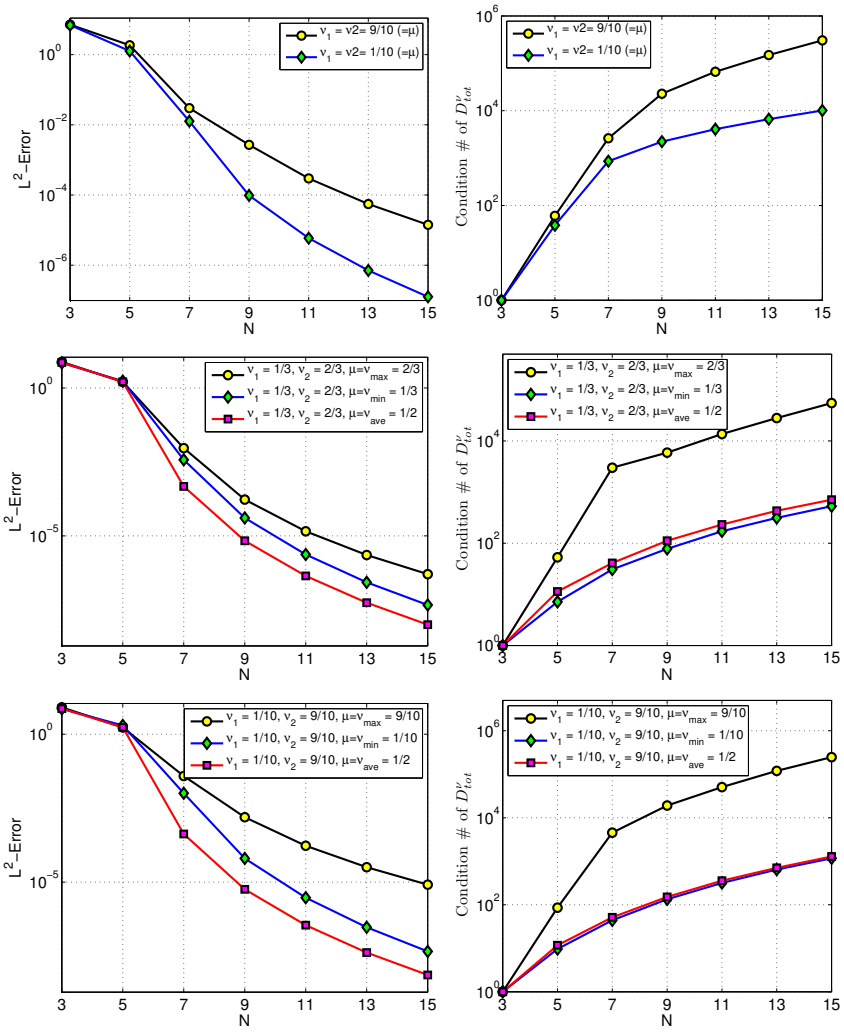

Figure 7.3: Steady-state fractional advection-diffusion: log-linear L^2-norm error of the numerical solution to $c\ {}_{-1}\mathcal{D}_x^{\nu_1} u(x) - K\ {}_{-1}\mathcal{D}_x^{1+\nu_2} u(x) = f(x)$, $x \in [-1, 1]$, versus N, employing different fractional orders ν_1 and ν_2 (left column), and the corresponding condition number of the linear system resulting form each choice of fractional order (right column).

Then, by requiring the corresponding residual to vanish at the collocation points $\{x_i\}_{i=2}^{N-1}$,

$$c\sum_{j=2}^{N-1}\mathbf{D}_{ij}^{\nu_1}\ u_N(x_j)\ -K\sum_{j=2}^{N-1}\mathbf{D}_{ij}^{1+\nu_2}\ u_N(x_j)-f(x_i)=0, \tag{7.41}$$

we obtain the following linear system

$$\mathbf{D}_{tot}^{\nu}\vec{\mathbf{u}_N}=\vec{\mathbf{f}}, \tag{7.42}$$

where $\mathbf{D}_{tot}^{\nu}=c\mathbf{D}^{\nu_1}-K\mathbf{D}^{1+\nu_2}$ of dimension $(N-2)\times(N-2)$, in which $\mathbf{D}^{1+\nu_2}$ is obtained from (11.26) or (11.21).

To demonstrate the performance of the collocation scheme for such application, we consider the forcing term

$$f(x)=\frac{\Gamma(\frac{128}{17})}{\Gamma(\frac{128}{17}-\nu_1)}\ (1+x)^{\frac{111}{17}-\nu_1}-(\frac{111}{17}-\nu_2)\frac{\Gamma(\frac{128}{17})}{\Gamma(\frac{128}{17}-\nu_2)}\ (1+x)^{\frac{94}{17}-\nu_2}, \tag{7.43}$$

for which the analytical solution to (7.40) is obtained as $u^{ext}(x)=(1+x)^{6+9/17}$. In Fig. 7.3, we show the log-linear L^2-norm error of the numerical solution to ${}_{-1}\mathcal{D}_x^{\nu_1}u(\,x\,)-\ {}_{-1}\mathcal{D}_x^{1+\nu_2}u(\,x\,)=f(x)\ ,\ x\in[-1,1]$, versus N, employing different fractional orders ν_1 and ν_2 (left column), and the corresponding condition number of the linear system resulting form each choice of fractional order (right column). In this figure, the first row is associated with the fractional order $\nu_1=\nu_2=\mu$, the middle row corresponds to the case where $\nu_1<\nu_2$ where the fractional interpolation parameter μ is taken as ν_{max}, ν_{min}, and ν_{ave}; and similarly, the bottom row corresponds to $\nu_1<\nu_2$ such that for this case $\nu_2-\nu_1$ becomes larger than one considered in the middle row.

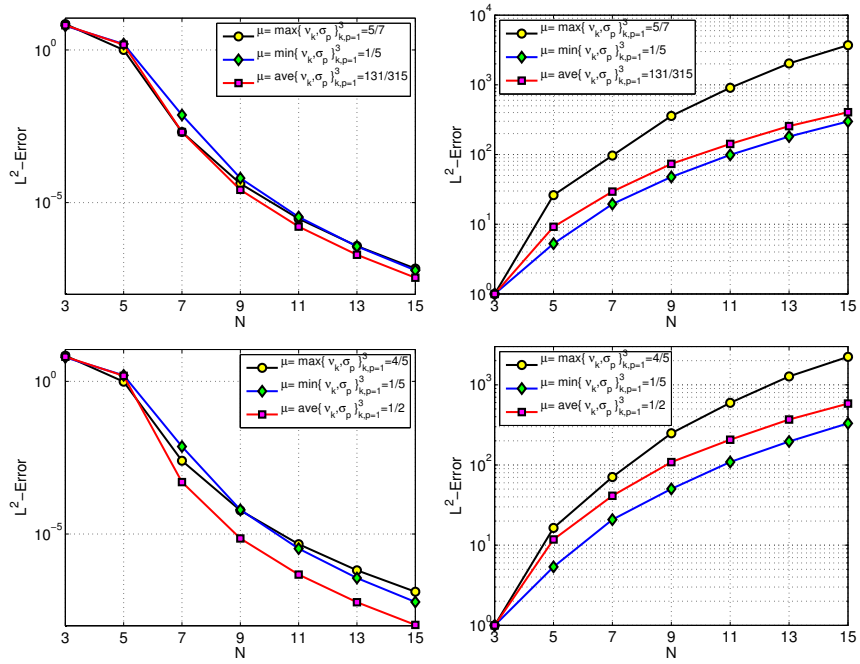

Figure 7.4: Steady-state multi-term problem: log-linear L^2-norm error of the numerical solution to (7.44), versus N, employing fractional orders (left column), and the corresponding condition number of the linear system resulting form each choice of fractional order (right column). Top row corresponds to the fractional orders $\nu_1 = \sigma_1 = 1/5$, $\nu_2 = \sigma_2 = 1/3$ and $\nu_3 = \sigma_3 = 5/7$; also bottom row corresponds to , $\nu_k = 1 - \sigma_k$, where $\sigma_1 = 1/5$, $\sigma_2 = 1/3$, $\sigma_3 = 5/7$.

The exponential decay of L^2-norm error with N is the first observation we make in Fig. 7.3. Here we employ the roots of ${}_{-1}\mathcal{D}_x^{\nu}[\ {}^{(1)}\mathcal{P}_M^{\nu}(\,x\,)\ ]$, (fractional) extrema of the Jacobi polyfractonomials, as our collocation/interpolation points. The second important observation is about the choice of the fractional interpolation parameter μ, since we have two different fractional orders ν_1 and ν_2. It was shown that among $\mu = \nu_{max}$, ν_{max}, and ν_{ave}, the average value i.e., $\mu = \nu_{ave}$ shows the fastest decay of error with N in Fig. 7.3 in addition to yielding almost the slowest growth of the condition number with N in the corresponding linear system.

Multi-term linear advection-diffusion-reaction equations

Next, we generalize (7.33) to a multi-term linear fractional differential equation as

$$\begin{aligned}\sum_{k=1}^{M_a} c_k \Big[{}_{-1}\mathcal{D}_x^{\nu_k} u(x) \Big] + \sum_{p=1}^{M_d} \mathcal{C}_k \Big[{}_{-1}\mathcal{D}_x^{1+\sigma_p} u(x) \Big] + \mathfrak{M}\, u(x) &= f(x),\ x \in [-1,1] \\ u(\pm 1) &= 0, \end{aligned} \tag{7.44}$$

where $\mathcal{C}_{M_d} \neq 0$, ν_k and $\sigma_p \in (0,1)$, moreover, $\{c_k\}_{k=1}^{M_a}$, $\{\mathcal{C}_p\}_{p=1}^{M_d}$ also $\mathfrak{M}$ are real constants given.

We follow similar steps and seek the solution to (7.44) as $u_N(x) = \sum_{j=2}^{N-1} u_N(x_j)\, h_j^{\mu}(x)$ by setting μ to some representative ν. Next, by requiring the corresponding residual to vanish at the collocation points $\{x_i\}_{i=2}^{N-1}$ (the roots of the Jacobi polyfractonomial), we obtain

$$\sum_{k=1}^{M_a} c_k \Big[{}_{-1}\mathcal{D}_x^{\nu_k} u(x) \Big]_{x=x_i} + \sum_{p=1}^{M_d} \mathcal{C}_k \Big[{}_{-1}\mathcal{D}_x^{1+\sigma_p} u(x) \Big]_{x=x_i} + \mathfrak{M}\, u(x_i) - f(x_i) = 0,$$

where the fractional differentiation matrices $\mathbf{D}^{\nu_k}$, $k = 1, 2, \cdots, M_a$ and $\mathbf{D}^{1+\sigma_p}$, $p = 1, 2, \cdots, M_d$, are obtained form (11.20) and (11.21). By doing so, the collocated fractional differential equation results in the following linear (algebraic) system

$$\mathbf{D}_{tot}^{\nu,\sigma}\ \vec{\mathbf{u}_N} = \vec{\mathbf{f}}, \tag{7.45}$$

where $\mathbf{D}_{tot}^{\nu,\sigma} = \sum_{k=1}^{M_a} \mathbf{D}^{\nu_k} + \sum_{p=1}^{M_d} \mathbf{D}^{1+\sigma_p} + \mathfrak{M}\, I$ represents the total fractional differentiation matrix whose dimension is $(N-2)\times(N-2)$, in which I denotes the identity matrix.

In Fig. 7.4 (left panel) we plot log-linear L^2-norm error of the numerical solution

to (7.44), versus N, corresponding to different fractional orders ν_k and σ_p. In this case, we take the exact solution to be $u^{ext}(x) = (1+x)^{6+9/17} - 2(1+x)^{5+9/17}$. These results once again confirm the exponential convergence of the fractional collocation method, and verify that the choice of fractional interpolation parameter μ as the algebraic mean of all fractional differential orders leads to the fastest exponential convergence. The corresponding condition number obtained for such average value, μ, leads to also a small growth with respect to N (see the right panel in Fig. 7.4).

7.4.2 Time-dependent FPDEs

We examine time-dependent FPDEs in which both spatial and temporal differential terms are considered as fractional-order. Specifically, we consider time- and space-fractional advection-diffusion equation, time- and sapce-fractional multi-term FPDEs, and finally time-dependent space-fractional nonlinear Burgers' equation.

Time- and space-fractional advection-diffusion

As the first time-dependent FPDE, we consider the following problem:

(7.46)

$$
\begin{aligned}
{}_0\mathcal{D}_t^{\tau} u(x,t) + c\,{}_{-1}\mathcal{D}_x^{\nu_1} u(x,t) - K\,{}_{-1}\mathcal{D}_x^{1+\nu_2} u(x,t) &= f(x,t), \quad x \in [-1,1],\, t \in [0,T], \\
u(\pm 1, t) &= 0, \\
u(x,0) &= 0,
\end{aligned}
$$

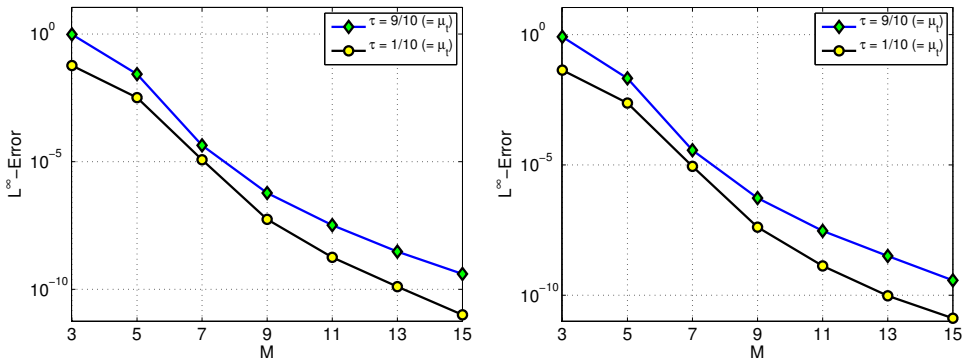

Figure 7.5: Time- and space- fractional advection-diffusion problem; log-linear L^2-norm error of the numerical solution to 7.46, versus N, corresponding to advective fractional order $\nu_1 = 1/3$ and $\nu_2 = 2/3$, i.e., total diffusive order $1+2/3$ (left), and $\nu_1 = 1/10$ and $\nu_2 = 9/10$ (right). In each case, we examine the time-fractional orders $\tau = 1/10$ and $9/10$, where the time-integration is performed for simulation time $T = 1$. Here, the left panel corresponds to the space-fractional orders $\nu_1 = 1/3$ and $\nu_2 = 2/3$, while the right panel corresponds to $\nu_1 = 1/10$ and $\nu_2 = 9/10$.

where $x \in [-1, 1]$ and $t \in [0, T]$, and the associated fractional orders τ, ν_1 and $\nu_2 \in (0, 1)$. We seek the solution of form

$$u_N^M(x,t) = \sum_{j=1}^{N} \sum_{m=1}^{M} u_N^M(x_j, t_m) h_j^{\mu_x}(x) l_m^{\mu_t}(t), \tag{7.47}$$

where $h_j^{\mu_x}(x)$ are the spatial fractional Lagrange basis functions with the representative fractional parameter μ_x, and $l_m^{\mu_t}(t)$ represent the corresponding temporal nodal basis functions with the representative parameter μ_t, constructed as

$$l_m^{\mu_t}(t) = \Big(\frac{t}{t_m}\Big)^{\mu_t} \prod_{\substack{q=1 \\ q \neq m}}^{M} \Big(\frac{t - t_q}{t_m - t_q}\Big), \;\; 2 \leq q \leq M, \tag{7.48}$$

where the collocation points can be taken as $t_i = (x_i+1)T/2$, where x_i are the spatial collocation points, such that $0 = t_1 < t_2 < \cdots < t_N = T$. By taking similar steps as in Sec. 7.3.1 and setting $\tau = \mu_t$, we can obtain the time-fractional differentiation matrix $\mathbf{D}^{\mu_t}$, whose entries are given as

$$\mathbf{D}_{ij}^{\mu_t} = \frac{1}{(t_m)^{\mu_t}} \sum_{m=1}^{M} \frac{\Gamma(m + \mu_t)}{\Gamma(m)} \beta_n^j \, P_{n-1}(\, x(t_i)\,). \tag{7.49}$$

Such temporal fractional interpolants satisfy the property $l_m^{\mu_t}(x_k) = \delta_{mk}$ at the time interpolation points. We note that the same β_n^j utilized for the space-fractional differentiation matrix are employed in (7.49). Next, we substitute (7.47) into (7.46) and take the interpolation and collocation points to be identical. Then, by the Kronecker property for both time- and space-fractional Lagrange interpolants we obtain:

$$\mathbf{U}\mathbf{D}^{\mu_t T} + [c\,\mathbf{D}^{\nu_1} - K\,\mathbf{D}^{1+\nu_2}]\,\mathbf{U} = \mathbf{F}, \tag{7.50}$$

in which $\mathbf{U}$ and $\mathbf{F}$ denote the matrix of approximate solution and load-matrix whose entries are $u_N^M(x_j, t_m)$ and $f(x_j, t_m)$, respectively. The linear system (7.50) can be viewed as a *Lyapunov* equation

$$\mathbf{A}\,\mathbf{U} + \mathbf{U}\mathbf{B} = \mathbf{F}, \tag{7.51}$$

where $\mathbf{A} = c\,\mathbf{D}^{\nu_1} - K\,\mathbf{D}^{1+\nu_2}$ and $\mathbf{B} = \mathbf{D}^{\mu_t T}$. Here, the superscript ^{T} represents the transpose operation.

Since we have already studied the spatial discretization of our scheme, the temporal accuracy is now examined in Fig. 7.5, where the aim is to show the exponential decay of the time-integration error with N, for which the exact solution is taken as $u^{ext}(x,t) = t^{6+2/3}\left((1+x)^{6+9/17} - 2(1+x)^{5+9/17}\right)$. We employ the fractional extrema of the Jacobi polyfractonomial as the time interpolation points and plot the log-linear L^2-norm error of the numerical solution to (7.46), versus N, corresponding to advection fractional order $\nu_1 = 1/3$ and $\nu_2 = 2/3$, i.e., total diffusive order $1+2/3$ (left), and $\nu_1 = 1/10$ and $\nu_2 = 9/10$ (right). In each case shown in Fig. 7.5, we examine the time-fractional orders $\tau = 1/10$ and $9/10$.

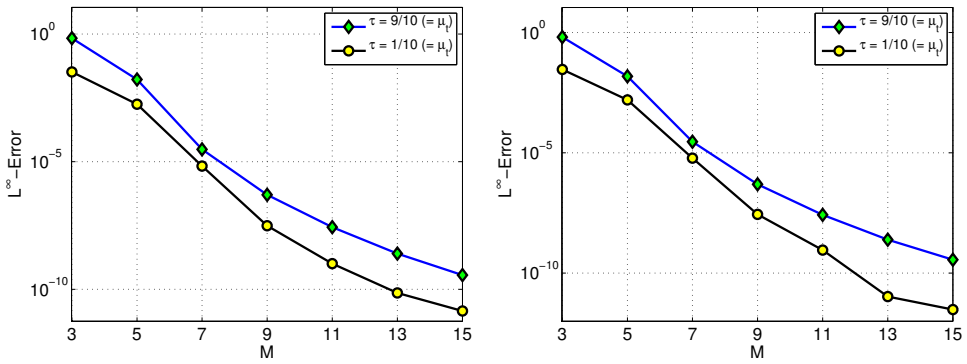

Figure 7.6: Time-and space-fractional multi-term problem; log-linear L^2-norm error of the numerical solution to 7.52, versus N, where the exact solution $u^{ext}(x,t) = t^{6+2/3}\,(\,(1+x)^{6+9/17} - 2(1+x)^{5+9/17}\,)$. The temporal fractional derivative order is τ, the multi-term advective fractional orders are shown by ν_k,$k = 1,2,3$, and the diffusive fractional orders are denoted by $1+\sigma_k$. The left figure corresponds to multi-term advective fractional orders $\nu_k = 1-\sigma_k$, $k = 1,2,3$ where $\sigma_1 = 1/5$, $\sigma_2 = 1/3$,and $\sigma_3 = 5/7$. The right figure is associated with the $\nu_k = \sigma_k$. In each case, we examine to time-fractional orders $\tau = 1/10$ and $9/10$, where the time-integration is performed for simulation time $T = 1$.

Time- and space-fractional multi-term FPDEs

Next, we generalize the fractional advection-diffusion problem (7.46) to a multi-term linear FPDE as

$$
\begin{aligned}
{}_0\mathcal{D}_t^{\,\tau} u(\,x,t\,) + \sum_{k=1}^{M_a} c_k \Big[\, {}_{-1}\mathcal{D}_x^{\,\nu_k} u(\,x,t\,)\Big] \quad + \qquad & (7.52)\\
\sum_{p=1}^{M_d} \mathcal{C}_k \Big[\, {}_{-1}\mathcal{D}_x^{\,1+\sigma_p} u(\,x,t\,)\Big] \;+\; \mathfrak{M}\, u(x,t) \;&=\; f(x,t), \quad x \in [-1,1],\, t \in [0,T],\\
u(\pm 1,t) \;&=\; 0,\\
u(x,0) \;&=\; 0,
\end{aligned}
$$

where $\mathcal{C}_{M_d} \neq 0$, τ, ν_k and $\sigma_p \in (0,1)$. In addition, $\{c_k\}_{k=1}^{M_a}$, $\{\mathcal{C}_p\}_{p=1}^{M_d}$ also $\mathfrak{M}$ are real constants given as before. Taking similar steps as in Sec. 7.4.2 leads to another Lyapunov matrix equation

$$\widetilde{\mathbf{A}}\,\mathbf{U} + \mathbf{U}\widetilde{\mathbf{B}} = \mathbf{F}, \qquad (7.53)$$

in which $\widetilde{\mathbf{A}} = \sum_{k=1}^{M_a} c_k \mathbf{D}^{\nu_k} + \sum_{p=1}^{M_d} \mathcal{C}_k \mathbf{D}^{1+\nu_p}$ and $\widetilde{\mathbf{B}} = \mathbf{B} = \mathbf{D}^{\mu_t T}$.

We confirm our observation made in the previous case in Fig. 7.6, where we plot log-linear L^2-norm error of the numerical solution to (7.52), versus N. On the left figure the distributed advective fractional orders are taken as $\nu_k = 1 - \sigma_k$, $k = 1, 2, 3$ where $\sigma_1 = 1/5$, $\sigma_2 = 1/3$,and $\sigma_3 = 5/7$. Instead, on the right figure, the associated fractional orders are $\nu_k = \sigma_k$. In each case, we examine to time-fractional orders $\tau = 1/10$ and $9/10$. We have taken the same exact solution as in the previous case, however, with a different corresponding forcing term $f(x, t)$, obtained using (7.8). We similarly observed that the algebraic mean of the fractional differentiation orders would be an appropriate candidate for μ, the fractional interpolation parameter.

Time-dependent space-fractional Burgers' equation

We shall show one of the most important advantage of our fractional collocation method that is the efficient treatment of the nonlinear fractional differential terms in FPDEs. As the last problem, we solve the following time-dependent space-fractional Burgers' equation

$$\begin{aligned} \frac{\partial u}{\partial t} + u(x,t)\ {}_{-1}\mathcal{D}_x^{\nu_1} u(\,x,t\,) - \epsilon\ {}_{-1}\mathcal{D}_x^{1+\nu_2} u(\,x,t\,) &= f(x,t), \quad x \in [-1,1],\, t \in [0,T], \\ u(\pm 1, t) &= 0, \\ u(x,0) &= 0, \end{aligned} \tag{7.54}$$

where ν_1 and $\nu_2 \in (0,1)$. The corresponding spatial discretization can be done in a similar fashion as shown in previous sections as

$$\frac{d\vec{\mathbf{u}_N}(t)}{dt} = -diag[\,\vec{\mathbf{u}_N}(t)\,]\mathbf{D}^{\nu_1}\vec{\mathbf{u}_N}(t) + \epsilon\ \mathbf{D}^{1+\nu_2}\vec{\mathbf{u}_N}(t) + \vec{\mathbf{f}}(t), \tag{7.55}$$

where $diag[\,\vec{\mathbf{u}_N}(t)\,]$ represents a diagonal matrix whose diagonal entries are the components of the solution vector $\vec{\mathbf{u}_N}(t)$. The time-integration of this system can be done using a fourth order Runge-Kutta (RK-4). In Table 8.1 we show the exponential decay of L^2-norm error of the numerical solution to (7.54) with N, corresponding to the fractional orders $\nu_1 = \nu_2 = 1/2$, and the simulation time $T = 1/2$. In our RK-4 multi-stage time-integration scheme, we utilize $\Delta t = 5\times 10^{-6}$. We have examined three values for ϵ: (i) $\epsilon = 0$ corresponding to the inviscid Burgers equation, (ii) $\epsilon = 10^{-4}$ corresponding to the viscous Burgers equation with comparatively small diffusivity, and (iii) $\epsilon = 10^{-3}$ corresponding to viscous Burgers equation with comparatively larger diffusivity. Here, we set the exact solution $u^{ext}(x,t) = exp(-t)\,(1-x)(1+x)^{5+9/17}$ for these test-cases and obtain the corresponding forcing term for each case is as:

$$\begin{aligned} f(x,t) = \sum_{q=1}^{\infty} \frac{(-1)^q \Gamma(q+1)}{(\Gamma+1-\tau)q!} t^{q-\tau} \quad &+ \\ \exp(-t)\, u^{ext}(x,t)\, \Big[\frac{2p_0}{p_0-\nu_1}(1+x)^{p_0-1-\nu_1} \quad &- \quad \frac{p_0+1}{p_0+1-\nu_1}(1+x)^{p_0-\nu_1}\Big] \\ -\epsilon\ \exp(-t)\Big[\frac{2p_0(p_0-1-\nu_2)}{p_0-\nu_2}(1+x)^{p_0-2-\nu_2} \quad &- \quad \frac{(p_0+1)(p_0-1-\nu_2)}{p_0+1-\nu_2}(1+x)^{p_0-1-\nu_2}\Big], \end{aligned} \tag{7.56}$$

where $p_0 = 6{+}9/17$, and we truncate the above infinite sum according to the machine precision.

Table 7.1: Exponential decay of L^2-norm error of the numerical solution to (7.54) with N, corresponding to the fractional orders $\nu_1 = \nu_2 = 1/2$, and the simulation time $T = 1/2$. In the RK-4 multi-stage time-integration scheme, we use $\Delta t = 5 \times 10^{-6}$.

N	Inviscid Burgres	Viscous Burgres ($\epsilon = 10^{-4}$)	Viscous Burgres ($\epsilon = 10^{-3}$)
3	1.8650958	1.8651994	1.8661323
5	0.5973899	0.6805485	0.6815204
7	2.03×10^{-4}	$2.41\ \times10^{-4}$	2.43×10^{-4}
9	8.71×10^{-6}	8.68×10^{-6}	8.51×10^{-6}

7.5 Discussion

We conclude the chapter by comparing the performance of FSCM with the finite difference method (FDM) developed in [111], where the fractional derivative ${}_0\mathcal{D}_t^\nu u(t)$ is represented as

$$ {}_0\mathcal{D}_t^\nu u(t) = \frac{1}{\Gamma(2-\nu)} \sum_{j=0}^{k} b_j \frac{u(t_{k+1-j}) - u(t_{k-j})}{(\Delta t)^\nu} + r_{\Delta t}^{k+1}, \tag{7.57} $$

where $r_{\Delta t}^{k+1} \leq C_u(\Delta t)^{2-\nu}$ and $b_j := (j+1)^{1-\nu} - j^{1-\nu}, j = 0, 1, \cdots, k$; a central difference method has been employed to approximate the kernel in the fractional derivative. Finite difference methods are usually easy schemes to implement, however, they are of low order of accuracy, which potentially leads to an enormous memory storage in solving FPDEs when relatively well-resolved solutions are needed. Here, we solve the simplest fractional-order differential equation of form

$$ \begin{aligned} {}_0\mathcal{D}_t^{\ \nu} u(t) &= f(t), \quad t \in [0, T], \\ u(0) &= 0. \end{aligned} \tag{7.58} $$

Table 7.2: CPU time (seconds) on a single 2.66 GHz Intel processor, corresponding to FSCM, PG spectral method, and FDM for solving ${}_0\mathcal{D}_t^{\nu} u(t) = f(t)$, and the exact solution is $u^{ext}(t) = t^6$. Here, N denotes the expansion order in FSCM and PG spectral method, also N_g represents the number of grid points in FDM, and the simulation time is set to $T = 1$.

		$(\nu = 1/10)$	
L^2-norm Error	FSCM	PG Spectral Method	FDM
$\mathcal{O}(10^{-4})$	$(N = 6)$ 0.474261	$(N = 6)$ 0.519422	$(N_g = 70)$ 0.412937
$\mathcal{O}(10^{-5})$	$(N = 7)$ 0.54725	$\times$	$(N_g = 260)$ 0.574912
$\mathcal{O}(10^{-6})$	$(N = 8)$ 0.726889	$(N = 7)$ 0.538418	$(N_g = 1000)$ 5.43267

		$(\nu = 1/2)$	
L^2-norm Error	FSCM	PG Spectral Method	FDM
$\mathcal{O}(10^{-4})$	$(N = 6)$ 0.490258	$(N = 6)$ 0.494925	$(N_g = 450)$ 1.20882
$\mathcal{O}(10^{-5})$	$(N = 7)$ 0.551916	$\times$	$(N_g = 2000)$ 21.9763
$\mathcal{O}(10^{-6})$	$(N = 8)$ 0.740887	$(N = 7)$ 0.501629	$(N_g = 7000)$ 285.797

		$(\nu = 9/10)$	
L^2-norm Error	FSCM	PG Spectral Method	FDM
$\mathcal{O}(10^{-4})$	$(N = 5)$ 0.434934	$\times$	$(N_g = 3500)$ 69.9344
$\mathcal{O}(10^{-5})$	$(N = 6)$ 0.497591	$(N = 6)$ 0.491425	$(N_g = 26000)$ 4714.55
$\mathcal{O}(10^{-6})$	$(N = 7)$ 0.531419	$(N = 7)$ 0.502424	Running Out of Memory!

where ν is taken as $1/10$, $1/2$, and $9/10$, also the simulation time is set to $T = 1$. Such a model-problem and the aforementioned FDM scheme are actually a building block for solving more complicated FPDEs, where the time-and space-fractional terms are discretized in a similar fashion. Moreover, in solving a multi-term FPDE with K fractional-order terms, one has to re-formulate the problem into a recurrence system of fractional-order problems resembling (7.58) (see e.g., [112]). However, as we have shown, our FSCM scheme solves any linear multi-term FPDE with the same ease and without resorting to re-formulating the original problem.

To highlight this fact, we want to compare the CPU time in FSCM and FDM scheme, in addition to a Petrov-Galerkin (PG) spectral method, developed in [189].

In this method, we seek an approximate solution of the form

$$u(t) \approx u_N(t) = \sum_{n=1}^{N} a_n \, {}^{(1)}\widetilde{\mathcal{P}}_n^{\mu}(t), \tag{7.59}$$

where a_n are the unknown expansion coefficients to be determined. By plugging (7.59) into (7.58), we obtain the residual $R_N(t)$ as

$$R_N(t) = {}_0\mathcal{D}_t^{\nu} u_N(t) - f(t)$$

to be L^2-orthogonal to all elements in the set of test functions $\{ {}^{(2)}\widetilde{\mathcal{P}}_k^{\mu}(\, x(t)\,) : \ k = 1, 2, \cdots, N\}$, which are the exact eigenfunctions of the fractional Sturm-Liouville eigen-problems (FSLP) of second kind [187]. This scheme yields a *diagonal* stiffness matrix, whose diagonal entries are given by $\gamma_k = (\frac{2}{T})^{2\mu-1} \ \left(\frac{k+\mu}{k}\right)^2 \frac{2}{2k-1}$. Consequently, we obtain the expansion coefficients as

$$a_k = \frac{1}{\gamma_k} \int_0^T f(t) \ \ {}^{(2)}\widetilde{\mathcal{P}}_k^{\mu}(\, x(t)\,)\, dt, \ \ k = 1, 2, \cdots, N. \tag{7.60}$$

In Table 7.2, we show the CPU time corresponding to FSCM, PG spectral method, and FDM for solving (7.58) corresponding to the following three level of L^2-norm error: $\mathcal{O}(10^{-4})$,$\mathcal{O}(10^{-5})$, and $\mathcal{O}(10^{-6})$. Here, the exact solution is taken as $u^{ext}(t) = t^6$, where by setting $T = 1$, the computational cost of each method is shown corresponding to fractional order $\nu = 1/10$ (top), $\nu = 1/2$ (middle), and $\nu = 9/10$ (bottom). Table 7.2 reveals that for the whole range ν, also for the whole range of error level of interest, our FSCM and PG spectral methods by far outperform FDM. Quantitatively, at the error level $\mathcal{O}(10^{-6})$, FSCM and PG methods perform roughly 7 and 386 times faster than FDM corresponding to $\nu = 1/10$ and $\nu = 1/2$, respectively. While we see that for such a simple model-problem and setting, FDM can

not achieve the error level $\mathcal{O}(10^{-6})$, because of the lack of memory. Instead, FSCM and PG spectral methods reach to the error $\mathcal{O}(10^{-6})$ in a half of a second. Finally, Table 4.1 shows that FSCM and PG spectral method perform almost equivalently in solving (7.58). However, we note that in this case, the linear system resulting from PG spectral method is diagonal. Therefore, in contrast to FSCM, the employment of PG spectral method in other problems such as linear FPDEs and multi-term FPDEs becomes computationally more expensive due to the extra cost of quadrature, while possessing the exponential accuracy.

Chapter Eight

Variable-Order Fractional PDEs

While several high-order methods have been developed for fractional PDEs (FPDEs) with fixed order, there are no such methods for FPDEs with field-variable order. These equations allow multiphysics simulations seamlessly, e.g. from diffusion to sub-diffusion or from wave dynamics transitioning to diffusion, by simply varying the fractional order as a function of space or time. We develop an exponentially accurate fractional spectral collocation method for solving linear/nonlinear FPDEs with field-variable order. Following the spectral theory, developed in [187] for fractional Sturm-Liouville eigenproblems, we introduce a new family of interpolants, called *left-/right-sided and central fractional Lagrange interpolants*. We employ the fractional derivatives of (left-/right-sided) Riemann-Liouville and Riesz type and obtain the corresponding fractional differentiation matrices by collocating the field-variable fractional orders. We solve several FPDEs including time- and space-fractional advection-equation, time- and space- fractional advection-diffusion equation, and finally the space-fractional Burgers' equation to demonstrate the performance of the method. In addition, we develop a spectral penalty method for enforcing inhomogeneous initial conditions. Our numerical results confirm the exponential-like convergence of the proposed fractional collocation methods.

8.1 Background

Recently, it has been demonstrated that in many dynamic processes, the underlying differential operators not only appear as fractional, but they also possess a dynamic nature in a sense that their order is *field-variable*, which may vary in time and/or space. For instance, several classes of random processes with variable-order fractional transition probability densities on unbounded domains have been studied in [94, 88]. Moreover, the notion of *variable-order* fractional calculus has been used

to dynamic modelling of heterogeneous physical systems. Examples are linear and nonlinear oscillators with viscoelastic damping by Coimbra [42], processing of geographical data using variable-order derivatives by Cooper and Cowan [43], signature verification through variable/adaptive fractional order differentiators by Tseng [172], constitutive laws in viscoelastic continuum mechanics by Ramirez et.al., [146], modeling of diffusive-convective effects on the oscillatory flows [136], anomalous diffusion problems by Sun et al. [165], fractional advection-diffusion problem by Chen et al., [37, 36], mobile-immobile advection-dispersion model by Zhang et al. [193], and chloride ions sub-diffusion in concrete structures by Chen et. al. [39].

Such an extension from fixed-order to variable-order operators provides an invaluable prospect in modeling complex phenomena, whose behaviour otherwise may not be properly understood. For instance, in Fig. 8.1 (right), we investigate the decaying solution to the following time- and space fractional diffusion problem

They introduced these polyfractonomials as the eigenfunctions of fractional Sturm-Liouville problems in [187], explicitly. Moreover, they employed these fractional bases to introduce a new class of fractional interpolants to develop efficient and spectrally accurate collocation methods in [190] for a variety of FODEs and FPDEs including multi-term FPDEs and the nonlinear space-fractional Burgers' equation. Employing the Jacobi polyfractonomials, Zayernouri and Karniadakis have recently developed a unified Petrov-Galerkin spectral method along with a unified fast solver in [183] that efficiently treats the whole family of elliptic, parabolic, and hyperbolic FPDEs in high-dimensions with spectral accuracy and in a unified fashion.

$$ {}_0^C\mathcal{D}_t^{\zeta(x)} u \;=\; \frac{\partial^{1+\nu} u}{\partial |x|^{1+\nu}}, \tag{8.1} $$

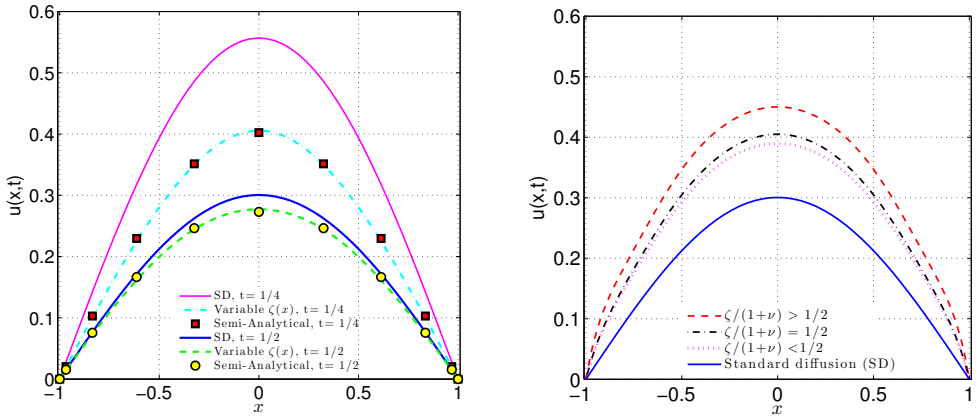

Figure 8.1: Variable-order (Left) versus fixed-order diffusion (Right). The initial condition is $u(x,0) = 1 - x^2$ and the solutions are obtained at $t = \frac{1}{2}$, where the space-fractional order is $(1+\nu) = 1.99$. While the fixed-order cases on the right plot exhibit the expected *sub-diffusion* process compared to the standard diffusion (SD) problem (i.e., when $\zeta = 1$ and $1+\nu = 2$), the variable-order test-case when $\zeta(x) = 1/(3|x| + 11/10)$ on the left plot exhibit, surprisingly, a *super-diffusion* behaviour.

subject to $u(x,0) = (1-x^2)$ and $u(\pm 1, t) = 0$, in the absence of any external forces. In (8.1), ${}_0^C\mathcal{D}_t^{\zeta}(\cdot)$ and $\frac{\partial^{1+\nu}(\cdot)}{\partial|x|^{1+\nu}}$ are fractional derivatives of Caputo and Riesz type, see section 8.2. Here, we set ζ and $\nu \in (0,1)$, highlighting the anomalous *sub-diffusion* character of the problem, compared to the standard diffusion denoted by SD, i.e., when $\zeta = \nu = 1$. We demonstrate the corresponding sub-diffusive behaviour in (8.1) by taking different but *fixed* values of ζ and ν and plotting the results in Fig. 8.1 (right) at $t = 1/2$. As expected, the corresponding curves all lag behind the standard diffusion. Surprisingly, when we allow the temporal order ζ to vary across the domain, as shown in Fig. 8.1 (left) at $t = 1/4$ and $t = 1/2$, we observe a *super-diffusive* behaviour even for $\zeta(x) \in (0,1)$; here, $\zeta(x) = 1/(3|x| + 11/10)$. In addition, we notice a more pronounced super-diffusion at earlier times in Fig. 8.1 (left). However, after a long time, the variable-order case becomes a sub-diffusion process.

The numerical approximation of variable-order FPDEs has been mostly developed using finite-difference methods (FDMs) (see [194, 158, 38, 157] and references

therein). Although easier to implement, the main challenge in FDM schemes is their limited accuracy interwoven with their inherent *local* character, while fractional derivatives are essentially *global* (nonlocal) differential operators. Hence, global schemes such as *Spectral Methods* (SM) may be more appropriate for discretizing fractional operators.

Recently, Zayernouri and Karniadakis [189] developed exponentially accurate Petrov-Galerkin spectral and spectral element methods for fractional differential equations, where they employed a new family of fractional bases, called *Jacobi Polyfractonomials*. They introduced these polyfractonomials as the eigenfunctions of fractional Sturm-Liouville problems in [187], explicitly given as

$$ {}^{(1)}\mathcal{P}_n^{\alpha,\beta,\mu}(\xi) = (1+\xi)^{-\beta+\mu-1} P_{n-1}^{\alpha-\mu+1,-\beta+\mu-1}(\xi), \quad \xi \in [-1,1], \tag{8.2} $$

with $\mu \in (0,1)$, $-1 \leq \alpha < 2-\mu$, and $-1 \leq \beta < \mu-1$, representing the eigenfunctions of the *singular* FSLP of first kind (SFSLP-I), and

$$ {}^{(2)}\mathcal{P}_n^{\alpha,\beta,\mu}(\xi) = (1-\xi)^{-\alpha+\mu-1} P_{n-1}^{-\alpha+\mu-1\,,\,\beta-\mu+1}(\xi), \quad \xi \in [-1,1], \tag{8.3} $$

where $-1 < \alpha < \mu - 1$ and $-1 < \beta < 2 - \mu$, and $\mu \in (0,1)$, denoting the eigenfunctions of the *singular* FSLP of *second* kind (SFSLP-II). Moreover, they employed these fractional bases to introduce a new class of fractional interpolants to develop efficient and exponentially accurate collocation methods in [190] for a variety of FODEs and FPDEs including multi-term FPDEs and the non-linear space-fractional Burgers' equation.

To the best of our knowledge, no high-order or spectral methods have been developed for variable-order FPDEs up to date. The main contribution of the present

study is the development of a new class of exponentially accurate fractional spectral collocation method for solving linear and nonlinear field-variable order in-time and in-space FPDEs. To this end, we introduce the *left-/right-sided* fractional Lagrange interpolants (FLIs) when spatial Riemann-Liouville derivatives are employed, in addition to the *central* FLIs when spatial Riesz derivatives are employed.

8.2 Preliminaries

We first provide some definitions from fractional calculus. Following [142], for a function $w(z) \in C^n[z_L, z_R]$, we denote by ${}_{z_L}\mathcal{D}_z^{\gamma} w(z)$ the *left-sided* Reimann-Liouville fractional derivative of order γ, when $n-1 \leq \gamma < n$, defined as

$$ {}^{RL}_{z_L}\mathcal{D}_z^{\gamma} w(z) = \frac{1}{\Gamma(n-\gamma)} \frac{d^n}{dz^n} \int_{z_L}^{z} \frac{w(s)}{(z-s)^{\gamma+1-n}}\, ds, \quad z \in [z_L, z_R], \tag{8.4} $$

where Γ represents the Euler gamma function, and as $\gamma \to n$, the *global* operator ${}^{RL}_{z_L}\mathcal{D}_z^{\gamma} \to d^n/dz^n$, recovering the *local* n-th order derivative with respect to z. We also denote by ${}^{RL}_{z}\mathcal{D}_{z_R}^{\gamma} w(z)$ the corresponding *right-sided* Reimann-Liouville fractional derivative of order $n-1 \leq \gamma < n$, defined as

$$ {}^{RL}_{z}\mathcal{D}_{z_R}^{\gamma} w(z) = \frac{1}{\Gamma(n-\gamma)} (-1)^n \frac{d^n}{dz^n} \int_{z}^{b} \frac{w(s)}{(s-z)^{\gamma+1-n}}\, ds, \quad z \in [z_L, z_R]. \tag{8.5} $$

Similarly, as $\gamma \to n$, the right-sided fractional derivative tends to the standard n-th order local derivative. We also recall from [142] a useful property of the Riemann-Liouville fractional derivatives. Assume that $0 < p \leq 1$, $0 < q \leq 1$ and $z > z_L$, then

$$ {}^{RL}_{z_L}\mathcal{D}_z^{p+q} w(z) = \left({}^{RL}_{z_L}\mathcal{D}_z^{p}\right)\left({}^{RL}_{z_L}\mathcal{D}_z^{q}\right) w(z) = \left({}^{RL}_{z_L}\mathcal{D}_z^{q}\right)\left({}^{RL}_{z_L}\mathcal{D}_z^{p}\right) w(z), \tag{8.6} $$

when $w(z_L) = 0$, and

$$ {}^{RL}_{z}\mathcal{D}^{p+q}_{z_R} w(z) = \left({}^{RL}_{z}\mathcal{D}^{p}_{z_R}\right)\left({}^{RL}_{z}\mathcal{D}^{q}_{z_R}\right) w(z) = \left({}^{RL}_{z}\mathcal{D}^{q}_{z_R}\right)\left({}^{RL}_{z}\mathcal{D}^{p}_{z_R}\right) w(z), \tag{8.7} $$

when $w(z_R) = 0$. Moreover, for $k > -1$, we have

$$ {}^{RL}_{z_L}\mathcal{D}^{\gamma}_{z}(z + z_L)^k = \frac{\Gamma(k+1)}{\Gamma(k+1-\gamma)}(z + z_L)^{k-\gamma} \tag{8.8} $$

and

$$ {}^{RL}_{z}\mathcal{D}^{\gamma}_{z_R}(z_R - z)^k = \frac{-\Gamma(k+1)}{\Gamma(k+1-\gamma)}(z_R - z)^{k-\gamma}, \tag{8.9} $$

if $\gamma \in (0, 1)$. In addition, let again $z = \frac{z_R+z_L}{2} + \frac{z_R-z_R}{2}\xi$ map $x \in [x_L, x_R]$ with $\xi \in [-1, 1]$, known as the *standard domain*, to $[z_L, z_R]$. Then,

$$ {}^{RL}_{z_L}\mathcal{D}^{\gamma}_{z} w(z) = \left(\frac{2}{z_R - z_L}\right)^{\gamma} \; {}^{RL}_{-1}\mathcal{D}^{\gamma}_{\xi} w\Big(z(\xi)\Big), \tag{8.10} $$

moreover,

$$ {}^{RL}_{z}\mathcal{D}^{\gamma}_{z_R} w(z) = \left(\frac{2}{z_R - z_L}\right)^{\gamma} \; {}^{RL}_{\xi}\mathcal{D}^{\gamma}_{1} w\Big(z(\xi)\Big), \tag{8.11} $$

which are useful in the derivation of the emerging differentiation matrices in our method.

The corresponding fractional derivatives of Caputo type, i.e., ${}^{C}_{z_R}\mathcal{D}^{\gamma}_{z} w(z)$ and ${}^{C}_{z}\mathcal{D}^{\gamma}_{z_R} w(z)$, are also defined by interchanging the order of differentiation and integration in (8.4) and (8.5) as

$$ {}^{C}_{z_L}\mathcal{D}^{\gamma}_{z} w(z) = \frac{1}{\Gamma(n-\gamma)} \int_{z_L}^{z} \frac{\frac{d^n w(s)}{ds^n}}{(z-s)^{\gamma+1-n}}\, ds, \quad z \in [z_L, z_R], \tag{8.12} $$

and

$$ {}^{C}_{z}\mathcal{D}^{\gamma}_{z_R} w(z) = \frac{(-1)^n}{\Gamma(n-\gamma)} \int_z^b \frac{\frac{d^n w(s)}{ds^n}}{(s-z)^{\gamma+1-n}}\, ds, \quad z \in [z_L, z_R], \tag{8.13} $$

which we will employ in FPDEs subject to non-homogeneous initial conditions. From the definition of the Caputo derivatives, the properties (8.8) and (8.9) become

$$ {}^{C}_{z_L}\mathcal{D}^{\gamma}_{z}(z+z_L)^k = \begin{cases} 0, & k < \gamma, \\ \frac{\Gamma(k+1)}{\Gamma(k+1-\gamma)}(z+z_L)^{k-\gamma}, & 0 < \gamma \leq k, \end{cases} \tag{8.14} $$

and

$$ {}^{C}_{z}\mathcal{D}^{\gamma}_{z_R}(z_R-z)^k = \begin{cases} 0, & k < \gamma, \\ \frac{-\Gamma(k+1)}{\Gamma(k+1-\gamma)}(z_R-z)^{k-\gamma}, & 0 < \gamma \leq k. \end{cases} \tag{8.15} $$

We denote by $\frac{\partial^\gamma u}{\partial |z|^\gamma}$ the *Riesz* fractional derivative of order γ, when $n-1 < \gamma < n$, defined in terms of left- and right-sided Riemann-Liouville fractional derivatives as

$$ \frac{d^\gamma u}{d|z|^\gamma} = C_\gamma \Big({}^{RL}_{z_L}\mathcal{D}^{\gamma}_{z} w(z) \; + \; {}^{RL}_{z}\mathcal{D}^{\gamma}_{z_R} w(z) \Big), \tag{8.16} $$

where $C_\gamma = -\frac{1}{2}\sec(\gamma\pi/2)$. It is easy to check that as $\gamma \to n$, asymptotically $\frac{d^\gamma(\cdot)}{d|z|^\gamma} \to d^n(\cdot)/dz^n$.

So far, we note that all the aforementioned fractional derivatives are of a *constant* order γ and are defined originally for the *univariate* function $w(z)$. In the sequel, we introduce a model problem, in which the fractional operators are defined through generalization of the given definitions to *multi-variate* functions, in which the corresponding fractional orders are *field* variables rather than constants.

8.3 Problem Definition

Let ζ, σ and $\nu : \mathbb{R}^2 \to \mathbb{R}$ be *continuous* functions. We study the following nonlinear variable-order time- and space-fractional FPDE for all $(x,t) \in [a,b] \times [0,T]$ as

$$
\begin{aligned}
{}^{RL}_{0}\mathcal{D}_t^{\zeta(x,t)} u + g(u)\, {}^{*}\mathcal{D}_x^{\sigma(x,t)} u &= K\, {}^{*}\mathcal{D}_x^{1+\nu(x,t)} u + f(u;x,t), && (8.17)\\
u(a,t) &= u(b,t) = 0, && (8.18)\\
u(x,0) &= 0, && (8.19)
\end{aligned}
$$

where $K > 0$ and $f(u;x,t)$ denotes the forcing- and/or reaction term. Moreover, the *temporal* order $\zeta(x,t) \in (0,1)$, the spatial *advection* order $\sigma(x,t), \in (0,1)$, and the spatial *diffusion* order $1+\nu(x,t) \in (1,2)$, i.e., $\nu(x,t) \in (0,1)$. We shall discuss the regularity of the aforementioned field variable orders in section 8.6. Here, ${}^{RL}_{0}\mathcal{D}_t^{\zeta(x,t)} u$ represents the $\zeta(x,t)$-th order left-sided *partial* time derivative of $u(x,t)$ of Riemann-Liouville type, defined as

$$
{}^{RL}_{0}\mathcal{D}_t^{\zeta(x,t)} u(x,t) = \frac{1}{\Gamma[1-\zeta(x,t)]} \frac{\partial}{\partial t} \int_0^t \frac{u(x,s)\; ds}{(t-s)^{\zeta(x,t)}}, \tag{8.20}
$$

based on (8.4). We consider the space-fractional derivatives ${}^{*}\mathcal{D}_x$, associated with the advection and the diffusion terms in (8.17), to be of either (i) Riemann-Liouville or (ii) Riesz type, when homogeneous initial/boundary conditions are imposed. Alternatively, when inhomogeneous initial conditions are enforced, we consider the temporal derivative to be of Caputo type.

(I) ${}^{*}\mathcal{D}_x$ of Riemann-Liouville type We define the corresponding advection partial fractional derivative ${}^{*}\mathcal{D}_x^{\sigma(x,t)} u$ of Riemann-Liouville type according to (8.4) and (8.5)

and based on the direction of the transport velocity as

$$
{}^{*}\mathcal{D}_x^{\sigma(x,t)}u(x,t) \equiv \begin{cases} {}_{a}^{RL}\mathcal{D}_x^{\sigma(x,t)}u = \frac{1}{\Gamma[1-\sigma(x,t)]}\frac{\partial}{\partial x}\int_a^x \frac{u(r,t)\,dr}{(x-r)^{\sigma(x,t)}}, & g>0, \\ \\ {}_{x}^{RL}\mathcal{D}_b^{\sigma(x,t)}u = \frac{1}{\Gamma[1-\sigma(x,t)]}(-\frac{\partial}{\partial x})\int_x^b \frac{u(r,t)\,dr}{(r-x)^{\sigma(x,t)}}, & g<0. \end{cases} \tag{8.21}
$$

In addition, we define the diffusion partial fractional derivative ${}^{*}\mathcal{D}_x^{1+\nu(x,t)}u$ of Riemann-Liouville type either as ${}_{a}^{RL}\mathcal{D}_x^{1+\nu(x,t)}u \equiv \frac{\partial}{\partial x}[{}_{a}^{RL}\mathcal{D}_x^{\nu(x,t)}u]$ or ${}_{x}^{RL}\mathcal{D}_b^{1+\nu(x,t)}u \equiv \frac{\partial}{\partial x}[{}_{x}^{RL}\mathcal{D}_b^{\nu(x,t)}u]$.

(II) ${}^{*}\mathcal{D}_x$ of Riesz type We alternatively define the corresponding advection partial fractional derivative ${}^{*}\mathcal{D}_x^{\sigma(x,t)}u$ of Riesz type as

$$
{}^{*}\mathcal{D}_x^{\sigma(x,t)}u(x,t) \equiv \frac{\partial^{\sigma(x,t)}u}{\partial|x|^{\sigma(x,t)}} = C_{\sigma(x,t)}\Big({}_{a}^{RL}\mathcal{D}_x^{\sigma(x,t)}u \;+\; {}_{x}^{RL}\mathcal{D}_b^{\sigma(x,t)}u\Big). \tag{8.22}
$$

Moreover, from (8.6) and (8.7), we define the diffusion partial fractional derivative ${}^{*}\mathcal{D}_x^{1+\nu(x,t)}u$ to be of Riesz type as

$$
{}^{*}\mathcal{D}_x^{1+\nu(x,t)}u(x,t) = C_{1+\nu(x,t)}\frac{\partial}{\partial x}\Big[{}_{a}^{RL}\mathcal{D}_x^{\nu(x,t)}u(x,t) + {}_{x}^{RL}\mathcal{D}_b^{\nu(x,t)}u(x,t)\Big]. \tag{8.23}
$$

In the following, we develop a fractional spectral collocation method for efficient solution of (8.17) based on the variable-order fractional differential operators defined here.

8.4 Fractional Lagrange Interpolants (FLIs)

We define a set of *interpolation points* on which the corresponding Lagrange interpolants are obtained. Specifically, we employ a new family of left- and right-sided space-time *fractional Lagrange interpolants* (FLI) rather than utilizing the standard algebraic/trigonometric polynomial Lagrange basis functions. We shall demonstrate that such a construction leads to efficient computation of the corresponding differentiation matrices in addition to efficient approximations. Denoting by u_N an approximation of the solution in terms of such interpolators, we formulate our collocation method by requiring the residual of the problem i.e.,

$$R_N(x,t) = {}^{RL}_{0}\mathcal{D}_t^{\zeta(x,t)} u_N + g(u)\, {}^{*}\mathcal{D}_x^{\sigma(x,t)} u_N - K\, {}^{*}\mathcal{D}_x^{1+\nu(x,t)} u_N - f(u_N; x, t), \quad (8.24)$$

to vanish on the same set of grid points called *collocation points*.

Our fractional spectral collocation scheme is inspired by a new spectral theory developed for fractional Sturm-Liouville eigen-problems (FSLP) in [187]. The idea is to represent the solution to (8.17) in terms of new fractional (non-polynomial) basis functions, called *Jacobi polyfractonomials*, which are the eigenfunctions of the FSLP of first and second kind, explicitly given in (8.2) and (8.3). So, depending on the choice of the spatial fractional derivative ${}^{*}\mathcal{D}_x$ in (8.17), we introduce the corresponding fractional Lagrange interpolants.

8.4.1 Construction of FLI when ${}^{*}\mathcal{D}_x \equiv {}^{RL}\mathcal{D}_x$

Let $\alpha = \beta = -1$ in (8.2) and (8.3), which corresponds to the *regular* eigenfunctions of first and second kind, given as

$$ {}^{(1)}\mathcal{P}_n^{\mu}(\xi) = (1+\xi)^{\mu} P_{n-1}^{-\mu,\mu}(\xi), \quad \xi \in [-1,1], \tag{8.25} $$

and

$$ {}^{(2)}\mathcal{P}_n^{\mu}(\xi) = (1-\xi)^{\mu} P_{n-1}^{\mu,-\mu}(\xi), \quad \xi \in [-1,1]. \tag{8.26} $$

where we recall that $\mu \in (0,1)$. From the properties of the eigensolutions in [187], the left-sided fractional derivatives of (11.16) and (8.26) are given as

$$ {}^{RL}_{-1}\mathcal{D}_{\xi}^{\mu}\left({}^{(1)}\mathcal{P}_n^{\mu}(\,\xi\,)\right) = {}^{RL}_{\xi}\mathcal{D}_{1}^{\mu}\left({}^{(2)}\mathcal{P}_n^{\mu}(\,\xi\,)\right) = \frac{\Gamma(n+\mu)}{\Gamma(n)} P_{n-1}(\,x\,), \tag{8.27} $$

where $P_{n-1}(\,x\,)$ denotes a Legendre polynomial of order $(n-1)$. Hence, in general, we can employ the univariate eigenfunctions (11.16) and (8.26) to construct the space-time *modal* basis functions needed. However, here we alternatively construct suitable *nodal* basis functions based on the transport velocity and the corresponding choice of the spatial derivatives ${}^{RL}_{a}\mathcal{D}_x$ or ${}^{RL}_{x}\mathcal{D}_b$; see (8.21).

Left-Sided FLIs when ${}^{*}\mathcal{D}_x \equiv {}^{RL}_{a}\mathcal{D}_x$

We seek solutions as a *nodal* expansion

$$ u_N(x,t) = \sum_{m=1}^{\mathcal{M}} \sum_{n=1}^{\mathcal{N}} u_N(x_m,t_n)\, L_m^{\mu}(x) \mathcal{T}_n^{\tau}(t), \tag{8.28} $$

where $L_m^{\mu}(x)$ represent the *left-sided* spatial FLIs and $\mathcal{T}_n^{\tau}(t)$ denote the *temporal* FLIs, which are defined on some interpolations points $a = x_1 < x_2 < \cdots < x_{\mathcal{M}} = b$ and $0 = t_1 < t_2 < \cdots < t_{\mathcal{N}} = T$ as

$$L_m^{\mu}(x) = \Big(\frac{x - x_1}{x_m - x_1}\Big)^{\mu} \prod_{\substack{k=1 \\ k \neq m}}^{\mathcal{M}} \Big(\frac{x - x_k}{x_m - x_k}\Big), \;\; 2 \leq m \leq \mathcal{M} - 1, \tag{8.29}$$

all of fractional order $(\mathcal{M} + \mu - 1)$, and

$$\mathcal{T}_n^{\tau}(t) = \Big(\frac{t}{t_n}\Big)^{\tau} \prod_{\substack{q=1 \\ q \neq n}}^{\mathcal{N}} \Big(\frac{t - t_q}{t_n - x_q}\Big), \;\; 2 \leq n \leq \mathcal{N}, \tag{8.30}$$

of fractional order $(\mathcal{N} + \tau - 1)$. Here, we call the superscript μ and τ as spatial and temporal *interpolation parameter*s, respectively. We set these constant fractional parameters prior to solving (8.17) from the variable orders given, i.e., τ, σ, and ν. Moreover, we note that the fractional interpolants satisfy the Kronecker delta property, i.e., $H_m^{\mu}(x_k) = \delta_{km}$ and $L_n^{\tau}(t_q) = \delta_{qn}$, at interpolation points.

Because of the homogeneous Dirichlet boundary/initial condition(s) in (8.17), we only construct $L_m^{\mu}(x)$ for $m = 2, 3, \cdots, \mathcal{M}$ when the maximum fractional order $1 + \nu \in (1, 2)$, where we set $u_N(x_1, t) = u_N(x_{\mathcal{M}}, t) = 0$. Moreover, when $\tau \in (0, 1)$, there are only $(\mathcal{N} - 1)$ fractional Lagrange interpolants $\mathcal{T}_n^{\tau}(t)$, $n = 2, 3, \cdots, \mathcal{N}$, since we impose $u_N(x, t_1) = 0$.

Right-Sided FLIs when ${}^{*}\mathcal{D}_x \equiv {}^{RL}_{x}\mathcal{D}_b$

In this case, we seek the solution as another *nodal* expansion given by

$$u_N(x,t) = \sum_{m=1}^{\mathcal{M}} \sum_{n=1}^{\mathcal{N}} u_N(x_m,t_n)\, R_m^{\mu}(x) \mathcal{T}_n^{\tau}(t), \tag{8.31}$$

where $R_m^{\mu}(x)$ represent the *right-sided* spatial FLIs, defined on the interpolations points as

$$R_m^{\mu}(x) = \Big(\frac{x_{\mathcal{M}} - x}{x_{\mathcal{M}} - x_m}\Big)^{\mu} \prod_{\substack{k=1 \\ k\neq m}}^{\mathcal{M}} \Big(\frac{x - x_k}{x_m - x_k}\Big), \;\; 2 \leq m \leq \mathcal{M}-1, \tag{8.32}$$

which are all again of fractional order $(\mathcal{M} + \mu - 1)$.

8.4.2 Central FLIs when ${}^{*}\mathcal{D}_x \equiv \frac{\partial}{\partial |x|}$ of Riesz Type

When the fractional derivatives in (8.17) are all of Riesz type, we seek the solution as

$$u_N(x,t) = \sum_{m=1}^{\mathcal{M}+1} \sum_{n=1}^{\mathcal{N}} u_N(x_m,t_n)\, h_m(x) \mathcal{T}_n^{\tau}(t), \tag{8.33}$$

where $h_m(x)$ represent the standard polynomial Lagrange interpolants, defined on the interpolations points as

$$h_m(x) = \prod_{\substack{k=1 \\ k\neq m}}^{\mathcal{M}+1} \Big(\frac{x - x_k}{x_m - x_k}\Big), \;\; 2 \leq m \leq \mathcal{M}, \tag{8.34}$$

which are all of order $\mathcal{M}$. The polynomial choice of $h_m(x)$ is mainly due to the *co-existence* of the left- and right-sided fractional derivatives in the definition of the Riesz derivatives in (8.22) and (8.23). Hence, compared to the structure of the FLIs in

(8.29) and (8.32), we call the FLIs presented in (8.33) *central* in-space interpolants. In fact, they can be viewed as the nodal representations of Legendre polynomials i.e., $P_{\mathcal{M}}(x)$, which simultaneously appear to be the regular eigenfucntions (11.16) and (8.26) asymptotically when $\mu \to 0$ setting $n = \mathcal{M} + 1$.

When the time-derivative is of Caputo type, which is a proper setting in which we can enforce the inhomogeneous initial conditions, we also use the standard Legendre bases in time, i.e.,

$$u_N(x,t) = \sum_{m=1}^{\mathcal{M}+1} \sum_{n=1}^{\mathcal{N}+1} u_N(x_m, t_n)\, h_m(x)\, h_n(t), \tag{8.35}$$

where

$$h_n(t) = \prod_{\substack{k=1 \\ k\neq n}}^{\mathcal{N}+1} \Big(\frac{t - t_k}{t_m - t_k} \Big), \;\; 1 \leq n \leq \mathcal{N} + 1, \tag{8.36}$$

which allows us to properly penalize the initial condition to the problem and develop a stable scheme.

8.5 Fractional Differentiation Matrices

We derive the corresponding spatial and temporal fractional differentiation matrices assuming that the collocation and interpolation points coincide. We first choose the suitable expansion among those given in (8.28), (8.31), or (8.33) based on the choice of the spatial fractional derivative ${}^{*}\mathcal{D}_x$. Then, we derive the corresponding differentiation matrices.

8.5.1 ${}^{*}\mathcal{D}_x$ of Left-Sided Riemann-Liouville Type

Whether left- or right-sided Riemann-Liouville derivatives are employed in (8.17), we obtain the corresponding to left- or right-sided fractional differentiation matrices of order $\sigma(x,t)$ and $1+\nu(x,t)$.

Theorem 8.5.1. *Let $\sigma = \sigma(x,t) \in C\Big([a,b]\times[0,T]\Big)$ and consider the affine mapping that maps $\xi \in [-1,1]$ to $x \in [a,b]$. Then, when ${}^{*}\mathcal{D}_x \equiv {}^{RL}_{a}\mathcal{D}_x$ in* (8.17)*, the left-sided spatial differentiation matrix ${}^{RL}\boldsymbol{D}^{\sigma}_{L}$ of Riemann-Liouville type, corresponding to the nodal FLI expansion* (8.28)*, is a three-dimensional matrix whose entries are given by*

$$\{{}^{RL}\boldsymbol{D}^{\sigma}_{L}\}_{ikm} = (\frac{2}{b-a})^{\sigma(x_i,t_k)} A_m \sum_{j=1}^{\mathcal{M}} \beta^{L}_{mj}\, F^{L,\sigma}_{j}\Big(x_i,t_k\Big), \tag{8.37}$$

where $i,m = 2,3,\cdots,\mathcal{M}$, $k = 2,3,\cdots,\mathcal{N}$, also $F^{L,\sigma}_{j}\Big(x(\xi),t\Big)$ is explicitly given as

$$F^{L,\sigma}_{j}\Big(x(\xi),t\Big) = \sum_{q=0}^{j-1} b^{\mu}_{jq}\,(1+\xi)^{q+\mu-\sigma}, \tag{8.38}$$

in which $A_m = (\frac{b-a}{2x_m-2a})^{\mu}$, and finally β^{L}_{mj} and b^{μ}_{jq} are the corresponding expansion coefficients, given a priori by (C.1) *and* (C.7).

Proof. Given in C.1. □

Remark 8.5.2. In standard collocation methods applied to constant/integer-order operators, the corresponding differentiation matrices are two-dimensional. The extra dimension appearing in the left-sided differentiation matrix ${}^{RL}\mathbf{D}^{\sigma}_{L}$ is due to the field-variable $\sigma(x,t)$, which makes the corresponding fractional differential operator vary across the computational domain. Consequently, by collocating the fractional order

on each collocation point (x_i, t_k), we must compute all the entries associated with the whole set of the spatial points indexed by " m". Therefore, it naturally renders the corresponding differentiation matrix three-dimensional. Interestingly, when $\sigma = \sigma(x)$, we reduce the dimension of ${}^{RL}\mathbf{D}_L^{\sigma}$ by one, and we obtain the entries of the two-dimensional differentiation matrix as

$$\{{}^{RL}\mathbf{D}_L^{\sigma}\}_{im} = (\frac{2}{b-a})^{\sigma(x_i)} A_m \sum_{j=1}^{\mathcal{M}} \beta_{mj}^{L}\, F_j^{L,\sigma}\Big(x_i\Big). \tag{8.39}$$

Moreover, when σ is constant, the differentiation matrix in (8.39) is further reduced to

$$\{{}^{RL}\mathbf{D}_L^{\sigma}\}_{im} = (\frac{2}{b-a})^{\sigma} A_m \sum_{j=1}^{\mathcal{M}} \beta_{mj}^{L} \frac{\Gamma(j+\sigma)}{\Gamma(j)} P_{j-1}(\,\xi_i\,), \tag{8.40}$$

previously given in [190], where $x_i = \frac{a+b}{2} + \frac{b-a}{2}\xi_i$.

The next theorem provides the corresponding left-sided differentiation matrix for the diffusion term in (8.17) when ${}^{*}\mathcal{D}_x^{1+\nu} \equiv {}_{a}^{RL}\mathcal{D}_x^{1+\nu}$.

Theorem 8.5.3. *Let $\nu = \nu(x,t) \in C\Big([a,b]\times[0,T]\Big)$ and consider the affine mapping the maps $\xi \in [-1,1]$ to $x \in [a,b]$. Then, the left-sided spatial differentiation matrix ${}^{RL}\boldsymbol{D}_L^{1+\nu}$ of Riemann-Liouville type, corresponding to the nodal FLI expansion* (8.28) *when ${}^{*}\mathcal{D}_x \equiv {}_{a}^{RL}\mathcal{D}_x$ in* (8.17)*, is a three-dimensional matrix whose entries are given by*

$$\{{}^{RL}\boldsymbol{D}_L^{1+\nu}\}_{ikm} = (\frac{2}{b-a})^{1+\nu(x_i,t_k)} A_m \sum_{j=1}^{\mathcal{M}} \beta_{mj}^{L} \mathcal{F}_j^{L,\nu}(x_i,t_k), \tag{8.41}$$

in which $A_m = (\frac{b-a}{2x_m-2a})^{\mu}$, $i,m = 2,3,\cdots,\mathcal{M}$, $k = 2,3,\cdots,\mathcal{N}$, and $\mathcal{F}_j^{L,\nu}\Big(x(\xi),t\Big)$ is

explicitly given by

$$\begin{aligned}\mathcal{F}_j^{L,\nu}\Big(x(\xi),t\Big) &= \mathbb{I}_{\{j\geq 1\}}\sum_{q=0}^{j-1}\mathbb{B}_{jq}^{\mu}\cdot(1+\xi)^{q+\mu-1-\nu(x_i,t_k)} \\ &+ \mathbb{I}_{\{j\geq 2\}}\sum_{q=0}^{j-2}B_{jq}^{\mu}\cdot(1+\xi)^{q+\mu-\nu(x_i,t_k)},\end{aligned} \tag{8.42}$$

where $\mathbb{B}_{jq}^{\mu}$ *and* B_{jq}^{μ} *are the corresponding expansion coefficients, given a priori by* (C.12) *and* (C.13).

Proof. Given in C.2. □

In analogy with Remark 8.5.2, we also appreciate the appearance of the extra dimension in the right-sided differentiation matrix ${}^{RL}\mathbf{D}_L^{1+\nu}$. Similarly, when $\nu = \nu(x)$, we reduce the dimension of ${}^{RL}\mathbf{D}_L^{1+\nu}$ by one and obtain the entries of the two-dimensional differentiation matrix as

$$\{{}^{RL}\mathbf{D}_L^{1+\nu}\}_{im} = (\frac{2}{b-a})^{1+\nu(x_i)}A_m\sum_{j=1}^{\mathcal{M}}\beta_{mj}^{L}\mathcal{F}_j^{L,\nu}(x_i). \tag{8.43}$$

Remark 8.5.4. We note that the coefficients β_{mj}^{L}, shown in (C.1), are obtained only *once* and are utilized as many times as needed to construct ${}^{RL}\mathbf{D}_L^{\sigma}$ and ${}^{RL}\mathbf{D}_L^{1+\nu}$ for any order σ, $\nu \in (0,1)$.

8.5.2 ${}^{*}\mathcal{D}_x$ of Right-Sided Riemann-Liouville Type

Following similar steps, presented in section 8.5.1, we now construct the corresponding right-sided *advection* differentiation matrix of order $\sigma(x,t)$ and the right-sided

diffusion differentiation matrix of order $1+\nu(x,t)$ when ${}^{*}\mathcal{D}_x \equiv {}^{RL}_{x}\mathcal{D}_b$ in the sequel.

Theorem 8.5.5. *Let $\sigma = \sigma(x,t) \in C\Big([a,b]\times[0,T]\Big)$ and consider the affine mapping that maps $\xi \in [-1,1]$ to $x \in [a,b]$. Then, when ${}^{*}\mathcal{D}_x \equiv {}^{RL}_{x}\mathcal{D}_b$ in* (8.17)*, the right-sided spatial differentiation matrix ${}^{RL}\boldsymbol{D}^{\sigma}_{R}$ of Riemann-Liouville type, corresponding to the nodal FLI expansion* (8.31)*, is a three-dimensional matrix whose entries are given by*

$$\{{}^{RL}\boldsymbol{D}^{\sigma}_{R}\}_{ikm} = (\frac{2}{b-a})^{\sigma(x_i,t_k)}\mathcal{A}_m \sum_{j=1}^{\mathcal{M}} \beta^{R}_{mj}\, F^{R,\sigma}_{j}\Big(x_i,t_k\Big) \tag{8.44}$$

in which $i,m = 2,3,\cdots,\mathcal{M}$, $k = 2,3,\cdots,\mathcal{N}$, also $F^{R,\sigma}_{j}\Big(x(\xi),t\Big)$ is explicitly given as

$$F^{R,\sigma}_{j}\Big(x(\xi),t\Big) = \sum_{q=0}^{j-1} c^{\mu}_{jq}\,(1-\xi)^{q+\mu-\sigma}, \tag{8.45}$$

in which $\mathcal{A}_m = 1/(\xi_{\mathcal{M}}-\xi_m)^{\mu}$, and finally β^{R}_{mj} and c^{μ}_{jq} are the corresponding expansion coefficients, given a priori by (C.14) *and* (C.19)*.*

Proof. Given in C.3. □

The next theorem provides the corresponding right-sided differentiation matrix for the diffusion term in (8.17) when ${}^{*}\mathcal{D}^{1+\nu}_{x} \equiv {}^{RL}_{x}\mathcal{D}^{1+\nu(x,t)}_{b}$.

Theorem 8.5.6. *Let $\nu = \nu(x,t) \in C\Big([a,b]\times[0,T]\Big)$ and consider the affine mapping that maps $\xi \in [-1,1]$ to $x \in [a,b]$. Then, the right-sided spatial differentiation matrix ${}^{RL}\boldsymbol{D}^{1+\nu}_{R}$ of Riemann-Liouville type, corresponding to the nodal FLI expansion* (8.31) *when ${}^{*}\mathcal{D}_x \equiv {}^{RL}_{x}\mathcal{D}_b$ in* (8.17)*, is a three-dimensional matrix whose entries are given*

by

$$\{{}^{RL}\boldsymbol{D}_R^{1+\nu}\}_{ikm} = (\frac{2}{b-a})^{1+\nu(x_i,t_k)}\mathcal{A}_m \sum_{j=1}^{\mathcal{M}} \beta_{mj}^R \mathcal{F}_j^{R,\nu}(x_i,t_k), \tag{8.46}$$

where $i, m = 2, 3, \cdots, \mathcal{M}$, $k = 2, 3, \cdots, \mathcal{N}$, *and* $\mathcal{F}_j^{R,\nu}\Big(x(\xi),t\Big)$ *is explicitly given by*

$$\begin{aligned} \mathcal{F}_j^{R,\nu}\Big(x(\xi),t\Big) &= \mathbb{I}_{\{j\geq 1\}} \sum_{q=0}^{j-1} \mathbb{C}_{jq}^{\mu} \cdot (1-\xi)^{q+\mu-1-\nu(x_i,t_k)} \\ &+ \mathbb{I}_{\{j\geq 2\}} \sum_{q=0}^{j-2} C_{jq}^{\mu} \cdot (1-\xi)^{q+\mu-\nu(x_i,t_k)}, \end{aligned} \tag{8.47}$$

in which C_{jq}^{μ} *and* $\mathbb{C}_{jq}^{\mu}$ *are the corresponding expansion coefficients, given a priori by* (C.25) *and* (C.24).

Proof. Given in C.4. □

8.5.3 ${}^{*}\mathcal{D}_x$ of Riesz Type

The following Lemma is useful in the derivation and construction of the Riesz spatial differentiation matrices.

Lemma 8.5.7. *[5] For* $\mu > 0$, $\alpha > -1$, $\beta > -1$, *and* $\forall \xi \in [-1, 1]$

$$(1+\xi)^{\beta+\mu} \frac{P_n^{\alpha-\mu,\beta+\mu}(\xi)}{P_n^{\alpha-\mu,\beta+\mu}(-1)} = \frac{\Gamma(\beta+\mu+1)}{\Gamma(\beta+1)\Gamma(\mu)P_n^{\alpha,\beta}(-1)} \int_{-1}^{\xi} \frac{(1+s)^{\beta}\ P_n^{\alpha,\beta}(s)}{(\xi-s)^{1-\mu}} ds, \tag{8.48}$$

and

$$(1-\xi)^{\alpha+\mu}\,\frac{P_n^{\alpha+\mu,\beta-\mu}(\xi)}{P_n^{\alpha+\mu,\beta-\mu}(+1)}=\frac{\Gamma(\alpha+\mu+1)}{\Gamma(\alpha+1)\Gamma(\mu)P_n^{\alpha,\beta}(+1)}\int_{\xi}^{1}\frac{(1-s)^{\alpha}\;P_n^{\alpha,\beta}(s)}{(s-\xi)^{1-\mu}}ds. \quad (8.49)$$

By the definition of the left-sided Riemann-Liouville integral ${}^{RL}_{-1}\mathcal{I}^{\mu}_{\xi}$ and evaluating the special end-values $P_n^{\alpha-\mu,\beta+\mu}(-1)$ and $P_n^{\alpha,\beta}(-1)$, we can re-write (8.48) as

$${}^{RL}_{-1}\mathcal{I}^{\mu}_{\xi}\Big\{(1+\xi)^{\beta}P_n^{\alpha,\beta}(\xi)\Big\}=\frac{\Gamma(n+\beta+1)}{\Gamma(n+\beta+\mu+1)}(1+\xi)^{\beta+\mu}\,P_n^{\alpha-\mu,\beta+\mu}(\xi).$$

Now, by taking the fractional derivative ${}^{RL}_{-1}\mathcal{D}^{\mu}_{\xi}$ on the when $\beta=-\mu$ and $\alpha=\mu$ we obtain

$${}^{RL}_{-1}\mathcal{D}^{\mu}_{\xi}\Big\{P_n(\xi)\Big\}=\frac{\Gamma(n+1)}{\Gamma(n-\mu+1)}(1+\xi)^{-\mu}P_n^{\mu,,-\mu}(\xi). \quad (8.50)$$

Similarly, by the definition of the right-sided Riemann-Liouville integral ${}^{RL}_{\xi}\mathcal{I}^{\mu}_{1}$ and evaluating the special end-values $P_n^{\alpha-\mu,\beta+\mu}(+1)$ and $P_n^{\alpha,\beta}(+1)$, we can re-write (8.49) as

$${}^{RL}_{\xi}\mathcal{I}^{\mu}_{1}\Big\{(1-\xi)^{\alpha}P_n^{\alpha,\beta}(\xi)\Big\}=\frac{\Gamma(n+\alpha+1)}{\Gamma(n+\alpha+\mu+1)}(1-\xi)^{\alpha+\mu}P_n^{\alpha+\mu,\beta-\mu}(\xi).$$

In a similar fashion, by taking the fractional derivative ${}^{RL}_{\xi}\mathcal{D}^{\mu}_{-1}$ on the both sides when $\alpha=-\mu$ and $\beta=\mu$ we obtain

$${}^{RL}_{\xi}\mathcal{D}^{\mu}_{1}\Big\{P_n(\xi)\Big\}=\frac{\Gamma(n+1)}{\Gamma(n-\mu+1)}(1-\xi)^{-\mu}P_n^{-\mu,\mu}(\xi). \quad (8.51)$$

Theorem 8.5.8. *Let $\sigma=\sigma(x,t)\in C\Big([a,b]\times[0,T]\Big)$ and consider the affine mapping that maps $\xi\in[-1,1]$ to $x\in[a,b]$. Then, when ${}^{*}\mathcal{D}_x\equiv\partial^{\sigma(x,t)}u/\partial|x|^{\sigma(x,t)}$ in* (8.17)*, the right-sided spatial differentiation matrix $\boldsymbol{D}^{\sigma}_{Riesz}$ of Riesz type, corresponding to the nodal FLI expansion* (8.33)*, is a three-dimensional matrix whose entries are given*

by

$$\{\boldsymbol{D}^{\sigma}_{Riesz}\}_{ikm} = \Big[(\frac{2}{b-a})^{\sigma(x,t)} C_{\sigma(x,t)}\Big]_{(x_i,t_k)} \sum_{j=1}^{\mathcal{M}} \widetilde{\beta}_{mj} \mathcal{Z}^{\sigma}_{j}(x_k,t_k), \tag{8.52}$$

in which $i,m = 2,3,\cdots,\mathcal{M}$, $k = 2,3,\cdots,\mathcal{N}$, $\xi = 2\frac{x-a}{b-a}$, *and* $\widetilde{\beta}_{mj}$ *are the corresponding expansion coefficients, given a priori by* (C.28). *Moreover,* $\mathcal{Z}^{\sigma}_{j}(x,t)$ *is explicitly given as*

$$\mathcal{Z}^{\sigma}_{j}(x,t) = \frac{\Gamma(j+1)}{\Gamma(j-\sigma(x_i,t_k)+1)}\Big[(1+\xi)^{-\sigma(x,t)} P^{\sigma,-\sigma}_{j}(\xi) \; + \; (1-\xi)^{-\sigma(x,t)} P^{-\sigma,\sigma}_{j}(\xi)\Big],$$

Proof. Given in C.5. □

Theorem 8.5.9. *Let* $\nu = \nu(x,t) \in C\Big([a,b]\times[0,T]\Big)$ *and consider the affine mapping that maps* $\xi \in [-1,1]$ *to* $x \in [a,b]$. *Then, when* ${}^{*}\mathcal{D}_{x} \equiv \partial^{1+\nu(x,t)}u/\partial|x|^{1+\nu(x,t)}$ *in* (8.17), *the right-sided spatial differentiation matrix* $\boldsymbol{D}^{1+\nu}_{Riesz}$ *of Riesz type, corresponding to the nodal FLI expansion* (8.33), *is a three-dimensional matrix whose entries are given by*

$$\{\boldsymbol{D}^{1+\nu(x,t)}_{Riesz}\}_{ikm} = \Big[(\frac{2}{b-a})^{1+\nu} C_{1+\nu}\Big]_{(x_i,t_k)} \sum_{j=1}^{\mathcal{M}} \widetilde{\beta}_{mj} \mathcal{W}^{\sigma}_{j}(x,t) \tag{8.53}$$

in which $i,m = 2,3,\cdots,\mathcal{M}$, $k = 2,3,\cdots,\mathcal{N}$, $\xi = 2\frac{x-a}{b-a}$, *and* $\mathcal{W}^{\sigma}_{j}(x,t)$ *is explicitly given as*

$$\mathcal{W}^{\nu}_{j} = (\frac{j+1}{2}) \sum_{q=\lceil\nu\rceil}^{j-1} \mathcal{C}_{j} \frac{(\frac{-1}{2})^{q}\Gamma(q+1)}{\Gamma(q+1-\nu(x,t))}\Big[(-1)^{j-1}(1+\xi)^{q-\nu(x,t)} - (1-\xi)^{q-\nu(x,t)}\Big].$$

Proof. Given in C.6. □

8.5.4 Temporal Differentiation Matrix ${}^{RL}\mathbf{D}_t^{\tau}$

We derive the temporal differentiation matrix ${}^{RL}\mathbf{D}_t^{\zeta}$ by taking ${}_0^{RL}\mathcal{D}_t^{\zeta(x,t)}u_N(x,t)$ and evaluating it the collocation points considering the fact that the spatial nodal bases $L_m^{\mu}(x)$, $R_m^{\mu}(x)$, and $h_m(x)$ all satisfy the Kronecker delta property at the collocation points. Hence, in the derivation of ${}^{RL}\mathbf{D}_t^{\zeta}$ any of the expansions (8.28), (8.31), or (8.33) can be used. Following similar steps in section 8.5.1, we obtain the temporal differentiation matrix corresponding to the following two cases:

Case I-A) Constant $\zeta = \tau \in (0,1)$. We map the interval $t \in [0,T]$ to the standard domain $\xi \in [-1,1]$ as usual, and use the property (11.17) to obtain

$$ {}_0^{RL}\mathcal{D}_t^{\zeta} u_N(\,x,t\,)\Big|_{(x_i,t_k)} = \sum_{n=2}^{\mathcal{N}} \{{}^{RL}\mathbf{D}_t^{\zeta}\}_{kn}\; u_N(x_i,t_n), $$

where $\{{}^{RL}\mathbf{D}_t^{\zeta}\}_{im}$ are the entries of the $(\mathcal{N}-1)\times(\mathcal{N}-1)$ *left-sided* temporal differentiation matrix ${}^{RL}\mathbf{D}_L^{\zeta}$ of Riemann-Liouville since, given by

$$ \{{}^{RL}\mathbf{D}_t^{\zeta}\}_{kn} = (\frac{2}{T})^{\zeta}\eta_n \sum_{j=1}^{\mathcal{N}} \beta_{nj}^{L} \frac{\Gamma(j+\zeta)}{\Gamma(j)} P_{j-1}(\,\xi_k\,), \tag{8.54} $$

where $\eta_n = \frac{T}{2t_n}$ and $\xi_k = \frac{2t_k}{T} - 1$.

Case I-B) The general $\zeta(x,t) \in (0,1)$. We obtain the corresponding temporal differentiation matrix of variable order $\zeta(x,t) \in (0,1)$, by evaluating ${}_0^{RL}\mathcal{D}_x^{\zeta(x,t)}u_N(x,t)$

at the collocation points (x_i, t_k) also by $L_m^{\mu}(x_i) = \delta_{im}$, we obtain

$$
\begin{aligned}
{}^{RL}_{0}\mathcal{D}_t^{\zeta(x,t)} u_N \Big|_{(x_i,t_k)} &= (\frac{2}{T})^{\zeta(x_i,t_k)} \sum_{n=2}^{\mathcal{N}} u_N(x_m, t_k)\eta_n \sum_{j=1}^{\mathcal{N}} \beta_{nj}^L \, F_j^{L,\tau}\Big(x_i, t_k\Big) \\
&= \sum_{n=2}^{\mathcal{N}} \{{}^{RL}\mathbf{D}_t^{\zeta}\}_{kni} u_N(x_i, t_n),
\end{aligned}
$$

where $\{{}^{RL}\mathbf{D}_L^{\zeta}\}_{kni}$ are the entries of the $(\mathcal{N}-1)\times(\mathcal{M}-1)\times(\mathcal{N}-1)$ *left-sided* temporal fractional differentiation matrix ${}^{RL}\mathbf{D}_t^{\zeta}$ of Riemann-Liouville sense, computed as

$$
\{{}^{RL}\mathbf{D}_t^{\zeta}\}_{ikn} = (\frac{2}{T})^{\zeta(x_i,t_k)} \eta_n \sum_{j=1}^{\mathcal{N}} \beta_{nj}^L \, F_j^{L,\tau}\Big(x_i, t_k\Big). \tag{8.55}
$$

We note that β_{nj}^L are the corresponding coefficients in the following expansion that are obtained once as

$$
\mathcal{G}_n(\xi) = \sum_{j=1}^{\mathcal{N}} \beta_{nj}^L P_{j-1}^{-\tau,\tau}(\xi), \tag{8.56}
$$

similar to what we showed in (C.1).

8.5.5 Temporal Differentiation Matrix ${}^{C}\mathbf{D}_t^{\tau}$

We recall that when the time-derivative is of Caputo type we employ the expansion (8.35).

Theorem 8.5.10. *Let $\zeta = \zeta(x,t) \in C\Big([a,b]\times[0,T]\Big)$ and consider the affine mapping that maps $\eta \in [-1,1]$ to $t \in [0,T]$. Then, when ${}^{*}\mathcal{D}_t \equiv {}^{C}_{0}\mathcal{D}_t$ in (8.17), the left-sided temporal differentiation matrix ${}^{C}\boldsymbol{D}^{\zeta}$ of Caputo type, corresponding to the nodal FLI expansion (8.35), is a three-dimensional matrix whose entries are given*

by

$$\{{}^{C}\boldsymbol{D}^{\zeta}\}_{ikm} = \Big[(\frac{2}{T})^{\zeta(x,t)}\Big]_{(x_i,t_k)} \sum_{j=1}^{\mathcal{N}} \widetilde{\beta}_{mj} \mathcal{Z}_j^{\zeta}(x_k,t_k), \tag{8.57}$$

when the solution to (8.17) *is assumed to be continuous in time, in which* $i, m = 2, 3, \cdots, \mathcal{M}$*,* $k = 1, 2, 3, \cdots, \mathcal{N}+1$*,* $\eta = \frac{2t}{T} - 1$*, and* $\widetilde{\beta}_{mj}$ *are the corresponding (temporal) expansion coefficients, given a priori similarly as in* (C.28)*. Moreover,* $\mathcal{Z}_j^{\zeta}(x,t)$ *is explicitly given as*

$$\mathcal{Z}_j^{\zeta}(x,t) = \frac{\Gamma(j+1)}{\Gamma(j-\zeta(x_i,t_k)+1)} \Big[(1+\eta)^{-\zeta(x,t)} P_j^{\zeta,-\zeta}(\eta)\Big].$$

Proof. See C.5. □

8.6 Numerical Tests

After the construction of the variable-order differentiation matrices of Riemann-Liouville and Riesz type, we now solve a number of FPDEs to investigate the performance of our schemes. We divide this section into two main parts. In the first part, we implement our variable-order collocation method in solving *linear* FPDEs such as time- and space-fractional *advection* equation, *diffusion*, and *advection-diffusion* problems. In the second part, we deal with *non-linear* FPDEs of field-variable order, namely the space-fractional nonlinear Burgers equation.

In all the numerical tests, we set collocation and interpolation points to be identical. Here, we adopt the choice of collocation points in [190], where we showed that the *fractional extrema* of ${}^{(1)}\mathcal{P}_n^{\mu}(\xi)$ and ${}^{(2)}\mathcal{P}_n^{\mu}(\xi)$, i.e., the zeros of Legendre polyno-

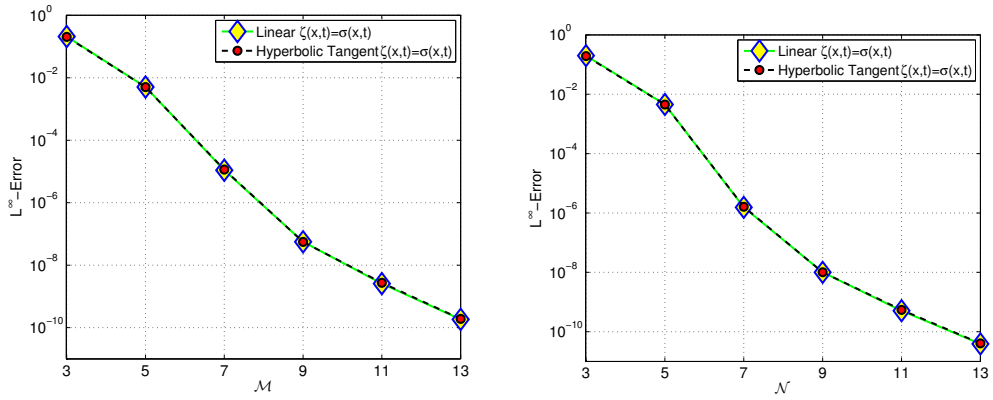

Figure 8.2: Time- and space-fractional linear advection problem with Riemann-Liouville spatial operators: (left) spatial p-refinement, and (right) temporal p-refinement. The exact solution is the fractional function $u^{ext}(x,t) = (1+x)^{6+9/17}\, t^{6+2/3}$, where $(x,t) \in [-1,1] \times [0,2]$; moreover, the temporal and spatial fractional orders are taken as the following field-variable functions, denoted as *linear* $\zeta(x,t) = \sigma(x,t) = (\frac{5+4x}{10})\,(\frac{1+4t}{10})$, and hyperbolic tangent $\zeta(x,t) = \sigma(x,t) = [1+\tanh(x)][1+\tanh(t-1)]/4$.

mials, are the best collocation points leading to the fastest rate of convergence. To demonstrate the accuracy of our methods, we adopt the L^∞ norm, normalized by the essential norm of the exact solution in each case.

8.6.1 Linear FPDEs with ${}^{*}\mathcal{D}_x \equiv {}^{RL}\mathcal{D}_x$

We first consider two examples of linear FPDEs, namely advection and advection-diffusion problems, in which the spatial fractional derivatives are all either of left- or right-sided Riemann-Liouville type.

Example 8.6.1. Fractional Advection Equation:

$$ {}^{RL}_{0}\mathcal{D}_t^{\zeta(x,t)} u + \theta \; {}^{RL}\mathcal{D}_x^{\sigma(x,t)} u \;=\; f(x,t), \quad (x,t) \in [-1,1] \times [0,2], \tag{8.58} $$

$$ u(x,0) \;=\; 0. \tag{8.59} $$

where we replace $g(u)$ in (8.17) with the constant advection velocity θ. Here,

${}^{RL}\mathcal{D}_x^{\sigma} \equiv {}^{RL}_{-1}\mathcal{D}_x^{\sigma}$ when $\theta > 0$, hence we set the boundary condition $u(-1,t) = 0$, and ${}^{RL}\mathcal{D}_x^{\sigma} \equiv {}^{RL}_{x}\mathcal{D}_1^{\sigma}$ when $\theta < 0$, and therefore we set $u(1,t) = 0$. Moreover in (8.58), $\zeta, \sigma : \mathbb{R}^2 \to \mathbb{R}$ are *continuous* functions. In fact, we deduce the continuity requirement in ζ and σ from the definition of the corresponding temporal and spatial differentiation matrices in (8.55) and (C.8), implying that each entry is assumed to be continuous from above and below. Let $\theta = 1$ and seek the solution of the form (8.28), where we set the interpolation parameters τ and μ to be the *mean-value* of $\zeta(x,t)$ and $\sigma(x,t)$ given by

$$\tau = \frac{1}{|\Omega|}\int_{\Omega} \zeta d\Omega, \tag{8.60}$$

and

$$\mu = \frac{1}{|\Omega|}\int_{\Omega} \sigma d\Omega, \tag{8.61}$$

receptively. This is analogous to the algebraic mean-value interpolation parameters in multi-term FODEs/FPDEs, studied in [190]. We have investigated that such mean-values also lead to efficient approximation of fractional operators of variable-orders. Next, by substituting $u_N(x,t)$ in (8.58), we require the residual

$$R_N(x,t) = {}^{RL}_{0}\mathcal{D}_t^{\zeta(x,t)} u_N + {}^{RL}_{-1}\mathcal{D}_x^{\sigma(x,t)} u_N - f(x,t), \tag{8.62}$$

to vanish at the collocation points (x_i, t_k), which leads to the following linear system:

$${}^{RL}\mathcal{S}_A \vec{\mathbf{u}} = \vec{\mathbf{b}}, \tag{8.63}$$

where ${}^{RL}\mathcal{S}_A$ is a $(\mathcal{M}-1)(\mathcal{N}-1) \times (\mathcal{M}-1)(\mathcal{N}-1)$ matrix, whose entries are given by

$$\begin{aligned} {}^{RL}\mathcal{S}_A\{I_{ik}\,,\, J_{mn}\} \;&=\; \{{}^{RL}\mathbf{D}_t^{\zeta}\}_{ikn}\,\delta_{im} \;+\; \{{}^{RL}\mathbf{D}_L^{\sigma}\}_{ikm}\delta_{kn}, \end{aligned} \tag{8.64}$$

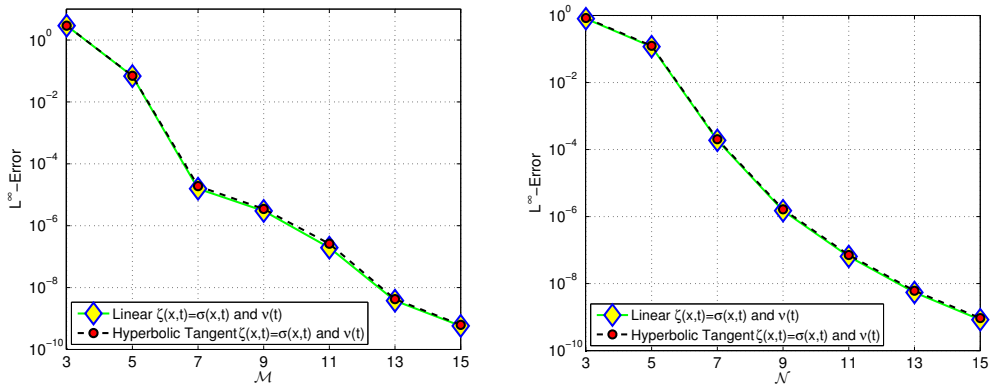

Figure 8.3: Time- and space-fractional linear advection-diffusion equation with Riemann-Liouville spatial operators: (left) spatial p-refinement, and (right) temporal p-refinement. The exact solution is given by the fractional $u^{ext}(x,t) = (1+x)^{6+9/17}\, t^{6+2/3}$, where $(x,t) \in [-1,1]\times[0,2]$; moreover, the temporal and spatial fractional orders are respectively taken as the following field-variable functions, denoted as *linear* $\zeta(x,t) = \sigma(x,t) = (\frac{5+4x}{10})\,(\frac{1+4t}{10})$ and $1+\nu(t) = 1+\frac{1+4t}{10}$, also hyperbolic tangent $\zeta(x,t) = \sigma(x,t) = [1+\tanh(x)][1+\tanh(t-1)]/4$ and $1+\nu(t) = [3+\tanh(t-1)]/2$.

where $I_{ik} = (i-2)(\mathcal{N}-1)+k-1$, $J_{mn} = (m-2)(\mathcal{N}-1)+n-1$, also $\{{}^{RL}\mathbf{D}_t^{\zeta}\}_{ikn}$ and $\{{}^{RL}\mathbf{D}_L^{\sigma}\}_{ikm}$ are given in (8.55) and (C.8), respectively. Moreover, $\vec{\mathbf{b}}$ represents the load vector whose components are obtained as

$$\vec{\mathbf{b}}\{I_{ik}\} = f(x_i, t_k), \tag{8.65}$$

and finally, the vector of unknown coefficients is defined as

$$\vec{\mathbf{u}}\{J_{mn}\} = u(x_m, t_n), \tag{8.66}$$

where $i,m = 2,3,\cdots,\mathcal{M}$ and $k,n = 2,3,\cdots,\mathcal{N}$.

In Fig. 8.2, we plot the exponential-like decay of L^{∞}-norm of the error in corresponding spatial and temporal p-refinement. We set the exact solution to be the following fractional function $u^{ext}(x,t) = (1+x)^{6+9/17}\, t^{6+2/3}$. Moreover, the temporal and spatial fractional orders are taken as the following field-variable functions, denoted as *linear* $\zeta(x,t) = \sigma(x,t) = (\frac{5+4x}{10})\,(\frac{1+4t}{10})$, and *hyperbolic tan-*

gent $\zeta(x,t) = \sigma(x,t) = [1+\tanh(x)][1+\tanh(t-1)]/4$. We obtain identical results when we choose $\theta = -1$, i.e., the wind blows from right to left, and therefore right-sided Riemann-Liouville fractional derivatives are employed, considering $u^{ext}(x,t) = (1-x)^{6+9/17}\, t^{6+2/3}$.

Example 8.6.2. Fractional Advection-Diffusion Equation:

$$
\begin{aligned}
{}^{RL}_{0}\mathcal{D}_t^{\zeta(x,t)} u + \theta\ {}^{RL}\mathcal{D}_x^{\sigma(x,t)} u &= {}^{RL}\mathcal{D}_x^{1+\nu(t)} u + f(x,t), \quad (x,t) \in [-1,1]\times[0,2], && (8.67)\\
u(\pm 1, t) &= 0 && (8.68)\\
u(x,0) &= 0. && (8.69)
\end{aligned}
$$

Here, ${}^{RL}\mathcal{D}_x^{\sigma} \equiv {}^{RL}_{-1}\mathcal{D}_x^{\sigma}$ and ${}^{RL}\mathcal{D}_x^{1+\nu} u \equiv {}^{RL}_{-1}\mathcal{D}_x^{1+\nu} u$ if $\theta > 0$, i.e., when the wind blows from left to right. Alternatively, we set ${}^{RL}\mathcal{D}_x^{\sigma} \equiv {}^{RL}_{x}\mathcal{D}_1^{\sigma}$ and ${}^{RL}\mathcal{D}_x^{1+\nu} u \equiv {}^{RL}_{x}\mathcal{D}_1^{1+\nu} u$ when $\theta < 0$. We note that in (8.67), $\zeta : \mathbb{R}^2 \to \mathbb{R}$ and $\sigma : \mathbb{R}^2 \to \mathbb{R}$ are continuous functions. In addition, $\nu : \mathbb{R} \to \mathbb{R}$ suffices to be *continuous* in order for the entries of the differentiation matrices to be well-defined. We first set $\theta = 1$ and seek the solution of the form (8.31), where we set the interpolation parameterμ to be the *mean-value* of $\sigma(x,t)$ given in (8.61). In a similar fashion, we can obtain the total average temporal interpolation parameter τ by including both $\zeta(x,t)$ and $\nu(t)$ into the averaging.

Having set the interpolation parameters, we substitute $u_N(x,t)$ in (8.67), and obtain the corresponding linear system by requiring the residual

$$
R_N(x,t) = {}^{RL}_{0}\mathcal{D}_t^{\zeta(x,t)} u_N + {}^{RL}_{-1}\mathcal{D}_x^{\sigma(x,t)} u_N + {}^{RL}_{-1}\mathcal{D}_x^{1+\nu(t)} u_N - f(x,t), \tag{8.70}
$$

to vanish at (x_i, t_k). It then leads to

$$ {}^{RL}\mathcal{S}_{AD}\vec{\mathbf{u}} = \vec{\mathbf{b}}, \tag{8.71} $$

where ${}^{RL}\mathcal{S}_{AD}$ is a $(\mathcal{M}-2)(\mathcal{N}-1)\times(\mathcal{M}-2)(\mathcal{N}-1)$ matrix, whose entries are given by

$$ {}^{RL}\mathcal{S}_{AD}\{I_{ik}\,,\,J_{mn}\} = \{{}^{RL}\mathbf{D}_t^{\zeta}\}_{ikn}\,\delta_{im} + \Big(\{{}^{RL}\mathbf{D}_L^{\sigma}\}_{ikm} - \{{}^{RL}\mathbf{D}_L^{1+\nu}\}_{ikm}\Big)\delta_{kn}, \tag{8.72} $$

in which $I_{ik} = (i-2)(\mathcal{N}-1)+k-1$, $J_{mn} = (m-2)(\mathcal{N}-1)+n-1$, also $\{{}^{RL}\mathbf{D}_L^{1+\nu}\}_{ikm}$ is given in (C.10), where $i, m = 2, 3, \cdots, \mathcal{M}-1$ and $k, n = 2, 3, \cdots, \mathcal{N}$.

In order to examine the temporal and spatial accuracy of our schemes for this model problem, we plot the L^{∞}-error versus expansion order in each case in Fig. 8.3. We set the exact solution again as $u^{ext}(x,t) = (1+x)^{6+9/17}\,t^{6+2/3}$, where the temporal and spatial fractional orders are taken as the field-variable functions, denoted as linear and hyperbolic tangent. Once again, we observe the exponential-like decays of error. We found identical convergence results in the case $\theta = -1$, where the corresponding spatial derivatives are of right-sided Riemann-Liouville type and $u^{ext}(x,t) = (1-x)^{6+9/17}\,t^{6+2/3}$.

8.6.2 Linear FPDEs with Riesz Derivatives

We consider two linear FPDEs with Riesz space-fractional derivatives of field-variable orders, namely as space- and time- fractional diffusion and advection-diffusion problems.

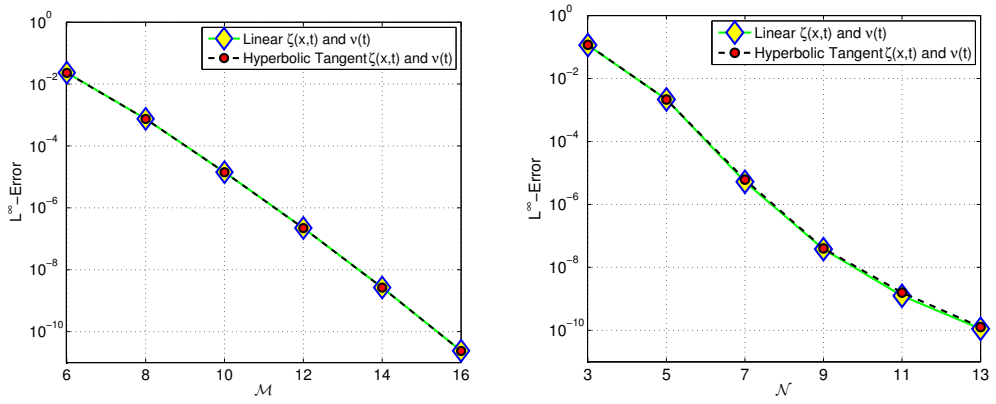

Figure 8.4: Time- and space-fractional linear diffusion equation with Riesz spatial operators: (left) spatial p-refinement, and (right) temporal p-refinement. The exact solution is given by the fractional $u^{ext}(x,t) = \sin(\pi x)\, t^{6+2/3}$, where $(x,t) \in [-1,1] \times [0,2]$; moreover, the temporal and spatial fractional orders are respectively taken as the following field-variable functions, denoted as *linear* $\zeta(x,t) = (\frac{5+4x}{10})\,(\frac{1+4t}{10})$ and $1+\nu(t) = 1+\frac{1+4t}{10}$, also hyperbolic tangent $\zeta(x,t) = [1+\tanh(x)][1+\tanh(t-1)]/4$ and $1+\nu(t) = [3+\tanh(t-1)]/2$.

Example 8.6.3. Fractional Diffusion Equation:

$$
\begin{aligned}
{}^{RL}_{0}\mathcal{D}_{t}^{\zeta(x,t)} u &= \frac{\partial^{1+\nu(t)}}{\partial |x|^{1+\nu(t)}}\, u + f(x,t), \quad (x,t) \in [-1,1] \times [0,T], && (8.73)\\
u(\pm 1, t) &= 0, && (8.74)\\
u(x,0) &= 0. && (8.75)
\end{aligned}
$$

Here, we examine the same linear and hyperbolic tangent $\zeta(x,t)$ and $\nu(t)$ as in previous section. Hence, by setting $\tau = \mu = 1/2$ as the average values for the aforementioned field-variable order, we seek the solution to (8.73) to be of the form (8.33). Next, we substitute $u_N(x,t)$ in (8.4), and require again the corresponding residual to vanish at (x_i, t_k) to construct

$$
{}^{Riesz}\mathcal{S}_D \vec{\mathbf{u}} = \vec{\mathbf{b}}, \tag{8.76}
$$

where ${}^{Riesz}\mathcal{S}_D$ is a $(\mathcal{M}-1)(\mathcal{N}-1) \times (\mathcal{M}-1)(\mathcal{N}-1)$ matrix, whose entries are given

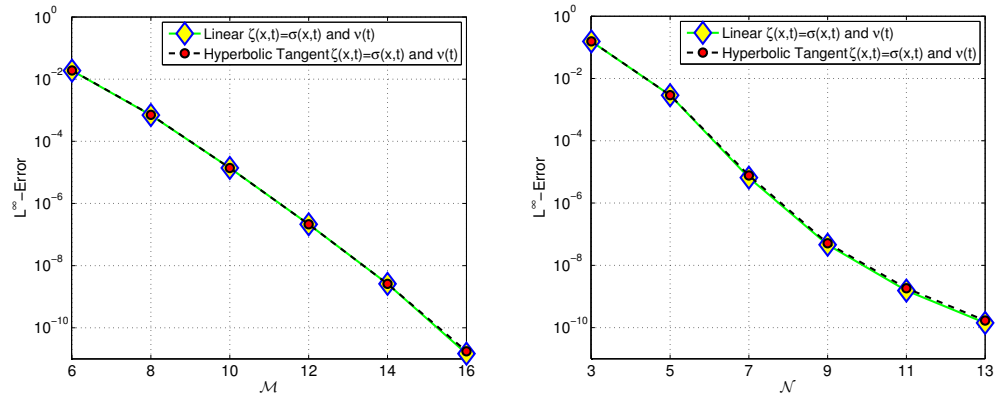

Figure 8.5: Time- and space-fractional linear advection-diffusion equation with Riesz spatial operators: (left) spatial p-refinement, and (right) temporal p-refinement. The exact solution is given by the fractional $u^{ext}(x,t) = \sin(\pi x)\, t^{6+2/3}$, where $(x,t) \in [-1,1] \times [0,2]$; moreover, the temporal and spatial fractional orders are respectively taken as the following field-variable functions, denoted as linear $\zeta(x,t) = \sigma(x,t) = (\frac{5+4x}{10})\,(\frac{1+4t}{10})$ and $1+\nu(t) = 1+\frac{1+4t}{10}$, also hyperbolic tangent $\zeta(x,t) = \sigma(x,t) = [1+\tanh(x)][1+\tanh(t-1)]/4$ and $1+\nu(t) = [3+\tanh(t-1)]/2$.

by

$$
{}^{Riesz}\mathcal{S}_D\{I_{ik}\,,\, J_{mn}\} \;=\; \{{}^{RL}\mathbf{D}_t^{\zeta}\}_{ikn}\,\delta_{im} \;-\; \{\mathbf{D}^{1+\nu}_{Riesz}\}_{ikm}\delta_{kn}, \tag{8.77}
$$

where $\{\mathbf{D}^{1+\nu}_{Riesz}\}_{ikm}$ is given in (C.35), in which $i,m = 2,3,\cdots,\mathcal{M}$ and $k,n = 2,3,\cdots,\mathcal{N}$. We note that in the nodal expansion (8.33), we consider $\mathcal{M}+1$, rather than $\mathcal{M}$ in the FLI (8.33), collocation points in the spatial dimension.

In a similar fashion, we plot the corresponding spatial and temporal p-refinement in Fig. 8.4, where we consider the exact solution this time to be $u^{ext}(x,t) = \sin(\pi x)\, t^{6+2/3}$, where we observe the exponential-like decay of the error versus the expansion order in each case.

Example 8.6.4. Fractional Advection-Diffusion Equation:

$$
\begin{aligned}
{}_{0}^{RL}\mathcal{D}_{t}^{\zeta(x,t)}u + \frac{\partial^{\sigma(x,t)}}{\partial|x|^{\sigma(x,t)}}\,u &= \frac{\partial^{1+\nu(t)}}{\partial|x|^{1+\nu(t)}}\,u + f(x,t), \quad (x,t)\in[-1,1]\times[0,2], && (8.78)\\
u(\pm 1,t) &= 0, && (8.79)\\
u(x,0) &= 0. && (8.80)
\end{aligned}
$$

We seek the solution to (8.78) to be of the form (8.33) and substitute it in (8.78). Then, we require the corresponding residual to vanish at (x_i, t_k) to obtain

$$
{}^{Riesz}\mathcal{S}_{AD}\vec{\mathbf{u}} = \vec{\mathbf{b}}, \tag{8.81}
$$

where the entries of ${}^{Riesz}\mathcal{S}_{AD}$ are given by

$$
{}^{Riesz}\mathcal{S}_{AD}\{I_{ik}\,,\,J_{mn}\} \;=\; \{{}^{RL}\mathbf{D}_{t}^{\zeta}\}_{ikn}\,\delta_{im} \;+\; \Big(\{\mathbf{D}_{Riesz}^{\sigma}\}_{ikm} \;-\; \{\mathbf{D}_{Riesz}^{1+\nu}\}_{ikm}\Big)\delta_{kn}, \tag{8.82}
$$

where $\{\mathbf{D}_{Riesz}^{\sigma}\}_{ikm}$ is given in (C.30), in which $i, m = 2, 3, \cdots, \mathcal{M}$ and $k, n = 2, 3, \cdots, \mathcal{N}$. Now, given the linear and hyperbolic tangent $\zeta(x,t)$ and $\nu(t)$ as in previous case, we set $\tau = \mu = 1/2$ as the average values for the aforementioned field-variable order.

In Fig. 8.5, we present the exponential-like decay of L^{∞}-error in the corresponding spatial and temporal p-refinement. The exact solution is again given by the fractional in-time function $u^{ext}(x,t) = \sin(\pi x)\, t^{6+2/3}$. As before, the temporal and spatial fractional orders are respectively taken as the following field-variable functions, denoted as linear $\zeta(x,t) = \sigma(x,t) = (\frac{5+4x}{10})\,(\frac{1+4t}{10})$ and $1+\nu(t) = 1+\frac{1+4t}{10}$,

also hyperbolic tangent $\zeta(x,t) = \sigma(x,t) = [1+\tanh(x)][1+\tanh(t-1)]/4$ and $1+\nu(t) = [3+\tanh(t-1)]/2$.

8.6.3 A Penalty Method for FPDEs

We consider the following variable-order in time and space diffusion equation subject to the initial condition $u(x,0) = g(x)$ and in absence of the any external forcing term.

Example 8.6.5.

$$
\begin{aligned}
{}_0^C\mathcal{D}_t^{\zeta(x,t)} u &= \frac{\partial^{1+\nu(x,t)}}{\partial |x|^{1+\nu(x,t)}}\, u, \quad \forall (x,t) \in [-1,1]\times[0,T], && (8.83)\\
u(\pm 1, t) &= 0, && (8.84)\\
u(x,0) &= g(x), && (8.85)
\end{aligned}
$$

In this example, $u(x,t)$ is assumed to be *continuous*, and we employ the time-derivative in (8.83) to be of Caputo type and the the spatial derivative of Riesz type. To enforce the inhomogeneous initial condition $u(x,0) = g(x)$, we present the following *penalty method* as follows: find $u_N(x,t) \approx u(x,t)$ such that

$$
\begin{aligned}
{}_0^C\mathcal{D}_t^{\zeta(x,t)} u_N &= \frac{\partial^{1+\nu(x,t)}}{\partial |x|^{1+\nu(x,t)}}\, u_N - \Xi Q^-(t)\Big[u_N(x,0) - g(x)\Big], && (8.86)\\
u(\pm 1, t) &= 0, && (8.87)
\end{aligned}
$$

where $Q^-(0) = 1$ and it vanishes at the rest of temporal collocation points $t \in (0,T]$. Next, we seek the solution u_N of the form

$$
u_N(x,t) = \sum_{m=2}^{\mathcal{M}} \sum_{n=1}^{\mathcal{N}+1} u_N(x_m,t_n)\, h_m(x)\, h_n(t), \tag{8.88}
$$

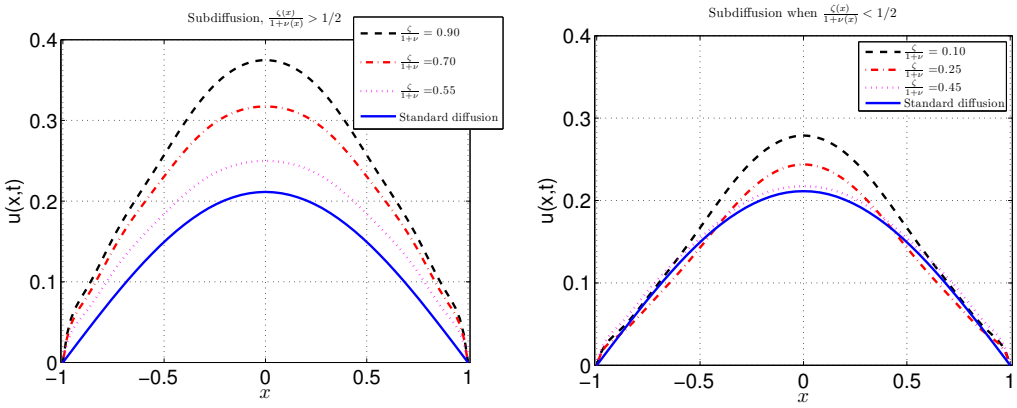

Figure 8.6: Variable-order diffusion problem: the initial condition is $u(x,0) = (1-x^2)^4$ and the solutions are obtained at $t = \frac{1}{2}$, where the space-fractional order is $(1+\nu(x)) \in (1,2)$ and the time-fractional order is $\zeta(x) \in (0,1)$, defined as spatial functions, where the ratio $\zeta(x)/(1+\nu(x))$ is greater than $1/2$ (left), and is smaller than $1/2$ (right). In these test-cases, the fractional orders $\zeta(x)$ and $\nu(x)$ are given as constant when $x \in [-1/2, 1/2]$ and they vary linearly towards the boundaries, such that they keep the ratio invariant.

where $h_n(t)$ are the standard Legendre polynomials defined in $[0,T]$. This scheme is consistent since as $u_N \to u$ the penalty term vanishes asymptotically. Moreover, the global (spectral) treatment of the fractional time-derivative results in the penalty method in (8.86) to be *unconditionally stable* when $\Xi > 0$, confirmed by our extensive numerical experiments. In fact, the bigger the penalty coefficient Ξ, the stronger enforcement of the initial condition is achieved. Hence, we set $\Xi = 10^{15}$, which enforces the initial condition up to the machine precision. The dimension of the problem then becomes $(\mathcal{M}-1) \times (\mathcal{N}+1)$ since $u_N(\pm 1, t_n) = 0$.

By substituting (8.88) in (8.83) and require the residual to vanish at the collocation points we obtain the following linear system

$$^{CR}\mathcal{S}_D \vec{\mathbf{u}} = \vec{\mathbf{b}}, \tag{8.89}$$

in which

$$
{}^{CR}\mathcal{S}_D\{I_{ik}\,,\,J_{mn}\} \;=\; \{{}^{C}\mathbf{D}_t^{\zeta}\}_{ikn}\;\delta_{im} \;-\; \{\mathbf{D}_{Riesz}^{1+\nu}\}_{ikm}\;\delta_{kn} + \Xi\delta_{mn}\delta_{1k}, \tag{8.90}
$$

and

$$
\vec{\mathbf{b}}\{I_{ik}\} = -\Xi g(x_i)\delta_{1k}, \tag{8.91}
$$

where $\{{}^{C}\mathbf{D}_t^{\zeta}\}_{ikn}$ is given in (8.57), in which $i, m = 2, 3, \cdots, \mathcal{M}$ and $k, n = 1, 2, \cdots, \mathcal{N}+1$. Here, the prescript CR recalls the Caputo and Riesz derivatives employed in the temporal and spatial dimensions, respectively.

In Fig. 8.6, we solve (8.86) subject to the initial condition is $u(x, 0) = (1 - x^2)^4$ and we plot the results at $t = \frac{1}{2}$, where the space-fractional order is $(1+\nu(x)) \in (1, 2)$ and the time-fractional order is $\zeta(x) \in (0, 1)$, defined as spatial functions, where the ratio $\zeta(x)/(1 + \nu(x))$ is greater than $1/2$ (left), and is smaller than $1/2$ (right). Here, we keep the fractional orders $\zeta(x)$ and $\nu(x)$ constant when $x \in [-1/2, 1/2]$ and allow them to decay linearly towards the boundaries, such that they keep the ratio invariant. The left plot reveals the sub-diffusion decay of the initial solution as expected. However, the right plot exhibits some *local super-diffusive* effects near the boundaries unexpectedly, which translates into faster decay compared to the standard diffusion. It is in contrast to the sub-diffusive nature of the problem when $\zeta \in (0, 1)$. Such a local effect can be associated with the way we define $\zeta(x)$ and $\nu(x)$, which is only x-dependent when $x \in [-1, -1/2]$ and $x \in [1/2, 1]$ and is constant in the middle domain. The polynomial order in time i.e., $\mathcal{N}$ and in space $\mathcal{M}$ are set to 18 is all simulations.

8.6.4 Nonlinear FPDEs

Here, we consider the nonlinear inviscid and viscous Burgers equation with field-variable orders in space.

Example 8.6.6. Inviscid and Viscous Burgers' Equation:

$$\frac{\partial u}{\partial t} + u\, {}^{*}\mathcal{D}_{x}^{\sigma(x,t)} u = K\ {}^{*}\mathcal{D}_{x}^{1+\nu(x,t)} u + f(u;x,t), \tag{8.92}$$

$$u(\pm 1, t) = 0, \tag{8.93}$$

$$u(x,0) = 0, \tag{8.94}$$

Depending on the type of the fractional derivatives ${}^{*}\mathcal{D}_{x}$, either of left-sided Riemann-Liouville or Riesz type, we seek the solution to (8.92) to be of the form

$$u_N(x,t_k) = \sum_{m=2}^{\mathcal{M}-1} u_N(x_m,t_k)\, L_m^{\mu}(x), \tag{8.95}$$

when ${}^{*}\mathcal{D}_{x} \equiv {}^{RL}\mathcal{D}_{x}$, given the homogeneous boundary conditions. Alternatively, we seek the solution to (8.92) to be of the form

$$u_N(x,t_k) = \sum_{m=2}^{\mathcal{M}} u_N(x_m,t_k)\, h_m(x), \tag{8.96}$$

when ${}^{*}\mathcal{D}_{x}$ is of Riesz type. In this case, we employ a third-order Adams-Bashforth scheme to carry out the time-integration of (8.92), where we partition the time interval $[0,T]$ into equidistant points such that $\Delta t = T/N_g$, in which N_g denotes the number of time-grid-points. Denoting by $\vec{u}_N^{\,j}$ the vector of solution at time $t_j = j\cdot\Delta t$,

we obtain the following fully discrete form

$$\frac{\vec{u}_N^{k+1} - \vec{u}_N^{k}}{\Delta t} = \sum_{q=1}^{\mathcal{J}} \alpha_q \Big(\Big[- diag(\vec{u}_N^{k+1-q}) \cdot \mathbf{D}^{\sigma} + K \ \mathbf{D}^{1+\nu} \Big] \cdot \vec{u}_N^{k+1-q} + \vec{f}^{k+1-q} \Big), \quad (8.97)$$

where $\vec{f}^{k+1-q} = f(\vec{x}, t_{k+1-q})$, $\mathcal{J}$ represents the order of the method and α_q are the coefficients of the $\mathcal{J}$-th order Adams-Bashforth method.

Remark 8.6.7. The differentiation matrices $\mathbf{D}^{\sigma}$ and $\mathbf{D}^{1+\nu}$ are now two-dimensional matrices. However, we note that the entries of these matrices must be updated in each iteration due to the temporal variability in the fractional orders $\sigma(x,t)$ and $\nu(x,t)$. To this end, we use (8.37) and (8.41) when ${}^{*}\mathcal{D}_x \equiv {}^{RL}\mathcal{D}_x$, where we substitute t_k by $(k+1-q)\Delta t$. In addition, when ${}^{*}\mathcal{D}_x$ is of Riesz type, we construct the two-dimensional matrices $\mathbf{D}^{\sigma}$ and $\mathbf{D}^{1+\nu}$ using (8.52) and (8.53) similarly by substituting t_k by $(k+1-q)\Delta t$ in each iteration.

In Table 8.1, we demonstrate the exponential decay of L^{∞}-norm error of the numerical solution to (8.92) with $\mathcal{M}$, where left-sided Riemann-Liouville and Riesz fractional derivatives are employed. Here we examine field-variable fractional orders $\sigma(x,t) = \nu(x,t) = (\frac{5+4x}{10})\,(\frac{1+4t}{10})$. When Riemann-Liouville derivatives are utilized, we set the exact solution to $u^{ext}(x,t) = t^3\,(1+x)^{6+2/3}$ and $\Delta t = 1/200$, and in the case of the Riesz fractional derivatives we set the exact solution $u^{ext}(x,t) = t^3\,\sin(\pi x)$ while $\Delta t = 1/600$. For both cases, the simulation time $T = 1$ and we employ a third-order Adams-Bashforth time-integration scheme.

Table 8.1: L^{∞}-norm error of the numerical solution to (8.92) with $\mathcal{M}$, corresponding to the fractional orders $\sigma(x,t) = \nu(x,t) = (\frac{5+4x}{10})\,(\frac{1+4t}{10})$, hence, we set $\mu = 1/2$, the mean-value. The top table corresponds to the case where left-sided Riemann-Liouville fractional derivatives are employed. In this case, the exact solution is $u^{ext}(x,t) = t^3\,(1+x)^{6+2/3}$, $x \in [-1,1]$ and we set $\Delta t = 1/200$. The bottom table corresponds to the case where Riesz fractional derivatives are used and the exact solution is $u^{ext}(x,t) = t^3 \sin(\pi x)$, $x \in [-1,1]$ and we set $\Delta t = 1/600$. In both cases, the simulation time $T = 1$, where in the third-order Adams-Bashforth time-integration scheme.

Left-Sided Riemann-Liouville ${}^{*}\mathcal{D}_x \equiv {}^{RL}\mathcal{D}_x$

$\mathcal{M}$	Inviscid Burgres ($K=0$)	Viscous Burgres ($K=1$)
5	1.88×10^{-1}	2.73×10^{-1}
7	8.12×10^{-4}	8.82×10^{-3}
9	1.44×10^{-5}	1.38×10^{-5}

Riesz Fractional Derivative ${}^{*}\mathcal{D}_x \equiv \frac{\partial}{\partial|x|}$

$\mathcal{M}$	Inviscid Burgres ($K=0$)	Viscous Burgres ($K=1$)
5	3.40×10^{-2}	1.42×10^{-1}
7	3.93×10^{-3}	9.68×10^{-3}
9	3.65×10^{-4}	6.32×10^{-4}

Chapter Nine

A Unified Petrov-Galerkin Spectral Method for FPDEs

Existing numerical methods for fractional PDEs suffer from low accuracy and inefficiency in dealing with three-dimensional problems or with long-time integrations. We develop a unified and spectrally accurate Petrov-Galerkin (PG) spectral method for a weak formulation of the general linear Fractional Partial Differential Equations (FPDEs) of the form ${}_0\mathcal{D}_t^{2\tau}u + \sum_{j=1}^{d} c_j[\ {}_{a_j}\mathcal{D}_{x_j}^{2\mu_j}u\ ] + \gamma\ u = f$, where 2τ, $\mu_j \in (0,1)$, in a $(1+d)$-dimensional *space-time* domain subject to Dirichlet initial and boundary conditions. We perform the stability analysis (in 1-D) and the corresponding convergence study of the scheme (in multi-D). The unified PG spectral method applies to the entire family of linear *hyperbolic*-, *parabolic*- and *elliptic*-like equations. We develop the PG method based on a new spectral theory for fractional Sturm-Liouville problems (FSLPs), recently introduced in [187]. Specifically, we employ the eigenfunctions of the FSLP of *first* kind (FSLP-I), called *Jacobi poly-fractonomial*s, as temporal/spatial bases. Next, we construct a different space for test functions from poly-fractonomial eigenfunctions of the FSLP of *second* kind (FSLP-II). Besides the high-order spatial accuracy of the PG method, we demonstrate its efficiency and spectral accuracy in time-integration schemes for solving time-dependent FPDEs as well, rather than employing algebraically accurate traditional methods, especially when $2\tau = 1$. Finally, we formulate a general fast linear solver based on the eigenpairs of the corresponding temporal and spatial mass matrices with respect to the stiffness matrices, which reduces the computational cost drastically. We demonstrate that this framework can reduce to *hyperbolic* FPDEs such as time- and space-fractional advection (TSFA), *parabolic* FPDEs such as time- and space-fractional diffusion (TSFD) model, and *elliptic* FPDEs such as fractional Helmholtz/Poisson equations with the same ease and cost. Several numerical tests confirm the efficiency and spectral convergence of the unified PG spectral method for the aforementioned families of FPDEs. Moreover, we demonstrate the computational efficiency of the new approach in higher-dimensions e.g., (1+3), (1+5) and (1+9)-dimensional prob-

lems.

9.1 Background

Existing numerical schemes for FPDEs suffer mainly from low accuracy and computational inefficiency in dealing with three-dimensional problems or with long-time integrations. Recently, a variety of numerical methods, originally developed for integer-order PDEs (see e.g., [64, 68, 195, 76]), have been extended to FPDEs. Such an extension is neither trivial nor straightforward. For instance, there is a lot of work done in developing Finite-Difference Methods (FDM) for FPDEs. Lubich [113, 114] introduced the idea of discretized fractional calculus and later Sanz-Serna [154] presented a first-order FDM algorithm for partial integro-differential equations. Since then, many works have aimed at improving the convergence rates of FDM schemes e.g., in time to $(\Delta t)^{2-\alpha}$ or $(\Delta t)^{3+\alpha}$, $\alpha \in (0,1)$ (see e.g.[104, 166, 111, 30]). The implementation of such FDM approaches is relatively easy. However, the bottleneck in the FDM approach is that the convergence is *algebraic* and the accuracy is limited. Moreover, we observe that the heavy cost and memory storage in computing the long-range history in two- and three-dimensional problems makes FDM schemes computationally inefficient. In fact, FDM is essentially a *local* approach which has been employed to approximate *non-local* fractional derivatives. This fact would suggest that *global* schemes, such as spectral methods (SM), are more consistent/adapted to the nature of FPDEs.

Sugimoto [163] employed Fourier SM in fractional Burgers' equation, and later Blank [25] adopted a spline-based collocation method for a class of FODEs. This approach was later employed by Rawashdeh [147] for solving fractional integro-

differential equations. Li and Xu [108, 109] developed a space-time spectral method for a time-fractional diffusion equation with spectral convergence, which was based on the early work of Fix and Roop [60]. Later on, Khader [86] proposed a Chebyshev collocation method for a space-fractional diffusion equation; also Piret and Hanert developed a radial basis function method for fractional diffusion equations [140]. Moreover, a Chebyshev spectral method [54], a Legendre spectral method [23], and an adaptive pseudospectral method [119] were proposed for solving fractional boundary value problems. In addition, generalized Laguerre spectral algorithms and Legendre spectral Galerkin method were developed by Baleanu et al. [13] and by Bhrawy and Alghamdi [22] for fractional initial value problems, respectively. The main challenge in these spectral methods is that the corresponding stiffness and mass matrices are *non-symmetric*, *dense* and they gradually become *ill-conditioned* when the fractional order tends to small values. Hence, carrying out long-time and/or adaptive integration using such SM schemes becomes intractable. To this end, Xu and Hesthaven [180] developed a stable multi-domain spectral penalty method for fractional partial differential equations. In all the aforementioned studies, the standard integer-ordered (polynomial) basis functions have been utilized.

Recently, Zayernouri and Karniadakis [189, 184] developed spectrally accurate Petrov-Galerkin spectral and spectral element methods for non-delay and delay fractional differential equations, where they employed a new family of fractional bases, called *Jacobi poly-fractonomials*. They introduced these poly-fractonomials as the eigenfunctions of fractional Sturm-Liouville problems in [187], explicitly given as

$$ {}^{(1)}\mathcal{P}_n^{\alpha,\beta,\mu}(\xi) = (1+\xi)^{-\beta+\mu-1} P_{n-1}^{\alpha-\mu+1,-\beta+\mu-1}(\xi), \quad \xi \in [-1,1], \tag{9.1} $$

with $\mu \in (0,1)$, $-1 \leq \alpha < 2-\mu$, and $-1 \leq \beta < \mu - 1$, which are representing the

eigenfunctions of the *singular* FSLP of first kind (SFSLP-I), and

$$^{(2)}\mathcal{P}_n^{\alpha,\beta,\mu}(\xi) = (1-\xi)^{-\alpha+\mu-1} P_{n-1}^{-\alpha+\mu-1\,,\,\beta-\mu+1}(\xi), \quad \xi \in [-1,1], \tag{9.2}$$

where $-1 < \alpha < \mu - 1$ and $-1 < \beta < 2 - \mu$, and $\mu \in (0,1)$, denoting the eigenfunctions of the *singular* FSLP of *second* kind (SFSLP-II). Moreover, Zayernouri and Karniadakis developed a space-time discontinuous Petrov-Galerkin (DPG) and a discontinuous Galerkin (DG) method for the hyperbolic time- and space-fractional advection equation in [188]. This approach was shown to be also applicable to problems of integer order time derivatives. In addition, they employed the aforementioned Jacobi poly-fractonomial bases to introduce a new class of *fractional Lagrange interpolants* for developing an efficient and spectrally accurate Fractional Spectral Collocation Method (FSCM) in [190] for a variety of FODEs and FPDEs including multi-term FPDEs and the nonlinear space-fractional Burgers' equation. Recently, the FSCM scheme has been further generalized to FPDEs of variable order in [185], in where the associate fractional order(s) can vary in the computational domain Ω. However, like all previous spectral methods, applying these schemes to higher-dimensional problems remains a great challenge.

In this paper, we develop a unified and spectrally accurate Petrov-Galerkin (PG) spectral method for the general FPDEs of the following weak form

$$({}_0\mathcal{D}_t^{\tau}\, u, {}_t\mathcal{D}_T^{\tau}\, v)_\Omega + \sum_{j=1}^{d} c_j ({}_{a_j}\mathcal{D}_{x_j}^{\mu_j}\, u, {}_{x_j}\mathcal{D}_{b_j}^{\mu_j}\, v)_\Omega + \gamma (u,v)_\Omega = (f,v)_\Omega,$$

where 2τ, $\mu_j \in (0,1)$, in a $(1+d)$-dimensional *space-time* domain subject to Dirichlet initial and boundary conditions. Such a weak form is equivalent to the strong form ${}_0\mathcal{D}_t^{2\tau} u + \sum_{j=1}^{d} c_{x_j}\, {}_{a_j}\mathcal{D}_{x_j}^{2\mu_j} u + \gamma\, u = f$, when u possesses enough smoothness. This method applies equally-well to the entire family of linear fractional *hyperbolic*,

parabolic and *elliptic* equations with the same ease. The main feature of this PG spectral methods is the *global* discretization of the temporal term, in addition to the spatial derivatives, rather than utilizing traditional low-order time-integration methods. Regarding the strong form, we note that there is a much larger and richer set of fractional derivative operators in $d > 1$ dimensions (see e.g., p.157 in [123]) to be considered in our future work. We essentially develop our PG method based on a new spectral theory for fractional Sturm-Liouville problems (FSLPs) [187]. Specifically, we employ the eigenfunctions of the FSLP of *first* kind (FSLP-I), called *Jacobi poly-fractonomial*s, as temporal/spatial bases. Next, we construct a different space for test functions from poly-fractonomial eigenfunctions of the FSLP of *second* kind (FSLP-II). We show that this choice of basis and test functions leads to a stable bilinear form; moreover, we perform the corresponding error analysis. In the present method, all the aforementioned matrices are constructed *exactly* and *efficiently*. Moreover, we formulate a new general fast linear solver based on the eigen-pairs of the corresponding temporal and spatial mass matrices with respect to the stiffness matrices, which significantly reduces the computational cost in higher-dimensional problems e.g., (1+3), (1+5) and (1+9)-dimensional FPDEs.

9.2 Preliminaries on Fractional Calculus

We first provide some definitions from fractional calculus. Following [142], for a univariate function $g(x) \in C^n[a,b]$, we denote by ${}_a\mathcal{D}_x^\nu g(x)$ the left-sided Reimann-Liouville fractional derivative of order ν, when $n-1 \leq \nu < n$, defined as

$$ {}_a\mathcal{D}_x^\nu g(x) = \frac{1}{\Gamma(n-\nu)} \frac{d^n}{dx^n} \int_a^x \frac{g(s)}{(x-s)^{\nu+1-n}}\, ds, \quad x \in [a,b], \tag{9.3} $$

where Γ represents the Euler gamma function, and as $\nu \to n$, the *global* operator ${}_a\mathcal{D}_x^\nu \to d^n/dx^n$, recovering the *local* n-th order derivative with respect to x. We also denote by ${}_x\mathcal{D}_b^\nu g(x)$ the corresponding right-sided Reimann-Liouville fractional derivative of order ν, defined as

$$ {}_b\mathcal{D}_x^\nu g(x) = \frac{1}{\Gamma(n-\nu)}(-1)^n \frac{d^n}{dx^n} \int_x^b \frac{g(s)}{(s-x)^{\nu+1-n}}\, ds, \quad x \in [a,b]. \tag{9.4} $$

Similarly, as $\nu \to n$, the right-sided fractional derivative tends to the standard n-th local one. The corresponding left- and right-sided fractional derivative of Caputo type can be also defined as (9.3) and (9.4), but with the order of integration and differentiation exchanged. However, these two sets of Riemann-Liouville and Caputo definitions are closely linked. By virtue of (9.3) and (9.4), we can define the corresponding partial fractional-derivative of a bivariate function.

Finally, we recall a useful property of the Riemann-Liouville fractional derivatives. Assume that $0 < p < 1$ and $0 < q < 1$ and $g(x_L) = 0 \;\; x > x_L$, then

$$ {}_{x_L}\mathcal{D}_x^{p+q} g(x) = \left({}_{x_L}\mathcal{D}_x^p\right)\left({}_{x_L}\mathcal{D}_x^q\right) g(x) = \left({}_{x_L}\mathcal{D}_x^q\right)\left({}_{x_L}\mathcal{D}_x^p\right) g(x). \tag{9.5} $$

9.3 Mathematical Formulation of Petrov-Galerkin Spectral Method

Let $u : \mathbb{R}^{d+1} \to \mathbb{R}$, for some positive integer d. For $u \in U$ (see e.g., (9.10)), we consider the following general weak form in $\Omega = [0,T] \times [a_1,b_1] \times [a_2,b_2] \times \cdots \times [a_d,b_d]$

as

$$({}_0\mathcal{D}_t^{\tau}\, u, {}_t\mathcal{D}_T^{\tau}\, v)_\Omega + \sum_{j=1}^{d} c_j({}_{a_j}\mathcal{D}_{x_j}^{\mu_j}\, u, {}_{x_j}\mathcal{D}_{b_j}^{\mu_j}\, v)_\Omega + \gamma(u,v)_\Omega = (f,v)_\Omega, \quad \forall v \in V, \quad (9.6)$$

where γ, c_j are constant, 2τ,$\mu_j \in (0,1)$, $j = 1, 2, \cdots, d$, subject to the following homogeneous Dirichlet initial and boundary conditions

$$\begin{aligned} u|_{t=0} &= 0, \quad \tau \in (0,1/2), \qquad (9.7)\\ u|_{x_j=a_j} &= 0, \quad \mu_j \in (0,1/2), \quad j = 1,2,\cdots,d \\ u|_{x_j=a_j} = u|_{x_j=b_j} &= 0, \quad \mu_j \in (1/2,1), \quad j = 1,2,\cdots,d. \end{aligned}$$

We note that the variational form (9.6) is equivalent to the following linear FPDE of order 2τ in time and $2\mu_j$ in the j-th spatial dimension, $j = 1, 2, \cdots, d$,

$$\begin{aligned} {}_0\mathcal{D}_t^{2\tau} u(t, x_1, x_2, \cdots, x_d) &+ \sum_{j=1}^{d} c_j[\, {}_{a_j}\mathcal{D}_{x_j}^{2\mu_j} u(t, x_1, x_2, \cdots, x_d)\,] \qquad (9.8)\\ &+ \gamma\, u(t, x_1, x_2, \cdots, x_d) = f(t, x_1, x_2, \cdots, x_d), \end{aligned}$$

when solution u is smooth enough.

We define the solution space U as

$$U := \Big\{ u : \Omega \to \mathbb{R} \,|\, u \in C(\Omega),\, \|u\|_U < \infty,\, and\, u|_{t=0} = u|_{x_j=a_j} = 0 \Big\}, \qquad (9.9)$$

if $\mu_j \in (0, 1/2)$ and

$$U := \Big\{ u : \Omega \to \mathbb{R} \,|\, u \in C(\Omega),\, \|u\|_U < \infty,\, s.t.\, u|_{t=0} = u|_{x_j=a_j} = u|_{x_j=b_j} = 0 \Big\} \qquad (9.10)$$

when $\mu_j \in (1/2, 1)$, in which

$$\|u\|_U = \Big\{ \| {}_0\mathcal{D}_t^\tau u\|^2 + \sum_{j=1}^{d} \| {}_{a_j}\mathcal{D}_{x_j}^{\mu_j} u\|^2 \, + \, \|u\|^2 \Big\}^{1/2}. \tag{9.11}$$

Correspondingly, we define the test space V as

$$V := \Big\{ v : \Omega \to \mathbb{R} \,|\, \|v\|_V < \infty, \, s.t. \, v|_{t=T} = v|_{x_j = b_j} = 0 \Big\}, \tag{9.12}$$

when $\mu_j \in (0, 1)$, in which

$$\|v\|_V = \Big\{ \| {}_t\mathcal{D}_T^\tau v\|^2 + \sum_{j=1}^{d} \| {}_{x_j}\mathcal{D}_{b_j}^{\mu_j} v\|^2 \, + \, \|v\|^2 \Big\}^{1/2}, \tag{9.13}$$

where by [60, 150], we can show that U and V are Hilbert spaces, moreover, the associated norms $\|\cdot\|_U$ and $\|\cdot\|_V$ are equivalent. Now, let $a : U \times V \to \mathbb{R}$ be a bilinear form, defined as

$$a(u, v) = ({}_0\mathcal{D}_t^\tau \, u, {}_t\mathcal{D}_T^\tau \, v)_\Omega + \sum_{j=1}^{d} c_j ({}_{a_j}\mathcal{D}_{x_j}^{\mu_j} \, u, \, {}_{x_j}\mathcal{D}_{b_j}^{\mu_j} \, v)_\Omega + \gamma(u, v)_\Omega. \tag{9.14}$$

Moreover, let $L \in V^*$, the dual space of V, be a continuous linear functional defined as

$$L(v) = (f, v), \quad \forall v \in V. \tag{9.15}$$

Now, the problem is to find $u \in U$ such that

$$a(u, v) = L(v), \quad \forall v \in V. \tag{9.16}$$

Next, we define $U_N \subset U$ and $V_N \subset V$ to be finite dimensional subspaces of U and V with $\dim(U_N) = \dim(V_N) = N$. Now, our PG spectral method reads as: find

$u_N \in U_N$ such that

$$a(u_N, v_N) = L(v_N), \quad \forall v_N \in V_N. \tag{9.17}$$

By representing u_N as a linear combination of points/elements in U_N i.e., the corresponding $(1 + d)$-dimensional space-time basis functions, the finite-dimensional problem (9.17) leads to a linear system known as *Lyapunov* matrix equation. For instance, if $d = 1$, i.e., 1-D in time and 1-D space, we obtain the corresponding Lyapunov equation in the space-time domain $[0, T] \times [a_1, b_1]$ as

$$S_\tau \mathcal{U} M_{\mu_1}^T + M_\tau \mathcal{U} S_{\mu_1}^T = F, \tag{9.18}$$

in which $\mathcal{U}$ is the matrix of unknown coefficients, S_τ and M_τ denote, respectively, the temporal stiffness and mass matrices; similarly, S_{μ_1} and M_{μ_1}, represent the spatial stiffness and mass matrices, and F is the corresponding load matrix.

In general, numerical solutions to such a linear system, originating from a fractional differential operator, become excessively expensive since the corresponding mass and stiffness matrices usually turn out to be *full* and *non-symmetric*. Moreover, we note that the size of the above linear system grows as the product of the degrees of freedom in each dimension. To address this problem in this paper, we present a new class of basis and test functions yielding stiffness matrices, which are either *diagonal* or *tridiagonal*. Similarly, by introducing proper quadrature rules, we compute exactly the corresponding mass matrices, which are *symmetric*. Such useful properties allow us to subsequently develop a general fast linear solver for (9.18) with a substantially reduced computational cost. To this end, we first introduce the corresponding finite-dimensional spaces of basis U_N and test functions V_N in our PG framework.

9.3.1 Space of Basis Functions (U_N)

We develop a PG spectral method for (9.8), subject to homogeneous Dirichlet initial and boundary conditions. We construct the basis function space as the space of some temporal and spatial functions to globally treat the time-dimension in addition to the spatial-dimensions. To this end, the new eigensolutions, introduced in [187], yield new sets of *basis* and *test* functions, properly suited for our Petrov-Galerkin framework. We represent the solution in the entire space-time computational domain Ω in terms of specially chosen basis functions, constructed as the tensor product of the the eigenfunctions in the following manner. Let

$$ {}^{(1)}\mathcal{P}_n^{\mu}(\xi) = (1+\xi)^{\mu}\ P_{n-1}^{-\mu,\mu}(\xi), \quad n = 1, 2, \cdots \quad x \in [-1, 1], \tag{9.19} $$

denote the eigenfunctions of the *regular* FSLP of first kind (RFSLP-I), corresponding to the case where $\alpha = \beta = -1$. We construct our basis for the spatial discretization using the univariate poly-fractonomials defined by

$$ \phi_m^{\mu}(\,\xi\,) = \sigma_m \begin{cases} {}^{(1)}\mathcal{P}_m^{\mu}(\,\xi\,), \quad m = 1, 2, \cdots, & \mu \in (0, 1/2], \\ \\ {}^{(1)}\mathcal{P}_m^{\mu}(\,\xi\,) \ - \ \epsilon_m^{\mu}\ {}^{(1)}\mathcal{P}_{m-1}^{\mu}(\,\xi\,), \quad m = 2, 3, \cdots & \mu \in (1/2, 1), \end{cases} \tag{9.20} $$

where $\sigma_m = 2+(-1)^m$ and the μ-dependent coefficient $\epsilon_{m_j}^{\mu} = (m-1-\mu)/(m-1)$. The definition reflects the fact that if $\mu \leq 1/2$ then only one boundary condition needs to be presented, whereas if $\mu > 1/2$ then two endpoint conditions are prescribed. Naturally, for the temporal basis functions only initial conditions are prescribed and as a consequence the basis functions for the temporal discretization are constructed

using the univariate poly-fractonomials

$$\psi_n^{\tau}(\eta) = \sigma_n \ {}^{(1)}\mathcal{P}_n^{\tau}(\,\eta\,), \quad \tau \in (0,1), \tag{9.21}$$

for $n \geq \lceil 2\tau \rceil$. With these notations established, we define the space-time trial space to be

$$U_N = span\Big\{ \Big(\psi_n^{\tau} \circ \eta\Big)(t) \prod_{j=1}^{d} \Big(\phi_{m_j}^{\mu_{x_j}} \circ \xi_j\Big)(x_j) \ : n = 1, \ldots, \mathcal{N},\, m_j = \lceil \sigma_j \rceil, \ldots, \mathcal{M}_j \Big\}, \tag{9.22}$$

where $\eta(t) = 2t/T - 1$ and $\xi_j(s) = 2\frac{s-a_j}{b_j-a_j} - 1$. The construction of the univariate functions ensures that $U_N \subset U$, since $\phi_m^{\mu}(-1) = 0$, for all $\mu \in (0,1)$, also $\phi_m^{\mu}(1) = 0$, for all $\mu \in (1/2, 1)$. Then, we shall approximate the solution to (9.8) in terms of a linear combination of elements in U_N, whose bases satisfy exactly the homogeneous initial and boundary condition in Ω.

9.3.2 Space of Test Functions (V_N)

Let the poly-fractonomials

$${}^{(2)}\mathcal{P}_k^{\mu}(\xi) = (1-\xi)^{\mu} \ P_{k-1}^{\mu,-\mu}(\xi), \quad k = 1, 2, \cdots, \xi \in [-1, 1], \tag{9.23}$$

denote the eigenfunctions of the *regular* FSLP of second kind (RFSLP-II), corresponding to the case $\alpha = \beta = -1$ in (9.2). Next, we construct our spatial test

functions using the univariate poly-fractonomials defined by

$$\Phi_k^{\mu}(\xi) = \widetilde{\sigma}_k \begin{cases} {}^{(2)}\mathcal{P}_k^{\mu}(\,\xi\,), \quad k = 1, 2, \cdots & \mu \in (0, 1/2], \\ \\ {}^{(2)}\mathcal{P}_k^{\mu}(\xi) \;+\; \epsilon_k^{\mu}\; {}^{(2)}\mathcal{P}_{k-1}^{\mu}(\xi), \quad k = 2, 3, \cdots & \mu \in (1/2, 1), \end{cases} \tag{9.24}$$

where $\widetilde{\sigma}_k = 2\,(-1)^k + 1$. Next, we define the temporal test functions using the univariate poly-fractonomials

$$\Psi_r^{\tau}(\eta) = \widetilde{\sigma}_r\, {}^{(2)}\mathcal{P}_r^{\tau}(\,\eta\,), \quad \tau \in (0, 1), \tag{9.25}$$

for all $r \geq \lceil 2\tau \rceil$. With these notations established, we define the space-time test space to be

$$V_N = span\Big\{ \Big(\Psi_r^{\tau} \circ \eta\Big)(t) \prod_{j=1}^{d} \Big(\Phi_{k_j}^{\mu_j} \circ \xi_j\Big)(x_j) \;:\; r = 1, \ldots, \mathcal{N},\; k_j = \lceil \sigma_j \rceil, \ldots, \mathcal{M}_j \Big\}. \tag{9.26}$$

Having defined the space of trial and test functions, we can now define the corresponding temporal/spatial stiffness and mass matrices.

Remark 9.3.1. We show later that the choice of σ_m in (9.20) and (9.21), also $\widetilde{\sigma}_k$ in (9.24) and (9.25), leads to the construction of *symmetric* spatial/temporal mass and stiffness matrices. We will exploit this property to formulate a general fast linear solver for the resulting linear system.

9.3.3 Stability and Convergence Analysis

The following theorems provide the stability analysis of the scheme when the pair of $U_N \subset U$ and $V_N \subset V$ are given as in (9.22) and (9.26), respectively. We first consider the discrete stability of the method for one-dimensional case.

Theorem 9.3.2. *The Petrov-Gelerkin spectral method for the problem*

$$\begin{aligned} {}_{-1}\mathcal{D}_x^{2\mu} u(x) &= f(x), \quad \forall x \in [-1,1], \\ u(-1) &= 0, \quad if\ 0 < \mu < 1/2, \\ u(\pm 1) &= 0, \quad if\ 1/2 < \mu < 1. \end{aligned} \tag{9.27}$$

is stable, i.e., the discrete inf-sup *condition*

$$\sup_{v_N \in V_N} \frac{a(u_N, v_N)}{\|v_N\|_V} \geq \beta \|u_N\|_U, \quad \forall u_N \in U_N \subset U, \tag{9.28}$$

holds with $\beta = 1$.

Proof. We note that in the absence of the time-derivative and since $\gamma = 0$, the corresponding norm defined on U (see Eq. 9.11) just reduces to $\|u\|_U = \| {}_{-1}\mathcal{D}_x^{\mu} u\|$. While $\| {}_{-1}\mathcal{D}_x^{\mu} u\|$ has been traditionally treated as a semi-norm in the literature (e.g., see [151, 108]), one can easily show that it satisfies all the properties of a norm since the Riemann-Liouville fractional derivative of a constant is non-zero. Correspondingly, in this one-dimensional setting, $\|v\|_V = \| {}_{x}\mathcal{D}_1^{\mu} v\|$.

Case I) $0 < \mu < 1/2$**:** we represent u_N as

$$u_N(x) = \sum_{n=1}^{N} \hat{u}_n (1+x)^{\mu} P_{n-1}^{-\mu,\mu}(x), \tag{9.29}$$

and choose v_N to be the following linear combination of elements in V_N as

$$v_N(x) = \sum_{k=1}^{N} \hat{u}_k (1-x)^{\mu} P_{k-1}^{\mu,-\mu}(x), \tag{9.30}$$

in which we employ the same coefficients $\hat{u}_k$ as in (9.29). Hence, we obtain

$$\begin{aligned}
& a(u_N, v_N) = \int_{-1} {}_{-1}\mathcal{D}_x^{\mu} u_N \; {}_x\mathcal{D}_1^{\mu} v_N \, dt \qquad (9.31)\\
= & \sum_{n=1}^{N} \hat{u}_n \sum_{k=1}^{N} \hat{u}_k \int_{-1} {}_{-1}\mathcal{D}_x^{\mu}[(1+x)^{\mu} P_{n-1}^{-\mu,\mu}(x)], {}_x\mathcal{D}_1^{\mu}[(1-x)^{\mu} P_{k-1}^{\mu,-\mu}(x)] \, dt \\
= & \sum_{n=1}^{N} \hat{u}_n \frac{\Gamma(n+\mu)}{\Gamma(n)} \sum_{k=1}^{N} \hat{u}_k \frac{\Gamma(k+\mu)}{\Gamma(k)} \int_{-1}^{1} P_{n-1}(x) P_{k-1}(x) \, dt \\
= & \sum_{n=1}^{N} \hat{u}_n^2 \Big(\frac{\Gamma(n+\mu)}{\Gamma(n)} \Big)^2 \, \frac{2n+1}{2} \\
= & \| {}_x\mathcal{D}_1^{\mu} v_N \|^2_{L^2([-1,1])} = \|v_N\|_V^2,
\end{aligned}$$

$$\sup_{v_N \in V_N} \frac{a(u_N, v_N)}{\|v_N\|_V} = \|u_N\|_U, \quad \forall u_N \in U_N, \tag{9.32}$$

which means that the stability is guaranteed for $\beta = 1$.

Case II) $1/2 < \mu < 1$**:** we expand u_N this time as

$$u_N(x) = \sum_{n=1}^{N} \hat{u}_n \Big[(1+x)^{\mu} P_{n-1}^{-\mu,\mu}(x) - \epsilon_n^{\mu} (1+x)^{\mu} P_{n-2}^{-\mu,\mu}(x) \Big], \tag{9.33}$$

and choose v_N to be the following linear combination of elements in V_N as

$$v_N(x) = \sum_{k=1}^{N} \hat{u}_k \Big[(1-x)^{\mu} P_{k-1}^{\mu,-\mu}(x) + \epsilon_k^{\mu} (1-x)^{\mu} P_{k-2}^{\mu,-\mu}(x) \Big], \tag{9.34}$$

where the coefficients $\hat{u}_k$ are the same as the ones in (9.33). Hence, it is easy to

again show that

$$\begin{aligned} a(u_N, v_N) &= \sum_{n=1}^{N} \hat{u}_n^2 \Big(\frac{\Gamma(n+\mu)}{\Gamma(n)}\Big)^2 \frac{2n+1}{2}(1-\epsilon_n^{\mu}\mathbb{I}_{\{1\le n\le N-1\}}) \\ &= \|\,{}_x\mathcal{D}_1^{\mu} v_N\|^2_{L^2([-1,1])} = \|v_N\|_V^2. \end{aligned} \tag{9.35}$$

□

Remark 9.3.3. We performed the discrete stability analysis for the 1-D case. The multi-D case is more involved and we will address it in a separate paper in future.

Theorem 9.3.4. *(Projection Error) In the weak form* (9.17)*, let* $\|\,{}_0\mathcal{D}_t^{r+\tau} u\|_{L^2(\Omega)} < \infty$ *and* $\|\,{}_{-1}\mathcal{D}_{x_j}^{r+\mu_j} u\|_{L^2(\Omega)} < \infty$ *for all* $j = 1, 2, \cdots, d$*, for some integer* $r \ge 1$*. Moreover, let* u_N *denote the projection of the exact solution* u*. Then,*

$$\|u - u_N\|_U^2 \le C\, N^{-2r}\Big(\|\,{}_0\mathcal{D}_t^{r+\tau} u\|^2_{L^2(\Omega)} + \sum_{j=1}^{d} \|\,{}_{-1}\mathcal{D}_{x_j}^{r+\mu_j} u\|^2_{L^2(\Omega)}\Big).$$

Proof. We first consider the one-dimensional problem (9.27). We expand the exact solution u, when $2\mu \in (0,1)$, in terms of the following infinite series of Jacobi poly-fractonomials

$$u(x) = \sum_{n=1}^{\infty} \hat{u}_n (1+x)^{\mu} P_{n-1}^{-\mu,\mu}(x). \tag{9.36}$$

Here, we would like to bound $\|u - u_N\|_U$ in terms of higher-order derivative We first note that

$${}_{-1}\mathcal{D}_x^{r+\mu} u(x) = \frac{d^r}{dx^r}[{}_{-1}\mathcal{D}_x^{\mu} u(x)] = \sum_{n=1}^{\infty} \hat{u}_n \frac{\Gamma(n+\mu)}{\Gamma(n)} \frac{d^r}{dx^r}[P_{n-1}(x)],$$

where

$$\frac{d^r}{dx^r}[P_{n-1}(x)] = \begin{cases} \frac{(n-1+r)!}{2r(n-1)!} P^{r,r}_{n-1-r}(x), & r \leq n, \\ 0, & r > n. \end{cases}$$

Hence,

$${}_{-1}\mathcal{D}^{r+\mu}_x u(x) = \sum_{n=r}^{\infty} \hat{u}_n \frac{\Gamma(n+\mu)}{\Gamma(n)} \frac{(n-1+r)!}{2r(n-1)!} P^{r,r}_{n-1-r}(x).$$

Therefore,

$$\begin{aligned} \|(1-x)^{r/2}(1+x)^{r/2}\, {}_{-1}\mathcal{D}^{r+\mu}_x u(x)\|^2 = \\ \int_{-1}^{1} (1-x)^r (1+x)^r \Big(\sum_{n=r}^{\infty} \hat{u}_n \frac{\Gamma(n+\mu)}{\Gamma(n)} \frac{(n-1+r)!}{2r(n-1)!} P^{r,r}_{n-1-r}(x) \Big)^2 = \\ \sum_{n=r}^{\infty} \Big(\hat{u}_n \frac{\Gamma(n+\mu)}{\Gamma(n)} \frac{(n-1+r)!}{2r(n-1)!} \Big)^2 \int_{-1}^{1} (1-x)^r (1+x)^r P^{r,r}_{n-1-r}(x) P^{r,r}_{n-1-r}(x) dx = \\ \sum_{n=r}^{\infty} \Big[\hat{u}_n \frac{\Gamma(n+\mu)}{\Gamma(n)} \frac{(n-1+r)!}{2r(n-1)!} \Big]^2 \frac{2^{2r+1}\,((n-1)!)^2}{(n-1-r)!(n-1+r)!} = \\ \sum_{n=r}^{\infty} \Big[\hat{u}_n \frac{\Gamma(n+\mu)}{\Gamma(n)} \Big]^2 \frac{2}{2n+1} \frac{(n-1+r)!}{(n-1-r)!}. \end{aligned}$$

We also note that $\frac{(n-1+r)!}{(n-1-r)!}$ is minimized when $n = N+1$. Hence,

$$\begin{aligned}
\|u-u_N\|_U^2 &= \sum_{n=N+1}^{\infty}\Big[\hat{u}_n\frac{\Gamma(n+\mu)}{\Gamma(n)}\Big]^2 \\
&\leq \sum_{n=N+1}^{\infty}\Big[\hat{u}_n\frac{\Gamma(n+\mu)}{\Gamma(n)}\Big]^2\frac{(n-1+r)!}{(n-1-r)!}\frac{(N-r)!}{(N+r)!} \\
&= \frac{(N-r)!}{(N+r)!}\sum_{n=N+1}^{\infty}\Big[\hat{u}_n\frac{\Gamma(n+\mu)}{\Gamma(n)}\Big]^2\frac{(n-1+r)!}{(n-1-r)!}, \\
&= \frac{(N-r)!}{(N+r)!}\|(1-x)^{r/2}(1+x)^{r/2}\,{}_{-1}\mathcal{D}_x^{r+\mu}u(x)\|^2 \\
&\leq \frac{(N-r)!}{(N+r)!}\|\,{}_{-1}\mathcal{D}_x^{r+\mu}u(x)\|^2 \\
&\leq c\,N^{-2r}\|\,{}_{-1}\mathcal{D}_x^{r+\mu}u(x)\|^2, \qquad (9.37)
\end{aligned}$$

where $r \geq 1$ and $2\mu \in (0,1)$. Similar steps are done for the case $2\mu \in (1,2)$ to obtain (9.37) noting that in either case, μ remains between 0 and 1.

Next, we consider the following *two-dimensional* problem in $\Omega = [-1,1]\times[-1,1]$:

$$\begin{aligned}
{}_{-1}\mathcal{D}_x^{2\mu_x}u(x,y) \;+\; {}_{-1}\mathcal{D}_y^{2\mu_y}u(x,y) &= f(x,y), \quad \forall (x,y)\in\Omega, \qquad (9.38)\\
u(-1,y) \;=\; u(x,-1) &= 0, \quad if\ 0<\mu_x,\mu_y<1/2,
\end{aligned}$$

whose corresponding weak form is given by

$$({}_{-1}\mathcal{D}_x^{\mu_x}u\,,\,{}_{x}\mathcal{D}_1^{\mu_x}v)_\Omega + ({}_{-1}\mathcal{D}_y^{\mu_y}u\,,\,{}_{y}\mathcal{D}_1^{\mu_y}v)_\Omega = (f,v)_\Omega. \qquad (9.39)$$

We represent the exact solution u when $2\mu_x, 2\mu_y \in (0,1)$, in terms of the following infinite series of tensor product Jacobi poly-fractonomials as

$$u(x,y) = \sum_{n=1}^{\infty}\sum_{m=1}^{\infty}\hat{u}_{nm}(1+x)^{\mu_x}P_{n-1}^{-\mu_x,\mu_x}(x)\,(1+y)^{\mu_y}P_{m-1}^{-\mu_y,\mu_y}(y). \qquad (9.40)$$

Hence,

$$
\begin{aligned}
{}_{-1}\mathcal{D}_x^{r+\mu_x} u &= \sum_{n=1}^{\infty}\sum_{m=1}^{\infty} \hat{u}_{nm} \frac{\Gamma(n+\mu_x)}{\Gamma(n)} \frac{(n-1+r)!}{2r(n-1)!} P_{n-1-r}^{r,r}(x)\,(1+y)^{\mu_y} P_{m-1}^{-\mu_y,\mu_y}(y) \qquad (9.41)\\
{}_{-1}\mathcal{D}_y^{r+\mu_y} u &= \sum_{n=1}^{\infty}\sum_{m=1}^{\infty} \hat{u}_{nm} (1+x)^{\mu_x} P_{n-1}^{-\mu_x,\mu_x}(x) \frac{\Gamma(m+\mu_y)}{\Gamma(m)} \frac{(m-1+r)!}{2r(m-1)!} P_{m-1-r}^{r,r}(y). \qquad (9.42)
\end{aligned}
$$

Moreover, taking $w_1(x) = (1-x)^{r/2}(1+x)^{r/2}$ and $w_2(y) = (1-y)^{-\mu_y/2}(1+y)^{-\mu_y/2}$, we have

$$
\begin{aligned}
&\|w_1(x)\, w_2(y)\, {}_{-1}\mathcal{D}_x^{r+\mu_x} u\|_{L^2(\Omega)}^2 = \\
&\quad \sum_{n=1}^{\infty}\sum_{m=1}^{\infty} \Big[\hat{u}_{nm} \frac{\Gamma(n+\mu_x)}{\Gamma(n)} \frac{(n-1+r)!}{2r(n-1)!}\Big]^2 . \int_{-1}^{+1} (1-x)^r (1+x)^r [P_{n-1-r}^{r,r}(x)]^2 dx \\
&\qquad\qquad . \int_{-1}^{+1} (1-y)^{-\mu_y} (1+y)^{\mu_y} [P_{m-1}^{-\mu_y,\mu_y}(y)]^2 dy \\
&= \sum_{n=1}^{\infty}\sum_{m=1}^{\infty} \Big[\hat{u}_{nm} \frac{\Gamma(n+\mu_x)}{\Gamma(n)}\Big]^2 \frac{2}{2n+1} . \frac{(n-1+r)!}{(n-1-r)!} \frac{2}{2m-1} \frac{\Gamma(m-\mu_y)\Gamma(m+\mu_y)}{(m-1)!\Gamma(m)} .
\end{aligned}
$$

Similarly,

$$
\begin{aligned}
&\|w_1(y)\, w_2(x)\, {}_{-1}\mathcal{D}_y^{r+\mu_y} u\|_{L^2(\Omega)}^2 = \\
&\quad \sum_{n=1}^{\infty}\sum_{m=1}^{\infty} \Big[\hat{u}_{nm} \frac{\Gamma(m+\mu_x)}{\Gamma(m)}\Big]^2 \frac{2}{2n-1} \frac{\Gamma(n-\mu_x)\Gamma(n+\mu_x)}{(n-1)!\Gamma(n)} \frac{2}{2m+1} \frac{(m-1+r)!}{(m-1-r)!} .
\end{aligned}
$$

We note that $u(x,y)$ can be decomposed into four contributions as

$$
u = \Big(\sum_{n=1}^{N}\sum_{m=1}^{N} + \sum_{n=1}^{N}\sum_{m=N+1}^{\infty} + \sum_{n=N+1}^{\infty}\sum_{m=1}^{N} + \sum_{n=N+1}^{\infty}\sum_{m=N+1}^{\infty} \Big) \hat{u}_{nm} \mathcal{P}_n^{\mu_x}(x) \mathcal{P}_m^{\mu_y}(y),
$$

or equivalently,

$$u - u_N = \Big(\sum_{n=1}^{N} \sum_{m=N+1}^{\infty} + \sum_{n=N+1}^{\infty} \sum_{m=1}^{N} + \sum_{n=N+1}^{\infty} \sum_{m=N+1}^{\infty} \Big) \hat{u}_{nm} \mathcal{P}_n^{\mu_x}(x) \mathcal{P}_m^{\mu_y}(y).$$

Next, we aim to bound $\|u - u_N\|_U$ in terms of higher-order derivative as

$$\begin{aligned} \|u - u_N\|_U^2 &\leq \| \sum_{n=1}^{N} \sum_{m=N+1}^{\infty} \hat{u}_{nm} \mathcal{P}_n^{\mu_x}(x) \mathcal{P}_m^{\mu_y}(y) \|_U^2 \\ &+ \| \sum_{n=N+1}^{\infty} \sum_{m=1}^{N} \hat{u}_{nm} \mathcal{P}_n^{\mu_x}(x) \mathcal{P}_m^{\mu_y}(y) \|_U^2 \\ &+ \| \sum_{n=N+1}^{\infty} \sum_{m=N+1}^{\infty} \hat{u}_{nm} \mathcal{P}_n^{\mu_x}(x) \mathcal{P}_m^{\mu_y}(y) \|_U^2, \end{aligned} \tag{9.43}$$

in which we note the symmetry between the first two terms on the right-hand side. Let us consider the second term first:

$$\begin{aligned} \| \sum_{n=N+1}^{\infty} \sum_{m=1}^{N} \hat{u}_{nm} \mathcal{P}_n^{\mu_x}(x) \mathcal{P}_m^{\mu_y}(y) \|_U^2 = \\ \| {}_{-1}\mathcal{D}_x^{\mu_x} \Big(\sum_{n=N+1}^{\infty} \sum_{m=1}^{N} \hat{u}_{nm} \mathcal{P}_n^{\mu_x}(x) \mathcal{P}_m^{\mu_y}(y) \Big) \|_{L^2(\Omega)}^2 + \\ \| {}_{-1}\mathcal{D}_y^{\mu_y} \Big(\sum_{n=N+1}^{\infty} \sum_{m=1}^{N} \hat{u}_{nm} \mathcal{P}_n^{\mu_x}(x) \mathcal{P}_m^{\mu_y}(y) \Big) \|_{L^2(\Omega)}^2, \end{aligned} \tag{9.44}$$

where

$$
\begin{aligned}
&\| {}_{-1}\mathcal{D}_x^{\mu_x}\Big(\sum_{n=N+1}^{\infty}\sum_{m=1}^{N} \hat{u}_{nm}\mathcal{P}_n^{\mu_x}(x)\mathcal{P}_m^{\mu_y}(y)\Big)\|_{L^2(\Omega)}^2 = \\
&\le \int_{-1}^{1}\int_{-1}^{1} w_2(y)\Big(\sum_{n=N+1}^{\infty}\sum_{m=1}^{N} \hat{u}_{nm}\frac{\Gamma(n+\mu_x)}{\Gamma(n)}P_{n-1}(x)\mathcal{P}_m^{\mu_y}(y)\Big)^2 \\
&\le \sum_{n=N+1}^{\infty}\sum_{m=1}^{N}\Big[\hat{u}_{nm}\frac{\Gamma(n+\mu_x)}{\Gamma(n)}\Big]^2\frac{2}{2n+1}\frac{2}{2m-1}\frac{\Gamma(m-\mu_y)\Gamma(m+\mu_y)}{(m-1)!\Gamma(m)} \\
&\le \frac{(N-r)!}{(N+r)!}\sum_{n=N+1}^{\infty}\sum_{m=1}^{N}\Big[\hat{u}_{nm}\frac{\Gamma(n+\mu_x)}{\Gamma(n)}\Big]^2\frac{2}{2n+1}\frac{(n-1+r)!}{(n-1-r)!}\frac{2}{2m-1}\frac{\Gamma(m-\mu_y)\Gamma(m+\mu_y)}{(m-1)!\Gamma(m)} \\
&\le \frac{(N-r)!}{(N+r)!}\| {}_{-1}\mathcal{D}_x^{1+\mu_x}u\|_{L^2(\Omega)}^2 \\
&\le cN^{-2r}\| {}_{-1}\mathcal{D}_x^{1+\mu_x}u\|_{L^2(\Omega)}^2.
\end{aligned}
$$

Following similar steps, we obtain

$$
\| {}_{-1}\mathcal{D}_y^{\mu_y}\Big(\sum_{n=N+1}^{\infty}\sum_{m=1}^{N} \hat{u}_{nm}\mathcal{P}_n^{\mu_x}(x)\mathcal{P}_m^{\mu_y}(y)\Big)\|_{L^2(\Omega)}^2 \le cN^{-2r}\| {}_{-1}\mathcal{D}_y^{r+\mu_y}u\|_{L^2(\Omega)}^2.
$$

Therefore, we obtain the following estimate for the second term on the right-hand side of (9.43)

$$
\| \sum_{n=N+1}^{\infty}\sum_{m=1}^{N} \hat{u}_{nm}\mathcal{P}_n^{\mu_x}(x)\mathcal{P}_m^{\mu_y}(y)\|_U^2 \le \tilde{c}N^{-2r}\Big(\| {}_{-1}\mathcal{D}_x^{r+\mu_x}u\|_{L^2(\Omega)}^2 + \| {}_{-1}\mathcal{D}_y^{r+\mu_y}u\|_{L^2(\Omega)}^2\Big) \tag{9.45}
$$

Moreover, by symmetry, we have the following results for the first term on the right-hand side of (9.43):

$$
\| \sum_{n=1}^{N}\sum_{m=N+1}^{\infty} \hat{u}_{nm}\mathcal{P}_n^{\mu_x}(x)\mathcal{P}_m^{\mu_y}(y)\|_U^2 \le \tilde{C}N^{-2r}\Big(\| {}_{-1}\mathcal{D}_x^{r+\mu_x}u\|_{L^2(\Omega)}^2 + \| {}_{-1}\mathcal{D}_y^{r+\mu_y}u\|_{L^2(\Omega)}^2\Big) \tag{9.46}
$$

It is easy to check that $\| \sum_{n=N+1}^{\infty}\sum_{m=N+1}^{\infty} \hat{u}_{nm}\mathcal{P}_n^{\mu_x}(x)\mathcal{P}_m^{\mu_y}(y)\|_U^2$ can be bounded by the first two terms on the right-hand side, hence, by substituting (9.45) and (9.46)

into (9.43), we finally obtain the following estimate

$$\|u - u_N\|_U^2 \leq CN^{-2r}\Big(\| \,{}_{-1}\mathcal{D}_x^{r+\mu_x} u\|_{L^2(\Omega)}^2 + \| \,{}_{-1}\mathcal{D}_y^{r+\mu_y} u\|_{L^2(\Omega)}^2\Big). \tag{9.47}$$

Such an error estimate can be isotropically tensor producted up for higher-dimensional problems to get the following estimate

$$\|u - u_N\|_U^2 \leq C\, N^{-2r}\Big(\| \,{}_{0}\mathcal{D}_t^{r+\tau} u\|_{L^2(\Omega)}^2 + \sum_{j=1}^{d} \| \,{}_{-1}\mathcal{D}_{x_j}^{r+\mu_j} u\|_{L^2(\Omega)}^2\Big), \tag{9.48}$$

in which N denotes the number of terms in the expansion in all $(d{+}1)$ dimensions. $\square$

Remark 9.3.5. Since the inf-sup condition holds (see Theorem 9.3.2), by the Banach-Nečas-Babuška theorem [56], the error in the numerical scheme is less than or equal to a constant times the projection error. Choosing the projection u_N in Theorem 9.3.4, we conclude the spectral accuracy of the scheme.

9.3.4 Implementation of PG Spectral Method

We now seek the solution to (9.8) in terms of a linear combination of elements in the space U_N of the form

$$u_N(x,t) = \sum_{n=\lceil 2\tau\rceil}^{\mathcal{N}} \sum_{m_1=\lceil 2\mu_1\rceil}^{\mathcal{M}_1} \cdots \sum_{m_d=\lceil 2\mu_d\rceil}^{\mathcal{M}_d} \hat{u}_{n,m_1,\cdots,m_d}\Big[\psi_n^{\tau}(t)\prod_{j=1}^{d}\phi_{m_j}^{\mu_j}(x_j)\Big] \tag{9.49}$$

in Ω. Next, we require the corresponding residual

$$R_N(t,x_1,\cdots,x_d) = {}_{0}\mathcal{D}_t^{2\tau}\Big(u_N\Big) + \sum_{j=1}^{d} c_j \;\, {}_{a_j}\mathcal{D}_{x_j}^{2\mu_j}\Big(u_N\Big) \;+ \gamma\, u_N - f \tag{9.50}$$

to be L^2-orthogonal to the elements in $v_N \in V_N$, which leads to the finite-dimensional variational form given in (9.17). Specifically, by choosing $v_N = \Psi_r^{\mu_t}(t) \prod_{j=1}^d \Phi_{k_j}^{\mu_{x_j}}(x_j)$, when $r = \lceil 2\tau \rceil, \ldots, \mathcal{N}$ and $k_j = \lceil 2\mu_j \rceil, \ldots, \mathcal{M}_j$, we obtain

$$\sum_{n=\lceil 2\tau \rceil}^{\mathcal{N}} \sum_{m_1=\lceil 2\mu_1 \rceil}^{\mathcal{M}_1} \cdots \sum_{m_d=\lceil 2\mu_d \rceil}^{\mathcal{M}_d} \hat{u}_{n,m_1,\cdots,m_d} \Big(\{S_\tau\}_{r,n} \{M_{\mu_1}\}_{k_1,m_1} \cdots \{M_{\mu_d}\}_{k_d,m_d} + \sum_{j=1}^d c_j \left[\{M_\tau\}_{r,n} \{M_{\mu_1}\}_{k_1,m_1} \cdots \{S_{\mu_j}\}_{k_j,m_j} \cdots \{M_{\mu_d}\}_{k_d,m_d} \right] + \gamma \{M_\tau\}_{r,n} \{M_{\mu_1}\}_{k_1,m_1} \cdots \{M_{\mu_d}\}_{k_d,m_d} \Big) = F_{r,k_1,\cdots,k_d}, \tag{9.51}$$

where S_τ and M_τ denote, respectively, the temporal stiffness and mass matrices, whose entries are defined as

$$\{S_\tau\}_{r,n} = \int_0^T {}_0\mathcal{D}_t^\tau \Big(\psi_n^\tau \circ \eta \Big)(t) \, {}_t\mathcal{D}_T^\tau \Big(\Psi_r^\tau \circ \eta \Big)(t) \, dt,$$

and

$$\{M_\tau\}_{r,n} = \int_0^T \Big(\Psi_r^\tau \circ \eta \Big)(t) \Big(\psi_n^\tau \circ \eta \Big)(t) \, dt.$$

Moreover, S_{μ_j} and M_{μ_j}, $j = 1, 2, \cdots, d$, are the corresponding spatial stiffness and mass matrices

$$\{S_{\mu_j}\}_{k_j,m_j} = \int_{a_j}^{b_j} {}_{a_j}\mathcal{D}_{x_j}^{\mu_j} \Big(\phi_{m_j}^{\mu_j} \circ \xi_j \Big)(x_j) \, {}_{x_j}\mathcal{D}_{b_j}^{\mu_j} \Big(\Phi_{k_j}^{\mu_j} \circ \xi_j \Big)(x_j) \, dx_j,$$

and

$$\{M_{\mu_j}\}_{k_j,m_j} = \int_{a_j}^{b_j} \Big(\Phi_{k_j}^{\mu_j} \circ \xi_j \Big)(x_j) \Big(\phi_{m_j}^{\mu_j} \circ \xi_j \Big)(x_j) \, dx_j,$$

respectively, to be exactly computed in the Appendix. Moreover, $F_{r,k_1,\cdots,k_d}$ is

$$\int_{\Omega} f(t,x_1,\cdots,x_d)\Big(\Psi_r^{\tau}\circ\eta\Big)(t)\prod_{j=1}^{d}\Big(\Phi_{k_j}^{\mu_j}\circ\xi_j\Big)(x_j)\,d\Omega. \tag{9.52}$$

Assuming that all the aforementioned stiffness and mass matrices are symmetric, we can render the linear system (9.51) as the following general Lyapunov equation

$$\begin{aligned}&\Big(\ S_\tau\otimes M_{\mu_1}\otimes M_{\mu_2}\cdots\otimes M_{\mu_d} \\ &+\sum_{j=1}^{d} c_j\ [\ M_\tau\otimes M_{\mu_1}\otimes\cdots\otimes M_{\mu_{j-1}}\otimes S_{\mu_j}\otimes M_{\mu_{j+1}}\cdots\otimes M_{\mu_d}\ ] \\ &\qquad +\gamma\ M_\tau\otimes M_{\mu_1}\otimes M_{\mu_2}\cdots\otimes M_{\mu_d}\Big)\mathcal{U}=F,\end{aligned} \tag{9.53}$$

in which $\otimes$ represents the Kronecker product, F denotes the multi-dimensional load matrix whose entries given in (9.52), and $\mathcal{U}$ is the corresponding multi-dimensional matrix of unknown coefficients whose entries are $\hat{u}_{n,m_1,\cdots,m_d}$.

In the Appendix, we investigate the properties of the aforementioned matrices in addition to presenting efficient ways of deriving the stiffness matrices explicitly and computing the mass matrices exactly through proper quadrature rules.

9.3.5 A New Fast FPDE Solver

So far, we have formulated a suitable Petrov-Galerkin variational framework for the general $(1+d)$-dimensional FPDE, given in (9.8), by choosing proper basis and test functions. The main advantage of such framework is that we can explicitly obtain the corresponding stiffness matrices to be symmetric diagonal/tridiagonal, and moreover, to exactly compute the mass matrices, which we showed to be symmetric. The

following result better highlights the benefit of this scheme, where we formulate a closed-form solution for the Lyapunov system (9.53) in terms of the generalised eigensolutions that can be computed very efficiently.

Theorem 9.3.6. *Let* $\{\vec{e}_{m_j}^{\mu_j}, \lambda_{m_j}^{\mu_j}\}_{m_j=\lceil 2\mu_j \rceil}^{\mathcal{M}_j}$ *be the set of general eigen-solutions of the spatial mass matrix* M_{μ_j} *with respect to the stiffness matrix* S_{μ_j}*. Moreover, let us assume that* $\{\vec{e}_n^{\tau}, \lambda_n^{\tau}\}_{n=\lceil 2\tau \rceil}^{\mathcal{N}}$ *are the set of general eigen-solutions of the temporal mass matrix* M_τ *with respect to the stiffness matrix* S_τ*. (I) if* $d > 1$*, then the multi-dimensional matrix of unknown solution* $\mathcal{U}$ *is explicitly obtained as*

$$\mathcal{U} = \sum_{n=\lceil 2\tau \rceil}^{\mathcal{N}} \sum_{m_1=\lceil 2\mu_1 \rceil}^{\mathcal{M}_1} \cdots \sum_{m_d=\lceil 2\mu_d \rceil}^{\mathcal{M}_d} \kappa_{n,m_1,\cdots,m_d}\ \vec{e}_n^{\tau} \otimes \vec{e}_{m_1}^{\mu_1} \otimes \cdots \otimes \vec{e}_{m_d}^{\mu_d}, \tag{9.54}$$

where the unknown $\kappa_{n,m_1,\cdots,m_d}$ *are given by*

$$\kappa_{n,m_1,\cdots,m_d} = \frac{(\vec{e}_n^{\tau}\, \vec{e}_{m_1}^{\mu_1} \cdots \vec{e}_{m_d}^{\mu_d})F}{\Big[(\vec{e}_n^{\tau^T} S_\tau \vec{e}_n^{\tau}) \prod_{j=1}^{d} (\vec{e}_{m_j}^{\mu_j^T} S_{\mu_j} \vec{e}_{m_j}^{\mu_j})\Big] \Lambda_{n,m_1,\cdots,m_d}}. \tag{9.55}$$

in which the numerator represents the standard multi-dimensional inner product, and $\Lambda_{n,m_1,\cdots,m_d}$ *are obtained in terms of the eigenvalues of all mass matrices as*

$$\Lambda_{n,m_1,\cdots,m_d} = \Big[(1+\gamma\ \lambda_n^{\tau}) \prod_{j=1}^{d} \lambda_{m_j}^{\mu_j} + \lambda_n^{\tau} \sum_{j=1}^{d} c_j\ (\prod_{s=1,s\neq j}^{d} \lambda_{m_s}^{\mu_s})\Big].$$

(II) If $d = 1$*, then the two-dimensional matrix of the unknown solution* $\mathcal{U}$ *is obtained as*

$$\mathcal{U} = \sum_{n=\lceil 2\tau \rceil}^{\mathcal{N}} \sum_{m_1=\lceil 2\mu_1 \rceil}^{\mathcal{M}_1} \kappa_{n,m_1}\ \vec{e}_n^{\tau}\ \vec{e}_{m_1}^{\mu_1^T},$$

where κ_{n,m_1} *is explicitly obtained as*

$$\kappa_{n,m_1} = \frac{\vec{e}_n^{\tau^T} F\, \vec{e}_{m_1}^{\mu_1}}{(\vec{e}_n^{\tau^T} S_\tau \vec{e}_n^{\tau})(\vec{e}_{m_1}^{\mu_1^T} S_{\mu_1} \vec{e}_{m_1}^{\mu_1}) \Big[\ \lambda_{m_1-1}^{\mu_1} \ +\ c_1\ \lambda_n^{\tau} \ +\ \gamma\ \lambda_n^{\tau} \lambda_{m_1}^{\mu_1}\Big]}.$$

Proof. Let us consider the following generalised eigenvalue problems

$$M_{\mu_j}\,\vec{e}_{m_j}^{\,\mu_j} \;=\; \lambda_{m_j}^{\mu_j}\,S_{\mu_j}\,\vec{e}_{m_j}^{\,\mu_j}, \quad m_j = \lceil 2\mu_j \rceil, \cdots, \mathcal{M}_j, \quad j = 1, 2, \cdots, d, \tag{9.56}$$

$$M_{\tau}\,\vec{e}_{n}^{\,\tau} \;=\; \lambda_{n}^{\tau}\,S_{\tau}\,\vec{e}_{n}^{\,\tau}, \quad n = \lceil 2\tau \rceil, 2, \cdots, \mathcal{N}. \tag{9.57}$$

We aim to represent the unknown coefficient matrix $\mathcal{U}$ in the expansion (9.49) in terms of the spatial and temporal eigenvectors as

$$\mathcal{U} = \sum_{n=\lceil 2\tau \rceil}^{\mathcal{N}} \sum_{m_1=\lceil 2\mu_1 \rceil}^{\mathcal{M}_1} \cdots \sum_{m_d=\lceil 2\mu_d \rceil}^{\mathcal{M}_d} \kappa_{n,m_1,\cdots,m_d}\;\vec{e}_{n}^{\,\tau} \otimes \vec{e}_{m_1}^{\,\mu_1} \otimes \cdots \otimes \vec{e}_{m_d}^{\,\mu_d}, \tag{9.58}$$

where the unknown $\kappa_{n,m_1,\cdots,m_d}$ are obtained as follows. We first take the multi-dimensional inner product of $\vec{e}_{q}^{\,\tau}\,\vec{e}_{p_1}^{\,\mu_1}\cdots\vec{e}_{p_d}^{\,\mu_d}$ on both sides of the Lyapunov equation (9.53) to obtain

$$\begin{aligned}(\,\vec{e}_{q}^{\,\tau}\,\vec{e}_{p_1}^{\,\mu_1}\,\vec{e}_{p_2}^{\,\mu_2}\cdots\vec{e}_{p_d}^{\,\mu_d})\Big[\; & S_{\tau}\otimes M_{\mu_1}\otimes\cdots\otimes M_{\mu_d} \\ & +\sum_{j=1}^{d} c_j\;[M_{\tau}\otimes M_{\mu_1}\otimes\cdots\otimes M_{\mu_{j-1}}\otimes S_{\mu_j}\otimes M_{\mu_{j+1}}\cdots\otimes M_{\mu_d}] \\ & +\gamma\; M_{\tau}\otimes M_{\mu_1}\otimes\cdots\otimes M_{\mu_d}\Big]\mathcal{U} = (\,\vec{e}_{q}^{\,\tau}\,\vec{e}_{p_1}^{\,\mu_1}\cdots\vec{e}_{p_d}^{\,\mu_d})F.\end{aligned}$$

Next, we substitute (9.58) and re-arrange the terms to obtain

$$\begin{aligned}
&\sum_{n=\lceil 2\tau\rceil}^{\mathcal{N}} \sum_{m_1=\lceil 2\mu_1\rceil}^{\mathcal{M}_1} \cdots \sum_{m_d=\lceil 2\mu_d\rceil}^{\mathcal{M}_d} \kappa_{n,m_1,\cdots,m_d} \\
&\Big(\vec{e}_q^{\,\tau^T} S_\tau \vec{e}_n^{\,\tau} \quad \vec{e}_{p_1}^{\,\mu_j^T} M_{\mu_1} \vec{e}_{m_1}^{\,\mu_j} \quad \cdots \quad \vec{e}_{p_d}^{\,\mu_j^T} M_{\mu_d} \vec{e}_{m_d}^{\,\mu_j} \\
+\sum_{j=1}^{d} c_j \; \vec{e}_q^{\,\tau^T} M_\tau \vec{e}_n^{\,\tau} \quad \vec{e}_{p_1}^{\,\mu_j^T} M_{\mu_1} \vec{e}_{m_1}^{\,\mu_j} \quad \cdots \quad \vec{e}_{p_j}^{\,\mu_j^T} S_{\mu_j} \vec{e}_{m_j}^{\,\mu_j} \quad \vec{e}_{p_{j+1}}^{\,\mu_{j+1}^T} M_{\mu_{j+1}} \vec{e}_{m_{j+1}}^{\,\mu_{j+1}} \quad \vec{e}_{p_d}^{\,\mu_j^T} M_{\mu_d} \vec{e}_{m_d}^{\,\mu_j} \\
+\gamma \; \vec{e}_q^{\,\tau^T} M_\tau \vec{e}_n^{\,\tau} \quad \vec{e}_{p_1}^{\,\mu_j^T} M_{\mu_1} \vec{e}_{m_1}^{\,\mu_j} \quad \vec{e}_{p_2}^{\,\mu_j^T} M_{\mu_2} \vec{e}_{m_2}^{\,\mu_j} \quad \cdots \quad \vec{e}_{p_d}^{\,\mu_j^T} M_{\mu_d} \vec{e}_{m_d}^{\,\mu_j} \Big) \\
&= (\, \vec{e}_q^{\,\tau} \, \vec{e}_{p_1}^{\,\mu_1} \, \vec{e}_{p_2}^{\,\mu_2} \cdots \vec{e}_{p_d}^{\,\mu_d}) F,
\end{aligned}$$

where we recall that $M_{\mu_j} \vec{e}_{m_j}^{\,\mu_j} = (\lambda_{m_j}^{\mu_j} S_{\mu_j} \vec{e}_{m_j}^{\,\mu_j})$ and $M_\tau \, \vec{e}_n^{\,\tau} = (\lambda_n^\tau \, S_\tau \, \vec{e}_n^{\,\tau})$. Hence,

$$\begin{aligned}
&\sum_{n=\lceil 2\tau\rceil}^{\mathcal{N}} \sum_{m_1=\lceil 2\mu_1\rceil}^{\mathcal{M}_1} \cdots \sum_{m_d=\lceil 2\mu_d\rceil}^{\mathcal{M}_d} \kappa_{n,m_1,\cdots,m_d} \\
&\Big(\vec{e}_q^{\,\tau^T} S_\tau \vec{e}_n^{\,\tau} \quad \vec{e}_{p_1}^{\,\mu_j^T} (\lambda_{m_1}^{\mu_1} S_{\mu_1} \vec{e}_{m_1}^{\,\mu_1}) \quad \vec{e}_{p_2}^{\,\mu_j^T} (\lambda_{m_2}^{\mu_2} S_{\mu_2} \vec{e}_{m_2}^{\,\mu_2}) \quad \cdots \quad (\lambda_{m_d}^{\mu_d} S_{\mu_d} \vec{e}_{m_d}^{\,\mu_d}) \\
+ \quad \sum_{j=1}^{d} c_j \; \vec{e}_q^{\,\tau^T} (\lambda_n^\tau \, S_\tau \, \vec{e}_n^{\,\tau}) \quad \vec{e}_{p_1}^{\,\mu_j^T} (\lambda_{m_1}^{\mu_1} S_{\mu_1} \vec{e}_{m_1}^{\,\mu_1}) \\
\cdots \quad \vec{e}_{p_j}^{\,\mu_j^T} S_{\mu_j} \vec{e}_{m_j}^{\,\mu_j} \quad \vec{e}_{p_{j+1}}^{\,\mu_{j+1}^T} (\lambda_{m_{j+1}}^{\mu_j+1} S_{\mu_{j+1}} \vec{e}_{m_{j+1}}^{\,\mu_{j+1}}) \cdots \vec{e}_{p_d}^{\,\mu_j^T} (\lambda_{m_d}^{\mu_d} S_{\mu_d} \vec{e}_{m_d}^{\,\mu_d}) \\
+ \quad \gamma \; \vec{e}_q^{\,\tau^T} (\lambda_n^\tau \, S_\tau \, \vec{e}_n^{\,\tau}) \quad \vec{e}_{p_1}^{\,\mu_j^T} (\lambda_{m_1}^{\mu_1} S_{\mu_1} \vec{e}_{m_1}^{\,\mu_1}) \quad \vec{e}_{p_2}^{\,\mu_j^T} (\lambda_{m_2}^{\mu_2} S_{\mu_2} \vec{e}_{m_2}^{\,\mu_2}) \; \cdots \; (\lambda_{m_d}^{\mu_d} S_{\mu_d} \vec{e}_{m_d}^{\,\mu_d}) \Big) \\
= \quad (\, \vec{e}_q^{\,\tau} \, \vec{e}_{p_1}^{\,\mu_1} \, \vec{e}_{p_2}^{\,\mu_2} \cdots \vec{e}_{p_d}^{\,\mu_d}) F.
\end{aligned}$$

or alternatively,

$$\begin{aligned}
&\sum_{n=\lceil 2\tau\rceil}^{\mathcal{N}} \sum_{m_1=\lceil 2\mu_1\rceil}^{\mathcal{M}_1} \cdots \sum_{m_d=\lceil 2\mu_d\rceil}^{\mathcal{M}_d} \kappa_{n,m_1,\cdots,m_d} \, (\vec{e}_q^{\,\tau^T} S_\tau \vec{e}_n^{\,\tau}) (\vec{e}_{p_1}^{\,\mu_j^T} S_{\mu_1} \vec{e}_{m_1}^{\,\mu_1}) \cdots (\vec{e}_{p_d}^{\,\mu_d^T} S_{\mu_d} \vec{e}_{m_d}^{\,\mu_d}) \\
&\times \Big[(1+\gamma \; \lambda_n^\tau) \prod_{j=1}^{d} \lambda_{m_j}^{\mu_j} + \lambda_n^\tau \sum_{j=1}^{d} c_j \; \Big(\prod_{s=1, s\neq j}^{d} \lambda_{m_s}^{\mu_s} \quad \Big) \Big] = (\, \vec{e}_q^{\,\tau} \, \vec{e}_{p_1}^{\,\mu_1} \, \vec{e}_{p_2}^{\,\mu_2} \cdots \vec{e}_{p_d}^{\,\mu_d}) F,
\end{aligned}$$

and since the spatial and temporal stiffness matrices S_{μ_j} and S_τ are diagonal (see Ap-

pendix), then $(\vec{e}_q^{\tau^T} S_\tau \vec{e}_n^{\tau}) = 0$ if $q \neq n$, also $(\vec{e}_{p_j}^{\mu_j^T} S_{\mu_j} \vec{e}_{m_j}^{\mu_j}) = 0$, if $p_j \neq m_j$, which completes the proof for the case $d > 1$. Following similar steps for the two-dimensional problem in the t-μ_1 domain, it is easy to see that if $d = 1$, the relationship for κ can be derived as

$$\kappa_{q,p_1} = \frac{\vec{e}_q^{\tau^T} F \, \vec{e}_{p_1}^{\mu_1}}{(\vec{e}_q^{\tau^T} S_\tau \vec{e}_q^{\tau})(\vec{e}_{p_1}^{\mu_1{}^T} S_{\mu_1} \vec{e}_{p_1}^{\mu_1}) \Big[\ \lambda_p^{\mu_1} \ + \ c_{\mu_1} \ \lambda_q^{\tau} + \gamma \ \lambda_q^{\tau} \lambda_p^{\mu_1} \Big]}. \tag{9.59}$$

□

Remark 9.3.7. If $\mu_j = \mu \neq \tau$ and $\mathcal{M}_j = \mathcal{M}$, $j = 1, 2, \cdots, d$, then the complexity of the calculations of (9.56) and (9.57) reduces to two linear generalised eigen-problems for space and time. Moreover, if $\mu = \tau$ and $\mathcal{M} = \mathcal{N}$, then we only need to solve a single one-dimensional eigen-problem $M_\mu \vec{e}_q = \lambda_q S_\mu \vec{e}_q$ once.

Remark 9.3.8. For time-independent (steady-state) problems, where the time-fractional derivative vanishes in (9.8), the same general framework holds. For such problems, the time-dependent basis and test functions in U_N and V_N consequently vanish, and we construct the d-dimensional basis space $\mathcal{U}_N$ in $\Omega = [a_1, b_1] \times \cdots \times [a_d, b_d]$ as

$$\mathcal{U}_N = span\Big\{ \prod_{j=1}^{d} \Big(\phi_{m_j}^{\mu_j} \circ \xi_j \Big)(x_j) \ : \ m_j = \lceil 2\mu_j \rceil, \ldots, \mathcal{M}_j \Big\}, \tag{9.60}$$

where we seek the solution in terms of elements in the space $\mathcal{U}_N$ of the form

$$u_N(\mu_1, \cdots, \mu_d) = \sum_{m_1 = \lceil 2\mu_1 \rceil}^{\mathcal{M}_1} \cdots \sum_{m_d = \lceil 2\mu_d \rceil}^{\mathcal{M}_d} \hat{u}_{m_1, \cdots, m_d} \prod_{j=1}^{d} \Big(\phi_{m_j}^{\mu_j} \circ \xi_j \Big)(x_j) \tag{9.61}$$

and test the problem against the elements in

$$\mathcal{V}_N = span\Big\{ \prod_{j=1}^{d} \Big(\Phi_{k_j}^{\mu_j} \circ \xi_j \Big)(x_j) \ : \ k_j = \lceil 2\mu_j \rceil, \ldots, \mathcal{M}_j \Big\}. \tag{9.62}$$

Subsequently, we obtain a similar Lyapunov equation as in (9.53) where M_τ no longer appears, however, M_{μ_j} and S_{μ_j} possess all the properties presented in Theorems (C.7.1) and (C.7.3) in Appendix.

Lemma 9.3.9. *If $d > 1$, in the absence of the fractional time-derivative in* (9.8)*, i.e., when S_τ vanishes, we obtain the matrix of unknown solution $\mathcal{U}$ in* (9.61) *as*

$$\mathcal{U} = \sum_{m_1=\lceil 2\mu_1 \rceil}^{\mathcal{M}_1} \cdots \sum_{m_d=\lceil 2\mu_d \rceil}^{\mathcal{M}_d} \kappa_{m_1,\cdots,m_d}\ \vec{e}_{m_1}^{\,\mu_1} \otimes \cdots \otimes \vec{e}_{m_d}^{\,\mu_d},$$

where the unknown $\kappa_{m_1,\cdots,m_d}$ is given by

$$\kappa_{m_1,\cdots,m_d} = \frac{(\vec{e}_{m_1}^{\,\mu_1} \cdots \vec{e}_{m_d}^{\,\mu_d})F}{\Big[\prod_{j=1}^{d}(\vec{e}_{m_j}^{\,\mu_j^T} S_{\mu_j} \vec{e}_{m_j}^{\,\mu_j})\Big]\Big[\gamma \prod_{j=1}^{d} \lambda_{m_j}^{\mu_j} + \sum_{j=1}^{d} c_j\ (\prod_{s=1,s\neq j}^{d} \lambda_{m_s}^{\mu_s}\ \ )\Big]}. \quad (9.63)$$

Proof. It follows the proof in Theorem 9.3.6. □

9.3.6 Computational Considerations

In Theorem 9.3.6, we assume that the eigenvectors and eigenvalues of each mass matrix with respect to the corresponding stiffness matrices are known. Therefore, employing the PG spectral method in a $(1 + d)$-dimensional problem when $(1 + d) \geq 2$ leads to efficient computations. Otherwise, the computational cost of the eigensolver, which is $\mathcal{O}(N^3)$ in practice, becomes dominant. As we shall demonstrate, this approach appears to be even more beneficial as $(1 + d)$ increases. In fact, the cost of the fast FPDE solver is associated with the following two steps: (i) the computation of $\kappa_{n,m_1,\cdots,m_d}$ in (9.55), and (ii) the cost of representing $\mathcal{U}$ in (9.54). In what follows, we show that the computational complexity of mathematical operations in our PG spectral method is $\mathcal{O}(N^{2+d})$, the dimension of the space-time domain Ω,

and if we assume $\mathcal{N} = \mathcal{M}_1 = \cdots = \mathcal{M}_d$.

Step (i): In order to compute the $(1+d)$-dimensional array κ in (9.55), we need to first calculate the numerator

$$(\vec{e}_q^{\,\tau}\, \vec{e}_{p_1}^{\,\mu_1} \cdots \vec{e}_{p_d}^{\,\mu_d})F = \sum_{i=\lceil 2\tau \rceil}^{\mathcal{N}} \sum_{s_1=\lceil 2\mu_1 \rceil}^{\mathcal{M}_1} \cdots \sum_{s_d=\lceil 2\mu_d \rceil}^{\mathcal{M}_d} \{\vec{e}_q^{\,\tau}\}_i \{\vec{e}_{p_1}^{\,\mu_1}\}_{s_1} \cdots \{\vec{e}_{p_d}^{\,\mu_d}\}_{s_d} \{F\}_{i,s_1,\cdots,s_d}, \tag{9.64}$$

for which naive computations for all the entries leads to a computational complexity $\mathcal{O}(N^{2(1+d)})$ that can be intractable when d increases. Alternatively, by performing *sum-factorization* (see [76]), the operation counts can be reduced to $\mathcal{O}(N^{2+d})$, including the *time-dimension* in our calculations. Following this technique we re-write the inner-product as

$$\begin{aligned} (\vec{e}_q^{\,\tau}\, \vec{e}_{p_1}^{\,\mu_1} \cdots \vec{e}_{p_d}^{\,\mu_d})F \quad &= \\ \sum_{i=\lceil 2\tau \rceil}^{\mathcal{N}} \{\vec{e}_q^{\,\tau}\}_i \sum_{s_1=\lceil 2\mu_1 \rceil}^{\mathcal{M}_1} \{\vec{e}_{p_1}^{\,\mu_1}\}_{s_1} \quad \cdots \quad &\sum_{s_{d-1}=\lceil 2\mu_{d-1} \rceil}^{\mathcal{M}_{d-1}} \{\vec{e}_{p_{d-1}}^{\,\mu_{d-1}}\}_{s_{d-1}} \sum_{s_d=\lceil 2\mu_d \rceil}^{\mathcal{M}_d} \{\vec{e}_{p_d}^{\,\mu_d}\}_{s_d} \{F\}_{i,s_1,\cdots,s_d}, \end{aligned} \tag{9.65}$$

in which we separately obtain the inner-most sum as

$$\mathcal{F}^d_{i,s_1,\cdots,s_{d-1},p_d} = \sum_{s_d=\lceil 2\mu_d \rceil}^{\mathcal{M}_d} \{\vec{e}_{p_d}^{\,\mu_d}\}_{s_d} \{F\}_{i,s_1,\cdots,s_d}, \tag{9.66}$$

and similarly we write the second inner-most sum as

$$\mathcal{F}^{d-1}_{i,s_1,\cdots,s_{d-2},p_{d-1},p_d} = \sum_{s_{d-1}=\lceil 2\mu_{d-1} \rceil}^{\mathcal{M}_{d-1}} \{\vec{e}_{p_{d-1}}^{\,\mu_{d-1}}\}_{s_{d-1}} \mathcal{F}^d_{i,s_1,\cdots,s_{d-1},p_d}. \tag{9.67}$$

Finally, we recursively obtain

$$\mathcal{F}^1_{i,p_1,\cdots,p_d} = \sum_{s_1=\lceil 2\mu_1 \rceil}^{\mathcal{M}_1} \{\vec{e}_{p_1}^{\,\mu_1}\}_{s_1} \mathcal{F}^2_{i,p_1,p_2,\cdots,p_d}. \tag{9.68}$$

We note that the operation count in computing the entries of $\mathcal{F}^{j}_{i,s_1,\cdots,s_{j-1},p_j,\cdots,p_d}$ in each recursion is $\mathcal{O}(N^{2+d})$. Now, by substituting (9.68) back into (9.65), we obtain the whole inner-product as

$$(\vec{e}_q^{\,\tau}\,\vec{e}_{p_1}^{\,\mu_1}\cdots\vec{e}_{p_d}^{\,\mu_d})F=\sum_{i=\lceil 2\tau\rceil}^{\mathcal{N}}\{\vec{e}_q^{\,\tau}\}_i\mathcal{F}^{1}_{i,p_1,\cdots,p_d}, \tag{9.69}$$

which is again of complexity $\mathcal{O}(N^{2+d})$. We observe that the total computational complexity of evaluating the inner product is $\mathcal{O}(N^{2+d})$. Moreover, the operation count for computing the denumerator in (9.55) and for each entry of $\kappa_{n,m_1,\cdots,m_d}$ is $\mathcal{O}(N)$. This is true since the stiffness matrix is either *diagonal* or *tridiagonal* due to the choice of our poly-fractonomial bases. Hence, the total complexity for computing the denumerator is again $\mathcal{O}(N^{2+d})$. We recall that we have already included the time-dimension into account, i.e., the space-time domain $\Omega\subset\mathbb{R}^{1+d}$. Hence, κ in (9.55) is obtained with cost $\mathcal{O}(N^{2+d})$.

Step (ii): In the computation of (9.54), we observe that sum-factorization technique helps to reduce the complexity to $\mathcal{O}(N^{2+d})$.

9.4 Special FPDEs and Numerical Tests

In section 9.3, we introduced general $(1+d)$-dimensional linear FPDEs, for which we developed a general Petrov-Galerkin spectral method in addition to the general fast solver. Here, we reduce this general framework to the special well-known (i) *hyperbolic* FPDEs such as the fractional advection equation, (ii) *parabolic* FPDEs such as the fractional sub-diffusion problems, and (iii) *elliptic* FPDEs such as the fractional Helmholtz/Poisson equations. In the following numerical examples, we carry out the

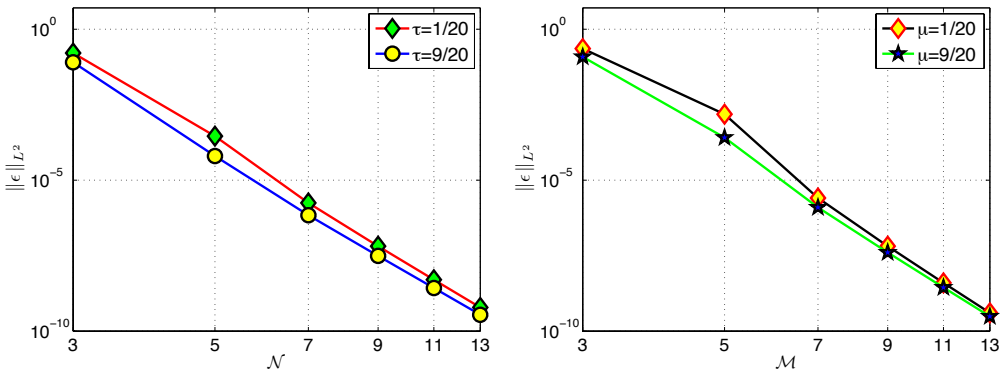

Figure 9.1: TSFA, temporal/spatial *p-refinement*: log-log L^2-error versus temporal and spatial expansion orders $\mathcal{N}$, $\mathcal{M}$. In the temporal p-refinement $\tau = 1/20$ and $9/20$ while $\mu = 1/4$, also in the spatial p-refinement, the spatial orders $\mu = 1/20$ and $9/20$ while $\tau = 1/4$. Here, the exact solution is $u^{ext}(x,t) = t^{6+2/7}\,(1+x)^{6+3/4}$.

spatial/temporal p-refinement test via fixing correspondingly the temporal/spatial expansion order fixed at 15.

9.4.1 Hyperbolic FPDEs

We consider the following hyperbolic FPDE

$$ {}_0\mathcal{D}_t^{2\tau} u(t,x) + c_x\,[\,{}_{-1}\mathcal{D}_x^{2\mu} u(t,x)\,] \;=\; f(t,x), \quad (t,x) \in [0,T]\times[-1,1], \quad (9.70) $$

subject to $u(x,0) = 0$ and $u(-1,t) = 0$ when $\tau, \mu \in (0, 1/2]$. In this case, the FPDE (9.70) appears as Time- and Space-Fractional Advection (TSFA) equation, where we set $c_x = 1$. We then seek the solution to (9.70) in terms of a linear combination of elements in U_N, now consisting of only two dimensions, i.e., time t and space x, of the form

$$ u_N(t,x) = \sum_{n=\lceil 2\tau\rceil}^{\mathcal{N}} \sum_{m=\lceil 2\mu\rceil}^{\mathcal{M}} \hat{u}_{n,m} \Big(\psi_n^{\tau} \circ \eta\Big)(t)\,\Big(\phi_m^{\mu} \circ \xi\Big)(x). \quad (9.71) $$

Next, we obtain the corresponding linear system of the Lyapunov equation after carrying out the Kronecker product as

$$S_\tau \, \mathcal{U} \, M_\mu + M_\tau \, \mathcal{U} \, S_\mu = F, \tag{9.72}$$

where we represent the unknown coefficient matrix $\mathcal{U}$ in terms of the spatial and temporal eigenvectors as

$$\mathcal{U} = \sum_{q=\lceil 2\tau \rceil}^{\mathcal{N}} \sum_{p=\lceil 2\mu \rceil}^{\mathcal{M}} \kappa_{q,p} \, \vec{e}_q^{\,\tau} \, \vec{e}_p^{\,\mu^T}, \tag{9.73}$$

for which $\kappa_{q,p}$ is followed by (9.59) setting $\gamma = 0$ as

$$\kappa_{q,p} = \frac{\vec{e}_q^{\,\tau^T} \, F \, \vec{e}_p^{\,\mu}}{(\, \vec{e}_q^{\,\tau^T} S_\tau \, \vec{e}_q^{\,\tau}) \cdot (\vec{e}_p^{\,\mu^T} S_\mu \, \vec{e}_p^{\,\mu}) \cdot (c_1 \; \lambda_q^\tau \; + \; \lambda_p^\mu)}. \tag{9.74}$$

In Fig. 9.1, we examine the TSFA problem (9.70) and study the p-refinement in both the temporal (left) and the spatial (right) dimensions. To demonstrate the spectral convergence of the PG spectral method, we plot the log-log L^2-error versus temporal and spatial expansion orders $\mathcal{N}$, $\mathcal{M}$. In the temporal p-refinement $\tau = 1/20$ and $9/20$ while $\mu = 1/4$; also in the spatial p-refinement, the spatial orders $\mu = 1/20$ and $9/20$ while $\tau = 1/4$. In this test, we set the simulation time to $T = 1$, while the exact solution is $u^{ext}(x,t) = t^{6+2/7} \, (1+x)^{6+3/4}$.

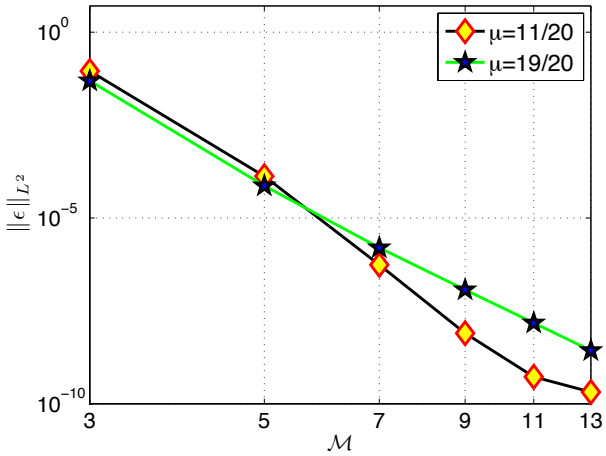

Figure 9.2: TSFD, spatial *p-refinement*: log-log L^2-error versus spatial expansion orders M. Here, the spatial orders $\mu = 11/20$ and $19/20$ while $\tau = 1/4$, and the exact solution is $u^{ext}(x,t) = t^{6+2/7}\,[\,(1+x)^{6+3/4} - 2^{38/35}\,(1+x)^{5+1/2}]$.

9.4.2 Parabolic FPDEs

First, we consider the following parabolic Time- and Space- Fractional Diffusion (TAFD) equation

$$\begin{aligned} {}_0\mathcal{D}_t^{2\tau} u(x,t) &= K\ {}_{-1}\mathcal{D}_x^{2\mu} u(x,t) + f(x,t), \quad (x,t) \in [0,T] \times [-1,1], \quad (9.75) \\ u(x,0) &= 0, \\ u(\pm 1,t) &= 0, \end{aligned}$$

where $\tau \in (0, 1/2]$, $\mu \in (1/2, 1)$, $K > 0$, which is a well-known model for anomalous *sub-diffusion* process. In this case, we seek the solution also of the form (9.71), and obtain a similar linear system as in (9.72), and hence we obtain

$$\kappa_{q,p} = \frac{\vec{e}_q^{\,\tau^T}\, F\, \vec{e}_p^{\,\mu}}{(\,\vec{e}_q^{\,\tau^T} S_\tau\, \vec{e}_q^{\,\tau}) \cdot (\vec{e}_p^{\,\mu^T} S_\mu\, \vec{e}_p^{\,x}) \cdot (\lambda_p^{\mu} - K\ \lambda_q^{\tau})}. \quad (9.76)$$

for $p = \lceil 2\tau \rceil, \cdots, \mathcal{N}$ and $q = \lceil 2\mu \rceil, \cdots, \mathcal{M}$. In Fig. 9.2, we solve the TSFD problem (9.75) and study the p-refinement in the spacial dimension. We plot the log-log L^2-

error versus the spatial expansion order $\mathcal{M}$. Similarly, in the spatial p-refinement, the spatial orders $\mu = 11/20$ and $19/20$ while $\tau = 1/4$. In both cases, the spectral convergence of the solution is achieved. Since, the exact solution is fixed in each case, the convergence rate corresponding to $\mu = 11/20$ appears to be larger than the case where $\mu = 19/20$ as expected. It is naturally due to the higher regularity requirement in the weak form corresponding to the second test-case. In the temporal p-refinement similar results were observed as in Fig.9.1 (left).

9.4.3 Elliptic FPDEs

We examine the well-known *elliptic Helmholtz/Poisson* equations, rendered fractional in two-dimensional (in space) domains. We choose the spatial computational domain as $\Omega = [-1, 1] \times [-1, 1]$, and consider the following problem

$$\begin{aligned} {}_{-1}\mathcal{D}_{x_1}^{2\mu_1} u(x_1, x_2) + {}_{-1}\mathcal{D}_{x_2}^{2\mu_2} u(x_1, x_2) + \gamma\, u(x_1, x_2) &= f(x_1, x_2), \quad \textit{in } \Omega, \\ u(x_1, x_2) &= 0, \quad \textit{on } \partial\Omega \end{aligned} \tag{9.77}$$

where $\gamma > 0$, $\mu_1, \mu_2 \in (1/2, 1)$, which reduces to the Space-Fractional Poisson equation when $\gamma = 0$. Here, we present a general scheme in addition to a linear fast solver for both problems.

We then seek the solution to (9.77) in terms of a linear combination of elements in U_N in absence of the time-basis, consisting of only two dimensions of the form

$$u_N(x_1, x_2) = \sum_{m_1=2}^{\mathcal{M}_1} \sum_{m_2=2}^{\mathcal{M}_2} \hat{u}_{m_1,m_2} \Big(\phi_{m_1}^{\mu_1} \circ \xi_1\Big)(x_1) \Big(\phi_{m_2}^{\mu_2} \circ \xi_2\Big)(x_2), \tag{9.78}$$

for which we represent the unknown coefficient matrix $\mathcal{U}$ in terms of the spatial

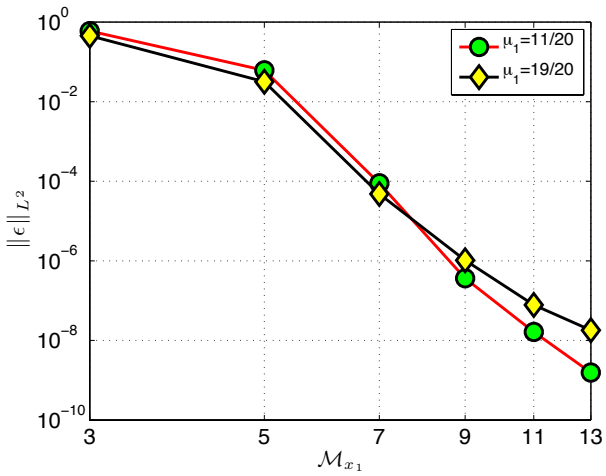

Figure 9.3: Space-fractional Helmholtz problem with $\gamma = 1$, spatial *p-refinement* in x-dimension: log-log L^2-error versus spatial expansion orders $\mathcal{M}_{x_1}$. Here, the spatial orders are $\mu_1 = 11/20$ and $19/20$ while $\mu_2 = 15/20$, is kept constant. The exact solution is $u^{ext}(x_1, x_2) = [\,(1+x_1)^{6+3/4} - 2^{5/4}\,(1+x_1)^{5+1/2}][\,(1+x_2)^{6+4/9} - 2^{73/63}\,(1+x_2)^{5+2/7}]$. A similar convergence curve is achieved in the p-refinement performed in the y-dimension, also for the case of $\gamma = 0$.

eigenvectors as

$$\mathcal{U} = \sum_{p_1=2}^{\mathcal{M}_1} \sum_{p_2=2}^{\mathcal{M}_2} \kappa_{p_1,p_2}\, \vec{e}_{p_1}^{\,\mu_1}\, \vec{e}_{p_2}^{\,\mu_2{}^T}, \tag{9.79}$$

where

$$\kappa_{p_1,p_2} = \frac{\vec{e}_{p_1}^{\,\mu_1{}^T}\, G\, \vec{e}_{p_2}^{\,\mu_2}}{(\vec{e}_{p_1}^{\,\mu_1{}^T} S_{\mu_1}\, \vec{e}_{p_1}^{\,\mu_1}) \cdot (\,\vec{e}_{p_2}^{\,\mu_2{}^T} S_{\mu_2}\, \vec{e}_{p_2}^{\,\mu_2}) \cdot (\,\lambda_{p_1}^{\mu_1} \,+\, \lambda_{p_2}^{\mu_2} \,+\, \gamma\, \lambda_{p_1}^{\mu_1}\, \lambda_{p_2}^{x_2}\,)}. \tag{9.80}$$

In Fig. 9.3, we solve the fractional Helmholzt problem (9.77) and study the p-refinement in the spacial x_1-dimension. To demonstrate the spectral convergence of the fast FPDE solver, we plot the log-log L^2-error versus the spatial expansion order $\mathcal{M}_{x_1}$. The spatial orders $\mu_1 = 11/20$ and $19/20$ while $\mu_2 = 15/20$. Similar to the spatial p-convergence in Fig.9.2, the convergence rate corresponding to $\mu_1 = 11/20$ appears to be larger than the case where $\mu_2 = 19/20$. We observe a similar p-refinement in the x_2-dimension as well.

9.4.4 Higher-Dimensional FPDEs

Next, we employ our PG method and the fast solver in even higher dimensional problems to exhibit the generality and efficiency of the scheme. In Table 9.1, the convergence results and CPU time of the unified PG spectral method in higher-dimensional problems are examined. Particularly, we employ this scheme to solve the time- and space- fractional advection equation (TSFA)

$$ {}_0\mathcal{D}_t^{2\tau} u + {}_{-1}\mathcal{D}_{x_1}^{2\mu_1} u + {}_{-1}\mathcal{D}_{x_2}^{2\mu_2} u + \cdots + {}_{-1}\mathcal{D}_{x_d}^{2\mu_d} u = f, $$

where $2\tau = 2\mu_j = 1/2$, subject to homogeneous Dirichlet boundary conditions in a four-dimensional (4-D), six-dimensional (6-D), and ten-dimensional (10-D) *space-time* hypercube domains. The error is measured by the essential norm $\|\epsilon\|_{L^\infty} = \|u - u^{ext}\|_{L^\infty}/\|u^{ext}\|_{L^\infty}$, which is stronger than the L^2-norm and is normalized by the essential norm of the exact solution $u^{ext}(t, \vec{x}) = [t\prod_{j=1}^{d}(1 + x_j)]^{2+2/5}$ for the sake of consistency. The CPU time (seconds) is measured on a single core Intel (Xeon X5550) 2.67GHz processor. In each step of the p-refinement, we uniformly increase the bases order by one in all dimensions. All the computations are performed in Mathematica 8. These simulations highlight that the unified PG spectral method is efficient even for a 10-D problem run on a PC in less than an hour!

9.4.5 Time-integration when $2\tau = 1$

We recall that our unified PG spectral method works equally well when the temporal time-derivative order $2\tau = 1$. In general, a first-order in time PDE/FPDE reads

$$ \frac{\partial u}{\partial t} = F(u; t, x_1, \cdots, x_d), \tag{9.81} $$

Table 9.1: Convergence study and CPU time of the unified PG spectral method employed in the time- and space- fractional advection equation (TSFA) ${}_0\mathcal{D}_t^{2\tau} u + \sum_{j=1}^{d} [{}_{-1}\mathcal{D}_{x_j}^{2\mu_j} u] = f$, where $2\tau = 2\mu_j = 1/2$, $j = 1, 2, \cdots, d$, subject to homogeneous Dirichlet boundary conditions in four-dimensional (4-D), six-dimensional (6-D), and ten-dimensional (10-D) *space-time* hypercube domains, where $D = 1 + d$. The error is measured by the essential norm $\|\epsilon\|_{L^\infty} = \|u - u^{ext}\|_{L^\infty} / \|u^{ext}\|_{L^\infty}$, which is normalized by the essential norm of the exact solution $u^{ext}(t, \vec{x}) = [t \prod_{j=1}^{d} (1 + x_j)]^{2+2/5}$, where $t \in [0, 1]$ and $x \in [-1, 1]^d$. The CPU time (seconds) is obtained on a Intel (Xeon X5550) 2.67GHz processor. In each step, we uniformly increase the bases order by one in all dimensions.

4-D TSFA

$\mathcal{N} = \mathcal{M}_1 = \cdots = \mathcal{M}_d$	$\|\epsilon\|_{L^\infty}$	CPU Time (seconds)
2	0.576869	0.006333
3	0.034706	0.015997
4	0.003990	0.041994
5	0.0009071	0.105984

6-D TSFA

$\mathcal{N} = \mathcal{M}_1 = \cdots = \mathcal{M}_d$	$\|\epsilon\|_{L^\infty}$	CPU Time (seconds)
2	0.741056	0.014748
3	0.055171	0.134313
4	0.006578	0.821208
5	0.001525	3.546791

10-D TSFA

$\mathcal{N} = \mathcal{M}_1 = \cdots = \mathcal{M}_d$	$\|\epsilon\|_{L^\infty}$	CPU Time (seconds)
2	0.903357	0.288956
3	0.095305	18.45320
4	0.0119229	370.1 ($\approx$ 6 min)
5	0.0028102	3332.4 ($\approx$ 55 min)

where the operator $F(u;t,x_1,\cdots,x_d)$ is given as

$$F(u;t,x_1,\cdots,x_d) = f(t,x_1,\cdots,x_d) - \sum_{j=1}^{d} c_j[\ {}_{a_j}\mathcal{D}_{x_j}^{2\mu_j} u\ ] + \gamma\ u,$$

in view of (9.8). Here, we regard the PG method as an alternative scheme for *spectrally* accurate time-integration for a general $F(u;t,x_1,\cdots,x_d)$, rather than utilizing existing *algebraically* accurate methods, including *multi-step* methods such as the Adams family and stiffly-stable schemes, also *multi-stage* approaches such as the Runge-Kutta method.

The idea of employing the PG spectral method when $2\tau = 1$ is simply based on the useful property (9.5) by which a full first-order derivative d/dt can be decomposed into a product of the sequential $(\frac{1}{2})$-th order derivatives ${}_0\mathcal{D}_t^{1/2}\ {}_0\mathcal{D}_t^{1/2}$, a result that is not valid in the standard (integer-order) calculus. Hence, by virtue of the *fractional* integration-by-parts, such a decomposition artificially induces *non-locality* to the temporal term in the corresponding weak form. Therefore, it provides an appropriate framework for *global* (spectral) treatment of the temporal term using our unified PG spectral method. To this end, we carry out the time-integration when $2\tau = 1$ in the following FPDE

$$\partial u/\partial t + \sum_{j=1}^{3} {}_{-1}\mathcal{D}_{x_j}^{2\mu_j} u = f$$

in $\Omega \subset \mathbb{R}^{1+3}$, where in general $\mu_j \in (0,1)$. Here, we set $\mu_j = 1/2$ for simplicity, which recovers the standard time-dependent advection equation in three-dimensional spatial domain.

In Table 9.2, we again measure the error by the normalized essential norm, where the exact solution is $u^{ext}(t,\vec{x}) = [t\prod_{j=1}^{3}(1+x_j)]^{6+2/5}$, where $t \in [0,1]$ and $x_j \in [-1,1]$, $j = 1,2,3$. Similar to the previous case, the CPU time (seconds) is obtained on a

Table 9.2: Time-Integration when $2\tau = 1$: $\partial u/\partial t + \sum_{j=1}^{3} [{}_{-1}\mathcal{D}_{x_j}^{2\mu_j} u] = f$ in $\Omega \subset \mathbb{R}^{1+3}$, where $t \in [0,1]$ and $x_j \in [-1,1]$, $j = 1,2,3$. Here, we set $\mu_j = 1/2$ to fully recover the standard time-dependent advection equation in three-dimensional spatial domain. However, in general $\mu_j \in (0,1)$. The error is measured by the essential norm $\|\epsilon\|_{L^\infty} = \|u - u^{ext}\|_{L^\infty} / \|u^{ext}\|_{L^\infty}$, which is normalized by the essential norm of the exact solution is $u^{ext}(t,\vec{x}) = [t \prod_{j=1}^{3}(1+x_j)]^{6+2/5}$. The CPU time (seconds) is obtained on a Intel (Xeon X5550) 2.67GHz processor. In each step, we uniformly increase the bases order by one in all dimensions.

Integer-Order Time-Integration

$\mathcal{N} = \mathcal{M}_1 = \mathcal{M}_2 = \mathcal{M}_3$	$\|\epsilon\|_{L^\infty}$	CPU Time (seconds)
3	0.6225970	0.051992
5	0.0336570	0.352947
7	1.34×10^{-5}	1.9737
9	1.06×10^{-7}	3.7894
11	3.52×10^{-9}	9.7365
13	2.54×10^{-10}	21.472

single-core Intel (Xeon X5550) 2.67GHz processor, where we uniformly increase the bases order by one in all dimensions in each step. In these simulations, we globally treat the time-axis in addition to other spatial dimensions. The CPU time and the spectral convergence strongly highlights the efficiency of our approach, where a 4-D problem (i.e., 1-D in time and 3-D in space) can be highly accurately solved in a fraction of minute!

9.5 Discussion

In practice, the enforcement of *periodic* boundary conditions to FPDEs is not possible since it is not clear how to define history (memory) for a periodic function. Moreover, we note that Riemann-Liouville fractional derivatives in time/space only allow us to impose homogeneous initial/boundary conditions to the corresponding FPDEs to be wellposed. However, we note that our PG spectral method is also applicable in

such problems in the following manner. When inhomogeneous Dirichlet conditions are enforced, the corresponding derivatives are usually replaced by *Caputo* fractional derivatives. We illustrate such a treatment in the following model problem posed subject to an inhomogeneous initial condition:

$$\begin{aligned} {}_0^C\mathcal{D}_t^{2\tau} u &= {}_{-1}\mathcal{D}_x^{2\mu} u + f(x,t), \\ u(x,0) &= g(x), \\ u(\pm 1, t) &= 0, \end{aligned} \tag{9.82}$$

in which $2\mu \in (1,2)$, $g(x) \in C^0([-1,1])$, and ${}_0^C\mathcal{D}_t^{2\tau}(\cdot)$ denotes the Caputo fractional derivative of order $2\tau \in (0,1)$, which is defined via interchanging the order of differentiation and integration in (9.3), see e.g., [142]. Now, we define $U(x,t) = u(x,t) - g(x)$, and taking into account that ${}_0^C\mathcal{D}_t^{2\tau} g(x) \equiv 0$. Then, by substituting $u = U + g$ into (9.82) and noting that ${}_0^C\mathcal{D}_t^{2\tau} U = {}_0\mathcal{D}_t^{2\tau} U$ due to the homogeneity of $U(x,0)$, we obtain the transformed problem as

$$\begin{aligned} {}_0\mathcal{D}_t^{2\tau} U &= {}_{-1}\mathcal{D}_x^{2\mu} U + \widetilde{f}(x,t), \\ U(x,0) &= 0, \\ U(\pm 1, t) &= 0, \end{aligned} \tag{9.83}$$

in which $\widetilde{f}(x,t) = f(x,t) + {}_{-1}\mathcal{D}_x^{2\mu} g(x)$. Therefore, we can treat such inhomogeneous conditions by our unified PG spectral method through homogenizing the problem and modifying the forcing term on the right-hand side. The same approach applies to inhomogeneous boundary conditions.

Chapter Ten

Distributed-Order Fractional Differential Equation

10.1 Background

Distributed-order fractional operators offer a rigorous tool for mathematical modelling of multi-physics phenomenon, in which the differential orders is distributed over a range of values rather than being just a fixed integer as it is in standard ODEs/PDEs [12, 35, 34]. There is a rapidly growing interest in the use of fractional derivatives in the construction of mathematical models which contain distributed order terms of the form

$$\int_{\sigma_1}^{\sigma_2} \phi(\sigma)\, {}_a^*\mathcal{D}_t^\sigma u(t) d\sigma = f(t), \quad t > a,$$

in papers [118, 52, 7, 8, 162], which show the range of potential applications of distributed order differential equations. Almost all of the numerical schemes developed for such models are of finite-difference methods. While the treatment of fractional differential equation with a fixed fractional order could be memory demanding due to the locality of these methods and their low-accuracy, the main challenge remains as the additional effect of distributive character of the differential order. This may lead to exceedingly growing cost (memory and CPU time) in simulation of such mathematical models.

We develop a spectrally-accurate fractional spectral collocation method for distributed fractional differential equations. This scheme is developed based on the recent spectral theory for fractional Sturm-Liouville problems (FSLPs), which has been recently developed in [187]. In the collocation scheme, We employ fractional Lagrange interpolants, which satisfy the Kronecker delta property at collocation points. Subsequently, we obtain the corresponding fractional differentiation matrices.

10.2 Definitions

We consider the standard domain $\xi \in [-1, 1]$. Then, the left-sided and right-sided Riemann-Liouville integrals of order σ, $n-1 < \sigma \leq n$, $n \in \mathbb{N}$, are defined (see e.g., [128, 142]), respectively, as

$$({}^{RL}_{-1}\mathcal{I}^{\sigma}_{\xi})u(\xi) = \frac{1}{\Gamma(n-\sigma)} \int_{-1}^{\xi} \frac{u(s)ds}{(\xi - s)^{1-\sigma}}, \quad \xi > -1. \tag{10.1}$$

The corresponding left-sided fractional derivatives of order σ are then defined, respectively, as

$$({}^{RL}_{-1}\mathcal{D}^{\sigma}_{\xi})u(\xi) = \frac{d^n}{d\xi^n}({}^{RL}_{-1}\mathcal{I}^{n-\sigma}_{\xi}u)(\xi) = \frac{1}{\Gamma(n-\sigma)} \frac{d^n}{dx^n} \int_{-1}^{\xi} \frac{u(s)ds}{(\xi - s)^{\sigma+1-n}}, \quad \xi > -1, \tag{10.2}$$

We recall a useful property of the Riemann-Liouville fractional derivatives. Assume that $0 < p < 1$ and $0 < q < 1$ and $g(x_L) = 0 \;\; x > x_L$, then

$${}_{x_L}\mathcal{D}^{p+q}_{x} g(x) = \left({}_{x_L}\mathcal{D}^{p}_{x}\right) \left({}_{x_L}\mathcal{D}^{q}_{x}\right) g(x) = \left({}_{x_L}\mathcal{D}^{q}_{x}\right) \left({}_{x_L}\mathcal{D}^{p}_{x}\right) g(x). \tag{10.3}$$

An alternative approach in defining the tempered fractional derivatives is to begin with the left-sided Caputo derivatives of order σ, $n-1 < \sigma \leq n$, $n \in \mathbb{N}$, defined respectively, as

$$({}^{C}_{-1}\mathcal{D}^{\sigma}_{\xi}u)(\xi) = ({}_{-1}\mathcal{I}^{n-\sigma}_{\xi} \frac{d^n u}{d\xi^n})(\xi) = \frac{1}{\Gamma(n-\mu)} \int_{-1}^{\xi} \frac{u^{(n)}(s)ds}{(\xi - s)^{\sigma+1-n}}, \quad \xi > -1. \tag{10.4}$$

By performing an affine mapping from the standard domain $[-1, 1]$ to the interval

$t \in [a, b]$, we obtain

$$
\begin{aligned}
{}^{RL}_{a}\mathcal{D}^{\sigma}_{t} u &= (\frac{2}{b-a})^{\sigma} ({}^{RL}_{-1}\mathcal{D}^{\sigma}_{\xi}) u(\xi), && (10.5)\\
{}^{C}_{a}\mathcal{D}^{\sigma}_{t} u &= (\frac{2}{b-a})^{\sigma} ({}^{C}_{-1}\mathcal{D}^{\sigma}_{\xi}) u(\xi), && (10.6)
\end{aligned}
$$

which help perform the operations in the standard domain only once for any given σ and efficiently utilize them on any arbitrary interval without resorting to repeat the calculations. Moreover, the corresponding relationships between the Riemann-Liouville and Caputo fractional derivatives in $[a, b]$ for any $\sigma \in (0, 1)$ are given by

$$
({}^{RL}_{a}\mathcal{D}^{\sigma}_{t}) u(t) = \frac{u(a)}{\Gamma(1-\sigma)(t-a)^{\sigma}} + ({}^{C}_{a}\mathcal{D}^{\sigma}_{t}) u(t). \tag{10.7}
$$

Next, following [6], we define the distributed fractional derivative. Let $f \in AC^{2}_{loc}([x_L, \infty))$. Then, the two forms of the distributed order fractional derivatives are defined.

(i) Let $\sigma \mapsto \phi(\sigma)$ be a continuous mapping in $[\sigma_1, \sigma_2]$, then we define the distributed-order fractional derivative as

$$
{}^{D}\mathcal{D}_{\phi} u(t) = \int_{\sigma_1}^{\sigma_2} \phi(\sigma)\, {}^{*}_{a}\mathcal{D}^{\sigma}_{t} u(t) d\sigma, \quad t > a, \tag{10.8}
$$

where ${}^{*}_{a}\mathcal{D}^{\sigma}_{t}$ can be either of Riemann-Liouville or Caputo sense.

(ii) Let $\sigma = \{\sigma_j\}_{j=0}^{k}$, $\sigma_j \in [\sigma_1, \sigma_2]$, be a continuous mapping in $[\sigma_1, \sigma_2]$, $j = 0, 1, \cdots, k$, then we define the distributed-order fractional derivative as

$$
{}^{D}\mathcal{D}_{\phi} u(t) = \sum_{j=0}^{k} {}^{*}_{a}\mathcal{D}^{\sigma_j}_{t} u(t) \quad t > a, \tag{10.9}
$$

which corresponds to the case (i) in which $\phi = \delta(\sigma - \sigma_j)$, $j = 0, 1, \cdots, k$, a Dirac delta function.

Next, we aim to solve the following differential equation of distributional order:

$$
\begin{aligned}
{}^{D}\mathcal{D}_{\phi} u(t) &= f(t; u), \quad \forall t \in (0, T], && (10.10)\\
u(0) &= 0, \quad \max(\sigma) \in (0, 1], && (10.11)\\
u(0) = \frac{du}{dt}|_{t=0} &= 0, \quad \max(\sigma) \in (1, 2], && (10.12)
\end{aligned}
$$

where $\max(\sigma) = \sigma_2$, the upper limit of the integral in (10.8). In the sequel, we present different approaches to discretize the aforementioned differential operator.

Remark 10.2.1. Due to (10.7), the Caputo and Riemann-Liouville fractional derivatives of order $\sigma \in (0, 1)$ coincide with each other when $u(a) = 0$. Therefore, in this study, we employ the definition of the distributed fractional derivatives (10.8) and (10.9), represented in terms of Riemann-Liouville derivatives.

10.3 Distributional Discretization

We denote by *distributional discretization* the following two-stage discretization; stage-I: in which we reduce the distributed order operator (10.8) to a sum (additive multi-term) form, and stage-II: where we represent the solution u in each term ${}^{RL}_{a}\mathcal{D}^{\alpha_j}_{t} u$ in the N-dimensional space by either a projection operator ${}^{RL}_{a}\mathcal{D}^{\alpha_j}_{t}(P_N u)$ or an interpolation operator ${}^{RL}_{a}\mathcal{D}^{\alpha_j}_{t}(\mathcal{I}_N u)$.

Specifically, by employing a proper Gauss (or Gauss-Lobatto) quadrature rule, the first stage renders the distributed-order operator a *multi-term* linear fractional

differential operator of set-order $\{\alpha_j\}$ as

$$ {}^{D}\mathcal{D}_{\phi}u(t) = \int_{\alpha_1}^{\alpha_2} \phi(\alpha)\, {}^{RL}_{a}\mathcal{D}_{t}^{\alpha}u(t)d\alpha \approx \sum_{j=0}^{Q-1} q_j\, {}^{RL}_{a}\mathcal{D}_{t}^{\alpha_j}u(t), \tag{10.13} $$

where $q_j = \omega_j\phi(\alpha_j)$, moreover, $\{\omega_j\}_{j=0}^{Q-1}$ and $\{\alpha_j\}_{j=0}^{Q-1}$ are the corresponding quadrature weights and points.

We perform the stage-II of discretization trough the spectral approximation of solution $u(t)$ in a finite-dimensional space. To this end, following the recent theory of fractional Sturm-Liouville eigen-problems (FSLP) in [187], we employ the corresponding eigenfunctions, known as *Jacobi Poly-fractonomial*s (of first kind) given in the standard domain $[-1, 1]$ by

$$ {}^{(1)}\mathcal{P}_n^{\mu_1}(\xi) = (1+\xi)^{\mu_1} P_{n-1}^{-\mu_1,\mu_1}(\xi), \quad \xi \in [-1, 1], \tag{10.14} $$

as *non-polynomial* basis functions consisting of a fractional term multiplied by the Jacobi polynomial $P_{n-1}^{-\mu_1,\mu_1}(\xi)$. However, we employ (11.16) in the corresponding *nodal* expansion. In the construction of the collocation method, the following lemma is useful.

Lemma 10.3.1. *Let $\sigma, \mu > 0$. The fractional derivative of the Jacobi poly-fractonomials of first ($i = 1$) and second kind ($i = 2$) are given by*

$$ {}^{RL}\mathcal{D}^{\sigma}\Big\{ {}^{(i)}\mathcal{P}_n^{\mu}(\xi)\Big\} \;=\; \frac{\Gamma(n+\mu)}{\Gamma(n+\mu-\sigma)}\, {}^{(i)}\mathcal{P}_n^{\eta}(\xi), \tag{10.15} $$

are also of Jacobi poly-fractonomial type, where ${}^{RL}\mathcal{D}^{\sigma} \equiv {}^{RL}_{-1}\mathcal{D}_x^{\sigma}$ when $i = 1$, ${}^{RL}\mathcal{D}^{\sigma} \equiv {}^{RL}_{x}\mathcal{D}_1^{\sigma}$ when $i = 1$, and $\eta = \mu - \sigma$.

Proof. Following [5] and for $\sigma > 0$, $\alpha > -1$, $\beta > -1$, and $\forall x \in [-1, 1]$ we have

$$(1+\xi)^{\beta+\sigma} \frac{P_n^{\alpha-\sigma,\beta+\sigma}(\xi)}{P_n^{\alpha-\sigma,\beta+\sigma}(-1)} = \frac{\Gamma(\beta+\sigma+1)}{\Gamma(\beta+1)\Gamma(\sigma)P_n^{\alpha,\beta}(-1)} \int_{-1}^{\xi} \frac{(1+s)^{\beta}\ P_n^{\alpha,\beta}(s)}{(x-s)^{1-\sigma}} ds, \quad (10.16)$$

and

$$(1-x)^{\alpha+\sigma} \frac{P_n^{\alpha+\sigma,\beta-\sigma}(x)}{P_n^{\alpha+\sigma,\beta-\sigma}(+1)} = \frac{\Gamma(\alpha+\sigma+1)}{\Gamma(\alpha+1)\Gamma(\sigma)P_n^{\alpha,\beta}(+1)} \int_{x}^{1} \frac{(1-s)^{\alpha}\ P_n^{\alpha,\beta}(s)}{(s-x)^{1-\sigma}} ds. \quad (10.17)$$

By the definition of the left-sided Riemann-Liouville integral ${}^{RL}_{-1}\mathcal{I}_x^{\sigma}$ and evaluating the special end-values $P_n^{\alpha-\sigma,\beta+\sigma}(-1)$ and $P_n^{\alpha,\beta}(-1)$, we can re-write (10.16) as

$${}^{RL}_{-1}\mathcal{I}_x^{\sigma}\Big\{(1+x)^{\beta} P_n^{\alpha,\beta}(x)\Big\} = \frac{\Gamma(n+\beta+1)}{\Gamma(n+\beta+\sigma+1)}(1+x)^{\beta+\sigma}\ P_n^{\alpha-\sigma,\beta+\sigma}(x),$$

where, by taking the fractional derivative ${}^{RL}_{-1}\mathcal{D}_x^{\sigma}$ on the both sides, we obtain

$${}^{RL}_{-1}\mathcal{D}_x^{\sigma}\Big\{(1+x)^{\beta+\sigma} P_n^{\alpha-\sigma,\beta+\sigma}(x)\Big\} = \frac{\Gamma(n+\beta+\sigma+1)}{\Gamma(n+\beta+1)}(1+x)^{\beta} P_n^{\alpha,\beta}(x). \quad (10.18)$$

Hence, taking $\beta+\sigma = \mu$, $\alpha-\sigma = -\mu$ in (10.18), and shifting from n to $n-1$, we obtain

$$\begin{aligned} {}^{RL}_{-1}\mathcal{D}_x^{\sigma}\Big\{\ {}^{(1)}\mathcal{P}_n^{\mu}(\xi)\Big\} &= \frac{\Gamma(n+\mu)}{\Gamma(n+\mu-\sigma)}(1+x)^{\mu-\sigma} P_{n-1}^{\sigma-\mu,\mu-\sigma}(x), \quad (10.19)\\ &= \frac{\Gamma(n+\mu)}{\Gamma(n+\mu-\sigma)}(1+x)^{\eta} P_{n-1}^{-\eta,\eta}(x),\\ &= \frac{\Gamma(n+\mu)}{\Gamma(n+\mu-\sigma)}\ {}^{(1)}\mathcal{P}_n^{\eta}(\xi), \end{aligned}$$

where $\eta = \mu - \sigma$. Moreover, by the definition of the right-sided Riemann-Liouville integral ${}^{RL}_{x}\mathcal{I}_1^{\sigma}$ and evaluating the special end-values $P_n^{\alpha-\sigma,\beta+\sigma}(+1)$ and $P_n^{\alpha,\beta}(+1)$, we

can re-write (10.17) as

$$ {}^{RL}_{x}\mathcal{I}_{1}^{\sigma}\Big\{(1-x)^{\alpha}P_{n}^{\alpha,\beta}(x)\Big\} = \frac{\Gamma(n+\alpha+1)}{\Gamma(n+\alpha+\sigma+1)}(1-x)^{\alpha+\sigma}P_{n}^{\alpha+\sigma,\beta-\sigma}(x). $$

In a similar fashion, by taking the fractional derivative ${}^{RL}_{x}\mathcal{D}_{-1}^{\sigma}$ on the both sides, we obtain

$$ {}^{RL}_{x}\mathcal{D}_{1}^{\sigma}\Big\{(1-x)^{\alpha+\sigma}P_{n}^{\alpha+\sigma,\beta-\sigma}(x)\Big\} = \frac{\Gamma(n+\alpha+\sigma+1)}{\Gamma(n+\alpha+1)}(1-x)^{\alpha}P_{n}^{\alpha,\beta}(x). \tag{10.20} $$

Next, by taking $\alpha+\sigma=\mu$, $\beta-\sigma=-\mu$ in (10.20), and again shifting from n to $n-1$ we have

$$ \begin{aligned} {}^{RL}_{x}\mathcal{D}_{1}^{\sigma}\Big\{\,{}^{(2)}\mathcal{P}_{n}^{\mu}(\xi)\Big\} &= \frac{\Gamma(n+\mu)}{\Gamma(n+\mu-\sigma)}(1-x)^{\mu-\sigma}P_{n-1}^{\mu-\sigma,\sigma-\mu}(x). \qquad (10.21)\\ &= \frac{\Gamma(n+\mu)}{\Gamma(n+\mu-\sigma)}(1-x)^{\eta}P_{n-1}^{\eta,-\eta}(x),\\ &= \frac{\Gamma(n+\mu)}{\Gamma(n+\mu-\sigma)}\,{}^{(2)}\mathcal{P}_{n}^{\eta}(\xi), \end{aligned} $$

and that completes the proof. □

Remark 10.3.2. Lemma 10.3.1 highlights that the structure of Jacobi poly-fractonomials is preserved under the action of fractional derivatives. Moreover, we note that when $\sigma=\mu$ in Lemma 10.3.1, the fractional derivative of Jacobi poly-fractonomials are obtained in terms of Legendre polynomials, which has been reported in [187]. Moreover, the importance of Lemma 10.3.1 lies in the construction the differentiation matrices with N less arithmetic operations. Employing this lemma, all the procedure ob obtaining the matrices go through without resorting to expand the polyfractonomials in order to calculate their fractional derivatives.

Table 10.1: Convergence study in L^∞-norm when the simulation time $T = 2$; (top) $u^{ext} = t^5$, $\phi(\alpha) = \Gamma(4-\alpha)/120$, and $f(t) = (t^5 - t^3)/\log(t)$ and (bottom) $u^{ext} = t^3$, $\phi(\alpha) = \Gamma(4-\alpha)\sinh(\alpha)/120$, and $6t(t^2 - \cosh(2)\log(t))/(\log(t^2) - 1)$.

$u^{ext} = t^5$, $\phi(\alpha) = \Gamma(6-\alpha)/120$

N	L^∞-Error ($\mu = 1 - 10^{-10}$)	L^∞-Error ($\mu = 7/10$)	L^∞-Error ($\mu = 1/10$)
2	$2.59 \times 10^{+1}$	$3.0 \times 10^{+1}$	$4.3 \times 10^{+1}$
4	6.81×10^{-1}	$1.10 \times 10^{+1}$	$2.51 \times 10^{+1}$
6	3.87×10^{-13}	1.43×10^{-3}	3.48×10^{-3}
8	1.10×10^{-14}	3.10×10^{-5}	8.38×10^{-5}
10	8.75×10^{-15}	2.12×10^{-6}	1.0×10^{-5}

$u^{ext} = t^3$, $\phi(\alpha) = \Gamma(4-\alpha)\sinh(\alpha)/120$

N	L^∞-Error ($\mu = 1 - 10^{-10}$)	L^∞-Error ($\mu = 7/10$)	L^∞-Error ($\mu = 1/10$)
2	5.74	8.84	19.91
4	5.30×10^{-12}	2.58×10^{-1}	1.01×10^{-1}
6	2.15×10^{-13}	1.52×10^{-3}	8.03×10^{-3}
8	2.68×10^{-14}	3.34×10^{-4}	1.83×10^{-3}
10	7.01×10^{-15}	1.12×10^{-4}	6.25×10^{-4}

10.4 Fractional Nodal Expansion

In our FSCM spatial discretization, we represent the solution via the following poly-fractonomial *nodal* expansion as

$$u_N(\xi) = \sum_{j=1}^{N} u_N(\xi_j)\, h_j^\mu(\xi), \tag{10.22}$$

where $h_j^\mu(\xi)$ represent *fractional Lagrange interpolants*, which are all of fractional order $(N + \mu - 1)$ and constructed using the aforementioned interpolations points $-1 = \xi_1 < \xi_2 < \cdots < \xi_N = 1$ as:

$$h_j^\mu(\xi) = \Big(\frac{\xi - x_1}{x_j - x_1}\Big)^\mu \prod_{\substack{k=1 \\ k\neq j}}^{N} \Big(\frac{\xi - x_k}{x_j - x_k}\Big), \;\; 2 \le j \le N. \tag{10.23}$$

Associated with the aforementioned FLIs, the corresponding fractional differentiation matrices $\mathbf{D}^\alpha$ and $\mathbf{D}^{1+\alpha}$, $\alpha \in (0, 1)$ are obtained in Chap 7.

In order to examine the convergence of the scheme, we consider two test cases: $u^{ext} = t^5$, $\phi(\alpha) = \Gamma(4-\alpha)/120$, and $f(t) = (t^5 - t^3)/\log(t)$. By taking the simulation time $T = 2$, we provide the convergence study in L^∞-norm in Table 10.1 (top). It is observed that the choice of μ has an important effect on the convergence behaviour of the scheme. For instance, since the exact solution is a polynomial, as $\mu \to 1$, we recover the exponential convergence capturing the exact solution. A similar observation is made when a different distribution $\phi(\alpha) = \Gamma(4-\alpha)\sinh(\alpha)/120$ is employed. In this case, $u^{ext} = t^3$ and the forcing term is given be $f(t)6t(t^2 - \cosh(2)\log(t))/(\log(t^2) - 1)$. The corresponding results are shown in Table 10.1 (bottom).

Since the exact solution is not always known and in contrast to the standard fractional ODEs where the forcing term gives some regularity information about the exact solution, in distributed-order problems such a prediction is rather difficult to make. Hence, the fractional parameter μ can play the role of a *fine-tuning knob* giving the possibility of searching for the best/optimal case, where the highest rate can be achieved with minimal degrees of freedom.

Chapter Eleven

Application to Keller-Segel Chemotaxis Equations

We develop an implicit-explicit (IMEX) splitting scheme for a one-dimensional space-fractional with integer-order time-derivative, in addition to time- and space-fractional Keller-Segel chemotaxis system. The fractional temporal derivative is of Caputo sense and the spatial derivatives are of Riemann-Liouville type. In this method, the diffusion term is treated implicitly while the nonlinear chemotaxis reaction term is evaluated explicitly. We carry out the time-integration in the prediction step employing a fractional finite difference scheme of observable order Δ^2. The spatial discretization is performed by employing an efficient and spectrally-accurate fractional spectral collocation method, in which the Lagrange interpolants are non-polynomials (fractional).

11.1 Background

The directed movement of cells and microorganisms in response to a diffusible chemical signal is referred to as chemotaxis [73]. Historically, the first mathematical model of chemotaxis was proposed by Evelyn Keller and Lee Segel in order to investigate the aggregation dynamics of the social amoeba *Dictyostelium discoideum* [80]. The model consisted of a nonlinear parabolic system of partial differential equations and is commonly referred to as the Keller-Segel model.

The Keller-Segel model has been analyzed extensively in the last three decades. A comprehensive review of mathematical results on dynamics, existence of solutions, and regularity can be found in the two articles by Horstmann [82, 83]. It is well known that in one dimension the Keller-Segel model is well-posed globally in time [81, 134, 169]. However, several results that appeared in the 1990's have demonstrated that in higher dimensions, the Keller-Segel model is well-posed only for "small" initial

data [138, 170, 173]. In the presence of "large" initial data, the solutions blow up; in other words, they do not remain bounded [45, 46, 81, 171]. Corrias and Perthame [100] showed that in d dimensions, the Keller-Segel model is critical in $L^{d/2}$, which is to say that the "smallness" or "largeness" of the initial data is determined in terms of the $L^{d/2}$ norm. Similar conditions were derived in [101] for a parabolic-elliptic variation of the Keller-Segel model.

Recent literature has also investigated the influence of substrate heterogeneity on the dynamics of the model. Specifically, Matzavinos and Ptashnyk [121] have investigated the one-dimensional Keller-Segel model in the context of a random heterogeneous domain. In [121], the diffusion and chemotaxis coefficients were assumed to be given by stationary ergodic random fields, and the authors applied stochastic two-scale convergence methods to derive the homogenized macroscopic equations. Matzavinos and Ptashnyk [121] also present numerical algorithms for approximating the homogenized asymptotic coefficients.

The influence of substrate heterogeneity was also investigated in [27, 103] by means of fractional calculus [128, 142]. Interestingly, Bournaveas and Calvez [27] have shown that the fractional one-dimensional Keller-Segel model exhibits dynamics similar to the classical two-dimensional model. In particular, Bournaveas and Calvez [27] have shown that the solutions of the fractional Keller-Segel model may blow up in finite time, even in the one-dimensional case. In view of these results, the need to develop accurate numerical methods for the fractional Keller-Segel model is apparent.

The use of spectral methods in FPDEs has been precipitated recently. Various approaches for solving fractional boundary value problems have been proposed, including a Chebyshev spectral method [54], a Legendre spectral method [23], and an adaptive pseudospectral method [119]. Similarly, spectral methods for fractional

initial value problems have been proposed, including generalized Laguerre spectral algorithms [13] and Legendre spectral Galerkin methods [22]. It is well known that long-time (and/or adaptive) integration using such spectral schemes becomes computationally intractable. To address this issue, Xu and Hesthaven [180] developed a stable multi-domain spectral penalty method for FPDEs.

A characteristic of these spectral approaches has been the use of standard integer-order (polynomial) basis functions. Recently, Zayernouri and Karniadakis [189, 184] developed spectrally accurate Petrov-Galerkin schemes for both non-delay and delay fractional differential equations. These schemes are based on fractional basis functions (i.e., basis functions of non-integer order), which are termed *Jacobi poly-fractonomials* and were introduced in [187] as the eigenfunctions of certain fractional Sturm-Liouville operators. A space-time discontinuous Petrov-Galerkin (DPG) method and a discontinuous Galerkin (DG) method for the time-space fractional advection equation were also introduced in [188]. In [190], Jacobi poly-fractonomials were used to define a new class of *fractional Lagrange interpolants*. These were subsequently employed to numerically solve various FODE and FPDE problems, including multi-term FPDEs and the space-fractional Burgers equation [190].

11.2 Definitions

Before defining the problem, we provide some preliminary definitions of fractional calculus following [128, 142]. The left-sided and right-sided Riemann-Liouville inte-

grals of order $\mu \in (0,1)$ are defined, respectively, as

$$({}_{x_L}\mathcal{I}_x^{\mu} f)(x) = \frac{1}{\Gamma(\mu)} \int_{x_L}^{x} \frac{f(s)ds}{(x-s)^{1-\mu}}, \quad x > x_L, \tag{11.1}$$

and

The corresponding inverse operators of (11.1), i.e., the left-sided fractional derivatives of order μ are then defined, respectively, as

$$({}_{x_L}\mathcal{D}_x^{\mu} f)(x) = \frac{d}{dx}({}_{x_L}\mathcal{I}_x^{1-\mu} f)(x) = \frac{1}{\Gamma(1-\mu)} \frac{d}{dx} \int_{x_L}^{x} \frac{f(s)ds}{(x-s)^{\mu}}, \quad x > x_L, \tag{11.2}$$

An alternative approach in defining the tempered fractional derivatives is to begin with the left-sided Caputo derivatives of order $\mu \in (0,1)$, defined respectively, as

$$({}_{x_L}^{C}\mathcal{D}_x^{\mu} f)(x) = ({}_{x_L}\mathcal{I}_x^{1-\mu} \frac{df}{dx})(x) = \frac{1}{\Gamma(1-\mu)} \int_{x_L}^{x} \frac{f'(s)ds}{(x-s)^{\mu}}, \quad x > x_L, \tag{11.3}$$

11.2.1 Problem Definitions

Let the time-derivative order $\tau \in (0,1]$. We consider the following nonlinear system of time- and space-fractional Keller-Segel chemotaxis equations in the interval $[-1,1]$ as

$$\begin{aligned} {}_0\mathcal{D}_t^{\tau} u(x,t) &= \mathcal{L}_x^{\sigma,\gamma,\beta} u(x,t) \\ u(x,0) &= 0, \\ u(\pm 1,t) &= 0, \end{aligned} \tag{11.4}$$

where

$$\mathcal{L}_x^{\sigma,\gamma,\beta}(\cdot) \equiv K\ {}_{-1}\mathcal{D}_x^{1+\sigma}(\cdot) - {}_{-1}\mathcal{D}_x^{\gamma}\Big[(\cdot)\ {}_{-1}\mathcal{D}_x^{\beta}\mathcal{C}(x,t)\Big] + f(x,t;u), \tag{11.5}$$

as coupled to the following elliptic fractional (in space) equation:

$$\begin{aligned} {}_{-1}\mathcal{D}_x^{2\beta}\mathcal{C}(x,t) &= -u(x,t) \\ \mathcal{C}(-1,t) &= 0 \\ \frac{\partial \mathcal{C}}{\partial x}|_{x=-1} &= 0 \end{aligned} \tag{11.6}$$

where the spatial orders $\beta \in (1/2, 1)$, and $\sigma, \lambda \in (0, 1)$, which leads to a $(1+\sigma)$-th order space-fractional FPDE. We note that we employ different temporal discretization methods depending on $\tau = 1$ or $\tau \in (0, 1)$.

11.3 Temporal Discretization

We consider a general fractional (in time and space) problem of the form

$$\begin{aligned} {}_0^C\mathcal{D}_t^{\tau}u(x,t) &= g(t;u), \quad \tau \in (0,1), t \in (0,T], \\ u(x,0) &= u_0, \end{aligned} \tag{11.7}$$

where $g(t;u)$ could in general be involved with the spatial operator. By the definition of the Caputo fractional derivative, we have

$${}_0^C\mathcal{D}_t^{\tau}u = \frac{1}{\Gamma(1-\tau)}\int_0^t \frac{\frac{\partial u}{\partial s}ds}{(t-s)^{\tau}} = H^k(t) + {}_{t_k}^C\mathcal{D}_t^{\tau}u \tag{11.8}$$

where $H^k(t) = \frac{1}{\Gamma(1-\tau)} \int_0^{t_k} \frac{\frac{\partial u}{\partial s} ds}{(t-s)^\tau}$. Moreover,

$$ {}^{C}_{t_k}\mathcal{D}^{\tau}_{t} u \;=\; {}^{C}_{t_k}\mathcal{D}^{\tau}_{t}(u - u_k + u_k) = {}^{C}_{t_k}\mathcal{D}^{\tau}_{t}(u - u_k) = {}^{RL}_{t_k}\mathcal{D}^{\tau}_{t}(u - u_k), \tag{11.9} $$

since $(u - u_k)$ vanishes at $t = t_k$. Next, by substituting (11.9) and (11.8) into (11.7), we obtain

$$ {}^{RL}_{t_k}\mathcal{D}^{\tau}_{t} u(x,t) \;=\; g(t;u) - H^k(t), \quad \tau \in (0,1), t \in (0,T]. \tag{11.10} $$

Applying the inverse operator ${}^{RL}_{t_k}\mathcal{I}^{\tau}_{t}(\cdot)$ to (11.10) and evaluating at $t = t_{k+1}$, we obtain:

$$ u_{k+1} - u_k \;=\; {}^{RL}_{t_k}\mathcal{I}^{\tau}_{t} g(t;u) - \mathcal{H}^k, \quad \tau \in (0,1), t \in (0,T], \tag{11.11} $$

where $\mathcal{H}^k = {}^{RL}_{t_k}\mathcal{I}^{\tau}_{t}(H^k)$, denoted as *history load*. Next, depending on how we extrapolate (in the explicit case) of interpolate (in the implicit case) the term ${}^{RL}_{t_k}\mathcal{I}^{\tau}_{t} g(t;u)$, we obtain the following explicit method

$$ \frac{u_{k+1} - u_k}{(\Delta t)^\tau} \;=\; \sum_{j=0}^{J} \beta_j g(t_{k-j}; u_{k-j}) - \frac{1}{(\Delta t)^\tau} \mathcal{H}^k \tag{11.12} $$

with $\beta_0 = 1/\Gamma(1+\tau)$ when $J = 0$ (1st-order extrapolation) and $\beta_0 = 1/\Gamma(1+\tau) + 2/\Gamma(2+\tau)$ and $\beta_1 = -2/\Gamma(2+\tau)$ (2nd-order extrapolation). Moreover, we obtain the following implicit method

$$ \frac{u_{k+1} - u_k}{(\Delta t)^\tau} \;=\; \sum_{j=0}^{J} \beta_j g(t_{k+1-j}; u_{k+1-j}) - \frac{1}{(\Delta t)^\tau} \mathcal{H}^k \tag{11.13} $$

with $\beta_0 = 1/\Gamma(1+\tau)$ when $J = 0$ (1st-order interpolation) and $\beta_0 = 2/\Gamma(2+\tau)$ and $\beta_1 = 1/\Gamma(1+\tau) - 1/\Gamma(2+\tau)$ (2nd-order interpolation). We note that when $\tau = 1$,

we recover the standard coefficients in the Adams-Bashforth and -Moulton methods. Finally, the history load $\mathcal{H}^k$ in each scheme is obtained as

$$\mathcal{H}^k = \frac{1}{\Gamma(\tau)\Gamma(2+\tau)} \sum_{j=1}^{k-1} (\frac{u_{j+1}-u_j}{\Delta t}) \mathcal{G}_j, \tag{11.14}$$

in which $\mathcal{G}_j$ is given by

$$\mathcal{G}_j = \sum_{q=1}^{N_q} w_q G_j(z_q), \tag{11.15}$$

where $\{w_q, z_q\}_{q=1}^{N_q}$ represent the Gauss-Lobatto-Jacobi weights and zeros corresponding to the weight function $(t_{k+1}-t)^{1-\tau}$, in addition, $G_j(t) = (t-t_j)^{1-\tau} - (t-t_{j+1})^{1-\tau}$.

In Table 11.1, we examine the performance of our schemes carrying out the time-integration of the ${}_0^C\mathcal{D}_t^\tau u(t) = f(t;u)$ subject to homogeneous initial conditions is performed. We examine both linear problem, in which $f(t;u) = u + [\Gamma(6 + 1/10)/\Gamma(6 + 1/10 - \tau)]t^{5+1/10-\tau} - t^{5+1/10}$ and a nonlinear case, in which $f(t;u) = \sin(u^2) + [\Gamma(6 + 1/10)/\Gamma(6 + 1/10 - \tau)]t^{5+1/10-\tau} - \sin(\ t^{2(5+1/10)}\ )$. We consider the exact solution $u^{ext} = t^{5+1/10}$.

11.4 Spatial Discretization via Fractional Spectral Collocation Method

In order to efficiently discretize the spatial terms, we employ a fractional spectral collocation method (FSCM), recently developed in [190], which is based on a new spectral theory developed for fractional Sturm-Liouville eigen-problems (FSLP) in [187]. To this end, we define a set of *interpolation points* $\{x_i\}_{i=1}^N$ on which the corre-

Table 11.1: Time-integration of the ${}_0^C\mathcal{D}_t^\tau u(t) = f(t;u)$ subject to homogeneous initial conditions: (upper table) linear problem, in which $f(t;u) = u + [\Gamma(6+1/10)/\Gamma(6+1/10-\tau)]t^{5+1/10-\tau} - t^{5+1/10}$; (lower table) nonlinear problem, in which $f(t;u) = \sin(u^2) + [\Gamma(6+1/10)/\Gamma(6+1/10-\tau)]t^{5+1/10-\tau} - \sin(\ t^{2(5+1/10)}\ )$. The exact solution $u^{ext} = t^{5+1/10}$.

(Linear Problem)

Δt	$\tau = 1/10$	Order	$\tau = 1/2$	Order	$\tau = 9/10$	Order
1/8	0.557552	1.21	0.237339	1.74	0.146352	1.89
1/16	0.240203	1.70	0.070809	1.98	0.039317	2.18
1/32	0.074064	1.90	0.017855	2.15	0.008697	2.69
1/64	0.019872	1.97	0.004016	2.36	0.001349	4.14
1/128	0.005063	-	0.000784	-	0.000077	-

(Nonlinear Problem)

Δt	$\tau = 1/10$	Order	$\tau = 1/2$	Order	$\tau = 9/10$	Order
1/8	0.368188	0.83	0.1996298	1.60	0.131686	1.86
1/16	0.206252	1.15	0.065989	1.96	0.036314	2.18
1/32	0.093031	1.63	0.016960	2.18	0.007975	2.74
1/64	0.029901	2.06	0.0037392	2.39	0.0011907	3.57
1/128	0.007163	-	0.000713	-	0.0000998	-

sponding Lagrange interpolants are constructed. Moreover, we require the residual to vanish on the same set of grid points called *collocation points* $\{y_i\}_{i=1}^{N}$.

11.4.1 Fractional Lagrange interpolants (FLIs)

We represent the solution at the time t_k in terms of new non-polynomial fractional basis functions, known as *Jacobi poly-fractonomials*, which are the explicit eigenfunctions of the FSLP of first kind, given as

$$ {}^{(1)}\mathcal{P}_n^{\,\mu}(x) = (1+x)^{\mu} P_{n-1}^{-\mu,\mu}(x), \quad x \in [-1,1]. \tag{11.16} $$

where the left-sided fractional derivative of (11.16) is given analytically as

$$ {}_{-1}\mathcal{D}_x^{\,\mu}\left({}^{(1)}\mathcal{P}_n^{\,\mu}(\,x\,)\right) \;=\; \frac{\Gamma(n+\mu)}{\Gamma(n)} P_{n-1}(\,x\,), \tag{11.17} $$

where $P_{n-1}(\,x\,)$ denotes a Legendre polynomial of order $(n-1)$. In our FSCM spatial discretization, we represent the solution at the time t_k via the following poly-fractonomial *nodal* expansion as

$$ u_N(x,t_k) = \sum_{j=1}^{N} u_N(x_j,t_k)\, h_j^{\mu}(x), \tag{11.18} $$

where $h_j^{\mu}(x)$ represent *fractional Lagrange interpolants*, which are all of fractional order $(N+\mu-1)$ and constructed using the aforementioned interpolations points $-1 = x_1 < x_2 < \cdots < x_N = 1$ as:

$$ h_j^{\mu}(x) = \Big(\frac{x-x_1}{x_j-x_1}\Big)^{\mu} \prod_{\substack{k=1 \\ k\neq j}}^{N} \Big(\frac{x-x_k}{x_j-x_k}\Big), \;\; 2 \le j \le N-1. \tag{11.19} $$

11.4.2 Spatial Differentiation Matrices $\mathbf{D}^{\sigma}$ and $\mathbf{D}^{1+\sigma}$, $\sigma \in (0,1)$

We note that FLIs satisfy the Kronecker delta property, i.e., $h_j^{\mu}(x_k) = \delta_{jk}$, at interpolation points, however they vary as a poly-fractonomial between x_k's. Moreover, associated with the aforementioned FLIs, the corresponding fractional differentiation matrices $\mathbf{D}^{\sigma}$ and $\mathbf{D}^{1+\sigma}$, $\sigma \in (0,1)$ are obtained as

$$\mathbf{D}_{ij}^{\sigma} = \frac{1}{(x_j+1)^{\mu}} \sum_{n=1}^{N} \beta_n^j \sum_{q=\lceil \sigma-\mu \rceil}^{n-1} b_{nq} \, (x_i+1)^{q+\mu-\sigma}. \tag{11.20}$$

and

$$\mathbf{D}_{ij}^{1+\sigma} = \frac{1}{(x_j+1)^{\mu}} \Big[\sum_{n=1}^{N} \beta_n^j \sum_{q=\lceil \sigma-\mu \rceil}^{n-1} b_{nq} (q+\mu-\sigma) \, (x_i+1)^{q+\mu-\sigma-1} \Big], \tag{11.21}$$

in which $\lceil \sigma - \mu \rceil$ denotes the ceiling of $\sigma - \mu$ and

$$b_{nq} = (-1)^{n+q-1} (\frac{1}{2})^q \begin{pmatrix} n-1+q \\ q \end{pmatrix} \begin{pmatrix} n-1+\mu \\ n-1-q \end{pmatrix} \frac{\Gamma(q+\mu+1)}{\Gamma(q+\mu-\sigma+1)}. \tag{11.22}$$

and the coefficients are obtained only *once* through the following poly-fractonomial expansion

$$\prod_{\substack{k=1 \\ k \neq j}}^{N} \Big(\frac{x-x_k}{x_j-x_k} \Big) = \sum_{n=1}^{N} \beta_n^j P_{n-1}^{-\mu,\mu}(x). \tag{11.23}$$

and can be computed efficiently since the Jacoi poly-fractonomials $P_{n-1}^{-\mu,\mu}(x)$ are orthogonal with respect to the weight function $w(x) = (1-x)^{-\mu}(1+x)^{-\mu}$. Hence, taking the polynomial $p_j(x) = \prod_{\substack{k=1 \\ k \neq j}}^{N} \Big(\frac{x-x_k}{x_j-x_k} \Big)$, the β_n^j are given exactly by the follow-

ing Guass-Lobatto-Jacobi quadrature rule:

$$\begin{aligned} \beta_n^j &= \frac{1}{\lambda_n}\int_{-1}^{1} w(x)p_j(x)P_{n-1}^{-\mu,\mu}(x)dx \\ &= \frac{1}{\lambda_n}\sum_{q=1}^{Q}\omega_q p_j(x_q)P_{n-1}^{-\mu,\mu}(x_q), \end{aligned} \tag{11.24}$$

where $\{x_q\}_{q=1}^{Q}$ and $\{\omega_q\}_{q=1}^{Q}$ are the associate quadrature points and weights corresponding to the Jacobi weight $w(x)$; moreover, λ_n denotes the orthogonality constant of the Jacobi poly-fractonomials given by $\lambda_n = \frac{2}{2k-1}\frac{\Gamma(n-\mu)\Gamma(n+\mu)}{(n-1)!\Gamma(n)}$.

Remark 11.4.1. When $\sigma = \mu$ (the interpolation parameter), the above differentiation matrices are simply obtained as

$$\mathbf{D}_{ij}^{\mu} = \frac{1}{(x_j+1)^{\mu}}\sum_{n=1}^{N}\frac{\Gamma(n+\mu)}{\Gamma(n)}\,\beta_n^j\,P_{n-1}(\,x_i\,). \tag{11.25}$$

and

$$\mathbf{D}_{ij}^{1+\mu} = \frac{1}{(x_j+1)^{\mu}}\sum_{n=2}^{N}\beta_n^j\Big[\frac{\Gamma(n+\mu)}{\Gamma(n)}\frac{n}{2}P_{n-2}^{1,1}(\,x_i\,)\Big]. \tag{11.26}$$

The right choice of the collocation/interpolation points is the key to obtaining efficient schemes resulting in well-conditioned linear systems. In [190], five different sets of collocation/interpolation points for the construction have been examined: (i) equidistant points, (ii) roots of the underlying poly-fractonomial bases ${}^{(1)}\widetilde{\mathcal{P}}_M^{\mu}(\,x\,) = (1+x)^{\mu}P_{M-1}^{-\mu,\mu}(x)$, (iii) roots of ${}_{-1}\mathcal{D}_x^{\mu}[\ {}^{(1)}\mathcal{P}_M^{\mu}(\,x\,)\ ]$, or equivalently roots of *Legendre* polynomial $P_{M-1}(x)$, (iv) Chebyshev roots $-\cos(\frac{(2j+1)}{M}\,\frac{\pi}{2})$, (v) Roots of $dT_{N+1}(x)/dx$, i.e., $-\cos(\frac{j\pi}{N-1})$, known as the *extrema* points of the Chebyshev polynomial $T_{N+1}(x)$ roots. It turns out that roots of ${}_{-1}\mathcal{D}_x^{\mu}[\ {}^{(1)}\mathcal{P}_M^{\mu}(\,x\,)\ ]$ that represents the (fractional) extrema of the Jacobi poly-fractonomial functions lead to the fasted

Table 11.2: Convergence study of the spatial operators. Here, $u^{ext}(x) = (2^{1/6}(1+x)^{4+1/3} - (1+x)^{4+1/2})$.

$\mu = 1/10$

N	${}^{RL}_{-1}\mathcal{I}^{\mu}_{x}u(x) = f(x)$	${}^{RL}_{-1}\mathcal{D}^{\mu}_{x}u(x) = f(x)$	${}^{RL}_{-1}\mathcal{D}^{1+\mu}_{x}u(x) = f(x)$	${}^{RL}_{-1}\mathcal{D}^{1+\mu}_{x}u(x) - u(x) = f(x)$
3	0.0143673	0.0175926	3.88583	0.368123
7	0.0000103311	0.0000106009	0.0000947525	0.000594943
11	2.31×10^{-8}	2.306×10^{-8}	4.18×10^{-7}	2.27×10^{-6}

$\mu = 1/2$

N	${}^{RL}_{-1}\mathcal{I}^{\mu}_{x}u(x) = f(x)$	${}^{RL}_{-1}\mathcal{D}^{\mu}_{x}u(x) = f(x)$	${}^{RL}_{-1}\mathcal{D}^{1+\mu}_{x}u(x) = f(x)$	${}^{RL}_{-1}\mathcal{D}^{1+\mu}_{x}u(x) - u(x) = f(x)$
3	0.043334	0.102084	0.866727	0.346067
7	0.00009786	0.0000794	0.0002552	0.00141853
11	1.54×10^{-6}	9.1×10^{-7}	5.8×10^{-6}	0.00002033

$\mu = 9/10$

N	${}^{RL}_{-1}\mathcal{I}^{\mu}_{x}u(x) = f(x)$	${}^{RL}_{-1}\mathcal{D}^{\mu}_{x}u(x) = f(x)$	${}^{RL}_{-1}\mathcal{D}^{1+\mu}_{x}u(x) = f(x)$	${}^{RL}_{-1}\mathcal{D}^{1+\mu}_{x}u(x) - u(x) = f(x)$
3	0.0528279	0.209984	0.423576	0.263411
7	0.000078243	0.0000256864	0.000969232	0.00179444
11	3.81×10^{-6}	7.43×10^{-7}	0.0000430498	0.0000925764

rate of convergence and minimal condition number of the resulting system.

11.4.3 Fractional-Order Time-Splitting Scheme

We propose the following splitting scheme as the following. In the prediction step, we split the original equation at t_k as:

$$\frac{u_p(x,t_{k+1})-u(x,t_k)}{(\Delta t)^\tau}=\sum_{j=1}^{J}\beta_j\Big(-{}_{-1}\mathcal{D}_x^{\gamma}\Big[u_p(x,t)\ {}_{-1}\mathcal{D}_x^{\beta}\mathcal{C}_p(x,t)\Big]+f(x,t_k;u_p)\Big)-\mathcal{H}^k, \tag{11.27}$$

subject to the homogeneous initial and boundary conditions. In the correction step we solve

$$\frac{u(x,t_{k+1})-u_p(x,t_{k+1})}{(\Delta t)^\tau}=K\sum_{j=0}^{J}\beta_j\Big({}_{-1}\mathcal{D}_x^{1+\sigma}u(x,t_{k+1-j})\Big), \tag{11.28}$$

In order to de-couple (11.27), using (11.6) we obtain

$$\begin{aligned}
{}_{-1}\mathcal{D}_x^{2\beta}\mathcal{C}(x,t) &= -u(x,t)=-\sum_{j=1}^{N}u(x_j,t_k)h_j^{\mu}(x)\\
&= -\sum_{j=1}^{N}u(x_j,t_k)\frac{1}{(x_j+1)^{\mu}}\sum_{n=1}^{N}\beta_n^j(1+x)^{\mu}P_{n-1}^{-\mu,\mu}(x)\\
&= -\sum_{j=1}^{N}(\frac{u(x_j,t_k)}{(x_j+1)^{\mu}}\sum_{n=1}^{N}\beta_n^j\ {}^{(1)}\mathcal{P}_n^{\mu}(x).
\end{aligned}$$

Since ${}^{(1)}\mathcal{P}_n^{\mu}(-1)=0$, we can analytically obtain

$${}_{-1}\mathcal{D}_x^{\beta}\mathcal{C}(x,t) = -\sum_{j=1}^{N}(\frac{u(x_j,t_k)}{(x_j+1)^{\mu}}\sum_{n=1}^{N}\beta_n^j\ {}_{-1}\mathcal{I}_x^{\beta}\Big[\ {}^{(1)}\mathcal{P}_n^{\mu}(x).\Big]$$

where ${}_{-1}\mathcal{I}_x^{\beta}\Big[\ {}^{(1)}\mathcal{P}_n^{\mu}(x).\Big]$ is obtained exactly as

$${}_{-1}\mathcal{I}_x^{\beta}\Big[\ {}^{(1)}\mathcal{P}_n^{\mu}(x)\Big]=\frac{1+1}{1}(1+x)^{\alpha+\mu}P_{n-1}^{-\beta-\mu,\beta+\mu}(x), \tag{11.29}$$

Hence, by plugging (11.29) into (11.29), we obtain the term ${}_{-1}\mathcal{D}_x^{\beta}\mathcal{C}(x,t_n)$ at an arbitrary time step n as

$$ {}_{-1}\mathcal{D}_x^{\beta}\mathcal{C}(x,t) = -\sum_{j=1}^{N}\Big(\frac{u(x_j,t_n)}{(x_j+1)^{\mu}}\sum_{n=1}^{N}\beta_n^j\frac{1+1}{1}(1+x)^{\alpha+\mu}P_{n-1}^{-\beta-\mu,\beta+\mu}(x). \tag{11.30}$$

By evaluating ${}_{-1}\mathcal{D}_x^{\beta}\mathcal{C}(x,t)$ at the spatial collocation points $\{x_k\}_{k=1}^{N}$ at any given time t_n, we obtain the following operational integration matrix

$$ {}_{-1}\mathcal{D}_x^{\beta}\mathcal{C}(x_j,t_n) = \sum_{k=1}^{N}\{\mathbb{I}^{\beta}\}_{kj}u(x_j,t_n), \tag{11.31}$$

in which $\mathbb{I}^{\beta}$ represents the fractional integration matrix whose entries are obtained as

$$ \{\mathbb{I}^{\beta}\}_{kj} = -\sum_{j=1}^{N}\Big(\frac{u(x_j,t_n)}{(x_j+1)^{\mu}}\sum_{n=1}^{N}\beta_n^j\frac{1+1}{1}(1+x_k)^{\alpha+\mu}P_{n-1}^{-\beta-\mu,\beta+\mu}(x_k). \tag{11.32}$$

In order to examine the accuracy of the spatial operators in this application, in Table 11.2, we solve a collection of fractional integral and differential equation in space.

In Table 11.3, we perform both fully explicit in addition to the IMEX time-integration of the Keller-Segel chemotaxis equation subject to homogeneous initial/boundary conditions. Here, $\sigma = \beta = 5/9$, $\gamma = 3/2$, $K = 1/300$. Here, the exact solution is $u^{ext}(t,x) = t^{5+1/2}(2^{1/6}(1+x)^{4+1/3} - (1+x)^{4+1/2})$ and the simulation time $T = 1$; (top) the full explicit scheme, and (bottom) the implicit-explicit (IMEX) splitting scheme. As expected, we observe at least a second order accuracy.

Table 11.3: IMEX time-integration of the Keller-Segel chemotaxis equation subject to homogeneous initial/boundary conditions. Here, $\sigma = \beta = 5/9$, $\gamma = 3/2$, $K = 1/300$. Here, the exact solution is $u^{ext}(t,x) = t^{5+1/2}(2^{1/6}(1+x)^{4+1/3} - (1+x)^{4+1/2})$ and the simulation time $T = 1$; (top) the full explicit scheme, and (bottom) the implicit-explicit (IMEX) splitting scheme.

Keller-Segel chemotaxis Eq. (Full Explicit)

Δt	$\tau = 1/10$	Order	$\tau = 1/2$	Order	$\tau = 9/10$	Order
1/8	0.080613	1.46	0.049351	1.78	0.035820	1.90
1/16	0.029303	1.80	0.014393	1.99	0.009619	2.13
1/32	0.008408	1.97	0.003604	2.17	0.002193	2.51
1/64	0.002148	1.95	0.000801	2.39	0.000385	4.29
1/128	0.000555	-	0.000153	-	0.000019	-

Keller-Segel chemotaxis Eq. (IMEX)

Δt	$\tau = 1/10$	Order	$\tau = 1/2$	Order	$\tau = 9/10$	Order
1/8	0.080213	1.43	0.0492818	1.78	0.035854	1.89
1/16	0.029787	1.68	0.0143615	1.99	0.009652	2.11
1/32	0.009284	1.85	0.003608	2.16	0.002230	2.40
1/64	0.00257	1.94	0.000808	2.36	0.000421	2.99
1/128	0.000669	-	0.000157	-	0.000053	-

Chapter Twelve

Galerkin Projection in Triangular/Tetrahedral Elements

In this chapter, we begin extending the concept of projection problem in one-dimensional cases, studied in chapter 2, to non-tensorial regions of multiple dimensions. Here, we examine triangle and tetrahedral in the standard domain. To this end, we construct the corresponding fractional modal basis function in terms of Jacobi polyfractonomials, introduced in chapter 2. This study is the first attempt in employing non-polynomial (fractional) basis functions in non-tensorial domains, which can lead to the formulation of FPDEs in complex geometries.

12.1 Background

An orthogonal, generalised tensor product, two-dimensional basis has been proposed by several authors, the first of which we believe to be Proriol in 1957 [143]. This basis has also been independently proposed by Karlin and McGregor [74] and Koornwinder [95] also by Dubiner [55]. These expansions are also known to be solutions to a singular Sturm Liouville problem [28, 96, 135, 178]. Moreover, Dubiner's paper also suggested a modified basis for C^0-continuous expansions and discussed the three-dimensional extension of the orthogonal expansion to a tetrahedral region. The derivation of a (C^0-continuous expansion in a tetrahedral region based on Dubiner's orthogonal expansion was first presented by Sherwin and Karniadakis [159, 77]. Very recently, Qiu et.al. have developed a nodal discontinuous Galerkin methods for fractional diffusion equations on 2-D domain with triangular meshes in [145].

We discuss non-tensorial expansions for simplex regions. An interesting characteristic of these expansions is that the individual expansion modes are not rotationally symmetric in the standard regions. Rotational symmetry has historically been an important consideration when constructing unstructured polynomial expansion

bases. The desire for rotational symmetry naturally motivates the use of rotationally-invariant barycentric coordinate systems. However, the use of the barycentric coordinate system can destroy much of the numerical efficiency associated with the standard tensor product expansion bases. One way to recover this efficiency is to design a coordinate system based on the mapping of a square to a triangle generating a collapsed coordinate system.

12.2 Non-Tensorial Expansions

The use of a collapsed coordinate system regains some of this efficiency but inherently destroys the rotational symmetry of each mode of the expansion. Nevertheless, these expansions span an identical polynomial space as the traditional unstructured expansions using barycentric coordinates. Therefore, in the absence of any integration error, they are equivalent to any other polynomial expansion bases used in a Galerkin approximation. The lack of rotational symmetry does not affect the multi-domain construction of the triangular expansion, although for tetrahedral domains it does impose a restriction on orientation of the elemental regions which can be trivially satisfied.

12.2.1 Collapsed 2-D Coordinate System

We provide the definition of a new collapsed coordinate system. Using the collapsed coordinate system we can then construct orthogonal expansions within simplex regions. Finally, since the orthogonal expansions cannot easily be tessellated into C^0-expansions, we discuss a set of modified expansions which have an interior and

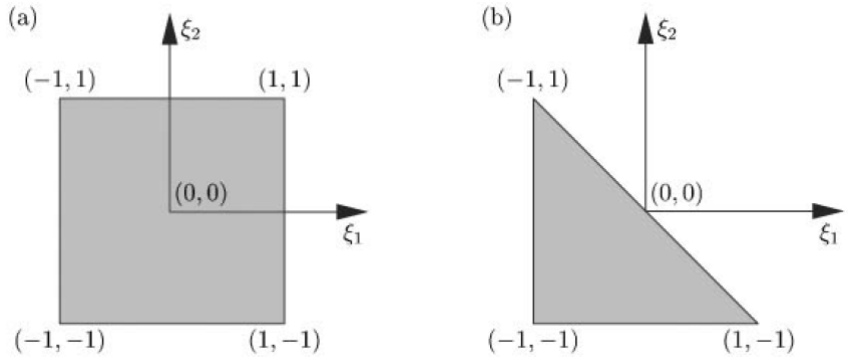

Figure 12.1: Standard regions for the (a) quadrilateral, and (b) triangular expansion in terms of the Cartesian coordinates (ξ_1, ξ_2).

boundary decomposition making them suitable for use in a global C^0-continuous expansion.

A suitable coordinate system, which describes the triangular region between constant independent limits, is defined by the transformation

$$\begin{aligned} \eta_1 &= 2\frac{1+\xi_1}{1-\xi_1} - 1, \\ \eta_2 &= \xi_2, \end{aligned} \tag{12.1}$$

and has the inverse transformation

$$\begin{aligned} \xi_1 &= \frac{(1+\eta_1)(1-\eta_2)}{2}, \\ \xi_2 &= \eta_2. \end{aligned} \tag{12.2}$$

These new local coordinates (η_1, η_2) define the standard triangular region by

$$\mathcal{T}^2 = \{(\eta_1, \eta_2) | -1 \leq \eta_1, \eta_2 \leq 1\}. \tag{12.3}$$

The definition of the triangular region in terms of the coordinate system (η_1, η_2)

is identical to the definition of the standard quadrilateral region in terms of the Cartesian coordinates (ξ_1, ξ_2). This suggests that we can interpret the transformation (12.1) as a mapping from the triangular region to a rectangular one.

12.2.2 Collapsed 3-D Coordinate System

If we consider the local coordinates (12.2) as independent axes then the coordinate system spans a rectangular region. Therefore, if we start with a hexahedral region and apply the inverse transformation(12.2) then we can derive a new local coordinate system in the tetrahedral region $\mathcal{T}^3$ in three dimensions, where $\mathcal{T}^3$ is defined as

$$\mathcal{T}^3 = \{(\eta_1, \eta_2)| -1 \leq \eta_1, \eta_2, \eta_3, \eta_1 + \eta_2 + \eta_3 \leq 1\}. \tag{12.4}$$

To reduce the hexahedron to a tetrahedron requires repeated application of the transformation (12.2), as illustrated in Fig. 12.2. Initially, we consider a hexahedral domain defined in terms of the local coordinate system (η_1, η_2, η_3), where all three coordinates are bounded by constant limits, that is, $-1 \leq \eta_1, \eta_2, \eta_3 \leq 1$. Applying the rectangle-to-triangle transformation (12.2) as illustrated in Fig. 12.2.

12.2.3 Barycentric Coordinate Systems

Barycentric coordinate systems have historically been used in unstructured domains because of their rotational symmetry. Unlike the quadrilateral or hexahedral regions, in a simplex region such as the triangle and tetrahedron, maintaining symmetry requires an extra (dependent) coordinate. This makes the tensor process construction

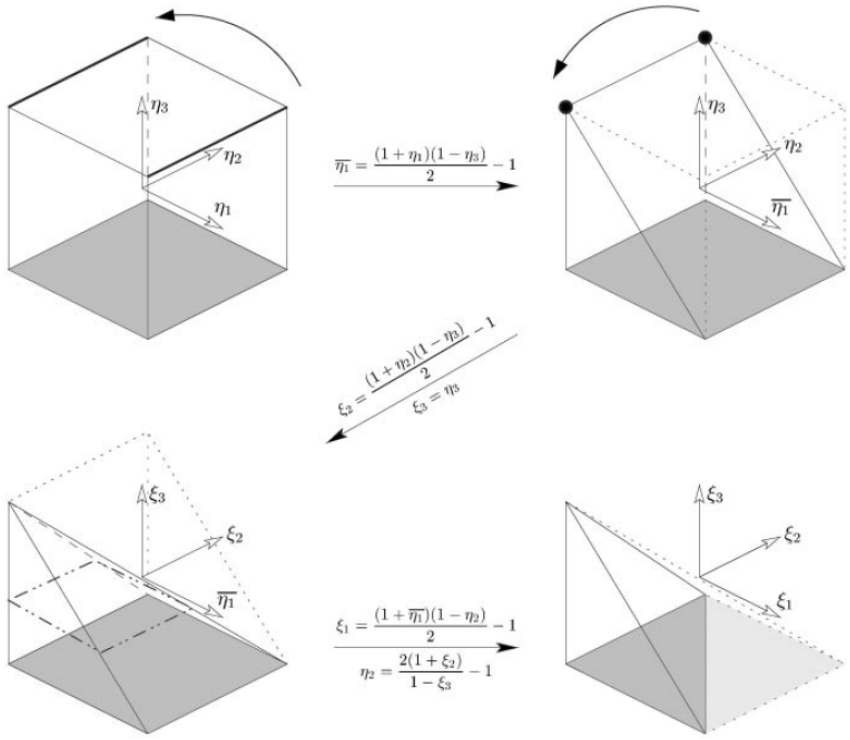

Figure 12.2: Hexahedron-to-tetrahedron transformation by repeatedly applying the rectangle-to-triangle mapping.

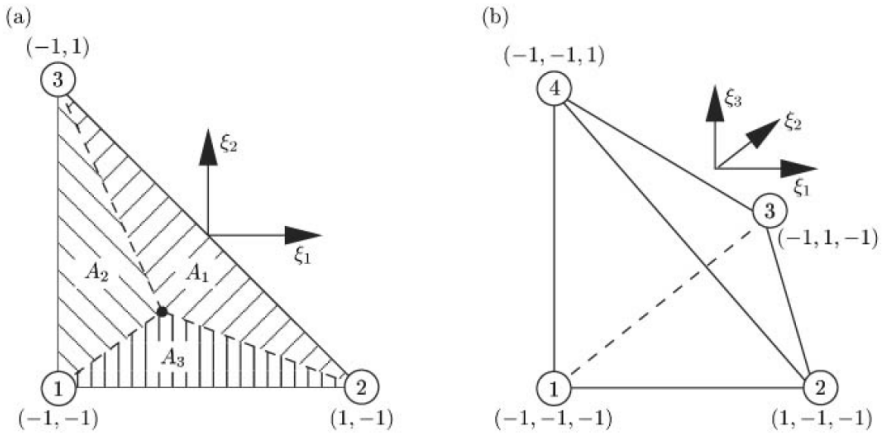

Figure 12.3: (a) The area coordinate system in the standard triangular region with coordinates L_1, L_2, and L_3; (b) The standard tetrahedral region for the definition of volume coordinates.

of expansions very difficult if not impossible. Barycentric coordinates will however be useful in defining the rotationally-symmetric non-tensorial expansions discussed in this section. We also define the relationship between the barycentric coordinates and volume coordinates and the collapsed coordinate systems. The area coordinate system is illustrated in Fig. 12.3 (a) for the standard triangle. Any point in the triangle is described by three coordinates L_1, L_2, and L_3, which can be interpreted as the ratio of the areas A_1, A_2, and A_3 over the total area $A = A_1 + A_2 + A_3$.

12.3 Fractional Modal Basis Functions

In this section, we construct a new class of fractional basis functions for non-tensorial domain based on Jacobi polyfractonomials. A similar approach can be found in the recent book of Bittencourt [24], where we now aim to employ non-polynomial functions in the construction of the bases along each direction L_i, $i = 1, 2, 3$, and 4 as

$$\phi_p^{(e)}(L_i) = \begin{cases} 1, & p = 0, \\ L_i, & p = P_i, \\ {}^{(1)}\mathcal{P}_n^{\mu_i}(2L_i - 1) & 1 < p < P_i, \end{cases} \tag{12.5}$$

where ${}^{(1)}\mathcal{P}_n^{\mu}(\xi) = (1+\xi)^{\mu}\ P_{n-1}^{-\mu,\mu}(\xi)$, denote the Jacobi polyfractonomial function introduced in Chap. 2.

12.3.1 Fractional Bases for Triangle Elements

Hence, the modal basis functions for triangles can be defined as the following; the vertex modes are given by

$$\begin{aligned}
\Phi^{(e)}_{P_1 00}(L_1, L_2, L_3) &= \phi^{(e)}_{P_1}(L_1)\phi^{(e)}_0(L_2)\phi^{(e)}_0(L_3) = L_1, \\
\Phi^{(e)}_{0P_2 0}(L_1, L_2, L_3) &= \phi^{(e)}_0(L_1)\phi^{(e)}_{P_2}(L_2)\phi^{(e)}_0(L_3) = L_2, \\
\Phi^{(e)}_{00P_3}(L_1, L_2, L_3) &= \phi^{(e)}_0(L_1)\phi^{(e)}_0(L_2)\phi^{(e)}_{P_3}(L_3) = L_3,
\end{aligned} \tag{12.6}$$

moreover, the edge modes for $P \geq 2$ and $0 < p, q, r < P$ are given by

$$\begin{aligned}
\Phi^{(e)}_{pq0}(L_1, L_2, L_3) &= \phi^{(e)}_p(L_1)\phi^{(e)}_q(L_2)\phi^{(e)}_0(L_3) \\
&= L_1^{\mu_1} L_2^{\mu_2} P^{-\mu_1,\mu_1}_{p-1}(2L1-1) P^{-\mu_2,\mu_2}_{q-1}(2L2-1), \quad (p+q=P) \\
\Phi^{(e)}_{p0r}(L_1, L_2, L_3) &= \phi^{(e)}_p(L_1)\phi^{(e)}_0(L_2)\phi^{(e)}_r(L_3) \\
&= L_1^{\mu_1} L_3^{\mu_2} P^{-\mu_1,\mu_1}_{p-1}(2L1-1) P^{-\mu_3,\mu_3}_{r-1}(2L3-1), \quad (p+r=P) \\
\Phi^{(e)}_{0qr}(L_1, L_2, L_3) &= \phi^{(e)}_0(L_1)\phi^{(e)}_q(L_2)\phi^{(e)}_r(L_3) \\
&= L_2^{\mu_2} L_3^{\mu_3} P^{-\mu_2,\mu_2}_{q-1}(2L2-1) P^{-\mu_3,\mu_3}_{r-1}(2L3-1), \quad (q+r=P).
\end{aligned} \tag{12.7}$$

Finally, the face modes for $P \geq 3$, $p + q + r = P$, and $0 < p, q, r < P - 1$ are given by

$$\begin{aligned}
\Phi^{(e)}_{pqr}(L_1, L_2, L_3) &= \phi^{(e)}_p(L_1)\phi^{(e)}_q(L_2)\phi^{(e)}_q(L_3) \\
&= L_1^{\mu_1} L_2^{\mu_2} L_3^{\mu_3} P^{-\mu_1,\mu_1}_{p-1}(2L1-1) P^{-\mu_2,\mu_2}_{q-1}(2L2-1) P^{-\mu_3,\mu_3}_{r-1}(2L3-1).
\end{aligned} \tag{12.8}$$

12.3.2 Fractional Bases for Tetrahedral Elements

The same tensorization procedure of triangle is applied to tetrahedral. For this purpose, the barycentric or volume coordinates presented in Fig. 12.3 (b) are employed. Given any interior point, we have four tetrahedrals with volumes V_1, V_2, V_3, and V_4, where the total volume $V = V_1 + V_2 + V_3 + V_4$. In order to obtain the fractional modal basis function in tetrahedral elements we employ (12.5) as the following; the vertex modes are obtained as

$$\begin{aligned}
\Phi^{(e)}_{P_1000}(L_1, L_2, L_3, L_4) &= \phi^{(e)}_{P_1}(L_1)\phi^{(e)}_0(L_2)\phi^{(e)}_0(L_4)\phi^{(e)}_0(L_4) = L_1, \qquad (12.9)\\
\Phi^{(e)}_{0P_200}(L_1, L_2, L_3, L_4) &= \phi^{(e)}_0(L_1)\phi^{(e)}_{P_2}(L_2)\phi^{(e)}_0(L_3)\phi^{(e)}_0(L_4) = L_2,\\
\Phi^{(e)}_{00P_30}(L_1, L_2, L_3, L_4) &= \phi^{(e)}_0(L_1)\phi^{(e)}_0(L_2)\phi^{(e)}_{P_3}(L_3)\phi^{(e)}_0(L_4) = L_3,\\
\Phi^{(e)}_{000P_4}(L_1, L_2, L_3, L_4) &= \phi^{(e)}_0(L_1)\phi^{(e)}_0(L_2)\phi^{(e)}_0(L_3)\phi^{(e)}_{P_4}(L_4) = L_4.
\end{aligned}$$

In addition, the edge modes are constructed for $P \geq 2$ and $0 < p, q, r, s < P$ as

$$
\begin{aligned}
\Phi^{(e)}_{pq00}(L_1, L_2, L_3, L_4) &= \phi^{(e)}_p(L_1)\phi^{(e)}_q(L_2)\phi^{(e)}_0(L_3)\phi^{(e)}_0(L_4) \qquad (12.10)\\
&= L_1^{\mu_1} L_2^{\mu_2} P^{-\mu_1,\mu_1}_{p-1}(2L1-1) P^{-\mu_2,\mu_2}_{q-1}(2L2-1), \quad (p+q=P),\\
\Phi^{(e)}_{p0r0}(L_1, L_2, L_3, L_4) &= \phi^{(e)}_p(L_1)\phi^{(e)}_0(L_2)\phi^{(e)}_r(L_3)\phi^{(e)}_0(L_4)\\
&= L_1^{\mu_1} L_3^{\mu_2} P^{-\mu_1,\mu_1}_{p-1}(2L1-1) P^{-\mu_3,\mu_3}_{r-1}(2L3-1), \quad (p+r=P),\\
\Phi^{(e)}_{0qr0}(L_1, L_2, L_3, L_4) &= \phi^{(e)}_0(L_1)\phi^{(e)}_q(L_2)\phi^{(e)}_r(L_3)\phi^{(e)}_0(L_4)\\
&= L_2^{\mu_2} L_3^{\mu_3} P^{-\mu_2,\mu_2}_{q-1}(2L2-1) P^{-\mu_3,\mu_3}_{r-1}(2L3-1), \quad (q+r=P),\\
\Phi^{(e)}_{p00s}(L_1, L_2, L_3, L_4) &= \phi^{(e)}_p(L_1)\phi^{(e)}_0(L_2)\phi^{(e)}_0(L_3)\phi^{(e)}_s(L_4)\\
&= L_1^{\mu_1} L_4^{\mu_4} P^{-\mu_1,\mu_1}_{p-1}(2L1-1) P^{-\mu_4,\mu_4}_{s-1}(2L4-1), \quad (p+s=P),\\
\Phi^{(e)}_{00rs}(L_1, L_2, L_3, L_4) &= \phi^{(e)}_0(L_1)\phi^{(e)}_0(L_2)\phi^{(e)}_r(L_3)\phi^{(e)}_s(L_4)\\
&= L_3^{\mu_3} L_4^{\mu_4} P^{-\mu_3,\mu_3}_{p-1}(2L3-1) P^{-\mu_4,\mu_4}_{s-1}(2L4-1), \quad (r+s=P),\\
\Phi^{(e)}_{0q0s}(L_1, L_2, L_3, L_4) &= \phi^{(e)}_0(L_1)\phi^{(e)}_q(L_2)\phi^{(e)}_0(L_3)\phi^{(e)}_s(L_4)\\
&= L_2^{\mu_2} L_4^{\mu_4} P^{-\mu_2,\mu_2}_{p-1}(2L2-1) P^{-\mu_4,\mu_4}_{s-1}(2L4-1), \quad (q+s=P),
\end{aligned}
$$

moreover the face modes for $P \geq 3$, $0 < p, q, r, s < P - 1$ are obtained as

$$\begin{aligned}
\Phi^{(e)}_{pqr0}(L_1, L_2, L_3, L_4) &= \phi^{(e)}_p(L_1)\phi^{(e)}_q(L_2)\phi^{(e)}_q(L_3)\phi^{(e)}_0(L_4) \qquad (12.11)\\
&= L_1^{\mu_1} L_2^{\mu_2} L_3^{\mu_3} P^{-\mu_1,\mu_1}_{p-1}(2L1-1) P^{-\mu_2,\mu_2}_{q-1}(2L2-1) P^{-\mu_3,\mu_3}_{r-1}(2L3-1),\\
\Phi^{(e)}_{pq0s}(L_1, L_2, L_3, L_4) &= \phi^{(e)}_p(L_1)\phi^{(e)}_q(L_2)\phi^{(e)}_0(L_3)\phi^{(e)}_s(L_4)\\
&= L_1^{\mu_1} L_2^{\mu_2} L_4^{\mu_4} P^{-\mu_1,\mu_1}_{p-1}(2L1-1) P^{-\mu_2,\mu_2}_{q-1}(2L2-1) P^{-\mu_4,\mu_4}_{r-1}(2L4-1),\\
\Phi^{(e)}_{p0rs}(L_1, L_2, L_3, L_4) &= \phi^{(e)}_p(L_1)\phi^{(e)}_0(L_2)\phi^{(e)}_r(L_3)\phi^{(e)}_s(L_4)\\
&= L_1^{\mu_1} L_3^{\mu_2} L_4^{\mu_4} P^{-\mu_1,\mu_1}_{p-1}(2L1-1) P^{-\mu_3,\mu_3}_{q-1}(2L3-1) P^{-\mu_4,\mu_4}_{r-1}(2L4-1),\\
\Phi^{(e)}_{0qrs}(L_1, L_2, L_3, L_4) &= \phi^{(e)}_0(L_1)\phi^{(e)}_q(L_2)\phi^{(e)}_r(L_3)\phi^{(e)}_s(L_4)\\
&= L_2^{\mu_1} L_3^{\mu_2} L_4^{\mu_4} P^{-\mu_2,\mu_2}_{p-1}(2L2-1) P^{-\mu_3,\mu_3}_{q-1}(2L3-1) P^{-\mu_4,\mu_4}_{r-1}(2L4-1).
\end{aligned}$$

Finally, the body (volume) modes for $P \geq 4$, $p+q+r+s = P$, and $< p, q, r, s < P-2$ are given by the general expression

$$\begin{aligned}
&\Phi^{(e)}_{pqrs}(L_1, L_2, L_3, L_4) = \phi^{(e)}_p(L_1)\phi^{(e)}_q(L_2)\phi^{(e)}_q(L_3)\phi^{(e)}_s(L_4) \qquad (12.12)\\
&= L_1^{\mu_1} L_2^{\mu_2} L_3^{\mu_3} L_4^{\mu_4} P^{-\mu_1,\mu_1}_{p-1}(2L1-1) P^{-\mu_2,\mu_2}_{q-1}(2L2-1) P^{-\mu_3,\mu_3}_{r-1}(2L3-1) P^{-\mu_4,\mu_4}_{s-1}(2L4-1).
\end{aligned}$$

12.4 Galerkin Projection

Now, we aim to examine the fractional basis functions in the Galerkin projection in triangular and tetrahedral elements. In addition, we carry out a multi-element projection operation in a L-shaped domain. The construction of the corresponding mass matrix is followed by [77].

To this end, we examine the Galerkin projection of two fractional functions $u^{ext} = (xy)^{2.5}(1-x-y)$ and $u^{ext} = \sin(x^{2.5})\sin(y^{2.5})(1-x-y)$ in a triangle element (single-

Table 12.1: Triangle Element; Galerkin projection (top): $u^{ext} = (xy)^{2.5}(1-x-y)$, and (bottom): $u^{ext} = \sin(x^{2.5})\sin(y^{2.5})(1-x-y)$.

	$u^{ext} = (xy)^{2.5}(1-x-y)$	
P	L^2-Error ($\mu = 1/10$)	L^2-Error ($\mu = 9/10$)
3	1.85×10^{-1}	9.02×10^{-2}
5	4.56×10^{-2}	1.12×10^{-3}
7	3.94×10^{-4}	4.13×10^{-5}
9	1.04×10^{-5}	7×10^{-6}
11	1.45×10^{-6}	2×10^{-6}

	$u^{ext} = \sin(x^{2.5})\sin(y^{2.5})(1-x-y)$	
P	L^2-Error ($\mu = 1/10$)	L^2-Error ($\mu = 9/10$)
3	1.86×10^{-1}	9.1×10^{-2}
5	4.64×10^{-2}	1.25×10^{-3}
7	4.12×10^{-4}	3.90×10^{-5}
9	1.03×10^{-5}	6.70×10^{-6}
11	1.4×10^{-6}	1.94×10^{-6}

Table 12.2: Tetrahedral Element; Galerkin projection (top): $u^{ext} = (xyz)^{2.5}(1-x-y-z)$, and (bottom): $u^{ext} = \sin(x^{2.5})\sin(y^{2.5})(1-x-y-z)$.

	$u^{ext} = (xyz)^{2.5}(1-x-y-z)$	
P	L^2-Error ($\mu = 1/10$)	L^2-Error ($\mu = 9/10$)
3	1.04×10^{-1}	4.63×10^{-2}
5	1.18×10^{-2}	2.66×10^{-2}
7	1.54×10^{-3}	5.44×10^{-4}
9	2.6×10^{-4}	1.22×10^{-5}
11	2.54×10^{-6}	3.90×10^{-7}

	$u^{ext} = \sin(x^{2.5})\sin(y^{2.5})\sin(z^{2.5})(1-x-y-z)$	
P	L^2-Error ($\mu = 1/10$)	L^2-Error ($\mu = 9/10$)
3	1.04×10^{-1}	4.67×10^{-2}
5	1.20×10^{-2}	2.68×10^{-3}
7	1.55×10^{-3}	5.54×10^{-4}
9	2.62×10^{-4}	1.18×10^{-5}
11	2.6×10^{-6}	3.88×10^{-7}

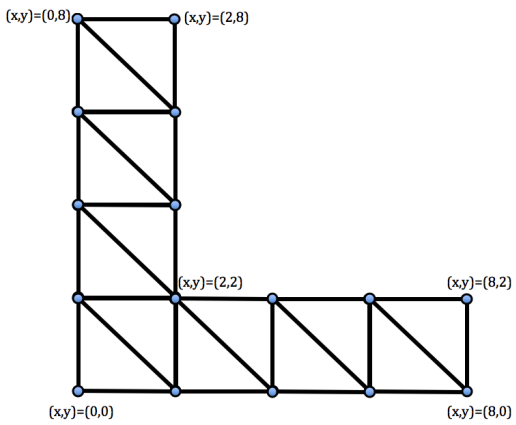

	$u(x,y)=\sin(x^{2.5})y$
P	$\mu=1/2$
3	$2.085\ \times 10^{-2}$
5	$2.666\ \times 10^{-3}$
7	6.505×10^{-4}
9	1.943×10^{-4}

Figure 12.4: Multi-element Galerkin projection in a L-shaped domain.

domain) in Table 12.1. We observe a spectral convergence in the standard L^2-norm. Moreover, we examine three-dimensional functions $u^{ext}=(xyz)^{2.5}(1-x-y-z)$ and $u^{ext}=\sin(x^{2.5})\sin(y^{2.5})(1-x-y-z)$ for projection onto a tetrahedral single-element in Table 12.2, we we achieve a similar spectral accuracy.

Finally, in Table 12.4, we perform the Galerkin projection of function $u(x,y)=\sin(x^{2.5})y$ in the L-shaped domain $\Omega=[0,8]\times[0,8]/[2,8]\times[2,8]$, partitioned to 14 triangle elements. The usefulness of domain decomposition (in capturing such a slightly more complicated domain in addition to the rate of convergence) can be observed in the left panel of Table 12.4.

Chapter Thirteen

Summary and Future Works

Fractional PDEs are the right mathematical models for many physical processes exhibiting self-similar structures, nonlocal interactions, and anomalous diffusion. However, the biggest challenge of employing these models is their global nature and memory-dependent characteristics. That is one important reason that over the past decades these global models have not been much utilized in science and engineering, and instead, simplifying Newtonian, Gaussian, and Brownian assumptions have been adopted at the cost of weakening the fidelity of resulting models. In fact, the inherent bottleneck of non-locality in fractional PDEs leads to excessive computer-memory storage requirements and insufficient computational accuracy. Utilization of local numerical methods, such as finite difference, can easily take days on a standard desktop computer, even for problems with a single dimension. Moreover, this challenge becomes even more severe when fractional PDEs are involved with multi-fractional order terms, nonlinear differential operators, or variable- and distributed-order derivatives in time and space, for which there existed no high-order numerical methods prior to our work. Given the aforementioned challenges in cases with low dimensionality, fractional PDEs in higher dimensions were computationally intractable, making real-world applications nearly impossible.

To overcome such barriers, in chapter 2, we introduced a regular fractional Sturm-Liouville problem of two kinds RFSLP-I and RFSLP-II of order $\nu \in (0, 2)$ with the fractional differential operators both of Riemann-Liouville and Caputo type, of the same fractional order $\mu = \nu/2 \in (0, 1)$. This choice, in turn, motivated a proper fractional integration-by-parts. In the first part of this chapter, we obtained the analytical eigensolutions to RFSLP-I &-II as non-polynomial functions, which we defined as Jacobi *poly-fractonomials*. These eigenfunctions were shown to be orthogonal with respect to the weight function, associated with the RFSLP-I &-II. In addition, these eigenfunctions were shown to be hierarchical, and a useful recursive

relation was obtained for each type of the eigenfunctions. Moreover, a detailed list of other important properties of such poly-fractonomials was presented at the end of the first part of this chapter.

Moreover, we extended the fractional operators to a new family of singular fractional Sturm-Liouville problems of two kinds, SFSLP-I and SFSLP-II, in the second part of the chapter. We showed that the regular boundary-value problems RFSLP-I&-II are indeed asymptotic cases for the singular counterparts SFSLP-I&-II. We also proved that the eigenvalues of the singular problems are real-valued and the eigenfunctions corresponding to distinct eigenvalues are orthogonal. Subsequently, we obtained the eigen-solutions to SFSLP-I &-II analytically, also as non-polynomial functions, which completed the whole family of the Jacobi poly-fractonomials. In a similar fashion, a number of useful properties of such eigensolutions was introduced. Finally in chapter 2, we analyzed the numerical approximation properties of the eigensolutions to RFSLP-I&-II and SFSLP-I&-II in a unified fashion. The exponential convergence in approximating fractal functions such as poly-fractonomials in addition to some other fractal functions such as fractional trigonometric functions highlighted the efficiency of the new fractal basis functions compared to Legendre polynomials.

In chapter 3, we first presented a regular tempered fractional Sturm-Liouville (TFSLP) problem of two kinds, regular TFSLP-I and regular TFSLP-II of order $\nu \in (0, 2)$ employing both tempered Riemann-Liouville and tempered Caputo fractional derivatives of order $\mu = \nu/2 \in (0, 1)$. We formulated the boundary-value problem by establishing the wellposedness of that, and then, proving that the eigenvalues of the regular tempered problems are real-valued and the corresponding eigenfunctions are orthogonal. Next, we excplicitly obtained the eigensolutions to the regular TFSLP-I & -II defined as *tempered Jacobi poly-fractonomials*. These eigenfunctions

were shown to be orthogonal with respect to the weight function associated with the regular TFSLP-I & -II. We also showed that when the tempering parameter $\tau = 0$, such eigenfunctions reduce to the regular Jacobi poly-fractonomials introduced in [187]. We demonstrated that such tempered eigensolutions enjoy many other attractive properties such as recurrence structure and having exact fractional derivatives and integrals. In addition, we extended the fractional operators to a new family of singular TFSLPs of two kinds, singular TFSLP-I and singular TFSLP-II. Subsequently, we obtained the eigensolutions to the singular TFSLP-I & -II analytically, also as non-polynomial functions, hence completing the whole family of the tempered Jacobi poly-fractonomials. Finally, we introduced the approximation properties of such eigenfunctions by introducing them as new basis (and test) functions. Moreover in chapter 3, we developed a Petrov-Galerkin spectral method for solving tempered fractional ODEs (TFODEs), for which the corresponding stability and convergence analysis were carried out. This work has been submitted [182].

In chapter 4, we developed spectrally accurate spectral methods of Petrov-Galerkin (PG) type for the fractional initial-value problems ${}_0\mathcal{D}_t^{\nu}u(t) = f(t)$ and the fractional final-value problem ${}_t\mathcal{D}_T^{\nu}u(t) = g(t)$, $\nu \in (0, 1)$, subject to Dirichlet initial/final conditions. We employed the recently developed spectral theory in [187] for fractional Sturm-Liouville problems, which provided the corresponding basis and test functions utilized in our schemes. We introduced the corresponding fractional basis functions, called *Jacobi-polyfractonomial*s, as the eigenfunctions of the FSLP of *first* kind (FSLP-I). Moreover in chapter 3, we employed another space of test functions as the span of polyfractonomial eigenfunctions of the FSLP of *second* kind (FSLP-II). In the aforementioned PG spectral methods, the basis functions satisfy the initial-/final-conditions exactly. Subsequently, we developed a Petrov-Gaerking discontinuous spectral method (DSM) for the aforementioned FIVPs and FFVPs, and finally

extended DSM to a discontinuous spectral element method (DSEM) for carrying out efficient longer time-integrations, but also performing possible discontinuity capturing and adaptive refinement. In both discontinuous schemes, we employed the basis and test functions which were *asymptotic* eigensolutions to FSLP-I&-II, belonging to the Jacobi family polynomials. We presented a variety of numerical tests for each case in chapter 4 to exhibit the exponential convergence of PG, DSM, and DSEM using p-refinement; we also investigated the algebraic convergence in DSEM when h-refinement is performed. In these numerical tests, we considered the exact solution to the FIVPs/FFVPs to be monomials t^p, smooth functions $t^q \sin(\pi t)$, and fractional functions $t^{p/q} \sin(\pi t^{r/s})$, where p, q, r and s were integers, or any combination of them. In DSEM, we furthermore highlighted the flexibility of the scheme in long-time/adaptive integration. We have also analyzed the computational complexity of these methods. For example, in Fig. 4.5 we present the condition number of the stiffness matrix in DSM and DSEM, which seems to grow roughly as $N^{3-\nu}$. For the case of PG spectral method, we recall that the stiffness matrix is diagonal due to the orthogonality property of the fractional bases.

In chapter 5, we developed spectrally accurate Petrov-Galerkin (PG) spectral and discontinuous spectral element methods for Fractional Differential Delay Equations (FDDEs) of form ${}_0\mathcal{D}_t^{\nu} u(t) = h(t) - A(t)u(t) - B(t)u(g_\tau(t))$. We demonstrated that the corresponding stiffness matrix is *diagonal*, also the corresponding mass and *delay* mass matrices are obtained exactly by employing proper quadrature rules. Hence, the total linear system becomes *full* in general, for which GMRES or GMRES(k) algorithms can be employed to solve the system. Moreover, we studied the wellposedness of the problem, also carried out the corresponding stability and convergence study of our PG spectral method. Subsequently, we developed a discontinuous Galerkin spectral method (DSM) along with *exact* quadrature rules for

the aforementioned matrices. We then extended DSM to a discontinuous spectral element method (DSEM) for efficient longer time-integrations and adaptive discontinuity capturing. We developed these schemes based on a new spectral theory for fractional Sturm-Liouville problems (FSLPs), recently presented in [187]. We examine a wide range of exact solutions with constant and time-dependent coefficients $A(t)$ and $B(t)$. We also considered the delay term $u(g_\tau(t))$ to be of $u(t-\tau)$, pantograph type $u(qt)$ and harmonic delay form $u(q\sin(\pi t))$. Consistently, in all the aforementioned test cases and schemes, spectral convergence of the L^2-norm error is achieved independent of the time-delay τ.

In chapter 6, we developed high-order methods for time- and space- Fractional Advection Equation (TSFAE) of the form (6.1), subject to Dirichlet initial/boundary conditions. We presented two highly accurate spectral element methods. We first developed the SM-DSEM scheme for carrying out the time-integration using a single time-domain spectral method (SM), and performing the spatial discretization using Discontinuous Spectral/*hp* Element Method (DSEM), when $\tau \in (0,1]$, $\nu \in (0,1)$. We accomplished this based on the new spectral theory for fractional Sturm-Liouville problems (FSLPs), presented in [187], which provides proper spaces of basis and test functions. For the particular case $\tau = 1$, we presented this PG-DG method as an exponentially accurate time-integration method, which outperforms the existing algebraically accurate backward and forward multi-step methods in terms of cost and accuracy. We subsequently extended the SM-DSEM to another method, *DSEM-DSEM*, in which both time-integration and spatial discretization are performed in an *hp*-element fashion, when $\tau \in (0,1)$, $\nu \in (0,1)$. We presented numerical tests in each case to demonstrate the exponential-like convergence of our methods employing *p*-refinement, in addition to the algebraic convergence in DSEM when *h*-refinement is performed.

In chapter 7, we developed an spectrally accurate fractional spectral collocation method (FSCM) for solving steady-state and time-dependent Fractional PDEs (FPDEs). First, we introduced *fractional Lagrange interpolants*, which satisfy the Kronecker delta property at collocation points. We performed such a construction following a spectral theory developed in [187] for fractional Sturm-Liouville eigen-problems. Moreover, we obtained the corresponding fractional differentiation matrices and solved a number of linear and nonlinear FPDEs to investigate the numerical performance of the fractional collocation method. To this end, we introduced new candidate choices for collocation/interpolation points, namely roots of Jacobi-polyfractonomial ${}^{(1)}\mathcal{P}_M^{\mu}(x)$ and roots of ${}_{-1}\mathcal{D}_x^{\mu}[\,{}^{(1)}\mathcal{P}_M^{\mu}(x)\,]$, denoted as (fractional) *extrema* of the Jacobi polyfractonomial. We compared these new sets of residual-vanishing points with other existing standard interpolation/collocation points such as roots of Chebyshev polynomials, extrema of Chebyshev polynomials, and equidistant points. We numerically demonstrated that the roots of ${}_{-1}\mathcal{D}_x^{\mu}[\,{}^{(1)}\mathcal{P}_M^{\mu}(x)\,]$ are the best among others leading to minimal condition number in the corresponding linear system and fastest decay of L^2-norm error.

We considered steady-state problems such as space-fractional advection-diffusion problem and generalized space-fractional multi-term problems; also time-dependent FPDEs such as time- and space-fractional advection-diffusion equation, time- and space- fractional multi-term FPDEs, and finally the space-fractional Burgers' equation. Our numerical results confirmed the exponential convergence of the fractional collocation method. We shall discuss the performance of FSCM in comparison with other approaches. In fact, among other high-order Galerkin spectral methods, also finite difference schemes developed for FPDEs, our FSCM scheme has a number of advantages including (i) ease of implementation, (ii) lower computational cost, and (iii) exponential accuracy. In the following we further elaborate on each of these

features.

In terms of computational cost, the computational complexity of mathematical operations in the construction of $\mathbf{D}^{\sigma}$ and $\mathbf{D}^{1+\sigma}$ can be shown to be of $\mathcal{O}(N^2)$. Moreover, the computational cost of the presented method for steady-state linear FODEs can be shown to be mainly associated with: (i) the construction of the differentiation matrices, and (ii) the linear system solver. Then, the computational cost of the presented scheme is asymptotically $\mathcal{O}(\,(M_a + M_d)N^2 + N^3)$ for such FODEs, where M_a and M_d represent the number of advection- and diffusion-looking terms, respectively. For time-dependent multi-term FPDEs presented, the cost of the scheme grows as $\mathcal{O}(\,(M_a + M_d)N^2 + (MN)^3)$, when a direct solver is employed.

In contrast to the standard Galerkin projection schemes, there is no quadrature performed in our FSCM. Moreover, the treatment of nonlinear terms in FSCM can be done with the same ease as in linear problems. This is significant because solving nonlinear FPDEs remains a challenge in Galerkin methods. In addition, although the employment of Galerkin methods in linear FPDEs becomes conceptually similar to FSCM, Galerkin spectral methods with the traditional (polynomial) basis functions do not always lead to exponential convergence as it does in our FSCM; such schemes. Another important barrier in Galerkin projection schemes is the difficulty of treating multi-term FPDEs, where no straightforward variational form can be efficiently obtained for such problems. In contrast, we have clearly shown that our FSCM requires no extra effort to solve such multi-term FPDEs. Despite the aforementioned advantages of FSCM, the drawback of FSCM is that there is no rigorous theoretical framework for collocation schemes in general.

In chapter 8, we developed a highly-accurate fractional spectral collocation method for solving linear and nonlinear FPDEs with field-variable temporal and/or spatial

fractional orders. To this end and corresponding to the type of spatial derivatives (either Riemann-Liouville or Riesz), we introduced a new family of interpolants, called *left-/right-sided and central fractional Lagrange interpolants*, which satisfy the Kronecker delta property at collocation points. We constructed such interpolators to approximate the aforementioned fractional operators of both (left-/right-sided) Riemann-Liouville and Riesz type. We obtained the corresponding fractional differentiation matrices exactly. We solved several variable-order FPDEs including time- and space-fractional advection-equation, time- and space- fractional advection-diffusion equation, and finally the space-fractional Burgers' equation. We also developed an unconditionally stable penalty method that efficiently treats FPDEs subject to inhomogeneous initial conditions. In our numerical examples, we demonstrated the exponential decay of L^∞-error in the aforementioned model problems.

In addition to the accuracy, the key idea to the efficiency in our approach was to collocate the fied-variable orders, as well as the resulting fractional FPDEs, at the collocation points. In fact, the C^0-continuity of the fractional order in fixed-order FDPEs allowed us to require only the C^0-continuity for the temporally and/or spatially-variable fractional orders in this study. This assumption made the point-wise evaluation of such field-variable orders at any arbitrary point well-defined in the space-time domain, hence, led us to circumvent the need for any quadrature rules that usually arise in spectral methods. To our experience, such numerical integrations become significantly costly when Galerkin/Petrov-Galerkin methods are employed, moreover, the resulting weak forms yield non-separable linear systems, which may lead to prohibitive computations in high dimensions.

In chapter 9, we developed a unified and spectrally accurate Petrov-Galerkin (PG) spectral method for a weak formulation of the general linear FPDE of the form ${}_0\mathcal{D}_t^{2\tau}u + \sum_{j=1}^{d} c_{x_j}[\ {}_{a_j}\mathcal{D}_{x_j}^{2\mu_j}u\ ] + \gamma\ u = f$, τ, $\mu_j \in (0,1)$, in a $(1+d)$-dimensional *space-*

time domain subject to Dirichlet initial and boundary conditions. We demonstrated that this scheme performs well for the whole family of linear *hyperbolic*-, *parabolic*- and *elliptic*-like equations with the same ease. We developed our PG method based on a new spectral theory for fractional Sturm-Liouville problems (FSLPs), recently introduced in [187]. In the present method, all the aforementioned matrices are constructed *exactly* and *efficiently*. We additionally performed the stability analysis (in 1-D) and the corresponding convergence study of the scheme (in multi-D). Moreover, we formulated a new general fast linear solver based on the eigen-pairs of the corresponding temporal and spatial mass matrices with respect to the stiffness matrices, which significantly reduces the computational cost in higher-dimensional problems e.g., (1+3), (1+5) and (1+9)-dimensional FPDEs.

In the p-refinement tests performed in the aforementioned problems, we kept the fractional order to be the middle-value (either 1/2 or 3/2) in the fixed direction, and we examined some limit fractional orders in the other direction. However, we numerically observe that if the fixed fractional order is taken to be closer to the limit values (i.e., either 0 or 1), the mode of spectral convergence remains unchanged but we achieve a different rate of convergence to be verified in our future theoretical analysis.

Alternating Direction Implicit (ADI) methods (see e.g., [75]) are another way of solving space-fractional FPDEs in higher dimensional problems. In this approach, a one-dimensional space-fractional FPDE solver with a low-order (finite-difference) time integrator can be employed to solve 2-D or 3-D problems. However, we note that ADI naturally cannot treat time- and space-fractional FPDEs. Moreover, the temporal rate of convergence in this approach is *algebraic* in contrast to the high accuracy in the spatial discretizations. Hence, the computational complexity of this approach becomes exceedingly large in higher-dimensional FPDEs.

Although the proposed unified PG method enjoys the high accuracy of the discretization in time and space in addition to its efficiency in solving higher-dimensional problems, treating FPDEs in complex geometries still remains a great challenge to be addressed in our future works. Moreover, special care should be taken when the FPDE of the interest is associated with variable coefficients and/or non-linearity. In [190], we have employed the fractional bases to construct a new class of fractional Lagrange interpolants i.e., fractional *nodal* rather than *modal* basis functions presented here, to develop efficient and spectrally accurate collocation methods for a variety of FODEs and FPDEs including non-linear space-fractional Burgers' equation.

In chapter 10, distributed-order fractional operators were considered. We developed a spectrally-accurate fractional spectral collocation method for distributed fractional differential equations. This scheme was developed based on the recent spectral theory for fractional Sturm-Liouville problems (FSLPs), which has been recently developed in [187]. In the collocation scheme, We employed fractional Lagrange interpolants, which satisfy the Kronecker delta property at collocation points. Subsequently, we obtained the corresponding fractional differentiation matrices. In addition to spectral accuracy in space, we were able to formulate an observable second order in time splitting method to be employed in other nonlinear problems such as Navier-Stokes equation in future. This chapter is under preparation for submission to SIAM Journal on multiscale simulations, [191].

In chapter 11, we developed an implicit-explicit (IMEX) splitting scheme for a one-dimensional space-fractional with integer-order time-derivative, in addition to time- and space-fractional Keller-Segel chemotaxis system. The fractional temporal derivative is of Caputo sense and the spatial derivatives are of Riemann-Liouville type. In this method, the diffusion term is treated implicitly while the nonlinear chemotaxis reaction term is evaluated explicitly. We carried out the time-integration

in the prediction step employing a fractional finite difference scheme of observable order Δ^2. The spatial discretization was performed by employing an efficient and spectrally-accurate fractional spectral collocation method, in which the Lagrange interpolants are non-polynomials (fractional). This chapter is also under preparation for submission to JCP, [186].

In chapter 12, we extended the concept of projection problem in one-dimensional cases, studied in chapter 2, to non-tensorial regions of multiple dimensions. We examined triangle and tetrahedral in the standard domain. To this end, we constructed the corresponding fractional modal basis function in terms of Jacobi polyfractonomials, introduced in chapter 2. This work was the first attempt in employing non-polynomial (fractional) basis functions in non-tensorial domains, which can lead to formulation of FPDEs in complex geometries.

13.1 Future Work

Many open issues remain in this field to be addressed in our future work. Here, we list some of them as follows:

- **Complex geometries:** the projection work we carried out in simplex domains (triangles and tetrahedrals) prepared the ground for our future development of high-order methods for FPDEs in complex geometries. To this end, there are a number of important issues to be addressed in future: i) the possibility of performing Petrov-Galerkin projection for possible improvement of efficiency, ii) construction of stiffness matrices in single and multi-element cases, iii) the enforcement of different types of boundary conditions, and iv) designing meshes,

which could minimize the complexity of history calculations in irregular domains.

- **Efficient adaptivity:** the fast convergence of spectral and spectral element methods relies on the smoothness of the solution. However, adaptivity is necessary for the region with low regularity, where the solution adopts certain types of singularities. Hence, effective adaptive strategies are necessary for both h- and p-convergence for certain problems.

- **High-performance computing:** we plan for strategic research efforts on high-performance computing of the developed high-order methods (spectral/hp element methods) for fractional fixed-, variable-, and distributed-order PDEs for a range of applications. To this end, we will develop open-source computational platforms for parallel computing for such models.

- **Uncertainty quantification:** uncertainties in our knowledge of physical properties of materials, as well as in topological (boundary) constrains is inevitable. Moreover, systems modeled by fractional PDEs could be subject to random excitements, which naturally cast underlying mathematical models in a stochastic framework. In addition, large data-driven simulations rely heavily on fine-tuning of differential orders (fixed, variable, and distributed) in fractional PDEs. This necessitates a systematic framework for uncertainty quantification (UQ) in fractional PDEs.

Appendix A

Derivation of the DSM and DSEM in Chapter 4

A.1 Derivation of the discontinuous spectral method (DSM)

Let $I = [0, T]$ be the time-domain and $\vartheta(t) \in \mathcal{V}_N$ be an arbitrary test function. Then, we obtain a variational form for the solution $u(t)$ by multiplying (4.1) by $\vartheta(t)$ and integrating in I as

$$\Big({}_0\mathcal{D}_t^{\nu} u(t)\,,\, \vartheta(t) \Big)_I = \Big(f(t)\,,\, \vartheta(t) \Big)_I. \tag{A.1}$$

On the left-hand side, by the definition of the left-sided fractional derivative we have

$$\begin{aligned}
\Big({}_0\mathcal{D}_t^{\nu} u(t)\,,\, \vartheta(t) \Big)_I &= \int_0^T \frac{1}{\Gamma(1-\nu)} \frac{d}{dt} \int_0^t \frac{u(s)ds}{(t-s)^{\nu}}\ \vartheta(t)dt, \qquad (A.2)\\
&= \frac{\vartheta(t)}{\Gamma(1-\nu)} \int_0^t \frac{u(s)ds}{(t-s)^{\nu}}\Big|_{t=0}^{t=T} - \int_0^T \frac{1}{\Gamma(1-\nu)} \int_0^t \frac{u(s)ds}{(t-s)^{\nu}}\ \frac{d}{dt}\vartheta(t)\,dt\\
&= \frac{\vartheta(T)}{\Gamma(1-\nu)} \int_0^T \frac{u(s)ds}{(T-s)^{\nu}} - \int_0^T \frac{1}{\Gamma(1-\nu)} \int_0^t \frac{u(s)ds}{(t-s)^{\nu}}\ \frac{d}{dt}\vartheta(t)\,dt\\
&= \frac{\vartheta(T)}{\Gamma(1-\nu)} \int_0^{0^+} \frac{u(s)ds}{(T-s)^{\nu}} + \frac{\vartheta(T)}{\Gamma(1-\nu)} \int_{0^+}^T \frac{u(s)ds}{(T-s)^{\nu}}\\
&- \int_0^T \frac{1}{\Gamma(1-\nu)} \int_0^t \frac{u(s)ds}{(t-s)^{\nu}}\ \frac{d}{dt}\vartheta(t)\,dt
\end{aligned}$$

where by carrying out the integration-by-parts in $\frac{\vartheta(T)}{\Gamma(1-\nu)} \int_0^{0^+} \frac{u(s)ds}{(T-s)^{\nu}}$ and assuming the exact solution $u \in C^1[0, T]$ we obtain

$$\begin{aligned}
\frac{\vartheta(T)}{\Gamma(1-\nu)} \int_0^{0^+} \frac{u(s)ds}{(T-s)^{\nu}} &= 0 \qquad (A.3)\\
&= \frac{\vartheta(T)\, T^{1-\nu}}{(1-\nu)\Gamma(1-\nu)}(u_D - u(0^+))\\
&+ \frac{\vartheta(T)}{\Gamma(1-\nu)} \int_0^{0^+} (T-s)^{1-\nu} \frac{du(s)}{ds}\, ds
\end{aligned}$$

where the second integral term in (A.3) is also identically zero. Now, by substituting the exact solution $u(t)$ by the approximate $u_N(t)$, we obtain

$$\frac{\vartheta(T)}{\Gamma(1-\nu)}\int_0^{0^+}\frac{u(s)ds}{(T-s)^\nu}\approx\frac{\vartheta(T)\,T^{1-\nu}}{(1-\nu)\Gamma(1-\nu)}(u_D-u_N(0^+)) \tag{A.4}$$

where $(u_D-u_N(0^+))\neq 0$, however, as $N\to\infty$ this jump discontinuity approaches zero. Now, by substituting (A.4) in (A.2), replacing u by u_N, and finally subtracting a zero term $\frac{\vartheta(0^+)}{\Gamma(1-\nu)}\int_{0^+}^{0^+}\frac{u_N(s)ds}{(0^+-s)^\nu}$, we obtain

$$\begin{aligned}
\Big({}_0\mathcal{D}_t^\nu u(t)\,,\,\vartheta(t)\Big)_I &\approx \Big({}_0\mathcal{D}_t^\nu u_N(t)\,,\,\vartheta(t)\Big)_I\\
&= \frac{\vartheta(T)\,T^{1-\nu}}{(1-\nu)\Gamma(1-\nu)}(u_D-u_N(0^+))\\
&+ \frac{\vartheta(T)}{\Gamma(1-\nu)}\int_{0^+}^{T}\frac{u_N(s)ds}{(T-s)^\nu}-\frac{\vartheta(0^+)}{\Gamma(1-\nu)}\int_{0^+}^{0^+}\frac{u_N(s)ds}{(0^+-s)^\nu}\\
&- \int_0^T\frac{1}{\Gamma(1-\nu)}\int_0^t\frac{u_N(s)ds}{(t-s)^\nu}\,\frac{d}{dt}\vartheta(t)\,dt\\
&= \frac{\vartheta(T^-)\,T^{1-\nu}}{(1-\nu)\Gamma(1-\nu)}(u_D-u_N(0^+))+\frac{\vartheta(t)}{\Gamma(1-\nu)}\int_{0^+}^{t}\frac{u_N(s)ds}{(t-s)^\nu}\Big|_{t=0^+}^{t=T}\\
&- \int_0^T\frac{1}{\Gamma(1-\nu)}\int_0^t\frac{u_N(s)ds}{(t-s)^\nu}\,\frac{d}{dt}\vartheta(t)\,dt\\
&= \Big({}_{0^+}\mathcal{D}_t^\nu u_N(t)\,,\,\vartheta(t)\Big)_I+\frac{\vartheta(T^-)\,T^{1-\nu}}{(1-\nu)\Gamma(1-\nu)}(u_D-u_N(0^+)),
\end{aligned}$$

where by by Lemma 6.3.4

$$\Big({}_0\mathcal{D}_t^\nu u_N(t)\,,\,\vartheta(t)\Big)_I=\Big({}_{0^+}\mathcal{D}_t^{\nu/2}u_N(t)\;,\;{}_t\mathcal{D}_T^{\nu/2}\vartheta(t)\Big)_I-\frac{\vartheta(T)T^{1-\nu}}{(1-\nu)\Gamma(1-\nu)}[\![u_N(0)]\!], \tag{A.5}$$

which completes the derivation of the DSM spectral method for FIVPs by substituting (A.5) into (A.1).

For the derivation of the DSM scheme (4.42) for FFVPs, we repeat the above

steps where this time the jump discontinuity occurs at the final-condition. However, we realize that there exists an easier way to do so that is performing the change of variable $\tilde{t} = T - t$ in (A.5) and the Lemma 6.3.4.

A.2 Derivation of the discontinuous spectral element method (DSEM)

Now, let $I_e = [t_{e-1/2}\,,\, t_{e+1/2}]$ be the e-th time-element and $\vartheta^e(t) \in \mathcal{V}_N$ be an arbitrary test function. Then, we obtain the corresponding variational form by multiplying (4.1) by $\vartheta^e(t)$, and integrating in I_e as

$$\Big({}_0\mathcal{D}_t^\nu u(t)\,,\, \vartheta^e(t) \Big)_{I_e} = \Big(f(t)\,,\, \vartheta^e(t) \Big)_{I_e}. \tag{A.6}$$

On the left-hand side, by the definition of the left-sided fractional derivative we have

$$\begin{aligned}
\Big({}_0\mathcal{D}_t^\nu u(t)\,,\, \vartheta^e(t) \Big)_{I_e} &= \Big(\frac{1}{\Gamma(1-\nu)} \frac{d}{dt} \int_0^t \frac{u(s)\,ds}{(t-s)^\nu}\,,\, \vartheta^e(t) \Big)_{I_e} \\
&= \Big(\frac{1}{\Gamma(1-\nu)} \frac{d}{dt} \int_0^{t_{e-1/2}^-} \frac{u(s)\,ds}{(t-s)^\nu}\,,\, \vartheta^e(t) \Big)_{I_e} \\
&+ \Big(\frac{1}{\Gamma(1-\nu)} \frac{d}{dt} \int_{t_{e-1/2}^-}^{t_{e-1/2}^+} \frac{u(s)\,ds}{(t-s)^\nu}\,,\, \vartheta^e(t) \Big)_{I_e} \\
&+ \Big(\frac{1}{\Gamma(1-\nu)} \frac{d}{dt} \int_{t_{e-1/2}^+}^{t} \frac{u(s)\,ds}{(t-s)^\nu}\,,\, \vartheta^e(t) \Big)_{I_e},
\end{aligned}$$

where by the same argument as in the derivation in A.1 and also by the definition of the left-sided fractional derivative in the last term we obtain

$$\begin{aligned}
\Big({}_0\mathcal{D}_t^{\nu} u(t)\,,\, \vartheta^e(t) \Big)_{I_e} &\approx \Big({}_0\mathcal{D}_t^{\nu} u_N(t)\,,\, \vartheta^e(t) \Big)_{I_e} \\
&= \Big({}_{t^+_{e-1/2}}\mathcal{D}_t^{\nu} u_N^e(t)\,,\, \vartheta^e(t) \Big)_{I_e} \\
&+ \frac{\vartheta^e(t^-_{e+1/2})(\Delta t)_e^{1-\nu}}{(1-\nu)\Gamma(1-\nu)} \Big(u_N^{e-1}(t^-_{e-1/2}) - u_N^e(t^+_{e-1/2}) \Big) \\
&+ \Big(\frac{1}{\Gamma(1-\nu)} \frac{d}{dt} \int_0^{t^-_{e-1/2}} \frac{u(s)\,ds}{(t-s)^{\nu}}\,,\, \vartheta^e(t) \Big)_{I_e}
\end{aligned} \tag{A.7}$$

where $(\Delta t)_e = t_{e+1/2} - t_{e-1/2}$, and we have replaced u in the last first and the second term by u_N and have left the last term unchanged for the following argument. Now, by Lemma 6.3.4, and the definition of the jump discontinuity we obtain

$$\begin{aligned}
\Big({}_0\mathcal{D}_t^{\nu} u_N(t)\,,\, \vartheta^e(t) \Big)_{I_e} &= \Big({}_{t^+_{e-1/2}}\mathcal{D}_t^{\nu/2} u_N^e(t)\,,\, {}_t\mathcal{D}^{\nu/2}_{t^-_{e+1/2}}\, \vartheta^e(t) \Big)_{I_e} \\
&- \frac{\vartheta^e(t^-_{e+1/2})(\Delta t)_e^{1-\nu}}{(1-\nu)\Gamma(1-\nu)} [\![u_N^e(t_{e-1/2})]\!] + \mathcal{H}_e\,.
\end{aligned} \tag{A.8}$$

We suppose that $u_N(t)$ is only unknown in the present element I_e and we have already solved for $u_N(t)$ in all the previous (past) time-elements. Hence the time-interval $[0, t^-_{e-1/2}]$, appearing in the last integral in (A.7), in fact represents a time-history interval. Consequently, we compute $\mathcal{H}_e$ in (A.8) by decomposing the time-history

interval $[0, t^-_{e-1/2}]$ into the *interior* past time-elements $I_\epsilon \equiv [t^+_{\epsilon-1/2}, t^-_{\epsilon+1/2}]$ as

$$\begin{aligned}
\mathcal{H}_e &= \Big(\frac{1}{\Gamma(1-\nu)} \frac{d}{dt} \int_0^{t^-_{e-1/2}} \frac{u_N(s)\, ds}{(t-s)^\nu} \,,\, \vartheta^e(t) \Big)_{I_e} \\
&= \Big(\sum_{\epsilon=1}^{e-1} \Big(\frac{1}{\Gamma(1-\nu)} \frac{d}{dt} \int_{t^-_{\epsilon-1/2}}^{t^+_{\epsilon-1/2}} \frac{u^\epsilon_N(s)\, ds}{(t-s)^\nu} \,,\, \vartheta^e(t) \Big)_{I_e} \\
&= \Big(\vartheta^e(t) \frac{1}{\Gamma(1-\nu)} \sum_{\epsilon=1}^{e-1} \int_{I_\epsilon} \frac{u^\epsilon_N(s) ds}{(t-s)^\nu} \Big) \Big|_{t=t^+_{e-1/2}}^{t=t^-_{e+1/2}} \\
&- \Big(\frac{1}{\Gamma(1-\nu)} \sum_{\epsilon=1}^{e-1} \int_{I_\epsilon} \frac{u^\epsilon_N(s) ds}{(t-s)^\nu} \,,\, \frac{d}{dt} \vartheta^e(t) \Big)_{I_e}
\end{aligned} \tag{A.9}$$

where u^ϵ_N denotes the known solution we have already solved for, and is well-defined only in element $I_\epsilon = [t^+_{\epsilon-1/2}, t^-_{\epsilon+1/2}]$. We note that u^ϵ_N is a polynomial of degree N. Therefore, u^ϵ_N has N continuous derivatives in I_ϵ. Accordingly, in order to reduce the double integral appearing in the last term in (A.9), we carry out integration-by-parts in $\int_{I_\epsilon} \frac{u^\epsilon_N(s) ds}{(t-s)^\nu}$ N times to obtain

$$\begin{aligned}
\frac{1}{\Gamma(1-\nu)} \sum_{\epsilon=1}^{e-1} \int_{I_\epsilon} \frac{u^\epsilon_N(s) ds}{(t-s)^\nu} &= \sum_{\epsilon=1}^{e-1} \sum_{\delta=0}^{N} \tau_\delta (t-s)^{\delta+1-\nu} u^{(\delta)\epsilon}_N(s) \Big|_{s=t^+_{\epsilon-1/2}}^{s=t^-_{\epsilon+1/2}} \\
&= \sum_{\epsilon=1}^{e-1} F^\epsilon_e(t) \\
&= F_e(t)
\end{aligned} \tag{A.10}$$

where $F_e(t)$ denotes the *flux function* associated to the element I_e in which $\tau_\delta = \frac{-1}{\Gamma(1-\nu) \prod_{m=0}^{\delta} (m+1-\nu)}$. Now, by substituting (A.10) we can efficiently compute the history term as

$$\mathcal{H}_e = \vartheta^e(t) F_e(t) \Big|_{t=t^+_{e-1/2}}^{t=t^-_{e+1/2}} - \Big(F_e(t) \,,\, \frac{d}{dt} \vartheta^e(t) \Big)_{I_e} \tag{A.11}$$

where the double-integral in (A.9) renders a convenient one-dimensional form in (A.11). It completes the derivation for the fractional discontinuous spectral element

scheme given in (5.79).

Now, we would like to shed more light on the meaning of such history term by re-representing the history term as

$$\mathcal{H}_e = \tag{A.12}$$
$$\frac{1}{\Gamma(1-\nu)}\sum_{\epsilon=1}^{e-1}\Big\{\vartheta^e(t^-_{e+1/2})\int_{t^+_{\epsilon-1/2}}^{t^-_{\epsilon+1/2}}\frac{u^\epsilon_N(s)ds}{(t^-_{e+1/2}-s)^\nu}-\vartheta^e(t^+_{e-1/2})\int_{t^+_{\epsilon-1/2}}^{t^-_{\epsilon+1/2}}\frac{u^\epsilon_N(s)ds}{(t^+_{e-1/2}-s)^\nu}\Big\}$$
$$-\frac{1}{\Gamma(1-\nu)}\sum_{\epsilon=1}^{e-1}\Big(\int_{I_\epsilon}\frac{u^\epsilon_N(s)ds}{(t-s)^\nu}\,,\,\frac{d}{dt}\vartheta^e(t)\Big)_{I_e},$$

Next, we continuously extend the solution u^ϵ_N from the corresponding element I_ϵ to the present element I_e, denoted by $u^{\epsilon*}_N$, such that $u^{\epsilon*}_N\Big|_{I_\epsilon} = u^\epsilon_N$. In the simplest extension which also sounds natural is to take right-end value of u^ϵ_N and consider this constant value in later elements upto I_e. Having such an extension defined, we can replace u^ϵ_N in (A.12) with $u^{\epsilon*}_N$ and re-write each expression in (A.12) in terms of the subtraction of two integrals as

$$\int_{t^+_{\epsilon-1/2}}^{t^-_{\epsilon+1/2}}\frac{u^\epsilon_N(s)ds}{(t^-_{e+1/2}-s)^\nu}=\int_{t^+_{\epsilon-1/2}}^{t^-_{e+1/2}}\frac{u^{\epsilon*}_N(s)ds}{(t^-_{e+1/2}-s)^\nu}-\int_{t^-_{\epsilon+1/2}}^{t^-_{e+1/2}}\frac{u^{\epsilon*}_N(s)ds}{(t^-_{e+1/2}-s)^\nu}, \tag{A.13}$$

$$\int_{t^+_{\epsilon-1/2}}^{t^-_{\epsilon+1/2}}\frac{u^\epsilon_N(s)ds}{(t^+_{e-1/2}-s)^\nu}=\int_{t^+_{\epsilon-1/2}}^{t^+_{e-1/2}}\frac{u^{\epsilon*}_N(s)ds}{(t^+_{e-1/2}-s)^\nu}-\int_{t^-_{\epsilon+1/2}}^{t^+_{e-1/2}}\frac{u^{\epsilon*}_N(s)ds}{(t^+_{e-1/2}-s)^\nu}, \tag{A.14}$$

and

$$\int_{I_\epsilon}\frac{u^\epsilon_N(s)ds}{(t-s)^\nu}=\int_{t^+_{\epsilon-1/2}}^{t}\frac{u^{\epsilon*}_N(s)ds}{(t-s)^\nu}-\int_{t^-_{\epsilon+1/2}}^{t}\frac{u^{\epsilon*}_N(s)ds}{(t-s)^\nu} \tag{A.15}$$

for any arbitrary $t \in I_e$. Now, by substituting (A.13)-(A.15) into (A.12), we obtain

(A.16)

$$\begin{aligned}\mathcal{H}_e = & \\ \sum_{\epsilon=1}^{e-1} \Big\{ \frac{\vartheta^e(t)}{\Gamma(1-\nu)} \int_{t^+_{\epsilon-1/2}}^{t} \frac{u_N^{\epsilon*}(s)ds}{(t-s)^\nu}\Big|_{t=t^+_{e-1/2}}^{t=t^-_{e+1/2}} - \frac{1}{\Gamma(1-\nu)} \Big(\int_{t^+_{\epsilon-1/2}}^{t} \frac{u_N^{\epsilon*}(s)ds}{(t-s)^\nu}, \frac{d}{dt}\vartheta^e(t) \Big)_{I_e} \Big\} \\ - \sum_{\epsilon=1}^{e-1} \Big\{ \frac{\vartheta^e(t)}{\Gamma(1-\nu)} \int_{t^-_{\epsilon+1/2}}^{t} \frac{u_N^{\epsilon*}(s)ds}{(t-s)^\nu}\Big|_{t=t^+_{e-1/2}}^{t=t^-_{e+1/2}} - \frac{1}{\Gamma(1-\nu)} \Big(\int_{t^-_{\epsilon+1/2}}^{t} \frac{u_N^{\epsilon*}(s)ds}{(t-s)^\nu}, \frac{d}{dt}\vartheta^e(t) \Big)_{I_e} \Big\},\end{aligned}$$

where by inverse integration-by-parts we obtain

(A.17)

$$\begin{aligned}\mathcal{H}_e &= \sum_{\epsilon=1}^{e-1} \Big(\frac{1}{\Gamma(1-\nu)} \frac{d}{dt} \int_{t^+_{\epsilon-1/2}}^{t} \frac{u_N^{\epsilon*}(s)ds}{(t-s)^\nu}, \vartheta^e(t) \Big)_{I_e} \\ &- \sum_{\epsilon=1}^{e-1} \Big(\frac{1}{\Gamma(1-\nu)} \frac{d}{dt} \int_{t^-_{\epsilon+1/2}}^{t} \frac{u_N^{\epsilon*}(s)ds}{(t-s)^\nu}, \vartheta^e(t) \Big)_{I_e}\end{aligned}$$

and by definition of the left-sided fractional derivative we obtain

$$\mathcal{H}_e = -\sum_{\epsilon=1}^{e-1} \Big\{ \Big(\ {}_{s^0_\epsilon}\mathcal{D}^\nu_t u_N^{\epsilon*}(t) \, , \, \vartheta^e(t) \Big)_{I_e} \Big|_{s^0_\epsilon=t^+_{\epsilon-1/2}}^{s^0_\epsilon=t^-_{\epsilon+1/2}}. \tag{A.18}$$

Appendix B

Derivation of the SM-DSEM in Chapter 6

B.1 Derivation of SM-DSEM Scheme

We partition the computational domain into N_{el} non-overlapping space-time elements, $\Omega_e = [x_{e-1/2}, x_{e+1/2}] \times [0, T]$. Next, we test the TSFAE (6.2) against some proper test function $v^e(x,t)$, then integrate over the sub-domain Ω_e and using Lemma 6.3.4 to carry out the temporal fractional integration-by-parts, we obtain

$$\Big({}_0\mathcal{D}_t^{\tau/2} u(x,t)\,,\, {}_t\mathcal{D}_T^{\tau/2} v^e(x,t) \Big)_{\Omega_e} + \theta \Big({}_0\mathcal{D}_x^{\nu} u(x,t)\,,\, v^e(x,t) \Big)_{\Omega_e} = \Big(f(x,t), v^e(x,t) \Big)_{\Omega_e}. \tag{B.1}$$

Due to our domain-decomposition, also the definition of the spatial fractional derivative with lower terminal beginning at $x = 0$, we obtain an equivalent yet more efficient expression as follows

$$\begin{aligned} \Big({}_0\mathcal{D}_x^{\nu} u(x,t)\,,\, v^e(x,t) \Big)_{\Omega_e} &= \Big(\frac{1}{\Gamma(1-\nu)} \frac{\partial}{\partial x} \int_{x_{e-1/2}^{+}}^{x} \frac{u(z,t)\,dz}{(x-z)^{\nu}}\,,\, v^e(x,t) \Big)_{\Omega_e} \\ &+ \Big(\frac{1}{\Gamma(1-\nu)} \frac{\partial}{\partial x} \int_{x_{e-1/2}^{-}}^{x_{e-1/2}^{+}} \frac{u(z,t)\,dz}{(x-z)^{\nu}}\,,\, v^e(x,t) \Big)_{\Omega_e} \\ &+ \Big(\frac{1}{\Gamma(1-\nu)} \frac{\partial}{\partial x} \int_{0}^{x_{e-1/2}^{-}} \frac{u(z,t)\,dz}{(x-z)^{\nu}}\,,\, v^e(x,t) \Big)_{\Omega_e}, \end{aligned} \tag{B.2}$$

where we can re-write (B.2) as

$$\begin{aligned} \Big({}_0\mathcal{D}_x^{\nu} u(x,t) \quad , \quad v^e(x,t) \Big)_{\Omega_e} &= \Big({}_{x_{e-1/2}^{+}}\mathcal{D}_x^{\nu} u(x,t)\,,\, v^e(x,t) \Big)_{\Omega_e} \\ &+ \Big(\frac{1}{\Gamma(1-\nu)} \frac{\partial}{\partial x} \int_{x_{e-1/2}^{-}}^{x_{e-1/2}^{+}} \frac{u(z,t)\,dz}{(x-z)^{\nu}}\,,\, v^e(x,t) \Big)_{\Omega_e} + \mathcal{H}_e^x, \end{aligned} \tag{B.3}$$

where the middle term can be obtained as

$$\Big(\frac{1}{\Gamma(1-\nu)} \frac{\partial}{\partial x} \int_{x^-_{e-1/2}}^{x^+_{e-1/2}} \frac{u(z,t)\,dz}{(x-z)^\nu}\,,\, v^e(x,t) \Big)_{\Omega_e} \approx \\ - \int_0^T \frac{v^e(x^-_{e+1/2},t)(\Delta x_e)^{1-\nu}}{(1-\nu)\Gamma(1-\nu)} [\![u(x_{e-1/2},t)]\!]\, dt, \tag{B.4}$$

where $(\Delta x_e)^{1-\nu} = (x_{e+1/2} - x_{e-1/2})^{1-\nu}$ and $[\![u(x_{e-1/2},t)]\!]$ denotes the jump discontinuity in the solution across the interface between elements Ω_e and I_{e-1} along the time-axis at $x = x_{e-1/2}$. We also obtain the history-load term H^x_e as

$$\mathcal{H}^x_e \;=\; \frac{1}{\Gamma(1-\nu)} \left(\sum_{\varepsilon=0}^{e-1} \frac{\partial}{\partial x} \int_{I_\varepsilon} \frac{u^\varepsilon(x,z)dz}{(x-z)^\nu}, v^e(x,t) \right)_{\Omega_e}. \tag{B.5}$$

Plugging (B.5), (B.4) in (B.3), then plugging (B.3) into (B.1) after carrying out the spatial fractional integration-by-parts using Lemma 6.3.5, we obtain

$$\Big({}_0\mathcal{D}^{\tau/2}_t u(x,t)\;,\; {}_t\mathcal{D}^{\tau/2}_T v^e(x,t) \Big)_{\Omega_e} + \theta \left({}_{x^+_{e-1/2}}\mathcal{D}^{\nu/2}_x u(x,t)\;,\; {}_x\mathcal{D}^{\nu/2}_{x^-_{e+1/2}} v^e(x,t) \right)_{\Omega_e} \\ - \frac{\theta(\Delta x)^{1-\nu}_e}{(1-\nu)\Gamma(1-\nu)} \int_0^T v^e(x^-_{e+1/2},t)\, [\![u^e(x_{e-1/2},t)]\!] dt + \mathcal{H}^x_e \\ = \Big(f(x,t), v^e(x,t) \Big)_{\Omega_e} \tag{B.6}$$

The variational (weak) form (B.6) is an infinite-dimensional problem. Seeking the solution in each sub-domain Ω_e of the form

$$u_{MN}(x,t) = \sum_{m=0}^{M} \sum_{n=1}^{N} \hat{u}_{mn} \tilde{P}^{\eta,0}_m(x^e)\; {}^{(1)}\tilde{\mathcal{P}}^\mu_n(t),$$

as linear combination of elements in the basis function space V^e, and plugging it into (B.6), we obtain the variational form (6.28). At last, we need to provide a more

efficient expression for the history-load term $\mathcal{H}_e^x$ in (B.5):

$$\mathcal{H}_e^x = \sum_{m,n}\sum_{\varepsilon=1}^{e-1}(M_t)_{jn}\frac{1}{\Gamma(1-\nu)}\Bigg(\int_{x_{\varepsilon-1/2}}^{x_{\varepsilon+1/2}}\frac{\hat{u}_{mn}^{\varepsilon}\tilde{P}_m^{\eta,0}(s)\ ds}{(x-s)^{\nu}}\tilde{P}_i^{0,\chi}(x)\Big|_{x=x_{e-1/2}^{+}}^{x=x_{e+1/2}^{-}} - \int_{x_{e-1/2}}^{x_{e+1/2}}\int_{x_{\varepsilon-1/2}}^{x_{\varepsilon+1/2}}\frac{\hat{u}_{mn}^{\varepsilon}\tilde{P}_m^{\eta,0}(s)\ ds}{(x-s)^{\nu}}\frac{d}{dx}\tilde{P}_i^{0,\chi}(x)dx\Bigg).$$

Since $\tilde{P}_m^{\eta,0}(s)$ are at most of degree M in each element Ω_e, we can carry out integration-by-parts M recursive times to eliminate the double integral. It leads to the history term shown in (6.39), where we reduce the calculation of the history term to a function evaluation and a one-dimensional integration carried out in the current element Ω_e. Finally, we obtain the history-load term $\mathcal{H}_e^x$ in a computationally efficient form as

$$(\mathcal{H}_e^x)_{ij} = \theta\ \sum_{m,n}\hat{u}_{mn}(M_t)_{jn}\left(F_e(x)P_i^{0,\nu/2}(x)\Big|_{x=x_{e-1/2}^{+}}^{x=x_{e+1/2}^{-}} - \int_{x_{e-1/2}}^{x_{e+1/2}}F_e(x)\frac{d}{dx}P_i^{0,\nu/2}(x)\ dx\right),$$

in which $F_e(x)$ represents the history function associated with the current element Ω_e

$$F_e(x) = \sum_{\varepsilon=1}^{e-1}F_e^{\varepsilon}(x)$$

consisting of all the past element contributions as

$$F_e^{\varepsilon}(x) \quad = \quad \sum_{m}\hat{u}_{mn}^{\varepsilon}\sum_{\delta=0}^{M}\tau_{\delta}(x-s)^{\delta+1-\nu}\tilde{P}_m^{\eta,0(\delta)}(s)\Big|_{s=s_{\varepsilon-1/2}^{+}}^{s=s_{\varepsilon+1/2}^{-}}, \tag{B.7}$$

where $\tilde{P}_m^{\eta,0(\delta)}(s)$ represents the δ-th derivative of $\tilde{P}_m^{\eta,0}(s)$, moreover, the coefficient $\tau_{\delta} = -1/\{\Gamma(1-\nu)\prod_{m=0}^{\delta}(m+1-\nu)\}$ decays in a factorial fashion with respect to δ.

Appendix C

Proof of Theorems in Chapter 8

C.1 Proof of Theorem 8.5.1 ($^{*}\mathcal{D}_x^{\sigma(x,t)} \equiv {}_a^{RL}\mathcal{D}_x^{\sigma(x,t)}$)

We substitute (8.29) in (8.28) and take the $\sigma(x,t)$-th order fractional derivative. We do this by mapping the interval $x \in [a,b]$ to the standard domain $\xi \in [-1,1]$ through $x(\xi) = \frac{b+a}{2} + \frac{b-a}{2}\xi$ and following (8.10) as

$$
\begin{aligned}
{}_a^{RL}\mathcal{D}_x^{\sigma(x,t)} u_N &= (\frac{2}{b-a})^{\sigma(x(\xi),t)}\, {}_{-1}\mathcal{D}_\xi^{\sigma(x(\xi),t)} u_N(\,x(\xi),t\,) \\
&= (\frac{2}{b-a})^{\sigma}\, {}_{-1}^{RL}\mathcal{D}_\xi^{\sigma}\Big\{ \sum_{m=2}^{\mathcal{M}}\sum_{n=1}^{\mathcal{N}} u_N(x_m,t_n)\, L_m^{\mu}(\,x(\xi)\,)\mathcal{T}_n^{\tau}(t)\Big\} \\
&= (\frac{2}{b-a})^{\sigma} \sum_{m=2}^{\mathcal{M}}\sum_{n=1}^{\mathcal{N}} u_N(x_m,t_n)\, {}_{-1}^{RL}\mathcal{D}_\xi^{\sigma}\Big\{ L_m^{\mu}(\,x(\xi)\,)\Big\}\mathcal{T}_n^{\tau}(t) \\
&= (\frac{2}{b-a})^{\sigma} \sum_{m=2}^{\mathcal{M}}\sum_{n=1}^{\mathcal{N}} u_N(x_m,t_n)\, {}_{-1}^{RL}\mathcal{D}_\xi^{\sigma}\Big\{ \Big(\frac{\xi-\xi_1}{\xi_m-\xi_1}\Big)^{\mu} \prod_{\substack{k=1\\k\neq m}}^{\mathcal{M}} \Big(\frac{\xi-\xi_k}{\xi_m-\xi_k}\Big)\Big\}\mathcal{T}_n^{\tau}(t) \\
&= (\frac{2}{b-a})^{\sigma} \sum_{m=2}^{\mathcal{M}}\sum_{n=1}^{\mathcal{N}} u_N(x_m,t_n)\, {}_{-1}^{RL}\mathcal{D}_\xi^{\sigma}\Big\{ (1+\xi)^{\mu}\mathcal{G}_m(\xi)\Big\} A_m\, \mathcal{T}_n^{\tau}(t)
\end{aligned}
$$

where $(2/(b-a))^{\sigma(x,t)}$ is a strictly positive function, $A_m = 1/(\xi_m+1)^{\mu}$ and $\mathcal{G}_m(\xi) = \prod_{\substack{k=1\\k\neq m}}^{\mathcal{M}} \Big(\frac{\xi-\xi_k}{\xi_m-\xi_k}\Big)$, $m = 2,3,\cdots,\mathcal{M}$, are all polynomials of order $(\mathcal{M}-1)$, which can be represented exactly in terms of Jacobi polynomials $P_{n-1}^{-\mu,\mu}(\xi)$ by

$$
\mathcal{G}_m(\xi) = \sum_{j=1}^{\mathcal{M}} \beta_{mj}^{L} P_{j-1}^{-\mu,\mu}(\xi). \tag{C.1}
$$

We note that the unknown coefficient matrix β_{mj}^{L} can be obtained analytically. The superscript ^{L} actually refers to the proper change of basis to the regular eigenfunctions of FSLP (11.16) whose *Left-sided* fractional derivative is given exactly in

(11.17). Next, by plugging (C.1) we obtain

$$
\begin{aligned}
{}^{RL}_{a}\mathcal{D}_{x}^{\sigma(x,t)}u_N &= (\frac{2}{b-a})^{\sigma}\sum_{m=2}^{\mathcal{M}}\sum_{n=1}^{\mathcal{N}} u_N(x_m,t_n)\ {}^{RL}_{-1}\mathcal{D}_{\xi}^{\sigma}\Big\{(1+\xi)^{\mu}\sum_{j=1}^{\mathcal{M}}\beta_{mj}^{L}P_{j-1}^{-\mu,\mu}(\xi)\Big\}A_m\,\mathcal{T}_n^{\tau}(t)\\
&= (\frac{2}{b-a})^{\sigma}\sum_{m=2}^{\mathcal{M}}\sum_{n=1}^{\mathcal{N}} u_N(x_m,t_n)\ \sum_{j=1}^{\mathcal{M}}\beta_{mj}^{L}\ {}^{RL}_{-1}\mathcal{D}_{\xi}^{\sigma}\Big\{(1+\xi)^{\mu}P_{j-1}^{-\mu,\mu}(\xi)\Big\}A_m\,\mathcal{T}_n^{\tau}(t)
\end{aligned}
$$

Hence, by (11.17) we obtain

$$
{}^{RL}_{a}\mathcal{D}_{x}^{\sigma(x,t)}u_N = (\frac{2}{b-a})^{\sigma}\sum_{m=2}^{\mathcal{M}}\sum_{n=1}^{\mathcal{N}} u_N(x_m,t_n)A_m\mathcal{T}_n^{\tau}(t)\sum_{j=1}^{\mathcal{M}}\beta_{mj}^{L}\ {}^{RL}_{-1}\mathcal{D}_{\xi}^{\sigma}\ {}^{(1)}\mathcal{P}_{j}^{\ \mu}(\xi). \quad \text{(C.2)}
$$

Case A-I) Constant $\sigma = \mu \in (0,1)$. We use the property (11.17) and obtain

$$
{}^{RL}_{a}\mathcal{D}_{x}^{\ \sigma}u_N = (\frac{2}{b-a})^{\sigma}\sum_{m=2}^{\mathcal{M}}\sum_{n=1}^{\mathcal{N}} u_N(x_m,t_n)A_m\mathcal{T}_n^{\tau}(t)\sum_{j=1}^{\mathcal{M}}\beta_{mj}^{L}\frac{\Gamma(j+\sigma)}{\Gamma(j)}P_{j-1}(\,\xi\,). \quad \text{(C.3)}
$$

Consequently, by evaluating ${}_{a}\mathcal{D}_{x}^{\ \sigma}u_N(\,x,t\,)$ at the collocation points (x_i,t_k) and recalling that $L_n^{\tau}(t_k)=\delta_{kn}$, we obtain

$$
\begin{aligned}
{}^{RL}_{a}\mathcal{D}_{x}^{\ \sigma}u_N(\,x,t\,)\Big|_{(x_i,t_k)} &= \\
(\frac{2}{b-a})^{\sigma}\sum_{m=2}^{\mathcal{M}}\sum_{n=1}^{\mathcal{N}} u_N(x_m,t_n)A_m\delta_{kn}\sum_{j=1}^{\mathcal{M}}\beta_{mj}^{L}\frac{\Gamma(j+\sigma)}{\Gamma(j)}P_{j-1}(\,\xi_i\,)&\\
= \sum_{m=2}^{\mathcal{M}}\{{}^{RL}\mathbf{D}_{L}^{\sigma}\}_{im}\ u_N(x_m,t_k),&
\end{aligned}
$$

where $\{{}^{RL}\mathbf{D}_{L}^{\sigma}\}_{im}$ are the entries of the $(\mathcal{M}-1)\times(\mathcal{M}-1)$ *left-sided* spatial differentiation matrix ${}^{RL}\mathbf{D}_{L}^{\sigma}$ of Riemann-Liouville type, given by

$$
\{{}^{RL}\mathbf{D}_{L}^{\sigma}\}_{im} = (\frac{2}{b-a})^{\sigma}A_m\sum_{j=1}^{\mathcal{M}}\beta_{mj}^{L}\frac{\Gamma(j+\sigma)}{\Gamma(j)}P_{j-1}(\,\xi_i\,). \quad \text{(C.4)}
$$

Case A-II) The general $\sigma(x,t) \in (0,1)$. Following [168] and [187], we first represent the polyfractonomial basis ${}^{(2)}\mathcal{P}_j^{\mu}(\xi)$ in terms of a sum and take a left-sided Riemann-Liouville fractional derivative, to obtain $F_j^{L,\sigma}$ as

$$\begin{aligned} F_j^{L,\sigma}\Big(x(\xi),t\Big) &\equiv {}_{-1}^{RL}\mathcal{D}_{\xi}^{\sigma}\Big\{ {}^{(1)}\mathcal{P}_j^{\mu}(\xi)\Big\} \\ &= {}_{-1}^{RL}\mathcal{D}_{\xi}^{\sigma}\Big\{ \sum_{q=0}^{j-1}(\frac{1}{2})^q(-1)^{q+j-1}\, b_{jq}^{\mu}\,(1+\xi)^{q+\mu}\Big\} \\ &= \sum_{q=0}^{j-1}(\frac{1}{2})^q(-1)^{q+j-1}\, b_{jq}^{*}\ {}_{-1}^{RL}\mathcal{D}_{\xi}^{\sigma}\Big\{(1+\xi)^{q+\mu}\Big\}, \end{aligned}$$

where $b_{jq}^{*} = \begin{pmatrix} j-1+q \\ q \end{pmatrix}\begin{pmatrix} j-1+\mu \\ j-1-q \end{pmatrix}$. Now, we obtain $F_j^{L,\sigma}\Big(x(\xi),t\Big)$ exactly using (8.8) as

$$F_j^{L,\sigma}\Big(x(\xi),t\Big) = \sum_{q=0}^{j-1} b_{jq}^{\mu}\,(1+\xi)^{q+\mu-\sigma}, \tag{C.5}$$

which leads to

$${}_{a}^{RL}\mathcal{D}_{x}^{\sigma(x,t)}u_N(x,t) = (\frac{2}{b-a})^{\sigma(x,t)}\sum_{m=2}^{\mathcal{M}}\sum_{n=1}^{\mathcal{N}} u_N(x_m,t_n)A_m\mathcal{T}_n^{\tau}(t)\sum_{j=1}^{\mathcal{M}}\beta_{mj}^{L}\,F_j^{L,\sigma}(x,t). \tag{C.6}$$

where

$$b_{jq}^{\mu} = (\frac{1}{2})^q(-1)^{q+j-1}\begin{pmatrix} j-1+q \\ q \end{pmatrix}\begin{pmatrix} j-1+\mu \\ j-1-q \end{pmatrix}\frac{\Gamma(q+\mu+1)}{\Gamma(q+\mu+1-\sigma)}. \tag{C.7}$$

Now, by evaluating ${}_{a}^{RL}\mathcal{D}_{x}^{\sigma(x,t)}u_N(x,t)$ at the collocation points (x_i,t_k) also by $L_n^{\tau}(t_k) =$

δ_{kn}, we obtain

$$\begin{aligned} {}^{RL}_{a}\mathcal{D}_{x}^{\sigma(x,t)} u_N\Big|_{(x_i,t_k)} &= (\frac{2}{b-a})^{\sigma(x_i,t_k)} \sum_{m=2}^{\mathcal{M}} u_N(x_m,t_k) A_m \sum_{j=1}^{\mathcal{M}} \beta_{mj}^{L}\, F_j^{L,\sigma}\Big(x_i,t_k\Big) \\ &= \sum_{m=2}^{\mathcal{M}} \{{}^{RL}\mathbf{D}_{L}^{\sigma}\}_{imk} u_N(x_m,t_k), \end{aligned}$$

where $\{{}^{RL}\mathbf{D}_{L}^{\sigma}\}_{ikm}$ are the entries of the $(\mathcal{M}-1)\times(\mathcal{N}-1)\times(\mathcal{M}-1)$ *left-sided* spatial fractional differentiation matrix ${}^{RL}\mathbf{D}_{L}^{\sigma}$ of Riemann-Liouville sense, computed as

$$\{{}^{RL}\mathbf{D}_{L}^{\sigma}\}_{ikm} = (\frac{2}{b-a})^{\sigma(x_i,t_k)} A_m \sum_{j=1}^{\mathcal{M}} \beta_{mj}^{L}\, F_j^{L,\sigma}\Big(x_i,t_k\Big) \tag{C.8}$$

where by re-arrangement $A_m = (\frac{b-a}{2x_m-2a})^{\mu}$. It completes the proof.

C.2 Proof of Theorem 8.5.3 $\left({}^{*}\mathcal{D}_{x}^{1+\nu(x,t)} \equiv {}^{RL}_{a}\mathcal{D}_{x}^{1+\nu(x,t)}\right)$

We switch the order of $\partial/\partial x$ and ${}^{RL}_{a}\mathcal{D}_{x}^{\nu(x,t)}$ to avoid the difficulties arising from taking the first partial derivative of the corresponding Euler gamma functions with respect to x. Hence,

$$\begin{aligned} {}^{RL}_{a}\mathcal{D}_{x}^{1+\nu(x,t)} u_N(x,t) &= {}^{RL}_{a}\mathcal{D}_{x}^{\nu(x,t)} \frac{\partial}{\partial x}\Big\{ u_N(\,x,t\,)\Big\} \\ = (\frac{2}{b-a})^{\nu(x,t)}\, {}^{RL}_{-1}\mathcal{D}_{\xi}^{\nu(x,t)} \Big\{ \sum_{m=2}^{\mathcal{M}} \sum_{n=1}^{\mathcal{N}} u_N(x_m,t_n) A_m \mathcal{T}_n^{\tau}(t) \sum_{j=1}^{\mathcal{M}} \beta_{mj}^{L} (\frac{2}{b-a}) \frac{\partial}{\partial \xi}\Big[\, {}^{(1)}\mathcal{P}_j^{\mu}(\xi)\Big]\Big\} \\ = (\frac{2}{b-a})^{(1+\nu(x,t))} \sum_{m=2}^{\mathcal{M}} \sum_{n=1}^{\mathcal{N}} u_N(x_m,t_n) A_m \mathcal{T}_n^{\tau}(t) \sum_{j=1}^{\mathcal{M}} \beta_{mj}^{L}\, {}^{RL}_{-1}\mathcal{D}_{\xi}^{\nu(x,t)} \Big\{ \frac{\partial}{\partial \xi}\Big[\, {}^{(1)}\mathcal{P}_j^{\mu}(\xi)\Big]\Big\}. \end{aligned}$$

Now, by substituting (11.16) we obtain

$$
\begin{aligned}
{}_{a}^{RL}\mathcal{D}_{x}^{1+\nu(x,t)}u_N(x,t) &= (\frac{2}{b-a})^{(1+\nu(x,t))}\sum_{m=2}^{\mathcal{M}}\sum_{n=1}^{\mathcal{N}}u_N(x_m,t_n)A_m\mathcal{T}_n^{\tau}(t)\cdot \\
\sum_{j=1}^{\mathcal{M}}\beta_{mj}^{L} &\Big[(\mu)\,{}_{-1}^{RL}\mathcal{D}_{\xi}^{\nu(x,t)}\Big\{(1+\xi)^{\mu-1}P_{j-1}^{-\mu,\mu}(\xi)\Big\} \\
&+ (\frac{j}{2})\,{}_{-1}^{RL}\mathcal{D}_{\xi}^{\nu(x,t)}\Big\{(1+\xi)^{\mu}P_{j-2}^{1-\mu,1+\mu}(\xi)\Big\}\Big]
\end{aligned}
\tag{C.9}
$$

in which the Jacobi polynomials $P_{j-1}^{-\mu,\mu}(\xi)$ and $P_{j-2}^{1-\mu,1+\mu}(\xi)$ can be represented in terms of the following sums

$$
\begin{aligned}
P_{j-1}^{-\mu,\mu}(\xi) &= \sum_{q=0}^{j-1}(\frac{1}{2})^{q}(-1)^{q+j-1}b_{jq}^{*}(1+\xi)^{q}, \quad j\geq 1 \\
P_{j-2}^{1-\mu,1+\mu}(\xi) &= \sum_{q=0}^{j-2}(\frac{1}{2})^{q}(-1)^{q+j-2}B_{jq}^{*}(1+\xi)^{q}, \quad j\geq 2
\end{aligned}
$$

respectively, where $B_{jq}^{*}=\begin{pmatrix} j+q \\ q \end{pmatrix}\begin{pmatrix} j-1+\mu \\ j-2-q \end{pmatrix}$. By substituting the Jacobi polynomials back into (C.9) and simplifying, it yields

$$
\begin{aligned}
{}_{a}^{RL}\mathcal{D}_{x}^{1+\nu(x,t)}u_N(x,t) &= (\frac{2}{b-a})^{1+\nu}\sum_{m=2}^{\mathcal{M}}\sum_{n=1}^{\mathcal{N}}u_N(x_m,t_n)A_m\mathcal{T}_n^{\tau}(t)\cdot \\
\sum_{j=1}^{\mathcal{M}}\beta_{mj}^{L} &\Big[(\mu)\mathbb{I}_{\{j\geq 1\}}\sum_{q=0}^{j-1}(\frac{1}{2})^{q}(-1)^{q+j-1}b_{jq}^{*}\,{}_{-1}^{RL}\mathcal{D}_{\xi}^{\nu(x,t)}\Big\{(1+\xi)^{q+\mu-1}\Big\} \\
&+ (\frac{j}{2})\mathbb{I}_{\{j\geq 2\}}\sum_{q=0}^{j-2}(\frac{1}{2})^{q}(-1)^{q+j-2}B_{jq}^{*}\,{}_{-1}^{RL}\mathcal{D}_{\xi}^{\nu(x,t)}\Big\{(1+\xi)^{q+\mu}\Big\}\Big].
\end{aligned}
$$

Now, by virtue of (8.8), we exactly obtain the variable-order fractional derivative of u_N as

$$
\begin{aligned}
{}^{RL}_{a}\mathcal{D}_{x}^{1+\nu(x,t)}u_N(x,t) &= (\frac{2}{b-a})^{1+\nu}\sum_{m=2}^{\mathcal{M}}\sum_{n=1}^{\mathcal{N}}u_N(x_m,t_n)A_m\mathcal{T}_n^{\tau}(t)\cdot \\
\sum_{j=1}^{\mathcal{M}}\beta_{mj}^{L} &\Big[(\mu)\mathbb{I}_{\{j\geq 1\}}\sum_{q=0}^{j-1}(\frac{1}{2})^q(-1)^{q+j-1}b_{jq}^{\mu}\frac{\Gamma(q+\mu)}{\Gamma(q+\mu-\nu(x,t))}(1+\xi)^{q+\mu-1-\nu} \\
&+ (\frac{j}{2})\mathbb{I}_{\{j\geq 2\}}\sum_{q=0}^{j-2}(\frac{1}{2})^q(-1)^{q+j-2}B_{jq}^{\mu}\frac{\Gamma(1+q+\mu)}{\Gamma(1+q+\mu-\nu(x,t))}(1+\xi)^{q+\mu-\nu}\Big].
\end{aligned}
$$

Next, by evaluating the above expression at the collocation points (x_i,t_k), we obtain

$${}_{a}\mathcal{D}_{x}^{1+\nu(x,t)}u_N(\,x,t\,)\Big|_{(x_i,t_k)} = \sum_{m=2}^{\mathcal{M}-1}\{{}^{RL}\mathbf{D}_{L}^{1+\nu}\}_{ikm}u_N(x_m,t_k)$$

in which $\{{}^{RL}\mathbf{D}_{L}^{1+\nu}\}_{ikm}$, when $\nu=\nu(x,t)$ are computed as

$$\{{}^{RL}\mathbf{D}_{L}^{1+\nu}\}_{ikm} = (\frac{2}{b-a})^{1+\nu(x_i,t_k)}A_m\sum_{j=1}^{\mathcal{M}}\beta_{mj}^{L}\mathcal{F}_j^{L,\nu}(x_i,t_k), \tag{C.10}$$

where $i,m=2,3,\cdots,\mathcal{M}$, $k=2,3,\cdots,\mathcal{N}$, and $\mathcal{F}_j^{L,\nu}\Big(x(\xi),t\Big)$ is explicitly given by

$$
\begin{aligned}
\mathcal{F}_j^{L,\nu}\Big(x(\xi),t\Big) &= \mathbb{I}_{\{j\geq 1\}}\sum_{q=0}^{j-1}\mathbb{B}_{jq}^{\mu}\cdot(1+\xi)^{q+\mu-1-\nu(x_i,t_k)} \\
&+ \mathbb{I}_{\{j\geq 2\}}\sum_{q=0}^{j-2}B_{jq}^{\mu}\cdot(1+\xi)^{q+\mu-\nu(x_i,t_k)},
\end{aligned} \tag{C.11}
$$

in which $j = 1, 2, \cdots, \mathcal{M}$, and $A_m = (\frac{b-a}{2x_m - 2a})^{\mu}$. Finally $\mathbb{B}_{jq}^{\mu}$ and B_{jq}^{μ} are the corresponding expansion coefficients, obtained as

$$\mathbb{B}_{jq}^{\mu} = \mu(\frac{1}{2})^q(-1)^{q+j-1} \begin{pmatrix} j-1+q \\ q \end{pmatrix} \begin{pmatrix} j-1+\mu \\ j-1-q \end{pmatrix} \frac{\Gamma(q+\mu)}{\Gamma(q+\mu-\nu(x_i,t_k))}, \qquad (C.12)$$

and

$$B_{jq}^{\mu} = \frac{j}{2}(\frac{1}{2})^q(-1)^{q+j-2} \begin{pmatrix} j+q \\ q \end{pmatrix} \begin{pmatrix} j-1+\mu \\ j-2-q \end{pmatrix} \frac{\Gamma(1+q+\mu)}{\Gamma(1+q+\mu-\nu(x_i,t_k))}. \qquad (C.13)$$

C.3 Proof of Theorem 8.5.5 ($^{*}\mathcal{D}_x^{\sigma(x,t)} \equiv {}_x^{RL}\mathcal{D}_b^{\sigma(x,t)}$)

We substitute (8.32) in (8.31) and take the $\sigma(x,t)$-th order fractional derivative as

$$\begin{aligned}
{}_x^{RL}\mathcal{D}_b^{\sigma(x,t)} u_N &= (\frac{2}{b-a})^{\sigma(x(\xi),t)} \, {}_{\xi}\mathcal{D}_1^{\sigma(x(\xi),t)} \Big\{ u_N(\, x(\xi), t\,) \Big\} \\
&= (\frac{2}{b-a})^{\sigma} \sum_{m=2}^{\mathcal{M}} \sum_{n=1}^{\mathcal{N}} u_N(x_m, t_n) \; {}_{\xi}^{RL}\mathcal{D}_1^{\sigma} \Big\{ R_m^{\mu}(\, x(\xi)\,) \Big\} \mathcal{T}_n^{\tau}(t) \\
&= (\frac{2}{b-a})^{\sigma} \sum_{m=2}^{\mathcal{M}} \sum_{n=1}^{\mathcal{N}} u_N(x_m, t_n) \; {}_{\xi}^{RL}\mathcal{D}_1^{\sigma} \Big\{ \Big(\frac{\xi_{\mathcal{M}} - \xi}{\xi_{\mathcal{M}} - \xi_m} \Big)^{\mu} \prod_{\substack{k=1 \\ k \neq m}}^{\mathcal{M}} \Big(\frac{\xi - \xi_k}{\xi_m - \xi_k} \Big) \Big\} \mathcal{T}_n^{\tau}(t) \\
&= (\frac{2}{b-a})^{\sigma} \sum_{m=2}^{\mathcal{M}} \sum_{n=1}^{\mathcal{N}} u_N(x_m, t_n) \; {}_{-1}^{RL}\mathcal{D}_{\xi}^{\sigma} \Big\{ (1-\xi)^{\mu} \mathcal{G}_m(\xi) \Big\} \mathcal{A}_m \, \mathcal{T}_n^{\tau}(t)
\end{aligned}$$

in which $\mathcal{A}_m = 1/(\xi_{\mathcal{M}} - \xi_m)^{\mu}$ and this time we can re-represent $\mathcal{G}_m(\xi), m = 2, 3, \cdots, \mathcal{M}$, in terms of another set of Jacobi polynomials $P_{n-1}^{\mu,-\mu}(\xi)$ exactly by

$$\mathcal{G}_m(\xi) = \sum_{j=1}^{\mathcal{M}} \beta_{mj}^{R} P_{j-1}^{\mu,-\mu}(\xi), \qquad (C.14)$$

where the superscript ^{R} in (C.14) now refers to the change of basis to the regular eigenfunctions of FSLP of second kind (8.26) whose *Right-sided* fractional derivative is given exactly in (11.17). We again highlight that the unknown coefficient matrix β^{R}_{mj} can be obtained analytically. Next, by plugging (C.1) we obtain

$$\begin{aligned} {}^{RL}_{x}\mathcal{D}^{\sigma(x,t)}_{b} u_N &= (\frac{2}{b-a})^{\sigma} \sum_{m=2}^{\mathcal{M}} \sum_{n=1}^{\mathcal{N}} u_N(x_m,t_n)\ {}^{RL}_{\xi}\mathcal{D}^{\sigma}_{1}\Big\{(1-\xi)^{\mu} \sum_{j=1}^{\mathcal{M}} \beta^{R}_{mj} P^{\mu,-\mu}_{j-1}(\xi)\Big\} \mathcal{A}_m\, \mathcal{T}^{\tau}_{n}(t) \\ &= (\frac{2}{b-a})^{\sigma} \sum_{m=2}^{\mathcal{M}} \sum_{n=1}^{\mathcal{N}} u_N(x_m,t_n) \sum_{j=1}^{\mathcal{M}} \beta^{R}_{mj}\ {}^{RL}_{\xi}\mathcal{D}^{\sigma}_{1}\Big\{(1-\xi)^{\mu} P^{\mu,-\mu}_{j-1}(\xi)\Big\} \mathcal{A}_m\, \mathcal{T}^{\tau}_{n}(t), \end{aligned}$$

Hence, by (11.17)

$${}^{RL}_{x}\mathcal{D}^{\sigma(x,t)}_{b} u_N = (\frac{2}{b-a})^{\sigma} \sum_{m=2}^{\mathcal{M}} \sum_{n=1}^{\mathcal{N}} u_N(x_m,t_n) \mathcal{A}_m \mathcal{T}^{\tau}_{n}(t) \sum_{j=1}^{\mathcal{M}} \beta^{R}_{mj}\ {}^{RL}_{\xi}\mathcal{D}^{\sigma}_{1}\Big\{\ {}^{(2)}\mathcal{P}^{\mu}_{j}(\xi)\Big\} \tag{C.15}$$

Case C-I) Constant $\sigma = \mu \in (0,1)$. By (11.17), we can directly obtain

$${}^{RL}_{x}\mathcal{D}^{\sigma}_{b} u_N = (\frac{2}{b-a})^{\sigma} \sum_{m=2}^{\mathcal{M}} \sum_{n=1}^{\mathcal{N}} u_N(x_m,t_n) \mathcal{A}_m \mathcal{T}^{\tau}_{n}(t) \sum_{j=1}^{\mathcal{M}} \beta^{R}_{mj} \frac{\Gamma(j+\sigma)}{\Gamma(j)} P_{j-1}(\,\xi\,), \tag{C.16}$$

which we evaluate (x_i, t_k) to obtain,

$$\begin{aligned} {}^{RL}_{x}\mathcal{D}^{\sigma}_{b} u_N(\,x,t\,)\Big|_{(x_i,t_k)} &= \\ (\frac{2}{b-a})^{\sigma} \sum_{m=2}^{\mathcal{M}} \sum_{n=1}^{\mathcal{N}} u_N(x_m,t_n) \mathcal{A}_m \delta_{kn} \sum_{j=1}^{\mathcal{M}} \beta^{R}_{mj} \frac{\Gamma(j+\sigma)}{\Gamma(j)} P_{j-1}(\,\xi_i\,) & \\ = \sum_{m=2}^{\mathcal{M}} \{{}^{RL}\mathbf{D}^{\sigma}_{R}\}_{im}\ u_N(x_m,t_k), & \end{aligned}$$

where $\{{}^{RL}\mathbf{D}^{\sigma}_{R}\}_{im}$ are the entries of the $(\mathcal{M}-1)\times(\mathcal{M}-1)$ *right-sided* spatial differ-

entiation matrix ${}^{RL}\mathbf{D}_R^{\sigma}$ of Riemann-Liouville since, given by

$$\{{}^{RL}\mathbf{D}_R^{\sigma}\}_{im} = (\frac{2}{b-a})^{\sigma}\mathcal{A}_m \sum_{j=1}^{\mathcal{M}} \beta_{mj}^{R} \frac{\Gamma(j+\sigma)}{\Gamma(j)} P_{j-1}(\,\xi_i\,). \tag{C.17}$$

Case C-II) The general $\sigma(x,t) \in (0,1)$. Following [187], we first represent the polyfractonomial basis ${}^{(2)}\mathcal{P}_j^{\mu}(\xi)$ in terms of the following sum then we take its right-sided Riemann-Liouville fractional derivative, denoted by $F_j^{R,\sigma}$, as

$$\begin{aligned} F_j^{R,\sigma}\Big(x(\xi),t\Big) &\equiv {}_{\xi}^{RL}\mathcal{D}_1^{\sigma}\Big\{\,{}^{(2)}\mathcal{P}_j^{\mu}(\xi)\Big\} \\ &= {}_{\xi}^{RL}\mathcal{D}_1^{\sigma}\Big\{\sum_{q=0}^{j-1}(\frac{-1}{2})^q\, b_{jq}^{\mu}\,(1-\xi)^{q+\mu}\Big\} \\ &= \sum_{q=0}^{j-1}(\frac{-1}{2})^q\, c_{jq}^{*}\;{}_{\xi}^{RL}\mathcal{D}_1^{\sigma}\Big\{(1-\xi)^{q+\mu}\Big\}, \end{aligned}$$

where $c_{jq}^{*} = \begin{pmatrix} j-1+q \\ q \end{pmatrix}\begin{pmatrix} j-1-\mu \\ j-1-q \end{pmatrix}$. Now, we obtain $F_j^{R,\sigma}\Big(x(\xi),t\Big)$ exactly using (8.9) as

$$F_j^{R,\sigma}\Big(x(\xi),t\Big) = \sum_{q=0}^{j-1} c_{jq}^{\mu}\,(1-\xi)^{q+\mu-\sigma}, \tag{C.18}$$

where

$$c_{jq}^{\mu} = -(\frac{-1}{2})^q \begin{pmatrix} j-1+q \\ q \end{pmatrix}\begin{pmatrix} j-1-\mu \\ j-1-q \end{pmatrix}\frac{\Gamma(q+\mu+1)}{\Gamma(q+\mu+1-\sigma)}, \tag{C.19}$$

which leads to

$${}_{x}^{RL}\mathcal{D}_b^{\sigma(x,t)}u_N(x,t) = (\frac{2}{b-a})^{\sigma(x,t)}\sum_{m=2}^{\mathcal{M}}\sum_{n=1}^{\mathcal{N}} u_N(x_m,t_n)\mathcal{A}_m\mathcal{T}_n^{\tau}(t)\sum_{j=1}^{\mathcal{M}}\beta_{mj}^{R}\,F_j^{R,\sigma}(x,t). \tag{C.20}$$

Now, by evaluating ${}^{RL}_{x}\mathcal{D}^{\sigma(x,t)}_{b} u_N(x,t)$ at the collocation points (x_i, t_k) we obtain

$$\begin{aligned} {}^{RL}_{x}\mathcal{D}^{\sigma(x,t)}_{b} u_N\Big|_{(x_i,t_k)} &= (\frac{2}{b-a})^{\sigma(x_i,t_k)} \sum_{m=2}^{\mathcal{M}} u_N(x_m,t_k)\mathcal{A}_m \sum_{j=1}^{\mathcal{M}} \beta^R_{mj}\, F_j^{R,\sigma}\Big(x_i,t_k\Big) \\ &= \sum_{m=2}^{\mathcal{M}} \{{}^{RL}\mathbf{D}^{\sigma}_{R}\}_{imk} u_N(x_m,t_k), \end{aligned}$$

where $\{{}^{RL}\mathbf{D}^{\sigma}_{R}\}_{ikm}$ are the entries of the $(\mathcal{M}-1)\times(\mathcal{N}-1)\times(\mathcal{M}-1)$ *right-sided* spatial fractional differentiation matrix ${}^{RL}\mathbf{D}^{\sigma}_{R}$ of Riemann-Liouville sense, computed as

$$\{{}^{RL}\mathbf{D}^{\sigma}_{R}\}_{ikm} = (\frac{2}{b-a})^{\sigma(x_i,t_k)} \mathcal{A}_m \sum_{j=1}^{\mathcal{M}} \beta^R_{mj}\, F_j^{R,\sigma}\Big(x_i,t_k\Big), \tag{C.21}$$

where by re-arrangement $\mathcal{A}_m = (\frac{b-a}{2b-2x_m})^{\mu}$. We recall from Remark 8.5.2 that if $\sigma = \sigma(x)$, we again reduce the dimension of ${}^{RL}\mathbf{D}^{\sigma}_{R}$ by one, hence, we can obtain the entries of the corresponding two-dimensional right-sided differentiation matrix as

$$\{{}^{RL}\mathbf{D}^{\sigma}_{R}\}_{im} = (\frac{2}{b-a})^{\sigma(x_i)} \mathcal{A}_m \sum_{j=1}^{\mathcal{M}} \beta^L_{mj}\, F_j^{R,\sigma}\Big(x_i\Big). \tag{C.22}$$

C.4 Proof of Theorem 8.5.6 $({}^{*}\mathcal{D}^{\sigma(x,t)}_{x} \equiv {}^{RL}_{x}\mathcal{D}^{1+\nu(x,t)}_{b})$

When the fractional order is both x- and t-dependent, to avoid the difficulties in computations of the first partial derivative in the corresponding gamma functions

with respect to x, we alternatively write ${}^{RL}_{x}\mathcal{D}_{b}^{1+\nu(x,t)}$ as

$$
\begin{aligned}
&{}^{RL}_{x}\mathcal{D}_{b}^{1+\nu(x,t)} u_N(x,t) = {}^{RL}_{x}\mathcal{D}_{b}^{\nu(x,t)} \frac{\partial}{\partial x}\Big\{ u_N(\,x,t\,)\Big\} \\
&= (\frac{2}{b-a})^{\nu}\, {}^{RL}_{\xi}\mathcal{D}_{1}^{\nu(x,t)}\Big\{ \sum_{m=2}^{\mathcal{M}}\sum_{n=1}^{\mathcal{N}} u_N(x_m,t_n)\mathcal{A}_m\mathcal{T}_n^{\tau}(t) \sum_{j=1}^{\mathcal{M}} \beta_{mj}^{L}\, (\frac{2}{b-a})\frac{\partial}{\partial\xi}\Big[\, {}^{(2)}\mathcal{P}_j^{\mu}(\xi)\Big]\Big\} \\
&\quad = (\frac{2}{b-a})^{1+\nu} \sum_{m=2}^{\mathcal{M}}\sum_{n=1}^{\mathcal{N}} u_N(x_m,t_n)\mathcal{A}_m\mathcal{T}_n^{\tau}(t) \sum_{j=1}^{\mathcal{M}} \beta_{mj}^{L}\ {}^{RL}_{\xi}\mathcal{D}_{1}^{\nu(x,t)}\Big\{ \frac{\partial}{\partial\xi}\Big[\, {}^{(2)}\mathcal{P}_j^{\mu}(\xi)\Big]\Big\}.
\end{aligned}
$$

Now, by substituting (8.26) we obtain

(C.23)

$$
\begin{aligned}
{}^{RL}_{x}\mathcal{D}_{b}^{1+\nu(x,t)} u_N(x,t) &= (\frac{2}{b-a})^{1+\nu} \sum_{m=2}^{\mathcal{M}}\sum_{n=1}^{\mathcal{N}} u_N(x_m,t_n)\mathcal{A}_m\mathcal{T}_n^{\tau}(t)\cdot \\
\sum_{j=1}^{\mathcal{M}} \beta_{mj}^{L} &\Big[\ (-\mu)\, {}^{RL}_{\xi}\mathcal{D}_{1}^{\nu(x,t)}\Big\{(1-\xi)^{\mu-1} P_{j-1}^{\mu,-\mu}(\xi)\Big\} \\
&+\ (\frac{j}{2})\, {}^{RL}_{\xi}\mathcal{D}_{1}^{\nu(x,t)}\Big\{(1-\xi)^{\mu} P_{j-2}^{1+\mu,1-\mu}(\xi)\Big\}\Big]
\end{aligned}
$$

in which the Jacobi polynomials $P_{j-1}^{\mu,-\mu}(\xi)$ and $P_{j-2}^{1+\mu,1-\mu}(\xi)$ can be represented in terms of the following sums

$$
\begin{aligned}
P_{j-1}^{\mu,-\mu}(\xi) &= \sum_{q=0}^{j-1} (\frac{-1}{2})^{q} c_{jq}^{\mu}\cdot(1-\xi)^{q}, \quad j\geq 1, \\
P_{j-2}^{1+\mu,1-\mu}(\xi) &= \sum_{q=0}^{j-2} (\frac{-1}{2})^{q} B_{jq}^{\mu}\cdot(1-\xi)^{q}, \quad j\geq 2,
\end{aligned}
$$

respectively. Now, by substituting the Jacobi polynomials back into (C.23) and simplifying, it yields

$$\begin{aligned}
{}^{RL}_{x}\mathcal{D}_{b}^{1+\nu(x,t)}u_N(x,t) &= (\frac{2}{b-a})^{1+\nu}\sum_{m=2}^{\mathcal{M}}\sum_{n=1}^{\mathcal{N}}u_N(x_m,t_n)\mathcal{A}_m\mathcal{T}_n^{\tau}(t)\cdot \\
\sum_{j=1}^{\mathcal{M}}\beta_{mj}^{L} &\Big[(-\mu)\mathbb{I}_{\{j\geq 1\}}\sum_{q=0}^{j-1}(\frac{-1}{2})^q c_{jq}^{*}\,{}^{RL}_{\xi}\mathcal{D}_1^{\nu(x,t)}\Big\{(1-\xi)^{q+\mu-1}\Big\} \\
&+ (\frac{j}{2})\mathbb{I}_{\{j\geq 2\}}\sum_{q=0}^{j-2}(\frac{-1}{2})^q C_{jq}^{*}\,{}^{RL}_{\xi}\mathcal{D}_1^{\nu(x,t)}\Big\{(1-\xi)^{q+\mu}\Big\}\Big].
\end{aligned}$$

where $C_{jq}^{*}=\begin{pmatrix} j+q \\ q \end{pmatrix}\begin{pmatrix} j-1+\mu \\ j-2-q \end{pmatrix}$. Now, by virtue of (8.9), we exactly obtain the variable-order fractional derivative of u_N as

$$\begin{aligned}
{}^{RL}_{x}\mathcal{D}_{b}^{1+\nu(x,t)}u_N(x,t) &= (\frac{2}{b-a})^{1+\nu}\sum_{m=2}^{\mathcal{M}}\sum_{n=1}^{\mathcal{N}}u_N(x_m,t_n)\mathcal{A}_m\mathcal{T}_n^{\tau}(t)\cdot \\
\sum_{j=1}^{\mathcal{M}}\beta_{mj}^{L} &\Big[\mathbb{I}_{\{j\geq 1\}}\sum_{q=0}^{j-1}\mathbb{C}_{jq}^{\mu}(1-\xi)^{q+\mu-1-\nu} \\
&+ \mathbb{I}_{\{j\geq 2\}}\sum_{q=0}^{j-2}C_{jq}^{\mu}(1-\xi)^{q+\mu-\nu}\Big].
\end{aligned}$$

where

$$\mathbb{C}_{jq}^{\mu}=(\mu)(\frac{-1}{2})^q\begin{pmatrix} j-1+q \\ q \end{pmatrix}\begin{pmatrix} j-1-\mu \\ j-1-q \end{pmatrix}\frac{\Gamma(q+\mu)}{\Gamma(q+\mu-\nu(x,t))} \tag{C.24}$$

and

$$C_{jq}^{\mu} = (\frac{-j}{2})(\frac{-1}{2})^{q} \begin{pmatrix} j+q \\ q \end{pmatrix} \begin{pmatrix} j-1+\mu \\ j-2-q \end{pmatrix} \frac{\Gamma(1+q+\mu)}{\Gamma(1+q+\mu-\nu(x,t))}. \tag{C.25}$$

Next, by evaluating the above expression at the collocation points (x_i, t_k), we obtain

$$\{{}^{RL}\mathbf{D}_{R}^{1+\nu}\}_{ikm} = (\frac{2}{b-a})^{1+\nu(x_i,t_k)} \mathcal{A}_m \sum_{j=1}^{\mathcal{M}} \beta_{mj}^{R} \mathcal{F}_{j}^{R,\nu}(x_i, t_k), \tag{C.26}$$

where $\mathcal{F}_{j}^{R,\nu}\Big(x(\xi), t\Big)$ is obtained as

$$\begin{aligned} \mathcal{F}_{j}^{R,\nu}\Big(x(\xi), t\Big) &= \mathbb{I}_{\{j\geq 1\}} \sum_{q=0}^{j-1} \mathbb{C}_{jq}^{\mu} \cdot (1-\xi)^{q+\mu-1-\nu(x_i,t_k)} \\ &+ \mathbb{I}_{\{j\geq 2\}} \sum_{q=0}^{j-2} C_{jq}^{\mu} \cdot (1-\xi)^{q+\mu-\nu(x_i,t_k)}, \end{aligned} \tag{C.27}$$

which completes the proof.

C.5 Proof of Theorem 8.5.8 (${}^{*}\mathcal{D}_{x}^{\sigma(x,t)} \equiv \partial^{\sigma(x,t)}u/\partial|x|^{\sigma(x,t)}$)

We substitute (8.34) in (8.33) and take the $\sigma(x,t)$-th order fractional derivative. Once again, we perform the affine mapping from $x \in [a,b]$ to $\xi \in [-1,1]$ as before an we obtain

$$\frac{\partial^{\sigma(x,t)}u_N(x,t)}{\partial|x|^{\sigma(x,t)}} = (\frac{2}{b-a})^{\sigma(x(\xi),t)} C_{\sigma(x(\xi),t)} \Big({}_{-1}\mathcal{D}_{\xi}^{\sigma} u_N + {}_{\xi}\mathcal{D}_{1}^{\sigma} u_N \Big)$$

$$= (\frac{2}{b-a})^{\sigma} C_{\sigma} \sum_{m=2}^{\mathcal{M}} \sum_{n=1}^{\mathcal{N}} u_N(x_m, t_n) \left({}^{RL}_{-1}\mathcal{D}_{\xi}^{\sigma} \Big\{ h_m(\, x(\xi)\,) \Big\} + {}^{RL}_{\xi}\mathcal{D}_{1}^{\sigma} \Big\{ h_m(\, x(\xi)\,) \Big\} \right) \mathcal{T}_{n}^{\tau}(t),$$

where $h_m(\,x(\xi)\,) \equiv h_m(\xi)$ are all polynomials of order $(\mathcal{M})$, which can be represented exactly in terms of Legendre polynomials $P_n(\xi)$ as

$$h_m(\xi) = \sum_{j=0}^{\mathcal{M}} \widetilde{\beta}_{mj} P_j(\xi). \tag{C.28}$$

We again note that the coefficient matrix $\widetilde{\beta}_{mj}$ can be obtained analytically. By plugging (C.28) we obtain

$$\frac{\partial^{\sigma(x,t)} u_N(x,t)}{\partial |x|^{\sigma(x,t)}} =$$
$$(\frac{2}{b-a})^{\sigma} C_\sigma \sum_{m=2}^{\mathcal{M}} \sum_{n=1}^{\mathcal{N}} u_N(x_m,t_n) \sum_{j=0}^{\mathcal{M}} \widetilde{\beta}_{mj} \Big({}_{-1}^{RL}\mathcal{D}_{\xi}^{\sigma} \Big\{ P_j(\xi) \Big\} + {}_{\xi}^{RL}\mathcal{D}_{1}^{\sigma} \Big\{ P_j(\xi) \Big\} \Big) \mathcal{T}_n^{\tau}(t),$$

where by exact evaluation of the left- and right-sided fractional derivatives of the Legendre polynomials in (10.18) and (10.20),

$$\frac{\partial^{\sigma(x,t)} u_N(x,t)}{\partial |x|^{\sigma(x,t)}} = (\frac{2}{b-a})^{\sigma} C_\sigma \sum_{m=2}^{\mathcal{M}} \sum_{n=1}^{\mathcal{N}} u_N(x_m,t_n) \Big\{$$
$$\sum_{j=\lceil \sigma(x,t) \rceil}^{\mathcal{M}} \widetilde{\beta}_{mj} \frac{\Gamma(j+1)}{\Gamma(j-\sigma+1)} \Big\{ (1+\xi)^{-\sigma} P_j^{\sigma,-\sigma}(\xi) + (1-\xi)^{-\sigma} P_j^{-\sigma,\sigma}(\xi) \Big\} \Big\} \mathcal{T}_n^{\tau}(t) \Big\}, \tag{C.29}$$

which we evaluate at the collocation points $u_N(x_i,t_k)$ to obtain

$$\frac{\partial^{\sigma(x,t)} u_N(x,t)}{\partial |x|^{\sigma(x,t)}} \Big|_{(x_i,t_k)} = \sum_{m=2}^{\mathcal{M}} \{\mathbf{D}_{Riesz}^{\sigma}\}_{ikm} u_N(x_m,t_k)$$

in which $\{\mathbf{D}_{Riesz}^{\sigma}\}_{ikm}$ are the entries of the three dimensional Riesz spatial differentiation matrix of order $\sigma(x_i,t_k)$, $\mathbf{D}_{Riesz}^{\sigma}$, given by

$$\{\mathbf{D}_{Riesz}^{\sigma}\}_{ikm} = \Big[(\frac{2}{b-a})^{\sigma(x,t)} C_{\sigma(x,t)} \Big]_{(x_i,t_k)} \sum_{j=1}^{\mathcal{M}} \widetilde{\beta}_{mj} \mathcal{Z}_j^{\sigma}(x_k,t_k), \tag{C.30}$$

where

$$\mathcal{Z}_j^{\sigma}(x,t) = \frac{\Gamma(j+1)}{\Gamma(j-\sigma(x_i,t_k)+1)}\Big[(1+\xi)^{-\sigma(x,t)}P_j^{\sigma,-\sigma}(\xi) \; + \; (1-\xi)^{-\sigma(x,t)}P_j^{-\sigma,\sigma}(\xi)\Big],$$

in which we recall that $\xi = 2\frac{x-a}{b-a}$.

C.6 Proof of Theorem 8.5.9 ($^{*}\mathcal{D}_x^{1+\nu(x,t)} \equiv \partial^{1+\nu(x,t)}u/\partial|x|^{1+\nu(x,t)}$)

We first take the fractional and then the first derivative of the solution to obtain

$$\begin{aligned}
&\frac{\partial^{1+\nu(x,t)}u_N(x,t)}{\partial|x|^{1+\nu(x,t)}} = C_{1+\nu}\Big\{ {}^{RL}_{a}\mathcal{D}_x^{\nu(x,t)} + {}^{RL}_{x}\mathcal{D}_b^{\nu(x,t)}\Big\}\Big(\frac{\partial u_N}{\partial x}\Big)\\
&= (\frac{2}{b-a})^{1+\nu}C_{1+\nu}\sum_{m=2}^{\mathcal{M}}\sum_{n=1}^{\mathcal{N}} u_N(x_m,t_n)\,\mathcal{T}_n^{\tau}(t)\,\Big\{ {}^{RL}_{-1}\mathcal{D}_{\xi}^{\nu} + {}^{RL}_{\xi}\mathcal{D}_1^{\nu}\Big\}\sum_{j=0}^{\mathcal{M}}\widetilde{\beta}_{mj}\frac{\partial}{\partial\xi}\Big\{P_j(\xi)\Big\},\\
&= (\frac{2}{b-a})^{1+\nu}C_{1+\nu}\sum_{m=2}^{\mathcal{M}}\sum_{n=1}^{\mathcal{N}} u_N(x_m,t_n)\mathcal{T}_n^{\tau}(t)\sum_{j=0}^{\mathcal{M}}\widetilde{\beta}_{mj}\mathcal{W}_j^{\nu},
\end{aligned} \tag{C.31}$$

in which we evaluate $\mathcal{W}_j^{\nu} \equiv (\frac{j+1}{2})\Big\{ {}^{RL}_{-1}\mathcal{D}_{\xi}^{\nu} + {}^{RL}_{\xi}\mathcal{D}_1^{\nu}\Big\}P_{j-1}^{1,1}(\xi)$ exactly by representing the Jacobi polynomial $P_{j-1}^{1,1}(\xi)$ as the following two alternative forms

$$P_{j-1}^{1,1}(\xi) \;=\; \sum_{q=0}^{j-1}\mathcal{C}_j(-1)^{q+j-1}(\frac{1}{2})^q(1+\xi)^q \tag{C.32}$$

$$\;=\; \sum_{q=0}^{j-1}\mathcal{C}_j(\frac{-1}{2})^q(1-\xi)^q \tag{C.33}$$

where $\mathcal{C}_j = \begin{pmatrix} j+1+q \\ q \end{pmatrix} \begin{pmatrix} j \\ j-1-q \end{pmatrix}$. Hence,

$$\begin{aligned}
\mathcal{W}_j^{\nu} &= (\frac{j+1}{2})({}_a^{RL}\mathcal{D}_x^{\nu(x,t)} + {}_x^{RL}\mathcal{D}_b^{\nu(x,t)})\Big\{P_{j-1}^{1,1}(\xi)\Big\} \\
&= (\frac{j+1}{2})\,{}_a^{RL}\mathcal{D}_x^{\nu(x,t)}\Big\{\sum_{q=0}^{j-1}\mathcal{C}_j(-1)^{q+j-1}(\frac{1}{2})^q(1+\xi)^q\Big\} \\
&+ (\frac{j+1}{2})\,{}_x^{RL}\mathcal{D}_b^{\nu(x,t)}\Big\{\sum_{q=0}^{j-1}\mathcal{C}_j(\frac{-1}{2})^q(1-\xi)^q\Big\},
\end{aligned}$$

by substituting $P_{j-1}^{1,1}(\xi)$ by (C.32) when taking the left-sided and by (C.33) when taking the right-sided Riemann-Liouville fractional derivative, respectively. Now, by (8.8) and (8.9), we obtain

$$\begin{aligned}
\mathcal{W}_j^{\nu} = (\frac{j+1}{2})\sum_{q=\lceil\nu\rceil}^{j-1}\mathcal{C}_j\frac{(\frac{-1}{2})^q\Gamma(q+1)}{\Gamma(q+1-\nu(x,t))}\Big[&(-1)^{j-1}(1+\xi)^{q-\nu(x,t)} \\
&-(1-\xi)^{q-\nu(x,t)}\Big]. \qquad \text{(C.34)}
\end{aligned}$$

Next, by substituting (C.34) into (C.31), evaluating it at the collocation points (x_i, t_k), ans using the Kronecker delta property $\mathcal{T}_n^{\tau}(t_k) = \delta_{kn}$, we obtain

$$\begin{aligned}
\frac{\partial^{1+\nu(x,t)}u_N(x,t)}{\partial|x|^{1+\nu(x,t)}}\Big|_{(x_i,t_k)} &= \Big[(\frac{2}{b-a})^{1+\nu}C_{1+\nu}\Big]_{(x_i,t_k)}\sum_{m=2}^{\mathcal{M}}u_N(x_m,t_k)\sum_{j=1}^{\mathcal{M}}\widetilde{\beta}_{mj}\mathcal{W}_j^{\nu} \\
&= \sum_{m=2}^{\mathcal{M}}\{\mathbf{D}_{Riesz}^{1+\nu(x,t)}\}_{ikm}u_N(x_m,t_k),
\end{aligned}$$

in which $\{\mathbf{D}_{Riesz}^{1+\nu(x,t)}\}_{ikm}$ denotes the x- and t-dependent fractional diffusion differentiation matrix of Riesz type, give by

$$\{\mathbf{D}_{Riesz}^{1+\nu(x,t)}\}_{ikm} = \Big[(\frac{2}{b-a})^{1+\nu} C_{1+\nu}\Big]_{(x_i,t_k)} \sum_{j=1}^{\mathcal{M}} \widetilde{\beta}_{mj} \mathcal{W}_j^{\nu}(x,t). \tag{C.35}$$

C.7 Construction of the Mass and Stiffness Matrices

Theorem C.7.1. *The temporal stiffness matrix S_τ corresponding to the time-fractional order $\tau \in (0,1)$ is a diagonal $\mathcal{N} \times \mathcal{N}$ matrix, whose entries are explicitly given as*

$$\{S_\tau\}_{n,n} = \widetilde{\sigma}_n \, \sigma_n \Big[\frac{\Gamma(n+\tau)}{\Gamma(n)}\Big]^2 \Big(\frac{2}{T}\Big)^{2\tau-1} \frac{2}{2n-1}, \quad n = 1, 2, \cdots, \mathcal{N}.$$

Proof. By the PG projection, the (r,n)-th entry of the stiffness matrix, $r, n = 1, 2, \cdots, \mathcal{N}$, is defined as

$$\{S_\tau\}_{r,n} \;=\; \int_0^T {}_t\mathcal{D}_T^\tau \Big(\Psi_r^\tau \circ \eta\Big)(t) \, {}_0\mathcal{D}_t^\tau \Big(\, \psi_n^\tau \circ \eta\Big)(t) \, dt, \tag{C.36}$$

Following [187], we obtain the Riemann-Liouville left-sided time-fractional derivative of the temporal basis as

$${}_0\mathcal{D}_t^\tau \Big(\, \psi_n^\tau \circ \eta\Big)(t) = \sigma_n \left(\frac{2}{T}\right)^\tau \frac{\Gamma(n+\tau)}{\Gamma(n)} P_{n-1}(\, 2t/T - 1\,), \tag{C.37}$$

where $P_{n-1}(\, 2t/T - 1\,)$ represents the $(n-1)$-th order *Legendre polynomial* in $t \in [0, T]$. Also, we obtain the right-sided time-fractional derivative of the temporal basis again following [187] as

$${}_t\mathcal{D}_T^\tau \Big(\Psi_r^\tau \circ \eta\Big)(t) = \widetilde{\sigma}_r \left(\frac{2}{T}\right)^\tau \frac{\Gamma(r+\tau)}{\Gamma(r)} P_{r-1}(\, 2t/T - 1\,). \tag{C.38}$$

Now, by plugging (C.37) and (C.38) into (C.36), we obtain

$$\begin{aligned}\{S_\tau\}_{r,n} &= \widetilde{\sigma}_r\,\sigma_n\frac{\Gamma(r+\tau)}{\Gamma(r)}\frac{\Gamma(n+\tau)}{\Gamma(n)}\Big(\frac{2}{T}\Big)^{2\tau}\int_0^T P_{r-1}(x(t))\,P_{n-1}(x(t))\,dt \quad \text{(C.39)}\\ &= \widetilde{\sigma}_r\,\sigma_n\frac{\Gamma(r+\tau)}{\Gamma(r)}\frac{\Gamma(n+\tau)}{\Gamma(n)}\Big(\frac{2}{T}\Big)^{2\tau-1}\int_{-1}^1 P_{r-1}(x)\,P_{n-1}(x)\,dx\\ &= \widetilde{\sigma}_r\,\sigma_n\frac{\Gamma(r+\tau)}{\Gamma(r)}\frac{\Gamma(n+\tau)}{\Gamma(n)}\Big(\frac{2}{T}\Big)^{2\tau-1}\frac{2}{2n-1}\delta_{rn},\end{aligned}$$

by the orthogonality of the Legendre polynomials, where δ_{rn} is the Kronecker delta functions. □

Theorem C.7.2. *(I) If $\mu_j \in (0, 1/2]$, the spatial stiffness matrix S_{μ_j} is a diagonal $\mathcal{M}_j \times \mathcal{M}_j$ matrix, whose entries are explicitly given as*

$$\{S_{\mu_j}\}_{k,k} = \widetilde{\sigma}_k\,\sigma_k\Big[\frac{\Gamma(k+\mu_j)}{\Gamma(k)}\Big]^2\Big(\frac{2}{L_j}\Big)^{2\mu_j-1}\frac{2}{2k-1}, \quad k = 1, 2, \cdots, \mathcal{M}_j.$$

(II) If $\mu_j \in (1/2, 1)$, S_{μ_j} is a symmetric tridiagonal $(\mathcal{M}_j-1)\times(\mathcal{M}_j-1)$ with entries, explicitly given as

$$\begin{aligned}\{S_{\mu_j}\}_{k,m} = b_k\,a_m\Big[\frac{\Gamma(k+\mu_j)}{\Gamma(k)}\Big]^2\Big(\frac{2}{L_j}\Big)^{2\mu_j-1}\frac{2}{2k-1}\Big(\delta_{k,m} - \epsilon_m^{\mu_j}\,\delta_{k,m-1}\Big) +\\ \epsilon_k^{\mu_j}\,b_k\,a_m\Big[\frac{\Gamma(k-1+\mu_j)}{\Gamma(k-1)}\Big]^2\Big(\frac{2}{L_j}\Big)^{2\mu_j-1}\frac{2}{2k-3}\Big(\delta_{k-1,m} - \epsilon_m^{\mu_j}\,\delta_{k-1,m-1}\Big),\end{aligned}$$

$k, m = 2, 3, \cdots, \mathcal{M}_j$ and $L_j = b_j - a_j$.

Proof. The first part, when $\mu_j \in (0, 1/2]$ is similar to the proof in Thm. C.7.1, however, carried out on the interval $[a_j, b_j]$ rather than $[0, T]$. Here, the μ_j-th order left-sided Riemann-Liouville fractional derivative of $\Big(\phi_{m_j}^{\mu_j} \circ \xi_j\Big)(x_j)$ is given following

[187] as

$$ {}_{a_j}\mathcal{D}_{x_j}^{\mu_j}\Big(\phi_m^{\mu_j}\circ\xi_j\Big)(x_j) = \begin{cases} B_m^{\mu_j}\ P_{m-1}\Big(\,\xi(x_j)\,\Big), & \mu_j\in(0,1/2], \\ \\ B_m^{\mu_j}\ P_{m-1}\Big(\,\xi(x_j)\,\Big)\ - C_m^{\mu_j}\ P_{m-2}\Big(\,\xi(x_j)\,\Big), & \mu_j\in(1/2,1), \end{cases} \tag{C.40} $$

for $m=\lceil 2\mu_j\rceil,\cdots,\mathcal{M}_j$ in the j-th spatial dimension, where the coefficient $B_{m_j}^{\mu_j}=\sigma_m\,(2/L_j)^{2\mu_j}\,\Gamma(m+\mu_j)/\Gamma(m)$ and $C_m^{\mu_j}=\sigma_m\,(2/L_j)^{2\mu_j}\,\epsilon_m^{\mu_j}\,\Gamma(m-1+\mu_j)/\Gamma(m-1)$; in addition, the μ_j-th order left-sided Riemann-Liouville fractional derivative of $\Big(\Phi_m^{\mu_j}\circ\xi_j\Big)(x_j)$ is obtained as

$$ {}_{x_j}\mathcal{D}_{b_j}^{\mu_j}\Big(\Phi_m^{\mu_j}\circ\xi_j\Big)(x_j) = \begin{cases} \mathcal{B}_k^{\mu_j}\ P_{k-1}\Big(\,\xi(x_j)\,\Big), & \mu_j\in(0,1/2], \\ \\ \mathcal{B}_k^{\mu_j}\ P_{k-1}\Big(\,\xi(x_j)\,\Big)\ - \mathcal{C}_k^{\mu_j}\ P_{k-2}\Big(\,\xi(x_j)\,\Big), & \mu_j\in(1/2,1), \end{cases} \tag{C.41} $$

for $k=\lceil 2\mu_j\rceil,\cdots,\mathcal{M}_j$ in the j-th spatial dimension, in which we set the coefficient $\mathcal{B}_k^{\mu_j}=\widetilde{\sigma}_k\,(2/L_j)^{2\mu_j}\,\Gamma(k+\mu_j)/\Gamma(k)$ and $\mathcal{C}_k^{\mu_j}=\widetilde{\sigma}_k\,(2/L_j)^{2\mu_j}\,\epsilon_k^{\mu_j}\,\Gamma(k-1+\mu_j)/\Gamma(k-1)$.

For the second part, when $\mu_j\in(1/2,1)$, the (k,m)-th entry of S_{μ_j} is

$$ \{S_{\mu_j}\}_{k,m} \;=\; \int_{a_j}^{b_j} {}_{x_j}\mathcal{D}_{b_j}^{\mu_j}\Big(\Phi_k^{\mu_j}\circ\xi_j\Big)(x_j)\ {}_{a_j}\mathcal{D}_{x_j}^{\mu_j}\Big(\phi_m^{\mu_j}\circ\xi_j\Big)(x_j)dx_j. $$

Next, by virtue of (C.40) and (C.41), also by an affine mapping from $[a_j,b_j]$ to the standard interval $[-1,1]$, we obtain

$$ \{S_{\mu_j}\}_{k,m} = (\frac{L_j}{2})\int_{-1}^{1} \Big[\ B_m^{\mu_j}\ P_{m-1}(\,\xi_j\,)\ - C_m^{\mu_j}\ P_{m-2}(\,\xi_j\,)\Big] \Big[\ \mathcal{B}_k^{\mu_j}\ P_{k-1}(\,\xi_j\,)\ - \mathcal{C}_k^{\mu_j}\ P_{k-2}(\,\xi_j\,)\Big] d\xi_j. $$

Hence, by the orthogonality of the Legendre polynomials we obtain

$$\begin{aligned}\{S_{\mu_j}\}_{k,m} = (\frac{L_j}{2}) \quad \Big[& \quad B_m^{\mu_j}\ \mathcal{B}_k^{\mu_j}\ \frac{2}{2k-1}\delta_{k,m} \\ & - \ C_m^{\mu_j}\ \mathcal{B}_k^{\mu_j}\ \frac{2}{2k-1}\delta_{k,m-1} \\ & + \ B_m^{\mu_j}\ \mathcal{C}_k^{\mu_j}\ \frac{2}{2k-3}\,\delta_{k-1,m} \\ & - \ C_m^{\mu_j}\ \mathcal{C}_k^{\mu_j}\ \frac{2}{2k-3}\,\delta_{k-1,m-1}\Big],\end{aligned}$$

which completes the proof, while the symmetry of the stiffness matrix can be easily checked. □

Theorem C.7.3. *The temporal and the spatial mass matrices M_τ as well as M_{μ_j} are symmetric. Moreover, their entries can be computed exactly by employing a Gauss-Lobatto-Jacobi (GLJ) rule with respect to the weight function $(1-\xi)^\alpha(1+\xi)^\alpha$, $\xi \in [-1,1]$, where $\alpha = \tau/2$ in the temporal and $\alpha = \mu_j$ for the spatial case.*

Proof. The entries of M_τ in our PG spectral method are defined as

$$\{M_\tau\}_{r,n} \ = \ \int_0^T \Big(\Psi_r^\tau \circ \eta\Big)(t)\Big(\psi_m^{\mu_t} \circ \eta\Big)(t)dt,$$

which be computed exactly as

$$\begin{aligned}\{M_\tau\}_{r,n} \ &= \ \widetilde{\sigma}_r\,\sigma_n\,(\frac{2}{T})^\tau \int_0^T t^\tau (T-t)^\tau P_{r-1}^{\tau,-\tau}(\,\eta(t)\,)\,P_{n-1}^{-\tau,\tau}(\,\eta(t)\,)\,dt \\ &= \ \widetilde{\sigma}_r\,\sigma_n\,\frac{T}{2}\int_{-1}^1 (1-\eta)^\tau(1+\eta)^\tau P_{r-1}^{\tau,-\tau}(\eta)\,P_{n-1}^{-\tau,\tau}(\eta)d\eta \\ &= \ \widetilde{\sigma}_r\,\sigma_n\,\frac{T}{2}\sum_{q=1}^{\mathcal{Q}} w_q\ P_{r-1}^{\tau,-\tau}(\eta_q)P_{n-1}^{-\tau,\tau}(\eta_q), \qquad \text{(C.42)}\end{aligned}$$

in which $\mathcal{Q} \geq \mathcal{N}+2$ represents the minimum number of GLJ quadrature points $\{\eta_q\}_{q=1}^{\mathcal{Q}}$, associated with the weigh function $(1-\eta)^\tau(1+\eta)^\tau$, for *exact* quadrature,

and $\{w_q\}_{q=1}^{Q}$ are the corresponding quadrature weights. From the exact discrete rule, recalling the definition of σ_n and $\widetilde{\sigma}_r$, employing the property of the Jacobi polynomials where $P_n^{\alpha,\beta}(-x) = (-1)^n P_n^{\beta,\alpha}(x)$, moreover, noting that $\{\eta_q\}_{q=1}^{\mathcal{Q}}$ and $\{w_q\}_{q=1}^{Q}$ are symmetric with respect to the reference point, it is easy to show that $\{M_\tau\}_{r,n} = \{M_\tau\}_{n,r}$.

The spatial mass matrix M_{μ_j}, when $\mu_j \in (0, 1/2]$, is also $\mathcal{M}_j \times \mathcal{M}_j$, whose entries are computed similarly as

$$\{M_{\mu_j}\}_{k,m} = \widetilde{\sigma}_k \, \sigma_m \, \frac{L_j}{2} \sum_{q=1}^{Q} w_q \; P_{k-1}^{\mu_j, -\mu_j}(\xi_q) P_{m-1}^{-\mu_j, \mu_j}(\xi_q), \tag{C.43}$$

in which $\mathcal{Q} \geq \mathcal{M}_j + 2$ represents the minimum number of GLJ quadrature points $\{\xi_q\}_{q=1}^{\mathcal{Q}}$, associated with the weigh function $(1-\xi)^{\mu_j}(1+\xi)^{\mu_j}$, for *exact* quadrature. We can also show that M_{μ_j} is symmetric and that the GJL rule is exact when $\mathcal{Q} \geq \mathcal{M}_j + 2$.

Finally, when $\mu_j \in (1/2, 1)$, the spatial mass matrix M_{μ_j}, becomes $(\mathcal{M}_j - 1) \times (\mathcal{M}_j - 1)$, whose entries are computed exactly as

$$\begin{aligned}
\{M_{\mu_j}\}_{k,m} &= \int_{a_j}^{b_j} \Big(\Phi_k^{\mu_j/2} \circ \xi \Big)(x_j) \Big(\phi_m^{\mu_j/2} \circ \xi \Big)(x_j) dx_j \\
&= \widetilde{\sigma}_{k_j} \, \sigma_{m_j} \Big[\int_{-1}^{1} {}^{(2)}\mathcal{P}_{k_j}^{\mu_j}(\,\xi(x_j)\,)\; {}^{(1)}\mathcal{P}_{m}^{\mu_x}(\,\xi(x_j)\,)\, dx_j \\
&- \epsilon_m^{\mu_x} \int_{-1}^{1} {}^{(2)}\mathcal{P}_{k_j}^{\mu_j}(\,\xi(x_j)\,)\; {}^{(1)}\mathcal{P}_{m_j-1}^{\mu_j}(\,\xi(x_j)\,)\, dx_j \\
&+ \epsilon_k^{\mu_x} \int_{-1}^{1} {}^{(2)}\mathcal{P}_{k_j-1}^{\mu_j}(\,\xi(x_j)\,)\, {}^{(1)}\mathcal{P}_{m_j}^{\mu_j}(\,\xi(x_j)\,)\, dx_j \\
&- \epsilon_{k_j}^{\mu_j} \, \epsilon_{m_j}^{\mu_j} \int_{-1}^{1} {}^{(2)}\mathcal{P}_{k_j-1}^{\mu_j}(\,\xi(x_j)\,)\, {}^{(1)}\mathcal{P}_{m_j-1}^{\mu_j}(\,\xi(x_j)\,) dx_j \Big],
\end{aligned}$$

where we note that all the above integrations share the same weight function by

construction. Hence, we obtain

$$\begin{aligned}\{M_{\mu_j}\}_{k,m} = \widetilde{\sigma}_{k_j}\,\sigma_{m_j}\frac{L_j}{2}\int_{-1}^{1} \quad & (1-\xi)^{\mu_j}\,(1+\xi)^{\mu_j} \\ & \Big[\quad P_{k-1}^{\mu_j,-\mu_j}(\xi)\quad P_{m-1}^{-\mu_j,\mu_j}(\xi) \\ & -\quad \epsilon_m^{\mu_x}\quad P_{k-1}^{\mu_j,-\mu_j}(\xi)\quad P_{m-2}^{-\mu_j,\mu_j}(\xi) \\ & +\quad \epsilon_k^{\mu_x}\quad P_{k-2}^{\mu_j,-\mu_j}(\xi)\quad P_{m-1}^{-\mu_j,\mu_j}(\xi) \\ & -\quad \epsilon_{k_j}^{\mu_j}\,\epsilon_{m_j}^{\mu_j}\quad P_{k-2}^{\mu_j,-\mu_j}(\xi)\quad P_{m-2}^{-\mu_j,\mu_j}(\xi)\Big]dx_j\end{aligned}$$

which leads to the following exact GLJ rule

$$\begin{aligned}\{M_{\mu_j}\}_{k,m} = \widetilde{\sigma}_{k_j}\,\sigma_{m_j}\frac{L_j}{2}\sum_{q=1}^{Q} w_q \quad & \Big[\quad P_{k-1}^{\mu_j,-\mu_j}(\xi_q)\quad P_{m-1}^{-\mu_j,\mu_j}(\xi_q) \\ & -\quad \epsilon_m^{\mu_x}\quad P_{k-1}^{\mu_j,-\mu_j}(\xi_q)\quad P_{m-2}^{-\mu_j,\mu_j}(\xi_q) \\ & +\quad \epsilon_k^{\mu_x}\quad P_{k-2}^{\mu_j,-\mu_j}(\xi_q)\quad P_{m-1}^{-\mu_j,\mu_j}(\xi_q) \\ & -\quad \epsilon_{k_j}^{\mu_j}\,\epsilon_{m_j}^{\mu_j}\quad P_{k-2}^{\mu_j,-\mu_j}(\xi_q)\quad P_{m-2}^{-\mu_j,\mu_j}(\xi_q)\Big],\end{aligned} \tag{C.44}$$

which is also exact when $\mathcal{Q} \geq \mathcal{M}_j + 2$, and the same argument on the symmetry of the matrix applies here. □

Bibliography

[1] Q. M. Al-Mdallal. An efficient method for solving fractional sturm–liouville problems. *Chaos, Solitons & Fractals*, 40(1):183–189, 2009.

[2] I. Ali, H. Brunner, and T. Tang. A spectral method for pantograph-type delay differential equations and its convergence analysis. *J. Comput. Math.*, 27(2-3):254–265, 2009.

[3] W. O. Amrein, A. M. Hinz, and D. B. Pearson. *Sturm-Liouville theory: past and present*. Birkhäuser Basel, 2005.

[4] A. A. M. Arafa, S. Z. Rida, and M. Khalil. The effect of anti-viral drug treatment of human immunodeficiency virus type 1 (HIV-1) described by a fractional order model. *Appl. Math. Model.*, 37(4):2189–2196, 2013.

[5] R. Askey and J. Fitch. Integral representations for jacobi polynomials and some applications. *Journal of Mathematical Analysis and Applications*, 26:411–437, 1969.

[6] T.M. Atanackovic, L. Oparnica, and S. Pilipović. Distributional framework for solving fractional differential equations. *Integral Transforms and Special Functions*, 20(3-4):215–222, 2009.

[7] T.M. Atanackovic, S. Pilipovic, and D. Zorica. Existence and calculation of the solution to the time distributed order diffusion equation. *Physica Scripta*, 2009(T136):014012, 2009.

[8] T.M. Atanackovic, S. Pilipovic, and D. Zorica. Time distributed-order diffusion-wave equation. i. volterra-type equation. *Proceedings of the Royal Society A: Mathematical, Physical and Engineering Science*, 465(2106):1869–1891, 2009.

[9] T.M. Atanackovic and B. Stankovic. Generalized wave equation in nonlocal elasticity. *Acta mechanica*, 208(1):1–10, 2009.

[10] B. Baeumer, D. A. Benson, M.M. Meerschaert, and S. W. Wheatcraft. Subordinated advection-dispersion equation for contaminant transport. *Water Resources Research*, 37(6):1543–1550, 2001.

[11] B. Baeumer and M. M. Meerschaert. Tempered stable Lévy motion and transient super-diffusion. *Journal of Computational and Applied Mathematics*, 233(10):2438–2448, 2010.

[12] RL Bagley and PJ Torvik. On the existence of the order domain and the solution of distributed order equations-part i. *International Journal of Applied Mathematics*, 2(7):865–882, 2000.

[13] D. Baleanu, A.H. Bhrawy, and T.M. Taha. Two efficient generalized laguerre spectral algorithms for fractional initial value problems. In *Abstract and Applied Analysis*, volume 2013. Hindawi Publishing Corporation, 2013.

[14] Eli Barkai, Ralf Metzler, and Joseph Klafter. From continuous time random walks to the fractional fokker-planck equation. *Physical Review E*, 61(1):132, 2000.

[15] E. Bas and F. Metin. Spectral properties of fractional sturm-liouville problem for diffusion operator. *arXiv preprint arXiv:1212.4761*, pages 1–11, 2012.

[16] A. Bellen and M. Zennaro. *Numerical methods for delay differential equations*. Numerical Mathematics and Scientific Computation. The Clarendon Press Oxford University Press, New York, 2003.

[17] M. Belmekki, K. Mekhalfi, and S.K. Ntouyas. Existence and uniqueness for semilinear fractional differential equations with infinite delay via resolvent operators. *Journal of Fractional Calculus and Applications*, 4(2):267–282, 2013.

[18] M. Benchohra and Z. Boutefal. Impulsive differential equations of fractional order with infinite delay. *Journal of Fractional Calculus and Applications*, 4(2):209–223, 2013.

[19] M. Benchohra, J. Henderson, S. K. Ntouyas, and A. Ouahab. Existence results for fractional order functional differential equations with infinite delay. *J. Math. Anal. Appl.*, 338(2):1340–1350, 2008.

[20] David A Benson, Stephen W Wheatcraft, and Mark M Meerschaert. Application of a fractional advection-dispersion equation. *Water Resources Research*, 36(6):1403–1412, 2000.

[21] S. Bhalekar and V. Daftardar-Gejji. A predictor-corrector scheme for solving nonlinear delay differential equations of fractional order. *Journal of Fractional Calculus and Applications*, 1(5):1–9, 2011.

[22] A.H. Bhrawy and M.A. Alghamdia. A new legendre spectral galerkin and pseudo-spectral approximations for fractional initial value problems. 2013, 2013.

[23] Ali H Bhrawy and Mohammed M Al-Shomrani. A shifted legendre spectral method for fractional-order multi-point boundary value problems. *Advances in Difference Equations*, 2012(1):1–19, 2012.

[24] Marco L Bittencourt. *Computational Solid Mechanics: Variational Formulation and High Order Approximation*. CRC Press, 2014.

[25] Luise Blank. *Numerical treatment of differential equations of fractional order*. Citeseer, 1996.

[26] Jean-Philippe Bouchaud and Antoine Georges. Anomalous diffusion in disordered media: statistical mechanisms, models and physical applications. *Physics reports*, 195(4):127–293, 1990.

[27] N. Bournaveas and V. Calvez. The one-dimensional Keller-Segel model with fractional diffusion of cells. *Nonlinearity*, 23:923–935, 2010.

[28] D. Braess and C. Schwab. Approximation on simplices with respect to weighted sobolev norms. *Journal of Approximation Theory*, 103(2):329–337, 2000.

[29] C. Canuto, M. Y. Hussaini, A. Quarteroni, and T. A. Zang. *Spectral methods*. Springer-Verlag, Berlin, 2006.

[30] J. Cao and C. Xu. A high order schema for the numerical solution of the fractional ordinary differential equations. *Journal of Computational Physics*, 238(1):154–168, 2013.

[31] Alfredo Raúl Carella. *Spectral Finite Element Methods for solving Fractional Differential Equations with applications in Anomalous Transport*. PhD thesis, Norwegian University of Science and Technology, 2012.

[32] A. Carpinteri and F. Mainardi. *Fractals and Fractional Calculus in Continum Mechanics*. Telos: Springer-Verlag, 1998.

[33] Á. Cartea and D. del Castillo-Negrete. Fluid limit of the continuous-time random walk with general Lévy jump distribution functions. *Physical Review E*, 76(4):041105, 2007.

[34] Aleksei V Chechkin, R Gorenflo, Igor M Sokolov, and V Yu Gonchar. Distributed order time fractional diffusion equation. *Fractional Calculus and Applied Analysis*, 6(3):259–280, 2003.

[35] AV Chechkin, R Gorenflo, and IM Sokolov. Retarding subdiffusion and accelerating superdiffusion governed by distributed-order fractional diffusion equations. *Physical Review E*, 66(4):046129, 2002.

[36] C. M. Chen, F. Liu, V. Anh, and I. Turner. Numerical simulation for the variable-order galilei invariant advection diffusion equation with a nonlinear source term. *Applied Mathematics and Computation*, 217(12):5729–5742, 2011.

[37] Chang-Ming Chen, Fawang Liu, Vo Anh, and Ian Turner. Numerical schemes with high spatial accuracy for a variable-order anomalous subdiffusion equation. *SIAM Journal on Scientific Computing*, 32(4):1740–1760, 2010.

[38] C.M. Chen, F. Liu, K. Burrage, and Y. Chen. Numerical methods of the variable-order rayleigh-stokes problem for a heated generalized second grade fluid with fractional derivative. *IMA Journal of Applied Mathematics*, pages 1–21, 2012.

[39] Wen Chen, Jianjun Zhang, and Jinyang Zhang. A variable-order time-fractional derivative model for chloride ions sub-diffusion in concrete structures. *Fractional Calculus and Applied Analysis*, 16(1):76–92, 2013.

[40] Y. Chen and T. Tang. Convergence analysis of the Jacobi spectral-collocation methods for Volterra integral equations with a weakly singular kernel. *Math. Comp.*, 79(269):147–167, 2010.

[41] W Chester. Resonant oscillations in closed tubes. *J. Fluid Mech*, 18(1):44–64, 1964.

[42] C.F.M. Coimbra. Mechanics with variable-order differential operators. *Annalen der Physik*, 12(11-12):692–703, 2003.

[43] G.R.J. Cooper and D.R. Cowan. Filtering using variable order vertical derivatives. *Computers & geosciences*, 30(5):455–459, 2004.

[44] R. V. Culshaw, S. Ruan, and G. Webb. A mathematical model of cell-to-cell spread of HIV-1 that includes a time delay. *J. Math. Biol.*, 46(5):425–444, 2003.

[45] Horstmann D. and Wang G. Blow-up in a chemotaxis model without symmetry assumptions. *European J. Appl. Math.*, 12:159–177, 2001.

[46] Horstmann D. and Winkler M. Boundedness vs blow-up in a chemotaxis system. *J. Diff. Eq.*, 215:52–107, 2005.

[47] D. del Castillo-Negrete, B. A. Carreras, and V. E. Lynch. Fractional diffusion in plasma turbulence. *Physics of Plasmas (1994-present)*, 11(8):3854–3864, 2004.

[48] W. Deng, J. Lü, and Ch. Li. Stability of N-dimensional linear systems with multiple delays and application to synchronization. *J. Syst. Sci. Complex.*, 19(2):149–156, 2006.

[49] W.H. Deng and J.S. Hesthaven. Local discontinuous Galerkin methods for fractional diffusion equations. *ESAIM: Mathematical Modelling and Numerical Analysis (Accepted)*, 2013.

[50] K. Diethelm and N. J. Ford. Analysis of fractional differential equations. *J. Math. Anal. Appl.*, 265(2):229–248, 2002.

[51] Kai Diethelm and Neville J Ford. Analysis of fractional differential equations. *Journal of Mathematical Analysis and Applications*, 265(2):229–248, 2002.

[52] Kai Diethelm and Neville J Ford. Numerical analysis for distributed-order differential equations. *Journal of Computational and Applied Mathematics*, 225(1):96–104, 2009.

[53] Kai Diethelm, Neville J Ford, and Alan D Freed. Detailed error analysis for a fractional adams method. *Numerical algorithms*, 36(1):31–52, 2004.

[54] E.H. Doha, A.H. Bhrawy, and S.S. Ezz-Eldien. A chebyshev spectral method based on operational matrix for initial and boundary value problems of fractional order. *Computers & Mathematics with Applications*, 62(5):2364–2373, 2011.

[55] M. Dubiner. Spectral methods on triangles and other domains. *Journal of Scientific Computing*, 6(4):345–390, 1991.

[56] Alexandre Ern. *Theory and practice of finite elements*, volume 159. Springer, 2004.

[57] T. Erneux. *Applied delay differential equations*, volume 3. Springer, 2009.

[58] V. S. Ertürk. Computing eigenelements of sturm-liouville problems of fractional order via fractional differential transform method. *Mathematical and Computational Applications*, 16(3):712, 2011.

[59] V. J. Ervin and J. P. Roop. Variational formulation for the stationary fractional advection dispersion equation. *Numer. Methods Partial Differential Equations*, 22(3):558–576, 2006.

[60] GJ Fix and JP Roof. Least squares finite-element solution of a fractional order two-point boundary value problem. *Computers & Mathematics with Applications*, 48(7):1017–1033, 2004.

[61] N. J. Ford and J. A. Connolly. Comparison of numerical methods for fractional differential equations. *Commun. Pure Appl. Anal.*, 5(2):289–306, 2006.

[62] L. Fox, D. F. Mayers, J. R. Ockendon, and A. B. Tayler. On a functional differential equation. *J. Inst. Math. Appl.*, 8:271–307, 1971.

[63] Rudolf Gorenflo, Francesco Mainardi, Daniele Moretti, and Paolo Paradisi. Time fractional diffusion: a discrete random walk approach. *Nonlinear Dynamics*, 29(1-4):129–143, 2002.

[64] Bertil Gustafsson, Heinz-Otto Kreiss, and Joseph Oliger. *Time dependent problems and difference methods*, volume 67. Wiley New York, 1995.

[65] J. K. Hale and Sjoerd M. Verduyn L. *Introduction to functional-differential equations*, volume 99 of *Applied Mathematical Sciences*. Springer-Verlag, New York, 1993.

[66] Emmanuel Hanert. A comparison of three eulerian numerical methods for fractional-order transport models. *Environmental fluid mechanics*, 10(1-2):7–20, 2010.

[67] Bruce I Henry and Susan L Wearne. Fractional reaction–diffusion. *Physica A: Statistical Mechanics and its Applications*, 276(3):448–455, 2000.

[68] Jan S Hesthaven, Sigal Gottlieb, and David Gottlieb. *Spectral methods for time-dependent problems*, volume 21. Cambridge University Press, 2007.

[69] J Huang, Y Tang, and L Vazquez. Convergence analysis of a block-by-block method for fractional differential equations. *Numer. Math. Theor. Methods Appl.*, 5(2):229–241, 2012.

[70] M Ichise, Y Nagayanagi, and T Kojima. An analog simulation of non-integer order transfer functions for analysis of electrode processes. *Journal of Electroanalytical Chemistry and Interfacial Electrochemistry*, 33(2):253–265, 1971.

[71] I. M. Jaimoukha and E. Kasenally. Krylov subspace methods for solving large Lyapunov equations. *SIAM Journal on Numerical Analysis*, 31(1):227–251, 1994.

[72] B. Jin and R. William. An inverse sturm-liouville problem with a fractional derivative. *Journal of Computational Physics*, 231:4954–4966, 2012.

[73] T. Jin and D. Hereld. *Chemotaxis: Methods and Protocols*. Springer, 2009.

[74] S. Karlin and J. McGregor. On some stochastic models in genetics. *Stochastic models in medicine and biology*, pages 245–279, 1964.

[75] G. E. Karniadakis and R. M. Kirby II. *Parallel scientific computing in C++ and MPI: a seamless approach to parallel algorithms and their implementation*. Cambridge University Press, 2003.

[76] G. E. Karniadakis and S. J. Sherwin. *Spectral/hp element methods for CFD*. Oxford University Press (2nd edition), 2005.

[77] George Em Karniadakis and Spencer J Sherwin. *Spectral/hp element methods for CFD*. Oxford University Press, 1999.

[78] E. Kaslik and S. Sivasundaram. Analytical and numerical methods for the stability analysis of linear fractional delay differential equations. *J. Comput. Appl. Math.*, 236(16):4027–4041, 2012.

[79] T. Kato and J. B. McLeod. The functional-differential equation $y'(x) = ay(\lambda x) + by(x)$. *Bull. Amer. Math. Soc.*, 77:891–937, 1971.

[80] E.F. Keller and L.A. Segel. Model for chemotaxis. *J. Theor. Biol.*, 30:225–234, 1971.

[81] E.F. Keller and L.A. Segel. Norm behaviour of solutions to a parabolic system of chemotaxis. *Math. Japon.*, 45:241–265, 1997.

[82] E.F. Keller and L.A. Segel. From 1970 until present: the Keller-Segel model in chemotaxis and its consequences I. *Jahresber. DMV*, 105:103–165, 2003.

[83] E.F. Keller and L.A. Segel. From 1970 until present: the Keller-Segel model in chemotaxis and its consequences I. *Jahresber. DMV*, 106:103–165, 2004.

[84] Jakob J Keller. Propagation of simple non-linear waves in gas filled tubes with friction. *Zeitschrift für angewandte Mathematik und Physik ZAMP*, 32(2):170–181, 1981.

[85] M. M. Khader, Talaat S. El Danaf, and A. S. Hendy. Efficient spectral collocation method for solving multi-term fractional differential equations based on the generalized Laguerre polynomials. *Journal of Fractional Calculus and Applications*, 3(13):1–14, 2012.

[86] MM Khader. On the numerical solutions for the fractional diffusion equation. *Communications in Nonlinear Science and Numerical Simulation*, 16(6):2535–2542, 2011.

[87] MM Khader and AS Hendy. The approximate and exact solutions of the fractional-order delay differential equations using legendre pseudospectral method. *International Journal of Pure and Applied Mathematics*, 74(3):287–297, 2012.

[88] K. Kikuchi and A. Negoro. On markov process generated by pseudodifferential operator of variable order. 2012.

[89] A. A. Kilbas, H. M. Srivastava, and J. J. Trujillo. *Theory and applications of fractional differential equations*, volume 204 of *North-Holland Mathematics Studies*. Elsevier Science B.V., Amsterdam, 2006.

[90] A. A. Kilbass, H. M. Srivastava, and J. J. Trujillo. *Theory and Applications of Fractional Differential Equations*. Amsterdam, Netherlands:Elsevier, 2006.

[91] Rainer Klages, Günter Radons, and Igor M Sokolov. *Anomalous Transport: Foundations and Applications*. Wiley-VCH, 2008.

[92] M. Klimek and O. P. Agrawal. Fractional Sturm-Liouville problem. *Computers & Mathematics with Applications*, 66(5):795–812, 2013.

[93] M. Klimek and O. P. Agrawal. On a regular fractional sturm-liouville problem with derivatives of order in $(0, 1)$. In *Proceedings of 2012, 13th International Carpathian Control Conference (ICCC), 978-1-4577-1868*, July 2012.

[94] T. Komatsu. On stable-like processes. *Probability theory and mathematical statistics (Tokyo, 1995)*, pages 210–219, 1995.

[95] Tom Koornwinder. Two-variable analogues of the classical orthogonal polynomials. In *Theory and application of special functions (Proc. Advanced Sem., Math. Res. Center, Univ. Wisconsin, Madison, Wis., 1975)*, pages 435–495. Academic Press New York, 1975.

[96] H.L. Krall and I.M. Sheffer. Orthogonal polynomials in two variables. *Annali di Matematica Pura ed Applicata*, 76(1):325–376, 1967.

[97] K. Krol. Asymptotic properties of fractional delay differential equations. *Appl. Math. Comput.*, 218(5):1515–1532, 2011.

[98] V. V. Kulish and J. L. Lage. Application of fractional calculus to fluid mechanics. *Journal of Fluids Engineering*, 124(3):803–806, 2002.

[99] Pankaj Kumar and Om Prakash Agrawal. An approximate method for numerical solution of fractional differential equations. *Signal Processing*, 86(10):2602–2610, 2006.

[100] Corrias L. and Perthame B. Critical space for the parabolic-parabolic Keller-Segel model in $\setminus^d$. *C.R. Acad. Sci. Paris*, Ser. I 342:745–750, 2006.

[101] Corrias L., Perthame B., and Zaag H. Global solutions of some chemotaxis and angiogenesis systems in high space dimensions. *Milan J. Math.*, 72:1–28, 2004.

[102] V. Lakshmikantham. Theory of fractional functional differential equations. *Nonlinear Anal.*, 69(10):3337–3343, 2008.

[103] T. A. Langlands and B. I. Henry. Fractional chemotaxis diffusion equations. *Physical Review E*, 81:051102, 2010.

[104] TAM Langlands and BI Henry. The accuracy and stability of an implicit solution method for the fractional diffusion equation. *Journal of Computational Physics*, 205(2):719–736, 2005.

[105] M. P. Lazarević and A. M. Spasić. Finite-time stability analysis of fractional order time-delay systems: Gronwall's approach. *Math. Comput. Modelling*, 49(3-4):475–481, 2009.

[106] Randall J LeVeque. *Finite volume methods for hyperbolic problems*, volume 31. Cambridge university press, 2002.

[107] Ch. Li and Y. Wang. Numerical algorithm based on Adomian decomposition for fractional differential equations. *Comput. Math. Appl.*, 57(10):1672–1681, 2009.

[108] X. Li and C. Xu. A space-time spectral method for the time fractional diffusion equation. *SIAM Journal on Numerical Analysis*, 47(3):2108–2131, 2009.

[109] X. Li and C. Xu. Existence and uniqueness of the weak solution of the space-time fractional diffusion equation and a spectral method approximation. *Communications in Computational Physics*, 8(5):1016, 2010.

[110] X. Li and Ch. Xu. A space-time spectral method for the time fractional diffusion equation. *SIAM J. Numer. Anal.*, 47(3):2108–2131, 2009.

[111] Y. Lin and C. Xu. Finite difference/spectral approximations for the time-fractional diffusion equation. *Journal of Computational Physics*, 225(2):1533–1552, 2007.

[112] F. Liu, M. M. Meerschaert, R. J. McGough, P. Zhuang, and Q. Liu. Numerical methods for solving the multi-term time-fractional wave-diffusion equation. *Fractional Calculus and Applied Analysis*, 16(1):9–25, 2013.

[113] Ch Lubich. On the stability of linear multistep methods for volterra convolution equations. *IMA Journal of Numerical Analysis*, 3(4):439–465, 1983.

[114] Ch Lubich. Discretized fractional calculus. *SIAM Journal on Mathematical Analysis*, 17(3):704–719, 1986.

[115] R. L. Magin. *Fractional Calculus in Bioengineering*. Redding, CT: Begell House Inc., 2006.

[116] F. Mainardi. Fractional diffusive waves in viscoelastic solids. *Nonlinear Waves in Solids*, pages 93–97, 1995.

[117] Francesco Mainardi. *Fractional calculus and waves in linear viscoelasticity: an introduction to mathematical models*. Imperial College Press, 2010.

[118] Francesco Mainardi, Gianni Pagnini, and Rudolf Gorenflo. Some aspects of fractional diffusion equations of single and distributed order. *Applied Mathematics and Computation*, 187(1):295–305, 2007.

[119] Mohammad Maleki, Ishak Hashim, Majid Tavassoli Kajani, and Saeid Abbasbandy. An adaptive pseudospectral method for fractional order boundary value problems. In *Abstract and Applied Analysis*, volume 2012. Hindawi Publishing Corporation, 2012.

[120] R. N. Mantegna and H. E. Stanley. Stochastic process with ultraslow convergence to a gaussian: the truncated lévy flight. *Physical Review Letters*, 73(22):2946, 1994.

[121] A. Matzavinos and M. Ptashnyk. Stochastic homogenization of the one-dimensional Keller-Segel chemotaxis system. *Submitted. Preprint available at http://arxiv.org/abs/1310.3430*, 2014.

[122] W. McLean and K. Mustapha. Convergence analysis of a discontinuous galerkin method for a sub-diffusion equation. *Numerical Algorithms*, 52(1):69–88, 2009.

[123] M. M. Meerschaert and A. Sikorskii. *Stochastic models for fractional calculus*, volume 43. Walter de Gruyter, 2011.

[124] M. M. Meerschaert and A. Sikorskii. *Stochastic models for fractional calculus*, volume 43. Walter de Gruyter studies in mathematics, 2012.

[125] M. M. Meerschaert, Y. Zhang, and B. Baeumer. Tempered anomalous diffusion in heterogeneous systems. *Geophysical Research Letters*, 35(17), 2008.

[126] R. Metzler and J. Klafter. The restaurant at the end of the random walk: recent developments in the description of anomalous transport by fractional dynamics. *Journal of Physics A: Mathematical and General*, 37(31):R161, 2004.

[127] Ralf Metzler and Joseph Klafter. The random walk's guide to anomalous diffusion: a fractional dynamics approach. *Physics reports*, 339(1):1–77, 2000.

[128] K. S. Miller and B. Ross. *An Introduction to the Fractional Calculus and Fractional Differential Equations*. New York, NY:John Wiley and Sons, Inc., 1993.

[129] M. L. Morgado, N. J. Ford, and P. M. Lima. Analysis and numerical methods for fractional differential equations with delay. *J. Comput. Appl. Math.*, 252:159–168, 2013.

[130] K. Mustapha and W. McLean. Superconvergence of a discontinuous Galerkin method for fractional diffusion and wave equations. *SIAM J. Numer. Anal.*, 51(1):491–515, 2013.

[131] A. Neamaty, R. Darzi, S. Zaree, and B. Mohammadzadeh. Haar wavelet operational matrix of fractional order integration and its application for eigenvalues of fractional sturm-liouville problem. *World Applied Sciences Journal*, 16(12):1668–1672, 2012.

[132] Z. Odibat. On Legendre polynomial approximation with the VIM or HAM for numerical treatment of nonlinear fractional differential equations. *J. Comput. Appl. Math.*, 235(9):2956–2968, 2011.

[133] T. Ohira and J. Milton. Delayed random walks: Investigating the interplay between delay and noise. In *Delay Differential Equations*, pages 1–31. Springer US, 2009.

[134] K. Osaki and A. Yagi. Finite dimensional attractor for one-dimensional Keller-Segel equations. *Funkcial. Ekvac.*, 44(3):441–469, 2001.

[135] R.G. Owens. Spectral approximations on the triangle. *Proceedings of the Royal Society of London. Series A: Mathematical, Physical and Engineering Sciences*, 454(1971):857–872, 1998.

[136] H.T.C. Pedro, M.H. Kobayashi, J.M.C. Pereira, and C.F.M. Coimbra. Variable order modeling of diffusive-convective effects on the oscillatory flow past a sphere. *Journal of Vibration and Control*, 14(9-10):1659–1672, 2008.

[137] T. Penzl. A cyclic low-rank smith method for large sparse Lyapunov equations. *SIAM Journal on Scientific Computing*, 21(4):1401–1418, 1999.

[138] B. Perthame. *Transport Equations in Biology*. Springer, NewYork, 2007.

[139] S. Picozzi and B. J. West. Fractional Langevin model of memory in financial markets. *Phys. Rev. E (3)*, 66(4):046118, 12, 2002.

[140] C. Piret and E. Hanert. A radial basis functions method for fractional diffusion equations. *J. Comp. Physics*, pages 71–81, 2012.

[141] I. Podlubny. Numerical solution of ordinary fractional differential equations by the fractional difference method. In *Advances in difference equations (Veszprém, 1995)*, pages 507–515. Gordon and Breach, Amsterdam, 1997.

[142] I Podlubny. *Fractional Differential Equations*. San Diego, CA, USA: Academic Press, 1999.

[143] J. Proriol. Sur une famille de polynomes á deux variables orthogonaux dans un triangle. *COMPTES RENDUS HEBDOMADAIRES DES SEANCES DE L ACADEMIE DES SCIENCES*, 245(26):2459–2461, 1957.

[144] J. Qi and S. Chen. Eigenvalue problems of the model from nonlocal continuum mechanics. *Journal of Mathematical Physics*, 52:073516, 2011.

[145] L. Qiu, W. Deng, and J. Hesthaven. Nodal discontinuous galerkin methods for fractional diffusion equations on 2d domain with triangular meshes. *arXiv preprint arXiv:1410.0796*, 2014.

[146] Lynnette ES Ramirez and Carlos FM Coimbra. A variable order constitutive relation for viscoelasticity. *Annalen der Physik*, 16(7-8):543–552, 2007.

[147] EA Rawashdeh. Numerical solution of fractional integro-differential equations by collocation method. *Applied mathematics and computation*, 176(1):1–6, 2006.

[148] W. H. Reed and T.R. Hill. Triangularmesh methodsfor the neutrontransportequation. *Los Alamos Report LA-UR-73-479*, 1973.

[149] M. Rivero, J. J. Trujillo, and M. P. Velasco. A fractional approach to the Sturm-Liouville problem. *Central European Journal of Physics*, 11(10):1246–1254, 2013.

[150] J. P. Roop. Variational solution of the fractional advection-dispersion equation, phd dissertation, clemson university, department of mathematical sciences, 2004.

[151] J. P. Roop. Computational aspects of fem approximation of fractional advection dispersion equations on bounded domains in r2. *Journal of Computational and Applied Mathematics*, 193(1):243–268, 2006.

[152] Y. Saad. *Numerical solution of large Lyapunov equations*. Research Institute for Advanced Computer Science, NASA Ames Research Center, 1989.

[153] F. Sabzikar, M. M. Meerschaert, and J. Chen. Tempered fractional calculus. *Journal of Computational Physics (in press)*, 2014.

[154] JM Sanz-Serna. A numerical method for a partial integro-differential equation. *SIAM journal on numerical analysis*, 25(2):319–327, 1988.

[155] E. Scalas, R. Gorenflo, and F. Mainardi. Fractional calculus and continuous-time finance. *Phys. A*, 284(1-4):376–384, 2000.

[156] R. Schumer, D. A. Benson, M. M. Meerschaert, and S. W. Wheatcraft. Eulerian derivation of the fractional advection-dispersion equation. *Journal of Contaminant Hydrology*, 48:69 – 88, 2001.

[157] S. Shen, F. Liu, V. Anh, I. Turner, and J Chen. A characteristic difference method for the variable-order fractional advection-diffusion equation. *Journal of Applied Mathematics and Computing*, pages 1–16, 2013.

[158] S. Shen, F. Liu, J. Chen, I. Turner, and V. Anh. Numerical techniques for the variable order time fractional diffusion equation. *Applied Mathematics and Computation*, 218(22):10861–10870, 2012.

[159] S. J. Sherwin and G. E. Karniadakis. A new triangular and tetrahedral basis for high-order (hp) finite element methods. *International Journal for Numerical Methods in Engineering*, 38(22):3775–3802, 1995.

[160] A. Si-Ammour, S. Djennoune, and M. Bettayeb. A sliding mode control for linear fractional systems with input and state delays. *Commun. Nonlinear Sci. Numer. Simul.*, 14(5):2310–2318, 2009.

[161] IM Sokolov, AV Chechkin, and J Klafter. Fractional diffusion equation for a power-law-truncated Lévy process. *Physica A: Statistical Mechanics and its Applications*, 336(3):245–251, 2004.

[162] T. Srokowski. Lévy flights in nonhomogeneous media: distributed-order fractional equation approach. *Physical Review E*, 78(3):031135, 2008.

[163] N Sugimoto. Burgers equation with a fractional derivative; hereditary effects on nonlinear acoustic waves. *J. Fluid Mech*, 225(631-653):4, 1991.

[164] N Sugimoto and T Kakutani. generalized burgers' equation for nonlinear viscoelastic waves. *Wave motion*, 7(5):447–458, 1985.

[165] H. G. Sun, W. Chen, and Y. Q. Chen. Variable-order fractional differential operators in anomalous diffusion modeling. *Physica A: Statistical Mechanics and its Applications*, 388(21):4586–4592, 2009.

[166] Zhi-zhong Sun and Xiaonan Wu. A fully discrete difference scheme for a diffusion-wave system. *Applied Numerical Mathematics*, 56(2):193–209, 2006.

[167] N. H. Sweilam, M. M. Khader, and A. M. S. Mahdy. Numerical studies for fractional-order Logistic differential equation with two different delays. *J. Appl. Math.*, pages Art. ID 764894, 14, 2012.

[168] Gabor Szegö. *Orthongonal Polynomials*, volume 23. AMS Bookstore, 1992.

[169] Hillen T. and Potapov A. The one-dimensional chemotaxis model: global existence and asymptotic profile. *Math. Meth. Appl. Sci.*, 27:1783–1801, 2004.

[170] Nagai T. Blow-up of radially symmetric solutions to a chemotaxis system. *Adv. Math. Sci. Appl.*, 5:581–601, 1995.

[171] Nagai T., Senba T., and K. Yoshida. Application of the Trundinger-Moser inequality to a parabolic system of chemotaxis. *Funkcial. Ekvac.*, 40(3):411–433, 1997.

[172] C.C. Tseng. Design of variable and adaptive fractional order fir differentiators. *Signal Processing*, 86(10):2554–2566, 2006.

[173] Jäger W. and Luckhaus S. On explosions of solutions to a system of partial differential equations modelling chemotaxis. *Trans. Amer. Math. Soc.*, 329:819–824, 1992.

[174] E.L. Wachspress. Iterative solution of the Lyapunov matrix equation. *Applied Mathematics Letters*, 1(1):87–90, 1988.

[175] Z. Wang, X. Huang, and G. Shi. Analysis of nonlinear dynamics and chaos in a fractional order financial system with time delay. *Comput. Math. Appl.*, 62(3):1531–1539, 2011.

[176] Z. Wang, X. Huang, and J. Zhou. A numerical method for delayed fractional-order differential equations: based on g-l definition. *Appl. Math. Inf. Sci.*, 7(2L):525–529, 2013.

[177] B. J. West, M. Bologna, and P. Grigolini. *Physics of Fractal Operators*. New York, NY: Springer Verlag., 2003.

[178] B.A. Wingate and M. A. Taylor. The natural function space for triangular and tetrahedral spectral elements. *Submitted to SIAM Journal on Numerical Analysis*, 1998.

[179] Q. Xu and J.S. Hesthaven. Discontinuous Galerkin method for fractional convection-diffusion equations. *arXiv:1304.6047*, 2013.

[180] Q. Xu and J.S. Hesthaven. Stable multi-domain spectral penalty methods for fractional partial differential equations. *Journal of Computational Physics*, 257:241–258, 2014.

[181] Y. Yan and Ch. Kou. Stability analysis of a fractional differential model of HIV infection of $CD4^+$ T-cells with time delay. *Math. Comput. Simulation*, 82(9):1572–1585, 2012.

[182] M. Zayernouri, M. Ainsworth, and G. E. Karniadakis. Tempered fractional Sturm-Liouville eigen-problems. *SIAM Journal on Scientific Computing (2014)-submitted*.

[183] M. Zayernouri, M. Ainsworth, and G. E. Karniadakis. A unified petrov-galerkin spectral method for fractional pdes. *Computer Methods in Applied Mechanics and Engineering,*, page http://dx.doi.org/10.1016/j.cma.2014.10.051, 2014.

[184] M. Zayernouri, W. Cao, Z. Zhang, and G. E. Karniadakis. Spectral and discontinuous spectral element methods for fractional delay equations. *SIAM Journal on Scientific Computing*, 36(6):B904–B929, 2014.

[185] M. Zayernouri and G. E. Karniadakis. Fractional spectral collocation methods for linear and nonlinear variable order fpdes. *J. Comp. Physics, A Special Issue on FPDEs, (2014)-Accepted*.

[186] M. Zayernouri and G. E. Karniadakis. Spectral methods for distributed-order differential equations. *J. Comp. Physics, (2014)-to be submitted*.

[187] M. Zayernouri and G. E. Karniadakis. Fractional Sturm-Liouville eigen-problems: theory and numerical approximations. *J. Comp. Physics*, 47-3:2108–2131, 2013.

[188] M. Zayernouri and G. E. Karniadakis. Discontinuous spectral element methods for time- and space-fractional advection equations. *SIAM Journal on Scientific Computing*, 36(4):B684–B707, 2014.

[189] M. Zayernouri and G. E. Karniadakis. Exponentially accurate spectral and spectral element methods for fractional odes. *J. Comp. Physics*, 257:460–480, 2014.

[190] M. Zayernouri and G. E. Karniadakis. Fractional spectral collocation method. *SIAM Journal on Scientific Computing*, 36(1):A40–A62, 2014.

[191] M. Zayernouri and A. Matzavinos. High-order methods for keller-segel chemotaxis equatios. *SIAM Journal on Multiscale Simulations-to be submitted*, 2014.

[192] A. Zettl. *Sturm-Liouville Theory*, volume 121. American Mathematical Soc., 2010.

[193] H. Zhang, F. Liu, M. S. Phanikumar, and M. M. Meerschaert. A novel numerical method for the time variable fractional order mobile–immobile advection–dispersion model. *Computers & Mathematics with Applications*, 2013.

[194] P. Zhuang, F. Liu, V. Anh, and I. Turner. Numerical methods for the variable-order fractional advection-diffusion equation with a nonlinear source term. *SIAM Journal on Numerical Analysis*, 47(3):1760–1781, 2009.

[195] O. C. Zienkiewicz, R. L. Taylor, and J. Z. Zhu. *The Finite Element Method: Its Basis and Fundamentals: Its Basis and Fundamentals*. Butterworth-Heinemann, 2005.